Cycle atmosphérique du mercure dans des zones reculées de l'Hémisphère Sud : cas de la couche limite marine subantarctique et du continent Antarctique

Hélène Angot

▶ **To cite this version:**

Hélène Angot. Cycle atmosphérique du mercure dans des zones reculées de l'Hémisphère Sud : cas de la couche limite marine subantarctique et du continent Antarctique. Océan, Atmosphère. Université Grenoble Alpes, 2016. Français. NNT : 2016GREAU014 . tel-01536102

HAL Id: tel-01536102
https://theses.hal.science/tel-01536102

Submitted on 10 Jun 2017

HAL is a multi-disciplinary open access archive for the deposit and dissemination of scientific research documents, whether they are published or not. The documents may come from teaching and research institutions in France or abroad, or from public or private research centers.

L'archive ouverte pluridisciplinaire **HAL**, est destinée au dépôt et à la diffusion de documents scientifiques de niveau recherche, publiés ou non, émanant des établissements d'enseignement et de recherche français ou étrangers, des laboratoires publics ou privés.

Communauté
UNIVERSITÉ Grenoble Alpes

THÈSE

Pour obtenir le grade de

DOCTEUR DE LA COMMUNAUTE UNIVERSITE GRENOBLE ALPES

Spécialité : **Sciences de la Terre, de l'Univers et de l'Environnement**

Arrêté ministériel : 7 août 2006

Présentée par

Hélène ANGOT

Thèse dirigée par **Aurélien DOMMERGUE**

préparée au sein du **Laboratoire de Glaciologie et Géophysique de l'Environnement**
dans **l'Ecole Doctorale Terre Univers Environnement**

Cycle atmosphérique du mercure dans des zones reculées de l'Hémisphère Sud : cas de la couche limite marine subantarctique et du continent Antarctique

Thèse soutenue publiquement le **7 novembre 2016**
devant le jury composé de :

Mme Catherine CHAUVEL
Directrice de Recherche au CNRS, ISTerre, Grenoble, Présidente
M. Alfonsó SAIZ-LOPEZ
Research Scientist, CSIC, Madrid, Espagne, Rapporteur
M. Jeroen SONKE
Directeur de Recherche au CNRS, GET, Toulouse, Rapporteur
Mme Céline MARI
Directrice de Recherche au CNRS, LA, Toulouse, Examinatrice
M. Aurélien DOMMERGUE
Maître de conférences à l'UGA, LGGE, Grenoble, Directeur de thèse

Remerciements

Ces trois années de thèse ont été une véritable aventure scientifique et humaine. Merci Aurélien pour ta confiance et ton soutien. Merci Olivier pour ta joie de vivre. Travailler avec vous deux a été un réel plaisir et ces trois années sont décidemment passées beaucoup trop vite.

Rien de tout cela n'aurait par ailleurs pu être possible sans le travail effectué par les Volontaires au Service Civique sur les bases d'Amsterdam, Dumont d'Urville et Concordia dans le cadre du programme GMOstral de l'IPEV. Merci donc à B. Brouillard, E. Coz, M. Le Dréau, A. Croguennoc, V. Lucaire, J. Chastain, J. Marais, N. Joly, I. Jouvie et M. De Florinier à AMS, N. Coillard, N. Vogel, B. Jourdain, D. Buiron, B. Laulier, J. Guilhermet, A. Thollot, S. Auguado, S. Oros et G. Dufresnes à DDU, et S. Aubin, A. Barbero, C. Lenormant, R. Jacob, N. Hueber et P. Serre à DC. L'interprétation des données recueillies n'aurait pu être possible sans l'aide précieuse de nombreux collaborateurs. Un merci tout particulier à Michel Legrand pour les longues heures passées à travailler sur DDU et à Hubert Gallée pour la mise à disposition des sorties MAR. Merci à Noelle Selin pour l'accueil au sein de son groupe au MIT au cours de l'été 2014 et à Shaojie Song pour la collaboration étroite initiée à cette occasion.

Merci aux membres du jury, Catherine Chauvel, Céline Mari, Alfonsó Saiz-Lopez et Jeroen Sonke pour l'intérêt porté à mes travaux.

Un merci tout particulier à toutes les personnes fantastiques rencontrées à bord du Marion Dufresne ou sur les différentes bases, et qui ont fait de mes trois missions sur l'Ile Amsterdam une expérience humaine d'une intensité incomparable.

Merci à Laure, pour tout, et ce depuis le tout premier jour de cette thèse. A Marion, co-bureau d'amour (instant love !), pour toutes ces joies et ces peines partagées. A Ilann, pour tous ces entraînements dans la joie parfois, la douleur souvent, et pour ce sourire niais qui te va si bien. A Julien B de Combloux (p'tit loup), pour toutes ces pauses thé. A Alban (p'tit biscuit aux jambes si douces), Etienne, Olivier P, Albane, Julien B de Belgique, Cyrille, Thomas, Elsa, Fanny, Chloé, Ruben, Delphine et Antho, Jean, Daminouchou, Thomas et Marie, pour tous ces bons moments partagés ensemble au labo ou sur Grenoble. A Beef, Nuria, Junior, JD, Geo, Wilou, Jenny, Kévin, Mélo, Galou, Elsa, Eva, Fabienne et Yo, pour tous ces moments partagés ensemble aux quatre coins du monde. A Nico, merci pour tant, pour tout.

Enfin, merci à ma famille. J'ai beau ne pas être souvent présente, sachez que vous m'accompagnez chaque jour dans mon cœur…

Résumé

Le mercure (Hg) est un métal émis dans l'atmosphère par des sources naturelles et anthropiques. Il est préoccupant à l'échelle mondiale de par sa propagation atmosphérique sur de longues distances, loin des sources d'émissions, sa persistance dans l'environnement, son potentiel de bioaccumulation dans les chaînes alimentaires aquatiques et ses effets néfastes sur la santé humaine. Les modèles atmosphériques, utilisés pour retracer son cheminement depuis les sources d'émissions jusqu'aux dépôts au sein des écosystèmes, sont entachés de fortes incertitudes en raison notamment de notre compréhension partielle des processus atmosphériques (réactions d'oxydo-réduction, dépôts, réémissions) et du manque de données d'observations à l'échelle planétaire. L'objectif de ces travaux de thèse est d'améliorer notre compréhension du cycle atmosphérique du Hg en trois sites reculés de l'Hémisphère Sud : l'île d'Amsterdam (AMS) en plein océan Indien, Concordia (DC) sur la calotte glaciaire antarctique et Dumont d'Urville (DDU) sur la côte Est du continent. Les données acquises à AMS démontrent une réactivité atmosphérique limitée du Hg dans cette région du globe. L'île étant faiblement et rarement influencée par des masses d'air continentales polluées, il s'agit d'un site clé pour la surveillance, sur le long terme, du bruit de fond atmosphérique aux moyennes latitudes de l'Hémisphère Sud. Les données acquises en Antarctique démontrent l'existence de processus inédits en termes de réactivité dans l'atmosphère et à l'interface air-neige. Les processus observés sur la calotte glaciaire influent par ailleurs sur le cycle du Hg à l'échelle continentale du fait des forts vents catabatiques. Ces avancées scientifiques permettront, à terme, de contraindre et d'améliorer les modèles atmosphériques globaux.

Mots-clés : Mercure ; Cycle atmosphérique ; Hémisphère Sud ; Antarctique ; Couche limite marine subantarctique.

Abstract

Mercury (Hg) is a metal emitted by both natural and anthropogenic sources. It is of global concern owing to its long-range atmospheric transport, its persistence in the environment, its ability to bioaccumulate in ecosystems, and its negative effects on human health. Large uncertainties associated with atmospheric models – that trace the link from emissions to deposition of Hg onto environmental surfaces – arise as a result of our incomplete understanding of atmospheric processes (oxidation pathways, deposition, and reemission) and of the scarcity of monitoring data at a global scale. The aim of this PhD work is to improve our understanding of the atmospheric Hg cycling at three remote sites of the Southern Hemisphere: Amsterdam Island (AMS) in the Indian Ocean, Concordia (DC) on the East Antarctic ice sheet, and Dumont d'Urville (DDU) on the East Antarctic coast. Data acquired at AMS suggest a limited atmospheric reactivity of Hg in this part of the globe. The advection of polluted continental air masses being scarce, AMS is a key site for the long-term monitoring of the atmospheric background in the Southern Hemisphere midlatitudes. Data acquired in Antarctica highlight the occurrence of unprecedented processes in the atmosphere and at the air-snow interface. Due to katabatic winds flowing out from the East Antarctic ice sheet down the steep vertical drops along the coast, processes observed at DC influence the cycle of atmospheric Hg on a continental scale. These scientific breakthroughs will ultimately lead to improved global transport and deposition models.

Keywords: Mercury; Atmospheric cycling; Southern Hemisphere; Antarctica; Subantarctic marine boundary layer.

Table des matières

1 Le mercure, une menace pour la santé humaine et les écosystèmes

1.1 Généralités sur le mercure

1.1.1 Propriétés physico-chimiques

Le mercure (Hg, du latin *hydrargyrum* signifiant argent liquide) est un métal argenté. Il s'agit du seul métal qui soit liquide dans les conditions standard de température et de pression (CSTP). Ses propriétés physico-chimiques (volatilité élevée, faible résistance électrique, coefficient de dilatation élevé, capacité à s'amalgamer avec divers métaux tels l'or, l'argent ou le palladium) en font un composé de choix pour diverses applications artisanales, industrielles ou médicales (voir section 1.1.2.).

De configuration électronique [Xe] $4f^{14}$ $5d^{10}$ $6s^2$, le mercure existe sous plusieurs degrés d'oxydation : 0 (mercure élémentaire, noté Hg(0)), +I (ion mercureux, noté Hg(I)) et +II (ion mercurique, noté Hg(II)). La forme élémentaire peut être oxydée en ions mercureux et mercuriques. Ces ions s'associent à d'autres éléments pour former des complexes inorganiques (p. ex. HgO, $HgCl_2$, $HgBr_2$) ou organométalliques (p. ex. CH_3HgCl, $Hg(CH_3)_2$), ou s'adsorbent sur des particules pour former du mercure particulaire (noté Hg(p)). Le mercure tend également à former des liaisons covalentes avec les composés soufrés tel le sulfure de mercure (HgS, nommé cinabre en minéralogie), espèce mercurielle la plus abondante au sein de la croûte terrestre (Rytuba, 2003).

Les propriétés et la réactivité chimique du mercure dépendent de son degré d'oxydation (Ariya et al., 2015). Une compilation des propriétés physico-chimiques d'une sélection d'espèces mercurielles inorganiques et organométalliques est présentée dans le Tableau 1-1. Celles-ci peuvent varier de plusieurs ordres de grandeur d'une espèce mercurielle à une autre. Hg(0) est ainsi peu soluble dans l'eau par rapport à une espèce divalente comme $HgCl_2$, mais plus volatil que HgO. Le coefficient de partage octanol/eau renseigne quant à la lipophilie des espèces considérées. Plus ce coefficient est élevé, plus l'espèce considérée est apte à franchir la barrière hémato-encéphalique et le placenta et à se bioaccumuler au sein des organismes vivants (voir section 1.3).

Le mercure, émis au sein des écosystèmes par des sources naturelles et anthropiques (voir section 1.1.3), existe donc sous différentes formes chimiques aux propriétés physico-chimiques diverses. Il en résulte un cycle biogéochimique très complexe (voir section 1.2).

Tableau 1-1: Propriétés physico-chimiques pour une sélection d'espèces mercurielles inorganiques et organométalliques. D'après Schroeder and Munthe (1998) et Ariya et al. (2015).

Espèces	Etat dans les CSTP	Solubilité dans l'eau à 25 °C (mol kg^{-1})	Coefficient de partage octanol/eau	Constante de Henry (Pa m^3 mol^{-1})
Hg(0)	Liquide	3×10^{-7}	4,2	729 (à 20 °C)
$HgCl_2$	Solide	0,27	0,5	$3,69\times10^{-5}$ (à 20 °C)
$Hg(CH_3)_2$	Liquide	Insoluble	180	646 (à 25 °C)
$HgBr_2$	Solide	0,017	-	-
HgO	Solide	2×10^{-4}	-	$3,76\times10^{-11}$ (à 25 °C)
HgS	Solide	Insoluble	-	-

1.1.2 Utilisations du mercure

Le mercure est utilisé par l'Homme depuis plusieurs milliers d'années. Le cinabre a ainsi très tôt été exploité afin d'en produire à des fins thérapeutiques, comme colorant ou pour amalgamer l'argent destiné à produire la monnaie. La mine d'Almadén en Espagne était ainsi déjà exploitée par les Romains (Selin, 2009). A l'heure actuelle, le mercure est encore très largement utilisé ; on en retrouve en petites quantités dans des batteries, des piles, des peintures, des composés électroniques, certains types de thermomètres, les ampoules à basse consommation d'énergie, certains pesticides et fongicides, dans le domaine médical (antiseptiques, amalgames dentaires) ou encore dans des produits cosmétiques à titre d'agent de conservation (UNEP, 2013a). L'utilisation du mercure dans certains secteurs de l'industrie (p. ex. électrolyseur à cathode de mercure dans l'industrie du chlore, catalyseur au mercure pour la production de chlorure de vinyle à partir d'acétylène) est désormais fortement réglementée (voir section 1.4). En revanche, il reste fortement utilisé dans le secteur artisanal de la mine aurifère engendrant une contamination importante de l'environnement (voir sections 1.1.3 et 1.3).

1.1.3 Les sources d'émissions de mercure

1.1.3.1 Sources naturelles

Le mercure peut être émis dans l'environnement *via* des processus naturels tels le dégazage de la croûte terrestre, les éruptions volcaniques, l'activité géothermale ou encore l'érosion des sols et des roches. Certaines régions du globe, situées à la frontière de plaques tectoniques, sont connues pour être naturellement riches en mercure (« the mercuriferous belts ») (Varekamp and Buseck, 1986). On estime à l'heure actuelle qu'à l'échelle mondiale, environ 10 % des émissions de mercure proviennent de sources naturelles (Amos et al., 2013). Cependant, les inventaires d'émissions naturelles sont entachés de fortes incertitudes (Pacyna et al., 2006; Ariya et al., 2015). Parmi ces émissions naturelles, on attribue 500 Mg an^{-1} aux

émissions primaires terrestres[1] (Lindqvist, 1991), 60 Mg an^{-1} aux émissions d'origine géothermique (Varekamp and Buseck, 1986) et 100-700 Mg an^{-1} aux émissions liées aux éruptions volcaniques (Nriagu and Becker, 2003; Pyle and Mather, 2003).

1.1.3.2 Sources anthropiques

Environ 30 % des émissions de mercure à l'échelle mondiale proviennent de sources anthropiques (Amos et al., 2013). Au cours du XX^{ème} siècle, la source anthropique principale fut la combustion de ressources fossiles (principalement du charbon, Figure 1-1a) (p. ex. Pacyna et al., 2010; Streets et al., 2011). Selon les dernières estimations (UNEP, 2013a), le secteur artisanal de la mine aurifère serait à présent la principale source à l'échelle mondiale, représentant 35 % des émissions anthropiques totales. Les chiffres liés aux émissions de mercure par ce secteur d'activité sont cependant soumis à caution compte tenu de la difficulté à obtenir des inventaires d'émissions fiables pour une activité qui est le plus souvent non réglementée, voire illégale.

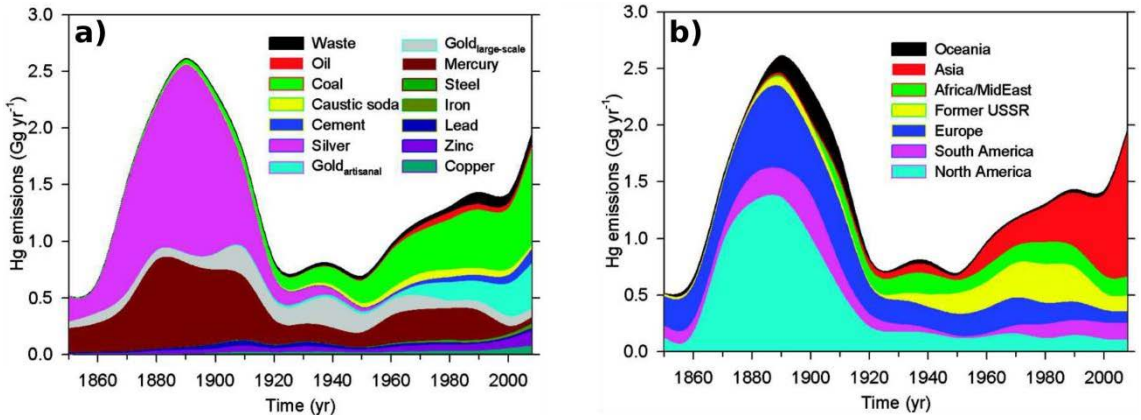

Figure 1-1: Evolution temporelle, de 1850 à 2008, des émissions anthropiques de mercure **a)** par type de source et **b)** par secteur géographique. D'après Streets et al. (2011).

D'après une étude menée par Streets et al. (2011), les émissions anthropiques de mercure à l'échelle mondiale ont culminé à 2600 Mg an^{-1} en 1890 (ruée vers l'or en Amérique du Nord). Les émissions ont par la suite diminué jusqu'à atteindre 700-800 Mg an^{-1} pendant l'entre-deux-guerres, avant d'augmenter progressivement à partir de 1950 jusqu'aux valeurs actuelles de l'ordre de 2000 Mg an^{-1}. Il est à noter que l'incertitude associée à ces estimations est de l'ordre de 25 à 30 % (Selin, 2009). Bien que le pic d'émissions anthropiques de mercure pendant la ruée vers l'or puisse être surestimé (Engstrom et al., 2014), leur augmentation depuis la fin de la seconde guerre mondiale est confirmée par l'analyse d'archives sédimentaires et glaciaires de par le monde (p. ex. Schuster et al., 2010; Beal et al., 2015; Kang et al., 2016). On estime à 350 Gg la quantité totale de mercure émise par les activités humaines depuis l'Antiquité (Streets et al., 2011). Les émissions anthropiques de mercure depuis l'Antiquité auraient engendré une augmentation des concentrations atmosphériques et des dépôts de mercure au sein des écosystèmes (voir section 1.2 pour le

[1] 1 Mg = 1 tonne ; 1 Gg = 1000 tonnes.

cycle biogéochimique du mercure) d'un facteur 7 à 10 à l'échelle mondiale (Amos et al., 2013; Serrano et al., 2013).

Les émissions anthropiques de mercure ont décliné en Amérique du Nord et en Europe au cours des dernières décennies (Figure 1-1b) grâce, notamment, aux politiques de réduction des émissions de soufre instaurées dans les années 1980 (Selin, 2009; Pudasainee et al., 2016). Cependant, comme le montre la Figure 1-1b, elles continuent d'augmenter en Asie en raison d'un développement économique galopant et d'une forte dépendance aux énergies fossiles. Plusieurs études ont montré que l'Asie est à l'heure actuelle la région la plus émettrice de mercure, comptant pour près de 50 % des émissions anthropiques mondiales (Streets et al., 2005; Lin et al., 2010b; Pirrone et al., 2010; Streets et al., 2011). Des études récentes ont par ailleurs proposé des projections pour 2050 à l'échelle mondiale, en se basant sur différents *scenarii* d'émissions anthropiques de mercure. Ces émissions pourraient diminuer jusqu'à 800 Mg an^{-1} en cas de mise en place de politiques contraignantes sur les émissions de mercure et de gaz à effet de serre (Rafaj et al., 2013), ou au contraire inexorablement augmenter jusqu'à 4860 Mg an^{-1} si aucune politique adaptée n'est mise en place (« business-as-usual scenario », Streets et al., 2009). Par ailleurs, la mise en place de technologies visant à limiter les émissions de mercure (notamment sur les centrales au charbon) pourrait engendrer une diminution des émissions sous forme de vapeurs de Hg(0) et une augmentation des émissions sous forme de Hg(II) (Streets et al., 2009), engendrant une modification du cycle atmosphérique du mercure du fait de la réactivité différente de ces deux espèces (voir section 1.2).

1.1.3.3 Réémissions

Le mercure émis *via* des sources naturelles et anthropiques circule au sein des différents réservoirs environnementaux (voir section 1.2 ci-dessous) pendant des centaines voire des milliers d'années avant d'être stocké dans les sédiments au fond des océans (Selin et al., 2008). Il en résulte des réémissions de mercure qui représentent 60 % des émissions annuelles (Amos et al., 2013). Les océans relargueraient ainsi chaque année entre 800 et 5500 Mg de mercure vers l'atmosphère (voir section 2.1.3.2.1). La végétation et les feux de biomasse seraient par ailleurs responsables de l'émission de 740 Mg an^{-1} (Smith-Downey et al., 2010) et 675 (± 240) Mg an^{-1} (Friedli et al., 2009b) de mercure, respectivement. Il est à noter que les émissions par les feux de biomasse suivent une distribution latitudinale et varient chaque année (De Simone et al., 2015).

1.2 Cycle du mercure au sein des écosystèmes

Le mercure se trouve dans l'atmosphère sous trois formes principales : Hg(0), qui représente plus de 90 % des espèces mercurielles atmosphériques (Slemr et al., 1985; Schroeder et al., 1991), Hg(II) et Hg(p). Avec un temps de vie estimé à 0,8-1,7 an (voir

section 2.1.1), Hg(0) est transporté sur de longues distances (des centaines de milliers de kilomètres, Figure 1-2) au sein de la troposphère. Les émissions sont ainsi transportées à l'échelle mondiale. *A contrario*, du fait d'une solubilité et d'une réactivité élevées (Tableau 1-1), les espèces divalentes gazeuses (Hg(II)) et particulaires (Hg(p)) se déposent plus rapidement puisqu'on estime qu'elles sont transportées sur quelques dizaines à quelques centaines de kilomètres seulement (Schroeder and Munthe, 1998).

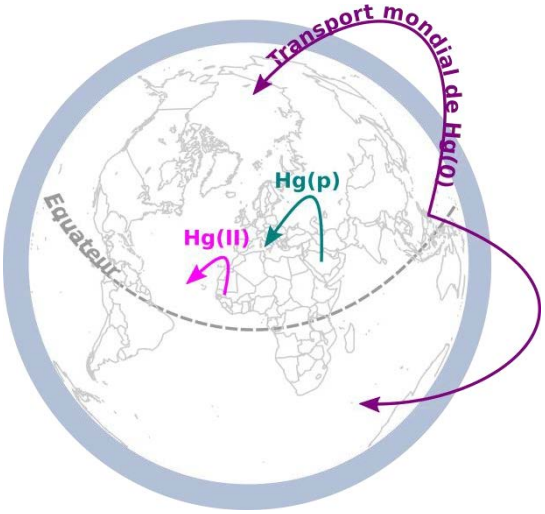

Figure 1-2: Transport troposphérique des espèces mercurielles. Hg(0) peut être transporté sur de très longues distances alors que Hg(II) et Hg(p) se déposent à proximité des sources d'émissions.

La Figure 1-3 présente une version simplifiée du cycle atmosphérique du mercure. Comme indiqué précédemment, le mercure se trouve principalement sous sa forme élémentaire gazeuse (Hg(0)) dans l'atmosphère. Il s'agit en outre de l'espèce mercurielle majoritairement émise par diverses sources naturelles et anthropiques (voir section 1.1.3). Hg(0) peut être oxydé en espèces divalentes (Hg(II) et Hg(p)) plus solubles et plus réactives, qui se déposent au sein des écosystèmes par voies sèches (sédimentation, adsorption *etc.*) et humides (précipitations). Une fois déposé, le mercure peut être réémis vers l'atmosphère (voir section 1.1.3.3) ou converti (dans les écosystèmes aquatiques) en CH_3Hg^+ ou $Hg(CH_3)_2$ (conjointement notés MeHg par la suite) *via* des processus biologiques (Jensen and Jernelov, 1969) ou abiotiques (Benoit et al., 2003) de méthylation. Le MeHg est un composé hautement toxique et bioaccumulable au sein des chaînes alimentaires. Les processus de bioaccumulation et de bioamplification permettent d'expliquer le gradient de concentration observé entre l'eau, de l'ordre du ng L^{-1} (ppt), et les poissons, de l'ordre du µg g^{-1} (ppm) (Morel et al., 1998). Dans les pays développés, la consommation de poisson constitue la principale source d'exposition de l'Homme au MeHg (Sunderland, 2007), celui-ci pouvant engendrer des effets néfastes sur le développement du système nerveux (voir section 1.3 ci-dessous).

La réactivité atmosphérique du mercure (réactions d'oxydo-réduction, processus de dépôts et réémissions) sera discutée plus en détails au sein de la section 2.1. L'atmosphère est un réservoir clé du cycle biogéochimique du mercure puisque c'est *via* cette dernière que les

émissions sont transportées à l'échelle planétaire et que le mercure, en étant oxydé, est déposé vers les écosystèmes et peut intégrer les chaînes alimentaires. Ce réservoir constitue le cœur de ces travaux de thèse.

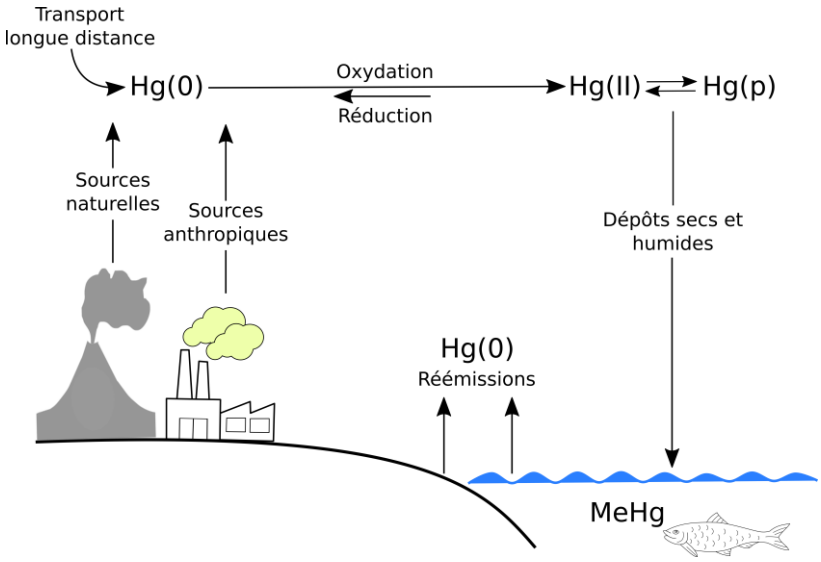

Figure 1-3: Schéma simplifié du cycle atmosphérique du mercure.

1.3 Impacts sur la santé humaine et animale

L'impact du mercure sur la santé dépend notamment du type d'espèce mercurielle (p. ex. Hg(0), MeHg), de la dose, de l'âge ou du stade de développement de la personne exposée, de la durée d'exposition, ainsi que du mode d'exposition (p. ex. inhalation, ingestion).

L'inhalation de vapeurs de Hg(0) peut engendrer des effets nocifs sur les systèmes nerveux, digestif et immunitaire, ainsi que sur les poumons et les reins (WHO, 2007). Les populations travaillant ou vivant à proximité d'exploitations aurifères artisanales sont particulièrement exposées à ce type de vapeurs (Wade, 2013; Gibb and O'Leary, 2014; Bose-O'Reilly et al., 2016; Nakazawa et al., 2016; Obiri et al., 2016; Riaz et al., 2016). Le Hg(0) émis vers l'atmosphère pouvant être oxydé, déposé au sein des écosystèmes et converti en MeHg, ces populations sont également exposées à des concentrations élevées en MeHg *via* leur alimentation (voir ci-après).

La découverte scientifique des risques pour la santé résultant d'une exposition au MeHg remonte à 1865 (Edwards, 1865). L'ataxie (troubles de la coordination des mouvements volontaires), la dysarthrie (troubles de l'articulation de la parole), la constriction du champ visuel, une déficience auditive et des troubles sensoriels furent alors listés parmi les symptômes d'intoxication au MeHg. Les connaissances scientifiques sur le MeHg et ses effets toxiques ont depuis progressé et ont fait l'objet de nombreuses publications (p. ex. Clarkson and Magos, 2006; Mergler et al., 2007; Choi and Grandjean, 2008; Li et al., 2010). Une série d'intoxications alimentaires de masse eut lieu suite à l'utilisation malencontreuse, pour

la fabrication de pain, de graines traitées par des fongicides au MeHg et autres composés d'éthylmercure : en Iraq en 1955-1956 et 1959-1960 (Jalili and Abbasi, 1961), au Pakistan en 1961 (Haq, 1963), au Guatemala en 1965 (Ordonez et al., 1966), et à nouveau en Iraq en 1970-1971 (Bakir et al., 1973). Dans les années 1950, la catastrophe de Minamata au Japon fut le premier incident d'empoisonnement au MeHg à grande échelle (Harada, 1995). Pendant plusieurs dizaines d'années, une usine pétrochimique installée dans la baie de Minamata rejeta des résidus de mercure et autres métaux lourds à la mer. S'ensuivit une contamination de tout l'écosystème aquatique, le MeHg s'accumulant au sein de la chaîne alimentaire. La maladie de Minamata, officiellement reconnue en 1956, atteignit principalement les pêcheurs et autres consommateurs réguliers de poisson. Des centaines de personnes moururent, des dizaines de milliers d'individus furent atteints de troubles neurologiques tandis que nombre d'enfants naquirent avec des malformations, handicaps ou troubles mentaux (Figure 1-4). D'autres cas d'empoisonnement au MeHg, bien que de moindre ampleur, survinrent par la suite à Niigata au Japon en 1965 (Takizawa and Osame, 2001) et au sein d'une tribu autochtone en Ontario (Canada) en 1969 (Harada et al., 2011).

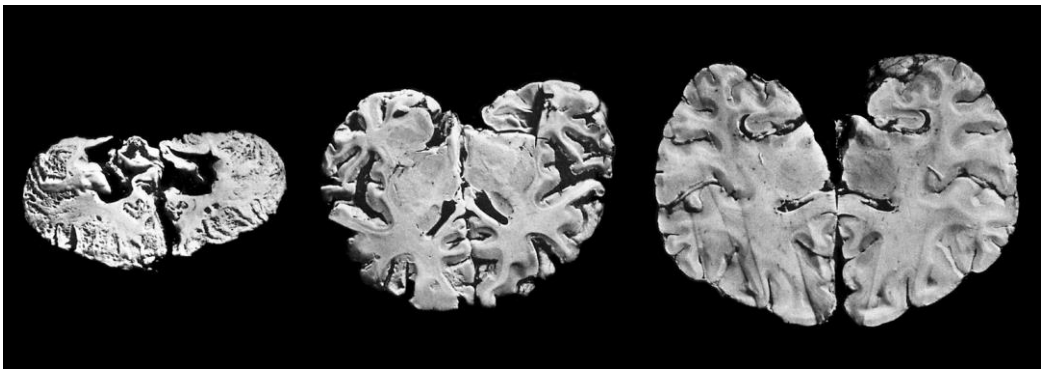

Figure 1-4: Echantillons de tissus cérébraux appartenant à des patients atteints de la maladie de Minamata (à gauche et au centre) illustrant les effets dévastateurs d'une exposition prolongée au MeHg. L'échantillon de gauche provient d'un enfant de sept ans décédé après quatre années d'exposition et celui du milieu d'un enfant de 8 ans décédé après 2,75 années d'exposition. L'échantillon de droite provient d'un individu sain de 30 ans. D'après Kessler (2013), © Robin Treadwell/Science Source.

Les exemples précédents relatent le cas d'expositions aiguës au MeHg. Les conséquences sur le développement post-natal de l'enfant de l'exposition *in utero* à de faibles doses de MeHg sont cependant toujours incertaines (Grandjean et al., 1997; Crump et al., 1998; Daniels et al., 2004; Axelrad et al., 2007; Karagas et al., 2012; Golding et al., 2016). Par ailleurs, la faune, *via* son alimentation, est également impactée par le MeHg. Plusieurs études ont ainsi montré que les concentrations présentes dans l'environnement suffisent à engendrer des problèmes d'ordre comportemental, neurochimique, hormonal ainsi que de reproduction chez différentes espèces (Scheuhammer, 1987; Wolfe et al., 1998; Evers et al., 2005; Scheuhammer et al., 2007).

Le poisson contient des n-3 polyacides gras insaturés à longue chaîne (n-3 PUFA), essentiels pour le développement cognitif (Mozaffarian and Rimm, 2006). Face au risque

d'intoxication au MeHg, limiter sa consommation de certaines espèces de poisson fortement accumulatrices de MeHg semble être la clé afin de limiter son exposition au mercure tout en bénéficiant des bienfaits de cette denrée (Chapman and Chan, 2000; Mahaffey et al., 2011; Jadán Piedra et al., 2016; Taylor et al., 2016). Les populations dépendant traditionnellement de la pêche, les Inuits par exemple (AMAP, 2015), sont en revanche directement impactées par cette contamination des chaînes alimentaires. Compte tenu du caractère planétaire du phénomène, une réduction significative des impacts du mercure n'est possible que *via* la mise en place de politiques adaptées à l'échelle internationale. Depuis la reconnaissance de la maladie de Minamata en 1956, il aura fallu près de 60 ans pour qu'une Convention Internationale sur le mercure ne voie le jour (voir section 1.4 ci-dessous). Ces décennies d'atermoiements peuvent se résumer par la citation suivante issue de Grandjean et al. (2010) : « Coupled with legal and political rigidity that demanded convincing documentation before considering prevention and compensation, types of uncertainty that are common in environmental research delayed the scientific consensus and were used as an excuse for deferring corrective action. Symptoms of methylmercury toxicity, such as tunnel vision, forgetfulness, and lack of coordination, also seemed to affect environmental health research and its interpretation ».

1.4 Contexte réglementaire

Les premières réglementations furent mises en place à l'échelle locale ou régionale et se concentrèrent sur l'exposition aiguë aux vapeurs de Hg(0) (Selin, 2011). A titre d'exemple, plusieurs états des Etats-Unis interdirent dans les années 1940 l'utilisation de mercure par les chapeliers (Wedeen, 1989). L'Organisation Mondiale de la Santé (OMS, WHO en anglais) fixa par la suite des seuils de tolérance dans l'air : 0,05 mg m^{-3} dans le cas d'une exposition occasionnelle (8 heures par jour, 225 jours par an) aux vapeurs de Hg(0), 0,015 mg m^{-3} dans le cas d'une exposition permanente (WHO, 1976). Il fallut cependant attendre le début des années 1990 pour que l'intérêt se porte sur l'exposition au mercure *via* des sources environnementales, et plus particulièrement sur l'exposition au MeHg *via* la consommation de poisson (Selin, 2011). La consommation de certaines espèces fut ainsi régulée dans certains pays en raison de leur teneur en MeHg (p. ex. EU, 2001b; Wood and Trip, 2001; EU, 2002; Endo et al., 2003). Malgré ces mesures préventives, une étude récente menée au sein de l'Union Européenne (UE, EU en anglais) montre que 200 000 enfants naissent chaque année avec des taux de mercure excédant les seuils définis par l'OMS (Bellanger et al., 2013). De même, une étude menée aux Etats-Unis montre que, chaque année, plus de 300 000 fœtus seraient exposés *in utero* à des taux de MeHg pouvant impacter le développement du système nerveux (Mahaffey et al., 2004). Il apparaît ainsi difficile de limiter notre exposition au mercure sans que les émissions ne soient régulées.

L'UE a initié sa stratégie sur le mercure au début des années 2000. Elle vise à réduire les sources de mercure dans les utilisations industrielles, à interdire son exportation, à améliorer

les pratiques de stockage et à réduire l'exposition de la population, surtout en ce qui concerne le MeHg dans les poissons. Deux Directives européennes (EU, 1996, 2001a) régissent les sources principales d'émission. La technique de l'électrolyse à mercure « ne peut en aucun cas être considérée comme une meilleure technique disponible » pour la production de chlore et de soude et les unités l'utilisant doivent être démantelées ou converties (EU, 2013). En revanche, l'UE n'impose pas, à l'heure actuelle, de limites d'émissions pour les centrales au charbon. La Directive 2007/51/EC (EU, 2007) régule quant à elle l'utilisation de mercure dans les thermomètres et baromètres. La Commission Européenne a par ailleurs réduit en 2011 les concentrations de mercure autorisées dans les ampoules à faible consommation d'énergie et renforcé les règlements concernant la collecte et le recyclage de matières dangereuses (EU, 2011). Le règlement 1102/2008 (EC, 2008), entré en vigueur en 2011, interdit les exportations de mercure métallique et de certains composés et mélanges de mercure et régule le stockage de cette substance dans des conditions optimales de sécurité. Le mercure fait également partie des substances dangereuses prioritaires désignées par la Directive Cadre sur l'Eau (EU, 2000, 2001c). Ceci engage notamment les cabinets dentaires à réduire et progressivement éliminer leurs émissions de mercure vers les eaux usées. Il n'existe en revanche pas de limite légale de mercure dans le cadre des Directives sur la Qualité de l'Air. La Directive 2004/107/EC (EU, 2004) impose seulement que les concentrations dans l'atmosphère soient mesurées en au moins un site rural tous les 100 000 km^2, et que l'incertitude élargie sur les mesures soit inférieure à 50 %.

Les risques engendrés par le mercure sur la santé humaine et l'environnement furent régulièrement discutés au cours de forums internationaux depuis les années 1970 (Selin and Selin, 2006). En 2001, le Programme des Nations Unies pour l'Environnement (PNUE, UNEP en anglais) décida d'initier un processus afin de définir si le mercure était ou non une menace mondiale. Il fut conclu fin 2002 qu'il y avait suffisamment de preuves attestant de sa dangerosité pour la santé humaine et l'environnement pour qu'une action conjointe à l'échelle internationale soit initiée (UNEP, 2002). Plusieurs pays parmi les plus gros émetteurs de mercure au monde, dont les Etats-Unis, la Chine et l'Inde, se montrèrent initialement réticents à la mise en place d'un tel traité (Appleton et al., 2009). Suite à l'élection en 2009 de B. Obama à la présidence des Etats-Unis, un consensus fut trouvé et les négociations démarrèrent à l'été 2010 (Selin, 2011; Kessler, 2013). En janvier 2013, le Comité de négociation intergouvernemental conclut sa cinquième session en s'accordant sur le texte d'une Convention Internationale sur le mercure, dite Convention de Minamata (UNEP, 2013b). La Convention fut adoptée par la Conférence de plénipotentiaires en octobre 2013 au Japon et ouverte à la signature. A ce jour, la Convention compte 128 signataires et a été ratifiée par 29 Parties. Elle entrera en vigueur dès qu'elle aura été ratifiée par au moins 50 Parties. L'objectif de la Convention est « de protéger la santé humaine et l'environnement contre les émissions et rejets anthropiques de mercure et de composés du mercure » (Article premier). Le déroulement des négociations ainsi que l'ensemble des décisions prises font l'objet de plusieurs publications scientifiques (p. ex. Andresen et al., 2012; Kessler, 2013; Selin, 2014a). La Convention est contraignante par bien des aspects. Les annexes A et B

listent par exemple les produits et procédés pour lesquels l'utilisation de mercure devra être abandonnée à court ou moyen terme. La Convention est en revanche plutôt souple en ce qui concerne les émissions. S'agissant de nouvelles sources atmosphériques, « chaque Partie exige l'utilisation des meilleures techniques disponibles et des meilleures pratiques environnementales pour contrôler, et dans la mesure du possible, réduire les émissions ». S'agissant des sources existantes vers l'atmosphère, les sols et les eaux, chaque Partie devra « contrôler et, dans la mesure du possible, réduire les émissions ». En outre, chaque Partie « peut élaborer un plan national énonçant les mesures à prendre (…) ainsi que les objectifs, les buts et les résultats escomptés ». A défaut de permettre une réduction des émissions de mercure, la Convention devrait au moins faciliter le ralentissement de l'augmentation programmée (voir section 1.1.3.2) des émissions au cours des décennies à venir (Selin, 2014a; Selin, 2014b). Les actions menées dans le cadre de la Convention au sein des exploitations aurifères artisanales et au niveau de la gestion des déchets devraient en revanche permettre de réduire de manière substantielle l'exposition des populations à l'échelle locale, notamment dans les pays en développement (Selin, 2014b).

1.5 Les modèles numériques, des outils pour prévoir l'évolution de la contamination des écosystèmes

Compte tenu de la complexité du cycle biogéochimique du mercure (voir section 1.2) et malgré des décennies de recherche scientifique sur le sujet, il demeure difficile d'évaluer les répercussions qu'auront les diverses réglementations mises en place de l'échelle locale à l'échelle internationale (voir section 1.4 ci-dessus) sur la contamination des écosystèmes et la santé des populations à court, moyen et long terme. L'Article 22 de la Convention de Minamata impose que l'efficacité de la Convention soit évaluée « au plus tard six ans après sa date d'entrée en vigueur et, par la suite, périodiquement ». Une étude récente d'Evers et al. (2016) propose diverses stratégies, notamment l'utilisation de bio-indicateurs, afin d'évaluer l'efficacité de la Convention à court (< 6 ans), moyen (6-12 ans) et long terme (> 12 ans). Il s'avère par ailleurs nécessaire de relier les politiques de réduction des émissions, en amont, avec l'ensemble de la chaîne transport-dépôt-bioaccumulation-exposition et les conséquences sur la santé humaine et animale, en aval. Depuis une dizaine d'années, des modèles atmosphériques globaux de chimie-transport sont développés pour retracer le cheminement du mercure depuis les émissions jusqu'aux dépôts au sein des écosystèmes (p. ex. Selin et al., 2007; Selin et al., 2008; Jung et al., 2009; Travnikov and Ilyin, 2009; Dastoor and Larocque, 2004). En parallèle, des modèles de la contamination de l'eau et de bioaccumulation sont utilisés pour étudier le devenir du mercure déposé au sein des écosystèmes aquatiques (p. ex. Knightes, 2008; Knightes et al., 2009). Enfin, les modèles pharmacocinétiques physiologiques (PBPK) permettent de prédire l'absorption, la distribution, la métabolisation et l'excrétion des différentes espèces mercurielles chez l'Homme ou l'animal (p. ex. Clewell et al., 1999; Young et al., 2001). Ces différents types de

modèles sont des outils précieux permettant de juger de l'efficacité potentielle des réglementations et de prévoir l'évolution de la contamination de notre environnement et des impacts sur la santé humaine. Les modèles atmosphériques globaux sont par exemple très fréquemment utilisés pour interpréter l'évolution des concentrations atmosphériques (Soerensen et al., 2012; Zhang et al., 2016) ou pour prévoir les émissions et dépôts futurs selon différents *scenarii* (Corbitt et al., 2011; Muntean et al., 2014; Giang and Selin, 2015). Compte tenu de l'importance relative des réémissions de mercure (~ 60 %, voir section 1.1.3.3), une diminution des émissions anthropiques n'aurait, à court terme, qu'une influence mineure sur la quantité de mercure circulant à l'échelle planétaire (Selin, 2014b). Il faudrait ainsi des années, voire des décennies, pour qu'une réduction des émissions anthropiques n'engendre une diminution des concentrations en MeHg dans les stocks de poisson (Mason et al., 2012). En considérant des émissions anthropiques constantes au cours des décennies à venir (scénario réaliste, voir section 1.4), on s'attend par exemple à une augmentation de près de 50 % des concentrations en mercure dans le secteur nord de l'océan Pacifique d'ici 2050 par rapport aux niveaux de 1995 (Sunderland et al., 2009). L'exposition des populations *via* la consommation de poisson pourrait ainsi s'aggraver dans les prochaines années (Sunderland and Selin, 2013). Même si les actions d'aujourd'hui n'ont pas d'impact à court terme, il est cependant bon de garder à l'esprit qu'elles en auront dans un futur plus ou moins lointain (Selin, 2014b).

Malgré une utilisation grandissante de ces modèles, la modélisation du cycle atmosphérique du mercure n'en demeure pas moins sujette à de nombreuses sources d'incertitudes (Kwon and Selin, 2016), pouvant notamment engendrer de fortes divergences entre les concentrations atmosphériques mesurées et les concentrations prédites par les modèles (Dastoor et al., 2008; Pan et al., 2008; Holmes et al., 2010; Zhang et al., 2012; Kos et al., 2013). Notre compréhension partielle des processus atmosphériques (réactions d'oxydo-réduction, dépôts, réémissions) est une des principales sources d'incertitudes des modèles atmosphériques actuels (Kwon and Selin, 2016). La validation de ces modèles globaux, primordiale pour orienter de manière judicieuse les futures réglementations sur le mercure, requiert par ailleurs des données d'observations à l'échelle planétaire. Le Chapitre 2 dresse un bilan de nos connaissances des différents processus atmosphériques et des données d'observations disponibles en 2013, au début de ces travaux de thèse.

2 Cycle atmosphérique du mercure : état et limites des connaissances

2.1 Transformations physico-chimiques du mercure dans l'atmosphère et échanges aux interfaces

2.1.1 Réactions d'oxydo-réduction dans l'atmosphère

2.1.1.1 Réactions en phase gazeuse

Hg(0) peut être oxydé en phase gazeuse par divers oxydants. Le temps de vie moyen de Hg(0) est estimé à 0,8-1,7 an dans la troposphère (Seigneur et al., 2006; Selin et al., 2007; Holmes et al., 2010). Deux types de mécanismes réactionnels sont proposés : oxydation directe de Hg(0) en Hg(II) ou oxydation en deux étapes *via* la formation de l'intermédiaire réactionnel Hg(I)Br (Goodsite et al., 2004; Goodsite et al., 2012). Il est à noter que, selon une étude théorique, Hg(I)Br se dissocie rapidement à température ambiante (en 10 secondes à 298 K et 1 atm, Goodsite et al., 2012). Hg(I)Br est en revanche suffisamment stable en régions polaires ou dans la haute troposphère pour que son oxydation en Hg(II) soit possible (Goodsite et al., 2004; Goodsite et al., 2012). Le Tableau 2-1 recense les principales réactions d'oxydation de Hg(0) en phase gazeuse ainsi que les constantes de réaction associées. La détermination expérimentale ou théorique de ces constantes est un exercice difficile et les sources d'incertitudes sont nombreuses (Subir et al., 2011; Ariya et al., 2015). Il en résulte des constantes de réaction pouvant varier d'un ou deux ordres de grandeurs d'une étude à une autre (Tableau 2-1). Il demeure également difficile de déterminer la (les) réaction(s) d'oxydation prépondérante(s) compte tenu de notre incapacité, à l'heure actuelle, à identifier la nature des espèces oxydées formées ($HgBr_2$, $HgCl_2$ *etc.*) (Gustin and Jaffe, 2010). Alors que des études suggèrent que les réactions d'oxydation par O_3 et OH sont trop lentes pour être pertinentes (Calvert and Lindberg, 2005; Hynes et al., 2009), ces réactions ont longtemps été considérées comme prépondérantes en phase gazeuse (p. ex. Lin et al., 2006; Selin et al., 2007). Des études de terrain et de modélisation ont par ailleurs montré que l'oxydation de Hg(0) par Br serait prédominante en régions polaires (voir ci-après), dans la haute troposphère ainsi qu'au sein de la couche limite marine (Hedgecock and Pirrone, 2001; Laurier et al., 2003; Laurier and Mason, 2007; Simpson et al., 2007b; Steffen et al., 2008; Holmes et al., 2009; Holmes et al., 2010; Soerensen et al., 2010b; Lyman and Jaffe, 2012). Dans le cas d'une oxydation en deux étapes, une oxydation de l'intermédiaire réactionnel Hg(I)Br par NO_2, HO_2, ClO, BrO ou I serait à privilégier par rapport à une oxydation par Br ou OH (Dibble et al., 2012; Wang et al., 2014).

L'oxydation de Hg(0) en phase gazeuse peut potentiellement se dérouler à n'importe quelle altitude au sein de l'atmosphère, le taux de conversion de Hg(0) en espèces oxydées dépendant notamment de la concentration en oxydants. Des études de terrain réalisées à haute altitude (voir section 2.2.1.1) ont cependant montré que la haute troposphère et la basse stratosphère sont des régions où l'oxydation de Hg(0) est particulièrement intense (Lyman and Jaffe, 2012; Weiss-Penzias et al., 2015).

Tableau 2-1: Principales réactions d'oxydation du mercure élémentaire en phase gazeuse et constantes de réaction associées (à 298 K et 1 atm).

Réaction	Constante de réaction (cm^3 $molec^{-1}$ s^{-1})	Référence
Hg(0) + OH → Hg(II)	$9{,}0\times10^{-14}$	Pal and Ariya (2004b)
	$8{,}7\times10^{-14}$	Sommar et al. (2001)
	$3{,}2\times10^{-13}$ $(T/298)^{-3{,}06}$	Goodsite et al. (2004)
	$< 1{,}2\times10^{-13}$	Bauer et al. (2003)
Hg(0) + O_3 → Hg(II)	3×10^{-20}	Hall (1995)
	$7{,}5\times10^{-19}$	Pal and Ariya (2004a)
	$6{,}2\times10^{-19}$	Snider et al. (2008)
Hg(0) + BrO → Hg(II)	$1{,}0\times10^{-13}$-$1{,}0\times10^{-15}$	Raofie and Ariya (2003)
Hg(0) + ClO → Hg(II)	$1{,}0\times10^{-17}$	Subir et al. (2011)
Hg(0) + H_2O_2 → Hg(II)	$< 8{,}5\times10^{-19}$	Tokos et al. (1998)
Hg(0) + Cl_2 → Hg(II)	$1{,}0\times10^{-17}$-$1{,}0\times10^{-19}$	Subir et al. (2011)
	$2{,}6\times10^{-18}$	Ariya et al. (2002)
Hg(0) + Br_2 → Hg(II)	$9{,}0\times10^{-17}$	Ariya et al. (2002)
	$2{,}8\times10^{-31}$	Balabanov et al. (2005)
Hg(0) + NO_3 → Hg(II)	4×10^{-15}	Sommar et al. (1997)
Hg(0) + Br → Hg(I)Br	$3{,}7\times10^{-13}$ $(T/298)^{-2{,}76}$	Goodsite et al. (2012)
	$3{,}6\times10^{-13}$	Donohoue et al. (2006)
	$1{,}1\times10^{-12}$ $(T/298)^{-2{,}37}$	Goodsite et al. (2004)
Hg(I)Br → Hg(0) + Br	$1{,}6\times10^{-9}$ $(T/298)^{-1{,}86}$ $e^{-7801/T}$	Dibble et al. (2012)
	$3{,}89\times10^{-11}$	Balabanov et al. (2005)
Hg(I)Br + Br → Hg(II)	$6{,}33\times10^{-11}$	Wang et al. (2014)
	$2{,}98\times10^{-11}$	Balabanov et al. (2005)
	$2{,}5\times10^{-10}$ $(T/298)^{-0{,}57}$	Goodsite et al. (2004)
Hg(I)Br + OH → Hg(II)	$6{,}33\times10^{-11}$	Wang et al. (2014)
Hg(I)Br + I → Hg(II)	$6{,}28\times10^{-11}$	Wang et al. (2014)
Hg(I)Br + BrO → Hg(II)	$1{,}09\times10^{-10}$	Wang et al. (2014)
Hg(I)Br + NO_2 → Hg(II)	$2{,}81\times10^{-11}$	Wang et al. (2014)
Hg(I)Br + HO_2 → Hg(II)	$8{,}2\times10^{-11}$	Wang et al. (2014)
Hg(I)Br + IO → Hg(II)	$4{,}9\times10^{-11}$	Wang et al. (2014)

Les mécanismes de réduction de Hg(II) et Hg(p) demeurent peu connus. D'après Schroeder et al. (1991), CO pourrait les réduire en phase gazeuse. Cependant, on considère communément que la réduction du mercure n'est possible qu'en phase aqueuse (Subir et al., 2011). Ces mécanismes en phase aqueuse sont détaillés au sein de la section 2.1.1.2.

Cas particulier des épisodes de déplétion atmosphérique de Hg(0)

Alors que le temps de vie moyen de Hg(0) est estimé à ~ 1 an (voir ci-avant), il peut être de l'ordre de 6 heures à 2,5 jours seulement lors d'épisodes de déplétion atmosphérique de Hg(0) (« atmospheric mercury depletion events (AMDEs) ») (Donohoue et al., 2006). Ces

AMDE se caractérisent par une chute brutale et simultanée des concentrations en Hg(0) et en O_3. Au cours de ces épisodes de déplétion, les concentrations en Hg(0) peuvent être proches de zéro pendant plusieurs heures. Les AMDE, découverts en 1995 à Alert (82°50 N, 62°50 W) (Schroeder et al., 1998), ont depuis été observés en de nombreux sites arctiques (Lindberg et al., 2001; Berg et al., 2003a; Poissant and Pilote, 2003; Skov et al., 2004; Steffen et al., 2005) et sur les côtes antarctiques (Ebinghaus et al., 2002b; Sprovieri et al., 2002; Temme et al., 2003; Brooks et al., 2008b; Nerentorp Mastromonaco et al., 2016). En régions polaires, ces AMDE ne sont observés qu'au printemps et sur la côte (Steffen et al., 2008). Aucun épisode de déplétion de ce type n'a ainsi jamais été observé à Summit (72°60 N, 38°50 W), station située au sommet de la calotte polaire au Groenland (Faïn et al., 2008). Il est à noter que des AMDE ont été observés aux abords de la mer Morte, lac salé du Proche-Orient (Peleg et al., 2007; Obrist et al., 2011).

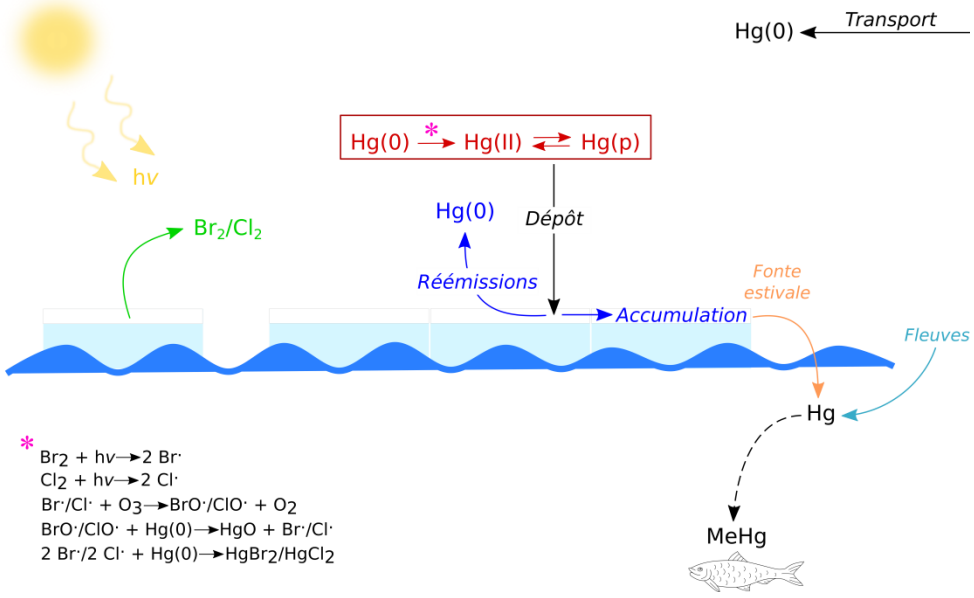

Figure 2-1: Cycle du mercure lors d'épisodes de déplétion atmosphérique de Hg(0) en régions polaires. Figure adaptée de celle de Steffen et al. (2008).

Bien que le mécanisme exact demeure incertain, les AMDE seraient dus à une oxydation par des espèces halogénées réactives (voir Figure 2-1) (Schroeder et al., 1998; Lu et al., 2001; Brooks et al., 2006b; Sommar et al., 2007). Plusieurs études réalisées en régions polaires ont ainsi montré que les AMDE et les déplétions d'O_3 semblent se dérouler de concert avec l'arrivée de masses d'air concentrées en BrO (p. ex. Lu et al., 2001; Ebinghaus et al., 2002b; Lindberg et al., 2002; Sprovieri et al., 2005a). Ces espèces réactives sont émises de manière épisodique (Pöhler et al., 2010) et à l'échelle locale (Bottenheim and Chan, 2006) par la glace de mer lors d'un phénomène connu sous le nom d'explosion de brome se déroulant au printemps aux hautes latitudes (Wennberg, 1999; Simpson et al., 2007b). Plusieurs études ont montré l'influence de la dynamique de la glace de mer, et notamment la présence de chenaux et zones d'eaux libres, sur la production d'espèces halogénées réactives et l'occurrence d'AMDE (Simpson et al., 2007a; Simpson et al., 2007b; Zhao et al., 2008; Moore et al., 2014). Il est à noter que les AMDE ne se déroulent que dans les couches basses

de la troposphère (1 km au maximum) et en l'absence de mélange vertical des masses d'air (Banic et al., 2003; Tackett et al., 2007). Au cours des AMDE, Hg(0) est massivement oxydé en Hg(II) et/ou Hg(p) (Lindberg et al., 2001; Poissant and Pilote, 2003; Obrist et al., 2011). En régions polaires, ces espèces oxydées sont alors déposées localement en surface du manteau neigeux (voir section 2.1.2 pour les mécanismes de dépôts). On estime qu'environ 100 tonnes de mercure sont ainsi déposées chaque année au sein des écosystèmes arctiques (Ariya et al., 2004; Skov et al., 2004; Dastoor et al., 2015). Ce mercure peut être rapidement réémis vers l'atmosphère sous forme de Hg(0) (voir section 2.1.3.2.2) ou s'accumuler, au moins en partie, au sein du manteau neigeux (Ferrari et al., 2005; Brooks et al., 2006a; Kirk et al., 2006; Sommar et al., 2007; Hirdman et al., 2009; Dommergue et al., 2010a; Larose et al., 2010). Outre la fonte estivale du manteau neigeux, il est à noter que les fleuves circumpolaires sont une source de mercure vers les écosystèmes aquatiques arctiques (Fisher et al., 2012).

2.1.1.2 Réactions en phase aqueuse atmosphérique

Tableau 2-2: Principales réactions d'oxydo-réduction en phase aqueuse et constantes de réaction associées.

Réaction	Constante de réaction	Référence
Oxydation		
$Hg(0) + O_3 \rightarrow Hg(II)$	$4{,}7\times10^{7}$ M^{-1} s^{-1}	Munthe (1992)
$Hg(0) + OH \rightarrow Hg(II)$	$2{,}4\times10^{9}$ M^{-1} s^{-1}	Gårdfeldt et al. (2001)
$Hg(0) + OH \rightarrow Hg(I)$	$2{,}4\times10^{10}$ M^{-1} s^{-1}	Lin and Pehkonen (1997)
$Hg(0) + HOCl \rightarrow Hg(II)$	$2{,}09\times10^{6}$ M^{-1} s^{-1}	Lin and Pehkonen (1998)
$Hg(0) + OCl^- \rightarrow Hg(II)$	$1{,}99\times10^{6}$ M^{-1} s^{-1}	Lin and Pehkonen (1998)
$Hg(0) + Br_2 \rightarrow Hg(II)$	0,20 M^{-1} s^{-1}	Wang and Pehkonen (2004)
$Hg(0) + HOBr \rightarrow Hg(II)$	0,28 M^{-1} s^{-1}	Wang and Pehkonen (2004)
$Hg(0) + OBr^- \rightarrow Hg(II)$	0,27 M^{-1} s^{-1}	Wang and Pehkonen (2004)
Réduction		
$Hg(II) + HO_2 \rightarrow Hg(I)$	0 $1{,}1\times10^{4}$ M^{-1} s^{-1}	Gårdfeldt and Jonsson (2003) Pehkonen and Lin (1998)
$Hg(II) + O_2^- \rightarrow Hg(I)$	0 $1{,}1\times10^{4}$ M^{-1} s^{-1}	Gårdfeldt and Jonsson (2003) Pehkonen and Lin (1998)
$HgSO_3 \rightarrow Hg(0)$	0,0106 s^{-1} 0,6 s^{-1}	Van Loon et al. (2000) Munthe et al. (1991)
$Hg(SO_3)_2^{2-} \rightarrow Hg(0)$	$<< 10^{-4}$ s^{-1}	Munthe et al. (1991)
$Hg(OH)_2 + h\nu \rightarrow Hg(0)$	$3{,}7\times10^{-7}$ s^{-1}	Xiao et al. (1994)

Bien que Hg(0) soit peu soluble dans l'eau (voir section 1.1.1), son oxydation en phase aqueuse par O_3 et OH est plus rapide qu'en phase gazeuse (Munthe, 1992; Lin and Pehkonen, 1997; Gårdfeldt et al., 2001). Le Tableau 2-2 recense les principales réactions d'oxydo-réduction en phase aqueuse. Il est à noter que les données sont rares et que l'étude de l'influence des conditions environnementales (pH, température, concentration en Cl^- *etc.*) sur les constantes de réaction n'est pas systématique (Subir et al., 2011). Dans l'atmosphère, ces réactions peuvent se produire en surface des gouttes d'eau (nuages, brouillard, pluie) ou des aérosols (constitués à 30-50 % en masse d'eau). La réduction de Hg(II) dépend de la nature des complexes formés (Munthe et al., 1991; Lin and Pehkonen, 1997). Plusieurs études ont montré qu'une réduction photochimique de Hg(II) est possible *via* un transfert de charge

ligand-métal (Griffiths and Anderson, 1991; Horváth and Vogler, 1994; Kunkely et al., 1997). Les réactions de photo-réduction des complexes dont la présence est peu probable au sein des gouttes d'eau (notamment les complexes HgI_2, HgI_3^- et HgI_4^{2-}) ne sont pas prises en compte dans les modèles atmosphériques (Lin and Pehkonen, 1999). L'atmosphère est un milieu hétérogène et une meilleure compréhension des réactions se déroulant en phase aqueuse ou sur différentes surfaces s'avère essentielle.

2.1.1.3 Réactions hétérogènes

Les nuages et les aérosols sont les principaux supports de réactions hétérogènes au sein de l'atmosphère (Subir et al., 2012). Les échanges aux interfaces air-écosystèmes terrestres et air-eau (océans, neige) seront décrits plus en détails au sein de la section 2.1.3. La Figure 2-2 illustre les différentes interactions physico-chimiques possibles entre les espèces mercurielles atmosphériques et un aérosol. Les espèces gazeuses peuvent s'adsorber sur les aérosols et subir des processus de chimie de surface, hétérogène ou multi-phase (Subir et al., 2012; Ariya et al., 2015). Il a par exemple été montré que les ions Cl^-, Br^- et I^- (qui forment des complexes stables avec Hg(II) (Clever et al., 1985)) s'adsorbent aux interfaces air-eau, notamment sur les aérosols marins (Jungwirth and Tobias, 2006; Petersen and Saykally, 2006). La taille (1 nm-100 µm) et la composition des aérosols étant variables (Prather et al., 2008), il s'avère difficile d'établir de manière systématique l'influence qu'ils peuvent avoir sur la spéciation des espèces mercurielles atmosphériques. Des études ont montré que l'adsorption de Hg(II) dépend fortement de la composition de l'aérosol (Rutter and Schauer, 2007a; Malcolm et al., 2009), de la température (Rutter and Schauer, 2007b) et de la concentration en aérosols (Amos et al., 2012). Des études de terrain et de modélisation ont par ailleurs suggéré l'existence d'une réduction de Hg(II) au sein des rejets des centrales au charbon (« in-plume reduction ») *via* une réaction hétérogène avec SO_2 (Edgerton et al., 2006; Lohman et al., 2006; Vijayaraghavan et al., 2008).

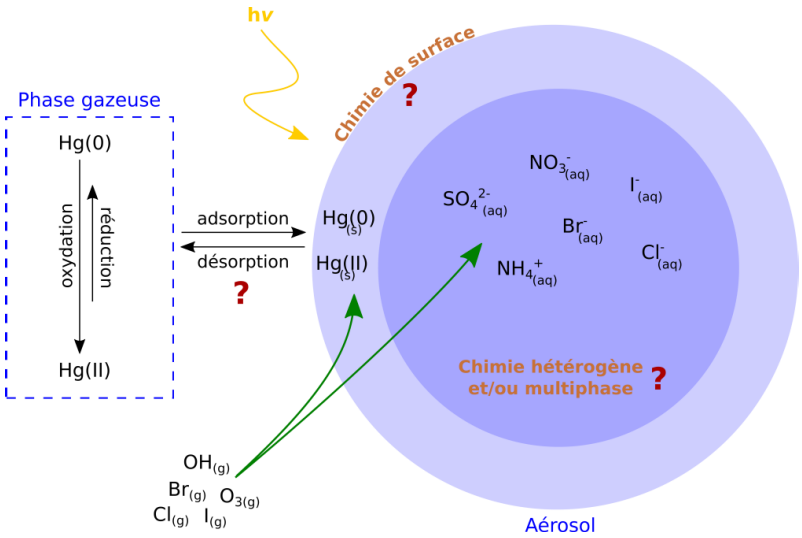

Figure 2-2: Interactions physico-chimiques possibles entre les espèces mercurielles atmosphériques et un aérosol. Figure adaptée de celle de Subir et al. (2012).

2.1.1.4 Bilan

Notre compréhension partielle des processus d'oxydo-réduction se déroulant au sein de la troposphère constitue l'une des principales sources d'incertitudes des modèles atmosphériques (Lin et al., 2006; Ariya et al., 2009; Holmes et al., 2010). Une synthèse des processus physico-chimiques implémentés au sein des principaux modèles atmosphériques régionaux et globaux a été établie par Ariya et al. (2015). O_3, OH et dans une moindre mesure Br sont les oxydants principaux et une réduction de Hg(II) en phase aqueuse au sein des nuages est souvent incluse. Les réactions de réduction entrent ainsi en compétition avec l'adsorption, le plus souvent réversible, de Hg(II) sur des particules. De l'état d'oxydation du mercure dans l'atmosphère dépend directement sa capacité à se déposer au sein des écosystèmes (voir section 2.1.2 ci-dessous).

2.1.2 Processus de dépôts

Comme indiqué précédemment (voir section 1.2), les différentes espèces mercurielles présentes dans l'atmosphère peuvent se déposer au sein des écosystèmes par voies sèches et humides. On estime à 2200-3200 Mg et 3700 Mg la quantité de mercure déposée chaque année au sein des écosystèmes terrestres et marins, respectivement (Mason et al., 2012; Selin, 2014b). La Figure 2-3 présente le cycle biogéochimique du mercure et notamment les flux annuels de dépôts calculés par Selin (2014b).

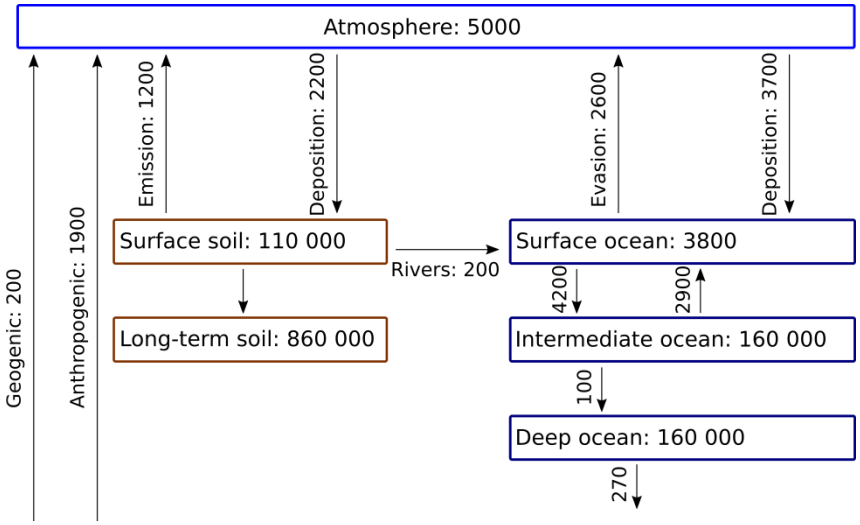

Figure 2-3: Cycle biogéochimique global du mercure. Les flux (flèches) sont exprimés en Mg an^{-1}, les stocks (cases) en Mg. D'après Selin (2014b).

2.1.2.1 Dépôts humides

La forme mercurielle dominante au sein des précipitations (pluie/neige) est Hg(II) sous forme dissoute et particulaire tandis que le MeHg représente ~ 0,5 à 2,5 % du total (Lindberg et al., 2007). Les dépôts humides de Hg(0) sont négligeables (Schroeder et al., 1991). Le flux de dépôts humides de mercure varie d'une région et d'une saison à l'autre en fonction des

conditions climatiques, de la chimie atmosphérique de la région d'intérêt et de la présence ou non de rejets anthropiques de mercure (Vanarsdale et al., 2005; Selin and Jacob, 2008; Prestbo and Gay, 2009). Plusieurs études ont ainsi montré que le flux de dépôts humides tend à être plus important à proximité de sources anthropiques du fait de l'assimilation directe par les gouttelettes de pluie du Hg(II) et du Hg(p) émis (p. ex. Dvonch et al., 1998; Munthe et al., 2001a). Le flux de dépôts humides est de l'ordre de 3 à 25 $\mu g\ m^{-2}\ an^{-1}$ en Amérique du Nord (Vanarsdale et al., 2005; Prestbo and Gay, 2009), où les stations de mesures sont nombreuses contrairement au reste du monde (voir section 2.2.1.2).

2.1.2.2 Dépôts secs

Les dépôts secs ayant lieu, par définition, à tout instant où il ne pleut/neige pas, ils sont quasi-permanents (environ 98 % du temps aux moyennes latitudes, Lindberg et al., 2007). Il s'agit donc d'une source non négligeable d'espèces mercurielles vers les écosystèmes aquatiques, marins et terrestres. La vitesse de dépôts secs de Hg(0) dépend du type de surface sous-jacente. Elle est de l'ordre de 0,1 à 0,4 $cm\ s^{-1}$ au-dessus de zones boisées, soit 3 ordres de grandeurs plus rapide qu'au-dessus de surfaces enneigées (Zhang et al., 2009). Les dépôts secs de Hg(0) sont souvent considérés comme négligeables pendant la journée en régions polaires car très lents et largement contrebalancés par les réémissions de Hg(0) par le manteau neigeux (voir section 2.1.3.2) (Zhang et al., 2009). Compte-tenu de leurs propriétés physico-chimiques (voir section 1.1.1), Hg(II) et Hg(p) se déposent plus rapidement. La vitesse de dépôts secs est ainsi de l'ordre de 0,5 à 6 $cm\ s^{-1}$ pour Hg(II) et de 0,02 à 2 $cm\ s^{-1}$ pour Hg(p) (Zhang et al., 2009). Dans certaines conditions, les dépôts secs peuvent être aussi, voire plus importants que les dépôts humides (Munthe et al., 2004; Sakata et al., 2006; Graydon et al., 2008; Enrico et al., 2016). Il est cependant à noter que l'incertitude sur ces différentes vitesses de dépôts secs est très élevée compte tenu du peu de données d'observations disponibles d'une part (voir section 2.2.1.2), et de la difficulté de la mesure d'autre part (Miller et al., 2005). La quantification des dépôts secs des différentes espèces mercurielles est délicate, notamment du fait de la lenteur du phénomène et de l'existence concomitante de processus de réémissions (Gustin, 2011).

2.1.3 Echanges d'espèces mercurielles aux interfaces avec l'atmosphère

La quantification des flux d'espèces mercurielles aux interfaces air-surface est primordiale pour une bonne caractérisation du cycle atmosphérique du mercure. Compte tenu de la semi-volatilité de Hg(0) et de l'occurrence de réactions d'oxydo-réduction au sein des différents compartiments environnementaux, le mercure subit un cycle continu de dépôts et réémissions (Lin and Pehkonen, 1999). Les échanges bidirectionnels d'espèces mercurielles sont complexes et dépendent des conditions environnementales, c'est-à-dire notamment de la température, de l'humidité, de la quantité de radiations solaires, de la capacité oxydante de l'atmosphère et de la surface d'intérêt, de la présence de végétation ou de turbulences atmosphériques (Zhu et al., 2016). Les processus de dépôts ayant été décrits ci-avant (voir section 2.1.2), cette partie est dédiée aux processus de réémissions de Hg(0). Il est à noter que

le flux de Hg(0) réémis par une surface est difficilement mesurable directement compte tenu des faibles gradients de concentration (Zhu et al., 2015b) et du fait qu'il n'existe pas, à l'heure actuelle, de protocole standard de mesure (Gustin, 2011; Zhu et al., 2015a; Zhu et al., 2016).

2.1.3.1 Interface air-écosystèmes terrestres

Différentes études ont montré que la réduction de Hg(II) en Hg(0) au sein des sols est favorisée par les UV-B et, dans une moindre mesure, par l'activité microbienne (Moore and Carpi, 2005; Choi and Holsen, 2009; Fritsche et al., 2008). L'évasion de Hg(0) des sols vers l'atmosphère est favorisée par des températures élevées et l'existence de turbulences atmosphériques (vent et friction de surface) (Carpi and Lindberg, 1997; Poissant and Casimir, 1998; Gustin et al., 2002), et dépend des caractéristiques du sol (composition, teneur en eau, pH) (Yang et al., 2007; Kocman and Horvat, 2010; Lin et al., 2010a). Par ailleurs, la matière organique présente dans les sols, de par sa capacité à former des complexes stables avec Hg(II), limite la réduction de Hg(II) et les réémissions de Hg(0) (Skyllberg et al., 2006; Yang et al., 2007). De même, la présence de végétation limite les réémissions de Hg(0) par les sols (Carpi et al., 2014). Par ailleurs, le rôle de la végétation comme source ou puits de mercure est toujours source de débat au sein de la communauté scientifique (Zhu et al., 2016). Les émissions de Hg(0) par la végétation ont longtemps été représentées dans les modèles comme une fonction du taux d'évapotranspiration (p. ex. Xu et al., 1999; Bash et al., 2004; Gbor et al., 2006; Shetty et al., 2008). Des études récentes ont cependant suggéré que le flux de Hg(0) à l'interface air-végétation est bidirectionnel et que la végétation peut être un puits net de mercure (Ericksen et al., 2003; Stamenkovic et al., 2008; Hartman et al., 2009). Les fractions de mercure réémis vers l'atmosphère après photo-réduction et de mercure assimilé biologiquement et accumulé au sein des plantes demeurent inconnues (Zhu et al., 2016). Une étude récente suggère que l'incertitude sur le flux de Hg(0) des écosystèmes terrestres vers l'atmosphère provient en grande partie de l'incertitude sur les échanges à l'interface air-plante (Agnan et al., 2016). D'après diverses études de modélisation, le flux de Hg(0) des écosystèmes terrestres vers l'atmosphère varierait entre -1300 et 3500 Mg an^{-1} (Holmes et al., 2010; Smith-Downey et al., 2010; Corbitt et al., 2011; Amos et al., 2013; Kikuchi et al., 2013; Lei et al., 2013; De Simone et al., 2014; Chen et al., 2015b).

2.1.3.2 Interface air-eau

2.1.3.2.1 Interface air-océan

Le flux de Hg(0) des océans vers l'atmosphère a été estimé entre 800 et 5500 Mg an^{-1} (Mason and Sheu, 2002; Strode et al., 2007; Sunderland and Mason, 2007; Soerensen et al., 2010b; Amos et al., 2013; Lei et al., 2013; Amos et al., 2014; De Simone et al., 2014; Zhang et al., 2014; Chen et al., 2015b) et représente au moins un tiers des émissions atmosphériques annuelles (chiffre variant selon les estimations, voir par exemple Figure 2-3). Ce flux est plus important sous les tropiques qu'aux moyennes latitudes (Strode et al., 2007; Soerensen et al., 2014) et dépend des conditions environnementales (p. ex. température,

intensité des radiations solaires) et des processus contrôlant la concentration en Hg(0) dans les eaux de surface (Zhu et al., 2016). La réduction de Hg(II) en Hg(0) dans les eaux de surface se fait *via* des processus photolytiques et biotiques tandis que l'oxydation de Hg(0) en Hg(II) se déroule *via* des processus photochimiques ou ne nécessitant pas de lumière (« dark oxidation ») (Mason et al., 1995; Amyot et al., 1997; Amyot et al., 2000; Lalonde et al., 2001; Mason et al., 2001; Whalin et al., 2007). La présence de ligands organiques ou inorganiques pouvant former des complexes stables avec Hg(II) influe directement sur la réduction de Hg(II) et sur le flux de Hg(0) émis vers l'atmosphère (Lamborg et al., 2004; Whalin et al., 2007). De même, la réduction de Hg(II) en Hg(0) entre en compétition avec les mécanismes de méthylation et de sorption sur la matière organique/sédimentation (Lamborg et al., 1999). De nombreuses études réalisées dans les océans Atlantique, Pacifique et Arctique, et dans les mers Méditerranée, Baltique et du Nord ont montré que les eaux superficielles sont saturées en Hg(0), engendrant un flux de l'océan vers l'atmosphère (pour une synthèse bibliographique, voir Sprovieri et al., 2010). Il est cependant à noter que des concentrations élevées en espèces divalentes ont été mesurées dans la couche limite atmosphérique marine en Méditerranée, Atlantique Nord et océan Pacifique, en raison d'une oxydation photochimique de Hg(0) en présence de composés halogénés (Mason et al., 2001; Wängberg et al., 2001; Hedgecock et al., 2003; Laurier et al., 2003; Pirrone et al., 2003; Sprovieri et al., 2003; Holmes et al., 2009). De plus amples informations concernant le cycle du mercure dans la couche limite marine et à l'interface air-océan peuvent être trouvées chez Strode et al. (2007), Holmes et al. (2009) et Soerensen et al. (2010a).

2.1.3.2.2 Interface air-manteau neigeux

Le manteau neigeux recouvre en moyenne 27 millions de km^2 entre 40° et 60° N, 18 millions de km^2 entre 60° et 90° N et près de 15 millions de km^2 en Antarctique (Pielke et al., 2004). Il est le siège de processus physiques, chimiques et photochimiques, et joue un rôle primordial sur le cycle atmosphérique de diverses espèces chimiques (Domine and Shepson, 2002). Un état des lieux des connaissances sur la réactivité du mercure au sein du manteau neigeux ainsi que sur les échanges à l'interface air-manteau neigeux a été réalisé par Durnford and Dastoor (2011) et est illustré et résumé par la Figure 2-4.

Les espèces mercurielles divalentes, et Hg(0) dans une moindre mesure (voir section 2.1.2), sont déposés à la surface du manteau neigeux par voies sèches et humides. Bien que la réduction de Hg(II) dans la couche de surface du manteau neigeux soit possible dans le noir (Ferrari et al., 2004; Faïn et al., 2007; Ferrari et al., 2008), elle est généralement photochimique (Sherman et al., 2010). Le taux de photo-réduction est corrélé à l'intensité de radiations solaires (Lalonde et al., 2002; Lalonde et al., 2003; Mann et al., 2015b) et à la température (Mann et al., 2015a). Il ne s'agirait pas d'une photolyse directe mais bien d'une réaction initiée par les radiations solaires (Lalonde et al., 2003) dans les UV-B, et dans une moindre mesure dans les UV-A ou le visible (Lalonde et al., 2003; Poulain et al., 2004; Dommergue et al., 2007; Faïn et al., 2007; Johnson et al., 2008). H_2O_2 (à pH neutre), $HO_2^{\cdot}$, les acides humiques ou l'acide oxalique sont régulièrement cités parmi les espèces pouvant

réduire Hg(II) (Dommergue et al., 2003b; Gårdfeldt and Jonsson, 2003; Lahoutifard et al., 2005; Dommergue et al., 2007; Faïn et al., 2008). Il est à noter qu'une fraction seulement des espèces divalentes déposées au sein du manteau neigeux est facilement réductible. Hg(p) serait moins réductible que Hg(II) mais les proportions exactes demeurent inconnues à l'heure actuelle (Durnford and Dastoor, 2011). Par ailleurs, de nombreuses études ont montré une corrélation entre la concentration en mercure total dans les couches superficielles du manteau neigeux et la présence d'halogénures (Cl^-, Br^-), suggérant une stabilisation de Hg(II) et une moindre production de Hg(0) (p. ex. Garbarino et al., 2002; Lalonde et al., 2003; Poulain et al., 2007; Larose et al., 2010).

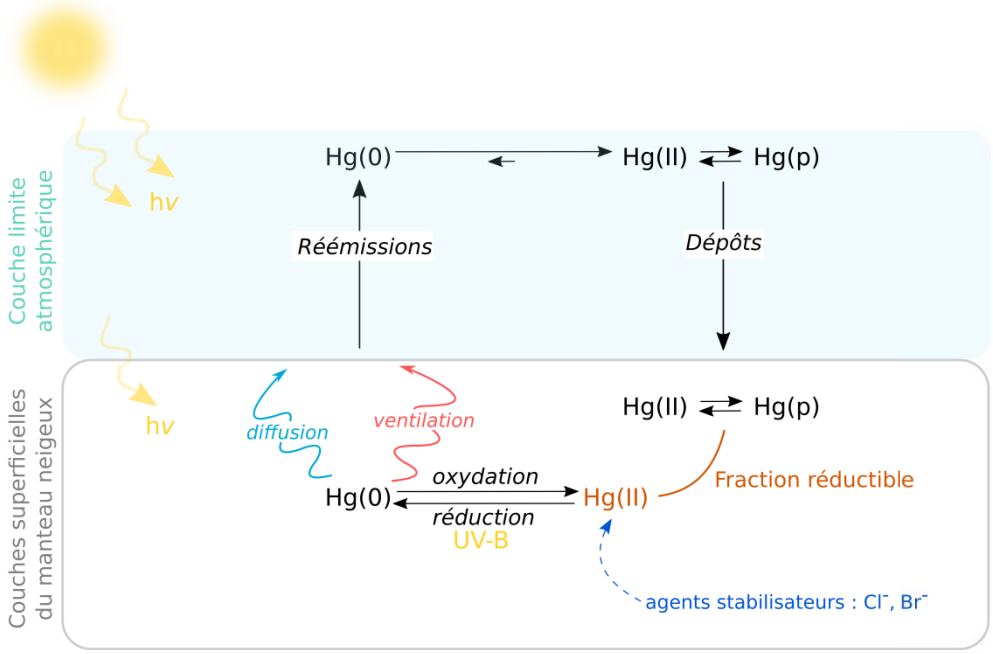

Figure 2-4: Processus physico-chimiques régissant le cycle du mercure dans les couches superficielles du manteau neigeux et à l'interface air-manteau neigeux.

Le Hg(0) produit en surface du manteau neigeux peut être ré-oxydé par H_2O_2 (à pH <7), Br^-, Br_2, O_3, OH^-, des alcènes ou des nitrates d'alkyle (Lalonde et al., 2003; Ferrari et al., 2004; Mann et al., 2005; Lahoutifard et al., 2006; Lin et al., 2006; Faïn et al., 2008). D'après Faïn et al. (2008), l'oxydation serait prépondérante au printemps et la réduction en été. La quantité de Hg(0) émise par le manteau neigeux vers l'atmosphère dépend directement de cet équilibre entre les réactions de réduction et d'oxydation. De nombreuses études ont mesuré un maximum de réémissions vers midi (Steffen et al., 2002; Ferrari et al., 2005; Brooks et al., 2006a; Sommar et al., 2007; Ferrari et al., 2008). Les réémissions de Hg(0) ne seraient en revanche pas directement corrélées à l'intensité de radiations solaires mais plutôt à la ventilation du manteau neigeux (Durnford and Dastoor, 2011), mécanisme permettant, avec la diffusion, de transporter le Hg(0) produit vers la surface (Albert and Shultz, 2002). Les réémissions de Hg(0) sont par ailleurs plus importantes en début de période de fonte du manteau neigeux (Dommergue et al., 2003a; Faïn et al., 2007; Sommar et al., 2007; Brooks et al., 2008b; Douglas et al., 2008).

2.2 Données d'observations

2.2.1 Les premiers grands réseaux d'observations

2.2.1.1 Espèces mercurielles atmosphériques

Les premières stations de mesures dédiées à l'analyse sur le long terme de Hg(0) furent mises en place au milieu des années 1990 en Europe, Asie, Amérique du Nord et Afrique du Sud (Baker et al., 2002; Blanchard et al., 2002; Ebinghaus et al., 2002a; Berg et al., 2004; Temme et al., 2004; Kim et al., 2005; Kock et al., 2005; Steffen et al., 2005). En 1996 le réseau de mesure CAMNet (« Canadian Atmospheric Mercury Measurement Network ») fut mis en place et 11 stations virent le jour à travers le Canada (Kellerhals et al., 2003). L'analyse des chroniques temporelles à Mace Head en Irlande (Ebinghaus et al., 2011) et en la plupart des stations du réseau CAMNet (Temme et al., 2007; Cole et al., 2013) suggère une diminution de l'ordre de 1,8 % par an des concentrations en Hg(0) depuis 1996. Ceci est corroboré par une diminution des dépôts humides de mercure en Amérique du Nord sur cette période (Prestbo and Gay, 2009). Cette diminution entre cependant en apparente contradiction avec l'augmentation des émissions au sein de l'Hémisphère Nord (Streets et al., 2011; Muntean et al., 2014). D'après Soerensen et al. (2012), cette diminution des concentrations atmosphériques pourrait s'expliquer par une diminution des concentrations en mercure des eaux de surface de l'Atlantique Nord et ainsi des réémissions océaniques de Hg(0). Une étude récente suggère cependant que la diminution des concentrations à Mace Head est de moins en moins marquée (Weigelt et al., 2015). Les données en provenance de Cape Point en Afrique du Sud suggèrent par ailleurs une diminution des concentrations en Hg(0) entre 1996 et 2004 et une augmentation depuis 2007 (Slemr et al., 2015). Des données complémentaires et en d'autres points du globe sont nécessaires pour confirmer, ou infirmer, ces premières tendances. Il est à noter que Cape Point et Troll en Antarctique étaient, avant la mise en place du programme GMOS (« Global Mercury Observation System », voir section 2.2.2 ci-après), les deux seules stations de mesures de l'Hémisphère Sud dédiées à l'analyse sur le long terme de Hg(0). Les seules autres données disponibles dans cette région du globe émanaient de campagnes océanographiques ponctuelles (pour une synthèse bibliographique, voir Soerensen et al., 2012). Il est à noter que les concentrations issues de ces campagnes sont très variables (p. ex. 0,72 ng m^{-3} dans le sud de l'océan Atlantique (Kuss et al., 2011) contre 2,20 ng m^{-3} dans le sud-est de l'océan Indien (Xia et al., 2010)) et peu représentatives car le plus souvent non filtrées d'une éventuelle pollution anthropique ou par le navire océanographique (Slemr et al., 2015). En se basant sur les données d'observations disponibles avant la mise en place du programme GMOS (voir section 2.2.2 ci-après) et grâce à l'utilisation de modèles numériques, des cartographies des concentrations en espèces mercurielles dans la couche limite atmosphérique ont été rendues disponibles (Figure 2-5). La communauté scientifique s'accordait par ailleurs sur un bruit de fond moyen en Hg(0) de l'ordre de 1,5-1,7 ng m^{-3} dans l'Hémisphère Nord, contre 1,1-1,3 ng m^{-3} dans l'Hémisphère Sud (Sprovieri et al., 2010).

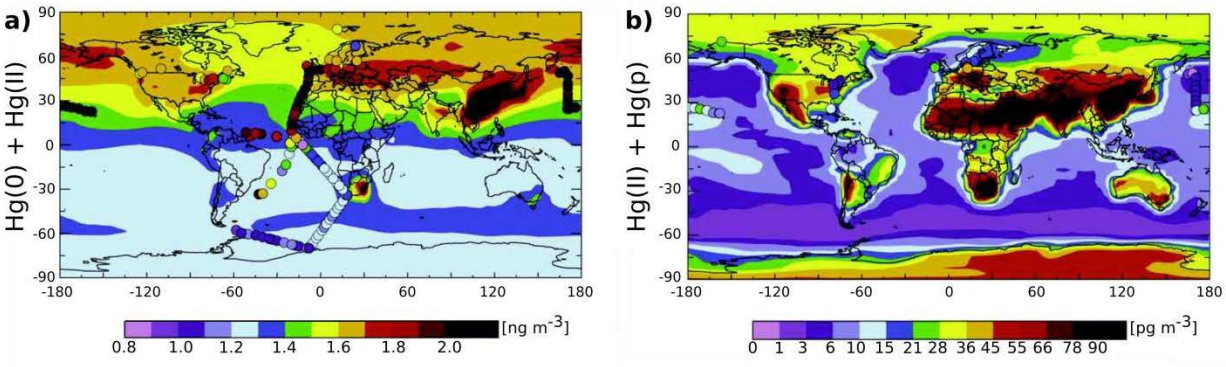

Figure 2-5: Concentrations moyennes annuelles en espèces mercurielles dans la couche limite atmosphérique d'après Selin et al. (2007). Les données issues du modèle GEOS-Chem sont en fond (année 2003) et comparées aux données d'observations (ronds) provenant de stations de mesures ou de campagnes océanographiques ponctuelles. **a)** Concentration moyenne en espèces gazeuses, c'est-à-dire somme des concentrations en Hg(0) et en Hg(II), **b)** concentration moyenne en espèces réactives, c'est-à-dire somme des concentrations en Hg(II) et Hg(p).

L'analyse sur le long terme des concentrations atmosphériques en espèces oxydées est rare (Figure 2-5b). Quelques stations du réseau CAMNet initièrent un tel suivi au début des années 2000 (Poissant et al., 2005; Cole et al., 2013; Steffen et al., 2014). En 2009, le réseau AMNet (« Atmospheric Mercury Network ») démarra et 30 stations furent installées à travers les Etats-Unis pour le suivi des concentrations en Hg(0), Hg(II) et Hg(p) (Gay et al., 2013). Bien que ces espèces ne constituent qu'une part infime des espèces mercurielles atmosphériques (p. ex. concentrations de l'ordre de quelques pg m^{-3} mesurées au Québec par Poissant et al. (2005)), leur suivi est primordial pour une meilleure compréhension du cycle atmosphérique du mercure (Sprovieri et al., 2010). Il est également à noter que l'ensemble des mesures de concentrations en Hg(0), Hg(II) et Hg(p) mentionnées ci-avant s'effectuent au sein de la couche limite atmosphérique (c'est-à-dire la partie de la troposphère directement soumise à l'influence de la surface terrestre). Une étude a cependant par exemple montré que le transport de masses d'air polluées entre l'Asie et les Etats-Unis s'effectue principalement au sein de la moyenne et haute troposphère (Jaffe et al., 2005). Les stations de mesures installées à haute altitude, telles que Mt. Bachelor aux Etats-Unis (Swartzendruber et al., 2006), Mauna Loa à Hawaï (Landis et al., 2005), Wank Mt. en Allemagne (Slemr et al., 2003), Lulin station à Taïwan (Sheu et al., 2010) ou le Pic du Midi en France (Fu et al., 2016a), sont très intéressantes pour étudier la spéciation du mercure à haute altitude puisque fréquemment situées dans la troposphère libre. Afin d'étendre la couverture spatiale des mesures, des campagnes aéroportées furent initiées en parallèle (p. ex. Ebinghaus and Slemr, 2000; Banic et al., 2003; Friedli et al., 2004). Celles-ci suggèrent, en accord avec les observations aux stations de haute altitude, que la haute troposphère et la basse stratosphère sont appauvries en Hg(0) et enrichies en espèces oxydées (Murphy et al., 2006; Talbot et al., 2007; Slemr et al., 2009; Lyman and Jaffe, 2012).

2.2.1.2 Dépôts

Les Etats-Unis et le Canada sont à la pointe en ce qui concerne le suivi des dépôts

humides. Dans le cadre du Programme National sur les Dépôts Atmosphériques (NADP), un réseau de mesure des dépôts de mercure (« Mercury Deposition Network » désormais AMNet, http://nadp.sws.uiuc.edu/mdn/) a été mis en place en 1995 après une année de tests (Vermette et al., 1995; Vermette et al., 1996). A ce jour, plus d'une centaine de stations ont été mises en place à travers les Etats-Unis et le Canada (p. ex. Mason et al., 2000; Keeler et al., 2005; Vanarsdale et al., 2005; Choi et al., 2008; Prestbo and Gay, 2009; Risch et al., 2012). En parallèle, des stations de mesures ont vu le jour en Europe (p. ex. Iverfeldt et al., 1995; Ebinghaus and Krüger, 1996; Wängberg et al., 2007) ainsi que dans d'autres régions de l'Hémisphère Nord (p. ex. Fu et al., 2010; Sanei et al., 2010; Sheu and Lin, 2013; Gichuki and Mason, 2014; Huang et al., 2015; Shanley et al., 2015). En revanche, les données de flux de dépôts humides étaient inexistantes dans l'Hémisphère Sud avant la mise en place du programme GMOS (voir section 2.2.2 ci-dessous). Les données de flux de dépôts secs des différentes espèces mercurielles atmosphériques sont quant à elles rares (Zhang et al., 2009). Des données supplémentaires de flux de dépôts (secs et humides) sont nécessaires pour améliorer notre compréhension du cycle du mercure (Mason and Sheu, 2002; Lindberg et al., 2007; Selin, 2009). De plus, afin de pouvoir juger de la capacité des réglementations mises en place à réduire de manière significative les dépôts de mercure au sein des écosystèmes, une très bonne compréhension des processus d'oxydation et de dépôts est primordiale (Sunderland et al., 2008; Selin, 2009). Il en découle la nécessité de mesurer de manière simultanée et en différents sites répartis sur l'ensemble de la planète les concentrations en espèces mercurielles atmosphériques (Hg(0), Hg(II) et Hg(p)) ainsi que les flux de dépôts (Sprovieri et al., 2010). Ce défi a en partie été relevé par le programme GMOS.

2.2.2 GMOS : un réseau mondial d'observations du mercure atmosphérique

D'après l'article suivant, disponible en intégralité en Annexe 1 :

Sprovieri, F., Pirrone, N., Bencardino, M., D'Amore, F., Carbone, F., Cinnirella, S., Mannarino, V., Landis, M., Ebinghaus, R., Weigelt, A., Brunke, E.-G., Labuschagne, C., Martin, L., Munthe, J., Wängerg, I., Artaxo, P., Morais, F., Cairns, W., Barbante, C., Diéguez, M., Garcia,, P. E., Dommergue, A., **Angot, H.**, Magand, O., Skov, H., Horvat, M., Kotnik, J., Read, K. A., Neves, L. M., Gawlik, B. M., Sena, F., Mashyanov, N., Obolkin, V. A., Wip, D., Feng, X. B., Zhang, H., Fu, X., Ramachandran, R., Cossa, D., Knoery, J., Marusczak, N., Nerentorp, M., Nordstrøm, C.: Atmospheric mercury concentrations observed at ground-based monitoring sites globally distributed in the framework of the GMOS network, Atmospheric Chemistry and Physics Discussions, doi: 10.5194/acp-2016-466, in review, 2016.

Bien qu'un certain nombre de stations de mesures ait été mis en place au cours des deux dernières décennies (voir section 2.2.1), il apparut indispensable, tant d'un point de vue politique que scientifique, de développer un réseau mondial d'observations. La motivation principale fut la suivante : rendre disponibles des données d'observations, cohérentes entre

elles, à l'échelle de la planète afin i) de valider les modèles atmosphériques régionaux et globaux et ii) d'évaluer l'évolution spatiale et temporelle des concentrations atmosphériques et des flux de dépôts et réémissions. C'est ainsi que naquit en 2010 le réseau mondial d'observations du mercure atmosphérique GMOS (« Global Mercury Observation System »), financé par l'Union Européenne (7ème programme cadre) et comprenant 24 partenaires institutionnels.

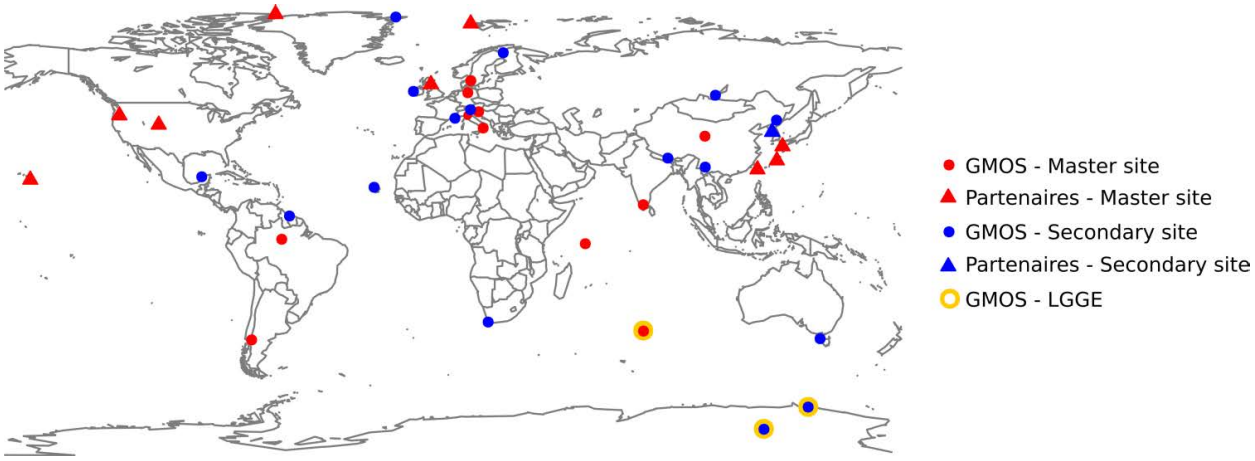

Figure 2-6: Situation géographique des différentes stations de mesures du réseau GMOS. Les trois stations cerclées d'or ont été mises en place par le Laboratoire de Glaciologie et Géophysique de l'Environnement (LGGE).

Ce réseau s'appuie sur des stations de mesures déjà existantes (voir section 2.2.1) et sur des stations nouvellement mises en place dans des régions du monde où les données étaient rares, notamment dans l'Hémisphère Sud (Sprovieri et al., 2010). Le réseau compte présentement près de 40 stations réparties sur l'ensemble de la planète, dont des stations situées au niveau de la mer (p. ex. Mace Head en Irlande, Calhau au Cap Vert, Cape Point en Afrique du Sud ou l'île d'Amsterdam au milieu de l'océan Indien), d'autres à haute altitude (p. ex. la station Everest-K2 au Népal à 5050 m ou la station Mt. Walinguan en Chine à 3816 m), ou encore en régions polaires (p. ex. Villum/Station Nord au Groenland, Pallas en Finlande, Concordia et Dumont d'Urville en Antarctique). La Figure 2-6 présente la position géographique des différentes stations, qu'elles soient directement gérées par le programme GMOS ou par des institutions partenaires. Il est à noter l'existence de deux types de stations, étiquetées « Master sites » ou « Secondary sites », en fonction des mesures qui y sont effectuées. Les « Master sites » analysent Hg(0), Hg(II) et Hg(p), et collectent les précipitations pour calculer le flux de dépôts humides, tandis que les « Secondary sites » analysent uniquement Hg(0). Outre la mise en place de stations de mesures, des campagnes océanographiques et aéroportées sont financées dans le cadre du programme GMOS. La Figure 2-7 résume l'organisation et les axes scientifiques du programme. De plus amples informations concernant GMOS peuvent être trouvées sur le site web suivant : www.gmos.eu.

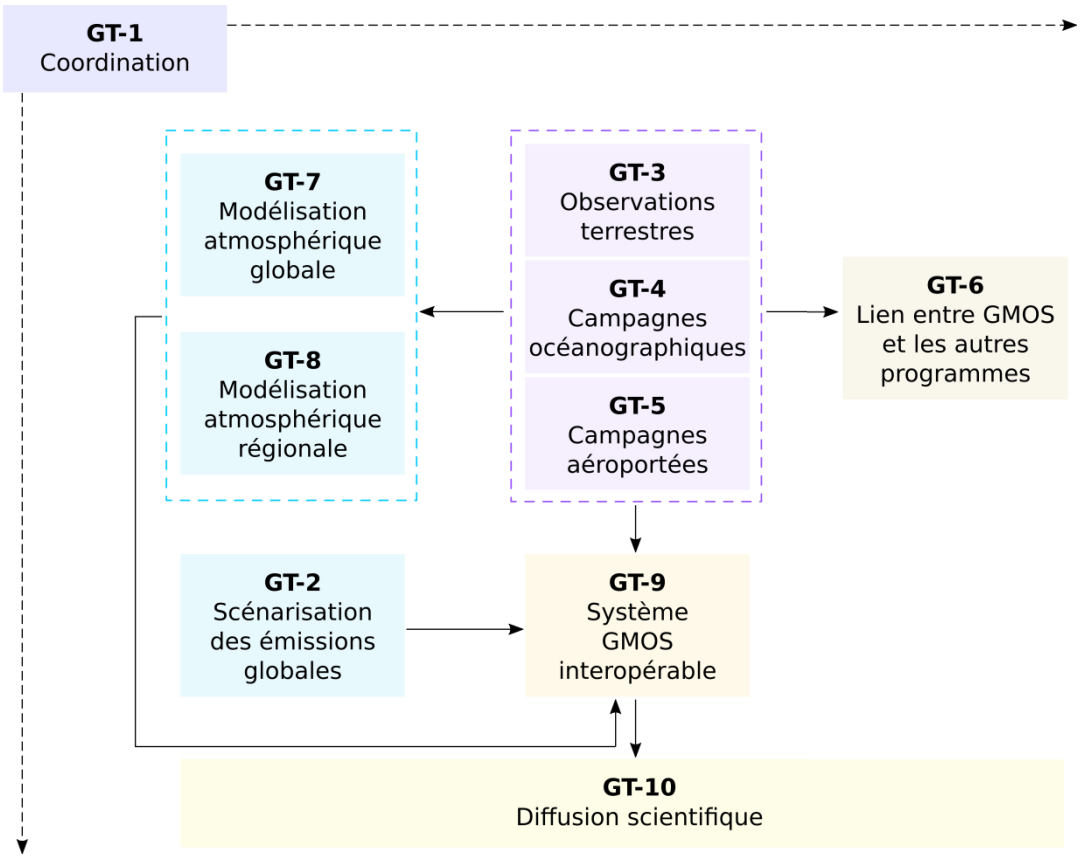

Figure 2-7: Organisation sous forme de groupes de travail (GT) et principaux axes scientifiques du programme GMOS.

2.3 Positionnement de l'étude dans le cadre des connaissances actuelles

Le mercure est une substance chimique préoccupante à l'échelle mondiale de par sa propagation atmosphérique sur de longues distances, loin des sources d'émission, sa persistance dans l'environnement, son potentiel de bioaccumulation dans les chaînes alimentaires aquatiques et ses effets néfastes sur la santé humaine (voir chapitre 1). Compte tenu de la complexité du cycle biogéochimique du mercure, il demeure difficile d'évaluer les répercussions qu'auront les diverses réglementations mises en place de l'échelle locale à l'échelle internationale (voir section 1.4) sur la contamination des écosystèmes et la santé des populations à court, moyen et long terme. Depuis une dizaine d'années, des modèles atmosphériques globaux sont développés pour retracer le cheminement du mercure des émissions aux dépôts au sein des écosystèmes. Ces modèles sont cependant entachés de fortes incertitudes en raison notamment de notre compréhension partielle des processus atmosphériques (réactions d'oxydo-réduction, dépôts, réémissions, voir section 2.1). Ces processus sont pourtant des étapes clés du cycle du mercure puisque c'est *via* l'atmosphère que les émissions sont transportées à l'échelle planétaire et que le mercure subit une oxydation préalable à son dépôt au sein des écosystèmes. La validation de ces modèles

globaux, primordiale pour orienter de manière judicieuse les futures réglementations sur le mercure, requiert par ailleurs des données d'observations à l'échelle planétaire.

Dans ce contexte, sous la houlette du programme GMOS et avec le soutien logistique et financier de l'Institut polaire français Paul-Emile Victor (IPEV, programme 1028 GMOstral), le Laboratoire de Glaciologie et de Géophysique de l'Environnement (LGGE) a installé trois stations de mesures dans l'Hémisphère Sud fin 2011 (voir Figure 2-6). La première a été installée en plein océan Indien sur l'île d'Amsterdam (AMS ; 37°48 S, 77°34 E, 55 m d'altitude). Les deux autres stations ont été implantées en Antarctique : à Dumont d'Urville sur la côte Est (DDU ; 66°40 S, 140°01 E, 43 m d'altitude) et à Concordia sur la calotte glaciaire (DC ; 75°06 S, 123°20 E, 3220 m d'altitude). L'objectif général de ces travaux de thèse est d'améliorer notre compréhension du cycle atmosphérique du mercure en ces régions reculées du globe.

Alors que les modèles atmosphériques se reposaient jusqu'alors essentiellement sur des données ponctuelles issues de campagnes océanographiques dans l'Hémisphère Sud (voir section 2.2.1.1 et Figure 2-5), la station d'AMS est l'endroit idéal pour capter un signal *a priori* peu influencé par les émissions anthropiques et documenter la réactivité atmosphérique du mercure dans la couche limite marine. Le chapitre 4 traite ainsi du cycle atmosphérique du mercure aux moyennes latitudes de l'Hémisphère Sud et répond aux questions suivantes : 1) Quelle est la réactivité atmosphérique du mercure dans la couche limite marine de ce secteur de l'océan Indien ? 2) Les flux de dépôts humides y sont-ils importants ? 3) Le signal enregistré sur AMS est-il significativement influencé par les émissions anthropiques ? 4) Ce signal est-il représentatif du bruit de fond atmosphérique aux moyennes latitudes de l'Hémisphère Sud ?

Alors que la réactivité atmosphérique du mercure est relativement bien connue en Arctique, avec notamment plus d'une centaine de publications sur les AMDE (voir section 2.1.1.1), les études sont plus rares en Antarctique. L'influence de ce continent sur le cycle biogéochimique du mercure demeure inconnue et est probablement sous-estimée par les modèles atmosphériques actuels (Dommergue et al., 2010b). D'après Brooks et al. (2008a), 60 tonnes de mercure seraient séquestrées chaque année sur le continent. De même, les mousses et les lichens antarctiques présentent des concentrations en mercure supérieures à celles retrouvées dans des zones polluées de l'Hémisphère Nord, suggérant des dépôts particulièrement importants d'espèces mercurielles sur le continent (Bargagli et al., 2005). La station norvégienne de Troll, située en Antarctique de l'ouest, était jusqu'alors la seule à fournir des chroniques pluriannuelles de concentrations en Hg(0) (Pfaffhuber et al., 2012). Plusieurs études ont cependant suggéré une capacité oxydante de l'atmosphère différente (halogènes *vs.* NO_x/OH) entre l'Ouest et l'Est du continent (Legrand et al., 2009; Grilli et al., 2013). La station de DDU est ainsi la première à permettre l'étude du cycle atmosphérique du mercure sur la côté Est de l'Antarctique. Une étude récente menée durant l'été austral a par ailleurs révélé une réactivité très importante du mercure sur la calotte glaciaire Antarctique, avec des cycles journaliers de dépôts et réémissions (Dommergue et al., 2012). La station de

DC permet désormais d'étudier le cycle annuel du mercure en Antarctique central. Le chapitre 5 traite ainsi du cycle atmosphérique du mercure sur le continent Antarctique et répond aux questions suivantes : 1) Quelle est la réactivité atmosphérique du mercure en Antarctique central et sur la côte Est ? 2) Quelle est l'influence du manteau neigeux sur le cycle atmosphérique du mercure ? 3) Quelle est l'influence potentielle du continent Antarctique sur le cycle du mercure à plus large échelle ?

Comment discuter du cycle atmosphérique du mercure à l'extrême sud de la planète sans essayer de dresser un parallèle avec la situation à l'extrême nord, en Arctique ? Le chapitre 6 propose ainsi une comparaison de la réactivité atmosphérique du mercure aux deux pôles. Un des objectifs du réseau GMOS étant de fournir des données de qualité pour la validation des modèles atmosphériques, ce chapitre propose également une comparaison des données d'observations en régions polaires avec les sorties de différents modèles globaux.

Avant d'entamer la discussion des résultats obtenus en ces trois sites de mesures, il apparaît indispensable de décrire au préalable, au sein du chapitre 3, les outils analytiques et les opérations de maintenance mis en place pour l'obtention de données de qualité.

3 Sites d'étude, outils analytiques et système de contrôle qualité

3.1 Sites d'étude

3.1.1 Ile d'Amsterdam

L'île d'Amsterdam (AMS) est une petite île française d'environ 55 km^2 située au beau milieu de l'océan Indien (Figure 3-1). Elle forme avec l'île Saint Paul, distante de 85 km, le district des îles Saint Paul et Amsterdam, l'un des cinq districts des Terres Australes et Antarctiques Françaises (TAAF). Située à 3400 km de Madagascar et à 5000 km de l'Afrique du Sud, AMS est l'une des îles les plus isolées au monde. Son isolement et éloignement de toute activité humaine en font un site de choix pour l'étude de la pollution de fond de l'atmosphère. L'installation d'une base scientifique (Figure 3-2a) remonte à décembre 1949, date à laquelle Martin de Viviès installa la première station météorologique. Depuis, une petite vingtaine de personnes hiverne chaque année. Le ravitaillement de la base est effectué quatre fois par an (Figure 3-3) par le navire *Marion Dufresne II*.

Figure 3-1: Localisation géographique des trois sites de mesures d'intérêt (en rouge). L'île d'Amsterdam (AMS) au milieu de l'océan Indien, Dumont d'Urville (DDU) sur la côte antarctique et la station Concordia (DC) sur le plateau antarctique. Le navire *Marion Dufresne II* effectue des rotations entre l'île de La Réunion (RUN), l'archipel de Crozet (CRO), l'archipel des Kerguelen (KER) et AMS. L'*Astrolabe* relie quant à lui Hobart (HBT) et DDU. AMS est située légèrement plus au sud que la ville du Cap (CPT) en Afrique du Sud.

Figure 3-2: Photographies des trois bases **a)** AMS, **b)** DDU et **c)** DC. © IPEV.

3.1.2 Continent Antarctique

3.1.2.1 Un continent consacré à la paix et à la science

L'Antarctique dispose d'un régime juridique unique basé sur le Traité sur l'Antarctique (1959), entré en vigueur en 1961. Au cours du XX^{ème} siècle, l'Argentine, l'Australie, le Chili, la France, la Norvège, la Nouvelle-Zélande et le Royaume-Uni eurent des revendications territoriales sur le continent. La Terre Adélie, zone de revendication française, forme un secteur angulaire entre les 136ème et 142ème méridiens de longitude Est et le pôle. L'Article IV du Traité stipule cependant qu'« aucun acte ou activité intervenant pendant la durée du présent Traité ne constituera une base permettant de faire valoir, de soutenir ou de contester une revendication de souveraineté territoriale dans l'Antarctique, ni ne créera des droits de souveraineté dans cette région ». Le Protocole au Traité sur l'Antarctique (1991), ou Protocole de Madrid, est entré en vigueur en 1998. Il fait de l'Antarctique une « réserve naturelle, consacrée à la paix et à la science » (Article 2). Toutes les activités relatives aux ressources minérales autres que la recherche scientifique sont interdites (Article 7). Toute activité doit en outre faire au préalable l'objet d'une étude d'impact sur l'environnement (Annexe I). Ce Protocole ne peut être modifié, jusqu'en 2048, qu'avec l'accord unanime de toutes les Parties consultatives au Traité sur l'Antarctique. Au cours de la dernière réunion consultative du Traité qui s'est tenue en juin 2011 à Buenos Aires, la Russie a cependant fait part de sa volonté de lancer des prospections de minerais et d'hydrocarbures pour l'horizon 2020 et à plus long terme (Foucart, 2011).

3.1.2.2 Base Dumont d'Urville

La base Dumont d'Urville (DDU, Figure 3-2b) en Terre Adélie, construite en 1956, est située sur l'île des Pétrels, dans l'archipel de Pointe Géologie, à 5 km du continent (Figure 3-1). Une trentaine de personnes hiverne chaque année. La base n'est accessible que durant l'été austral et est ravitaillée par quatre rotations du navire l'*Astrolabe*, au départ du port d'Hobart en Tasmanie. La base annexe de Cap Prud'homme, située sur le continent à 5 km de l'île des Pétrels, permet l'organisation de convois terrestres (raids) pour ravitailler la base Concordia située à 1100 km à l'intérieur du continent (voir section 3.1.2.3 ci-dessous).

3.1.2.3 Station Concordia

Parmi les 40 stations scientifiques permanentes établies en Antarctique, 37 sont implantées sur la côte. Les stations Amundsen-Scott (Etats-Unis), Vostok (Russie) et Concordia (Franco-Italienne) sont les seules stations continentales permanentes. La station Concordia (DC, Figure 3-2c) est située à 3220 m d'altitude et à 1100 km de DDU. Active depuis 1997, elle permet chaque année, et ce depuis 2005, l'hivernage d'une quinzaine de personnes. La base est ravitaillée par des raids terrestres depuis la base côtière annexe de Cap Prud'homme durant l'été austral (voir section 3.1.2.2 ci-dessus).

3.1.3 Logistique en régions isolées

Compte tenu de l'isolement des trois sites d'étude, une logistique bien rodée est nécessaire. Les mesures (voir section 3.2) sont réalisées par des volontaires au service civique employés par l'IPEV qui hivernent sur les différentes bases pour une durée de 14 mois (Figure 3-3). Les hivernants sont formés avant leur départ (formation initiale au LGGE) puis pendant la campagne d'été. Cette période permet une passation de consignes entre anciens et nouveaux hivernants. Un membre de l'équipe se rend également sur place afin de terminer la formation du nouvel hivernant et d'effectuer des opérations de maintenance sur les instruments de mesures (voir section 3.3). J'ai ainsi participé à trois campagnes d'été sur AMS durant ma thèse dans le cadre du programme IPEV-GMOstral 1028.

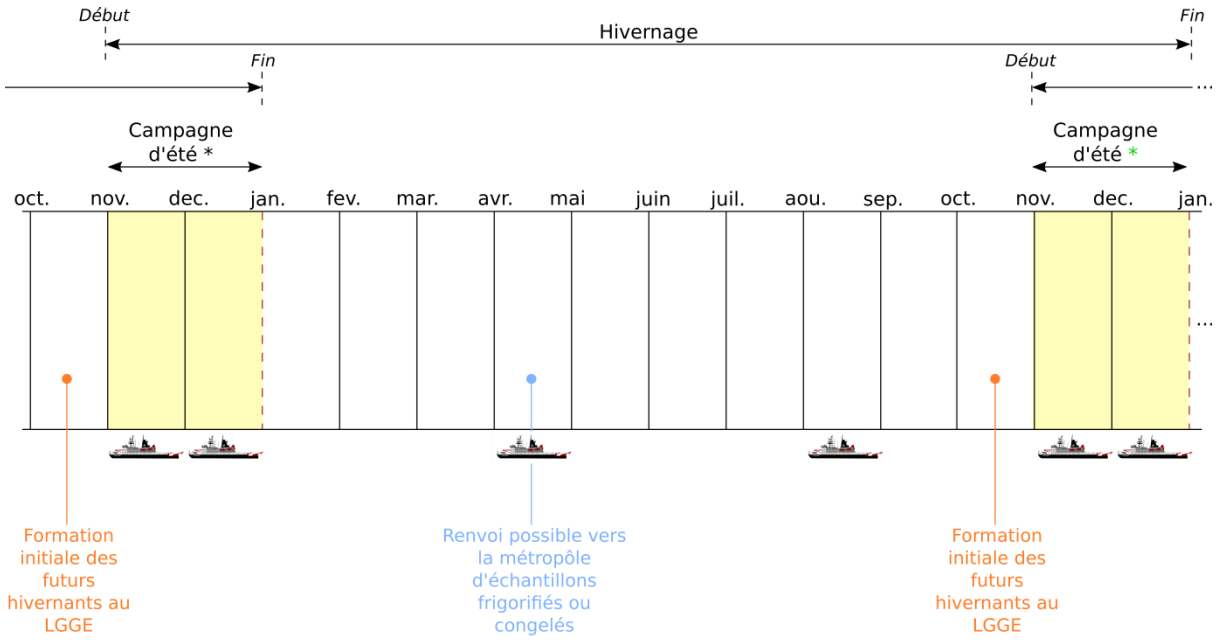

Figure 3-3: Exemple de chronogramme sur AMS. L'hivernage se déroule de novembre d'une année à fin décembre de l'année suivante. Le *Marion Dufresne II* effectue quatre rotations dans l'année permettant la relève des équipes, le ravitaillement de la base et l'envoi de matériel scientifique. Les campagnes d'été permettent une passation de consignes entre les anciens et nouveaux hivernants.

3.2 Outils analytiques

3.2.1 Espèces mercurielles atmosphériques

3.2.1.1 Remarques préliminaires

Comme indiqué précédemment (voir p. ex. section 1.2), le mercure se trouve dans l'atmosphère sous trois formes principales : Hg(0), Hg(II) et Hg(p). Pour rappel, AMS est un « Master site » tandis que DC et DDU sont des « Secondary sites ». Ainsi, seule l'analyse de Hg(0) est réalisée en Antarctique alors que Hg(0), Hg(II) et Hg(p) sont mesurés à AMS. En outre, les précipitations y sont collectées pour calculer le flux de dépôts humides (voir section 3.2.2.1).

Le TGM (« Total Gaseous Mercury », mercure gazeux total) est défini opérationnellement comme la fraction de mercure gazeux passant au travers d'un filtre de porosité 0,45 µm (Munthe et al., 2001b). Il est composé de Hg(0) et de Hg(II) (Figure 3-4). Certaines études rapportent ainsi des concentrations en TGM et non en Hg(0) (p. ex. Ebinghaus et al., 1999). On estime cependant qu'en régions éloignées de toute source anthropique, le TGM est composé à plus de 98 % de Hg(0) (Munthe et al., 2001b; Gustin et al., 2015). Pour les sites dédiés à l'étude de la pollution de fond de l'atmosphère, le programme GMOS a ainsi choisi la terminologie Hg(0) et non TGM (Sprovieri et al., 2016b). Pour les sites, tel AMS, disposant d'un instrument permettant l'analyse des trois espèces mercurielles atmosphériques (voir ci-après), la question ne se pose pas et l'instrument analyse bel et bien du Hg(0). Pour les sites polaires, tels DDU et DC, on estime communément que la présence d'un filtre de porosité 0,45 µm en amont de l'analyseur et l'utilisation d'une ligne d'échantillonnage non chauffée suffisent à s'assurer de l'analyse de Hg(0) et non de TGM (Steffen et al., 2002; Temme et al., 2003; Steffen et al., 2008). Du fait des dispositifs mis en place, on considère que nos trois sites mesurent du Hg(0) et non du TGM.

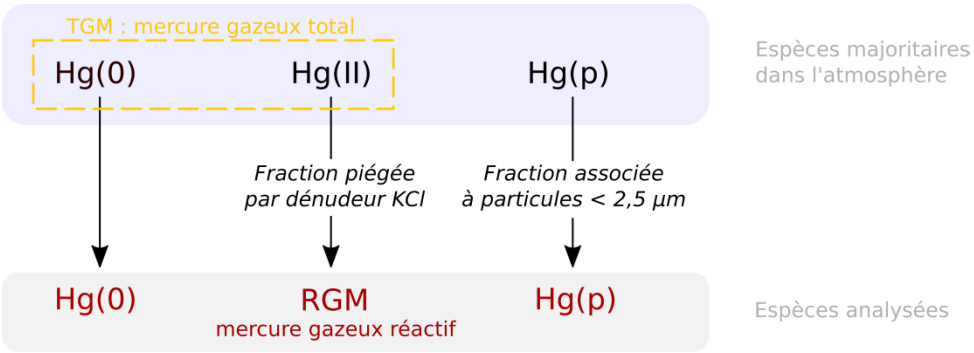

Figure 3-4: Bilan des espèces majoritairement présentes dans l'atmosphère et effectivement analysées par nos instruments de mesures.

On nomme communément RGM (« Reactive Gaseous Mercury », mercure gazeux réactif) la fraction de mercure divalent gazeux mesurée par les instruments actuellement disponibles (voir ci-après). La spéciation exacte du RGM demeure inconnue mais des études de terrain et

en laboratoire suggèrent la présence de composés gazeux tels $HgCl_2$, $HgBr_2$, HgO, $HgSO_4$, $Hg(NO_2)_2$ et $Hg(OH)_2$ (Gustin et al., 2013). On considère par la suite que le RGM contient toutes les formes divalentes gazeuses piégées par un dénudeur enduit de KCl (Figure 3-4). De même, Hg(p) correspond au mercure associé à des particules de diamètre inférieur à 2,5 µm (Figure 3-4). Le fait que le RGM et le Hg(p) soient définis opérationnellement engendre *a fortiori* des biais. Ceux-ci seront discutés au sein de la section 3.2.1.4.

3.2.1.2 Analyse du mercure élémentaire

A la fin des années 1990 différents instruments automatiques de mesures ont vu le jour (Urba et al., 1995; Tekran, 1998) et ont, petit à petit, supplanté les techniques manuelles d'échantillonnage (Brosset, 1987). Tous ces instruments donnent des résultats comparables (Ebinghaus et al., 1999; Munthe et al., 2001b) mais le Tekran® 2537 (Tekran, 1998), instrument utilisé en nos trois sites de mesures, est le plus répandu (Sprovieri et al., 2016b). L'air ambiant est aspiré pendant la durée souhaitée (5-15 min en fonction des sites) par l'intermédiaire d'une pompe interne à l'appareil (débit de 0,8-1,0 L min^{-1} en fonction des sites). Le mercure contenu dans l'air est alors amalgamé sur un piège en or, avant d'être désorbé sous forme élémentaire *via* la chauffe du piège. La présence de deux pièges en or permet une alternance des phases d'échantillonnage et de désorption et ainsi une analyse continue de l'air ambient. Le Hg(0) est ensuite analysé par spectrométrie d'absorption atomique en vapeur froide (« cold vapor atomic fluorescence spectrometer (CVAFS) ») à 253,7 nm (Fitzgerald and Gill, 1979; Bloom and Fitzgerald, 1988). L'instrument est alimenté par un flux d'argon et la limite de détection est de 0,10 ng m^{-3} (Tekran, 2011). Il possède en outre une source interne de calibration (voir section 3.3) et est protégé en amont par deux filtres PTFE (polytétrafluoroéthylène) de porosité 0,45 µm (un en entrée de la ligne de prélèvement et un en amont immédiat de l'instrument).

3.2.1.3 Analyse des espèces oxydées

L'analyse des espèces oxydées (RGM et Hg(p)) a été réalisée à AMS grâce à un instrument automatisé de chez Tekran®, communément appelé « unité de spéciation ». Deux modules (1130 et 1135) installés sur le toit de la station, à 6 m au-dessus du sol, permettent la collecte du RGM et du Hg(p), respectivement (Figure 3-5). Ces modules sont reliés au Tekran® 2537, qui permet l'analyse sous forme de Hg(0) (voir ci-après), *via* une ligne chauffée en PTFE de 10 m de long. Cette ligne est en permanence chauffée à 50 °C car les espèces divalentes sont très réactives et ont tendance à s'adsorber sur les surfaces présentes (Landis et al., 2002). Une donnée de RGM et de Hg(p) est disponible toutes les 4 h (3 h de collecte, 1 h d'analyse). Il est à noter que pendant les 3 h de collecte, l'analyse de Hg(0) se poursuit en parallèle (une donnée toutes les 5 min). L'air ambiant est aspiré à 10 L min^{-1} et passe au travers d'un impacteur permettant de filtrer les particules les plus grossières (diamètre > 2,5 µm) afin de ne pas endommager le module 1130. Tandis que le RGM est adsorbé sur un dénudeur en quartz enrobé de KCl au sein du module 1130, les particules de diamètre < 2,5 µm sont piégées par un filtre régénérable en quartz (RPF) au sein du module

1135. A la fin de la période de collecte, tout l'instrument est purgé par de l'air zéro (c'est-à-dire exempt de mercure) fourni par le module pompe. Le RPF puis le dénudeur sont alors successivement portés à 800 °C et 500 °C, respectivement, afin de permettre la décomposition thermique du Hg(p) et du RGM et l'analyse sous forme de Hg(0).

Figure 3-5: Schéma de la ligne d'échantillonnage et d'analyse du mercure divalent gazeux et particulaire. D'après Landis et al. (2002).

3.2.1.4 Biais

De plus en plus d'indices suggèrent que la mesure du RGM et du Hg(p) par une unité de spéciation souffre de biais et interférences importants (Lyman et al., 2010b; Gustin et al., 2013; Jaffe et al., 2014). Plusieurs études ont montré que le piégeage des espèces divalentes gazeuses par un dénudeur enduit de KCl n'est pas optimal (Gustin et al., 2013; Huang et al., 2013), engendrant une sous-estimation des concentrations en Hg(II) d'un facteur 1,3 à 3,7 (Huang et al., 2013). D'autres études suggèrent par ailleurs des artéfacts de mesure pour le Hg(p) engendrés par la température et le temps de collecte (Malcolm and Keeler, 2007; Rutter et al., 2008; Lynam and Keeler, 2005). La collecte et l'analyse sélective des particules de diamètre < 2,5 µm amène de plus à s'interroger quant à la possible sous-estimation des concentrations en Hg(p) (Kos et al., 2013), particulièrement en milieu océanique où le mercure s'associe surement préférentiellement avec des aérosols marins relativement grossiers (2-10 µm, Talbot et al., 2011; Feddersen et al., 2012). En parallèle, une fraction de Hg(II) pourrait ne pas être piégée par le dénudeur et être collectée, en aval, par le RPF, engendrant une surestimation de la concentration en Hg(p) (Gustin et al., 2013). Il est à noter

qu'il n'existe, à l'heure actuelle, aucune technique de calibration de l'unité de spéciation qui soit robuste et facilement utilisable sur le terrain (Gustin et al., 2015). Ceci s'explique notamment par la multiplicité des espèces divalentes, leur faible concentration atmosphérique et leur réactivité. Bien que la précision de la mesure de la concentration en RGM ait été estimée à 15 % (Landis et al., 2002), une étude poussée de l'influence des conditions environnementales (p. ex. concentration en ozone, humidité relative) s'avère nécessaire.

Malgré ces limitations, l'instrumentation décrite ci-avant est, à l'heure actuelle, la seule permettant l'analyse simultanée et automatique des trois espèces mercurielles atmosphériques. Ce système a par ailleurs permis de révolutionner nos connaissances sur le cycle atmosphérique du mercure en permettant une analyse à haute fréquence temporelle. Des techniques alternatives sont actuellement en cours de développement. Celles-ci seront discutées au sein des chapitres suivants.

3.2.2 Dépôts de mercure

3.2.2.1 Collecteur de précipitations

Le collecteur de précipitations installé sur AMS (Figure 3-6) est de type « wet only » (NSA 171 de chez Eigenbrodt®), c'est-à-dire qu'il ne s'ouvre que lorsque des précipitations sont détectées par un capteur de pluie. Les échantillons sont collectés pendant une période d'une semaine à un mois en fonction des saisons et du cumul de précipitations. Ils sont conservés dans un triple sac Ziploc® et congelés avant d'être rapatriés en métropole. L'analyse du mercure total contenu dans les échantillons a été réalisée par nos partenaires italiens du CNR-IIA (« Instituto del Consiglio Nazionale delle Ricerche, Istituto sull'inquinamento atmosferico ») selon la méthode 1631 de l'US EPA (2002). Les procédures opératoires standard mises en place pour la collecte des échantillons sont détaillées au sein de la section 3.3.

Figure 3-6: Collecteur de précipitations de type "wet only" installé à AMS. *Marion Dufresne II*, navire ravitailleur des TAAF, en arrière-plan. © Isabelle Jouvie.

3.2.2.2 Echantillons de neige de surface

A défaut de collecter les précipitations, des échantillons de neige de surface ont été collectés en Antarctique. 11 échantillons ont ainsi été collectés entre DC et DDU au cours d'un raid scientifique en février 2009 et analysés par la suite au LGGE. De plus, des échantillons ont été prélevés chaque semaine à DC entre février 2013 et janvier 2014. De plus amples informations concernant la collecte et l'analyse de ces échantillons seront données au sein du chapitre 5.

3.2.3 Bilan des données disponibles

La Figure 3-7 résume l'ensemble des données disponibles aux trois sites de mesures. Il est à noter que nous avons parfois dû faire face à des soucis d'ordre technique. Compte tenu de l'éloignement des stations et de l'impossibilité de faire parvenir rapidement des pièces de rechange en cas de problème, les instruments ont pu rester éteints de quelques semaines à près d'un an (DC en 2014). Le fonctionnement de l'unité de spéciation à AMS a, par ailleurs, été quelque peu erratique au court de l'année 2015 en raison d'une corrosion importante des modules situés en extérieur et de soucis électroniques, certes de courte durée, mais récurrents. L'unité de spéciation, éteinte à partir de septembre 2015, a été définitivement démontée au cours de ma campagne d'été de novembre-décembre 2015. De même, le Tekran® 2537 présent à DDU, stoppé dès juin 2015, a été définitivement rapatrié lors de la campagne d'été suivante. A l'heure où ces lignes sont écrites, l'analyse de Hg(0) à AMS et DC est toujours en cours ainsi que la collecte des précipitations à AMS.

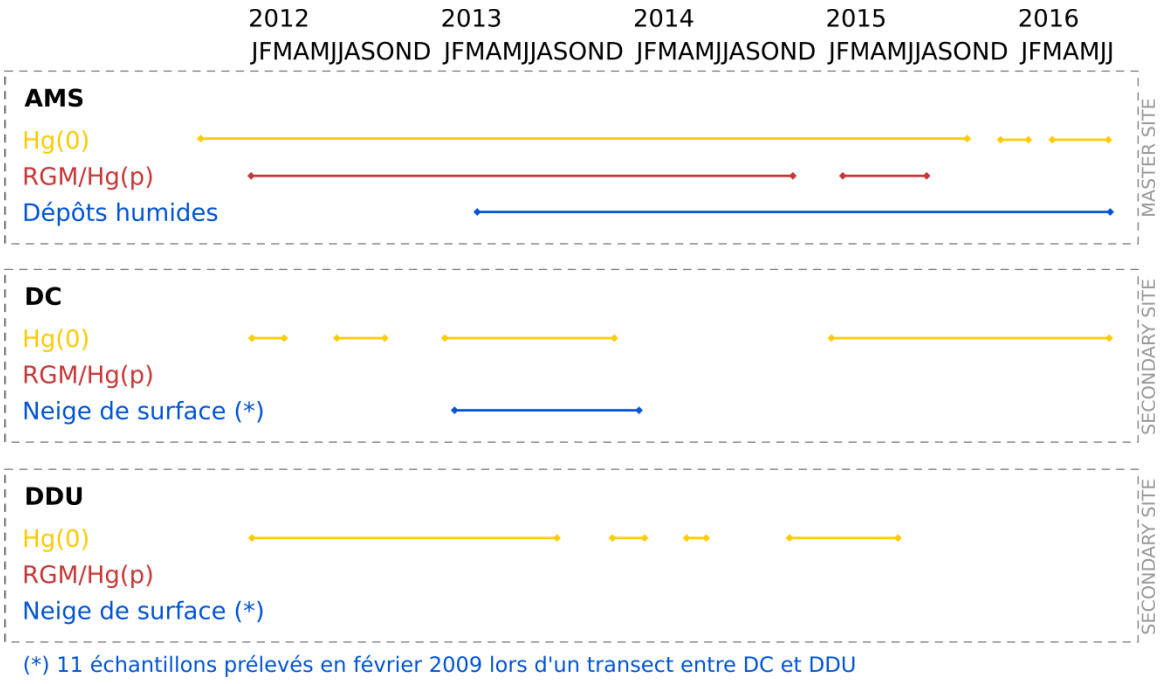

Figure 3-7: Bilan des données disponibles aux trois sites de mesures (en date de fin juillet 2016). Un trait plein signifie que des données sont disponibles pour le mois considéré, un blanc qu'aucune donnée n'a été enregistrée.

3.3 Système de contrôle qualité

3.3.1 Procédures Opératoires Standard pour la gestion des instruments

Des procédures opératoires standard (POS) pour la gestion des différents instruments sont distribuées aux hivernants en charge des expérimentations sur les trois sites. Elles synthétisent les opérations de maintenance à effectuer ainsi que les protocoles à suivre. L'opérateur doit, *a minima*, effectuer une visite hebdomadaire sur site afin de vérifier un certain nombre de paramètres, remplir une fiche de contrôle d'assurance-qualité (« fiche de maintenance », Annexe 2) et nous envoyer les données de la semaine. Les sections ci-après synthétisent l'ensemble des opérations de maintenance réalisées périodiquement.

3.3.1.1 Tekran® 2537

Le Tableau 3-1 résume les opérations de maintenance réalisées par les hivernants sur les analyseurs de Hg(0) à AMS, DC et DDU. Il est à noter que la préparation des ensembles porte-filtre + filtre est réalisée selon une procédure précise incluant notamment un nettoyage du porte-filtre à l'acide.

Tableau 3-1: Synthèse des opérations de maintenance réalisées par les hivernants sur les analyseurs de mercure élémentaire gazeux à AMS, DC et DDU.

Opérations de maintenance
Opérations hebdomadaires
1- Compléter la fiche de maintenance
2- Envoyer les données de la semaine et la fiche de maintenance par courriel
Opérations mensuelles
1- Installer un nouvel ensemble porte-filtre + filtre PTFE sur la ligne de prélèvement en entrée de l'analyseur
2- Vérifier l'absence de fuites sur la ligne
Opérations trimestrielles
1- Installer un nouvel ensemble porte-filtre + filtre PTFE sur la ligne « air zéro » en entrée de l'analyseur
2- Vérifier l'absence de fuites sur la ligne
3- Réaliser une calibration manuelle de l'analyseur
4- Mesurer le débit de pompage de l'analyseur
5- Vérifier le bon fonctionnement des bobines chauffantes entourant les pièges en or
6- Vérifier l'état de la pompe
Si nécessaire
1- Nettoyer ou changer la ligne de prélèvement
2- Changer la bonbonne d'air zéro
3- Remplacer les bobines chauffantes entourant les pièges en or
4- Changer la bouteille d'argon et vérifier l'absence de fuites
5- Effectuer la maintenance de la pompe
6- Installer une nouvelle paire de pièges en or
7- Nettoyer ou installer de nouvelles valves PTFE
8- Nettoyer ou remplacer la cellule de détection
9- Optimiser la position ou remplacer la lampe UV

Comme indiqué ci-avant (voir section 3.2.1.2), le Tekran® 2537 possède une source interne de perméation permettant la calibration automatique de l'instrument toutes les 25 à 69 h (en fonction des sites). Celle-ci peut cependant se dégrader avec le temps et il est nécessaire de s'assurer périodiquement de son bon fonctionnement au moyen d'une calibration externe

manuelle. Cette calibration externe, effectuée en moyenne deux à trois fois par an sur chacun des sites (Tableau 3-1) à l'aide d'une valise de calibration (Tekran® 2505) et d'une micro-seringue Hamilton®, fait l'objet d'un protocole strict adapté de celui développé par Dumarey et al. (1985). Elle consiste en l'injection (au moins 10 répétitions) d'un volume connu de vapeurs de mercure à une température donnée. Le débit d'air prélevé par l'instrument est également régulièrement contrôlé (chaque trimestre) à l'aide d'un débitmètre (Definer 220 de chez DryCal®) préalablement calibré.

3.3.1.2 Unité de spéciation

Le Tableau 3-2 résume les opérations de maintenance réalisées par les hivernants sur l'unité de spéciation à AMS. La préparation d'un dénudeur et d'un RPF propres, d'une nouvelle union GL14-GL18 et d'un nouvel impacteur font l'objet de protocoles précis, détaillés dans les POS. Les hivernants sont formés au cours de la campagne d'été à la réalisation de ces opérations. Comme précisé précédemment (voir section 3.2.1.4), il n'existe pas, à l'heure actuelle, de technique de calibration de l'unité de spéciation. En revanche, de même que pour le Tekran® 2537 (voir section 3.3.1.1 ci-dessus), le débit d'air prélevé au niveau de l'impacteur est régulièrement contrôlé (Tableau 3-2).

Tableau 3-2: Synthèse des opérations de maintenance réalisées par les hivernants sur l'unité de spéciation à AMS.

Opérations de maintenance
Opérations hebdomadaires
1- Compléter la fiche de maintenance
Opérations bimensuelles
1- Installer un dénudeur enduit de KCl propre
2- Installer un impacteur propre
3- Installer un nouvel ensemble porte-filtre + filtre quartz sur la ligne de prélèvement
4- Vérifier l'absence de fuites sur la ligne
Opérations mensuelles
1- Installer un nouvel ensemble porte-filtre + filtre PTFE sur la ligne « air zéro »
2- Installer un RPF propre
3- Installer une union GL14-GL18 propre
Opérations trimestrielles
1- Changer les joints PTFE de l'union GL14-GL18
Opérations semestrielles
1- Mesurer le débit de pompage au niveau de l'impacteur
Opérations annuelles
1- Changer le coude PTFE en sortie du RPF
2- Changer la ligne PTFE reliant le coude et le porte-filtre situé en aval immédiat sur la ligne de prélèvement
Si nécessaire
1- Nettoyer ou changer les lignes PTFE
2- Changer les bonbonnes d'air zéro du module de pompage 1130
3- Effectuer la maintenance de la pompe du module de pompage 1130

3.3.1.3 Collecteur de précipitations

Les procédures mises en place à AMS (Tableau 3-3) sont en accord avec les normes européennes et les procédures recommandées par l'EMEP (« European Monitoring and Evaluation Programme ») (EMEP, 2001; NEN-EN 15853, 2010). Elles ont par ailleurs été

validées lors d'un séminaire à Bruxelles en Avril 2011 par l'ensemble des partenaires impliqués dans le programme GMOS.

Tableau 3-3: Synthèse des opérations de maintenance réalisées par les hivernants sur le collecteur de précipitations à AMS.

Opérations de maintenance
Opérations hebdomadaires
1- Vérifier qu'il n'y a pas de toiles d'araignée devant le capteur, le nettoyer si besoin
2- Tester le bon fonctionnement du capteur en passant la main devant
Opérations hebdomadaires à bimensuelles en hiver, mensuelles en été
1- Changer la bouteille de collecte
2- Installer un système de prélèvement propre
3- Stocker la bouteille récupérée au congélateur (dans un triple sac Ziploc®)
Opérations mensuelles
1- Changer les bains de détergent alcalin et d'acide nitrique
Opérations bimestrielles
1- Réaliser un « blanc terrain »
2- Réaliser un « blanc bouteille »
Opérations semestrielles
1- Réaliser un « blanc transport »
Opérations annuelles
1- Nettoyer le compartiment interne du collecteur
2- Nettoyer l'extérieur du collecteur
3- Changer le joint d'étanchéité en silicone entre l'entonnoir et le collecteur
4- Vérifier la tension de la chaîne et l'ajuster si besoin
5- Huiler la chaîne et le tube actionneur du couvercle
Si nécessaire
1- Réaliser un « blanc eau milliQ » lorsqu'une nouvelle production d'eau milliQ débute au laboratoire

Le système de prélèvement (entonnoir, lignes PTFE, bouchon connecteur), illustré par la Figure 3-8, est minutieusement nettoyé à l'acide entre chaque échantillon. Le protocole de nettoyage inclut notamment des rinçages à l'eau milliQ et des trempages dans des bains de détergent alcalin (5 % v/v) et d'acide nitrique (3,5 % v/v). Les bouteilles destinées à l'échantillonnage des précipitations sont préparées en amont par nos partenaires du CNR-IIA. Elles contiennent de l'acide chlorhydrique (0,8 % v/v) permettant la stabilisation de l'échantillon en attendant l'analyse. Comme précisé auparavant, l'analyse du mercure total contenu dans les échantillons a été réalisée en Italie.

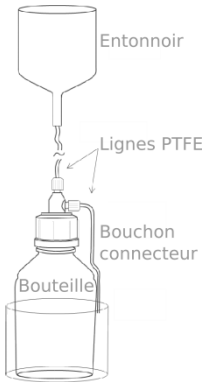

Figure 3-8: Schéma du système de collecte des précipitations.

Comme indiqué dans le Tableau 3-3, différents types de blancs sont régulièrement réalisés. Un « blanc terrain » correspond au versement de 1000 mL d'eau milliQ dans une bouteille, pour analyse ultérieure, au travers d'un système de prélèvement propre nouvellement installé dans le collecteur. Au contraire, un « blanc bouteille » correspond au versement d'eau milliQ directement dans une bouteille, pour analyse ultérieure, sans passer par le système de prélèvement. Rien n'est ajouté dans un « blanc transport » : la bouteille, préalablement préparée par le CNR-IIA, est directement congelée sur AMS avant d'être renvoyée en Italie pour analyse. Enfin, un « blanc eau milliQ » correspond au versement d'eau milliQ (préparée sur AMS) directement dans une bouteille. Un tel blanc est réalisé à chaque fois que le système d'eau milliQ est relancé afin de s'assurer de la bonne qualité de l'eau utilisée pour le nettoyage du système de collecte.

3.3.2 Validation/invalidation des données atmosphériques et suivi des performances des instruments

Les données brutes (niveau 0) nous parviennent chaque semaine par courriel. Il s'agit alors de procéder à leur validation/invalidation (Figure 3-9) et de s'assurer du bon fonctionnement des instruments (voir ci-après).

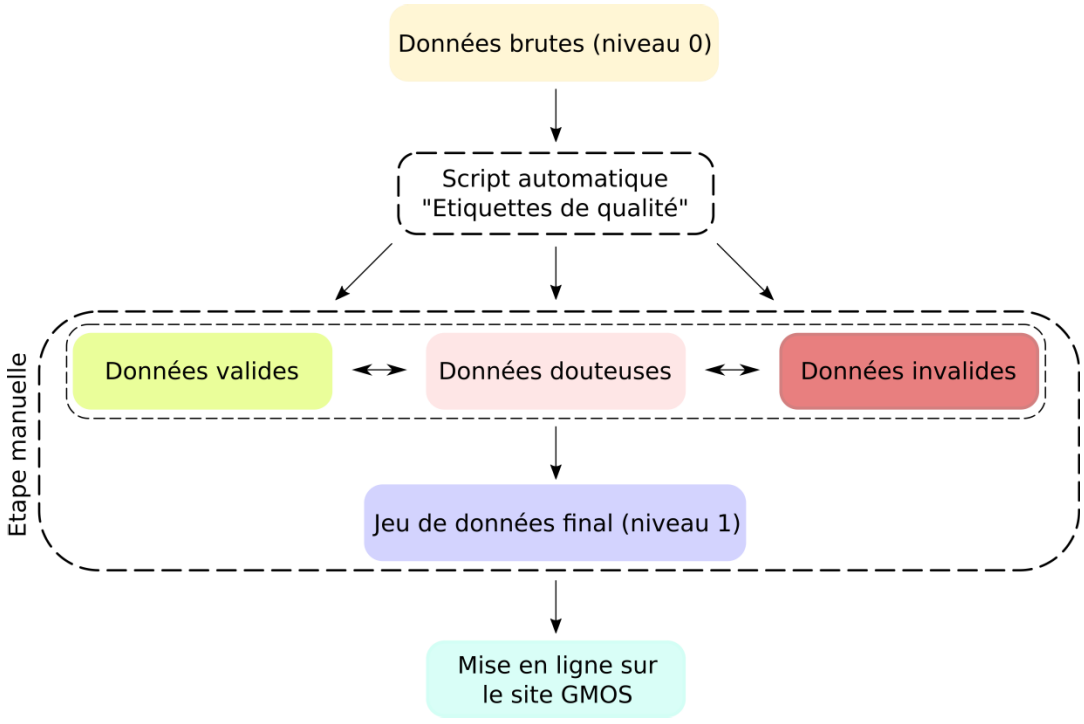

Figure 3-9: Schéma du processus de validation/invalidation des données mis en place pour la gestion des trois sites de mesures.

La première étape consiste en un étiquetage automatique des données *via* l'utilisation d'un script développé au LGGE par Manuel Barret. Ce script se base sur les fichiers bruts de données, sur les informations renseignées chaque semaine par l'hivernant dans la fiche de maintenance et sur une série d'étiquettes de qualité (Tableau 3-4). Ces dernières sont inspirées

de celles utilisées dans le cadre des réseaux AMNet et CAMNet (Steffen et al., 2012). La validation/invalidation finale des données est cependant réalisée manuellement, une expertise humaine étant nécessaire pour analyser les cas litigieux et identifier d'éventuels soucis non fléchés automatiquement.

Tableau 3-4: Exemples d'étiquettes de qualité utilisées dans le script automatique de prétraitement des données développé au LGGE.

Etiquettes	Description
A1	Biais > 10 % sur 10 mesures de Hg(0) consécutives
A2	Biais > 15 % sur 10 mesures de Hg(0) consécutives
BL1	Tension ligne de base < 0,150 ou > 0,300 V
BL2	Déviation ligne de base > 0,100 mV
E5	Biais > 50 % sur mesures consécutives même piège
E0	Première donnée Hg(0) après cycle désorption
V1	Volume de collecte hors gamme (± 2 %)
G1	Cycle de désorption RGM incorrect
P1	Cycle de désorption Hg(p) incorrect
S1	Blanc de désorption ≠ 0

A titre d'exemple, les étiquettes de qualité G1, P1 et S1, relatives aux cycles de désorption des espèces divalentes, permettent d'identifier un cycle anormal et d'invalider automatiquement les données. Pour rappel, les espèces divalentes sont collectées pendant 3 h puis désorbées et analysées (cycle d'une heure) sous forme de Hg(0). Le Tableau 3-5 illustre les différentes étapes d'un cycle de désorption. Les étapes A-C et K-L permettent de purger les lignes du système afin d'éliminer tout mercure résiduel. Comme c'est le cas dans le cadre du réseau AMNet (Steffen et al., 2012), nous utilisons la concentration (en pg m^{-3}) de l'étape C comme blanc analytique. Les concentrations en Hg(p) et RGM (en pg m^{-3}) sont alors calculées selon les équations 3-1 et 3-2. Il est à noter que pour qu'un cycle de désorption soit valide, il faut que la concentration en Hg(p) et RGM lors de la première étape de désorption (E et H, respectivement) soit supérieure à 70 % de la concentration finale.

$$Hg(p) = E + F + G - (3 \times C) \quad \text{(Eq. 3-1)}$$

$$RGM = H + I + J - (3 \times C) \quad \text{(Eq. 3-2)}$$

Tableau 3-5: Etapes d'un cycle de désorption au sein de l'unité de spéciation pour l'analyse du RGM et du Hg(p) sous forme de Hg(0).

N° Tekran	Type de mesure	Label	Description
1	Air zéro	A	Ligne purgée avec de l'air zéro. Début du cycle de désorption.
1	Air zéro	B	
1	Air zéro	C	
2	Chauffe pyrolyseur	D	Chauffe pyrolyseur enclenchée.
3	Hg(p)	E	Début chauffe RPF.
3	Hg(p)	F	
3	Hg(p)	G	
4	RGM	H	Début chauffe dénudeur.
4	RGM	I	
4	RGM	J	
1	Air zéro	K	Refroidissement actif (ventilateurs).
1	Air zéro	L	Fin du cycle de désorption. Reprise du mode collecte.

Un certain nombre de paramètres sont par ailleurs vérifiés semaine après semaine afin de nous assurer du fonctionnement optimal des analyseurs de Hg(0) (Figure 3-10). En cas de nécessité, les hivernants interviennent pour réaliser un réglage de l'instrument ou changer une (ou plusieurs) pièce(s).

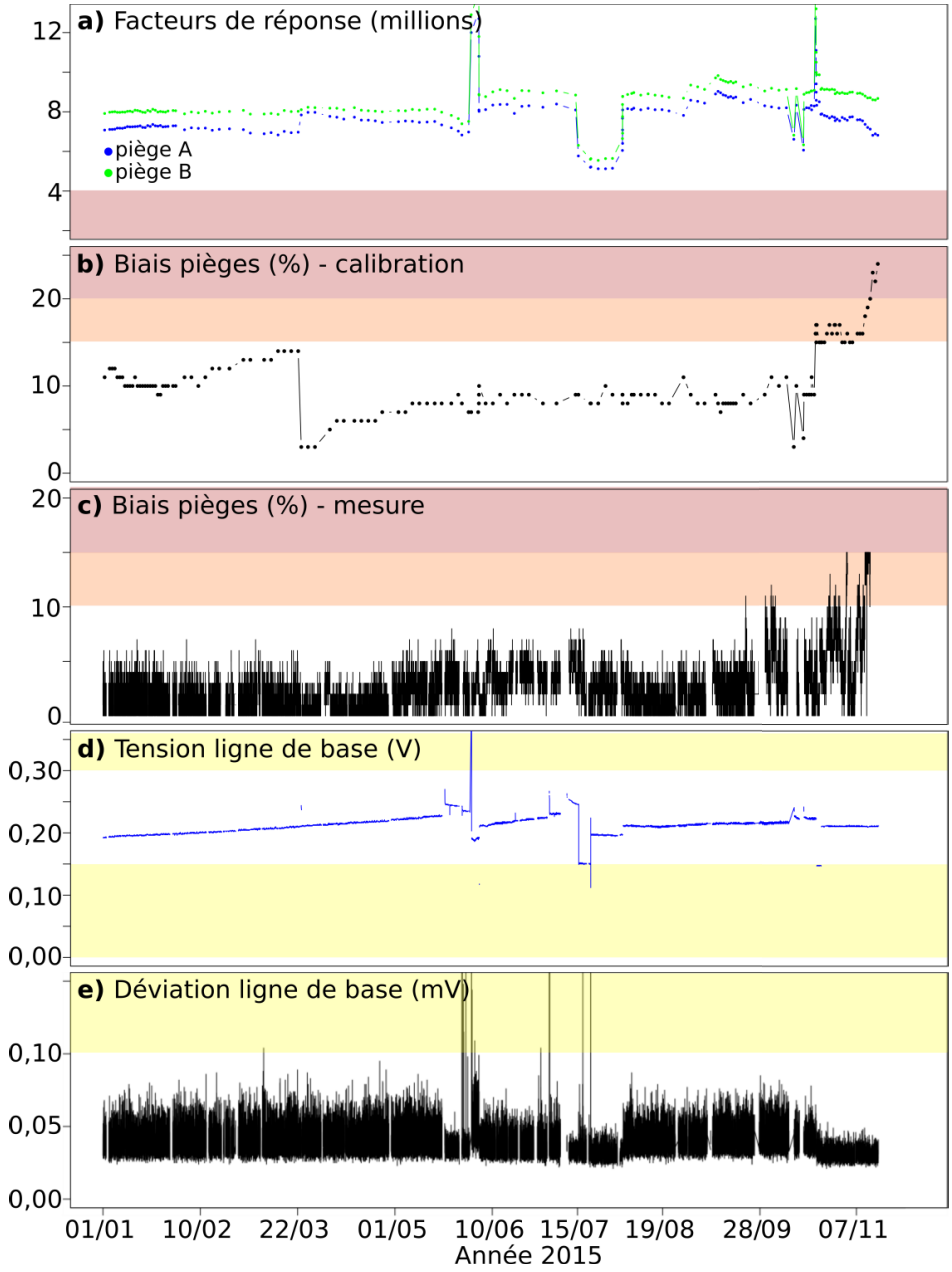

Figure 3-10: Variation de différents paramètres permettant de juger du bon fonctionnement de l'instrument (exemple ici de l'année 2015 à AMS) : **a)** facteurs de réponse des deux pièges en or lors de la calibration interne, **b)** biais entre les deux pièges en or lors de la calibration interne, **c)** biais entre les deux pièges en or lors de la mesure de Hg(0), **d)** tension de la ligne de base de l'instrument et **e)** déviation de la ligne de base. Les zones en jaune signifient qu'un réglage de l'instrument doit être opéré. Les zones en orange signifient que la vigilance est de mise tandis que les zones en rouge engendrent une invalidation des données et nécessitent très probablement une intervention de l'opérateur (remplacement de la paire de pièges en or ou des bobines chauffantes).

3.3.3 Erreurs systématiques sur la mesure de Hg(0)

Le Tekran® 2537 est un instrument complexe et les erreurs systématiques sur la mesure de Hg(0) dépendent des procédures mises en place, des performances de l'instrument ainsi que du niveau d'expérience des opérateurs (Slemr et al., 2015). Les calibrations internes, réalisées toutes les 25 à 69 h selon les sites (voir section 3.3.1.1), permettent de limiter les biais engendrés par l'usure des composants électroniques et le vieillissement du matériel de collecte et de détection. La source interne de perméation est en outre contrôlée plusieurs fois par an *via* des calibrations externes manuelles (voir section 3.3.1.1). Les injections manuelles par un opérateur expérimenté sont généralement répétables (~ 3 %) et on tolère un biais de 5 % entre calibrations interne et externe. Il s'avère difficile, en pratique, de quantifier la déviation par rapport à une performance idéale de l'appareil ; déviation engendrée par la désactivation progressive des pièges en or, un biais entre les pièges, une contamination résiduelle des lignes ou la présence d'éventuelles fuites (Steffen et al., 2012). L'erreur systématique sur la mesure de Hg(0) peut en revanche être estimée grâce aux différents exercices d'intercomparaison (EI) réalisés de par le monde (Slemr et al., 2015). Lors d'un EI réalisé à Mace Head en Irlande (Ebinghaus et al., 1999) trois analyseurs Tekran® 2537 révélèrent un biais moyen de 0,02-0,11 ng m^{-3}. Considérant une concentration moyenne de 1,75 ng m^{-3} pendant la durée de l'intercomparaison, cela représente un biais maximal de l'ordre de 6 %. L'analyse en parallèle de Hg(0) par deux Tekran® 2537 pendant quatre jours en Toscane révéla par ailleurs un biais moyen de 9 % (Munthe et al., 2001b). Hg(0) fut également mesuré pendant 28 jours par 5 analyseurs à la station allemande de Waldhof (Aas, 2006). Les concentrations médianes mesurées furent 2,02, 1,88, 1,77, 1,70 et 1,69 ng m^{-3}. Le biais moyen fut donc d'environ 8 % alors que le biais maximal atteignit environ 18 % (par rapport aux concentrations moyennes). En se basant sur ces résultats expérimentaux, on peut estimer à environ 10 % l'incertitude moyenne sur la mesure de Hg(0), jusqu'à 20 % dans les cas extrêmes (Slemr et al., 2015).

Les outils analytiques et le système de contrôle qualité ayant été présentés, il est à présent temps d'entamer la discussion des résultats obtenus à AMS (chapitre 4) et en Antarctique (chapitre 5) de sorte à répondre aux questions soulevées au sein de la section 2.3.

4 Cycle atmosphérique du mercure aux moyennes latitudes de l'Hémisphère Sud

Ce chapitre décrit nos avancées concernant la compréhension du cycle atmosphérique du mercure aux moyennes latitudes de l'Hémisphère Sud. La section 4.1 propose une description et interprétation des concentrations en espèces mercurielles atmosphériques acquises à AMS. Cette section s'appuie sur un article publié présentant les données de janvier 2012 à décembre 2013. Un résumé, en français, des principaux résultats et conclusions issus de cet article est disponible au sein de la section 4.1.5. Les données acquises depuis janvier 2014 y sont également présentées. Les flux de dépôts humides font l'objet de la section 4.2. La section 4.3 propose quant à elle une mise en perspective de ces données, l'objectif étant de répondre à la question suivante : dans quelle mesure le signal enregistré à AMS est-il représentatif du bruit de fond atmosphérique aux moyennes latitudes de l'Hémisphère Sud et permet-il de mieux contraindre les modèles atmosphériques actuels ?

4.1 Cycle atmosphérique du mercure au niveau de l'île d'Amsterdam (37°48 S, 77°34 E)

D'après :

Angot, H., Barret, M., Magand, O., Ramonet, M., and Dommergue, A.: A 2-year record of atmospheric mercury species at a background Southern Hemisphere station on Amsterdam Island, Atmospheric Chemistry and Physics 14, 11461-11473, 2014.

Abstract

Although essential to fully understand the cycling of mercury at the global scale, mercury species records in the Southern Hemisphere are scarce. Under the framework of the "Global Mercury Observation System" (GMOS) project, a monitoring station has been set up on Amsterdam Island (37°48 S, 77°34 E) in the remote southern Indian Ocean. For the first time in the Southern Hemisphere, a 2-year record of gaseous elemental mercury (Hg(0)), reactive gaseous mercury (RGM) and particle-bound mercury (Hg(p)) is presented. Hg(0) concentrations were remarkably steady (1.03 ± 0.08 ng m^{-3}) while RGM and Hg(p) concentrations were very low and exhibited a strong variability (mean: 0.34 pg m^{-3} [range:

< detection limit-4.07 pg m^{-3}] and mean: 0.67 pg m^{-3} [range: < detection limit-12.67 pg m^{-3}], respectively). Despite the remoteness of the island, wind sector analysis, air mass back trajectories and the observation of radonic storms highlighted a long-range contribution from the southern African continent to the Hg(0) and Hg(p) budgets from July to September during the biomass burning season. Low concentrations of Hg(0) were associated with southerly polar and marine air masses from the remote southern Indian Ocean. This unique data set provides new baseline Hg(0) concentrations in the Southern Hemisphere midlatitudes while mercury speciation along with upcoming wet deposition data will help to improve our understanding of mercury cycle in the marine boundary layer.

4.1.1 Introduction

Due to its toxicity, persistence, bioaccumulative nature, and long-range transport, mercury (Hg) is a global threat to ecosystems and human health. Since the 70's, multiple regulations have been implemented to tackle the exposure of populations to this contaminant. In 2013, the United Nations Environment Programme (UNEP) opened for signature a new legally-binding treaty on mercury, giving birth to the Minamata Convention on mercury (UNEP, 2013b). However, research gaps limiting mercury reduction policies at regional or global scale remain. For example, the policy effectiveness at reducing deposition of mercury requires a better knowledge of the chemistry of atmospheric mercury species (Selin, 2014b).

According to recent estimates (Amos et al., 2013) while 10 % of annual global emissions of atmospheric mercury currently come from natural geological sources – *e.g.*, volcanic emissions or mercury-containing rocks –, 30 % are produced by a variety of anthropogenic activities – *e.g.*, coal combustion, cement production, waste incineration or artisanal and small-scale gold mining –, and reemissions of previously released mercury account for the remaining 60 %. Gaseous elemental mercury (GEM, Hg(0)) is the dominant form of atmospheric mercury (Lindberg and Stratton, 1998). It can be oxidized by ozone or free radicals into highly reactive and water-soluble divalent species (Hg(II)) and/or particle-bound mercury (Hg(p)) (Lin and Pehkonen, 1999) that can be deposited through wet and dry processes (Lindqvist and Rodhe, 1985).

In remote areas far from any local sources, atmospheric deposition has been recognized as the main source of mercury to the ocean (Lindberg et al., 2007). Mercury can then be re-emitted back to the atmosphere via gas exchange (Schroeder and Munthe, 1998) and modeling studies suggest that reemission from oceans is a major contributor to atmospheric concentrations of Hg(0), particularly in the Southern Hemisphere where oceans were shown to contribute more than half of the surface atmospheric concentration (Strode et al., 2007). To better understand the cycling of mercury at the global scale a coordinated global monitoring network is needed (Pirrone et al., 2013), along with long-term records of atmospheric mercury species in the Southern Hemisphere and at background sites (Sprovieri et al., 2010). To date observations in the Southern Hemisphere mainly rely on a few oceanographic campaigns (*e.g.*, Lamborg et al., 1999; Temme et al., 2003a; Witt et al., 2010) and on-going ground-

based monitoring surveys at the Cape Point station in South Africa (Slemr et al., 2008) and at Troll, Dumont d'Urville and Concordia stations in Antarctica (Pfaffhuber et al., 2012; Dommergue et al., 2013a; Dommergue et al., 2013b).

In this context, a monitoring station has been set up on Amsterdam Island, a remote island in the southern Indian Ocean, under the framework of the European Union-financed project "Global Mercury Observation System" (GMOS, http://www.gmos.eu/). The 2-year record of elemental, divalent and particle-bound mercury concentrations presented here is, to the best of the authors' knowledge, the first reported in the Southern Hemisphere midlatitudes. Along with mercury species, ancillary parameters were analyzed to categorize air masses reaching the station based on their source region. The main objective of this study is to investigate to what extent observations at Amsterdam Island could define Southern Hemisphere midlatitudes background conditions and provide new constraints in multi-scale mercury species cycling models.

4.1.2 Materials and Methods

4.1.2.1 Sampling site description

Amsterdam Island (AMS) is a small island (55 km^2) located in the southern Indian Ocean (37°48 S, 77°34 E), 3400 km and 5000 km downwind from the nearest lands, Madagascar and South Africa, respectively (Figure 3-1). Instrumentation dedicated to the study of atmospheric mercury is located at the Pointe Bénédicte station, at the northwest end of the island, 55 m above sea level and 2 km west of the scientific base (30 residents at most). Other monitoring activities are performed at the station for various atmospheric compounds such as ozone (Gros et al., 1998), carbon monoxide (Gros et al., 1999), total aerosol number concentration (Sciare et al., 2001), or carbonaceous aerosol (Sciare et al., 2009).

4.1.2.2 Ancillary parameters

Meteorological data – air temperature, relative humidity, barometric pressure, wind speed, and wind direction – were provided by the local meteorological station. Radon 222 and 220 (Rn) are monitored with a precision of 10 % on a 2-hour basis. The method is described in detail by Polian et al. (1986) and Kritz et al. (1990). It is assumed that ^{222}Rn and ^{220}Rn are in radioactive equilibrium with their short-lived daughters so that ^{222}Rn and ^{220}Rn concentrations can be calculated by measuring the concentration of their short-lived decay products. Upon formation these short-lived daughters are quickly and irreversibly scavenged by aerosols and sampled by filtration. The detection then relies on the measurement over time of the decrease of alpha radioactivity of these aerosols.

O_3 measurements have been performed at the Pointe Bénédicte station since 1994, halfway up on a 20-m high tower (Gros et al., 1998). Unfortunately, 2012 and 2013 data are not available due to technical problems.

A new cavity ring-down spectroscopy (CRDS) analyzer was installed at the Pointe Bénédicte station in 2012 for in-situ measurements of CH_4. This instrument (G2301, Picarro) is calibrated once a month with four reference gases (NO11-2004 scale for CH_4).

7-days air mass back trajectories were calculated at 60 meters above sea level, approximate sampling height for mercury analysis, using the HYSPLIT (HYbrid Single-Particle Lagrangian Integrated Trajectory) model accessed via NOAA Air Resources Laboratory READY (Real-time Environmental Applications and Display sYstem) website (Draxler and Rolph, 2013; Rolph, 2013). Calculated back trajectories always have some uncertainty, arising for example from the possible errors in input meteorological fields and the numerical methods (Yu et al., 2009), and increasing with time along the path (Stohl, 1998). As suggested by Jaffe et al. (2005) it should be noted that back trajectories only give a general indication of the source region.

Fire counts and chlorophyll-a data west of Amsterdam Island were obtained via the FIRMS MODIS Fire Archive Download (Davies et al., 2009) and the Giovanni online data system developed and maintained by the NASA GES DISC, respectively.

4.1.2.3 Mercury analyzers

Since January 2012 we have monitored 3 atmospheric mercury species: Hg(0), Hg(p) (< 2.5 µm) and reactive gaseous mercury (RGM), the latter consisting of various oxidized gaseous Hg(II) compounds and hereafter defined as all forms of mercury sampled using a KCl-coated denuder (Landis et al., 2002).

Atmospheric mercury species measurements were performed using a Tekran mercury speciation unit (Tekran 1130 and 1135) coupled to a Tekran 2537B analyzer (Tekran Inc., Toronto, Canada). Concentrations are expressed in ng m^{-3} (Hg(0)) or pg m^{-3} (Hg(p) and RGM), at standard temperature and pressure (273.15 K, 1013.25 hPa). Hg(0) was determined at sub ng m^{-3} levels using a gas-phase mercury analyzer, based on the amalgamation of mercury onto a gold cartridge followed by a thermal desorption and a detection by an integrated cold vapor atomic fluorescence spectrometer (CVAFS) at 253.7 nm (Fitzgerald and Gill, 1979; Bloom and Fitzgerald, 1988). The presence of two gold cartridges allowed alternating sampling and desorption modes and thus a continuous analysis of Hg(0) in the sample air stream. In order to protect the two gold cartridges against deleterious compounds such as acid gases and halogen compounds, and against particulate matter, the sample air stream – after exiting the speciation unit – was pre-filtered through a sodalime trap and a 0.2 µm PTFE filter.

The speciation unit was located on the roof top of the station, the sampling inlet being at 6 m above the ground, and connected to the 2537B analyzer through a 10 m-long PTFE heated line (50 °C). The sampling resolution was 5 min for Hg(0) and 4 hours for RGM and Hg(p), with sampling flow rates of 1 L min^{-1} and 10 L min^{-1}, respectively. Measurements were achieved through a multi-step procedure as described elsewhere (Lindberg et al., 2002) using

an impactor inlet (2.5 µm cut-off aerodynamic diameter at 10 L min^{-1}), a KCl-coated quartz annular denuder in the 1130 unit, and a quartz regenerable particulate filter (RPF) in the 1135 unit.

Quality assurance and quality control procedures

Fortnightly to monthly routine maintenance operations on the denuder, RPF, sodalime trap and filters, along with thorough cleaning steps and weekly site visits enabled the collection of contamination-free air samples. The accuracy of flow measurements was checked twice a year with a calibrated flow meter (Definer 220). An automatic calibration step of the 2537B analyzer was carried out every 69 hours with an internal mercury permeation source. The accuracy of this permeation source was annually checked against manual injections of saturated mercury vapor taken from a temperature controlled vessel, using a Tekran 2505 mercury vapor calibration unit and a Hamilton digital syringe, and following a strict procedure adapted from Dumarey et al. (1985). Both routine and exceptional maintenance were compiled and archived via a software program developed at the LGGE. This software program also enabled a rapid data processing in order to produce clean time-series of Hg(0), Hg(p) and RGM. Screening criteria for data validation/invalidation were inspired by standard operative protocols used by the Canadian Atmospheric Mercury Measurement Network (CAMNet) and the Atmospheric Mercury Network (AMNet) (Steffen et al., 2012). To ensure uniformity across the network, GMOS is currently developing a quality control (QC) software and an intercomparison with the AMNet QC software will be undertaken.

The best estimate of the detection limit (DL) for Hg(0) measurements was 0.10 ng m^{-3} (Tekran, 2011) and ten injections of 15 µL of saturated mercury vapor were performed to check the repeatability of the system response. The system gave a relative expanded uncertainty of 1 % (95 % confidence level). Validated 5-minute Hg(0) data subsets were compiled into hourly-average data when the hourly recovery rate exceeded 50 % (number of valid data records collected *vs.* that possible over the reporting period).

RGM and Hg(p) sampling resolution was shifted from 3 to 4 hours after a few days due to very low concentrations, and the detection limit therefore decreased from 0.42 pg m^{-3} to 0.28 pg m^{-3} based on the sampling volumes and Hg(0) detection limit (Wang et al., 2014). The mean of the distributions was estimated using the Kaplan-Meier cumulative proportion-based method. It provides more reliable results for data sets containing below-detection limit values than the substitution method, *i.e.* replacement of below-detection limit values by a constant equal to 0, 0.5 DL or DL (Helsel, 2005). 75 % and 50 % of RGM and Hg(p) measurements, respectively, were below the limits of detection resulting in differences for mean values up to 60 % and 15 %, respectively, comparing Kaplan-Meier and normally averaged data sets. Values 3.3 times above the stated detection limits, *i.e.* reliably quantified, will be discussed thereafter and referred to as RGM and Hg(p) events (3 % and 18 % of RGM and Hg(p) measurements, respectively).

There is growing evidence that RGM and Hg(p) measurements might suffer from significant biases and interferences (Lyman et al., 2010b; Gustin et al., 2013; Jaffe et al., 2014). Several studies highlighted the inefficient collection of gaseous oxidized mercury compounds with a KCl-coated denuder in the Tekran technique (Gustin et al., 2013; Huang et al., 2013), leading to an underestimation of reactive mercury concentrations by a factor 1.3 to 3.7 (Huang et al., 2013). Other studies suggested sampling artifacts for Hg(p) measurements due to temperature or sampling duration (Malcolm and Keeler, 2007; Rutter et al., 2008). Moreover, the upper size cut-off diameter at 2.5 µm raises concerns about mercury associated with large (> 2.5 µm) particle fractions (Kos et al., 2013), especially in the marine environment where mercury is likely mainly contained in coarse sea salt aerosols (Talbot et al., 2011; Feddersen et al., 2012). There is no robust calibration technique of the Tekran speciation unit and no certified reference material available. The precision of RGM measurements – shown to be of 15 % under given conditions (Landis et al., 2002) – should be assessed in various sampling environments (*e.g.*, varying ozone/relative humidity conditions). Given the limitations of the RGM and Hg(p) measurements, data reported in this study should thus only be directly compared with the existing Tekran-based literature, as suggested by Wang et al. (2014). An extensive data set has been gathered worldwide using the Tekran speciation technique, which is the best available automated method. Future interference and calibration tests are fundamental to validate measurements and quantify uncertainties (Kos et al., 2013), and might enable us to correct RGM and Hg(p) data. Until then, orders of magnitude and variability in time and space of Tekran-based RGM and Hg(p) concentrations can be used as first estimates by policy makers or to evaluate atmospheric models.

4.1.3 Results and Discussion

4.1.3.1 Meteorological data

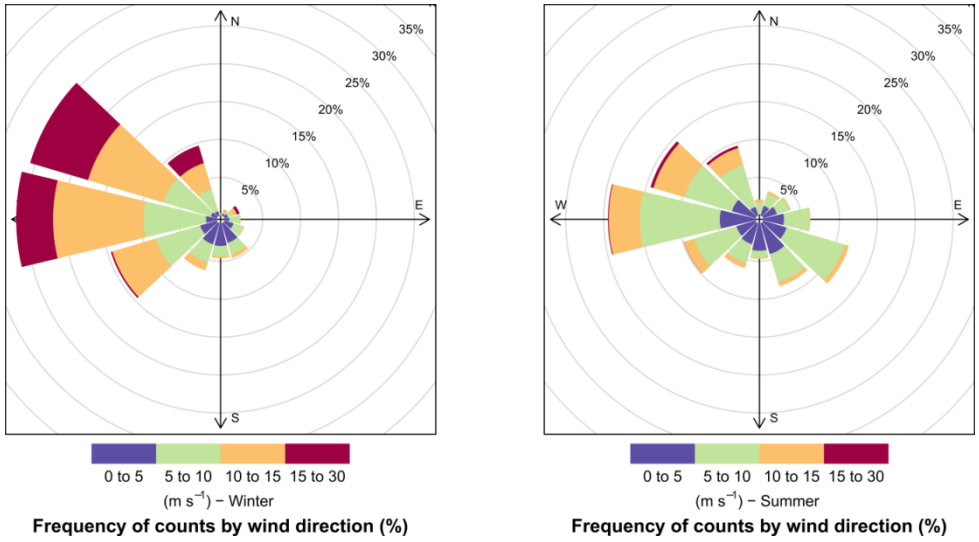

Figure 4-1: Wind direction and wind speed (m s^{-1}) in winter (July to September) and summer (December to February) at the Pointe Bénédicte station. N: North, E: East, S: South, W: West.

Climate is mild oceanic, with frequent presence of clouds. Seasonal boundaries were defined as follows: winter from July to September and summer from December to February, in line with other studies performed at Amsterdam Island (NGuyen et al., 1990; Gros et al., 1998; Sciare et al., 2009). During the two-year period under discussion here (January 2012 until December 2013), the monthly median air temperature ranged from 11 °C in austral winter to 17 °C in austral summer, while the monthly median relative humidity remained high and ranged from 65 to 85 % most of the year. Precipitation was very frequent with total precipitation of 1262 mm in 2012 and 1128 mm in 2013, in good agreement with the 1124 mm 40-year average reported by Miller et al. (1993). Wind speed remained comparatively high throughout the year (from 5 to 15 m s^{-1}); strong northwesterly winds peaked during winter months (July to September) when the roaring forties were at a maximum (Figure 4-1).

4.1.3.2 Hg(0) concentrations

4.1.3.2.1 Seasonality and contribution from biomass burning

Hg(0) concentrations were very steady with an average hourly mean concentration of 1.03 ± 0.08 ng m^{-3} (mean ± standard deviation, range: 0.72–1.55 ng m^{-3}; n = 10 285, Figure 4-2). Hg(0) data are lower than concentrations reported in the Northern Hemisphere but well within the expected range for a remote marine site in the Southern Hemisphere (Sprovieri et al., 2010). Indeed, Witt et al. (2010) measured a mean TGM (Total Gaseous Mercury defined as the sum of gaseous mercury species) concentration of 1.24 ± 0.06 ng m^{-3} in the Indian Ocean at latitudes ranging from 9 to 21° S, while TGM concentrations ranged from 1.20 to 1.40 ng m^{-3} at the Cape Point station, South Africa (34°21 S, 18°29 E) between 1995 and 2004 (Slemr et al., 2008) and Hg(0) concentrations amounted to 0.93 ± 0.19 ng m^{-3} at Troll station in Antarctica (Pfaffhuber et al., 2012). Hg(0) concentrations measured at Amsterdam Island are furthermore highly consistent with data reported by Wang et al. (2014) in the marine boundary layer over the equator at Galápagos Islands (0°57 S, 90°58 W; 1.08 ± 0.17 ng m^{-3}) despite occasional influence of northern hemispheric air at this station. A comprehensive comparison of mercury concentrations measured in the Southern Hemisphere is given in Slemr et al. (2015).

Whereas TGM and Hg(0) concentrations at the Cape Point station and at Galápagos Islands, respectively, showed a seasonal variation (Slemr et al., 2008; Wang et al., 2014), with minimum in winter and maximum in summer, Hg(0) data at Amsterdam Island followed an opposite trend, with slightly but significantly higher concentrations in winter (July to September) than in summer (December to February) (1.06 ± 0.09 ng m^{-3} *vs.* 1.04 ± 0.07 ng m^{-3}, p value < 2.2×10^{-16}, Mann-Whitney test, Figure 4-3a). This seasonality of Hg(0) concentrations is in agreement with more frequent air masses originating from southern Africa (northwesterly winds) from July to September. In order to further test this hypothesis Hg(0) data were sorted according to wind direction imposing a strict criterion on wind speed (> 8 m s^{-1}) to remove any local influence (Monfray et al., 1987). With north at 0°, southerly (S) winds ranged from 100 to 250° and northwesterly (NW) winds from 250 to 300°. Hg(0)

concentrations monitored during periods of NW flow were shown to be significantly higher than during S flow (1.05 ± 0.08 ng m^{-3} (n = 2 833) *vs.* 1.01 ± 0.08 ng m^{-3} (n = 822), *p* value < 2.2×10^{-16}, Mann-Whitney test, Figure 4-3b).

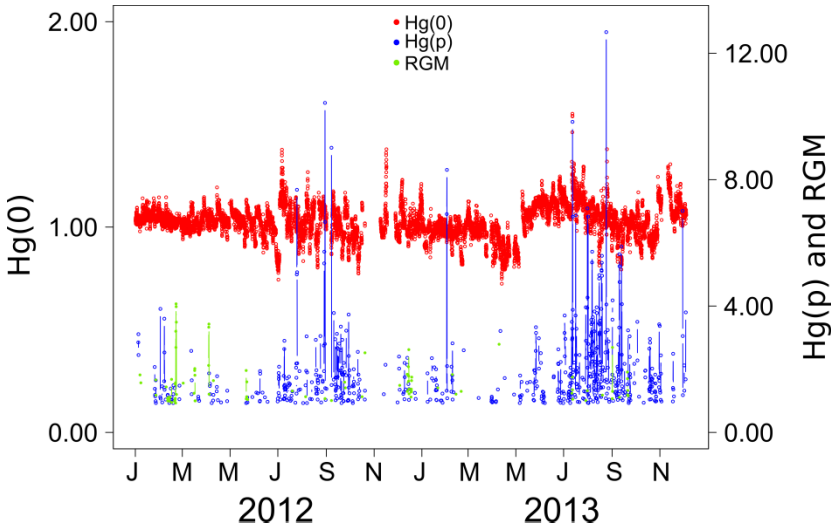

Figure 4-2: Particle-bound mercury (Hg(p), blue) and reactive gaseous mercury (RGM, green) concentrations (pg m^{-3}), and hourly averaged gaseous elemental mercury (Hg(0), red) concentrations (ng m^{-3}) measured at Amsterdam Island from January 2012 to December 2013.

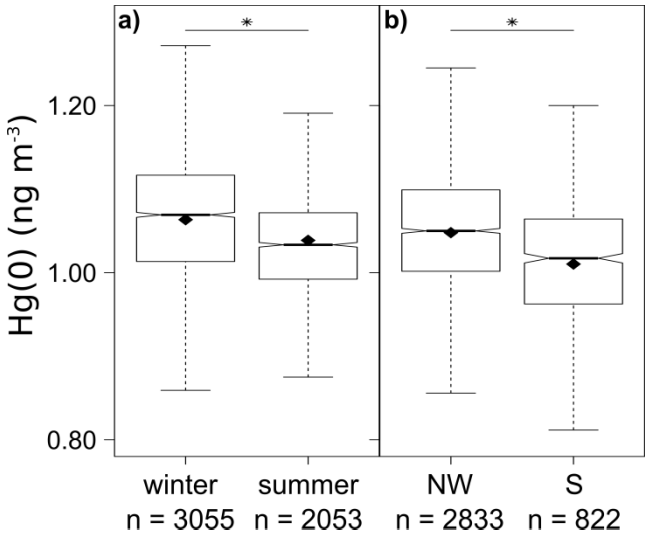

Figure 4-3: Hourly averaged gaseous elemental mercury (Hg(0)) concentrations (ng m^{-3}) measured at Amsterdam Island: **a)** in winter (July-September) or summer (December-February), and **b)** under northwesterly (NW) or southerly (S) winds. ◆: mean, *: statistically significant difference, n: number of hourly averaged data, bottom and top of the box: first and third quartiles, band inside the box: median, ends of the whiskers: lowest (highest) datum still within 1.5 interquartile range of the lower (upper) quartile. Outliers are not represented.

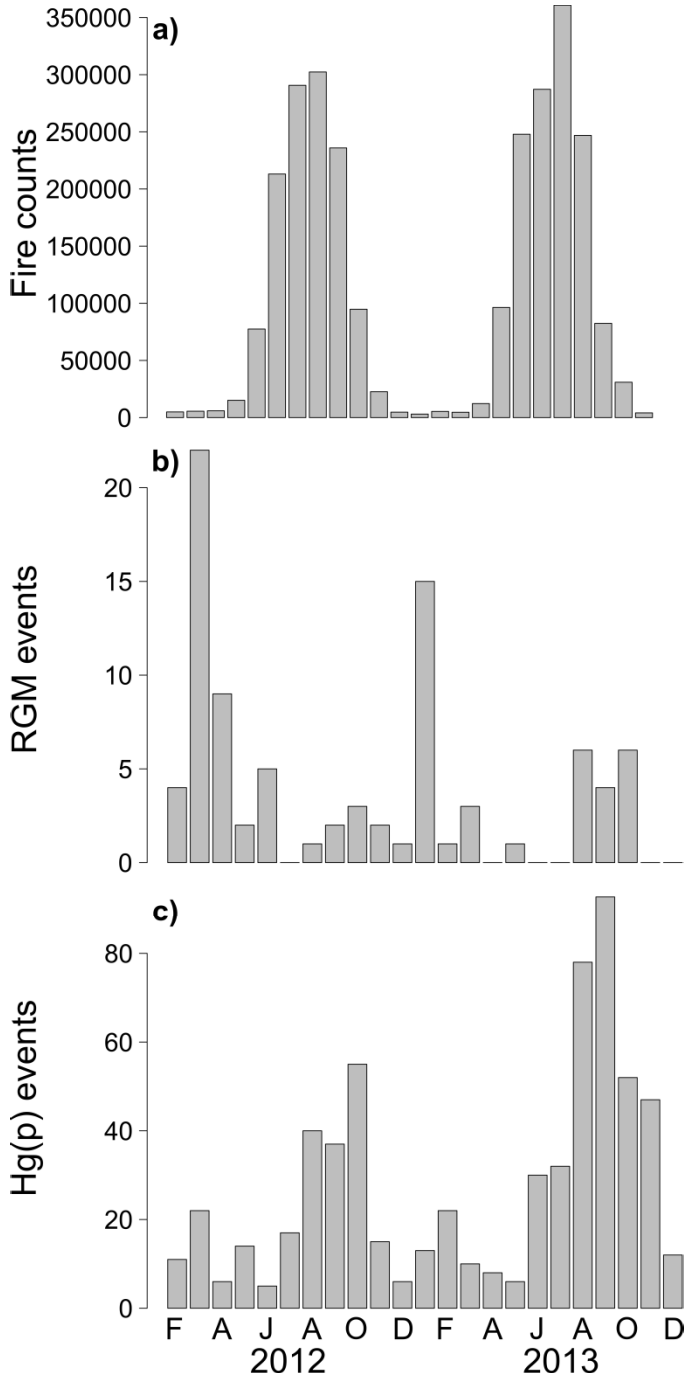

Figure 4-4 : Monthly **a)** fire counts west of Amsterdam Island (latitude: 3-53° S, longitude: 10-73° E) in 2012 and 2013. Data courtesy of FIRMS MODIS Fire Archive Download. **b**) Reactive gaseous mercury (RGM) events, *i.e.* number of measurements above quantification limit, at Amsterdam Island from February 2012 to December 2013. **c)** Particle-bound mercury (Hg(p)) events, *i.e.* number of measurements above quantification limit, at Amsterdam Island from February 2012 to December 2013.

The Hg(0) budget on the island could be enhanced from July to September by long-range transport during the burning season in southern Africa. 2012 and 2013 satellite observations of fires west of Amsterdam Island (latitude ranging from 3 to 53° S and longitude from 10 to 73° E) showed that the burning season extended from May to October, peaking between June and September (Figure 4-4a), in line with observations reported by Cooke et al. (1996). This

observation is also supported by the concomitant seasonal maxima on Amsterdam Island of CO (Gros et al., 1999), equivalent black carbon, non-sea-salt potassium and oxalate (Sciare et al., 2009), the latter two being commonly used as tracers for biomass burning.

4.1.3.2.2 Short-time variations

The atmosphere at Amsterdam Island could define background marine boundary layer conditions, with minimum perturbation from anthropogenic influences. However, as reported by Balkanski and Jacob (1990), the rapid export of air from southern Africa to the subantarctic Indian Ocean could constitute a major source of pollution to southern midlatitudes. The influence of continental air mass advection on Hg(0) concentrations was thus investigated.

The background variability of Hg(0) concentrations was assessed following a procedure adapted from Gros et al. (1999) calculating the difference, dHg(0), between hourly Hg(0) concentrations and the monthly mean. dHg(0) events higher than ± 0.18 ng m^{-3}, 3 times the mean monthly standard deviation of dHg(0) measurements, were further investigated.

^{222}Rn, decay product of ^{238}U with a 3.8 day half-life, is particularly well suited as a tracer of continental air over the oceans (Balkanski and Jacob, 1990). On the other hand, ^{220}Rn and its daughter ^{212}Pb, due to 54 s and 10.6 h half-lives, respectively, can only be attributed to local outgassing from Amsterdam Island's soil and not to any marine nor remote continental source (Polian et al., 1986). Therefore, ^{222}Rn activities below 100 mBq m^{-3} are considered as typical for marine air (Brunke et al., 2004), whereas air with ^{222}Rn activity above 100 mBq m^{-3} along with a ^{220}Rn (^{212}Pb) activity below 3.7 mBq m^{-3} is considered to be significantly influenced by a remote continent (Gros et al., 1999; Williams et al., 2001). Rapid and sharp variations of ^{222}Rn activity, referred to as "radonic storms" (Lambert et al., 1970), could be observed at Amsterdam Island, usually peaking around 400 mBq m^{-3}, and exceptionally reaching 1000 mBq m^{-3}. The occurrence of radonic storms was about 4 % in 2012 and 7 % in 2013.

The local production of radon on Amsterdam Island can explain the radonic storm occurring on December 13, 2012 (Figure 4-5a). As reported by Polian et al. (1986), it is associated with low wind speeds (below 5 m s^{-1}) and meteorological conditions corresponding to a low atmospheric eddy diffusion. The back trajectory ending on December 13, 2012 on Amsterdam Island (Figure 4-6) meanders over the ocean, and low south-eastern/eastern winds prevailed ahead of ^{222}Rn and ^{220}Rn peaks, in good agreement with an influence from the island and local radon exhausts. The associated high Hg(0) event (dHg(0) > 0.18 ng m^{-3}; Figure 4-5c) was significantly positively correlated with ^{222}Rn and ^{220}Rn activities ($r = 0.83$, p value = 0.005 and $r = 0.80$, p value = 0.010 respectively, Spearman test) and can therefore be attributed to a local non-anthropogenic source as no noteworthy activity occurred at the sampling station nor on the scientific base.

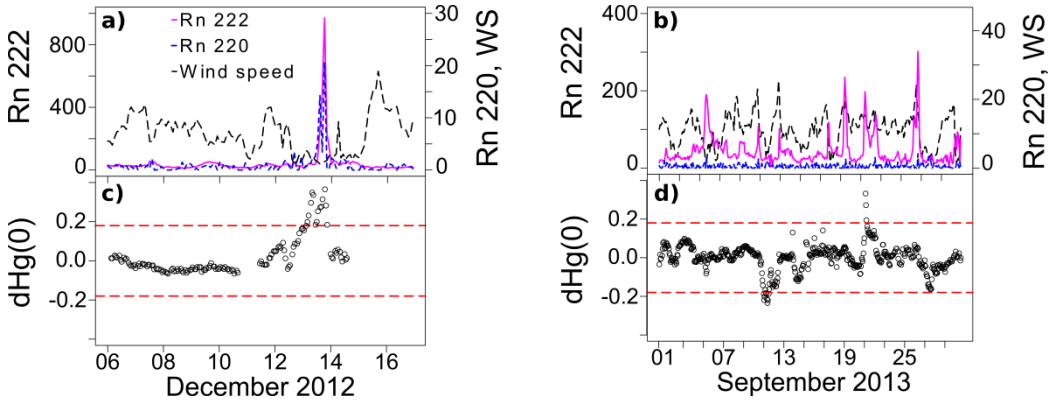

Figure 4-5: Examples of ^{222}Rn (mBq m^{-3}) peaks observed at Amsterdam Island along with ^{220}Rn (mBq m^{-3}) activity and wind speed (WS, m s^{-1}): **a)** in December 2012, **b)** in September 2013. Background variability (dHg(0), ng m^{-3}) of Hg(0) concentrations observed at Amsterdam Island in: **c)** December 2012, **d)** September 2013. Dotted lines represent 3 times the mean monthly standard deviation of dHg(0) measurements.

About 50 % of sharp high Hg(0) events (dHg(0) > 0.18 ng m^{-3}) were associated with ^{222}Rn peaks, strong winds and ^{220}Rn activities below 3.7 mBq m^{-3}, and therefore ascribed to continental air mass advection. For example, the high Hg(0) event occurring on September 21, 2013 (Figure 4-5d) was associated with a ^{222}Rn peak of about 200 mBq m^{-3}, a ^{220}Rn activity below 3.7 mBq m^{-3} and 15 m s^{-1} winds (Figure 4-5b). This high Hg(0) event was significantly positively correlated with ^{222}Rn activities but not correlated with ^{220}Rn activities ($r = 0.81$, p value = 9.3×10^{-5} and $r = -0.27$, p value = 0.295 respectively, Spearman test). The back trajectory ending on September 21, 2013 on Amsterdam Island (Figure 4-6) passes near the southern African continent and Madagascar, confirming the continental origin of the air at the time of enhanced ^{222}Rn activity and Hg(0) concentrations. Although the back trajectory indicates no direct passage over the continent, a continental origin of the air is not unlikely since that range of ^{222}Rn activities has already been measured for trajectories calculated to have passed more than 100 km away from mainland Australia (Whittlestone et al., 1998).

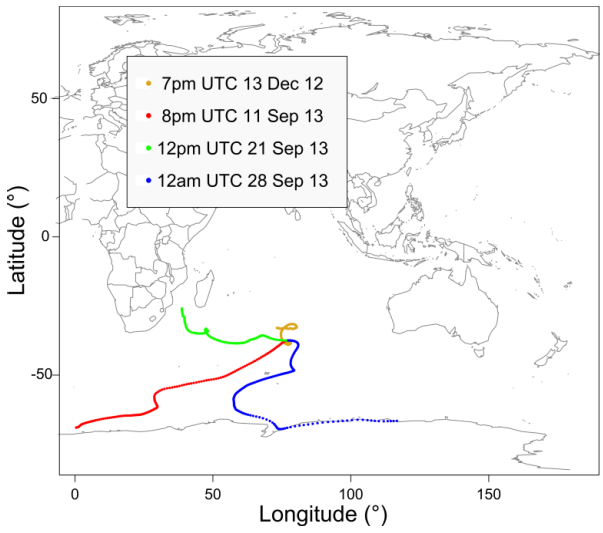

Figure 4-6: 7-days back trajectories ending on Amsterdam Island on December 13, 2012, September 11, 2013, September 21, 2013 and September 28, 2013. Data courtesy of NOAA.

As for high Hg(0) events, continental induced radonic storms mainly occurred between June and October reflecting the seasonality of wind direction at Amsterdam Island and of long-range transport from the southern African continent.

As illustrated on Figure 4-5d and Figure 4-6, low Hg(0) events (dHg(0) < 0.18 ng m^{-3}) were well correlated with trajectories passing over Antarctica. This continent being almost all ice-covered, local emission of ^{222}Rn and ^{220}Rn is low (Polian et al., 1986) explaining why low Hg(0) events are not associated with any ^{222}Rn peak.

These short-term variations suggest that cleaner air masses originate from the remote southern Indian Ocean while NW air masses are influenced by continental southern Africa, as previously assumed by several authors (Miller et al., 1993; Gros et al., 1999; Williams et al., 2001).

4.1.3.2.3 Southern Hemisphere midlatitudes baseline concentrations for modeling studies

The monthly means, medians and standard deviations are given in Table 4-1. Over the 2 years the occurrence of high and low Hg(0) events was less than 1 % and these events did not significantly affect the monthly and annual means. Medians have been calculated for each month and differ in average from the arithmetical means by 0.90 % which is less than the relative expanded uncertainty of the system response. The difference between mean and median did not show any seasonal variation.

Table 4-1: Summary of monthly Hg(0) data at AMS. n: number of hourly averaged data.

Month	Mean (ng m^{-3})	Median (ng m^{-3})	Standard deviation (ng m^{-3})	Range (ng m^{-3})	n
2012					
January	1.04	1.04	0.02	1.01-1.09	60
February	1.06	1.05	0.03	0.98-1.14	457
March	1.02	1.02	0.02	0.94-1.15	459
April	1.03	1.02	0.04	0.95-1.15	474
May	1.04	1.03	0.04	0.94-1.19	468
June	1.02	1.03	0.04	0.90-1.13	451
July	0.99	1.01	0.08	0.74-1.17	519
August	1.05	1.03	0.09	0.83-1.38	501
September	1.04	1.06	0.07	0.80-1.27	442
October	1.01	1.01	0.07	0.84-1.17	416
November	0.94	0.94	0.07	0.77-1.12	184
December	1.01	0.99	0.08	0.93-1.38	255
2013					
January	1.03	1.02	0.07	0.90-1.23	474
February	0.98	0.98	0.03	0.85-1.09	417
March	0.98	0.99	0.06	0.82-1.13	457
April	0.98	0.99	0.05	0.81-1.10	385
May	0.89	0.89	0.05	0.72-1.03	437
June	1.08	1.08	0.05	0.96-1.23	414
July	1.12	1.12	0.04	1.00-1.25	551
August	1.12	1.11	0.07	0.97-1.55	534
September	1.05	1.05	0.07	0.81-1.38	508
October	1.00	1.01	0.06	0.79-1.17	515
November	0.99	0.98	0.08	0.85-1.24	516
December	1.10	1.08	0.06	0.98-1.31	390

Hg(0) concentrations at Amsterdam Island can be considered as baseline concentrations and be used as is in modeling studies. However, a slight but significant seasonal cycle was highlighted and despite the remoteness of the station an influence of biomass burning was observed from July to September. Biomass burning affects all the midlatitude belt of the Southern Hemisphere at least and can be considered as a widespread pollution (Fishman et al., 1991; Gros et al., 1999). Biomass burning slightly contributes to the background Hg(0) level in this region and should be carefully considered in modeling studies when dealing with seasonality of Hg(0) concentrations in the Southern Hemisphere midlatitudes.

4.1.3.3 Oxidized mercury species: seasonality and sources

A 2-year record of RGM and Hg(p) concentrations is presented hereafter – the longest ever reported in the Southern Hemisphere. Concentrations at Amsterdam Island were very low – at the lower end of the range reported during oceanographic campaigns (Laurier et al., 2003; Temme et al., 2003; Laurier and Mason, 2007) –, and exhibited a strong variability (Figure 4-2). RGM and Hg(p) mean concentrations amounted to 0.34 pg m^{-3} [range: < DL-4.07 pg m^{-3}] and 0.67 pg m^{-3} [range: < DL-12.67 pg m^{-3}], respectively. Such low RGM and Hg(p) concentrations at Amsterdam Island could be explained by the very frequent drizzle efficiently scavenging oxidized mercury species. To further investigate the latter assumption, a precipitation collector was set up on the island at the beginning of 2013 in order to analyze mercury species in rainwater.

4.1.3.3.1 Reactive gaseous mercury

RGM can be emitted from point sources or originate from oxidation of Hg(0). Due to its short lifetime RGM can only be transported tens to hundreds of kilometers in the boundary layer (Schroeder and Munthe, 1998). Monitoring of primary emitted RGM at Amsterdam Island is therefore unlikely. RGM in the marine boundary layer has been reported to originate from a photochemically driven oxidation of Hg(0) (Hedgecock and Pirrone, 2001; Hedgecock et al., 2003; Laurier et al., 2003) or through entrainment from the free troposphere (Holmes et al., 2009). Oxidation pathways of Hg(0) involving ozone (O_3), the hydroxyl radical (OH), atomic bromine (Br) or nitrogen dioxide (NO_2), or a combination of them, have been suggested by modeling and field studies (Holmes et al., 2010; Wang et al., 2014). Our understanding of RGM production mechanisms at Amsterdam Island is still limited and no anti-correlation between RGM and Hg(0) concentrations, suggesting an in-situ Hg(0) oxidation, was found.

A slight but significant seasonal trend in RGM concentrations was highlighted (1.34 ± 0.45 pg m^{-3} in winter (July to September) *vs.* 1.58 ± 0.35 pg m^{-3} in summer (December to February), p value = 0.01, Mann-Whitney test), and RGM events occurred about 55 % of the time between December and March (Figure 4-4b), in line with an enhanced photochemistry in summer. While a significant negative correlation between CH_4 and air temperature was observed (r = -0.638, p value < 2.2×10^{-16}, Spearman test), consistent with its photochemical

destruction by the hydroxyl radical (Khalil and Rasmussen, 1983), no correlation was found between RGM concentrations and air temperature, or any other meteorological parameter. The lack of correlation between RGM concentrations and other parameters may come from the small number of RGM measurements above quantification limit (n = 87).

More frequent RGM events between December and March could also be in line with an enhanced biological activity in summer. The production of halogen species, photochemically oxidizing Hg(0), could be driven by biological activity (Gschwend et al., 1985). Unlike the oceanic region surrounding Amsterdam Island, an area located in a southwest upwind sector covering the subtropical front (Figure 4-7) is highly productive, with a marine productivity (characterized by chlorophyll-a concentration) peaking from December to January and sometimes in March-April (Sciare et al., 2009), in agreement with peaks of RGM events. Similarly, marine organic aerosol concentrations at Amsterdam Island have been shown to be directly related to the seasonal cycle of chlorophyll-a (Sciare et al., 2009) and dimethylsulfide (DMS) concentrations peaking in summer have been reported on the island, in line with an enhanced biological activity (NGuyen et al., 1990; Sciare et al., 1999). While enhanced photochemistry and biological activity in summer might explain more frequent RGM events at Amsterdam Island between December and March, further field studies are needed to fully understand divalent mercury formation pathways.

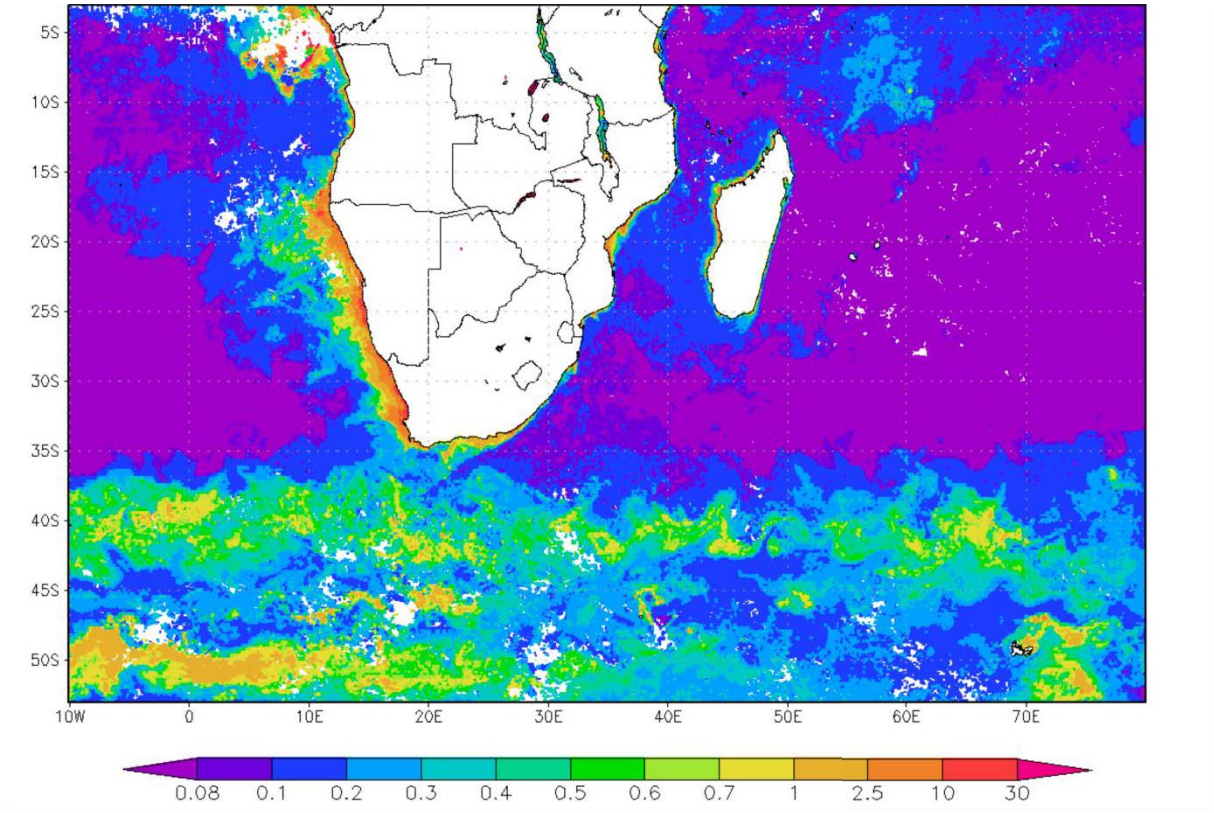

Figure 4-7: SeaWIFS chlorophyll-a map (January 2013, in mg m^{-3}) of the Indian sector of the Austral Ocean. The oceanic region located southwest of Amsterdam Island is highly productive in summer and potentially produces halogen species. Data courtesy of Giovanni online data system.

4.1.3.3.2 Particle-bound mercury

Hg(p) is associated with airborne particles – *e.g.*, dust, soot, sea-salt aerosols, or ice crystal –, or originates from the adsorption of reactive mercury onto atmospheric particles (Lu and Schroeder, 2004). Field and modeling studies (Rutter and Schauer, 2007b; Amos et al., 2012; Steffen et al., 2014) suggested that the partitioning of mercury onto particles might be driven by air temperature and aerosol particle loadings.

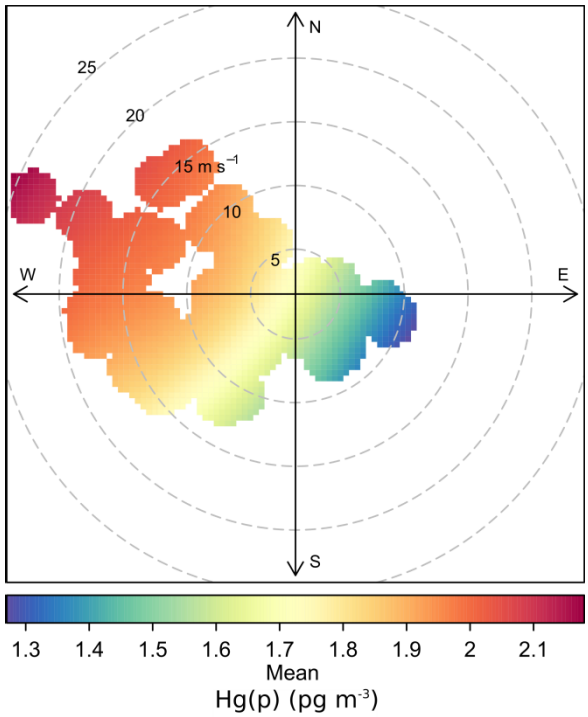

Figure 4-8: Particle-bound mercury (Hg(p)) concentrations (pg m^{-3}) according to wind speed ($m.s^{-1}$) and direction. N: North, E: East, S: South, W: West.

Hg(p) concentrations at Amsterdam Island followed a seasonal trend with significantly higher concentrations in winter (July to September) than in summer (December to February) (2.18 ± 1.56 ng m^{-3} *vs*.1.79 ± 1.15 pg m^{-3}, *p* value = 0.027, Mann-Whitney test). Higher Hg(p) concentrations were recorded during the strongest NW winds episodes (Figure 4-8), suggesting an enhanced long-range transport of Hg(p) from continental southern Africa during strong NW winds episodes. The higher number of Hg(p) events in 2013 (Figure 4-4c) is in good agreement with about twice as many continental induced radonic storms observed at Amsterdam Island in 2013 than in 2012. Hg(p) events occurred about 55 % of the time between August and October in 2012 and 2013 (Figure 4-4c) and were significantly positively correlated with fire counts west of Amsterdam Island (r = 0.56, *p* value = 0.005, Spearman test). This result is consistent with other observations of enhanced Hg(p) concentrations during wildfires (Finley et al., 2009). However, biomass fire counts reached a maximum between June and September while Hg(p) events peaked later, between August and October. The seasonality of aerosol optical depth (AOD) in the Southern Hemisphere Africa biomass burning region was extensively monitored by the Cimel sun-sky radiometer at the AERONET

site in Mongu, Zambia. 1995 to 2009 measurements highlighted that the monthly means of Level 2 direct sun-measured 500 nm AOD at Mongu reached a peak from August to October (Eck et al., 2013), in line with the Hg(p) events peak observed at Amsterdam Island. This time lag between seasonal peaks in fire counts and emissions has already been pointed out by Swap et al. (2003), but its origin remains unclear. It has been attributed either to unusual synoptic conditions favoring eastward transport of pollution over measurement sites (Stein et al., 2003; Swap et al., 2003) or to undetected/highly emissive denser wooded vegetation burns at the end of the fire season (Edwards et al., 2006).

4.1.4 Conclusion

Wind sector analysis, air mass back trajectories and the observation of radonic storms led to the important conclusion that despite the remoteness of Amsterdam Island the rapid export of air from the southern African continent during the biomass burning season contributes to Hg(0) and Hg(p) budgets on the island. Low Hg(0) concentrations are associated with southerly polar and marine air masses from the remote southern Indian Ocean. This data set provides a new insight into baseline concentrations of mercury species in the Southern Hemisphere midlatitudes and new measurement constraints on the mercury cycle, opening the way for new avenues in future modeling studies. Our understanding of mercury cycle in the marine boundary layer over Amsterdam Island is still limited. It represents a real challenge given harsh weather conditions – with a very frequent drizzle most certainly scavenging oxidized species –, and technical and logistical limitations. Further studies involving wet deposition, simultaneous measurements of other trace gases, and interference and calibration tests of the Tekran speciation unit are needed to improve our understanding of deposition processes and oxidation mechanisms.

Acknowledgements

This work contributes to the EU-FP7 project Global Mercury Observation System (GMOS). Logistical and financial support was provided by the French Polar Institute IPEV (Program 1028, GMOStral). Financial support was also provided by a grant from Labex OSUG@2020 (ANR10 LABX56) and LEFE CNRS/INSU (program SAMOA). We deeply thank the overwintering staff: B. Brouillard, J. Chastain, E. Coz, A. Croguennoc, M. Le Dréau and V. Lucaire, and AD acknowledges the Institut Universitaire de France. We also gratefully acknowledge the MODIS mission scientists and associated NASA personnel for the production of the data used in this research effort, and the NOAA Air Resources Laboratory (ARL) for the provision of the READY website (http://www.ready.noaa.gov**)** used in this publication.

4.1.5 Compléments d'information

4.1.5.1 Résumé des principaux résultats et conclusions de l'article

Bien qu'essentielles à la bonne compréhension du cycle du mercure à l'échelle planétaire, les données de concentrations en espèces mercurielles atmosphériques sont rares au sein de l'Hémisphère Sud (voir section 2.2.1.1). Dans le cadre du programme GMOS, une station de mesures a été mise en place sur l'île d'Amsterdam (AMS) au beau milieu de l'océan Indien (37°48 S, 77°34 E). L'article ci-avant propose, pour la première fois dans cet hémisphère, une série temporelle de deux ans (2012-2013) de concentrations en Hg(0), RGM et Hg(p) (Figure 3-4 pour un rappel des définitions). Les concentrations en Hg(0) se sont révélées très stables au cours de cette période (1,03 ± 0,08 ng m^{-3}) (moyenne ± écart-type) et 40 à 50 % inférieures aux valeurs mesurées dans l'Hémisphère Nord. Les concentrations en espèces divalentes sont quant à elles au niveau des limites de détection instrumentales (de l'ordre du pg m^{-3}), révélant une réactivité *a priori* limitée dans cette zone de l'océan Indien. Compte tenu des conditions météorologiques (bruine très fréquente pouvant lessiver les espèces divalentes) et des limites de la technique d'analyse utilisée (voir section 3.2.1.4), ces faibles concentrations en espèces divalentes doivent être confirmées (ou infirmées) par l'analyse des flux de dépôts humides (voir section 4.2 ci-dessous).

AMS est l'une des îles les plus isolées au monde. L'analyse des rétro-trajectoires de masses d'air et des données de concentrations en radon (traceur de masses d'air continentales) ont toutefois mis en évidence l'influence occasionnelle du continent africain sur les concentrations en Hg(0) et Hg(p) mesurées à AMS, tout particulièrement entre juillet et septembre pendant la saison des feux de biomasse. Cette conclusion sera rediscutée au sein de la section 4.3 à la lumière d'une étude récente sur les dépôts de mercure engendrés par les feux de biomasse (De Simone et al., 2016a). L'article présenté ci-avant montre par ailleurs que les masses d'air en provenance du sud de l'océan Indien et du continent Antarctique sont quant à elles associées à des concentrations légèrement plus faibles en Hg(0). Malgré l'influence occasionnelle de masses d'air d'origine continentale (sud-africaine ou antarctique), il apparaît important de souligner la stabilité remarquable du signal en Hg(0) enregistré entre janvier 2012 et décembre 2013 (1,03 ± 0,08 ng m^{-3}). La stabilité du signal à plus long terme est discutée au sein de la section 4.1.5.2 ci-dessous.

4.1.5.2 Données ultérieures à l'article

L'article présenté ci-avant propose une interprétation des données de concentrations en espèces mercurielles atmosphériques acquises entre janvier 2012 et décembre 2013. Comme indiqué au sein de la section 3.2.3, des données de concentrations en espèces divalentes sont disponibles jusqu'en août 2015 tandis que la mesure de Hg(0) est toujours en cours. L'ensemble des données acquises à AMS entre janvier 2012 et fin juillet 2016 est présenté sur la Figure 4-9.

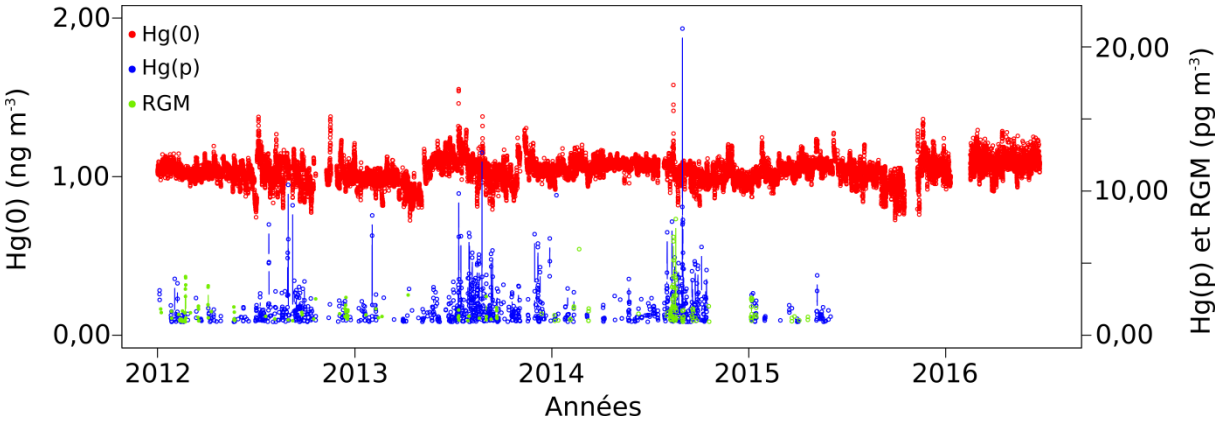

Figure 4-9: Concentrations en Hg(p) et RGM (en pg m^{-3}) et concentrations moyennes (pas de temps horaire, en ng m^{-3}) en Hg(0) enregistrées à AMS entre janvier 2012 et fin juillet 2016. La mesure de la concentration en Hg(0) est toujours en cours. Le peu de données de concentrations en espèces divalentes en 2015 s'explique par le fonctionnement erratique de l'unité de spéciation avant son arrêt définitif fin août 2015 et les nombreuses données sous la limite de quantification.

Comme indiqué précédemment, la concentration moyenne (± écart-type) en Hg(0) est de 1,03 ± 0,08 ng m^{-3} entre janvier 2012 et décembre 2013. Les mesures effectuées depuis montrent que les concentrations en Hg(0) demeurent stables, avec une concentration moyenne de 1,05 ± 0,05 ng m^{-3} en 2014, 1,01 ± 0,07 ng m^{-3} en 2015 et 1,08 ± 0,06 ng m^{-3} entre janvier et fin juillet 2016. Il est à noter que pour l'année 2016 le dispositif instrumental est différent des années précédentes. En effet, comme indiqué au sein de la section 3.2.3, l'unité de spéciation a été désinstallée en décembre 2015. L'analyseur Tekran® 2537 est désormais relié à une cloche de prélèvement *via* une ligne PTFE chauffée de 10 m de long (Figure 4-10). Cette cloche de prélèvement accueille une membrane échangeuse de cations (polyéthersulfone (PES), porosité 0,45 µm, diamètre 47 mm) censée piéger les espèces divalentes. L'analyseur est en outre protégé, en amont immédiat, par un filtre PTFE de porosité 0,2 µm. Le protocole mis en place ainsi que les tests d'assurance qualité réalisés ou à réaliser sont décrits au sein de l'Annexe 3 ; tout laisse à penser que nous analysons bien du Hg(0) et non du TGM avec le dispositif actuel (Figure 3-4 pour un rappel des définitions). Les données 2014 confirment par ailleurs les faibles concentrations en espèces divalentes ainsi que le pic de concentrations en Hg(p) entre juillet et septembre (Figure 4-9).

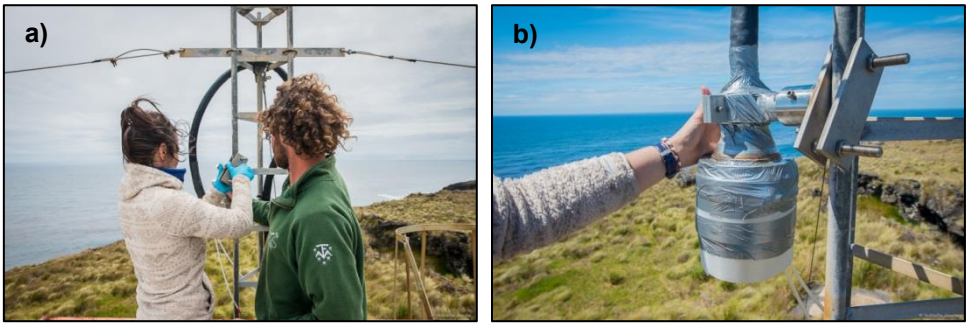

Figure 4-10: **a)** Installation en décembre 2015 de la ligne chauffée et de la cloche de prélèvement sur le toit du bâtiment à AMS, **b)** cloche de prélèvement. © Isabelle Jouvie.

4.2 Flux de dépôts humides des espèces mercurielles atmosphériques

D'après l'article suivant, disponible en intégralité en Annexe 4 :

Sprovieri, F., Pirrone, N., Bencardino, M., D'Amore, F., **Angot, H.**, Barbante, C., Brunke, E.-G., Cabrera, F. A., Cairns, W., Comero, S., Diéguez, M. D. C., Dommergue, A., Ebinghaus, R., Feng, X. B., Fu; X., Garcia, P. E., Gawlik, B. M., Hageström, U., Hansson, K., Horvat, M., Kotnik, J., Labuschagne, C., Magand, O., Martin, L., Mashyanov, N., Mkololo, T., Munthe, J., Obolkin, V., Islas, M. R., Sena, F., Somerset, V., Spandow, P., Vardè, M., Walters, C., Wängberg, I., Weigelt, A., Yang, X., Zhang, H.: Five-year records of total mercury deposition flux at GMOS sites in the Northern and Southern Hemispheres, Atmospheric Chemistry and Physics Discussions, doi: 10.5194/acp-2016-517, in review, 2016.

Le flux de dépôts humides de mercure (F_w en µg m^{-2} an^{-1}) est calculé selon l'équation 4-1 comme le produit de la concentration moyenne pondérée en mercure total dans les échantillons collectés (C_{Hg} en ng L^{-1}) et la quantité de précipitations dans chaque échantillon (P_i en L m^{-2}).

$$F_w = C_{Hg} \sum_{i=1}^{i=n} P_i \times {}^{1}/_{1000} \qquad \text{(Eq. 4-1)}$$

La Figure 4-11 présente les flux de dépôts humides de mercure et le cumul de précipitations à AMS ainsi qu'en 16 autres sites GMOS. A AMS, le flux annuel est de 2,0 µg m^{-2} en 2013 et 1,6 µg m^{-2} en 2014. Ces flux sont dans la gamme basse des flux mesurés aux différents sites GMOS (Figure 4-11a). A titre de comparaison, les flux sont de 3,1 (2013) et 3,8 µg m^{-2} (2014) à Cape Grim (CPG) en Tasmanie, 0,9 (2013) et 1,7 µg m^{-2} (2014) à Ny-Ålesund (NYA) au Spitzberg, 4,8 (2013) et 4,1 µg m^{-2} (2014) à Mace Head (MHE) en Irlande ou encore 7,2 (2013) et 10,0 µg m^{-2} (2014) à Iskrba (ISK) en Slovénie. A l'inverse, avec près de 850 mm par an, les cumuls de précipitations à AMS font partie de la gamme haute (Figure 4-11b). Ces résultats suggèrent une concentration moyenne pondérée en mercure total peu élevée à AMS. Celle-ci est en effet de 2,3 ng L^{-1} en 2013 et 1,8 ng L^{-1} en 2014. A titre de comparaison, elle est de 4,0 (2013) et 6,7 ng L^{-1} (2014) à CPG, 4,1 (2013) et 5,7 ng L^{-1} (2014) à NYA ou encore 8,2 (2013) et 6,6 ng L^{-1} (2014) à MHE. En termes de saisonnalité, aucune différence significative n'est observée à AMS au niveau des concentrations en mercure total (*p* value > 0,5, Mann-Whitney test). Compte tenu des faibles concentrations atmosphériques en espèces divalentes mesurées entre janvier 2012 et l'été 2015 avec l'unité de spéciation (voir section 4.1), ces teneurs en mercure total dans les précipitations confortent l'idée d'une réactivité atmosphérique du mercure limitée dans cette zone de l'océan Indien. Les échantillons de précipitations collectés entre janvier 2015 et mars 2016 sont actuellement en cours d'analyse au CNR-IIA. Les résultats à venir devraient permettre de confirmer que, pour une troisième année consécutive, les concentrations en mercure total et les flux de dépôts humides associés sont faibles.

Figure 4-11: **a)** Flux de dépôts humides (µg m^{-2} an^{-1}) et **b)** cumul de précipitations (mm) en 17 sites GMOS entre 2011 et 2015. NYA : Ny-Ålesund au Spitzberg, PAL : Pallas en Finlande, RAO : Råö en Suède, MHE : Mace Head en Irlande, LIS : Listvyanka en Russie, CMA : Col Margherita en Italie, ISK : Iskrba et Slovénie, MCH : Mont Changbai en Chine, LON : Longobucco en Italie, MWA : Mont Waliguan en Chine, MAL : Mont Ailao en Chine, SIS : Sisal au Mexique, CST : Celestún au Mexique, AMS : île d'Amsterdam, CPT : Cape Point en Afrique du Sud, CGR : Cape Grim en Tasmanie, BAR : Bariloche en Argentine.

4.3 Discussion

4.3.1 Contribution au signal enregistré sur AMS des émissions par les feux de biomasse

Malgré l'isolement géographique d'AMS, l'observation d'orages radoniques suggère que des masses d'air en provenance du sud de l'Afrique peuvent occasionnellement venir

perturber le signal de concentrations en Hg(0) et Hg(p) enregistré à AMS (voir section 4.1). Les feux de biomasse sont une source importante de mercure vers l'atmosphère (Friedli et al., 2009a; De Simone et al., 2015). Alors qu'on considère généralement les émissions par les feux de biomasse sous forme de Hg(0) uniquement (De Simone et al., 2015), certaines études ont montré que la fraction de Hg(p) varierait en fait de l'ordre de quelques % à près de 30 % (p. ex. Obrist et al., 2007; Finley et al., 2009). Notre méconnaissance de la spéciation exacte au sein des émissions engendre de fortes incertitudes quant aux dépôts de mercure, notamment à l'échelle régionale, le temps de vie des deux espèces étant significativement différent (voir section 1.2). Une étude récente s'intéresse ainsi à l'influence de la composition en Hg(p) des émissions par les feux de biomasse sur les dépôts de mercure (De Simone et al., 2016a). Un ensemble de simulations a été effectué, les variables étant le mécanisme d'oxydation de Hg(0), la fraction de Hg(p) et l'inventaire d'émissions utilisé. Les dépôts de mercure résultants de cet ensemble sont présentés sur la Figure 4-12a. Les résultats de cette étude montrent que l'inclusion d'une fraction de Hg(p) dans les émissions par les feux de biomasse engendre un dépôt plus important (en rouge) près des zones d'émissions et notamment au niveau de l'océan Indien. Cette étude conforte l'idée avancée ci-avant selon laquelle les feux de biomasse peuvent occasionnellement venir perturber le signal de concentrations en espèces mercurielles enregistré à AMS. La Figure 4-12b montre par ailleurs que la contribution aux dépôts de mercure des feux de biomasse par rapport aux émissions anthropiques est supérieure à 25 % dans tout l'Hémisphère Sud et est proche de 40 % au niveau d'AMS. Dans un contexte de régulation forte des émissions anthropiques (voir section 1.4) on s'attend cependant à ce que la contribution relative aux dépôts de mercure des feux de biomasse augmente progressivement au fil des ans (De Simone et al., 2016a).

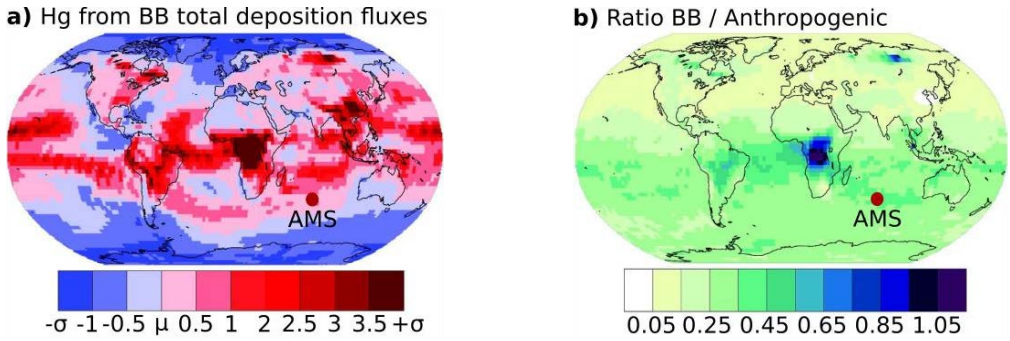

Figure 4-12: Distribution géographique des dépôts de mercure émis par les feux de biomasse (BB) résultant d'un ensemble de simulations pour l'année 2013 **a)** en termes de moyenne (μ) et d'écart-type (σ) de l'ensemble. La comparaison de cet ensemble de simulations avec un autre ensemble n'incluant que des émissions anthropiques montre **b)** la distribution géographique de la contribution aux dépôts de mercure des feux de biomasse par rapport aux émissions anthropiques. D'après De Simone et al. (2016a).

4.3.2 Bruit de fond atmosphérique aux moyennes latitudes de l'Hémisphère Sud

D'après l'article suivant, disponible en intégralité en Annexe 5 :

Slemr, F., **Angot, H.**, Dommergue, A., Magand, O., Barret, M., Weigelt, A., Ebinghaus, R., Brunke, E.-G., Pfaffhuber, K. A., Edwards, G., Howard, D., Powell, J., Keywood, M., Wang, F.: Comparison of mercury concentrations measured at several sites in the Southern Hemisphere, Atmospheric Chemistry and Physics, 15, 3125-3133, 2015.

Comme indiqué précédemment au sein de la section 2.2.1, notre compréhension du cycle atmosphérique du mercure dans l'Hémisphère Sud reposait jusqu'il y a peu encore essentiellement sur des données ponctuelles issues de campagnes océanographiques (Figure 2-5). Il est à noter que les concentrations en Hg(0) issues de ces campagnes sont très variables (p. ex. 0,72 ng m^{-3} dans le sud de l'océan Atlantique (Kuss et al., 2011) contre 2,20 ng m^{-3} dans le sud-est de l'océan Indien (Xia et al., 2010)) et peu représentatives car le plus souvent non filtrées d'une éventuelle pollution anthropique ou par le navire océanographique. La présente étude vise à comparer le signal enregistré par quatre stations situées aux moyennes latitudes de l'Hémisphère Sud et permettant l'analyse sur le long terme de Hg(0) : AMS, Cape Point (CPT) en Afrique du Sud, Cape Grim (CGR) en Tasmanie et Troll (TR) en Antarctique (Figure 4-13). Il s'agit de stations permettant la mesure du bruit de fond atmosphérique (AMS, TR), c'est-à-dire peu influencées par les émissions anthropiques, ou de stations (CPT, CGR) disposant de données complémentaires (p. ex. CO, ^{222}Rn, direction du vent, teneur en aérosols) permettant de filtrer les données.

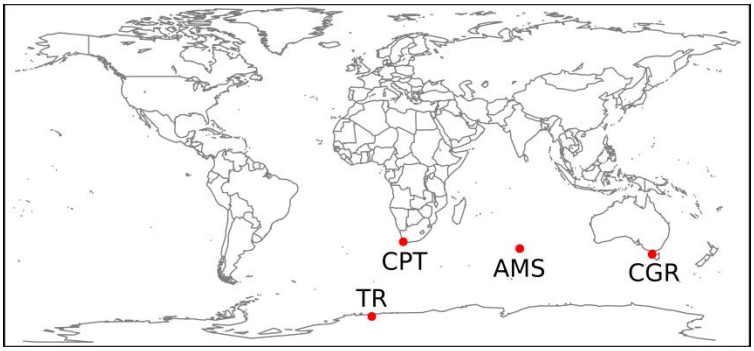

Figure 4-13: Localisation géographique des quatre sites de mesures d'intérêt. CPT : Cape Point en Afrique du Sud, TR : Troll en Antarctique, AMS : île d'Amsterdam et CGR : Cape Grim en Tasmanie.

Le Tableau 4-2 présente les concentrations moyennes et médianes en Hg(0) mesurées aux quatre sites d'intérêt entre 2011 et 2013. Les concentrations à CGR sont ~ 15 % plus faibles qu'aux trois autres sites. En revanche, les concentrations moyennes mesurées à CPT, AMS et TR sont homogènes. L'écart maximal observé entre les moyennes annuelles aux quatre sites est de l'ordre de 0,2 ng m^{-3}. Considérant une erreur systématique sur la mesure de l'ordre de 10 % (voir section 3.3.3), la variabilité moyenne maximale de la concentration en Hg(0) aux moyennes latitudes de l'Hémisphère Sud serait de ~ 0,1 ng m^{-3}. Ces résultats montrent que les concentrations en Hg(0) sont bien plus uniformes aux moyennes latitudes de l'Hémisphère Sud que ce que les diverses campagnes océanographiques laissaient présager. La station d'AMS est ainsi représentative du bruit de fond atmosphérique à ces latitudes. Cette station se

révèle être un site clé pour la surveillance, sur le long terme, des effets sur les concentrations en Hg(0) des réglementations instaurées dans le cadre de la Convention de Minamata (voir section 1.4). En ce sens, la station d'AMS est précieuse et permet notamment le suivi en continu, depuis 35 ans, de la concentration en CO_2 par le service national d'observation ICOS-France (« Integrated Carbon Observation System ») du Laboratoire des Sciences du Climat et de l'Environnement (LSCE, CNRS/CEA/UVSQ) avec le soutien de l'IPEV. Légère digression de ma part mais alors qu'AMS est la station où l'on relève les concentrations en CO_2 les plus basses au monde (hors cycles saisonniers), la concentration vient d'y franchir, en mai dernier, la barre symbolique des 400 ppmv (CNRS, 2016).

Tableau 4-2: Tableau récapitulatif des concentrations en Hg(0) mesurées aux quatre sites d'intérêt. Il est à noter qu'à CGR, en 2011, des données ne sont disponibles que pour les mois de septembre, octobre et décembre et qu'en 2013, l'instrument n'a pas fonctionné en avril, mai et octobre.

Site	moyenne ± écart-type	médiane
2011		
CPT	0,92 ± 0,11	0,93
AMS	-	-
CGR	0,96 ± 0,15	0,98
TR	1,03 ± 0,19	1,06
2012		
CPT	1,02 ± 0,10	1,02
AMS	1,03 ± 0,07	1,03
CGR	0,87 ± 0,13	0,85
TR	1,05 ± 0,16	1,04
2013		
CPT	1,05 ± 0,16	1,04
AMS	1,03 ± 0,10	1,03
CGR	0,85 ± 0,11	0,86
TR	0,97 ± 0,16	1,00

Les données de concentrations atmosphériques en espèces mercurielles (voir section 4.1) et de flux de dépôts humides (voir section 4.2) enregistrées à AMS devraient par ailleurs permettre de mieux contraindre les modèles atmosphériques dans cette région du globe (voir section 4.3.1.3 ci-dessous).

4.3.3 Des données d'observations à disposition des modélisateurs

Des simulations multi-modèles récentes (UNEP, 2015), réalisées dans le cadre du programme GMOS, proposent une distribution géographique de la concentration moyenne en Hg(0) ainsi que des dépôts de mercure pour l'année 2013 (Figure 4-14). Ces simulations suggèrent une concentration moyenne en Hg(0) de l'ordre de 1,1-1,2 ng m^{-3} aux moyennes et hautes latitudes de l'Hémisphère Sud et un dépôt total de mercure de l'ordre de 6 à 10 µg m^{-2} an^{-1} dans le secteur d'AMS. Même en considérant une erreur systématique sur les données d'observations de l'ordre de 10 % (voir section 3.3.3), la valeur simulée surestime d'environ

10 % les concentrations en Hg(0) mesurées à AMS, CPT et TR (voir section 4.3.1.2). Au vu des conditions météorologiques dans le secteur d'AMS (bruine très fréquente) il semble peu probable que le flux de dépôts secs soit plus important que le flux de dépôts humides. Même en considérant des flux de dépôts secs et humides du même ordre de grandeur, les dépôts totaux atteignent difficilement les 3-4 µg m^{-2} an^{-1} à AMS contre 6-10 µg m^{-2} an^{-1} simulés. Il apparaît ainsi indispensable de contraindre les modèles atmosphériques actuels avec les données d'observations enregistrées à AMS et aux autres stations sud-hémisphériques.

Figure 4-14: Distribution géographique pour l'année 2013 **a)** de la concentration moyenne en Hg(0) (en ng m^{-3}) et **b)** des dépôts totaux de mercure (en µg m^{-2} an^{-1}). D'après UNEP (2015).

Le paragraphe à suivre s'appuie sur l'article suivant, disponible en intégralité en Annexe 6 :

Song, S., Selin, N. E., Soerensen, A. L., **Angot, H.**, Artz, R., Brooks, S., Brunke, E.-G., Conley, G., Dommergue, A., Ebinghaus, R., Holsen, T. M., Jaffe, D. A., Kang, S., Kelley, P., Luke, W. T., Magand, O., Marumoto, K., Pfaffhuber, K. A., Ren, X., Sheu, G.-R., Slemr, F., Warneke, T., Weigelt, A., Weiss-Penzias, P., Wip, D. C., Zhang, Q.: Top-down constraints on atmospheric mercury emissions and implications for global biogeochemical cycling, Atmospheric Chemistry and Physics, 15, 7103-7125, 2015.

Cet article propose une modélisation inverse à l'échelle planétaire afin de contraindre les émissions atmosphériques actuelles. Cette étude se base sur des simulations numériques réalisées à l'aide du modèle atmosphérique GEOS-Chem (v9-02) et sur des données d'observations acquises de par le monde. L'optimisation des émissions résulte en une meilleure simulation des concentrations en Hg(0) dans l'Hémisphère Sud (Figure 4-15a). Contrairement aux observations (en noir), la simulation de référence (en bleu) prédit une forte variation saisonnière de la concentration en Hg(0) avec un maximum en hiver (~ 1,3 ng m^{-3}) et un minimum en été (~ 0,9 ng m^{-3}). L'optimisation des émissions (en rouge) engendre une diminution des concentrations hivernales, en accord avec les observations. Ce résultat s'explique par une modification de la saisonnalité des émissions océaniques, plus importantes en été et moins importantes en hiver après optimisation des émissions (Figure 4-15b). La saisonnalité des émissions océaniques au sein de l'Hémisphère Sud sera à nouveau abordée au sein du chapitre 6. L'optimisation des émissions réalisée dans cette étude a également permis d'optimiser certains paramètres clés du modèle atmosphérique GEOS-Chem (en vert). Cette

étude est une preuve supplémentaire, s'il en était encore besoin, que les données d'observations acquises à AMS et aux autres sites GMOS permettent de contraindre et d'améliorer les modèles atmosphériques.

Figure 4-15: **a)** Concentrations moyennes mensuelles en Hg(0) dans l'Hémisphère Sud (en ng m^{-3}). Les données d'observations (en noir) proviennent d'AMS, CPT et TR**.** Les barres d'erreur noires correspondent à l'incertitude totale sur les données d'observations. **b)** Emissions océaniques mensuelles dans l'Hémisphère Sud (en Mg $mois^{-1}$). La partie grisée et les barres d'erreur rouges correspondent à une incertitude 1σ pour les simulations de référence et d'optimisation des émissions, respectivement. Données d'observations en noir, simulation de référence en bleu, simulation après optimisation des émissions en rouge et simulation après optimisation de certains paramètres au sein de GEOS-Chem en vert. D'après Song et al. (2015).

5 Cycle atmosphérique du mercure sur le continent antarctique

Ce chapitre décrit nos avancées concernant la compréhension du cycle atmosphérique du mercure en Antarctique. La section 5.1 propose une description et interprétation des concentrations en Hg(0) enregistrées sur la calotte glaciaire à DC. Cette section s'appuie sur un article publié présentant les données de janvier 2012 à décembre 2013. Un résumé, en français, des principaux résultats et conclusions issus de cet article est disponible au sein de la section 5.1.6. Les données acquises ultérieurement y sont également présentées. La section 5.2 propose quant à elle une description et interprétation des concentrations en Hg(0) enregistrées à DDU, sur la côte Est du continent, entre janvier 2012 et mai 2015. Cette section s'appuie également sur un article publié. Un résumé, en français, des principaux résultats et conclusions est disponible au sein de la section 5.2.6. Pour rappel, l'objectif de ce chapitre est de répondre aux questions suivantes : 1) Quelle est la réactivité atmosphérique du mercure en Antarctique central et sur la côte Est ? 2) Quelle est l'influence du manteau neigeux sur le cycle atmosphérique du mercure ? 3) Quelle est l'influence potentielle du continent Antarctique sur le cycle biogéochimique du mercure à plus large échelle ?

5.1 Cycle atmosphérique du mercure sur le plateau antarctique

D'après :

Angot, H., Magand, O., Helmig, D., Ricaud, P., Quennehen, B., Gallée, H., Del Guasta, M., Sprovieri, F., Pirrone, N., Savarino, J., Dommergue, A.: New insights into the atmospheric mercury cycling in central Antarctica and implications on a continental scale, Atmospheric Chemistry and Physics 16, 8249-8264, 2016.

Abstract

Under the framework of the GMOS project (Global Mercury Observation System) atmospheric mercury monitoring has been implemented at Concordia Station on the high-altitude Antarctic Plateau (75°06 S, 123°20 E, 3220 m above sea level). We report here the first year-round measurements of gaseous elemental mercury (Hg(0)) in the atmosphere and in snowpack interstitial air on the East Antarctic ice sheet. This unique data set shows evidence of an intense oxidation of atmospheric Hg(0) in summer (24 h daylight) due to the high oxidative capacity of the Antarctic Plateau atmosphere in this period of the year.

Summertime Hg(0) concentrations exhibited a pronounced daily cycle in ambient air with maximal concentrations around midday. Photochemical reactions and chemical exchange at the air-snow interface were prominent, highlighting the role of the snowpack on the atmospheric mercury cycle. Our observations reveal a 20 to 30 % decrease of atmospheric Hg(0) concentrations from May to mid-August (winter, 24 h darkness). This phenomenon has not been reported elsewhere and possibly results from the dry deposition of Hg(0) onto the snowpack. We also reveal the occurrence of multi-day to week-long atmospheric Hg(0) depletion events in summer, not associated with depletions of ozone, and likely due to a stagnation of air masses above the plateau triggering an accumulation of oxidants within the shallow boundary layer. Our observations suggest that the inland atmospheric reservoir is depleted in Hg(0) in summer. Due to katabatic winds flowing out from the Antarctic Plateau down the steep vertical drops along the coast and according to observations at coastal Antarctic stations, the striking reactivity observed on the plateau most likely influences the cycle of atmospheric mercury at a continental scale.

5.1.1 Introduction

Mercury biomagnifies in its methylated form in aquatic food webs to elevated levels in freshwater and marine fish, causing adverse health effects to wildlife and humans (Mason et al., 2012). In 2013, the Minamata Convention (UNEP, 2013b) was adopted and opened for signature to reduce the exposure of populations to this worldwide contaminant. Gaseous elemental mercury (Hg(0)), the most abundant form of mercury in the atmosphere, is efficiently transported around the globe, and even remote areas receive significant inputs of anthropogenic mercury by long-range atmospheric transport, as recently reported in modeling and observational studies (Weiss-Penzias et al., 2007; Lin et al., 2010b).

Hg(0) can be oxidized into highly reactive and water-soluble gaseous and/or particulate divalent species (Hg(II) and Hg(p), respectively) (Lin and Pehkonen, 1999) leading to the formation and subsequent deposition of reactive mercury onto environmental surfaces (Hedgecock and Pirrone, 2004). Upon deposition, mercury can be re-emitted back to the atmosphere or may enter the food chain through the conversion of Hg(II) to its methylated form (Driscoll et al., 2013). Effects and toxicity of mercury depends on this complex cycle, which is still not fully understood, and are only indirectly related to regional and global emissions (Driscoll et al., 2013). A better understanding of atmospheric mercury chemistry will lead to improved global transport and deposition models and could help refine pollution-control strategies around the world.

New oxidation pathways, discovered in 1995 in the Arctic (Schroeder et al., 1998) and highlighting the influence of halogen radicals on Hg(0) oxidation in spring, changed our understanding of the mercury cycle. While the Arctic has been extensively monitored, there is still much to be learned from the Antarctic continent where studies are scarce (Dommergue et al., 2010b), especially on the high altitude plateau (Figure 5-1). The Antarctic Plateau – ice-covered area of ~ 7 million km^2 – was first considered to be chemically inactive and a giant

cold trap for atmospheric species (*e.g.*, Lambert et al., 1990). It turned out to be highly photochemically active (Davis et al., 2001; Grannas et al., 2007) during the sunlit period with oxidant concentrations approaching those of tropical or urban midlatitude environments (Eisele et al., 2008; Kukui et al., 2014). Earlier studies (Brooks et al., 2008a; Dommergue et al., 2012) – the only two mercury studies ever carried out on the high-altitude Antarctic Plateau with modern instruments – also suggested, based on short-term observations (a few weeks) in summer, an intense reactivity of mercury on the plateau at the air-snow interface. In this context, and under the framework of the GMOS project (Global Mercury Observation System, www.gmos.eu), atmospheric mercury was continuously monitored at Concordia Station (DC, Figure 5-1) since 2012 and, for the first time, Hg(0) has been monitored year-round in both the snow interstitial air and the overlying atmosphere in 2013. Given harsh weather conditions (see section 5.1.2.1), and technical and logistical limitations, presenting such a record is in itself an important achievement. The main objective of this study is to provide new insights into the year-round cycling of gaseous mercury on the Antarctic Plateau.

5.1.2 Experimental Section

5.1.2.1 Sampling site

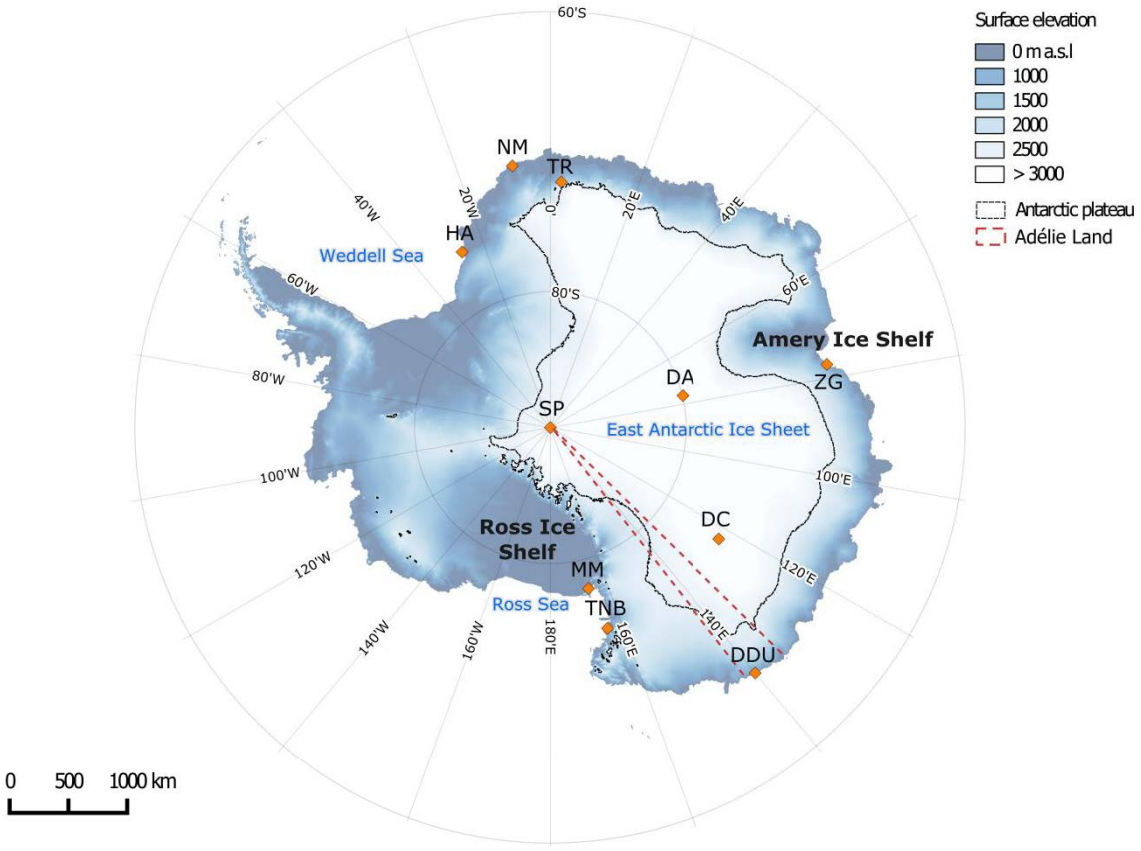

Figure 5-1: Map of Antarctica showing surface elevation (meters above sea level, m a.s.l.) and the position of various stations: Halley (HA), Neumayer (NM), Troll (TR), Zhongshan Station (ZG), Dome A (DA), South Pole (SP), Concordia Station (DC), Dumont d'Urville (DDU), McMurdo (MM), and Terra Nova Bay (TNB). The black line shows the periphery of the high altitude plateau (> 2500 m a.s.l.), and the red dotted line Adélie Land (from 136° E to 142° E).

Year-round measurements of gaseous mercury were conducted in 2012 and 2013 at the French/Italian Concordia Station (75°06 S, 123°20 E, 3220 m above sea level), located on the Antarctic Plateau, 1100 km away from the nearest coast of East Antarctica (Figure 5-1). DC is a regional topographic maximum on the plateau; the surface terrain slopes do not exceed 1 % (Genthon et al., 2010). The air temperature ranges between -20 °C in summer and -70 °C in winter, with an annual mean value of -45 °C (Pietroni et al., 2012). There is permanent daylight in summer and permanent darkness in winter. Snow accumulation is ~ 10 cm year^{-1} (Genthon et al., 2013).

5.1.2.2 Sampling instrumentation

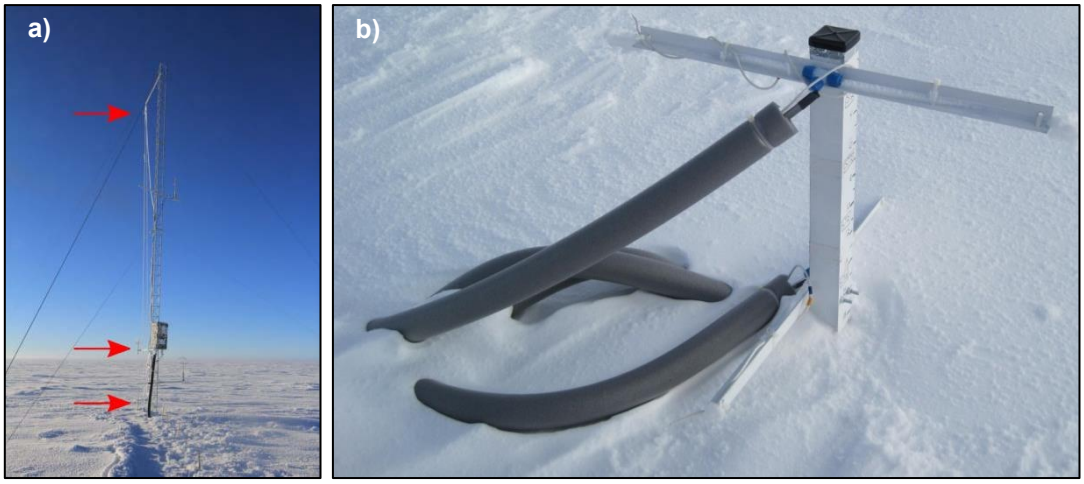

Figure 5-2: Photographs showing **a)** the meteorological tower with the three gas inlets (red arrows) at 1070 cm, 210 cm, and 25 cm above the snow surface (© B. Jourdain), and **b)** one of the snow towers with the two sampling inlets above the snowpack at 50 and 10 cm (© D. Helmig).

Instrumentation was located in a below-surface shelter at the edge of the "clean area", 800 m away from the main camp and upwind with respect to the dominant wind direction (south west). In 2012, year-round measurements were performed in the atmospheric boundary layer at about 500 cm above the snow surface. In 2013, measurements were performed in both the atmosphere and in snowpack interstitial air for several trace gases including gaseous mercury and ozone (O_3). Sampling instrumentation included one 10 m meteorological tower for above-surface gradient sampling and two multi-inlet snow sampling manifolds ("snow towers") for measuring trace gases at various depths in interstitial air (Bocquet et al., 2007; Seok et al., 2009). The 10 m meteorological tower was installed ~ 15 m upwind of the underground instrument shelter. It accommodated three gas inlets at 1070 cm, 210 cm, and 25 cm above the snow surface (Figure 5-2a). Trace gas measurements were acquired on each snow tower at six height levels: 50 and 10 cm above the snow surface, and 10, 30, 50, and 70 cm below the snow surface (Figure 5-2b). Sampling lines were purged continuously at 5 L min^{-1} on the meteorological tower and intermittently at ~ 2-3 L min^{-1} on the snow towers. On each snow

tower, inlets were fitted with a small glass fiber filter in PTFE housing (25 mm Acrodisc syringe filters, Pall Life Sciences, Ann Arbor, Michigan, USA) to prevent snow crystals from entering the PFA sampling lines. Sampling lines were inside insulation tubing and the temperature of the sampling lines was maintained at a level 5-10 °C warmer than the snowpack temperature with a heat trace to prevent water vapor from freezing and clogging the lines. An automatic sampling pattern was implemented: trace gases were collected sequentially from the uppermost inlets on the meteorological tower to deepest levels of the snow towers. Measurements were taken for 10 min from each inlet.

5.1.2.3 Gaseous mercury measurements

Measurements were performed using a Tekran 2537A analyzer (Tekran Inc., Toronto, Canada) based on the amalgamation of mercury onto a gold cartridge followed by thermal desorption and detection by an integrated cold vapor atomic fluorescence spectrometer (CVAFS) at 253.7 nm (Fitzgerald and Gill, 1979; Bloom and Fitzgerald, 1988). The presence of two gold cartridges allowed alternating sampling and desorption modes and thus a continuous analysis in the pre-filtered (0.45 µm PTFE filter) and unheated sample air stream. The sampling resolution was 5 min with a sampling flow rate of 0.8 L min^{-1}. Concentrations are expressed in nanograms per cubic meter at standard temperature and pressure (273.15 K, 1013.25 hPa). Using both a 0.45 µm PTFE filter at the entrance inlet of the sample line, and an unheated ¼"PTFE sample line, we assume that only Hg(0) (*vs.* total gaseous mercury, defined as the sum of gaseous mercury species) was efficiently collected and subsequently analyzed in this study (Steffen et al., 2002; Temme et al., 2003; Steffen et al., 2008).

Quality assurance and quality control procedures

An automatic calibration step of the Tekran 2537A analyzer was carried out every 25 h with an internal mercury permeation source. External calibrations were performed twice a year by manually injecting saturated mercury vapor taken from a temperature-controlled vessel (Tekran 2505 mercury vapor calibration unit, Hamilton digital syringe). As described by Angot et al. (2014), bi-monthly to monthly routine maintenance operations were performed. A software program was developed at the LGGE (Laboratoire de Glaciologie et Géophysique de l'Environnement) in accordance with quality control practice in well-established North American networks (Steffen et al., 2012). Based on various flagging criteria (Munthe et al., 2011; D'Amore et al., 2015), it enabled rapid data processing in order to produce clean time series of Hg(0). The detection limit is estimated at 0.10 ng m^{-3} (Tekran, 2011). Based on experimental evidence, the average systematic uncertainty for Hg(0) measurements is of ~ 10 % (Slemr et al., 2015).

5.1.2.4 Surface snow sampling and analysis

Surface snow samples (first cm) were collected weekly from February 2013 to January 2014 using acid cleaned PTFE bottles and clean sampling procedures. Upon collection,

samples were stored in the dark at -20 °C. Field blanks, carried out by opening and closing a bottle containing mercury-free water, were regularly conducted. Surface snow samples and field blanks were analyzed for total mercury using a Tekran Model 2600. The instrument was calibrated with the NIST SRM-3133 mercury standard. Quality assurance and quality control included the analysis of analytical blanks, replicates, and internal standards (reference waters for mercury: HG102-2 at 22 ng L^{-1} from Environment Canada). The limit of quantification – calculated as 10 times the standard deviation of a set of three analytical blanks – amounted to 0.3 ng L^{-1} with a relative accuracy of ± 8 %.

5.1.2.5 Ancillary parameters

Ozone

Measurements were performed using a UV absorption monitor (Thermo Electron Corporation, Franklin, MA), model 49I in 2012 (Legrand et al., 2016b) and model 49C in 2013. In 2013, the instrument was calibrated against the standard of the National Oceanic and Atmospheric Administration Global Monitoring Division, Boulder, Colorado.

Air mass back trajectories

Air mass back trajectories were computed using the Lagrangian model FLEXPART (Stohl et al., 1998; Stohl and Thomson, 1999; Stohl et al., 2005) run in the backward mode and driven by NCEP (National Center for Environmental Predictions) GFS (Global Forecast System) final meteorological fields. Simulations were done every day at 1200 UTC in 2012 and 2013. For each simulation, 20000 pseudo-particles were released by the model around the position of DC and tracked for 5 days in three layers of altitude (0-0.1, 0.1-4 and 4-10 km above ground level). Simulations at an altitude of 4-10 km were computed in order to investigate the potential occurrence of upper troposphere/lower stratosphere intrusions. For each 1 h time step, the model produced a normalized particle residence time (in seconds) within an output grid of 0.5×0.5°. The sum of the 5 days outputs provided potential emission sensitivities (PES, in seconds) for the three layers of altitude. PES in a particular grid cell is proportional to the particle residence time in that cell. It should be noted that, in Antarctica, the meteorological data driving the FLEXPART transport model rely on sparse measurements. Consequently, the trajectories calculated in this region are often associated with relatively high uncertainties.

Height of the boundary layer and shortwave radiation

The height of the boundary layer and downwelling shortwave radiation were calculated by the MAR regional atmospheric model (Modèle Atmosphérique Régional). MAR was developed at the LGGE for polar regions and the simulations have been evaluated against meteorological observations made at DC (Gallée and Gorodetskaya, 2010; Gallée et al., 2015).

Meteorological data

Temperature, wind speed and direction were recorded at six height levels on a 45 m tower. The general observation set up is described by Genthon et al. (2010).

Ice precipitation

A tropospheric depolarization lidar (light detection and ranging) operating at 523 nm provided tropospheric profiles of aerosol and clouds every 5 min, allowing detection of water/ice clouds, snow drift, diamond dust and pollution plumes.

Tropospheric temperature and integrated water vapor

A H_2O Antarctica Microwave Stratospheric and Tropospheric Radiometers (HAMSTRAD) instrument was used for the detection of the 60 GHz oxygen and the 183 GHz water vapor lines, allowing measurement of tropospheric temperature and water vapor profiles, respectively, together with integrated water vapor (IWV) every 7 min. The instrument is fully automated and a liquid nitrogen calibration is performed twice per year (Ricaud et al., 2015)

Eddy diffusivity and friction velocity

The Eddy diffusivity was calculated as follows (Xiao et al., 2014) where k (set to 0.40) is the von Karman constant, u_* the friction velocity (m s^{-1}), z the measurement height (m), and φ_h the Obukhov stability function:

$$K = k\, u_*\, z/\varphi_h \qquad \text{(Eq. 5-1)}$$

According to Frey et al. (2013), the stability function was $\varphi_h = 0.95 + 4.62\, z/L$ for stable conditions above snow (King and Anderson, 1994), and $\varphi_h = 0.95(1 - 11.6\ z/L)^{-0.5}$ for unstable conditions (Hoegstroem, 1988). u_* and L (the Obukhov length (m)) were computed from the three-dimensional wind components (*u*, *v*, *w*) and temperature measured by a Metek sonic anemometer mounted at 8 m above the snow surface.

5.1.3 Results and Discussion

5.1.3.1 Hg(0) concentrations in ambient air

The record of atmospheric Hg(0) over the entire 2012-2013 period is displayed in Figure 5-3a. Hg(0) concentrations ranged from below 0.10 to 2.30 ng m^{-3}, with average values amounting to 0.76 ± 0.24 ng m^{-3} in 2012, and to 0.81 ± 0.28 ng m^{-3}, 0.84 ± 0.27 ng m^{-3}, and 0.82 ± 0.26 ng m^{-3} in 2013 at 25, 210, and 1070 cm above the snow surface, respectively. No significant difference was observed between annual averages of Hg(0) concentrations measured at the three inlets of the meteorological tower in 2013 (p value = 3.1×10^{-14}, Mann-Whitney test). It should be noted that Hg(0) concentrations at the three inlets were significantly different in winter only (see section 5.1.3.1.4). These mean annual Hg(0)

concentrations are lower than annual averages reported at near-coastal or coastal Antarctic stations (*i.e.*, 0.93 ± 0.19 ng m^{-3} for Hg(0) at TR (Pfaffhuber et al., 2012) and 1.06 ± 0.24 ng m^{-3} for total gaseous mercury at NM (Ebinghaus et al., 2002b)).

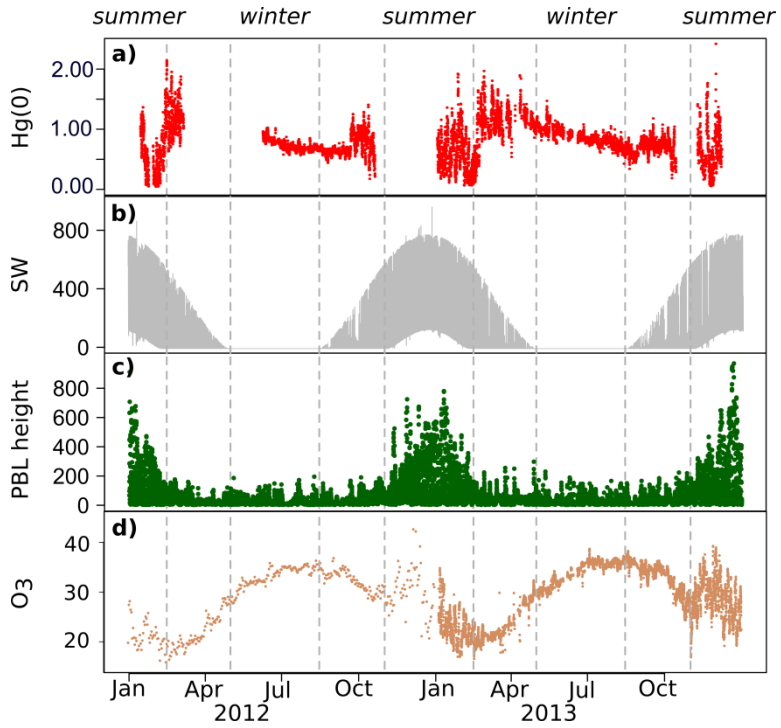

Figure 5-3: Annual variation in 2012 and 2013 of **a)** hourly averaged Hg(0) concentrations (in ng m^{-3}) at 500 cm and 25 cm above the snow surface in 2012 and 2013, respectively, **b)** downwelling shortwave (SW) radiation (in W m^{-2}), **c)** planetary boundary layer (PBL) height (in m), and **d)** ozone (O_3, daily mean in 2012 and hourly mean in 2013) mixing ratios (in ppbv). The vertical dashed lines represent seasonal boundaries.

The seasonal boundaries are defined according to the transitions in downwelling shortwave radiation (Figure 5-3b) as follows: winter from May to mid-August, spring from mid-August to October, summer from November to mid-February, and fall from mid-February to April. Unlike in winter, Hg(0) concentrations were highly variable during the sunlit period with concentrations ranging from below 0.10 ng m^{-3} to 1.50-2.00 ng m^{-3}, up to twice the average background levels recorded in the Southern Hemisphere midlatitudes (Slemr et al., 2015). These seasonal features, in good agreement with observations at other Antarctic stations (Ebinghaus et al., 2002b; Pfaffhuber et al., 2012), suggest the existence of a photochemically induced reactivity of atmospheric mercury during the sunlit period. The mechanisms which cause the seasonal variation of Hg(0) concentrations are discussed in the following sections.

5.1.3.1.1 Spring

First discovered in the Arctic (Schroeder et al., 1998), atmospheric Hg(0) depletion events (AMDEs) result from an oxidation by reactive bromine species released during springtime so-called “bromine explosions” in coastal regions (Durnford and Dastoor, 2011 and references

therein) and are concurrent with tropospheric O_3 depletion events (Simpson et al., 2007b). Despite the distance of DC from the coast (1100 km), a Hg(0) depletion event was observed on 11 September 2013 due to a maritime air transport event (Figure 5-4a). During this event, Hg(0) concentrations dropped from 0.85 to 0.56 ng m^{-3} and exhibited a strong positive correlation with O_3 mixing ratios (rho = 0.94, *p* value = 5×10^{-7}).

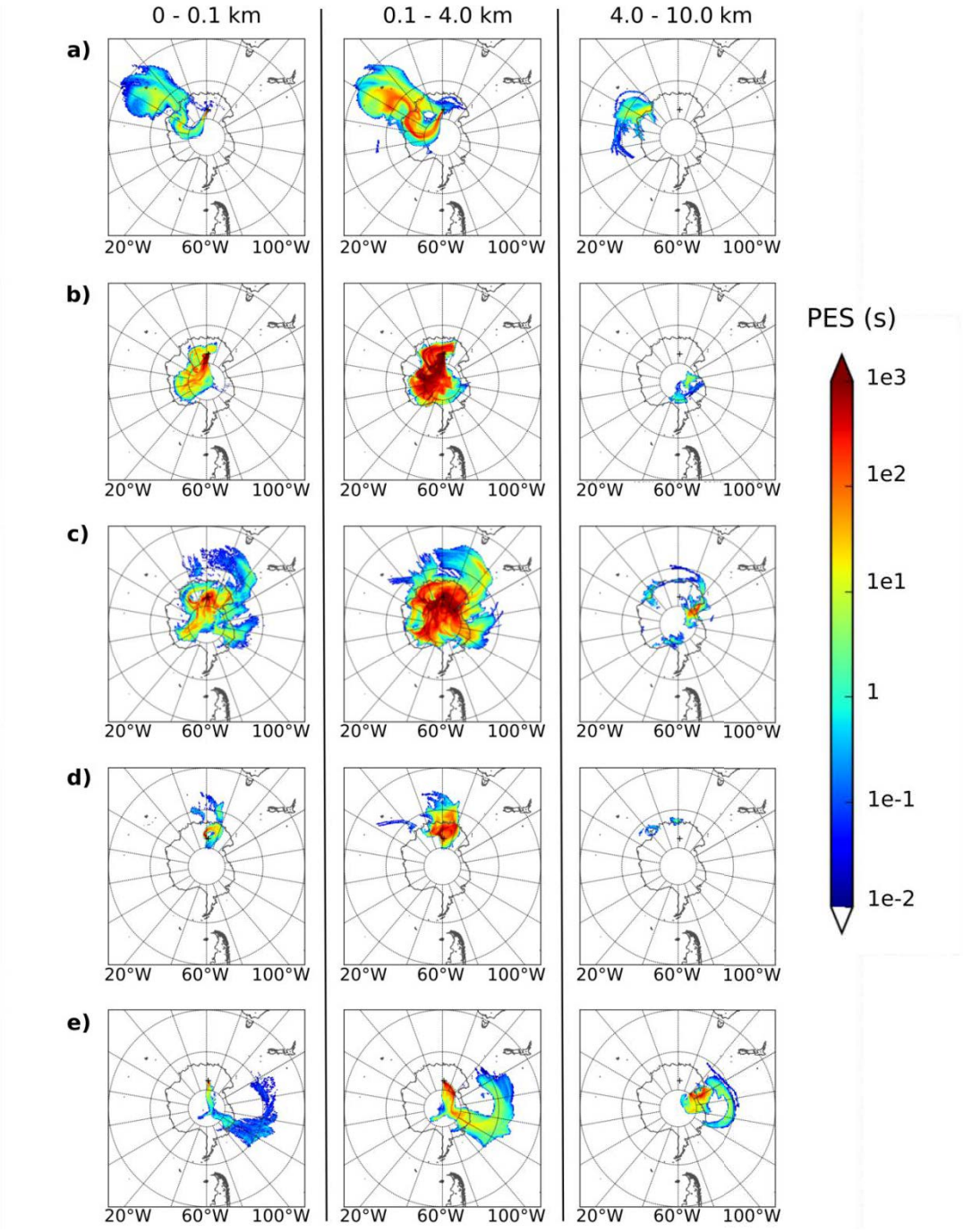

Figure 5-4: Back trajectories for the three layers of altitude colored according to the potential emission sensitivity (PES, in seconds) **a)** on 11 September 2013, **b)** from 19 January to 8 February 2012, **c)** from 5 to 20 February 2013, **d)** on 10 February 2012, and **e)** on 22 February 2013. Note that PES in a particular grid cell is proportional to the particle residence time in that cell.

5.1.3.1.2 Summertime

a) Oxidation of Hg(0) in ambient air and Hg(II) deposition onto snowpack

In summer, the mean atmospheric Hg(0) concentration was 0.69 ± 0.35 ng m^{-3} (mean ± standard deviation). This means that Hg(0) concentrations are ~ 25 % lower than levels recorded at the same period of the year at coastal Antarctic stations (Ebinghaus et al., 2002b; Sprovieri et al., 2002; Pfaffhuber et al., 2012). Total mercury concentrations in surface snow samples were highly variable (median value: 4.8 ng L^{-1}, range: < detection limit–73.8 ng L^{-1}, Figure 5-5) and were higher in summer (median value: 10.4 ng L^{-1}, range: 1.3–73.8 ng L^{-1}), suggesting that divalent mercury species were preferentially deposited onto the snowpack in this period of the year. The lower Hg(0) concentrations in ambient air along with high total mercury concentrations in surface snow samples suggest an intense oxidation of Hg(0) in ambient air in summer, followed by the deposition of oxidation products on surface snow. This hypothesis is further supported by elevated oxidized mercury concentrations measured on the Antarctic Plateau at SP in summer (0.10–1.00 ng m^{-3}) by Brooks et al. (2008a).

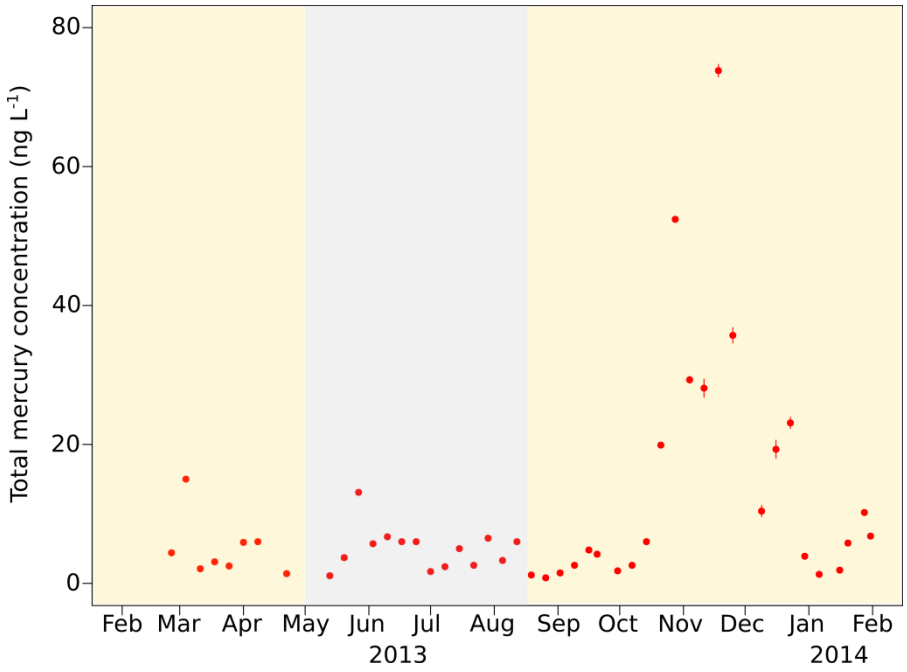

Figure 5-5: Total mercury concentration (ng L^{-1}), along with standard errors, in surface snow samples collected weekly at Concordia Station from February 2013 to January 2014. Dark period (winter) highlighted in grey, sunlit period highlighted in yellow. Total mercury concentrations were elevated (up to 74 ng L^{-1}) in November-December 2013 (summer). All samples were analyzed in replicates of three. Standard errors are frequently smaller than the width of the dots.

The oxidative capacity of the Antarctic Plateau atmosphere is elevated in summer, as evidenced by several studies (Davis et al., 2001; Grannas et al., 2007; Eisele et al., 2008; Kukui et al., 2014), likely explaining this intense oxidation of Hg(0) in ambient air. Among these oxidants, NO_2, RO_2, and OH are particularly abundant at DC in summer (Frey et al., 2013; Kukui et al., 2014) and a recent study provided as a first estimate a BrO mixing ratio of

2-3 pptv near the ground during sunlight hours (Frey et al., 2015). Given the current understanding of mercury oxidation and the lack of continuous halogens measurements, we were not able to identify the exact mechanism for the reactivity observed at DC. A two-step oxidation mechanism, favored at cold temperatures, is worth being considered further. The initial recombination of Hg(0) and Br is followed by the addition of a second radical (*e.g.*, I, Cl, BrO, ClO, OH, NO_2, or HO_2) in competition with thermal dissociation of the HgBr intermediate (Goodsite et al., 2004; Wang et al., 2014). According to Dibble et al. (2012), HO_2, NO, NO_2, and NO_3 bind Hg(0) too weakly to initiate its oxidation in the gas phase and reactions of the HgBr intermediate with NO_2, HO_2, ClO, and BrO are more important than with Br and OH. Further modeling or laboratory chamber studies investigating the fate of Hg(0) in the presence of various potential oxidants are needed to improve our understanding of the mechanisms.

b) Multi-day depletion events of atmospheric Hg(0)

From 19 January to 8 February 2012 and from 5 to 20 February 2013 we observed Hg(0) depletion events. The mechanism seems however different from springtime AMDEs (see section 5.1.3.1.1). While atmospheric Hg(0) concentrations dropped and remained low (0.39 ± 0.19 ng m^{-3} from 19 January to 8 February 2012, 0.41 ± 0.21 ng m^{-3} from 5 to 20 February 2013) for several weeks (Figure 5-3a, Figure 5-6a, and Figure 5-6e), O_3 showed no abnormal variability (Figure 5-6d, Figure 5-6h). These depletion events occurred as air masses stagnated over the Antarctic Plateau (Figure 5-4b, Figure 5-4c) according to our FLEXPART simulations. This stagnation of air masses is confirmed in 2013 (Figure 5-6f, Figure 5-6g) by a decrease of temperature at 10 m a.g.l. (from -29 ± 3 °C in January to -43 ± 4 °C during the Hg(0) depletion event) and a low integrated water vapor (0.40 ± 0.13 kg m^{-2} during the Hg(0) depletion event *vs.* 0.77 ± 0.20 kg m^{-2} in January). In both 2012 and 2013, depletions of Hg(0) ended when air masses started moving out of the plateau (Figure 5-4d, Figure 5-4e).

While previous studies attributed high Hg(II) concentrations in the Antarctic summer to subsiding upper tropospheric air (Holmes et al., 2006; Brooks et al., 2008a), potential emission sensitivities suggest that the depletions of Hg(0) reported here were unlikely concomitant with upper troposphere/lower stratosphere intrusions (Figure 5-4b, Figure 5-4c, PES at 4-10 km). This is also confirmed by stable O_3 mixing ratios. High altitude vertical profiles of Hg(0) should be carried out to rule out this hypothesis of subsiding upper tropospheric air. We suggest that these Hg(0) depletion events observed at DC result from processes occurring within the shallow boundary layer. Since O_3 was not depleted during these events, Hg(0) depletion cannot be accounted for by bromine oxidation alone. FLEXPART simulations along with integrated water vapor and temperature measurements indicate that these Hg(0) depletion events occurred as air masses stagnated over the Antarctic Plateau. As highlighted in the previous section, the oxidative capacity is high in summer on the plateau (Davis et al., 2001; Grannas et al., 2007; Eisele et al., 2008; Kukui et al., 2014).

This air mass stagnation might favor an accumulation of oxidants within the shallow boundary layer (< 300 m in average), leading to an oxidation of Hg(0) stronger than usual.

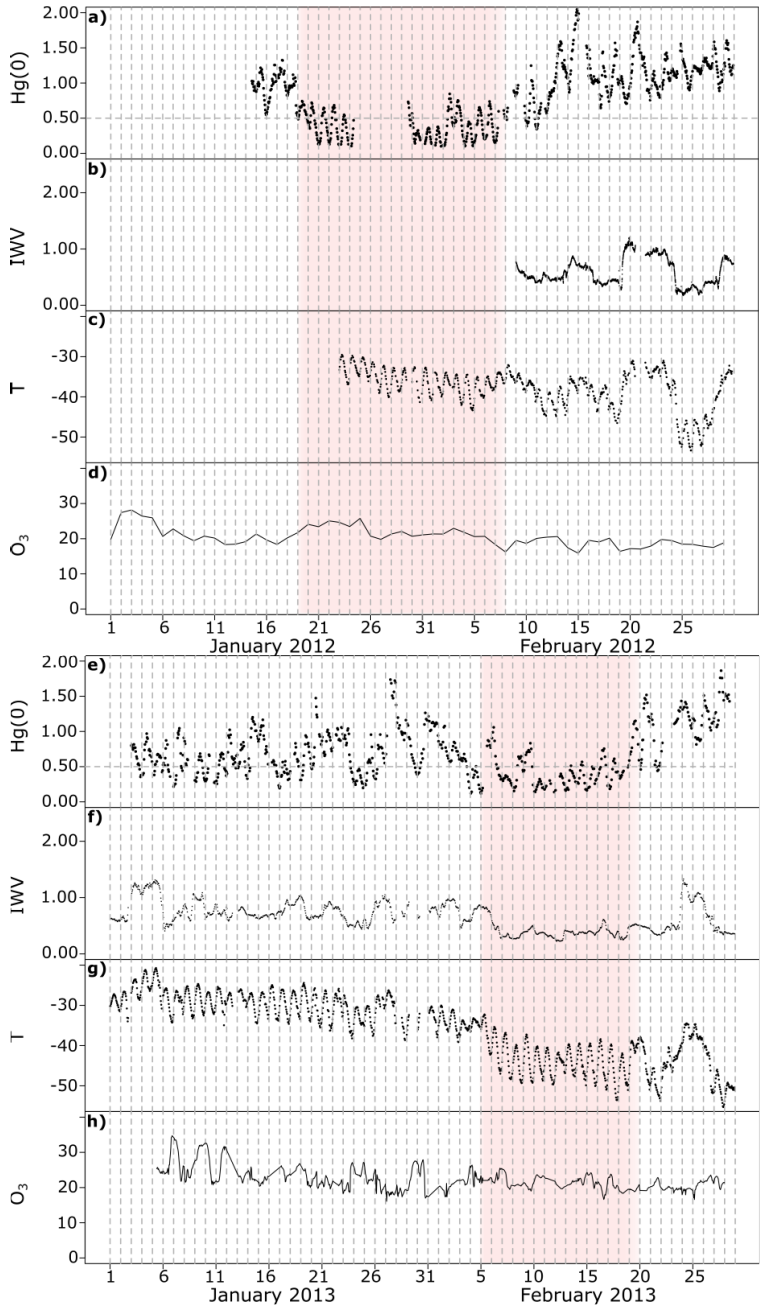

Figure 5-6: Top: January and February 2012 cycle of **a)** hourly averaged Hg(0) concentrations (in ng m^{-3}) at 500 cm above the snow surface, **b)** integrated water vapor (IWV, kg m^{-2}), **c)** Temperature (in °C) at 10 m above ground level, and **d)** ozone (O_3, daily mean) mixing ratios (ppbv). Hg(0) was low from 19 January to 8 February (period highlighted in red) while O_3 showed no abnormal variability. Bottom: January and February 2013 cycle of the following: **e)** hourly averaged Hg(0) concentrations (in ng m^{-3}) at 210 cm above the snow surface, **f)** integrated water vapor (IWV, kg m^{-2}), **g)** Temperature (in °C) at 10 m above ground level, and **h)** ozone (O_3, hourly mean) mixing ratio (ppbv). Hg(0), IWV, and temperature were low from 5 to 20 February (period highlighted in red) while O_3 showed no abnormal variability. Note that Hg(0) concentrations exhibited the same pattern at the three inlets of the meteorological tower from 5 to 20 February 2013.

c) Hg(0) diurnal cycle

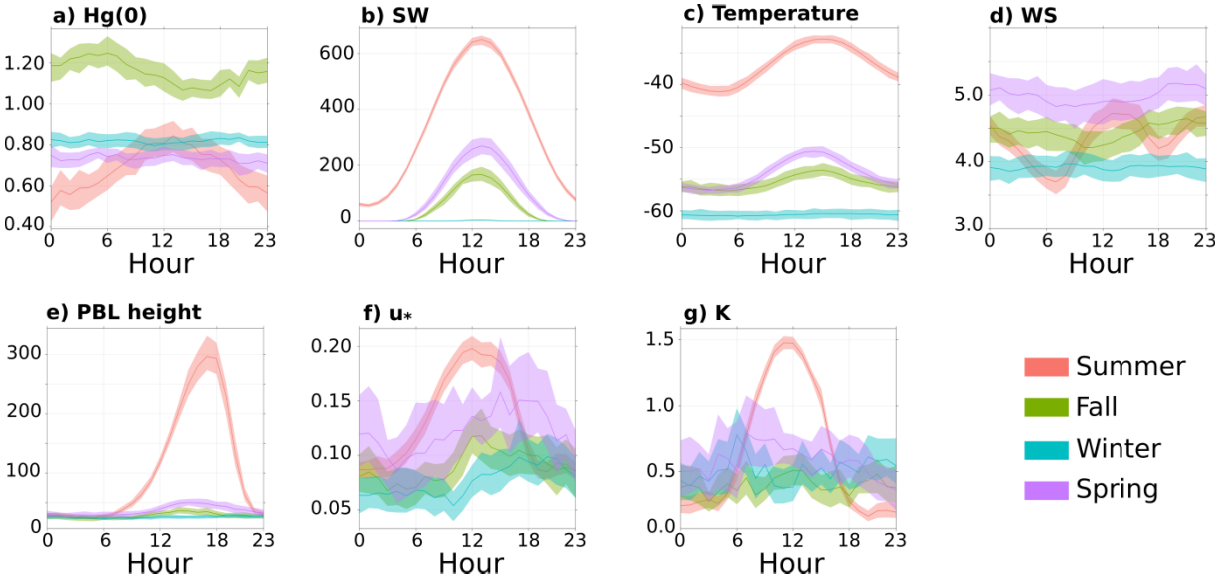

Figure 5-7: Hourly (local time) mean variation, along with the 95 % confidence interval for the mean, of: **a)** Hg(0) concentration (in ng m^{-3}) at 25 cm above the snow surface, **b)** downwelling shortwave (SW) radiation (in W m^{-2}) according to the MAR model simulations, **c)** temperature (in °C) at 3 m above the snow surface, **d)** wind speed at 3 m above the snow surface (in m s^{-1}), **e)** planetary boundary layer (PBL) height (in m) according to the MAR model simulations, **f)** friction velocity (u_*, in m s^{-1}), and **g)** Eddy diffusivity (K, in m^2 s^{-1}) in summer (red), fall (green), winter (blue), and spring (purple). Note that the hourly mean variation of Hg(0) concentration in summer is similar at the three inlets of the meteorological tower.

Based on a week of measurements made at DC in January 2009, Dommergue et al. (2012) reported that atmospheric Hg(0) exhibited a significant daily cycle with maximal concentrations around noon. We show that this daily cycle occurred throughout the summer, with low atmospheric Hg(0) concentrations (~ 0.50 ng m^{-3}) when solar radiation was minimum and a maximum (~ 0.80 ng m^{-3}) around noon (Figure 5-7a). Such a pronounced daily cycle has never been observed at other Antarctic stations (Dommergue et al., 2010b; Pfaffhuber et al., 2012). Several studies showed that Hg(0) emission from the snowpack maximizes near midday (e.g., Steffen et al., 2002; Ferrari et al., 2005; Brooks et al., 2006a; Faïn et al., 2007; Ferrari et al., 2008; Johnson et al., 2008). As suggested by Durnford and Dastoor (2011), the noon emission does not necessarily reflect maximum concentrations of cryospheric Hg(0) around midday (Hg(0) concentration peaked in the afternoon at 10 cm below the snow surface, see section 5.1.3.2.1) and could be driven by ventilation generated by atmospheric thermal convection. Stable boundary layers are almost ubiquitous in polar regions due to radiation cooling (Anderson and Neff, 2008). However, convective boundary layers have been observed in summer at polar domes at DC (King et al., 2006) and Summit in Greenland (Cohen et al., 2007). Figure 5-7 displays the hourly mean variation of several parameters. As illustrated by Figure 5-7c and Figure 5-7d, and in agreement with earlier observations (Argentini et al., 2005; Pietroni et al., 2012; Argentini et al., 2013), there was a strong diurnal cycle in near-surface temperature and wind speed in summer at DC. These

observations are typical for locations where a convective boundary layer develops as a response to daytime heating (King et al., 2006), as can be seen in Figure 5-7e. In a convective boundary layer, vertical mixing is enhanced during convective hours (Anderson and Neff, 2008), as shown in Figure 5-7f and Figure 5-7g by increasing values for the friction velocity (u_*, indicative of the strength of the mixing processes in the surface layer (Neff et al., 2008)) and the Eddy diffusivity (K). Similarly, several studies highlighted that the atmospheric turbulence at DC in summer influences the vertical flux and concentration profiles of various atmospheric species (Legrand et al., 2009; Dommergue et al., 2012; Kerbrat et al., 2012; Frey et al., 2013).

In summary, the observed summertime Hg(0) diurnal cycle in ambient air might be due to a combination of factors: i) the intense oxidation of Hg(0) in ambient air due to the high oxidative capacity on the plateau – as evidenced by low mean Hg(0) concentrations (see section 5.1.3.1.2), ii) subsequent Hg(II) deposition onto snowpack – as evidenced by elevated total mercury levels in surface snow samples (see section 5.1.3.1.2), and iii) emission of Hg(0) from the snowpack during convective hours. Figure 5-8 summarizes the processes that govern mercury exchange at the air-snow interface. Redox processes occurring within the snowpack are discussed in details in section 5.1.3.2.

5.1.3.1.3 Fall

In fall, Hg(0) concentrations in ambient air no longer peaked around midday (Figure 5-7a) and were in average 67 % higher than during the summer, exceeding levels recorded at lower latitudes in the Southern Hemisphere (Slemr et al., 2015). In this period of the year, the boundary layer lowered to ~ 50 m in average (Figure 5-3c) and no longer exhibited a pronounced diurnal cycle (Figure 5-7e). We believe that the shallow boundary layer could cause Hg(0) concentrations in ambient air to build up to where they exceeded levels recorded at lower latitudes in the Southern Hemisphere because Hg(0) – emitted from the snowpack – was dispersed into a reduced volume of air, limiting the dilution. Similarly, NO_x mixing ratios are enhanced when the boundary layer is shallow (Neff et al., 2008; Frey et al., 2013). Elevated Hg(0) concentrations were also likely favored by the fact that oxidation in ambient air was weaker under lower solar radiation.

5.1.3.1.4 Winter

While stable concentrations were expected in winter given the absence of photochemistry, our observations reveal a 20 to 30 % decrease of atmospheric Hg(0) concentrations from May to mid-August (Figure 5-3a). Conversely, Hg(0) concentrations remained stable at NM and TR from late fall through winter (Ebinghaus et al., 2002b; Pfaffhuber et al., 2012). This decreasing trend observed in winter might be due to several mechanisms, including gas-phase oxidation, heterogeneous reactions, or dry deposition of Hg(0).

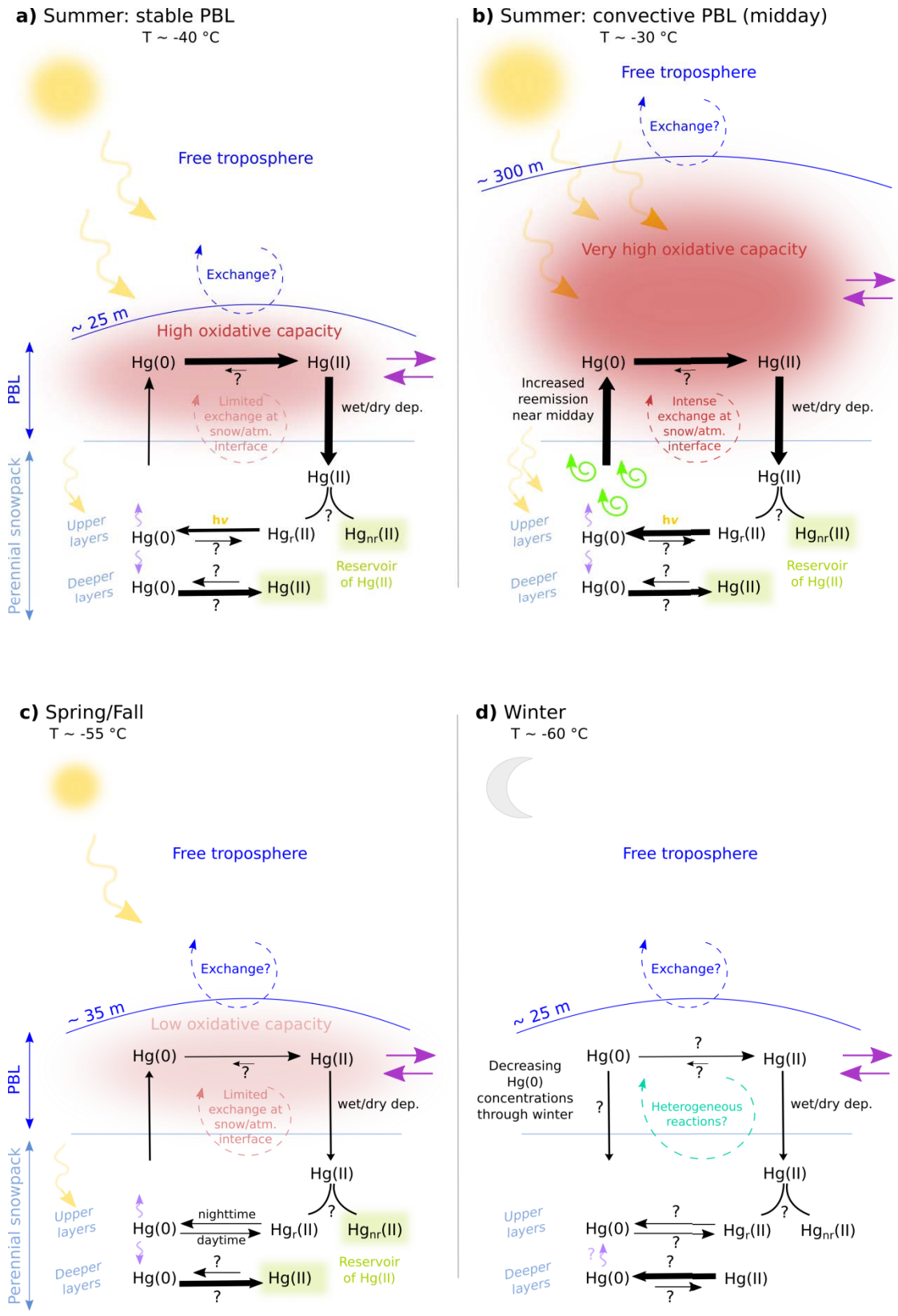

Perennial snowpack:
Upper layers: first 10 cm
Deeper layers: below 50 cm
diffusion
ventilation

Hg(II): divalent mercury species (gaseous and/or particulate)
$Hg_r(II)$: reducible divalent mercury
$Hg_{nr}(II)$: non reducible divalent mercury
$Hg_r(II) + Hg_{nr}(II)$ = total mercury in snow samples
Long-range transport of mercury species (import/export)

Figure 5-8: Schematic diagram illustrating the processes that govern the Hg(0) budget at DC **a)** in summer under stable Planetary Boundary Layer (PBL) conditions, **b)** in summer under convective PBL conditions, **c)** in spring/fall, and **d)** in winter. In summer, Hg(0) is intensely oxidized due to the high oxidative capacity of the boundary layer and a large amount of divalent mercury species deposit onto the snowpack. A fraction of deposited mercury can be reduced (the reducible pool, $Hg_r(II)$) in the upper layers of the snowpack and subsequently re-emitted to the atmosphere as Hg(0). Hg(0) emission from the snowpack maximizes near midday likely due to increased ventilation as a response to daytime heating. Oxidation of Hg(0) dominates in the deeper layers of the snowpack likely leading to the formation of a Hg(II) reservoir. In spring/fall, the balance of reduction and oxidation processes within the upper layers of the snowpack differs from summertime: oxidation dominates during the day, reduction at night. In winter, Hg(0) is produced in the deeper layers of the snowpack likely as a result of the reduction of Hg(II) species accumulated during the sunlit period. Ambient Hg(0) concentrations exhibit a 20 to 30 % decrease through winter possibly due to dry deposition of Hg(0).

Several studies suggested the involvement of nitrate radicals in the night-time oxidation of Hg(0) (Mao and Talbot, 2012; Peleg et al., 2015). However, as previously mentioned, Dibble et al. (2012) indicated that NO_3 binds Hg(0) too weakly to initiate its oxidation in the gas phase. Another potential oxidant is O_3, with this reactant reaching a maximum in the winter (Figure 5-3d). However, according to some theoretical studies (*e.g.*, Hynes et al., 2009), reaction (R1) is unlikely to proceed as a homogeneous reaction. Several experimental studies confirmed the major product of reaction (R1) to be solid mercuric oxide, HgO (s) and not HgO (g) (e.g., Pal and Ariya, 2004a; Ariya et al., 2009), suggesting that pure gas-phase oxidation of elemental mercury by O_3 may not occur in the atmosphere. However, Calvert and Lindberg (2005) proposed an alternative mechanism that would make this reaction potentially viable in the atmosphere (Subir et al., 2011). The reaction may start with the formation of a metastable HgO_3 (g) molecule which then decomposes to OHgOO (g) and thereafter transforms to HgO (s) and O_2 (g).

$$Hg(0)\,(g) + O_3\,(g) \rightarrow HgO\,(g) + O_2\,(g) \qquad \text{(R1)}$$

As suggested by Subir et al. (2011), the influence of heterogeneous surfaces of water droplets, snow, ice, and aerosols should be taken into account when attempting to describe mercury chemistry in the atmosphere. O'Concubhair et al. (2012) showed that freezing an acidic solution containing nitrite or hydrogen peroxide can oxidize dissolved gaseous mercury in the dark. Nitrous acid and hydrogen peroxide are present on the Antarctic Plateau (Huey et al., 2004; Hutterli et al., 2004). As suggested by Dommergue et al. (2012), similar processes could occur in the snow or on surface hoar at DC in winter. In 2013, the height of measurement had a significant influence on the decline over time of Hg(0) concentrations (ANCOVA test, p value < 0.05), with a steeper decrease at 25 cm than at 1070 cm. Additionally, wintertime Hg(0) concentrations were significantly lower at 25 cm than at 1070 cm (p value < 0.05, Mann-Whitney test). These results suggest that snowpack may act as a sink for mercury, enhancing the deposition rate due to heterogeneous reactions, through absorption of oxidation products, and/or physical sorption/condensation of Hg(0) on surface snow.

The observed declining trend could also be attributed to the dry deposition of Hg(0) onto the snowpack. The dry deposition velocity is defined according to equation 5-2 (Joffre, 1988) as the ratio between the deposition flux F (ng m^{-2} s^{-1}) and the concentration C (ng m^{-3}). Denoting the height of the boundary layer h and the Hg(0) concentration at the beginning of winter C_0, the evolution of the concentration versus time is thus given by the ordinary differential equation 5-3. During winter (t = 107 days), the Hg(0) concentration gradually decreased from C_0 ~ 1.03 ng m^{-3} to C ~ 0.73 ng m^{-3} at 25 cm above the snowpack, in a mixing layer of 25 m high. According to equation 5-3, the associated dry deposition velocity is 9.3×10^{-5} cm s^{-1}. This result is in very good agreement with dry deposition velocities reported for Hg(0) over snow (Cobbett et al., 2007; Zhang et al., 2009).

$$v_d = {}^{F}/_{C} \qquad \text{(Eq. 5-2)}$$

$$C = C_0\, e^{-(v_d/h)t} \qquad \text{(Eq. 5-3)}$$

In spite of the observed decreasing trend of Hg(0) concentrations in ambient air, total mercury concentrations in surface snow samples did not significantly increase over time in winter (Figure 5-5). Using a snow density of 300 kg m^{-3} a loss of 0.30 ng m^{-3} over a period of 3 months in a mixing layer of 25 m high would lead to a 2.5 ng L^{-1} increase in the first cm of the snowpack. Given the variability of chemical species deposition onto the snow surface, and the occurrence of either fresh snowfall or blowing snow, this 2.5 ng L^{-1} increase over a period of three months could not be detected in our weekly surface snow samples.

Despite the overall decreasing trend in winter, Hg(0) concentration exhibited abrupt increases when moist and warm air masses from lower latitudes occasionally reached Concordia Station. This is, for example, evidenced on 13 June 2012 by an increase of 0.25 ng m^{-3} of the Hg(0) concentration, an increase of temperature at 10 m a.g.l. from -63 to -26 °C, and a high integrated water vapor column (Figure 5-9).

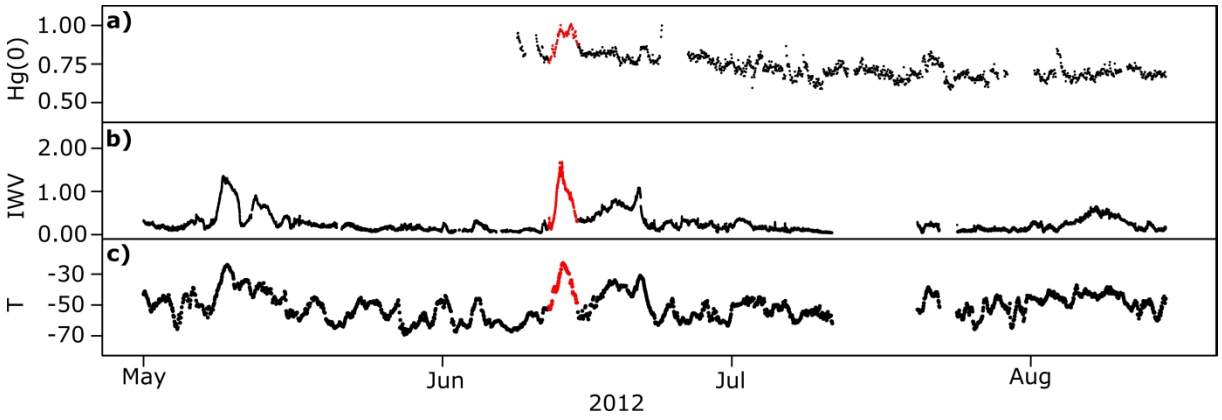

Figure 5-9: Year 2012 wintertime record of **a)** hourly averaged Hg(0) concentrations (in ng m^{-3}) at 500 cm above the snow surface, **b)** integrated water vapor (IWV, kg m^{-2}), and **c)** Temperature (T, °C) at 10 m above ground level. Hg(0), temperature, and IWV increased from June 12 to 15 (in red) suggesting transport of moist and warm air masses originating from lower latitudes.

5.1.3.2 Hg(0)/Hg(II) redox conversions within the snowpack

The 2013 record of Hg(0) in the snow interstitial air (SIA) is displayed in Figure 5-10. Figure 5-11 depicts the mean Hg(0) concentration at various heights above and below the snow surface (in the interstitial air of the snow) for all seasons.

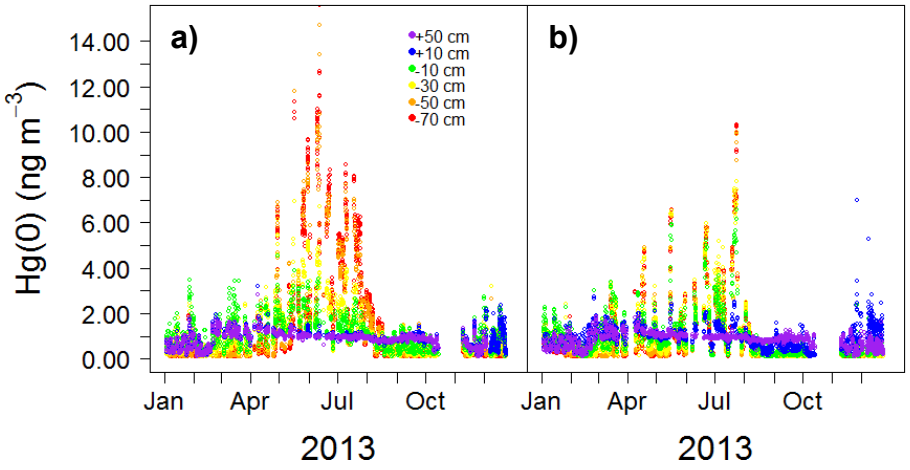

Figure 5-10: Annual variation of hourly averaged Hg(0) concentrations (in ng m^{-3}) in the snow interstitial air collected at the various inlets of the two snow towers: **a)** snow tower #1, **b)** snow tower #2. Note that we regularly experienced technical problems on snow tower #2 leading to missing values.

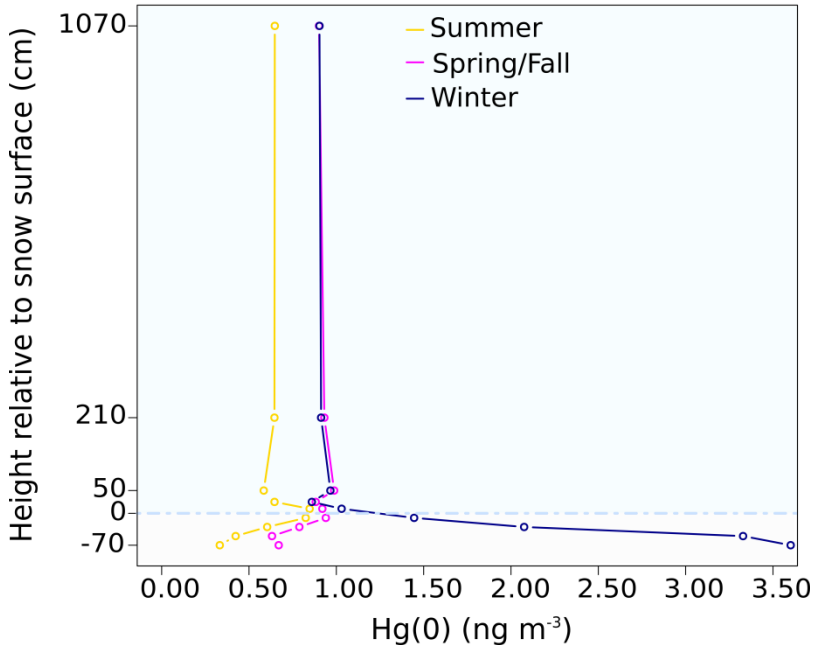

Figure 5-11: Mean Hg(0) concentration (ng m^{-3}) measured at various heights above and below the snow surface (cm) at Concordia Station in summer (yellow), spring/fall (purple), and winter (dark blue). The horizontal light blue dashed line represents the snow surface.

5.1.3.2.1 Sunlit period

During the sunlit period (summer, spring/fall), Hg(0) concentration peaked in the upper layers of the snowpack and then decreased with depth, with levels in the SIA dropping below atmospheric values.

Hg(0) is generally produced in the upper layers of the snowpack – as the result of a photolytically initiated reduction of Hg(II) (Lalonde et al., 2003) – and diffuses upward and downward. According to our observations, Hg(0) concentration peaked at ~ 10 cm below the snow surface (Figure 5-11). Similarly, Brooks et al. (2008a) reported Hg(0) concentrations peaking at a depth of 3 cm at SP. Below the top layer, the actinic flux decreases exponentially with depth (King and Simpson, 2001; Domine et al., 2008). The light penetration depth (*e*-folding depth) is the depth at which the actinic flux's magnitude is 1/*e* of its incident value (Perovich, 2007). It is estimated that ~ 85 % of the photoreduction occurs in the top two *e*-folding depths (King and Simpson, 2001). At DC, the *e*-folding depth is ~ 10 cm at 400 nm for the wind pack layers (France et al., 2011), which supports our observations. Reduced mercury can concurrently be reoxidized within the snowpack. Below the top layer, Hg(0) concentration in the SIA dropped with depth (Figure 5-11) suggesting that oxidation dominated in the deepest layers – in good agreement with observations within the snowpack at Kuujjuarapik/Whapmagoostui, Québec, Canada (Dommergue et al., 2003a) – leading to the formation of a Hg(II) reservoir.

The amount of Hg(0) emitted from the snowpack to the atmosphere (see section 5.1.3.1.2) depends on the balance of reduction and oxidation processes within the upper layers of the snowpack (Durnford and Dastoor, 2011). Figure 5-12 depicts the hourly mean atmospheric and interstitial air Hg(0) concentrations. Our observations indicate that summertime Hg(0) concentration in the upper layers of the snowpack exhibited a diurnal cycle and peaked in the afternoon (Figure 5-12a). Conversely, in spring/fall, Hg(0) concentration reached a maximum at night and a minimum near midday in the upper layers of the snowpack (Figure 5-12b). The balance of reduction and oxidation processes within the upper layers of the snowpack suddenly shifted in summer. Similarly, Faïn et al. (2008) found that reduction dominated during summer and oxidation in spring in the upper layers of the snowpack at Summit, Greenland.

It is worth noting that Hg(0) concentration in the SIA was occasionally very high. For instance, on 24 February 2013, Hg(0) concentration reached 3.00 ng m^{-3} at a depth of 10 cm. During this event, ice precipitation was observed at DC with depolarization values greater than 30 % (data not shown). This suggests that the presence of ice crystals could enhance the dry deposition of Hg(II) species onto the snow surface leading to increased Hg(0) formation in the upper layers of the snowpack. Indeed, due to an elevated specific surface area, mercury-capture efficiency of ice crystals is high (Douglas et al., 2008). Unfortunately, due to a low sampling frequency of surface snow samples (weekly), total mercury concentrations cannot

be used to study further the relationship between the occurrence of ice precipitation events and dry deposition of mercury species.

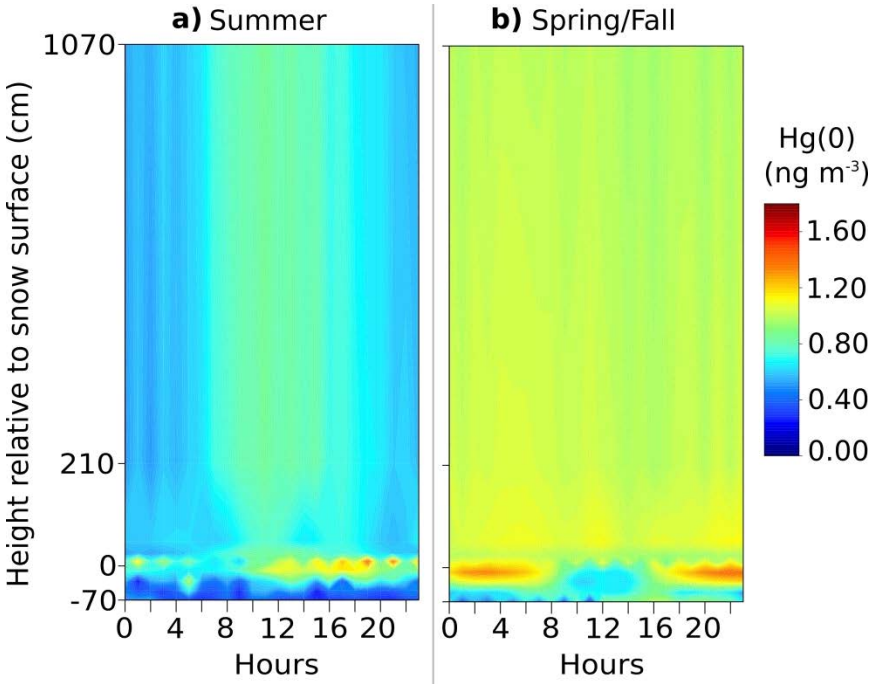

Figure 5-12: Hourly (local time) mean atmospheric and interstitial air Hg(0) concentrations in **a)** summer, and **b)** spring/fall. The vertical axis is the height of measurement relative to the snow surface (in cm). Color contours show Hg(0) concentrations (in ng m^{-3}). Concentrations at 25, 210, and 1070 cm above the snow surface were acquired on the meteorological tower while concentrations at 50, 10, -10, -30, -50 cm, and -70 cm were collected on snow tower #1. Data were cubic spline interpolated using software R.

5.1.3.2.2 Winter

Contrarily to the sunlit period, Hg(0) concentration increased with depth in the SIA in winter (Figure 5-10 and Figure 5-11). The average Hg(0) concentration amounted to 3.60 ng m^{-3} at a depth of 70 cm and was observed at a temperature of about -60 °C and not related to any change in atmospheric composition. Our observations are in agreement with earlier studies indicating that reduction of Hg(II) species is possible in the dark (Ferrari et al., 2004; Faïn et al., 2007; Ferrari et al., 2008). The production of Hg(0) might be due to the reduction of Hg(II) species accumulated in the deepest layers of the snowpack during the sunlit period (see section 5.1.3.2.1). This shift from oxidation to reduction in the deepest layers of the snowpack at the beginning of winter remains unexplained.

5.1.4 Implications on a continental scale

Depletion events of atmospheric Hg(0) that have been observed in the Arctic and at various coastal Antarctic stations have been associated with O_3 depletions, where Hg(0) and O_3 concentrations are positively correlated (Simpson et al., 2007b). Increases in both Hg(II) and Hg(p) have been reported in conjunction with decreases of Hg(0) (Lu et al., 2001;

Lindberg et al., 2002; Aspmo et al., 2005). Conversely, low Hg(0) concentrations that were not correlated or anti-correlated with O_3 were observed at NM and TR (Temme et al., 2003; Pfaffhuber et al., 2012), while elevated Hg(II) concentrations (up to 0.33 ng m^{-3}) were recorded at TNB in the absence of Hg(0)/O_3 depletion (Sprovieri et al., 2002). The intense oxidation of Hg(0) in summer (see section 5.1.3.1.2) and multi-day Hg(0) depletion events observed at DC in January/February (see section 5.1.3.1.2) are expected to result in the build-up of an inland atmospheric reservoir enriched in Hg(II) and depleted in Hg(0) in the summer. Due to strong katabatic winds flowing out from the Antarctic Plateau – generated by the negative buoyant force that develops in the stable cooled layer along the ice sheet slopes (Gallée and Pettré, 1998) –, a fraction of this inland atmospheric reservoir can be transported toward the coastal margin. The influence of the flows from the Antarctic Plateau on coastal locations varies depending on the location. As demonstrated by Parish and Bromwich (1987) and Parish and Bromwich (2007), the volume of air moving off inland Antarctica toward the coastal margin displays significant spatial variability due to the topographic slope and orientation of the underlying ice sheets. Northward transport of air from the plateau is enhanced in a few locations called confluence zones – *e.g.*, the broad region upslope from the Ross Ice Shelf at 175° E and the area near Adélie Land at 142° E – but can be sporadically observed elsewhere explaining the aforementioned observations at NM, TR, or TNB. Monitoring atmospheric mercury at a coastal station situated close to a confluence zone could provide new insights regarding the extent of the transport of reactive air masses from the Antarctic Plateau. This topic is addressed in a companion paper (Angot et al., 2016a). The Antarctic continent shelters unconventional atmospheric pathways of mercury reactivity both in winter and in summer. Its role should be taken into account in the modeling of the global geochemical cycle of mercury.

5.1.5 Conclusion

Mean summertime atmospheric Hg(0) concentration was ~ 25 % lower compared to values recorded at other Antarctic stations at the same period of the year, suggesting an intense oxidation of atmospheric Hg(0) within the shallow boundary layer as a result of the high oxidative capacity of the Antarctic Plateau atmosphere in this period of the year. This hypothesis is further supported by high total mercury concentrations in surface snow samples measured at the station (up to 74 ng L^{-1}). Our results confirm short-term observations by Brooks et al. (2008a) and Dommergue et al. (2012) of chemical exchange at the air-snow interface. During the sunlit period, Hg(0) concentration peaked in the upper layers of the snowpack. Summertime Hg(0) concentration in ambient air exhibited a pronounced diurnal cycle likely due to large emissions from the snowpack as a response to daytime snowpack ventilation. Our observations also reveal a decrease of atmospheric mercury concentrations in winter (24 h darkness) possibly due to the dry deposition of Hg(0). Interestingly, this decreasing trend has never been observed elsewhere. Additionally, Hg(0) concentrations increased with depth in the snow interstitial air in winter likely due to a dark reduction of Hg(II) species accumulated within the snowpack during the sunlit period. Finally, we reveal

the occurrence of multi-day to week-long depletion events of Hg(0) in ambient air in summer, that are not associated with depletion of O_3, and likely result from a stagnation of air masses on the plateau triggering an accumulation of oxidants in the shallow boundary layer. This behaviour is radically different from what is usually observed in the Arctic where only mercury depletion events that were associated with O_3 depletion (and with a $Hg(0)/O_3$ correlation) have been highlighted so far. According to observations at coastal Antarctic stations (see section 5.1.4), the reactivity observed at DC can be transported at a continental scale by strong katabatic winds. Our understanding of the atmospheric mercury chemistry on the Antarctic Plateau is currently limited by the lack of continuous halogens measurements. Our findings point out new directions for future kinetic, observational, and modeling studies.

Data availability

Mercury data reported in this paper are available upon request at http://sdi.iia.cnr.it/geoint/publicpage/GMOS/gmos_historical.zul.

Acknowledgements

Mercury data reported in this paper are available upon request at http://sdi.iia.cnr.it/geoint/publicpage/GMOS/gmos_historical.zul. We thank A. Barbero and the rest of the overwintering crew: S. Aubin, C. Lenormant, and R. Jacob. We also gratefully acknowledge M. Barret for the development of a QA/QC software program, L. Bonato for the analysis of total mercury in surface snow samples, D. Liptzin for the calculation of the Obukhov length and friction velocity, M. Legrand for the 2012 ozone data, C. Genthon for the meteorological data, E. Vignon for helpful discussion, and B. Jourdain and X. Faïn for their help in the field. This work contributed to the EU-FP7 project Global Mercury Observation System (GMOS – www.gmos.eu) and has been supported by a grant from Labex OSUG@2020 (Investissements d'avenir – ANR10 LABX56), and the Institut Universitaire de France. BQ and PR acknowledge ANR CLIMSLIP and HAMSTRAD Program 910, respectively. Logistical and financial support was provided by the French Polar Institute IPEV (Program 1028, GMOstral and Program 1011, SUNITEDC), and a grant from the U.S. National Science Foundation (NSF, PLR#1142145). Computing resources for FLEXPART simulations were provided by the IPSL CICLAD/CLIMSERV mesocenter. Meteorological data were obtained thanks to LEFE/IMAGO programs CLAPA and GABLS4, IPEV program CALVA/1013, and Observatoire des Sciences de l'Univers de Grenoble (GLACIOCLIM observatory).

5.1.6 Compléments d'information

5.1.6.1 Résumé des principaux résultats et conclusions de l'article

L'article ci-avant propose, pour la première fois sur la calotte glaciaire antarctique, une série temporelle de deux ans de mesures de concentrations en Hg(0). Il s'agit également de la première étude proposant la mesure, sur une année complète, des concentrations en Hg(0) à différentes profondeurs dans l'air du manteau neigeux. En été, le jour est perpétuel et la capacité oxydante de la couche limite atmosphérique très élevée (Eisele et al., 2008; Kukui et al., 2014). Les données acquises à DC montrent que la concentration moyenne en Hg(0) à cette période de l'année y est ~ 25 % plus basse qu'aux stations côtières. Ce résultat suggère une oxydation intense de Hg(0) en présence de concentrations élevées en oxydants. Cette hypothèse est par ailleurs confortée par les concentrations élevées en mercure total (jusqu'à 74 ng L^{-1}) mesurées au cours de cette étude en surface du manteau neigeux à DC et celles en espèces divalentes mesurées à Pôle Sud (Brooks et al., 2008a). Les données acquises à DC confirment par ailleurs l'hypothèse d'échanges estivaux d'espèces mercurielles à l'interface air-neige avancée par Brooks et al. (2008a) et Dommergue et al. (2012). La concentration en Hg(0) est maximale dans les couches de surface du manteau neigeux. En raison de l'existence de processus de réémissions, il en résulte, chaque jour à la mi-journée, une concentration maximale dans la couche limite atmosphérique. En hiver, la nuit est perpétuelle et les données acquises à DC révèlent une diminution progressive des concentrations atmosphériques en Hg(0). Le dépôt sec de Hg(0) au cours de l'hiver est une des hypothèses privilégiées pour expliquer ce phénomène inédit et les données d'observations suggèrent une vitesse de dépôt de 9.3×10^{-5} cm s^{-1}, vitesse en accord avec la littérature (Zhang et al., 2009). Les données acquises au sein du manteau neigeux pendant la période hivernale montrent par ailleurs une augmentation des concentrations en Hg(0) avec la profondeur, probablement en raison de la réduction des espèces oxydées accumulées au cours de l'année. Enfin, les données acquises à DC révèlent l'existence d'épisodes de déplétion de Hg(0) pouvant durer plusieurs semaines. Contrairement aux AMDE couramment observés au printemps sur la côte en régions polaires (voir section 2.1.1.1), ces épisodes de déplétion se déroulent en été et ne sont pas concomitants avec des déplétions d'ozone. L'analyse des rétro-trajectoires suggère une stagnation des masses d'air au-dessus du plateau antarctique pouvant engendrer une accumulation d'oxydants au sein de la couche limite atmosphérique et ainsi la déplétion de Hg(0). Cette étude révèle ainsi des processus inédits en termes de réactivité sur le plateau antarctique. L'existence de forts vents catabatiques s'écoulant du plateau vers les côtes suggère que les processus observés à DC sur la calotte glaciaire pourraient influer sur le cycle du mercure à l'échelle continentale. Les épisodes de vents catabatiques étant une constante du climat de la côte de Terre Adélie, les données enregistrées à DDU devraient permettre d'évaluer dans quelle mesure les processus observés sur le plateau antarctique influent sur le cycle du mercure à plus large échelle. Cette question fait l'objet de la section 5.2.

5.1.6.2 Données ultérieures à l'article

L'article présenté ci-avant propose une interprétation des données de concentrations en Hg(0) acquises entre janvier 2012 et décembre 2013. Comme indiqué au sein de la section 3.2.3, les mesures sont toujours en cours à DC. L'ensemble des données acquises entre janvier 2012 et fin juillet 2016 est présenté sur la Figure 5-13.

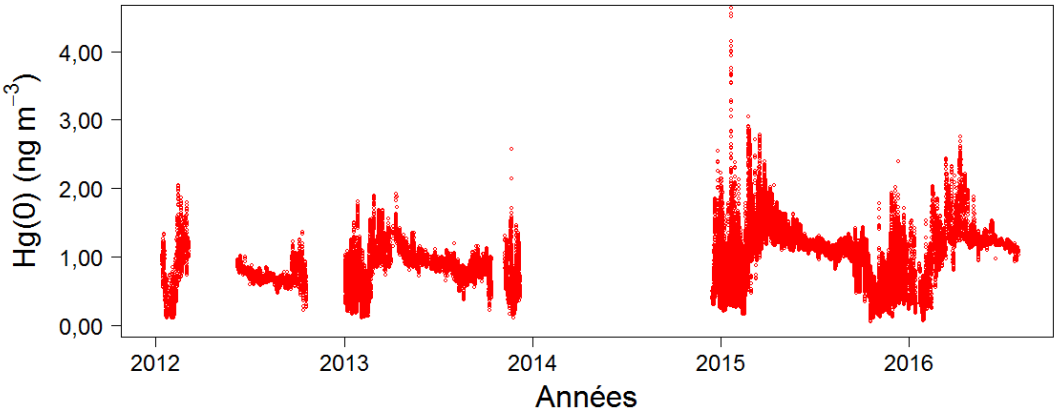

Figure 5-13: Concentrations moyennes en Hg(0) (pas de temps horaire, en ng m^{-3}) enregistrées à DC entre janvier 2012 et fin juillet 2016. Les données de l'année 2013 sont celles à 210 cm. Une défaillance de l'instrument de mesures explique l'absence de données en 2014.

Comme indiqué précédemment, la concentration moyenne (± écart-type) en Hg(0) est de 0,76 ± 0,24 ng m^{-3} en 2012 et de 0,84 ± 0,27 ng m^{-3} en 2013 (à 210 cm). Les mesures effectuées depuis montrent une concentration moyenne de 1,06 ± 0,41 ng m^{-3} en 2015 et de 1,18 ± 0,39 ng m^{-3} entre janvier et fin juillet 2016. Les concentrations plus élevées en 2015 et 2016 peuvent s'expliquer, au moins en partie, par la mise en place d'un nouvel instrument de mesures suite à la panne de 2014. Ceci sera discuté plus en détails au sein du chapitre 6. Il est toutefois intéressant de noter que le cycle saisonnier (concentrations très variables en été, décroissance progressive en hiver) est systématiquement observé. De même qu'à AMS (voir section 4.1.5.2), une membrane échangeuse de cations (polyéthersulfone (PES), porosité 0,45 µm, 47 mm de diamètre), censée piéger les espèces divalentes, a été installée en décembre 2015 en entrée de ligne de prélèvement. Les premiers résultats sont décrits au sein de la section 5.1.6.3.1 tandis que le protocole mis en place ainsi que les tests d'assurance qualité réalisés ou à réaliser sont décrits au sein de l'Annexe 3.

5.1.6.3 Travaux en cours

5.1.6.3.1 Utilisation de filtres PES pour le suivi des concentrations en espèces divalentes

Des tests ont été réalisés au cours de la campagne d'été 2014 à DC et les premiers résultats nous sont parvenus fin 2015. Trois filtres PES ont successivement été installés en amont de la ligne de prélèvement et analysés par la suite au laboratoire Géosciences Environnement Toulouse (GET, digestion du filtre à l'eau régale inverse et analyse par spectroscopie de fluorescence atomique (Tekran® 2600)). L'analyse a révélé les

concentrations moyennes suivantes en mercure divalent pour les trois périodes de collecte : 479, 378 et 454 pg m^{-3}. Ces concentrations sont dans la gamme de celles mesurées à Pôle Sud par Brooks et al. (2008a) et confirment notre hypothèse de concentrations élevées en espèce divalentes en été à DC. Considérant un bruit de fond atmosphérique en Hg(0) + Hg(II) de l'ordre de 1,0-1,1ng m^{-3} dans l'Hémisphère Sud (voir Chapitre 4) et une concentration moyenne estivale en Hg(0) de l'ordre de 0,7 ng m^{-3} à DC (voir section 5.1.3.1.2), ces concentrations en espèces divalentes pourraient permettre de boucler le bilan de concentrations en espèces mercurielles atmosphériques. Si les tests d'assurance qualité s'avèrent concluants (résultats attendus courant 2017), ces filtres pourraient permettre d'étudier plus finement le cycle journalier des concentrations en espèces divalentes.

5.1.6.3.2 Développement d'un modèle de boîte

Les mesures de concentrations en Hg(0) effectuées à DC ont permis de mettre en évidence le dynamisme du cycle atmosphérique du mercure en été. Les données acquises dans la couche limite atmosphérique ainsi qu'à différentes profondeurs dans l'air du manteau neigeux suggèrent par ailleurs l'existence de processus de réémissions quotidiens de Hg(0) par les couches superficielles du manteau neigeux. Notre compréhension des processus d'oxydo-réduction et de réémissions est cependant limitée. Dans le cadre d'une collaboration entre le Massachussetts Institute of Technology (MIT) et le LGGE (MISTI Global Seed Funds), un modèle de boîte est actuellement en cours de développement. Ce projet, mené par Shaojie Song doctorant au MIT, a pour objectif d'identifier les facteurs contribuant à la réactivité unique observée en été sur la calotte glaciaire antarctique. Cette collaboration permet de tirer profit du savoir-faire du MIT en termes de modélisation du cycle du mercure et de l'expertise des équipes du LGGE en termes d'observations et de modélisation des milieux polaires.

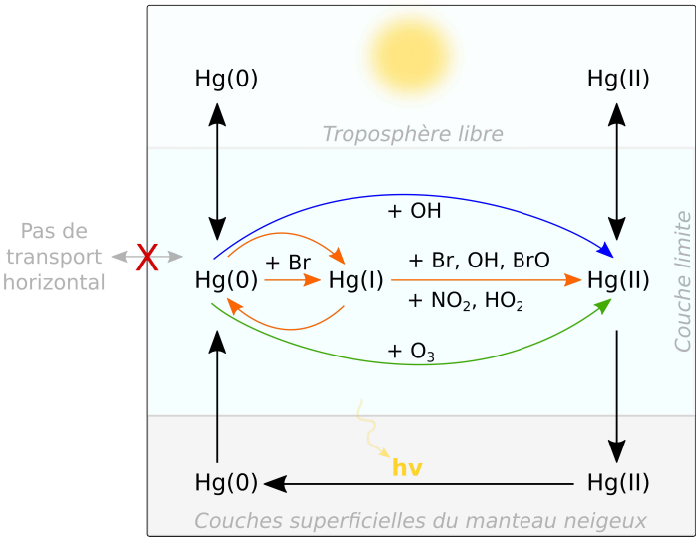

Figure 5-14: Paramétrisation du modèle de boîte en cours de développement dans le cadre d'une collaboration entre le MIT et le LGGE. L'objectif est d'étudier les réactions d'oxydo-réduction au sein de la couche limite atmosphérique à DC ainsi que les échanges d'espèces mercurielles entre la couche limite et la troposphère libre d'une part et la couche limite et les couches superficielles du manteau neigeux d'autre part.

La paramétrisation du modèle de boîte est résumée par la Figure 5-14. Les paramètres d'entrée du modèle incluent notamment les données d'observations *in situ* de concentrations en Hg(0), O_3 et NO_2 ainsi que de température et pression. La hauteur de la couche limite est simulée par MAR (Modèle Atmosphérique Régional) développé au LGGE (Gallée et al., 2015). Les concentrations en OH, RO_2 et BrO sont issues de la littérature (Kukui et al., 2014; Frey et al., 2015) et leur cycle diurne dépend du rayonnement solaire (ondes courtes). Ce modèle devrait permettre d'affiner notre compréhension des processus de réémissions à l'interface air-neige et d'évaluer les différents mécanismes d'oxydation et constantes de réactions associées.

5.2 Cycle atmosphérique du mercure en Antarctique de l'Est

D'après :

Angot, H., Dion, I., Vogel, N., Legrand, M., Magand, O., Dommergue, A.: Atmospheric mercury record at Dumont d'Urville, East Antarctic coast: continental outflow and oceanic influences, Atmospheric Chemistry and Physics 16, 8265-8279, 2016.

Abstract

Under the framework of the Global Mercury Observation System (GMOS) project, a 3.5-year record of atmospheric gaseous elemental mercury (Hg(0)) has been gathered at Dumont d'Urville (DDU, 66°40 S, 140°01 E, 43 m above sea level) on the East Antarctic coast. Additionally, surface snow samples were collected in February 2009 during a traverse between Concordia Station located on the East Antarctic Plateau and DDU. The record of atmospheric Hg(0) at DDU reveals particularities that are not seen at other coastal sites: a gradual decrease of concentrations over the course of winter, and a daily maximum concentration around midday in summer. Additionally, total mercury concentrations in surface snow samples were particularly elevated near DDU (up to 194.4 ng L^{-1}) as compared to measurements at other coastal Antarctic sites. These differences can be explained by the more frequent arrival of inland air masses at DDU than at other coastal sites. This confirms the influence of processes observed on the Antarctic Plateau on the cycle of atmospheric mercury at a continental scale, especially in areas subject to recurrent katabatic winds. DDU is also influenced by oceanic air masses and our data suggest that the ocean plays a dual role on Hg(0) concentrations. The open ocean may represent a source of atmospheric Hg(0) in summer whereas the sea-ice surface may provide reactive halogens in spring that can oxidize Hg(0). This paper also discusses implications for coastal Antarctic ecosystems and for the cycle of atmospheric mercury in high southern latitudes.

5.2.1 Introduction

The Antarctic continent is one of the last near-pristine environments on Earth and still relatively unaffected by human activities. Except for pollutants released from Antarctic Research stations (*e.g.*, Hale et al., 2008; Chen et al., 2015a) and by marine and air-borne traffic (Shirsat and Graf, 2009), only the long-lived atmospheric contaminants reach this continent situated far from anthropogenic pollution sources. With an atmospheric lifetime on the order of 1 year (Lindberg et al., 2007), gaseous elemental mercury (Hg(0)) is efficiently transported worldwide. Hg(0) is the most abundant form of mercury in the atmosphere (Lindberg and Stratton, 1998). It can be oxidized into highly reactive and water-soluble gaseous divalent species (Hg(II)) – that can bind to existing particles and form particulate mercury (Hg(p)) – leading to the deposition of reactive mercury onto various environmental surfaces through wet and dry processes (Lindqvist and Rodhe, 1985; Lin and Pehkonen, 1999). Upon deposition, Hg(II) can be reduced and re-emitted back to the atmosphere as Hg(0) (Schroeder and Munthe, 1998). Assessing mercury deposition and reemission pathways remains difficult due to an insufficient understanding of the involved physic-chemical processes.

Only sparse measurements of atmospheric mercury have been performed in Antarctica and there are still many gaps in our understanding of its cycle at the scale of this vast continent (~ 14 million km^2) (Dommergue et al., 2010b). To date, observations were made over 1 year at the coastal site of Neumayer (NM, Ebinghaus et al., 2002b; Temme et al., 2003) and during summer campaigns at Terra Nova Bay (TNB, Sprovieri et al., 2002) and McMurdo (MM, Brooks et al., 2008b). More recently, multi-year records have been obtained at Troll (TR) situated approximately 220 km from the coast at 1275 m a.s.l. (Pfaffhuber et al., 2012) and Concordia Station located at Dome C (denoted DC, 3220 m a.s.l.) (Angot et al., 2016b). Under the framework of the GMOS project (Global Mercury Observation System, www.gmos.eu), atmospheric monitoring of Hg(0) has been implemented at Dumont d'Urville (DDU) located in Adélie Land (Figure 5-1) and we here report the obtained 3.5-year record of atmospheric Hg(0) that represents the first multi-year record of Hg(0) available for the East Antarctic coast. In this paper, the Hg(0) record from DDU is discussed in terms of influence of marine versus inland air masses, and compared to records available at other coastal (NM, TNB, MM) or near-coastal (TR) stations. In parallel, total mercury was determined in surface snow samples collected during a traverse between DC and DDU in February 2009. These results provide new insight into the transport and deposition pathways of mercury species in East Antarctica.

5.2.2 Experimental Section

5.2.2.1 Sampling site and prevailing meteorological conditions

From January 2012 to May 2015, Hg(0) measurements were performed at DDU station located on a small island (Ile des Pétrels) about 1 km offshore from the Antarctic mainland. A

detailed description of the sampling site ("Labo 3") has been given by Preunkert et al. (2013) while the climatology of this coastal station has been detailed by König-Langlo et al. (1998). The average surface air temperature ranges from -1 °C in January to -17 °C in winter, with a mean annual temperature of -12 °C. The annual mean surface wind speed is 10 m s^{-1}, with no clear seasonal variations. Due to the strong katabatic effects, the most frequent surface wind direction is 120° E-160° E.

5.2.2.2 Methods

5.2.2.2.1 Hg(0) measurements

Hg(0) measurements were performed using a Tekran 2537B (Tekran Inc., Toronto, Canada). The sampling resolution ranged from 10 to 15 minutes with a sampling flow rate of 1.0 L min^{-1}. Concentrations are reported here as hourly averages and are expressed in nanograms per cubic meter at standard temperature and pressure (273.15 K, 1013.25 hPa). Setting a 0.2 µm PTFE filter and a 10 m-long unheated sampling line on the front of the analyzer inlet, we assume that mainly Hg(0) (instead of total gaseous mercury, defined as the sum of gaseous mercury species) was efficiently collected and subsequently analyzed by the instrument (Steffen et al., 2002; Temme et al., 2003; Steffen et al., 2008).

External calibrations were performed twice a year by manually injecting saturated mercury vapor taken from a temperature-controlled vessel, using a Tekran 2505 mercury vapor calibration unit and a Hamilton digital syringe, and following a strict procedure adapted from Dumarey et al. (1985). As described by Angot et al. (2014), fortnightly to monthly routine maintenance operations were performed. A software program was developed at the LGGE (Laboratoire de Glaciologie et Géophysique de l'Environnement) following quality control practice commonly applied in North American networks (Steffen et al., 2012). Based on various flagging criteria (Munthe et al., 2011; D'Amore et al., 2015), it enabled rapid data processing in order to produce clean time series of Hg(0). According to the instrument manual, the detection limit is 0.10 ng m^{-3} (Tekran, 2011).

5.2.2.2.2 Snow sampling and analysis

Eleven surface snow samples (the upper 3 cm) were collected during a traverse between DC and DDU conducted in February 2009. As described by Dommergue et al. (2012), samples were collected using acid cleaned PTFE bottles and clean sampling procedures. After sampling, samples were stored in the dark at -20 °C. Field blanks were made by opening and closing a bottle containing mercury-free distilled water. Total mercury (Hg_{tot}) in snow samples was analyzed using a Tekran Model 2600. Hg_{tot} includes species such as $HgCl_2$, $Hg(OH)_2$, HgC_2O_4, stable complexes such as HgS and Hg(II) bound to sulfur in humic compounds, or some organomercuric species (Lindqvist and Rodhe, 1985). The instrument was calibrated with the NIST SRM-3133 mercury standard. Quality assurance and quality control included the analysis of analytical blanks, replicates, and internal standards (reference waters for mercury: HG102-2 at 22 ng L^{-1} from Environment Canada). The limit of

quantification – calculated as 10 times the standard deviation of a set of 3 analytical blanks – was 0.3 ng L^{-1} and the relative accuracy ± 8 %.

Surface snow samples collected during traverses may have limited spatial and temporal representativeness given the variability of chemical species deposition onto the snow surface, and the occurrence of either fresh snowfall or blowing snow. The (in)homogeneity of surface snow samples was investigated at MM by Brooks et al. (2008b). Surface (3-5 cm) snow samples were collected daily (n = 14) at different snow patches. Hg_{tot} concentrations averaged 67 ± 21 ng L^{-1}. This result indicates that the spatial and temporal representativeness of surface snow samples collected in Antarctica can be satisfactory and gives us confidence that spatial differences in Hg_{tot} concentrations reported in section 5.2.3.2.2 are not due to samples inhomogeneity.

5.2.2.2.3 Ancillary parameters

O_3 was continuously monitored with a UV absorption monitor (Thermo Electron Corporation model 49I, Franklin, Massachusetts) (Legrand et al., 2009). Collected at 15-s intervals, the data are reported here as hourly averages.

Back trajectories were computed using the HYSPLIT (Hybrid Single-Particle Lagrangian Integrated Trajectory) model (Draxler and Rolph, 2013). Meteorological data from Global Data Assimilation Process (available at ftp://arlftp.arlhq.noaa.gov/pub/archives/gdas1) were used as input, and the model was run every hour in backward mode for 5 days at 0, 200, and 500 m above the model ground level. Three typical situations prevail at DDU: strong katabatic winds flowing out from the Antarctic ice sheet situated south of the station, pure marine air masses, or continental/marine mixed air masses with easterly winds due to the arrival near the site of low-pressure systems (König-Langlo et al., 1998). Oceanic origin was attributed to air masses having traveled at least 1 day over the ocean and less than 3 days out of 5 over the high-altitude Antarctic Plateau. Conversely, plateau origin refers to air masses having traveled at least 3 days over the high-altitude Antarctic Plateau and less than 1 day out of 5 over the ocean. Finally, mixed origin refers to air masses having traveled less than 1 and 3 days out of 5 over the ocean and the high-altitude Antarctic Plateau, respectively. It should be noted that uncertainties associated with calculated backward trajectories arise from possible errors in input meteorological fields and numerical methods (Yu et al., 2009), and increase with time along the way (Stohl, 1998). According to Jaffe et al. (2005), back trajectories only give a general indication of the source region. Despite these limitations, back trajectories remained very similar at the three levels of altitude arrival at the site and we only use here those arriving at the model ground level. This method also gave consistent results with respect to the origin of various chemical species including O_3 (Legrand et al., 2009), HCHO (Preunkert et al., 2013), NO_2 (Grilli et al., 2013), and sea-salt aerosol (Legrand et al., 2016a)

5.2.2.3 Local contamination

Pollution plumes due to the station activities (*e.g.*, combustion, vehicular exhaust) occasionally reached the sampling site. Such local pollution events can be easily identified for instance by the fast decrease of O_3 or increase of HCHO mixing ratios (Legrand et al., 2009; Preunkert et al., 2013). We used a criterion based on wind direction and sudden drops of O_3 mixing ratios to filter the raw data (*i.e.*, collected at 5 min intervals) and discard Hg(0) data impacted by local pollution. Raw Hg(0) data above 1.60 ng m^{-3}, corresponding to the mean + 3 standard deviation, obtained when the wind was blowing from 30° W to 70° E (*i.e.*, the sector where main station activities are located), and accompanied by a drop of O_3 were discarded from the data set. Using this criterion, only 0.1 % of raw Hg(0) data was discarded, the Hg(0) record being very weakly impacted by pollution plumes.

5.2.3 Results and Discussion

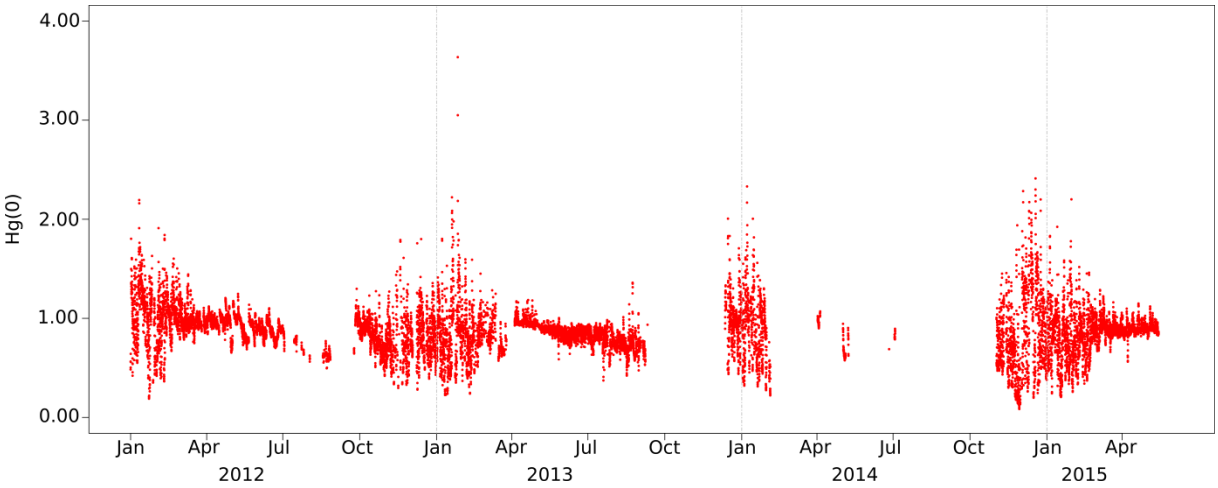

Figure 5-15: Hourly averaged Hg(0) concentrations (ng m^{-3}) measured at DDU from January 2012 to May 2015. Missing data are due to instrument failure or QA/QC invalidation. Hg(0) concentrations were highly variable during the sunlit period as compared to wintertime (May-August) suggesting a photochemically induced reactivity in this period of the year.

The record of atmospheric Hg(0) from January 2012 to May 2015 is displayed in Figure 5-15. Hourly averaged Hg(0) concentrations ranged from 0.10 to 3.61 ng m^{-3}, with an average value of 0.87 ± 0.23 ng m^{-3} (mean ± standard deviation). This mean annual Hg(0) concentration is in good agreement with the value of 0.93 ± 0.19 ng m^{-3} (4-year average) reported by Pfaffhuber et al. (2012) at TR, but lower than the concentration of 1.06 ± 0.24 ng m^{-3} (12-month average) reported by Ebinghaus et al. (2002b) at NM. While the same device was used at the three stations, the measurements may target different mercury species depending on their configuration (*e.g.*, heated/unheated sample line). The difference between total gaseous mercury and Hg(0) data can be rather substantial since gaseous oxidized mercury (Hg(II)) concentrations of up to ~ 0.30 ng m^{-3} were reported in spring/summer at several coastal Antarctic stations (Sprovieri et al., 2002; Temme et al., 2003; Brooks et al.,

2008b). To allow a more accurate comparison of data available at the various Antarctic stations, more harmonized sampling protocols are needed. Seasonal boundaries have been defined as follows: summer refers to November-February, fall to March-April, winter to May-August, and spring to September-October. Though being arbitrary, this dissection was done by considering the time period over which the halogen chemistry (September-October) or the OH/NO_x chemistry (November-February) is dominant at DDU (see sections 5.2.3.1.2 and 5.2.3.2.2). The mechanisms which cause the seasonal variation of Hg(0) concentrations are discussed in the following sections.

5.2.3.1 From winter darkness to spring sunlight

5.2.3.1.1 Continental outflow and advection from lower latitudes in winter

A gradual 20 % decrease in Hg(0) concentrations from 0.89 ± 0.09 in average in May to 0.72 ± 0.10 ng m^{-3} in August (Figure 5-16a) was observed at DDU. Conversely, concentrations remained rather stable at NM and TR in winter with mean values of 1.15 ± 0.08 and 1.00 ± 0.07 ng m^{-3}, respectively (Ebinghaus et al., 2002b; Pfaffhuber et al., 2012). Pfaffhuber et al. (2012) suggested that this stability of Hg(0) concentrations at TR is related to a lack of oxidation processes during the polar night.

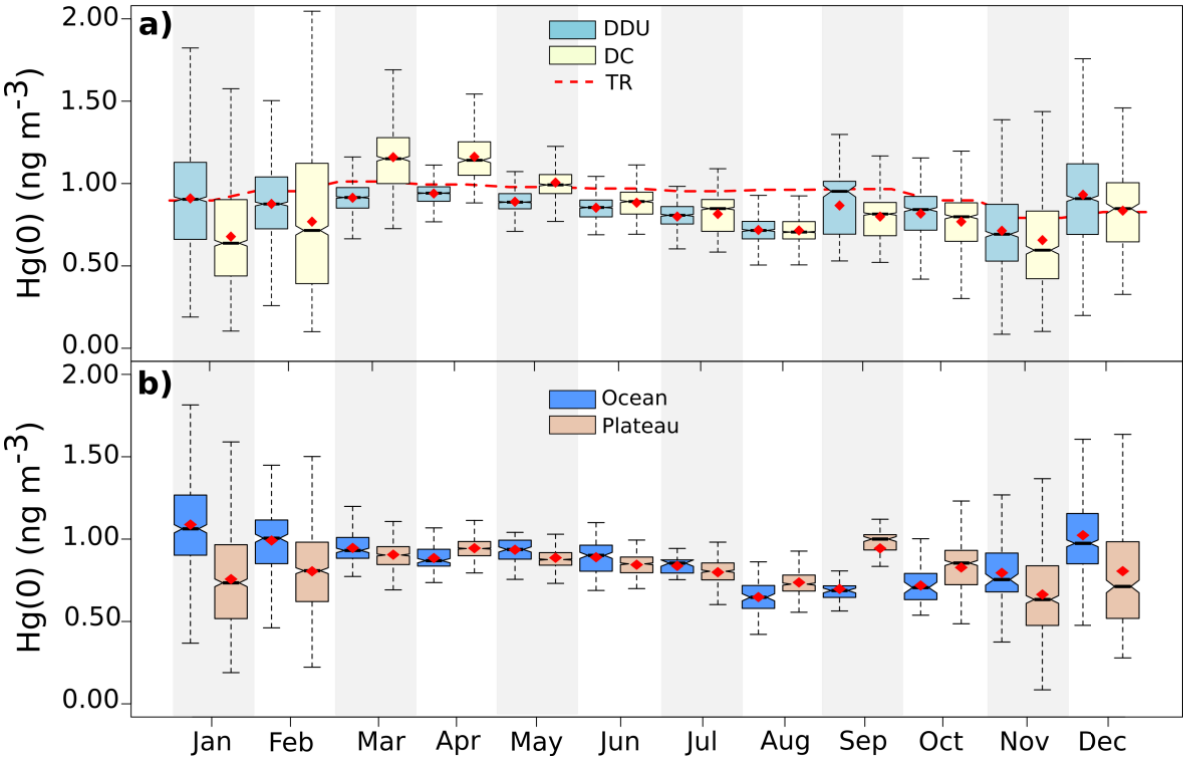

Figure 5-16: Box and whisker plot presenting the monthly Hg(0) concentration distribution **a)** from all the data collected at DDU and DC along with the monthly mean recorded at TR, and **b)** from all the data collected at DDU associated with air masses originating from the ocean or the Antarctic Plateau according to the HYSPLIT simulations. ◆ mean, bottom and top of the box: first and third quartiles, band inside the box: median, ends of the whiskers: lowest (highest) datum still within the 1.5 interquartile range of the lowest (upper) quartile. Outliers are not represented.

A local reactivity at DDU – absent at other coastal stations – seems unlikely. Angot et al. (2016b) showed evidence of a gradual 30 % decrease of Hg(0) concentrations at DC at the same period of the year (Figure 5-16a), probably due to a gas-phase oxidation, heterogeneous reactions, or dry deposition of Hg(0) onto the snowpack. Since the decreasing trend observed in winter is less pronounced at DDU than at DC, it most likely results from reactions occurring within the shallow boundary layer on the Antarctic Plateau, subsequently transported toward the coastal margins by katabatic winds. This assumption is supported by the HYSPLIT model simulations showing prevalence in winter (62 ± 23 %) of air masses originating from the Antarctic Plateau reaching DDU (Figure 5-17). The export of inland air masses towards the coastal regions is not uniform across Antarctica and is concentrated in a few locations – "confluence zones" – such as the Amery Ice Shelf region, the area near Adélie Land at 142°, the broad region upslope from the Ross Ice Shelf, and the eastern side of the Antarctic Peninsula at ~ 60° W (Figure 5-1) (Parish and Bromwich, 1987, 2007). Given its geographic location, DDU in Adélie Land lies close to a confluence zone explaining the extent of the transport of air masses from the Antarctic Plateau. Conversely, several studies showed that stations such as NM and HA are not significantly impacted by air masses originating from the Antarctic Plateau (Helmig et al., 2007; Legrand et al., 2016b), consistently explaining why Hg(0) concentrations did not decrease at NM and TR throughout winter (Ebinghaus et al., 2002b; Pfaffhuber et al., 2012).

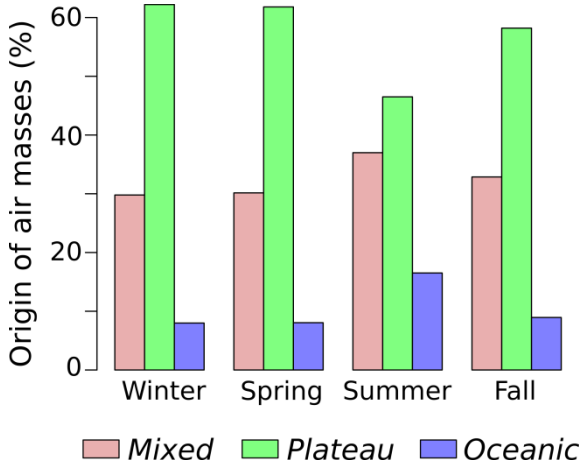

Figure 5-17: Mean percentage (%) of continental/oceanic mixed air masses (pink), and of air masses originating from the Antarctic Plateau (green) or the ocean (blue) according to the HYSPLIT model simulations in winter (May to August), spring (September to October), summer (November to February), and fall (March to April).

Despite the overall decreasing trend in winter, Hg(0) concentrations sporadically exhibited abrupt increases when warm air masses from lower latitudes reached DDU. As illustrated by Figure 5-18, Hg(0) concentration for example increased from 0.72 (8 June 2012) to 1.10 ng m^{-3} (14 June 2012) with increasing temperature, and a significant positive correlation was found between the two parameters ($r = 0.88$, p value < 0.0001, Spearman test). This result is supported by an enhanced fraction of oceanic air masses reaching DDU at that time according to the HYSPLIT model simulations (Figure 5-18d). Consistently, aerosol

data gained in the framework of the French environmental observation service CESOA (http://www-lgge.obs.ujf-grenoble.fr/CESOA/spip.php?rubrique3) dedicated to the study of the sulfur cycle at middle and high southern latitudes indicate a mean sodium concentration of 450 ng m^{-3} between 10 and 14 June 2012 (not shown) instead of 112 ± 62 ng m^{-3} over the other days of this month. It can be noted that the mean Hg(0) concentration in June 2012 was 0.95 ± 0.04 ng m^{-3} at TR (Slemr et al., 2015), and 1.02 ± 0.04 ng m^{-3} on Amsterdam Island (37°48 S, 77°34 E, Angot et al., 2014). These values are consistent with the increase seen at DDU in air masses arriving from lower latitudes.

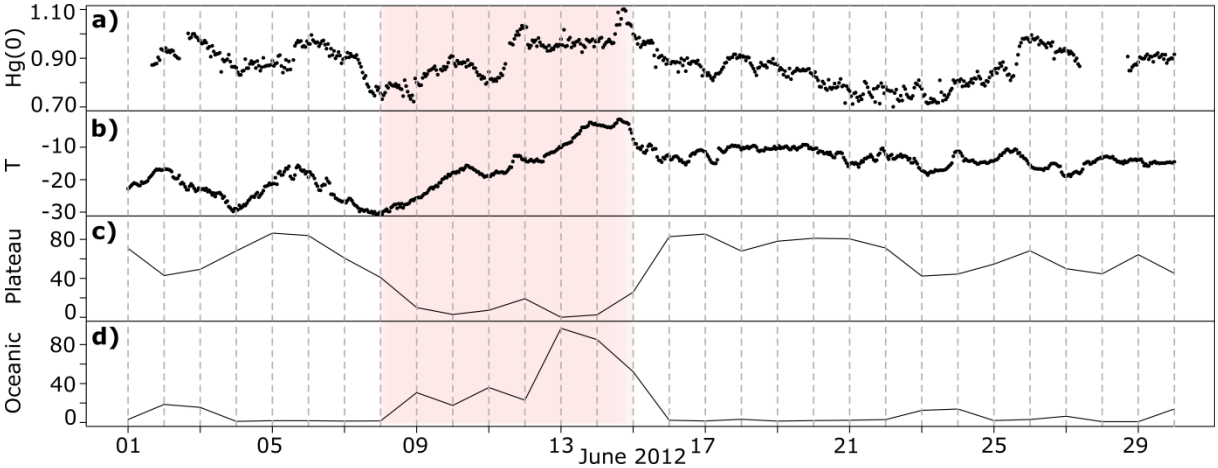

Figure 5-18: June 2012 variation of **a)** Hg(0) concentration (ng m^{-3}), **b)** temperature (°C), **c)** daily averaged percentage (%) of air masses originating from the Plateau (HYSPLIT model simulations), and **d)** daily averaged percentage (%) of air masses originating from the ocean (HYSPLIT model simulations). From 8 to 14 June (period highlighted in red), both Hg(0) and temperature increased suggesting an advection of air masses from midlatitudes, as confirmed by an elevated percentage of oceanic air masses.

5.2.3.1.2 The ice-covered ocean as a sink for Hg(0) in spring

First discovered in the Arctic in 1995 (Schroeder et al., 1998), atmospheric mercury depletion events (AMDEs) have been subsequently observed after polar sunrise (mainly from early September to the end of October) at coastal or near-coastal Antarctic stations at NM (Ebinghaus et al., 2002b), TNB (Sprovieri et al., 2002), MM (Brooks et al., 2008b), and TR (Pfaffhuber et al., 2012). These events, characterized by abrupt decreases of Hg(0) concentrations below 1.00 ng m^{-3} in the Arctic and 0.60 ng m^{-3} in Antarctica (Pfaffhuber et al., 2012), result from the oxidation of Hg(0) by reactive bromine species (e.g., Schroeder et al., 1998; Lu et al., 2001; Brooks et al., 2006a; Sommar et al., 2007). At DDU, Hg(0) data covering the spring time period are scarce (Figure 5-15) and we can just emphasize that the absence of Hg(0) drops in October 2012 tends to suggest that AMDEs, if exist, are not very frequent at DDU. Ozone depletion events (ODEs) are found to be less frequent and far less pronounced at DDU compared to other coastal stations such as NM and HA (Legrand et al., 2009; Legrand et al., 2016b). Based on the oxygen and nitrogen isotope composition of airborne nitrate at DDU, Savarino et al. (2007) concluded to an absence of significant implication of BrO in the formation of nitric acid at this site, contrarily to what is usually

observed in the Arctic where high levels of BrO are measured at polar sunrise (Morin et al., 2008). All these observations are consistent with a less efficient bromine chemistry in East compared to West Antarctica due to a less sea-ice coverage, as also supported by GOME-2 satellite observations of the tropospheric BrO column (Theys et al., 2011; Legrand et al., 2016a). Additionally, air masses originating from the Antarctic Plateau prevailed (62 ± 23 %, Figure 5-17) in spring at DDU according to the HYSPLIT model simulations. This can also explain, to some extent, the lack of AMDE-observations at DDU.

Despite the absence of large AMDEs at DDU, springtime oceanic air masses were associated with low Hg(0) concentrations (0.71 ± 0.11 ng m^{-3}, Figure 5-16b). A slight but significant negative correlation was found between Hg(0) concentrations in spring and the daily averaged percentage of oceanic air masses reaching DDU (r = -0.38, *p* value = 0.01, Spearman test) while a significant positive correlation was observed between springtime Hg(0) concentrations and O_3 mixing ratios in these oceanic air masses (r up to 0.65, *p* value < 0.0001, Spearman test). Therefore, though being not as pronounced as AMDEs observed at other coastal stations, we cannot rule out that the rather low background Hg(0) levels observed in spring at DDU are due to a weak effect of the bromine chemistry.

5.2.3.2 High variability of Hg(0) concentrations in summer

Hg(0) concentrations were highly variable during the sunlit period as compared to wintertime (Figure 5-15). Figure 5-19 displays processes that may govern the atmospheric mercury budget at DDU in summer, as discussed in the following sub-sections.

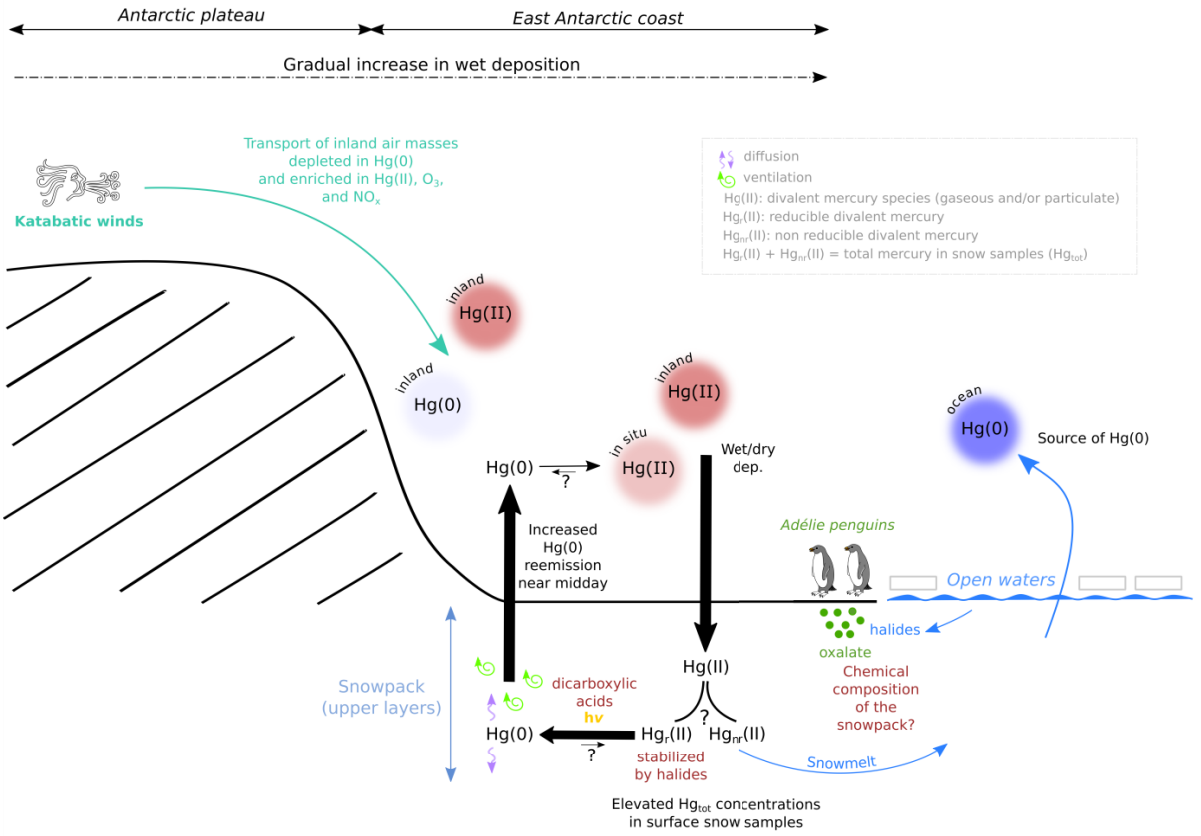

Figure 5-19: Schematic diagram illustrating the processes that may govern the mercury budget at DDU in summer. Katabatic winds transport inland air masses enriched in oxidants and Hg(II) toward the coastal margins. Hg(II) species deposit onto the snowpack by wet and dry processes leading to elevated concentrations of total mercury in surface snow samples. A fraction of deposited mercury can be reduced (the reducible pool, $Hg_r(II)$) in the upper layers of the snowpack and subsequently re-emitted to the atmosphere as Hg(0). Hg(0) emission from the snowpack maximizes near midday likely as a response to daytime heating. The chemical composition of the snowpack (halides, dicarboxylic acids) may influence the reduction rate of Hg(II) species within the snowpack. The ocean may be a net source of Hg(0) to the atmosphere.

5.2.3.2.1 Diurnal cycle of Hg(0) in ambient air

Figure 5-20 displays the monthly mean diurnal cycle of Hg(0) concentrations at DDU. Undetected from March to October, a diurnal cycle characterized by a noon maximum was observed in summer (November to February). Interestingly, Pfaffhuber et al. (2012) did not observe any diurnal variation in Hg(0) concentrations at TR and there is no mention of a daily cycle at NM, TNB, and MM (Ebinghaus et al., 2002b; Temme et al., 2003; Sprovieri et al., 2002; Brooks et al., 2008b).

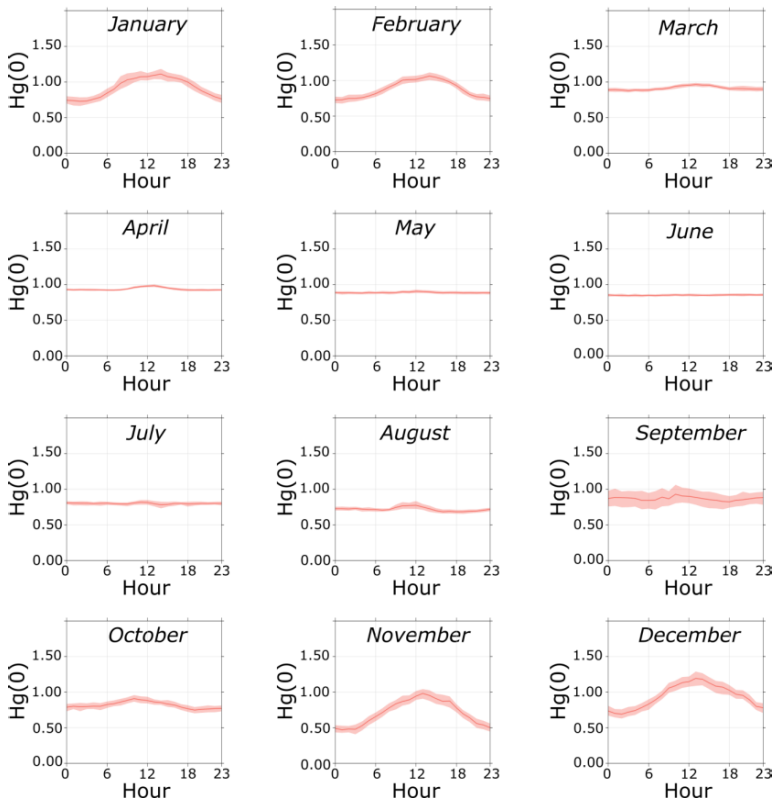

Figure 5-20: Monthly mean diurnal cycle of Hg(0) concentrations (in ng m^{-3}) along with the 95 % confidence interval for the mean, calculated from all the data collected at DDU (January 2012-May 2015). Hours are in local time (UTC+10). Hg(0) concentrations exhibit a strong diurnal cycle in summer (November to February).

Hg(0) concentrations at DDU were sorted according to wind speed and direction. With north at 0°, oceanic winds ranged from 270 to 110° E, coastal winds from 110 to 130° E,

katabatic winds from 160 to 180° E, and continental winds from 130 to 160° E and from 180 to 270° E. Summertime Hg(0) concentrations exhibited a diurnal cycle regardless of wind speed and direction (Figure 5-21). This result indicates that the observed diurnal cycle involves a local source of Hg(0) around midday which is, moreover, specific to DDU since the diurnal cycle is not observed at other coastal stations.

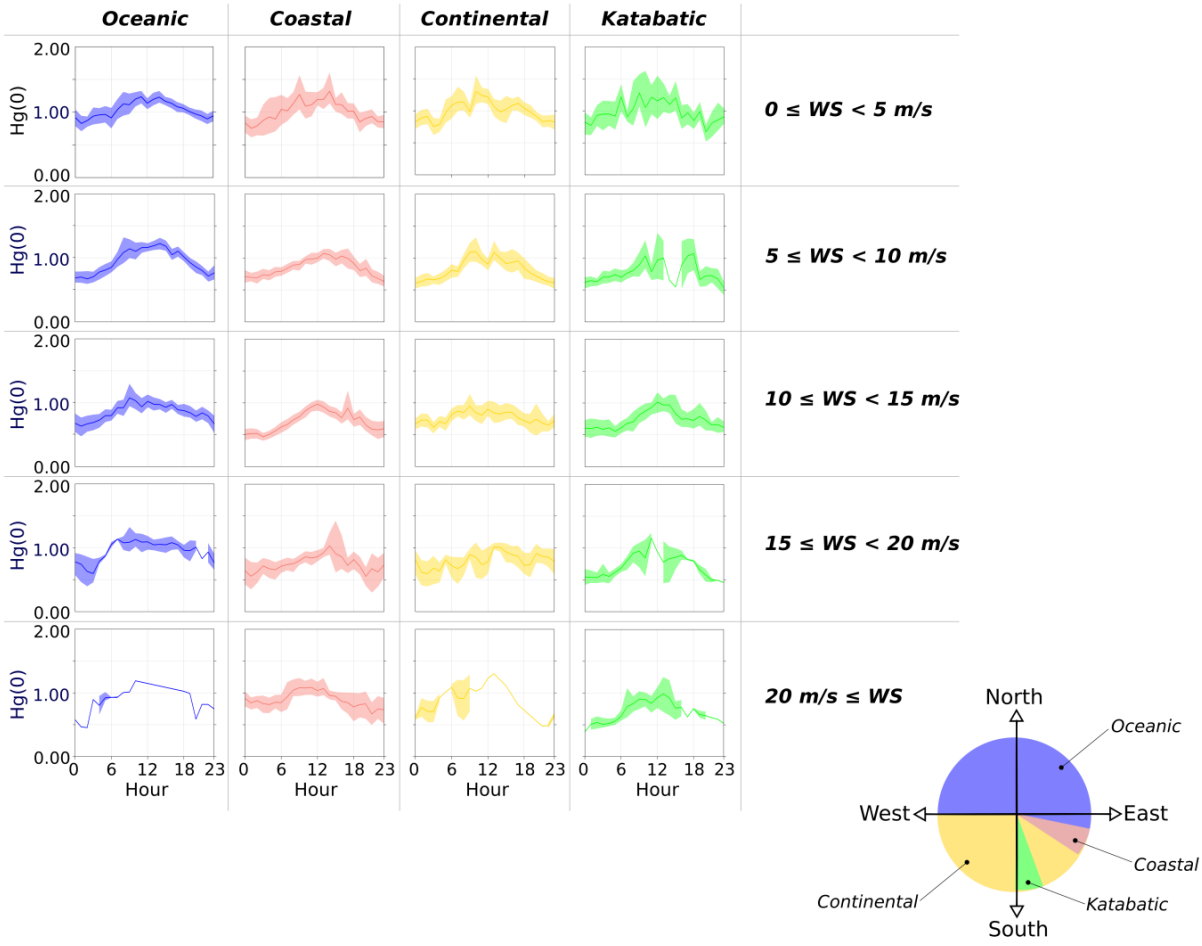

Figure 5-21: Summertime (November to February) mean diurnal cycle of Hg(0) concentrations (in ng m^{-3}), along with the 95 % confidence interval for the mean, depending on wind direction and wind speed. With north at 0°, oceanic winds ranged from 270 to 110°, coastal winds from 110 to 130°, katabatic winds from 160 to 180°, and continental winds from 130 to 160° and from 180 to 270°. Hours are in local time (UTC+10). Hg(0) concentrations exhibit a diurnal cycle regardless of wind speed and direction.

a) Role of penguin emissions

Large colonies of Adélie penguins nest on islands around DDU from the end of October to late February, with a total population estimated at 60 000 individuals (Micol and Jouventin, 2001). Several studies highlighted that the presence of these large colonies at DDU in summer significantly disturbs the atmospheric cycle of several species including ammonium and oxalate (Legrand et al., 1998), carboxylic acids and other oxygenated volatile organic compounds (Legrand et al., 2012), and HCHO (Preunkert et al., 2013). In a study

investigating sediment profiles excavated from ponds and catchments near penguin colonies in the Ross Sea region, Nie et al. (2012) measured high mercury content in penguin excreta (guano). Similarly, elevated total mercury concentrations were measured in ornithogenic soils (*i.e.*, formed by accumulation of guano) of the Fildes and Ardley peninsulas of King George Island (De Andrade et al., 2012). When soil temperature rises above freezing in summer at DDU, oxalate is produced together with ammonium following the bacterial decomposition of uric acid in ornithogenic soils (Legrand et al., 1998 and references therein). Dicarboxylic acids such as oxalic acid were shown to promote the light-driven reduction of Hg(II) species in aqueous systems and ice (Gårdfeldt and Jonsson, 2003; Si and Ariya, 2008; Bartels-Rausch et al., 2011). Emissions of Hg(0) from snow-covered ornithogenic soils are expected to peak early and late summer – following the reduction of Hg(II) species in the upper layers of the snowpack –, as also seen in the oxalate concentrations at DDU (Legrand et al., 1998). Furthermore the rise of temperature at noon would strengthen Hg(0) emissions from ornithogenic soils, possibly contributing to the observed diurnal cycle from November to February.

b) Possible role of the "sea breeze"

In summer, the surface wind direction sometimes changes from 120-160° E to North as temperature rises over midday (Pettré et al., 1993; Gallée and Pettré, 1998), giving birth to an apparent sea breeze. This phenomenon usually lasts half a day or less and air masses cannot be referred to as oceanic (see section 5.2.2.2.3). Legrand et al. (2001) and Legrand et al. (2016b) observed increasing atmospheric dimethylsulfide (DMS) and chloride concentrations, respectively, during sea breeze events. However, our results indicate that Hg(0) concentrations did not tend to increase systematically with the occurrence of a sea breeze (Figure 5-22).

c) Role of snowpack emissions

Angot et al. (2016b) reported a daily cycle in summer at DC with maximal Hg(0) concentrations around midday. This daily cycle atop the East Antarctic ice sheet was attributed to: i) an intense oxidation of Hg(0) in the atmospheric boundary layer due to the high level of oxidants present there (Davis et al., 2001; Grannas et al., 2007; Eisele et al., 2008; Kukui et al., 2014), ii) Hg(II) dry deposition onto the snowpack, and iii) increased emission of Hg(0) from the snowpack around midday as a response to daytime heating following photoreduction of Hg(II) in the upper layers of the snowpack. Even if DDU is located on snow free bedrock for most of the summer season, the same mechanism could apply since the station is surrounded by vast snow-covered areas. However, such a dynamic cycle of deposition/reemission at the air-snow interface requires the existence of a summertime atmospheric reservoir of Hg(II) species nearby DDU. This question is addressed in the following sub-section.

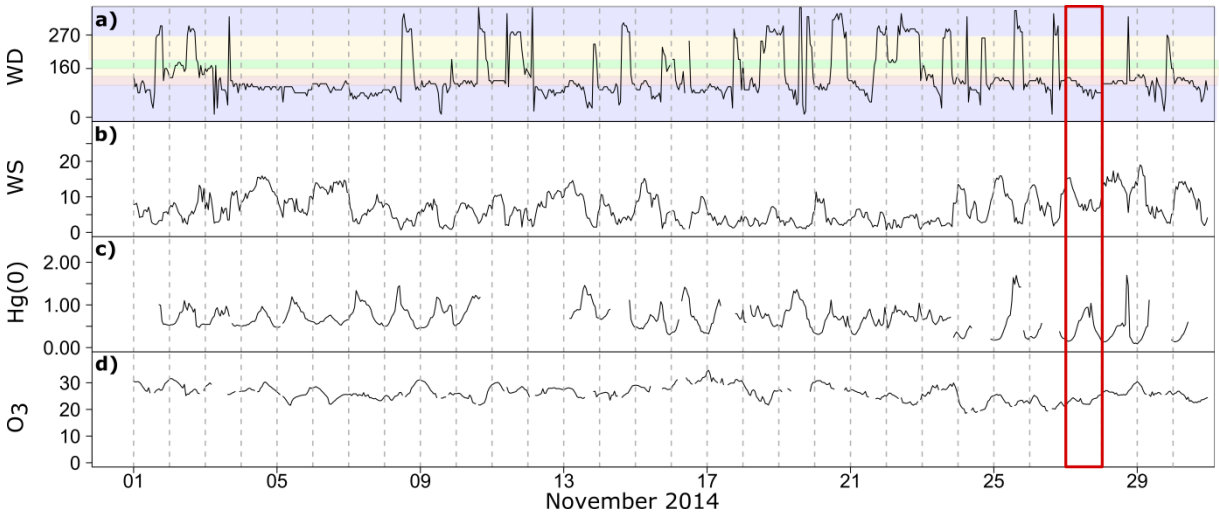

Figure 5-22: November 2014 variation of **a)** wind direction (WD, in °), **b)** wind speed (WS, in m s^{-1}), **c)** Hg(0) concentration (in ng m^{-3}), and **d)** O_3 mixing ratio (in ppbv). With north at 0°, oceanic winds ranged from 270 to 110° (purple), coastal winds from 110 to 130° (pink), katabatic winds from 160 to 180° (green), and continental winds from 130 to 160° and from 180 to 270° (yellow). On 27 November 2014 (period framed in red), a sea breeze is observed around midday: WD changes from ~ 120-130° to below 110° while WS decreases. Both Hg(0) concentrations and O_3 mixing ratios are not higher than during the previous days.

5.2.3.2.2 Transport of reactive air masses from the Antarctic Plateau

Several previous studies pointed out that the major oxidants present in the summer atmospheric boundary layer at coastal Antarctic sites differ in nature from site to site: halogens chemistry prevails in the West, OH/NO_x chemistry in the East (Legrand et al., 2009; Grilli et al., 2013). Measurements made at HA in summer indicate a BrO mixing ratio of 3 pptv (Saiz-Lopez et al., 2007), a NO_2 mixing ratio of about 5 pptv (Bauguitte et al., 2012), and a 24 h average value of 3.9×10^5 radicals cm^{-3} for OH (Bloss et al., 2007). Conversely, BrO levels are at least lower by a factor of 2 at DDU (Legrand et al., 2016a) and Grilli et al. (2013) reported a daily mean of 20 pptv for NO_2 in summer at DDU while Kukui et al. (2012) reported a 24 h average value of 2.1×10^6 radicals cm^{-3} for OH. Large OH/NO_x concentrations at DDU compared to HA were attributed to the arrival of air masses originating from the Antarctic Plateau where the OH/NO_x chemistry is very efficient (Legrand et al., 2009; Kukui et al., 2012).

Goodsite et al. (2004) and Wang et al. (2014) suggested a two-step oxidation mechanism for Hg(0), favored at cold temperatures. The initial recombination of Hg(0) and Br is followed by the addition of a second radical (*e.g.*, I, Cl, BrO, ClO, OH, NO_2, or HO_2) in competition with the thermal dissociation of the HgBr intermediate. Using the rate constants calculated by Wang et al. (2014) for the reactions of BrO, NO_2, and OH with the HgBr intermediate, we found that BrO is the most efficient oxidant of HgBr at HA (lifetime of 1.9 min against 2.2 min with NO_2 and 11 days with OH). At DDU the situation is reversed with a lifetime of the HgBr intermediate of 0.5 min with NO_2, 3.9 min with BrO (assuming the presence of 1.5 pptv of BrO in summer at DDU (Legrand et al., 2016a)), and 2 hours with OH. These results

suggest that the formation of Hg(II) species at DDU could be promoted by oxidants transported from the Antarctic Plateau towards the coast.

In addition to oxidants, inland air masses may transport mercury species. Low Hg(0) concentrations (0.76 ± 0.30 ng m^{-3}) at DDU were associated with transport from the Antarctic Plateau in summer (November to February, Figure 5-16b). A significant negative correlation was found in summer between Hg(0) concentrations and the daily averaged percentage of air masses originating from the Antarctic Plateau (r = -0.49, *p* value < 0.0001, Spearman test). Brooks et al. (2008a) reported elevated concentrations of oxidized mercury species at SP in summer (0.10–1.00 ng m^{-3}). Similarly, Angot et al. (2016b) observed low Hg(0) concentrations at the same period of the year at DC (0.69 ± 0.35 ng m^{-3}, *i.e.*, ~ 25 % lower than at NM, TNB and MM). Angot et al. (2016b) also reported the occurrence of multi-day to week-long Hg(0) depletion events (mean Hg(0) concentration ~ 0.40 ng m^{-3}) likely due to a stagnation of air masses above the plateau triggering an accumulation of oxidants within the shallow boundary layer. These observations indicate that inland air masses reaching DDU in summer are depleted in Hg(0) and enriched in Hg(II).

Transect from central to coastal Antarctica

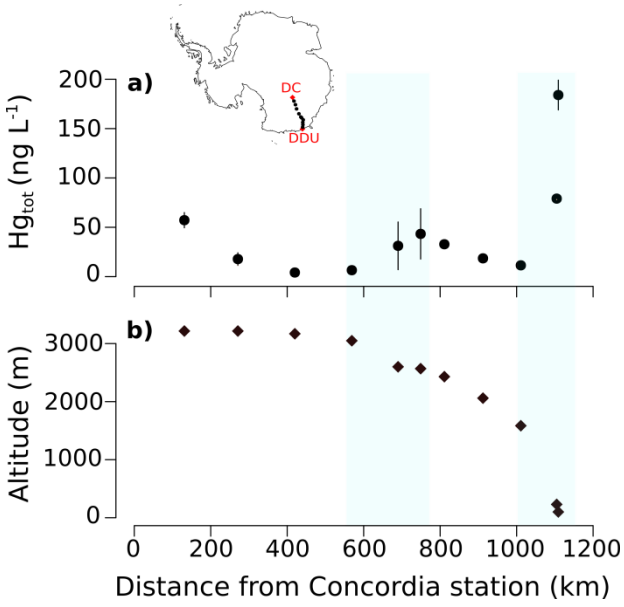

Figure 5-23: **a)** Total mercury concentration in surface snow samples (Hg_{tot} in ng L^{-1}) along with standard deviation and **b)** altitude (m) *vs.* distance from Concordia station (DC) during the traverse from DC to DDU. Hg_{tot} concentrations increased in areas highlighted in blue, characterized by steeper slopes and higher snow accumulation values.

The Hg_{tot} concentration of snow samples collected in summer 2009 between DC and DDU (see section 5.2.2.2.2) ranged from 4.2 to 194.4 ng L^{-1} (Figure 5-23). The closest sample from DC exhibited a Hg_{tot} concentration of 60.3 ± 8.1 ng L^{-1} (n = 3), in very good agreement with concentrations found in surface snow samples collected in summer at DC (up to 73.8 ± 0.9 ng L^{-1}, Angot et al., 2016b). As illustrated by Figure 5-23, Hg_{tot} concentrations increased between 600-800 km and 1000-1100 km from DC in areas characterized by steeper slopes and

higher snow accumulation values. Several studies reported a gradual increase in snow accumulation from DC toward the coast (Magand et al., 2007; Verfaillie et al., 2012; Favier et al., 2013), in good agreement with a gradual increase in humidity (Bromwich et al., 2004). These results suggest that the wet deposition of Hg(II) species was enhanced near the coast, resulting in elevated Hg_{tot} concentrations in surface snow samples. Additionally, the presence of halides such as chloride in snow can reduce the reduction rate of deposited Hg(II) species by competing with the complexation of Hg(II) with dicarboxylic acids (Si and Ariya, 2008) resulting in higher Hg_{tot} concentrations in coastal snowpacks (Steffen et al., 2015). It is worth noting that the Hg_{tot} concentrations between DC and DDU were higher than the values measured in summer along other expedition routes in East Antarctica. Han et al. (2011) measured very low Hg_{tot} concentrations (< 0.4–10.8 pg g^{-1}) along a ~ 1500 km transect in east Queen Maud Land, and Hg_{tot} concentrations ranged from 0.2 to 8.3 ng L^{-1} along a transect from ZG to DA (Figure 5-1) (Li et al., 2014). Unfortunately none of the samples collected during these two traverses were truly coastal – the most seaward samples were collected at altitudes of 948 and 622 m, respectively – preventing a direct comparison with the concentration measured near DDU. The mean Hg_{tot} concentration of 67 ± 21 ng L^{-1} reported by Brooks et al. (2008b) at MM is the only truly coastal value available in Antarctica and is lower than the value reported here near DDU.

The advection of inland air masses enriched in both oxidants and Hg(II) likely results in the build-up of an atmospheric reservoir of Hg(II) species at DDU – as confirmed by elevated Hg_{tot} concentrations in surface snow samples –, confirming the hypothesis of a dynamic cycle of deposition/reemission at the air-snow interface.

5.2.3.2.3 The ocean as a source of Hg(0)

DDU is located on a small island with open ocean immediately around from December to February. It should be noted that during summers 2011/2012, 2012/2013, and 2013/2014, areas of open waters were observed but with a significant unusual large amount of sea ice. Sea ice maps can be obtained from:

http://www.iup.uni-bremen.de:8084/amsr2data/asi_daygrid_swath/s6250/ (Spreen et al., 2008).

According to Figure 5-16b, Hg(0) concentrations in oceanic air masses were elevated from December to February (1.04 ± 0.29 ng m^{-3}), and a significant positive correlation was found between Hg(0) concentrations and the daily averaged percentage of oceanic air masses in summer ($r = 0.50$, p value < 0.0001, Spearman test). While in winter the ice cover limited mercury exchange at the air-sea interface (Andersson et al., 2008) leading to the build-up of mercury-enriched waters, large emissions of Hg(0) from the ocean likely occurred in summer. According to Cossa et al. (2011), total mercury concentrations can be one order of magnitude higher in under-ice seawater than those measured in open ocean waters. The authors attributed this build-up of mercury-enriched surface waters to the massive algal production at basal sea ice in spring/summer triggering a large production of Hg(0), and to the mercury enrichment in

brine during the formation of sea ice. Elevated Hg(0) concentrations in oceanic air masses are consistent with observations in the Arctic where Hg(0) concentrations in ambient air peak in summer due to oceanic evasion and snowmelt re-volatilization (Dastoor and Durnford, 2014). Additionally, evasion from meltwater ponds formed on the remaining sea ice and observed around the station may contribute to the increase in Hg(0) concentrations (Aspmo et al., 2006; Durnford and Dastoor, 2011)

5.2.4 Implications

5.2.4.1 For coastal Antarctic ecosystems

The reactivity of atmospheric mercury is unexpectedly significant in summer on the Antarctic Plateau as evidenced by elevated Hg(II) and low Hg(0) concentrations (Brooks et al., 2008a; Dommergue et al., 2012; Angot et al., 2016b). This study shows that katabatic/continental winds can transport this inland atmospheric reservoir toward the coastal margins where Hg(II) species tend to deposit due to increasing wet deposition (Figure 5-23). However, the post-deposition dynamics of mercury and its ultimate fate in ecosystems remain unknown. Bargagli et al. (1993) and Bargagli et al. (2005) showed evidence of enhanced bioaccumulation of mercury in soils, mosses, and lichens collected in ice-free areas around the Nansen Ice Sheet (Victoria Land, upslope from the Ross Ice Shelf), suggesting an enhanced deposition of mercury species. Interestingly, four large glaciers join in the Nansen Ice Sheet region and channel the downward flow of air masses from the Antarctic Plateau toward Terra Nova Bay, generating intense katabatic winds. The monthly mean wind speed is about 16 m s^{-1} in this area (Bromwich, 1989). Along with an enhanced deposition of mercury during AMDEs, the wind might as well be responsible for the advection of inland air masses enriched in Hg(II) species as observed in our case study. As already pointed out by Bargagli et al. (2005), coastal Antarctic ecosystems may become a sink for mercury, especially in view of increasing anthropogenic emissions of mercury in Asia (Streets et al., 2009).

5.2.4.2 For the cycle of atmospheric mercury in high southern latitudes

The influence of the Antarctic continent on the global geochemical cycle of mercury remains unclear (Dommergue et al., 2010b). This study shows that the reactivity observed on the Antarctic Plateau (Brooks et al., 2008a; Dommergue et al., 2012; Angot et al., 2016b) influences the cycle of atmospheric mercury at a continental scale, especially downstream of the main topographic confluence zones. The question is whether the katabatic airflow propagation over the ocean is important. According to Mather and Miller (1967), the katabatic flow draining from the Antarctic Plateau merges with the coastal polar easterlies under the action of the Coriolis force. The near-surface flow takes the form of an anticyclonic vortex (King and Turner, 1997), limiting the propagation of katabatic flows over the ocean.

5.2.5 Conclusion

We presented here a 3.5-year record of Hg(0) concentrations at DDU: the first multi-year record on the East Antarctic coast. Our observations reveal a number of differences with other costal or near coastal Antarctic records. In winter, observations showed a gradual 20 % decrease in Hg(0) concentrations from May to August, a trend never observed at other coastal sites. This is interpreted as a result of reactions occurring within the shallow boundary layer on the Antarctic Plateau, subsequently efficiently transported at that site by katabatic winds. In summer, the advection of inland air masses enriched in oxidants and Hg(II) species likely results in the build-up of an atmospheric reservoir of Hg(II) species at DDU, at least partly explaining the elevated (up to 194.4 ng L^{-1}) Hg_{tot} concentrations measured in surface snow samples near the station during a traverse between DC and DDU. Additionally, Hg(0) concentrations in ambient air exhibited a diurnal cycle in summer at DDU – phenomenon never observed at other coastal Antarctic stations. Several processes may contribute to this diurnal cycle, including a local chemical exchange at the air-snow interface in the presence of elevated levels of Hg(II) species in ambient air, and emissions from ornithogenic soils present at the site. Our data also highlight the fact that the Austral Ocean may be a net source for mercury in the summer. Even though AMDEs are likely very rare at DDU compared to other coastal stations, we cannot exclude that the sea-ice present offshore DDU at the end of winter influenced springtime Hg(0) levels. Finally, having shown that the reactivity observed on the Antarctic Plateau influences the cycle of atmospheric mercury on the East Antarctic coast, this study raises concern for coastal Antarctic ecosystems there.

Data availability

Mercury data reported in this paper are available upon request at http://sdi.iia.cnr.it/geoint/publicpage/GMOS/gmos_historical.zul.

Acknowledgements

We thank the overwintering crew: S. Aguado, D. Buiron, N. Coillard, G. Dufresnes, J. Guilhermet, B. Jourdain, B. Laulier, S. Oros, and A. Thollot. We also gratefully acknowledge M. Barret for the development of a QA/QC software program, Météo France for the meteorological data, and Susanne Preunkert who helped to validate contamination-free ozone data. This work contributed to the EU-FP7 project Global Mercury Observation System (GMOS – www.gmos.eu) and has been supported by a grant from Labex OSUG@2020 (Investissements d'avenir – ANR10 LABX56), and the Institut Universitaire de France. Logistical and financial support was provided by the French Polar Institute IPEV (Program 1028, GMOstral).

5.2.6 Compléments d'information

5.2.6.1 Résumé des principaux résultats et conclusions de l'article

L'article ci-avant propose, pour la première fois sur la côte Est du continent antarctique, une série temporelle pluriannuelle de mesures de concentrations en Hg(0). Les données acquises à DDU mettent en lumière un certain nombre de différences avec les observations aux autres stations côtières antarctiques. Premièrement, en hiver, une diminution progressive des concentrations atmosphériques en Hg(0) est observée. Ce phénomène, jamais observé auparavant sur la côte antarctique, n'est pas sans rappeler celui observé à DC sur la calotte glaciaire (voir section 5.1). Nous faisons l'hypothèse de processus se déroulant dans la couche limite atmosphérique sur le plateau antarctique, les masses d'air étant ensuite transportées jusqu'à DDU par les vents catabatiques. Dans un second temps, en été cette fois, les données acquises à DDU suggèrent que l'advection de masses d'air en provenance de la calotte glaciaire engendre un transfert d'oxydants et de Hg(II) vers la côte. Cette hypothèse est confortée par les concentrations élevées (jusqu'à 194.4 ng L^{-1}) en mercure total dans les échantillons de neige de surface prélevés sur la côte et par les concentrations en divers oxydants mesurées à DDU (Legrand et al., 2009; Grilli et al., 2013). Contrairement à ce qui est observé aux autres stations côtières antarctiques, un cycle diurne est observé en été à DDU, avec des concentrations en Hg(0) maximales à la mi-journée. Cela n'est à nouveau pas sans rappeler le cycle diurne observé à DC sur la calotte glaciaire en raison d'échanges d'espèces mercurielles à l'interface air-neige en présence de concentrations atmosphériques élevées en Hg(II) (voir section 5.1). Les données acquises à DDU mettent également en évidence le fait que l'océan Austral est une source de Hg(0) en été.

5.2.6.2 Dépôts de mercure au sein des écosystèmes côtiers et influence à plus large échelle

Les données acquises à DC et DDU ainsi que les observations à TNB, NM et TR (Sprovieri et al., 2002; Temme et al., 2003; Pfaffhuber et al., 2012) mettent en évidence l'influence, du fait des vents catabatiques, de la réactivité observée sur la calotte glaciaire sur le cycle atmosphérique du mercure à l'échelle continentale. Les espèces mercurielles divalentes, transportées vers les côtes, se déposent au sein des écosystèmes. Dans des zones fréquemment balayées par les vents catabatiques, Bargagli et al. (1993) ont ainsi retrouvé des taux de mercure dans les lichens supérieurs à ceux mesurés dans l'Hémisphère Nord. Ces résultats laissent à penser que les écosystèmes côtiers pourraient agir comme des puits de mercure. L'influence des vents catabatiques sur le cycle atmosphérique du mercure à l'échelle continentale pose également question à plus large échelle. D'après Mather et Miller (1967), la propagation des vents catabatiques sur l'océan Austral est limitée. L'article ci-avant s'achève par la conclusion suivante : l'influence de la réactivité observée sur la calotte glaciaire sur le cycle atmosphérique du mercure serait ainsi limitée au continent antarctique et mineure à plus large échelle. Il semble cependant nécessaire de se pencher plus avant sur cette question.

Au cours d'une campagne océanographique entre Hobart (HBT) en Tasmanie et le continent antarctique, Cossa et al. (2011) ont mesuré des concentrations croissantes en mercure total (Hg_{tot}) et réactif (Hg_R) dans les eaux de surface en s'approchant du continent. Des concentrations supérieures à 2 pmol L^{-1} ont ainsi été mesurées dans les zones AZ et SZ (Figure 5-24a). Les auteurs attribuent notamment ces résultats à une source atmosphérique de mercure (non identifiée) à proximité du continent antarctique. L'export estival de mercure réactif de la calotte glaciaire vers les zones côtières par les vents catabatiques pourrait s'avérer être une hypothèse intéressante. Les concentrations en Hg_{tot}, Hg_R et MeHg se sont par ailleurs révélées supérieures dans les eaux AABW que dans les eaux AAIW (Figure 5-24b). Ceci s'explique par la densité plus importante, engendrée par l'expulsion de sels lors de la formation de la glace de mer, des masses d'eaux riches en mercure. Ces masses d'eaux enrichies en mercure étant par la suite transférées vers le nord, répondre à la question de l'influence de la réactivité du mercure en Antarctique sur le cycle biogéochimique à plus large échelle n'est pas si trivial. Il pourrait être intéressant de réaliser des simulations à l'aide de modèles couplés océan-atmosphère.

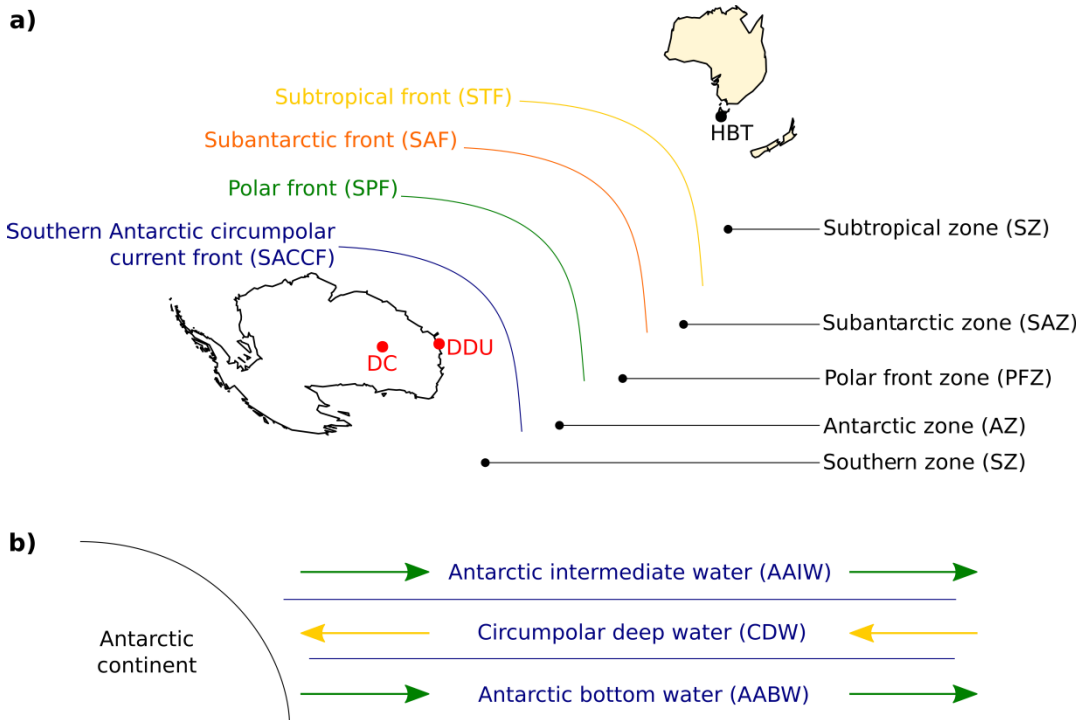

Figure 5-24: **a)** Position relative des différents fronts de l'océan Austral et **b)** Position relative des différentes masses d'eaux constituant l'océan Austral et direction des courants (flèches). Les schémas ne sont pas à l'échelle. D'après Cossa et al. (2011).

6 Cycle atmosphérique du mercure en régions polaires : avancées et limites des connaissances

Le chapitre 5, dédié au continent antarctique, a permis de démontrer l'existence de processus inédits en termes de réactivité du mercure dans l'atmosphère et à l'interface air-neige. Cependant, comment discuter du cycle atmosphérique du mercure à l'extrême sud de la planète sans essayer de dresser un parallèle avec la situation à l'extrême nord, en Arctique ? Le présent chapitre propose ainsi une comparaison de la réactivité atmosphérique du mercure aux deux pôles. Un des objectifs du réseau GMOS et de ces travaux de thèse étant de fournir des données de qualité pour la validation des modèles atmosphériques, ce chapitre propose également une comparaison des données d'observations en régions polaires avec les sorties de différents modèles globaux. Ce chapitre, qui s'appuie sur un article publié, permet de dresser un bilan de nos connaissances concernant le cycle atmosphérique du mercure en régions polaires. Un résumé, en français, des principaux résultats et conclusions est disponible au sein de la section 6.5.

D'après :

Angot, H., Dastoor, A., De Simone, F., Gårdfeldt, K., Gencarelli, C. N., Hedgecock, I. M., Langer, S., Magand, O., Mastromonaco, M. N., Nordstrøm, C., Pfaffhuber, K. A., Pirrone, N., Ryjkov, A., Selin, N. E., Skov, H., Song, S., Sprovieri, F., Steffen, A., Toyota, K., Travnikov, O., Yang, X., Dommergue, A.: Chemical cycling and deposition of atmospheric mercury in polar regions: review of recent measurements and comparison with models, Atmospheric Chemistry and Physics 16, 10735-10763, 2016.

Abstract

Mercury (Hg) is a worldwide contaminant that can cause adverse health effects to wildlife and humans. While atmospheric modeling traces the link from emissions to deposition of Hg onto environmental surfaces, large uncertainties arise from our incomplete understanding of atmospheric processes (oxidation pathways, deposition, and reemission). Atmospheric Hg reactivity is exacerbated in high latitudes and there is still much to be learned from polar regions in terms of atmospheric processes. This paper provides a synthesis of the atmospheric Hg monitoring data available in recent years (2011-2015) in the Arctic and in Antarctica along with a comparison of these observations with numerical simulations using four cutting-

edge global models. The cycle of atmospheric Hg in the Arctic and in Antarctica presents both similarities and differences. Coastal sites in the two regions are both influenced by springtime atmospheric Hg depletion events and by summertime snowpack reemission and oceanic evasion of Hg. The cycle of atmospheric Hg differs between the two regions primarily because of their different geography. While Arctic sites are significantly influenced by northern hemispheric Hg emissions especially in winter, coastal Antarctic sites are significantly influenced by the reactivity observed on the East Antarctic ice sheet due to katabatic winds. Based on the comparison of multi-model simulations with observations, this paper discusses whether the processes that affect atmospheric Hg seasonality and interannual variability are appropriately represented in the models, and identifies research gaps in our understanding of the atmospheric Hg cycling in high latitudes.

6.1 Introduction

Mercury (Hg) can be emitted to the atmosphere by natural geological sources (*e.g.*, volcanic emissions) and a variety of anthropogenic activities (*e.g.*, coal combustion, artisanal and small-scale gold mining) (UNEP, 2013a). The dominant form of atmospheric mercury is gaseous elemental mercury (Hg(0)) (Lindberg and Stratton, 1998). Hg(0) has an atmospheric lifetime of 0.5 to 1 year (Selin, 2009) and can therefore be transported worldwide. It can be oxidized into highly reactive and water-soluble gaseous and particulate divalent species (Hg(II) and Hg(p), respectively) that can deposit onto environmental surfaces (*e.g.*, land, surface oceans) through wet and dry processes (Lindqvist and Rodhe, 1985). Upon deposition, mercury can be re-emitted to the atmosphere or converted – in aquatic systems – to methylmercury (Driscoll et al., 2013). Anthropogenic activities have altered the global geochemical cycle of mercury, enhancing the amount of mercury circulating in the atmosphere and surface oceans by at least a factor of 3 (Lamborg et al., 2014; Amos et al., 2015).

Methylmercury is a worldwide contaminant of seafood that can cause adverse effects on the developing nervous system of vulnerable populations (AMAP, 2015). The Minamata Convention on mercury – a global treaty to protect human health and the environment from mercury – was opened for signature in October 2013 (UNEP, 2013b). To date, the Convention has been signed by 128 countries and ratified by 29. It will enter into force once it is ratified by 50 nations. As noted in the preamble of the Convention, Arctic ecosystems and indigenous communities are particularly vulnerable due to the biomagnification of mercury and contamination of traditional foods. In order to reduce mercury effects, the pathway from emissions to human and environmental impacts needs to be traced. Atmospheric modeling provides a first step by tracing the link from emissions to deposition onto environmental surfaces. Deposition of mercury in a particular region depends on the magnitude and speciation of domestic and foreign emissions, and on the oxidative capacity of the atmosphere that transforms Hg(0) to deposited divalent species (UNEP, 2015). Deposition is partly offset

by the re-volatilization of a fraction of deposited mercury. Large uncertainties associated with the models arise as a result of our incomplete understanding of atmospheric processes (*e.g.*, oxidation pathways, deposition, and reemission) (Kwon and Selin, 2016). Atmospheric mercury reactivity is exacerbated in high latitudes and there is still much to be learned from polar regions in terms of atmospheric processes.

First discovered in 1995 (Schroeder et al., 1998), atmospheric mercury depletion events (AMDEs) are observed in springtime throughout the Arctic (Lindberg et al., 2001; Berg et al., 2003a; Poissant and Pilote, 2003; Skov et al., 2004; Steffen et al., 2005) as a result of the oxidation of Hg(0) by reactive bromine species (Lu et al., 2001; Brooks et al., 2006a; Sommar et al., 2007). AMDEs can lead to a deposition of ~ 100 tons of mercury per year to the Arctic (Ariya et al., 2004; Skov et al., 2004; Dastoor et al., 2015). The fate of mercury deposited onto the snowpack during AMDEs is still a matter of debate in the scientific mercury community (Steffen et al., 2008). Several studies reported significant reemission (e.g., Ferrari et al., 2005; Brooks et al., 2006a; Kirk et al., 2006; Sommar et al., 2007; Dommergue et al., 2010a) although a fraction of mercury may likely accumulate within the snowpack (Hirdman et al., 2009; Larose et al., 2010). While the Arctic has been extensively monitored – with hundreds of publications focusing on AMDEs – measurements are sporadic in Antarctica. To the best of the author's knowledge, only 11 studies dealing with atmospheric mercury in Antarctica (and using modern instrument) have been published (Ebinghaus et al., 2002b; Sprovieri et al., 2002; Temme et al., 2003; Brooks et al., 2008a; Brooks et al., 2008b; Dommergue et al., 2012; Pfaffhuber et al., 2012; Angot et al., 2016a; Angot et al., 2016b; Nerentorp Mastromonaco et al., 2016; Wang et al., 2016). The earliest studies showed the occurrence of AMDEs in coastal Antarctica after polar sunrise. The latest studies highlighted new atmospheric processes in the Antarctic boundary layer – both in winter and summertime – leading to the formation and subsequent deposition of reactive mercury. In the meantime, several studies showed that the Antarctic Plateau plays a key role in influencing the cycle of atmospheric mercury at a continental scale.

The first objective of this paper is to provide a synthesis of the atmospheric mercury monitoring data available in recent years (2011-2015) in polar regions. Secondly, we provide a comparison of these observations with numerical simulations of atmospheric mercury concentrations using cutting-edge global models. Finally, this paper identifies research gaps in our understanding and modeling of the atmospheric mercury cycling in high latitudes.

6.2 Experimental section

6.2.1 Measurements of atmospheric species

6.2.1.1 Definitions

Hg(0), Hg(II), and Hg(p) are the most abundant mercury species in the atmosphere.

Atmospheric Hg(0) is easily and accurately measured in polar regions (Steffen et al., 2008; Dommergue et al., 2010b). Hg(p) and reactive gaseous mercury (RGM) – the latter consisting of various gaseous Hg(II) compounds – are operationally defined. Total gaseous mercury (TGM) refers to the sum of Hg(0) and Hg(II), and reactive mercury (RM) to the sum of RGM and Hg(p).

6.2.1.2 Instrumentation

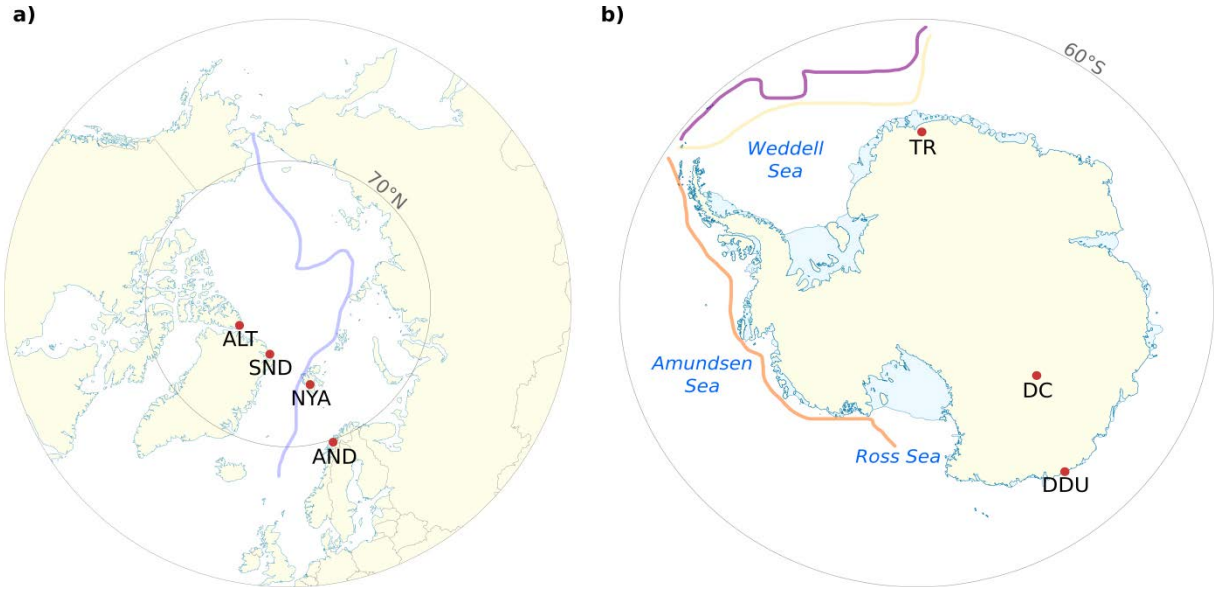

Figure 6-1: Location of **a)** Arctic and **b)** Antarctic ground-based sites whose data are reported in this paper: Alert (ALT), Villum Research Station at Station Nord (SND), Zeppelin station at Ny-Ålesund (NYA), Andøya (AND), Troll (TR), Concordia Station at Dome C (DC), and Dumont d'Urville (DDU). Additionally, the approximate path of cruises performed in recent years (2011-2015) is given: CHINARE 2012 in the Arctic on board the Chinese vessel Xuelong (in blue), ANT XXIX/6-7 (denoted ANT in the paper) over the Weddell Sea on board R/V Polarstern (in yellow and purple), and OSO 10/11 (denoted OSO in the paper) over Ross and Amundsen Seas onboard icebreaker Oden (in orange).

Measurements of atmospheric mercury species were performed at various sites in the Arctic and in Antarctica over the 2011-2015 period (Figure 6-1). All Hg(0) measurements reported in this paper were performed using a Tekran gas-phase analyzer (Model 2537), and all RGM and Hg(p) measurements using a Tekran speciation unit (1130/1135) (Table 6-1). The Tekran 2537 analyzer is based on the amalgamation of mercury onto a gold cartridge followed by a thermal desorption and detection by an integrated cold vapor atomic fluorescence spectrometer (CVAFS) at 253.7 nm (Fitzgerald and Gill, 1979; Bloom and Fitzgerald, 1988). The analysis of Hg(0) is semi-continuous and the presence of two gold cartridges allows alternating sampling and desorption modes. At all sampling sites, the sample air stream was prefiltered either through a Tekran speciation unit or through a soda lime trap and/or a PTFE (polytetrafluoroethylene) filter (Table 6-1). Some researchers report ambient air collected at polar sites as TGM (Ebinghaus et al., 2002b), instead of Hg(0), but the PTFE

filter on the front of the analyzer inlet most likely removes RGM and thus only Hg(0) is collected and analyzed (Steffen et al., 2002; Steffen et al., 2008). Due to the extremely cold and dry air in Antarctica, no heated sampling line was used and no soda lime was applied at TR, DC, and DDU. Collected at 5 to 15 min intervals at the various sites, Hg(0) measurements are reported here as hourly averages. RGM and Hg(p) measurements at ALT and ANT were performed using a Tekran speciation unit – connected to a 2537 analyzer through a PTFE heated sampling line – through a multistep procedure as described elsewhere (Lindberg et al., 2002) using an impactor inlet (2.5 µm cut-off aerodynamic diameter at 10 L min^{-1}), a KCl-coated quartz annular denuder in the 1130 unit, and a quartz regenerable particulate filter (RPF) in the 1135 unit.

Table 6-1: Summary of the instrumentation used at the various polar sites to measure atmospheric mercury species. The flow rate is in L min^{-1} and the resolution (Resol.) in minutes unless stated otherwise. S. line means sampling line.

Code	Elevation	Analyte	Instrumentation	Flow rate	Resol.	Filter	S. line
ALT	195	Hg(0)	Tekran 2537A	1.0	5	speciation unit	heated
		Hg(p), RGM	1130 and 1135	10.0	2 h		
SND	30	Hg(0)	Tekran 2537A	1.5	5	soda lime	heated
NYA	474	Hg(0)	Tekran 2537A	1.5	5	2 µm PTFE, soda lime	heated
AND	10	Hg(0)	Tekran 2537A	1.5	5	2 µm PTFE, soda lime	heated
TR	1275	Hg(0)	Tekran 2537A	1.5	5	2 µm PTFE	unheated
DC	3220	Hg(0)	Tekran 2537A	0.8	5-15	0.45 PTFE	unheated
DDU	43	Hg(0)	Tekran 2537B	1.0	10-15	0.20 PTFE	unheated
ANT	20	Hg(0)	Tekran 2537A	1.0	5	speciation unit	heated
		Hg(p), RGM	1130 and 1135	10.0	2 h		
OSO	15	Hg(0)	Tekran 2537A	1.0	5	0.45 PTFE	unheated

Quality assurance and quality control procedures

Auto-calibrations of the 2537 analyzers were performed every 25 to 72 hours at the various sites using an internal mercury permeation source. The accuracy of this permeation source was checked at least once per year against manual injections using a Tekran 2505 mercury vapor calibration unit and following a strict procedure adapted from Dumarey et al. (1985). The detection limit for Hg(0) measurements is 0.10 ng m^{-3} according to the instrument manual (Tekran, 2011). Based on experimental evidence, the average systematic uncertainty for Hg(0) measurements is of ~ 10 % (Slemr et al., 2015). There is no robust calibration technique of the Tekran speciation unit and no certified reference material available. There is growing evidence that RGM and Hg(p) might suffer from significant biases and interferences (Lyman et al., 2010b; Gustin et al., 2013; Jaffe et al., 2014; Huang et al., 2013; Kos et al., 2013), and that RGM concentrations might be underestimated by as much as a factor of 2-13 (Gustin et al., 2016). Despite these limitations, the Tekran speciation unit is currently the best available automated method, and Hg(p) and RGM measurements can be used as first estimates to evaluate atmospheric models. Maintenance operations on the Tekran 2537/1130/1135 instruments and screening criteria for data validation/invalidation were performed according to the directives of the standard operational procedure from CAMNet (Canadian Mercury Measurement Network), AMNet (United States Atmospheric Mercury

Network), or GMOS (Global Mercury Observation System) (Steffen et al., 2012; D'Amore et al., 2015).

6.2.2 Global mercury simulations

The current study is based on multi-model simulations performed as part of the Mercury Modeling Task Force under the GMOS project (Travnikov et al., in preparation). Four global models (ECHMERIT, GEM-MACH-Hg, GEOS-Chem, and GLEMOS) were applied for evaluating monthly-averaged atmospheric mercury concentrations and deposition at various Arctic and Antarctic ground-based sites for the year 2013. Additionally, GEM-MACH-Hg and GEOS-Chem provided hourly averaged data from 2011 to 2014 to allow investigations of interannual variability. A brief description of the parameterization of the four models is given below. The models differ significantly in their description of mercury atmospheric chemistry and their parameterization of processes specific to polar regions (*i.e.*, AMDEs, oceanic evasion, and reemissions from the snowpack).

6.2.2.1 ECHMERIT

ECHMERIT is a fully coupled model, based on the atmospheric general circulation model ECHAM5, and a mercury chemistry module, developed at the Institute for Atmospheric Pollution of the National Research Council (CNR-IIA) of Italy (Jung et al., 2009; De Simone et al., 2014; De Simone et al., 2016b). The base mechanism includes oxidation of Hg(0) by OH and O_3 in the gas and aqueous (in-cloud) phases (reactions R1 to R3). Rate constants of reactions (R1) to (R3) are from Sommar et al. (2001), Hall (1995), and Munthe (1992), respectively.

$$\mathrm{Hg(0) + OH \rightarrow Hg(II)} \qquad \text{(R1)}$$

$$\mathrm{Hg(0) + O_3 \rightarrow Hg(II)} \qquad \text{(R2)}$$

$$\mathrm{Hg(0)_{(aq)} + O_{3(aq)} \rightarrow Hg(II)_{(aq)}} \qquad \text{(R3)}$$

Oxidant fields (OH/O_3) are imported from MOZART (Model for Ozone and Related Chemical Tracers) (Emmons et al., 2010). In the base run used for this work bromine chemistry is not included, and there is no parameterization of AMDEs. ECHMERIT implements dynamically calculated ocean emissions for all ice-free basins, including polar regions, as described in De Simone et al. (2014), and a prompt reemission of 60 % of deposited mercury over ice (Selin et al., 2008).

6.2.2.2 GEM-MACH-Hg

GEM-MACH-Hg is a mercury version of the Environment and Climate Change Canada's (ECCC's) current operational air quality forecast model – Global Environmental Multi-scale – Modelling air-quality and Chemistry (GEM-MACH). GEM-MACH-Hg is an online model,

meaning that the meteorology is simulated in-step with the chemistry, and includes representation of physicochemical processes of mercury based on the ECCC's previous mercury model, GRAHM (Dastoor and Larocque, 2004; Dastoor et al., 2008; Durnford et al., 2010; Durnford et al., 2012; Kos et al., 2013; Dastoor et al., 2015). The horizontal resolution of the model for this study is $1° \times 1°$ latitude/longitude. Hg(0) is oxidized in the atmosphere by OH (R1) and bromine (reactions (R4) to (R6), X = Br or BrO). The rate constant of (R1) is from Sommar et al. (2001), but scaled down by a coefficient of 0.34 to take into account possible dissociation reactions (Tossell, 2003; Goodsite et al., 2004). Rate constants of reactions (R4) to (R6) are from Donohoue et al. (2006), Dibble et al. (2012), and Goodsite et al. (2004), respectively. Aqueous-phase reduction reactions are not included.

$$\mathrm{Hg(0) + Br \rightarrow Hg(I)Br} \qquad \text{(R4)}$$

$$\mathrm{Hg(I)Br \rightarrow Hg(0) + Br} \qquad \text{(R5)}$$

$$\mathrm{Hg(I)Br + X \rightarrow Hg(II)X} \qquad \text{(R6)}$$

OH fields are from MOZART (Emmons et al., 2010) while BrO is derived from 2007-2009 satellite observations of BrO vertical columns. The associated Br concentration is then calculated from photochemical steady state according to Eq. 6 - 1, where J_{BrO} is the BrO photolysis frequency, and $k_1 = 2.1\times10^{-11}$ cm^3 $molecule^{-1}$ s^{-1} and $k_2 = 1.2\times10^{-12}$ cm^3 $molecule^{-1}$ s^{-1} are the rate coefficients for the $BrO + NO \rightarrow Br + NO_2$ and $Br + O_3 \rightarrow BrO + O_2$ reactions, respectively (Platt and Janssen, 1995).

$$[Br]/[BrO] = J_{BrO} + k_1[NO]/k_2[O_3] \qquad \text{(Eq. 6-1)}$$

Durnford et al. (2012) developed and implemented a dynamic multilayer snowpack/meltwater parameterization allowing the representation of deposition and reemission of mercury. Oceanic evasion of Hg(0) is activated if there is open water and the temperature at the air-sea interface is -4 °C or greater (Dastoor and Durnford, 2014). In addition, Hg(0) released from sea-ice melting is also taken into account. The parameterization of AMDEs is based on Br production and chemistry and snow reemission of Hg(0) (Dastoor et al., 2008).

6.2.2.3 GEOS-Chem

GEOS-Chem (v9-02) is a global chemical transport model driven by assimilated meteorological data from the NASA GMAO Goddard Earth Observing System (Bey et al., 2001). It couples a 3-D atmosphere (Holmes et al., 2010), a 2-D mixed layer slab ocean (Soerensen et al., 2010b), and a 2-D terrestrial reservoir (Selin et al., 2008) with a horizontal resolution of $2° \times 2.5°$ latitude/longitude. Three mercury tracers (Hg(0), Hg(II), and Hg(p)) are tracked in the atmosphere (Amos et al., 2012). Mercury fluxes at terrestrial and ocean surfaces are described in Song et al. (2015). A two-step oxidation mechanism initialized by Br

atoms is used (reactions (R4) to (R6), X = Br or OH). Br fields are archived from a full-chemistry GEOS-Chem simulation (Parrella et al., 2012) while rate constants of reactions (R4) to (R6) are from Donohoue et al. (2006), Balabanov et al. (2005), and Goodsite et al. (2012), respectively. Some model setups related to polar regions are implemented in v9-02 of the model as described in details in Holmes et al. (2010). 5 pptv of BrO – at the low end of concentrations reported by Neuman et al. (2010) – is added in the springtime Arctic (Antarctic) boundary layer during March-May (August-October) over areas with sea ice, sunlight, stable conditions, and temperatures below -5 °C. The associated Br concentration is then calculated from photochemical steady state according to Eq. 6-2 assuming that O_3 is depleted to 2 ppbv. Additionally, a snowpack reservoir is added. It accumulates deposited mercury and releases it as Hg(0) under sunlit conditions in a temperature-dependent way.

6.2.2.4 GLEMOS

GLEMOS (Global EMEP Multi-media Modelling System) is a multi-scale chemical transport model developed for the simulation of environmental dispersion and cycling of different chemicals including mercury (Travnikov and Ilyin, 2009). The model simulates atmospheric transport, chemical transformations, and deposition of three mercury species (Hg(0), Hg(II), and Hg(p)). The atmospheric transport of tracers is driven by meteorological fields generated by the Weather Research and Forecast (WRF) modeling system (Skamarock et al., 2007) fed by the operational analysis data from ECMWF. The model in the base configuration has a horizontal resolution of $1° \times 1°$. The base mechanism includes oxidation of Hg(0) by OH (R1) and O_3 (R2) in the atmosphere. Rate constants are from Sommar et al. (2001) and Hall (1995), respectively. The model also includes in-cloud oxidation of Hg(0) by OH, O_3, and Cl with associated rate constants from Gårdfeldt et al. (2001), Munthe (1992), and Lin and Pehkonen (1999), respectively. In-cloud reduction by SO_3^{2-} is also implemented, with an associated rate constant from Petersen et al. (1998). Reactant fields are imported from MOZART (Emmons et al., 2010).

The parameterization of AMDEs in polar regions is based on Br chemistry following the two-step mechanism (R4)-(R6) described in Holmes et al. (2010). Br concentrations are extracted from p-TOMCAT (parallel-Tropospheric Off-Line Model of Chemistry and Transport) results (Yang et al., 2005). GLEMOS includes an empirical parameterization of prompt reemission from snow. It is assumed that reemission occurs only from newly deposited mercury in the presence of solar radiation. Two competing processes are considered: photoreduction and ageing of deposited mercury with the characteristic times of 1 day and 10 days, respectively. It is also assumed that all reduced mercury is immediately re-emitted back to the atmosphere. The aged fraction of mercury does not undergo reduction and is accumulated within the snowpack. No mercury evasion from the ocean is implemented.

6.2.3 Goodness-of-fit statistics between modeled and observed data

The Nash-Sutcliffe efficiency (NSE; Nash and Sutcliffe, 1970) indicates how well the plot

of observed versus simulated data fits the 1:1 line – NSE = 1 corresponding to the perfect match. NSE is defined according to Eq. 6-2 as 1 minus the sum of the absolute squared differences between the simulated and observed values normalized by the variance of the observed values. The root-mean square error (RMSE), calculated according to Eq. 6-3, gives the standard deviation of the model prediction error (in the same units of simulated and observed values). A smaller value indicates better model performance. The percent bias (PBIAS, in %) measures the average tendency of the simulated values to be larger or smaller than their observed ones. The optimal value of PBIAS is 0. PBIAS is calculated according to Eq. 6-4. NSE, RMSE, and PBIAS were calculated by using the R package "hydroGOF" (Zambrano-Bigiarini, 2014).

$$NSE = 1 - \frac{\sum_{i=1}^{N}(O_i - S_i)^2}{\sum_{i=1}^{N}(O_i - \bar{O})^2} \qquad \text{(Eq. 6-3)}$$

$$RMSE = \sqrt{\frac{1}{N} \sum_{i=1}^{N}(S_i - O_i)^2} \qquad \text{(Eq. 6-4)}$$

$$PBIAS = 100 \frac{\sum_{i=1}^{N}(S_i - O_i)}{\sum_{i=1}^{N} O_i} \qquad \text{(Eq. 6-5)}$$

6.3 Results and Discussion

6.3.1 Arctic sites

6.3.1.1 Observations

Figure 6-2 shows monthly box plots of all data collected at the four Arctic sites. The average Hg(0) value in the Arctic over the 2011-2014 period is 1.46 ± 0.33 ng m^{-3}. This concentration falls within the range of what is observed in the Northern Hemisphere (Sprovieri et al., 2016b). The highest mean is at AND (1.55 ± 0.15 ng m^{-3} over the 2011-2015 period), which is closer to European industrialized areas than other sites and experiences less frequent and pronounced AMDEs in spring (see section 6.3.1.1.2). There is a clear Hg(0) concentration gradient (except from June to August): AND > NYA > SND > ALT.

The Hg(0) concentration data from the four Arctic sites for the period 2011-2015 are presented as monthly box and whisker plots in Figure 6-3. Information regarding annually and monthly based statistics at the three sites can be found in Table 6-2 and Table 6-3, respectively. The annual medians at NYA and AND (Table 6-2) suggest a low inter annual variability in the distribution of Hg(0) concentrations. Conversely, there is a high degree of

interannual variability at ALT and SND driven by the intensity of spring and summertime processes. This will be addressed in the following sections.

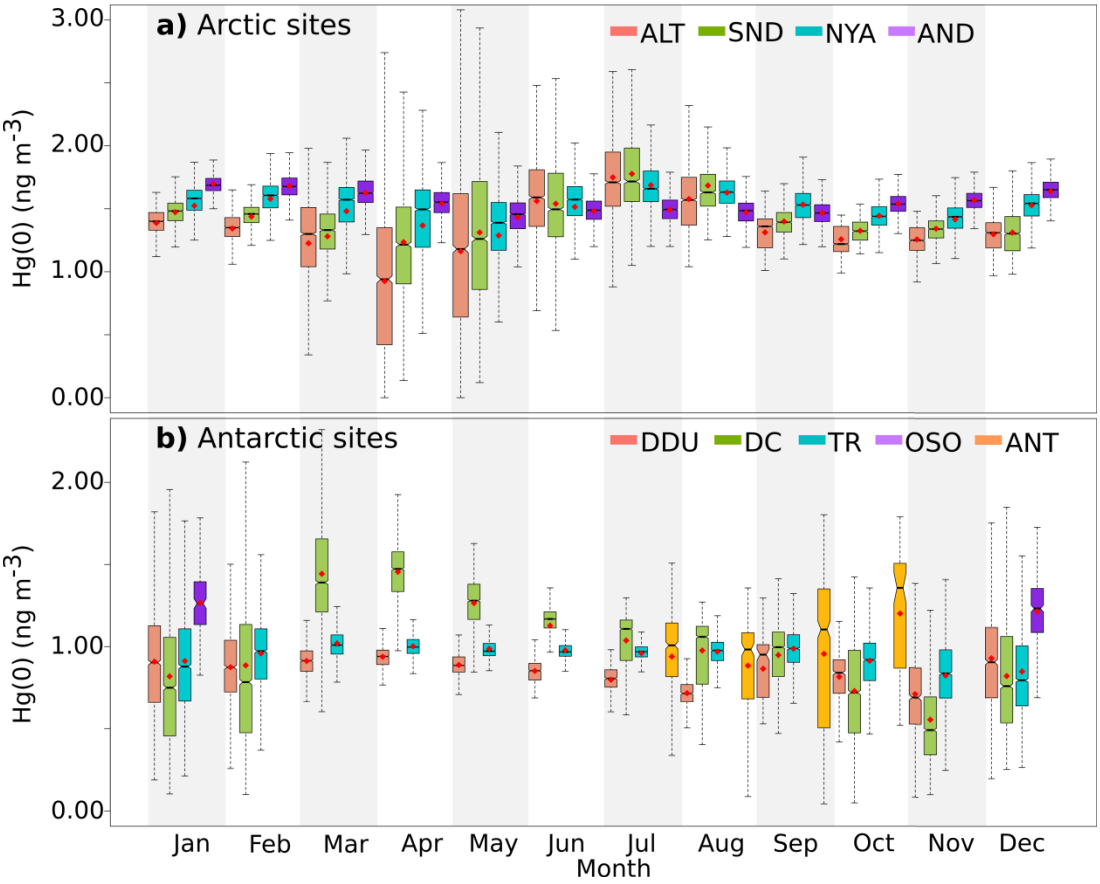

Figure 6-2: Box and whisker plots presenting the monthly Hg(0) concentration distribution at **a)** Arctic sites: ALT (red), SND (green), NYA (turquoise), AND (purple), and **b)** Antarctic sites: DDU (red), DC (green), TR (turquoise), during the OSO (purple) and ANT (orange) cruises. ◆: mean. Bottom and top of the box: first and third quartiles. Band inside the box: median. Ends of the whiskers: lowest (highest) datum still within the 1.5 interquartile range of the lowest (upper) quartile. Outliers are not represented.

The mean seasonal variation of Hg(0) concentrations at ground-based Arctic sites is displayed in Figure 6-4a. Summer refers to June-August, fall to September-November, winter to December-February, and spring to March-May. Hg(0) concentrations exhibit a strong and consistent seasonal pattern year after year, as already reported by others (Steffen et al., 2005; Berg et al., 2013). Hg(0) concentrations reach a distinct maximum in summer at ALT, SND, and NYA (mean concentrations of 1.63 ± 0.37, 1.63 ± 0.37, and 1.60 ± 0.23 ng m^{-3}, respectively). In late summer the concentrations start to decrease and reach in fall a mean value of 1.28 ± 0.12 ng m^{-3} at ALT, 1.36 ± 0.11 ng m^{-3} at SND, and 1.46 ± 0.16 ng m^{-3} at NYA. In winter, concentrations increase slightly and are significantly higher than in fall at the three sites (p value < 0.0001 at the three sites, Mann-Whitney test). Springtime reflects the lowest Hg(0) concentrations with mean values of 1.11 ± 0.58 ng m^{-3} at ALT, 1.28 ± 0.51 ng m^{-3} at SND, and 1.38 ± 0.38 ng m^{-3} at NYA. The seasonal cycle is more pronounced at ALT than at SND and NYA. In contrast, lower concentrations were found in the Chukchi Sea in

July (1.17 ± 0.38 ng m^{-3}) than in September (1.51 ± 0.79 ng m^{-3}) during the CHINARE 2012 expedition (Yu et al., 2014).

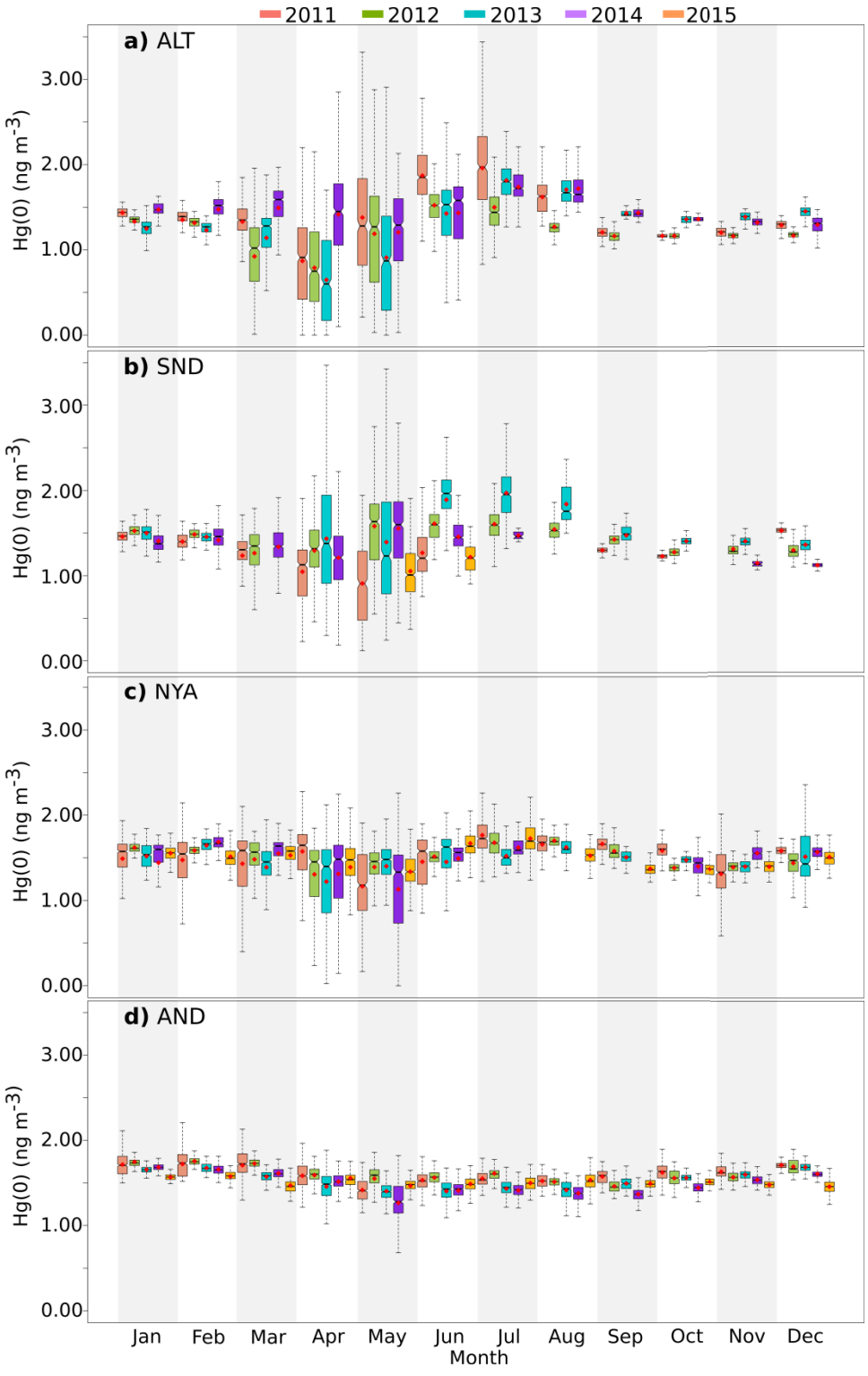

Figure 6-3: Box and whisker plots presenting the monthly Hg(0) concentration distribution at Arctic sites **a)** ALT, **b)** SND, **c)** NYA, and **d)** AND in 2011 (pink), 2012 (green), 2013 (turquoise), 2014 (purple), and 2015 (orange). ◆: mean. Bottom and top of the box: first and third quartiles. Band inside the box: median. Ends of the whiskers: lowest (highest) datum still within the 1.5 interquartile range of the lowest (upper) quartile. Outliers are not represented.

Hg(0) concentrations at AND exhibit an opposite seasonal cycle with a significantly (*p* value < 0.0001, Mann-Whitney test) higher mean concentration in winter (1.67 ± 0.11 ng m^{-3}) than in summer (1.48 ± 0.12 ng m^{-3}), in line with the seasonality reported at Pallas, Finland (67°22 N, 26°39 E) (Berg et al., 2001; Sprovieri et al., 2016b). The mechanisms which cause the seasonal variation of Hg(0) concentrations at Arctic sites are discussed in the following sections.

Table 6-2: Annually based statistics (number of hourly averaged data (n), mean, median, standard deviation (SD)) of Hg(0) concentrations (in ng m^{-3}) at ground-based polar sites over the 2011-2015 period. Note that 2013 data at DC refer to concentrations recorded at 210 cm above the snowpack. The 2015 data coverage is May to June at SND and January to May at DDU (see Table 6-3). na: not available due to QA/QC invalidation, instrument failure, or because the QA/QC validation is currently in progress (2015 data).

	ALT	SND	NYA	AND	TR	DC	DDU
2011							
n	8040	4712	8173	7444	5978	na	na
mean	1.39	1.26	1.51	1.61	0.95	na	na
median	1.35	1.34	1.59	1.61	0.99	na	na
SD	0.45	0.32	1.61	0.15	0.20	na	na
2012							
n	8447	7932	8181	8428	7808	3761	5949
mean	1.21	1.44	1.51	1.61	0.98	0.76	0.91
median	1.21	1.44	1.54	1.61	0.97	0.70	0.92
SD	0.35	0.26	0.21	0.13	0.15	0.24	0.20
2013							
n	8048	6605	6980	7862	8197	2900	5121
mean	1.31	1.57	1.47	1.53	0.90	0.84	0.85
median	1.39	1.49	1.52	1.56	0.93	0.87	0.85
SD	0.46	0.44	0.30	0.15	0.15	0.27	0.19
2014							
n	8358	4991	6730	8146	7421	na	1958
mean	1.45	1.36	1.48	1.50	0.95	na	0.85
median	1.45	1.36	1.57	1.51	1.00	na	0.82
SD	0.33	0.35	0.33	0.16	0.21	na	0.38
2015							
n	na	1059	8342	7146	3670	8383	3114
mean	na	1.11	1.49	1.50	0.94	1.06	0.86
median	na	1.11	1.49	1.50	0.93	1.12	0.87
SD	na	0.32	0.21	0.10	0.31	0.41	0.19

6.3.1.1.1 Wintertime advection of Hg from midlatitudes

Several studies highlighted that the Arctic is significantly influenced by atmospheric pollution from midlatitudes – phenomenon known as Arctic haze – during wintertime (Barrie et al., 1981; Heintzenberg et al., 1981; Shaw, 1982; Heidam et al., 1999; Heidam et al., 2004; Bourgeois and Bey, 2011; Nguyen et al., 2013). Dastoor and Larocque (2004) used an online model to explain the observed seasonal variations in atmospheric mercury circulation and showed frequent episodes of mercury transport from midlatitudes sources to the Arctic in winter. Similarly, Hirdman et al. (2009) attributed the highest 10 % of all wintertime Hg(0) data at NYA to transport of air masses especially from Europe. Higher Hg(0) concentrations in winter compared to fall at ALT, SND, and NYA can therefore be attributed to the

meteorological differences in the seasonal circulation patterns (Dastoor and Larocque, 2004). Higher concentrations in winter at AND compared to the three other Arctic sites can be attributed to the powerful advection of air masses from Europe at this site (Durnford et al., 2010).

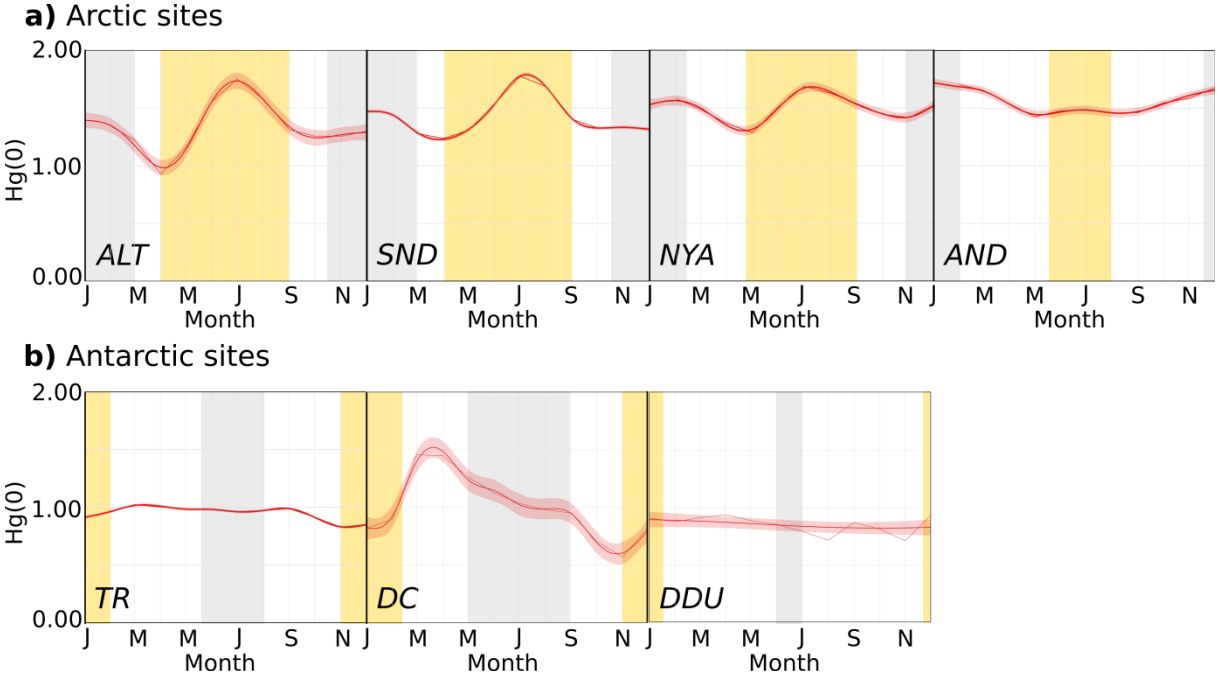

Figure 6-4: Seasonal variation (monthly mean along with the 95 % confidence interval for the mean) of Hg(0) concentrations (in ng m^{-3}) at **a)** Arctic and **b)** Antarctic ground-based sites. Periods highlighted in yellow refer to 24-h sunlight and periods highlighted in gray to 24-h darkness. Summer refers to June-August (November-February), fall to September-November (March-April), winter to December-February (May-August), and spring to March-May (September-October) at Arctic (Antarctic) sites.

6.3.1.1.2 Springtime AMDEs

AMDEs in the Arctic are defined as Hg(0) concentrations below 1.00 ng m^{-3} (Steffen et al., 2005; Cobbett et al., 2007). Based on this threshold, AMDEs occur in 39 %, 28 %, 15 %, and 1 % of the 2011-2014 springtime observations at ALT, SND, NYA, and AND, respectively. The fact that ALT experiences stronger and more frequent AMDEs than other Arctic sites could be due to air mass circulation patterns. Several studies indicated that a large fraction of the AMDEs reported at NYA and AND are suspected to result from the long-range transport of air masses containing depleted Hg(0) from areas over the Arctic Ocean (Gauchard et al., 2005; Sommar et al., 2007; Berg et al., 2008; Steen et al., 2011; Berg et al., 2013). A statistical analysis on the results from a Lagrangian particle dispersion model (FLEXPART) and Hg(0) concentrations measured at NYA was performed by Hirdman et al. (2009) to identify source regions of high- and low-Hg air masses. The authors concluded that the lowest 10 % of the Hg(0) data at NYA in spring were strongly associated with transport across the sea-ice covered Arctic Ocean at low altitudes – areas where elevated BrO concentrations are seen in the atmospheric column by satellite observations (*e.g.*, Lindberg et al., 2002).

Similarly, a correlation of AMDEs with wind direction at ALT supports the origin of depletion events over the Arctic Ocean (Cole and Steffen, 2010). The less frequent and pronounced AMDEs at AND may be explained by the fact that this site is farther away from the source areas of AMDEs (Berg et al., 2008).

Over the 2011-2015 period, AMDEs at NYA are evenly distributed between April and May (38 % of the time in both cases), with fewer in March and June (14 and 10 % of the time, respectively). This result is in good agreement with the distribution reported by Berg et al. (2013) over the 2000-2009 period. Conversely, AMDEs are more frequent in April (41 %) than in May (32 %) at ALT, while less frequent in April (34 %) than in May (43 %) at SND. Interestingly, the analysis of the ALT data set from 1995 to 2007 by Cole and Steffen (2010) revealed that, over time, the month of maximum AMDE activity shifted from May to April. In contrast, the analysis of the NYA data set from 2000 to 2009 by Berg et al. (2013) did not evidence such a change in the timing of AMDEs. The reason for this shift in timing of AMDEs at ALT is not fully understood but could be due to local meteorology (Cole and Steffen, 2010). The authors found that the length, magnitude, and frequency of AMDEs decreased with increasing local temperature. These results are consistent with earlier studies on the temperature dependence of the halogen chemistry initiating AMDEs and ozone depletion events (Koop et al., 2000; Adams et al., 2002; Tarasick and Bottenheim, 2002; Sander et al., 2006) and with a modeling study reporting that increasing surface air temperature decreases the frequency of AMDEs (Chen et al., 2015c) . However, considering the fact that AMDEs observed at Arctic sites often result from the transport of depleted air masses, local temperature might not be the key explanatory parameter. Moore et al. (2014) showed that AMDEs and ozone depletion events near Barrow, Alaska, are directly linked to sea-ice dynamics. According to the authors, depletion events are favored by consolidated sea-ice cover but both Hg(0) and O_3 concentrations immediately recover to near-background concentrations when air masses cross open leads within a day before measurements. The authors attributed this recovery of concentrations to changes in boundary layer dynamics induced by sea-ice leads, causing significant convective mixing with non-depleted air masses aloft. Further work is needed to establish the degree to which sea-ice dynamics across the Arctic might influence the interannual variability of AMDEs at the various Arctic sites. Indeed, AMDEs occurred at ALT in 36 % (2011), 51 % (2012), 50 % (2013), and 21 % (2014) of the springtime observations, at SND in 37 % (2011), 16 % (2012), 36 % (2013), and 19 % (2014) of the springtime observations, and finally at NYA in 18 % (2011), 13 % (2012), 16 % (2013), 20 % (2014), and 6 % (2015) of the springtime observations.

Several studies reported RGM and Hg(p) concentrations during AMDEs at Arctic sites (Lindberg et al., 2002; Berg et al., 2003a; Steffen et al., 2003; Aspmo et al., 2005; Gauchard et al., 2005; Sprovieri et al., 2005a; Steen et al., 2011; Wang, 2015). Figure 6-5 shows box plots of the monthly concentrations of RGM and Hg(p) at ALT over the 2011-2014 period. A distinct annual cycle is highlighted in this figure. Hg(p) concentrations increase from November through February likely due to the Arctic haze (Steffen et al., 2014), reach a maximum in March and April due to AMDEs, and then decrease. RGM

concentrations peak in spring and then gradually decrease. The production of RGM in June and July – after the AMDEs season – is observed every year and remains unexplained (Steffen et al., 2014). While Hg(p) is the dominant species in early spring, a clear shift is observed, from the predominance of Hg(p) to RGM in AMDEs occurring toward the end of spring. This shift has already been evidenced at Churchill, Manitoba (Kirk et al., 2006), ALT (Cobbett et al., 2007), and NYA (Steen et al., 2011), and has been shown to repeat year after year at ALT (Steffen et al., 2014). Steffen et al. (2014) suggested that this shift is due to temperature and particle availability. Using a detailed air-snowpack model for interactions of bromine, ozone and mercury in the springtime Arctic, Toyota et al. (2014) proposed that Hg(p) is mainly produced as $HgBr_4^{2-}$ through uptake of RGM into bromine-enriched aerosols after ozone is significantly depleted in the air mass. In addition, Toyota et al. (2014) provided the temperature dependence of these reactions, which needs to be verified experimentally. Based on 10 years of data, Steffen et al. (2014) also reported higher levels of mercury in the snow when the atmospheric conditions favored the formation of RGM. This springtime shift from the predominance of Hg(p) to RGM in AMDEs likely directly impacts the amount of mercury deposited onto the snowpack. This will be further discussed in section 6.3.1.2.2.

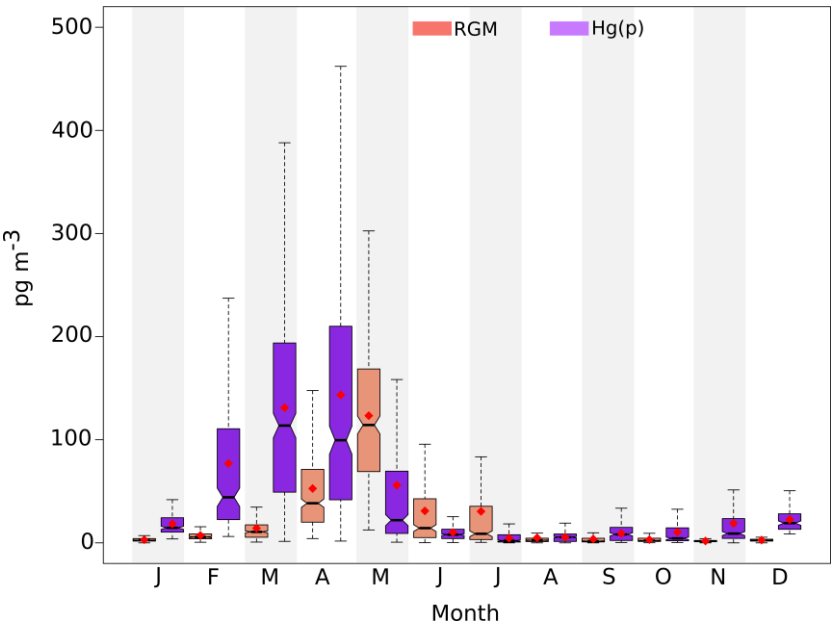

Figure 6-5: Box and whisker plots presenting the monthly RGM (in red) and Hg(p) (in violet) concentration distribution (in pg m^{-3}) at ALT over the 2011-2014 period. ◆: mean. Bottom and top of the box: first and third quartiles. Band inside the box: median. Ends of the whiskers: lowest (highest) datum still within the 1.5 interquartile range of the lowest (upper) quartile. Outliers are not represented.

Table 6-3: Monthly based statistics (number of hourly averaged Hg(0) data (n), mean (μ), median (md), standard deviation (σ)) of Hg(0) concentrations (in ng m^{-3}) at ground-based polar sites over the 2011-2015 period. Note that 2013 data at DC refer to concentrations recorded at 210 cm above the snowpack. na: not navailable due to QA/QC invalidation, instrument failure, or because the QA/QC validation is currently in progress (2015 data).

	ALT				SND				NYA				AND			
	n	μ	md	σ	n	μ	md	σ	n	μ	md	σ	n	μ	md	σ
2011																
Jan	736	1.44	1.44	0.06	698	1.46	1.46	0.07	739	1.49	1.58	0.26	627	1.72	1.71	0.14
Feb	664	1.35	1.39	0.22	631	1.40	1.40	0.08	661	1.48	1.55	0.31	446	1.72	1.73	0.14
Mar	740	1.33	1.35	0.33	613	1.24	1.30	0.28	548	1.43	1.59	0.38	673	1.71	1.73	0.21
Apr	720	0.87	0.91	0.52	621	1.05	1.13	0.36	719	1.58	1.65	0.31	631	1.59	1.59	0.16
May	647	1.38	1.28	0.73	622	0.91	0.91	0.44	709	1.17	1.18	0.42	494	1.42	1.41	0.13
Jun	690	1.87	1.85	0.31	434	1.27	1.21	0.35	716	1.46	1.58	0.28	658	1.53	1.53	0.11
Jul	672	1.96	1.97	0.48	na	na	na	na	647	1.77	1.73	0.27	676	1.55	1.54	0.09
Aug	724	1.62	1.63	0.19	na	na	na	na	663	1.66	1.68	1.15	606	1.52	1.53	0.08
Sep	670	1.21	1.20	0.06	458	1.30	1.30	0.04	715	1.66	1.66	0.12	444	1.58	1.59	0.09
Oct	719	1.16	1.16	0.02	107	1.23	1.23	0.03	669	1.59	1.60	0.12	728	1.62	1.64	0.10
Nov	395	1.20	1.21	0.06	na	na	na	na	681	1.32	1.34	0.30	719	1.64	1.62	0.11
Dec	663	1.29	1.30	0.06	528	1.52	1.53	0.05	706	1.59	1.59	0.06	742	1.71	1.71	0.06
2012																
Jan	595	1.33	1.36	0.10	744	1.53	1.53	0.07	595	1.62	1.61	0.06	720	1.75	1.74	0.07
Feb	685	1.32	1.33	0.07	696	1.48	1.49	0.07	696	1.59	1.59	0.06	696	1.76	1.75	0.05
Mar	722	0.92	1.02	0.41	744	1.26	1.35	0.29	726	1.48	1.59	0.28	744	1.73	1.73	0.08
Apr	695	0.79	0.75	0.49	319	1.29	1.32	0.41	550	1.31	1.45	0.37	720	1.59	1.60	0.12
May	698	1.19	1.27	0.59	703	1.58	1.63	0.52	697	1.39	1.46	0.26	744	1.55	1.59	0.16
Jun	720	1.52	1.52	0.24	719	1.61	1.60	0.22	698	1.52	1.50	0.10	720	1.56	1.57	0.09
Jul	728	1.50	1.44	0.33	744	1.61	1.59	0.22	734	1.68	1.68	0.17	412	1.61	1.61	0.07
Aug	744	1.27	1.26	0.09	593	1.54	1.53	0.12	678	1.70	1.69	0.09	744	1.52	1.52	0.06
Sep	657	1.16	1.16	0.06	631	1.43	1.42	0.07	713	1.58	1.56	0.10	720	1.46	1.45	0.07
Oct	742	1.16	1.16	0.04	601	1.28	1.27	0.06	664	1.38	1.39	0.05	744	1.56	1.56	0.10
Nov	718	1.16	1.17	0.06	694	1.31	1.28	0.09	700	1.40	1.41	0.08	720	1.57	1.57	0.07
Dec	743	1.16	1.18	0.05	744	1.29	1.27	0.11	730	1.45	1.47	0.15	744	1.70	1.67	0.09
2013																
Jan	468	1.25	1.27	0.12	729	1.50	1.51	0.13	483	1.51	1.54	0.13	717	1.66	1.66	0.05
Feb	671	1.23	1.27	0.14	378	1.46	1.45	0.06	596	1.65	1.67	0.10	671	1.68	1.67	0.06
Mar	664	1.14	1.28	0.40	na	na	na	na	671	1.39	1.45	0.30	725	1.57	1.59	0.07
Apr	707	0.65	0.60	0.49	582	1.43	1.38	0.63	689	1.22	1.40	0.51	680	1.46	1.49	0.20
May	739	0.91	0.87	0.67	744	1.39	1.23	0.75	744	1.40	1.48	0.33	732	1.41	1.40	0.10
Jun	696	1.43	1.53	0.59	719	1.89	1.96	0.50	686	1.45	1.63	0.42	713	1.41	1.43	0.13
Jul	742	1.82	1.80	0.23	709	1.97	1.95	0.28	206	1.52	1.50	0.13	717	1.43	1.45	0.12
Aug	720	1.71	1.67	0.15	538	1.84	1.76	0.23	716	1.63	1.60	0.12	622	1.42	1.43	0.11
Sep	720	1.43	1.41	0.04	412	1.47	1.49	0.13	690	1.51	1.51	0.07	266	1.50	1.49	0.08
Oct	744	1.36	1.36	0.04	502	1.41	1.40	0.05	687	1.48	1.48	0.06	739	1.56	1.56	0.05
Nov	605	1.36	1.36	0.02	597	1.40	1.39	0.17	298	1.40	1.41	0.07	545	1.60	1.61	0.05
Dec	646	1.32	1.33	0.07	694	1.36	1.36	0.09	514	1.52	1.44	0.31	735	1.69	1.69	0.05
2014																
Jan	743	1.47	1.47	0.07	719	1.41	1.37	0.16	701	1.44	1.60	0.36	688	1.69	1.68	0.04
Feb	671	1.48	1.52	0.16	672	1.42	1.46	0.23	584	1.69	1.67	0.10	656	1.66	1.66	0.06
Mar	744	1.49	1.59	0.31	694	1.34	1.34	0.33	703	1.55	1.64	0.24	718	1.62	1.61	0.07
Apr	675	1.42	1.45	0.60	718	1.21	1.21	0.47	688	1.31	1.49	0.49	677	1.52	1.52	0.11
May	702	1.21	1.29	0.50	722	1.56	1.60	0.50	709	1.13	1.33	0.54	534	1.27	1.28	0.26
Jun	712	1.43	1.58	0.39	718	1.46	1.45	0.25	689	1.49	1.56	0.25	664	1.41	1.43	0.12
Jul	732	1.74	1.72	0.21	28	1.47	1.46	0.05	666	1.62	1.59	0.15	714	1.41	1.42	0.10
Aug	744	1.72	1.65	0.21	na	na	na	na	na	na	na	na	725	1.38	1.38	0.09
Sep	720	1.43	1.42	0.06	na	na	na	na	na	na	na	na	711	1.37	1.37	0.08
Oct	605	1.36	1.36	0.02	na	na	na	na	586	1.40	1.44	0.14	740	1.45	1.45	0.06
Nov	646	1.32	1.33	0.07	50	1.14	1.13	0.05	660	1.56	1.56	0.09	582	1.54	1.54	0.06
Dec	664	1.29	1.31	0.10	670	1.12	1.12	0.04	744	1.57	1.58	0.08	737	1.61	1.60	0.05
2015																
Jan	na	na	na	na	na	na	na	na	730	1.56	1.56	0.10	139	1.57	1.57	0.04
Feb	na	na	na	na	na	na	na	na	665	1.52	1.50	0.14	560	1.58	1.59	0.06
Mar	na	na	na	na	na	na	na	na	701	1.53	1.58	0.19	585	1.47	1.46	0.09
Apr	na	na	na	na	na	na	na	na	707	1.39	1.48	0.37	607	1.56	1.54	0.15
May	na	na	na	na	672	1.05	1.01	0.37	742	1.34	1.34	0.23	741	1.47	1.48	0.08
Jun	na	na	na	na	387	1.22	1.21	0.16	616	1.67	1.64	0.20	703	1.49	1.48	0.09
Jul	na	na	na	na	na	na	na	na	720	1.73	1.70	0.20	729	1.50	1.50	0.09
Aug	na	na	na	na	na	na	na	na	682	1.53	1.54	0.12	568	1.54	1.52	0.12
Sep	na	na	na	na	na	na	na	na	616	1.67	1.64	0.20	703	1.49	1.48	0.09
Oct	na	na	na	na	na	na	na	na	707	1.37	1.37	0.07	665	1.52	1.51	0.05
Nov	na	na	na	na	na	na	na	na	682	1.40	1.41	0.08	568	1.48	1.49	0.05
Dec	na	na	na	na	na	na	na	na	702	1.52	1.51	0.11	628	1.46	1.46	0.09

	TR				DC				DDU			
	n	μ	md	σ	n	μ	md	σ	n	μ	md	σ
2011												
Jan	671	0.85	0.86	0.25	na	na	na	na	na	na	na	na
Feb	656	0.98	1.06	0.25	na	na	na	na	na	na	na	na
Mar	735	1.06	1.05	0.11	na	na	na	na	na	na	na	na
Apr	711	1.01	1.01	0.05	na	na	na	na	na	na	na	na
May	718	0.99	0.99	0.03	na	na	na	na	na	na	na	na
Jun	614	0.98	0.99	0.04	na	na	na	na	na	na	na	na
Jul	733	0.98	0.98	0.05	na	na	na	na	na	na	na	na
Aug	169	0.92	0.92	0.04	na	na	na	na	na	na	na	na
Sep	na	na	na	na	na	na	na	na	na	na	na	na
Oct	na	na	na	na	na	na	na	na	na	na	na	na
Nov	254	0.59	0.71	0.34	na	na	na	na	na	na	na	na
Dec	717	0.87	0.86	0.29	na	na	na	na	na	na	na	na
2012												
Jan	497	1.07	1.08	0.28	259	0.61	0.57	0.33	576	1.06	1.09	0.32
Feb	660	1.03	1.00	0.23	593	0.93	1.00	0.42	670	1.01	1.03	0.23
Mar	744	0.97	0.97	0.05	67	1.14	1.14	0.26	635	0.97	0.95	0.09
Apr	712	0.97	0.96	0.04	na	na	na	na	668	0.97	0.98	0.08
May	649	0.97	0.97	0.03	na	na	na	na	696	0.92	0.94	0.11
Jun	654	0.95	0.94	0.04	423	0.82	0.81	0.06	663	0.88	0.88	0.08
Jul	487	0.87	0.87	0.06	624	0.70	0.70	0.05	101	0.79	0.79	0.07
Aug	670	1.01	1.02	0.07	682	0.66	0.67	0.05	107	0.63	0.62	0.05
Sep	612	1.08	1.08	0.08	682	0.72	0.66	0.14	131	0.99	1.00	0.09
Oct	744	1.02	1.01	0.12	431	0.79	0.81	0.20	719	0.82	0.84	0.14
Nov	699	0.94	0.94	0.15	na	na	na	na	428	0.76	0.74	0.24
Dec	680	0.90	0.88	0.22	na	na	na	na	555	0.82	0.80	0.21
2013												
Jan	711	0.97	0.96	0.24	762	0.69	0.64	0.30	644	0.88	0.84	0.37
Feb	665	0.93	0.97	0.21	585	0.68	0.59	0.41	450	0.81	0.81	0.23
Mar	727	0.98	1.00	0.08	487	1.16	1.15	0.19	215	0.81	0.77	0.15
Apr	704	0.98	0.97	0.05	271	1.16	1.14	0.16	635	0.96	0.95	0.04
May	688	0.94	0.94	0.03	464	1.01	0.99	0.10	725	0.88	0.88	0.04
Jun	718	0.95	0.95	0.02	297	0.93	0.93	0.05	661	0.83	0.83	0.05
Jul	713	0.96	0.96	0.03	554	0.89	0.89	0.05	639	0.80	0.81	0.09
Aug	679	0.90	0.91	0.05	591	0.75	0.75	0.08	655	0.73	0.73	0.10
Sep	670	0.87	0.87	0.06	616	0.85	0.85	0.08	82	0.68	0.68	0.06
Oct	710	0.79	0.76	0.12	245	0.75	0.79	0.17	na	na	na	na
Nov	606	0.76	0.76	0.18	431	0.66	0.60	0.33	na	na	na	na
Dec	606	0.78	0.76	0.20	213	0.84	0.85	0.24	415	0.98	0.97	0.25
2014												
Jan	427	0.70	0.62	0.31	na	na	na	na	585	0.91	0.92	0.33
Feb	414	0.89	0.90	0.17	na	na	na	na	26	0.42	0.41	0.13
Mar	708	1.09	1.09	0.16	na	na	na	na	na	na	na	na
Apr	681	1.06	1.07	0.04	na	na	na	na	50	0.97	0.98	0.04
May	542	1.07	1.08	0.05	na	na	na	na	84	0.68	0.63	0.10
Jun	680	1.03	1.03	0.05	na	na	na	na	na	na	na	na
Jul	693	1.00	1.00	0.03	na	na	na	na	17	0.82	0.81	0.03
Aug	672	1.02	1.02	0.05	na	na	na	na	na	na	na	na
Sep	670	0.99	0.99	0.06	na	na	na	na	na	na	na	na
Oct	662	0.91	0.91	0.19	na	na	na	na	na	na	na	na
Nov	586	0.76	0.76	0.24	na	na	na	na	569	0.67	0.65	0.30
Dec	686	0.79	0.72	0.33	240	0.87	0.78	0.43	626	1.00	0.99	0.45
2015												
Jan	648	0.94	0.83	0.41	710	0.88	0.81	0.51	711	0.82	0.82	0.31
Feb	520	0.95	0.92	0.25	652	0.93	0.78	0.59	664	0.81	0.81	0.21
Mar	na	na	na	na	734	1.50	1.47	0.31	695	0.90	0.89	0.09
Apr	na	na	na	na	717	1.49	1.49	0.16	715	0.89	0.88	0.06
May	na	na	na	na	648	1.31	1.30	0.11	329	0.90	0.89	0.05
Jun	na	na	na	na	717	1.20	1.18	0.06	na	na	na	na
Jul	na	na	na	na	744	1.14	1.14	0.05	na	na	na	na
Aug	na	na	na	na	740	1.10	1.10	0.07	na	na	na	na
Sep	na	na	na	na	718	1.03	1.05	0.15	na	na	na	na
Oct	714	0.94	0.96	0.21	725	0.71	0.69	0.32	na	na	na	na
Nov	695	0.91	0.90	0.26	680	0.54	0.48	0.29	na	na	na	na
Dec	712	0.91	0.79	0.41	598	0.81	0.76	0.33	na	na	na	na

6.3.1.1.3 Summer enhancement of Hg(0) concentrations

According to Dastoor and Larocque (2004), advection of mercury from midlatitudes to the Arctic is insignificant in summer due to weak airflow movements and to a confined polar front. The increase of Hg(0) concentrations in summer could be due to the reemission of mercury deposited during springtime AMDEs. However, the comparison of the magnitude of the springtime depletion and the magnitude of the summer enhancement at ALT suggests otherwise. Mean springtime Hg(0) concentrations are lower – suggesting more intense and/or frequent AMDEs – in 2012 (0.97 ± 0.53 ng m^{-3}) and 2013 (0.89 ± 0.57 ng m^{-3}) than in 2011 (1.19 ± 0.59 ng m^{-3}) and 2014 (1.37 ± 0.50 ng m^{-3}), while mean summertime concentrations are higher – suggesting more reemission – in 2011 (1.81 ± 0.37 ng m^{-3}) and 2014 (1.63 ± 0.31 ng m^{-3}) than in 2012 (1.43 ± 0.27 ng m^{-3}) and 2013 (1.65 ± 0.41 ng m^{-3}). Therefore, the summer enhancement of Hg(0) concentrations is generally attributed to emissions from snow and ice surfaces (Poulain et al., 2004; Sprovieri et al., 2005b; Sprovieri et al., 2005a; Sprovieri et al., 2010; Douglas et al., 2012) and/or to evasion from the ice-free surface waters of the Arctic Ocean (Aspmo et al., 2006; Andersson et al., 2008; Hirdman et al., 2009; Fisher et al., 2013; Dastoor and Durnford, 2014; Yu et al., 2014; Soerensen et al., 2016). Inhomogeneous distributions of Hg(0) were observed over the Arctic Ocean during the CHINARE 2012 (Yu et al., 2014) and the Beringia 2005 (Sommar et al., 2010) expeditions. Both studies reported a rapid increase of concentrations in air when entering the ice-covered waters, highlighting the influence of sea-ice dynamics on Hg(0) concentrations. The atmospheric mercury model (GRAHM) used by Dastoor and Durnford (2014) simulated a first peak in Hg(0) concentrations driven by re-volatilization from snowpack/meltwaters, followed by a second peak driven by oceanic evasion – the timing of the peaks varying with location and year. Additional field and modeling studies suggested that some of the mercury in surface ocean waters may come from riverine input (Fisher et al., 2012; Yu et al., 2014; Soerensen et al., 2016).

As can be seen in Figure 6-3, Hg(0) concentrations are significantly higher (p value < 0.0001, Mann-Whitney test) during summer 2011 at ALT (1.81 ± 0.37 ng m^{-3}) than during the following summers (1.57 ± 0.35 ng m^{-3} on average). At SND, Hg(0) concentrations peak in summer 2013 (1.91 ± 0.37 ng m^{-3} *vs.* 1.52 ± 0.26 ng m^{-3} in average during summers 2011, 2012, and 2014). One possible explanation for this interannual variability is sea-ice extent. Daily sea-ice maps can be obtained from http://www.iup.uni-bremen.de/iuppage/psa/2001/amsrop.html (Spreen et al., 2008). ALT and SND are both surrounded by multi-year ice. During summer 2011, the Hall Basin – waterway between Greenland and Canada's northernmost island where ALT is located – was ice free. During summer 2013, sea-ice extent was particularly low in the Greenland Sea – between Greenland and the Svalbard archipelago. These large areas of ice-free surface waters might have led to enhanced oceanic evasion near ALT and SND in 2011 and 2013, respectively. Indeed, Yu et al. (2014) reported a negative correlation between TGM and salinity over an Arctic ice-covered region, suggesting that ice melting would enhance TGM concentrations. This

hypothesis is further supported by wind data obtainable from the two links below. At ALT, the summertime dominant wind direction is from northeast but with frequent and strong winds from south/southwest (Hall Basin), in line with results reported by Bilello (1973) and Cobbett et al. (2007). At SND, the dominant wind direction is from southwest but the direction becomes more variable in summer with winds also occurring from south and east (Bilello, 1973; Nguyen et al., 2013). However, a comprehensive and systematic analysis of air mass back-trajectories and sea-ice extent is required to further investigate parameters responsible for the observed interannual variability.

http://climate.weather.gc.ca/historical_data/search_historic_data_e.html
http://villumresearchstation.dk/data/

NYA is normally surrounded by open water in the summer. Therefore, oceanic emissions are expected to act as a significant local source to NYA, while being a regional and diffuse source at ALT and SND (Cole et al., 2013). However, the summer enhancement of Hg(0) concentrations is weaker at NYA than at ALT and SND (Figure 6-4). The western coast of Spitsbergen island, where NYA is located, was ice-free year-round over the period of interest possibly preventing the buildup of mercury-enriched ice-covered surface waters in winter and intense evasion in summer. Additionally, a comparative study was carried out at NYA with measurements at both 12 m a.s.l. and 474 m a.s.l. While Aspmo et al. (2005) found no significant difference between Hg(0) concentrations at the two elevations, several studies (Berg et al., 2003b; Sprovieri et al., 2005b; Sommar et al., 2007) reported that Hg(0) concentrations at 12 m a.s.l. were higher in magnitude and exhibited a higher variability than at 474 m a.s.l. Evidence of volatile mercury evasion from snow and water surfaces was also obtained, suggesting a cycling of mercury near the surface. Zeppelin station at 474 m a.s.l. is typically positioned over or at the top of the marine boundary layer of the fjord valley (Sommar et al., 2007) likely, at least partly, explaining why the summer enhancement of Hg(0) concentrations is weaker at NYA.

In contrast to observations at ALT, SND, and NYA, Hg(0) concentrations reach a minimum in summer at AND. Transport of air masses from Europe is dominant at AND (Durnford et al., 2010) and could mask any variability induced by oceanic evasion. The mean Hg(0) concentration in summer at AND (1.48 ± 0.12 ng m^{-3} over the 2011-2015 period) is consistent with the value of ~ 1.42 ng m^{-3} reported at Pallas, Finland, over the 2013-2014 period (Sprovieri et al., 2016b).

6.3.1.2 Comparison with models

Table 6-4 displays goodness-of-fit statistics between monthly-averaged modeled and observed data in 2013. Except at ALT, modeled Hg(0) concentrations are biased low suggesting that the four global models tend to underestimate sources of Hg(0). The ability of the four models to reproduce the observed seasonality of Hg(0) concentrations at Arctic sites in 2013 is shown in Figure 6-6a and discussed in the following sections. As mentioned in

section 6.2.2, GEM-MACH-Hg and GEOS-Chem provided hourly averaged data from 2011 to 2014. The interannual variability of the monthly Hg(0) concentration distribution at Arctic sites as simulated by the two models is displayed in Figure 6-7a while Table 6-5 shows the percent bias between hourly averaged modeled and observed data on a seasonal basis from 2011 to 2014.

Table 6-4: Goodness-of-fit statistics between monthly averaged (year 2013) modeled and observed Hg(0) data at all ground-based sites: Nash-Sutcliffe efficiency (NSE, quantity without unit), root-mean square error (RMSE, in ng m^{-3}), and percent bias (PBIAS, in %).

	ALT	SND	NYA	AND	TR	DC	DDU
GLEMOS							
NSE	0.12	-0.83	0.00	-2.76	-1.83	-0.28	-6.10
RMSE	0.29	0.29	0.11	0.20	0.13	0.19	0.24
PBIAS	4.9	-12.0	-6.3	-8.3	14.0	16.2	25.4
GEOS-Chem							
NSE	0.32	-0.85	-1.82	-2.50	-4.76	-1.07	-8.15
RMSE	0.25	0.29	0.18	0.19	0.19	0.25	0.27
PBIAS	1.3	-13.7	-9.7	-12.2	3.0	7.5	16.9
GEM-MACH-Hg							
NSE	0.49	-0.17	-0.40	-0.26	-2.98	-1.08	-4.87
RMSE	0.22	0.23	0.13	0.12	0.16	0.25	0.22
PBIAS	4.1	-9.0	-4.4	-4.1	10.2	16.3	16.7
ECHMERIT							
NSE	-0.27	-2.85	-4.16	-6.24	-2.50	-0.32	-0.85
RMSE	0.34	0.42	0.25	0.28	0.15	0.20	0.12
PBIAS	-10.0	-22.7	-15.5	-16.7	-11.8	-6.6	-5.1

6.3.1.2.1 Seasonal variation

a) Winter

All the models (except ECHMERIT) overestimate Hg(0) concentrations at ALT in January and February 2013, but reproduce well the average value in December 2013 (Figure 6-6a). It is worth noting that the observed mean value in January/February 2013 (1.24 ± 0.13 ng m^{-3}) is lower than the value observed in December 2013 (1.45 ± 0.07 ng m^{-3}) and lower than the hemispheric background (1.30-1.60 ng m^{-3} according to Sprovieri et al. (2016b)). Additionally, the observed mean value in January/February 2013 is at the low end of values reported in this period of the year at ALT from 2011 to 2014 (Figure 6-3, 1.40 ± 0.16 ng m^{-3} in 2011, 1.32 ± 0.09 ng m^{-3} in 2012, and 1.47 ± 0.12 ng m^{-3} in 2014). The interannual variability of observed Hg(0) concentrations at ALT is not captured by models. Modeled Hg(0) concentrations in January/February range from 1.48 ± 0.03 in 2014 to 1.54 ± 0.03 ng m^{-3} in 2011 and 2012 with GEOS-Chem and from 1.54 ± 0.06 in 2012 to 1.58 ± 0.04 ng m^{-3} in 2013 with GEM-MACH-Hg. Similarly, the interannual variability of modeled Hg(0) concentrations is low at other Arctic sites (Figure 6-7a). The wintertime interannual variability of observed Hg(0) concentrations might be driven by meteorology and mercury emissions in midlatitudes. However, the AMAP/UNEP (2010) global inventory of mercury anthropogenic emissions (annual mean emission fields) was used for all simulated years

(2011-2014) in both GEOS-Chem and GEM-MACH-Hg, preventing the consideration of interannual changes in anthropogenic emissions.

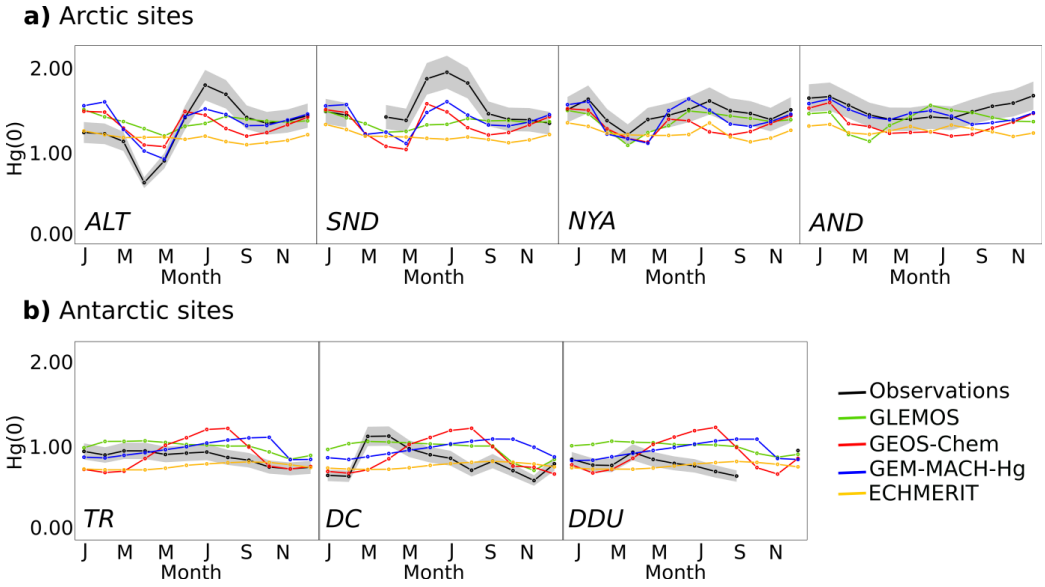

Figure 6-6: Year 2013 monthly averaged Hg(0) concentrations (in ng m^{-3}) at **a)** Arctic and **b)** Antarctic ground-based sites: observations (in black) and concentrations according to the four global models (GLEMOS in green, GEOS-Chem in red, GEM-MACH-Hg in blue, ECHMERIT in yellow). The gray shaded regions indicate a 10 % uncertainty for observations.

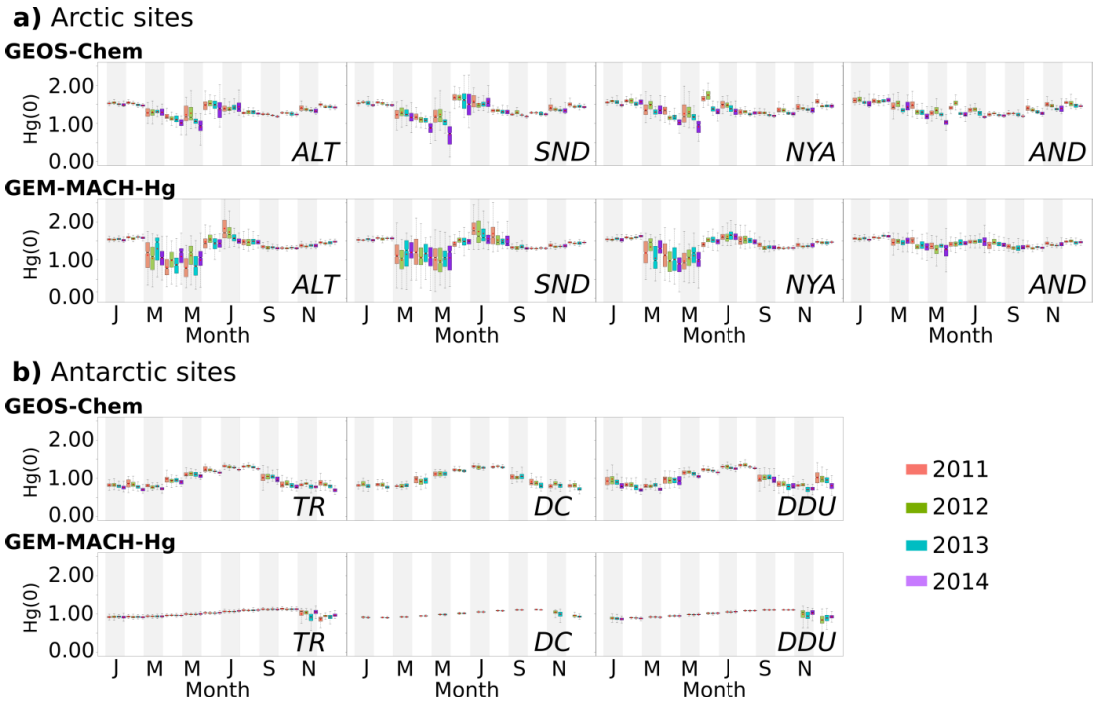

Figure 6-7: Box and whisker plots presenting the monthly Hg(0) concentration distribution at **a)** Arctic and **b)** Antarctic ground-based sites as simulated by GEOS-Chem and GEM-MACH-Hg in 2011 (pink), 2012 (green), 2013 (turquoise), and 2014 (purple). ◆: mean. Bottom and top of the box: first and third quartiles. Band inside the box: median. Ends of the whiskers: lowest (highest) datum still within the 1.5 interquartile range of the lowest (upper) quartile. Outliers are not represented.

Table 6-5: Percent bias (in %) between hourly averaged modeled and observed Hg(0) data at all ground-based sites. Summer refers to Jun-Aug (Nov-Feb), fall to Sep-Nov (Mar-Apr), winter to Dec-Feb (May-Aug), and spring to Mar-May (Sep-Oct) at Arctic (Antarctic) sites. na: not available due to QA/QC invalidation or instrument failure.

	GEOS-Chem				GEM-MACH-Hg			
	2011	2012	2013	2014	2011	2012	2013	2014
Summer								
ALT	-23.9	-1.9	-15.4	-17.1	-12.3	11.1	-9.2	-10.0
SND	34.3	-3.8	-22.0	4.6	11.6	1.4	-17.5	3.4
NYA	-8.9	-7.3	-14.7	-15.6	-5.9	-4.4	-0.2	-1.0
AND	-13.2	-10.4	-11.9	-14.1	-7.2	-6.8	3.2	3.0
TR	-1.1	-14.0	-8.9	-5.6	4.0	-1.9	6.3	23.6
DC	na	1.7	15.6	na	na	8.7	35.6	na
DDU	na	0.1	0.0	-8.3	na	-3.4	-1.7	8.4
Fall								
ALT	9.4	11.7	-9.8	-9.5	13.4	14.7	-3.6	-3.0
SND	-3.3	-1.5	-9.1	23.4	2.7	-0.5	-5.0	26.8
NYA	-11.1	-7.9	-14.4	-12.0	-9.3	-8.4	-9.7	-8.5
AND	-12.6	-11.1	-15.0	-12.1	-13.4	-12.5	-13.9	-6.5
TR	-13.1	-12.0	-10.9	-24.6	-7.8	-1.4	-2.9	-11.6
DC	na	-31.5	-22.6	na	na	-18.6	-43.4	na
DDU	na	-9.6	1.1	-19.9	na	-3.2	2.1	-4.4
Winter								
ALT	11.8	18.5	11.7	3.3	12.8	19.2	16.2	8.0
SND	5.5	5.5	4.2	11.6	5.1	4.8	5.5	15.3
NYA	4.1	0.1	-3.0	-4.0	1.3	-1.4	-1.4	-1.5
AND	-7.6	-9.0	-8.0	-7.6	-10.1	-11.1	-7.2	-6.7
TR	25.3	29.8	29.6	14.1	5.8	9.2	11.3	2.8
DC	na	79.9	39.3	na	na	48.4	17.8	na
DDU	na	38.5	50.4	49.4	na	15.4	26.9	40.4
Spring								
ALT	3.2	27.4	29.7	-21.8	-23.0	9.3	11.8	-24.0
SND	12.3	-11.6	-25.5	-33.3	4.2	-27.7	-23.0	-18.8
NYA	-5.8	-5.3	-9.7	-17.8	-23.8	-17.0	-21.5	-20.4
AND	-11.5	-13.8	-12.4	-16.7	-9.3	-16.0	-5.5	-7.6
TR	na	-9.0	13.0	-7.7	na	7.5	36.5	18.1
DC	na	32.6	22.9	na	na	48.8	34.5	na
DDU	na	3.2	73.6	na	na	31.9	62.8	na

b) Spring

Springtime reflects the lowest Hg(0) concentrations at ALT, SND, and NYA due to the occurrence of AMDEs (see section 6.3.1.1.2). This minimum is well reproduced by GEM-MACH-Hg, GEOS-Chem, and GLEMOS at all three stations, but not reproduced by ECHMERIT (Figure 6-6a). It should be noted that there is no parameterization of AMDEs in the latter. Interestingly, GLEMOS predicts a similar springtime minimum at AND in contradiction with the seasonal pattern observed at this station (see section 6.3.1.1.2). This discrepancy can likely be attributed to uncertainties in Br fields extracted from p-TOMCAT.

As discussed in section 6.3.1.1.2, AMDEs were less frequent at ALT in 2014. This lower occurrence frequency is fairly well reproduced by GEM-MACH-Hg (61 % (2011), 43 % (2012), 53 % (2013), and 36 % (2014)), but not at all by GEOS-Chem (4 % (2011), 6 %

(2012), 13 % (2013), and 37 % (2014)). A temperature dependence of BrO concentrations is implemented in GEM-MACH-Hg and Br_2 is assumed to occur only over consolidated sea-ice which would change with changing meteorological conditions. Conversely, a constant value of 5 pptv of BrO is added in the springtime Arctic boundary layer into GEOS-Chem v9-02. However, updates to Arctic mercury processes will be implemented in v11-01 based on Fisher et al. (2012) and Fisher et al. (2013) (http://wiki.seas.harvard.edu/geos-chem/index.php/Mercury#Updates_to_Arctic_Hg_processes). BrO concentrations will depend on temperature according to a relationship chosen to optimize spring Hg(0) concentrations and the shift of peak depletion at ALT from May to April (see section 6.3.1.1.2). It should also be noted that GEOS-Chem relies on GEOS-5 and GEOS-FP meteorological fields in 2011-2013 and 2014, respectively. Simulations in polar regions can be very sensitive to subtle changes in meteorological fields, especially during the AMDEs season, which could at least partly explain the interannual variability of modeled AMDEs occurrence frequencies.

Based on the work by Moore et al. (2014) showing the impact of sea-ice leads on AMDEs (AMDEs might be favored by consolidated sea-ice cover, see section 6.3.1.1.2), real-time distribution of sea-ice dynamics including presence of leads is needed. Contrarily to conclusions by Moore et al. (2014), a recent modeling study (Chen et al., 2015c) carried out using GEOS-Chem v9-02 – but including an ice/snow module and riverine inputs as described by Fisher et al. (2012) and Fisher et al. (2013) – showed that increasing sea-ice lead occurrence increases the frequency of AMDEs. These contradictory results highlight the fact that further work is needed regarding the degree to which sea-ice dynamics across the Arctic alters mercury chemistry in spring.

c) Summer

All the models (except ECHMERIT in which polar processes are not implemented) capture, to some extent, the summertime Hg(0) enhancement. GLEMOS clearly underestimates summertime mean concentrations at ALT and SND (Figure 1-3a). This can be attributed to missing reemissions and/or oceanic evasion. As mentioned is section 6.3.1.1.3, Dastoor and Durnford (2014) suggested two distinct summertime maxima: the first one supported by re-volatilization from snowpack/meltwaters occurring from the end of May to mid-June at ALT, and in June at NYA; the second one supported by oceanic evasion from mid-July to early August at ALT and NYA. GEOS-Chem gives a summer maximum in June instead of July at ALT, SND and NYA. This time lag might result from to the fact that oceanic evasion from the Arctic Ocean is not implemented in v9-02. v11-01 of the model will include, among other updates, new present-day (2009) fields for net primary productivity (NPP) based on Jin et al. (2012), a UV-B dependence for Hg(II) reduction in seawater based on results of O'Driscoll et al. (2006), updated Hg(0) emissions from snow, and a source of mercury from the snowpack to the Arctic Ocean at the onset of snowmelt. In order for the models to reproduce the interannual variability of Hg(0) concentrations, real-time distribution

of areas of ice-free surface waters along with the type of surface (ice/snow/snow-free bedrock) are needed.

6.3.1.2.2 Reactive mercury and deposition

Year 2013 modeled monthly-averaged RM concentrations and wet/dry deposition are displayed in Figure 6-8a. GEOS-Chem, GEM-MACH-Hg, and GLEMOS predict increased RM concentrations in spring, during the AMDEs season, consistent with the observed pattern at ALT (Figure 6-5) and NYA (Wang, 2015). The fact that ECHMERIT does not capture the spring enhancement is not surprising since the model does not implement any chemistry specific to polar regions. GLEMOS also predicts a RM spring maximum at AND, in line with the modeled Hg(0) spring minimum at this site (Figure 6-6a). As discussed in section 6.3.1.2.1, this can likely be attributed to uncertainties in Br fields extracted from p-TOMCAT. Long-term measurements of RM in the Arctic are scarce and limited to ALT and NYA (data not presented here). According to Figure 6-8a, all four models underestimate RM concentrations at ALT from at least January to April 2013. Similarly, the comparison of modeled RM concentrations at NYA with annual averages reported by Steen et al. (2011) and Wang (2015) suggests an underestimation of the concentrations by GEOS-Chem, GEM-MACH-Hg, and ECHMERIT.

According to the models, deposition of mercury peaks in spring at ALT and SND, consistent with the RM spring maximum. The deposition of mercury during AMDEs depends on temperature, relative humidity and aerosol contribution (Cobbett et al., 2007), and is higher when the atmospheric conditions favor the formation of RGM over Hg(p) (see section 6.3.1.1.2). Therefore, as suggested by Steffen et al. (2015), prevailing atmospheric conditions must be fully characterized in order to accurately evaluate the deposition of mercury. GEOS-Chem and GLEMOS both predict higher dry deposition in spring at NYA. Wet deposition is largely driven by precipitation – RM being readily scavenged by rain or snow, whereas dry deposition depends on the boundary layer stability and the type of the underlying surface (Cadle, 1991). Deposition of mercury in the Arctic is typically inferred from concentrations of total mercury in the snowpack (e.g., Steffen et al., 2014) or from a Hg(0) flux gradient method (Steffen et al., 2002; Brooks et al., 2006a; Cobbett et al., 2007; Steen et al., 2009), and not through direct measurement of wet and dry deposition, making it difficult to evaluate the accuracy of models predictions. To the best of our knowledge, NYA is the only site out of the four Arctic sites where wet deposition measurements have been reported (Sprovieri et al., 2016a). From May to December 2013, the observed net wet deposition flux is equal to 0.9 µg m^{-2} while modeled fluxes amount to 1.7, 3.2, 2.8, and 2.4 µg m^{-2} according to GLEMOS, GEOS-Chem, GEM-MACH-Hg, and ECHMERIT, respectively. All four models overestimate the wet deposition flux. Interestingly, all four models also overestimate the amount of precipitation (by a factor of 2.0, 2.2, 2.1, and 1.1, respectively; data not shown). Several studies showed that the form of precipitation (rain *vs.* snow) influences the collection efficiency of the sampler. Lynch et al. (2003) and Prestbo and Gay (2009) found that the annual collection efficiency is 89 % and 87.1 ± 6.5 %, respectively, at cold weather sites in

the United States and Canada experiencing snowfall in winter *vs.* 98.8 ± 4.3 % at warm weather sites (Prestbo and Gay, 2009). Assuming an annual 89 % collection efficiency of snow at NYA does not narrow the gap between observed and modeled amounts of precipitation. However, an annual 89 % collection efficiency at NYA seems generous considering that snow falls year-round and that strong wind (> 10 m s^{-1}) and blowing snow are frequent, especially in winter (Maturilli et al., 2013).

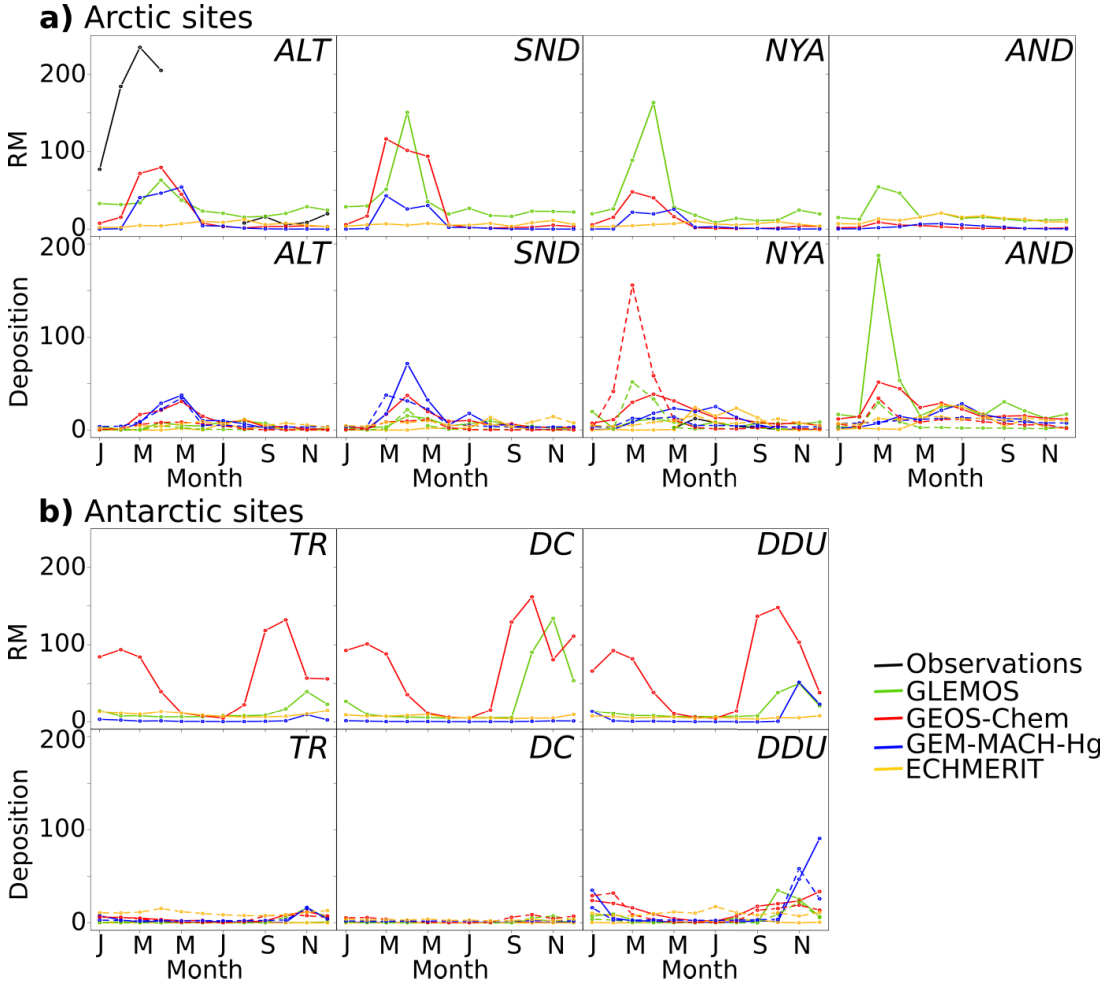

Figure 6-8: Year 2013 monthly averaged mean reactive mercury (RM) concentrations (in pg m^{-3}) along with mean wet (solid line) and dry (dashed line) deposition (in ng m^{-2} day^{-1}) at **a)** Arctic and **b)** Antarctic ground-based sites: observations (in black) and concentrations according to the four global models (GLEMOS in green, GEOS-Chem in red, GEM-MACH-Hg in blue, ECHMERIT in yellow). Note that RM (wet deposition) observations are available at ALT (NYA) only.

6.3.2 Antarctic sites

6.3.2.1 Observations

Figure 6-2b shows monthly box plots of all data collected in Antarctica (ground-based sites and cruises). Hg(0) concentrations from the ANT cruises displayed in Figure 6-2b refer to data collected when R/V Polarstern operated within the marginal sea-ice region (from 8

July to 23 July 2013, from 25 July to 9 August 2013, and from 28 August to 5 October 2013) (Nerentorp Mastromonaco et al., 2016). Similarly, Hg(0) concentrations from the OSO cruise refer to data collected at latitude > 60° S. Hg(0) concentrations measured during the ANT and OSO cruises are somewhat higher than values at ground-based Antarctic sites. The average value at Antarctic sites is 0.96 ± 0.32 ng m^{-3}, *i.e.* 35 % lower than the average value at Arctic sites (see section 6.3.1.1). This result is consistent with the north-to-south Hg(0) decreasing gradient reported by Sprovieri et al. (2016b), and with values reported at southern hemisphere midlatitudes sites (Angot et al., 2014; Slemr et al., 2015).

The Hg(0) concentration data from the three Antarctic ground-based sites for the period 2011-2015 are presented as monthly box and whisker plots in Figure 6-9. Information regarding annually and monthly based statistics at the three sites can be found in Table 6-2 and Table 6-3, respectively. The annual medians for 2011-2015 at TR and 2012-2015 at DDU (Table 6-2) suggest a low inter annual variability in the distribution of Hg(0) concentrations. Conversely, Hg(0) concentrations are notably higher in 2015 than in 2012 and 2013 at DC. This trend is more apparent from Figure 6-9b, especially from March to September. It is worth noting that in 2015 measurements were performed at a different location within the "clean area" (the instrument was moved from one shelter to another). Additionally, following the January 2014 instrument failure, a new Tekran instrument operated in 2015. The combination of these two elements likely, at least partly, explains the offset observed in 2015. Despite this offset, the seasonal trends of Hg(0) repeat from year to year at DC (see below).

The mean seasonal variation of Hg(0) concentrations at Antarctic ground-based sites is displayed in Figure 6-4b. Summer refers to November-February, fall to March-April, winter to May-August, and spring to September-October. At TR, the Hg(0) concentrations are significantly (p value < 0.0001, Mann-Whitney test) higher in winter (0.98 ± 0.06 ng m^{-3}) than in summer (0.89 ± 0.29 ng m^{-3}), in good agreement with the seasonal variation reported at TR by Pfaffhuber et al. (2012) from February 2007 to June 2011, and at Neumayer (NM) by Ebinghaus et al. (2002b). Contrarily, Hg(0) concentrations at DDU are slightly but significantly (p value < 0.0001, Mann-Whitney test) higher in summer (0.88 ± 0.32 ng m^{-3}) than in winter (0.84 ± 0.11 ng m^{-3}). On the high-altitude Antarctic Plateau at DC, Hg(0) concentrations exhibit a distinct maximum in fall (1.45 ± 0.27 ng m^{-3}) and a minimum in summer (0.78 ± 0.46 ng m^{-3}). The mechanisms which cause the seasonal variation of Hg(0) concentrations at Antarctic sites are discussed in the following sections.

6.3.2.1.1 The winter mysteries

Hg(0) concentrations at TR remain at a fairly constant level of 0.98 ± 0.06 ng m^{-3} on average from April to August (Figure 6-2b). This result is in good agreement with observations at Neumayer (Ebinghaus et al., 2002b). Pfaffhuber et al. (2012) attributed this phenomenon to the lack of photochemical oxidation processes during the polar night. Conversely, Hg(0) concentrations exhibit a gradual 30 % decrease at DC, from 1.48 ± 0.19 on average in April to 0.98 ± 0.20 ng m^{-3} in August. This decreasing trend remains unexplained

and possibly results from the dry deposition of Hg(0) onto the snowpack (Angot et al., 2016b). In 2013, measurements were performed at various height levels above the snow surface. Interestingly, Angot et al. (2016b) reported a steeper decrease of Hg(0) concentrations close to the snow surface suggesting that the snowpack may act as a sink for mercury. Similarly, a gradual 20 % decrease in Hg(0) concentrations is observed at DDU, from 0.94 ± 0.07 on average in April to 0.72 ± 0.10 ng m^{-3} in August (Figure 6-2b). Based on an analysis of air mass back trajectories, Angot et al. (2016a) suggested that this decreasing trend at DDU most likely results from reactions occurring within the shallow boundary layer on the Antarctic Plateau, subsequently transported toward the coastal margins by katabatic winds. DDU is influenced most of the time by inland air masses whereas several studies showed that stations such as NM are not significantly impacted by air masses originating from the Antarctic Plateau (Helmig et al., 2007; Legrand et al., 2016b) explaining why concentrations remain rather stable at NM and TR throughout winter.

Hg(0) concentration exhibits abrupt increases when moist and warm air masses from lower latitudes occasionally reach the three ground-based Antarctic stations. At DDU, such events are concomitant with an enhanced fraction of oceanic air masses reaching the site according to the HYSPLIT model simulations, and with increased sodium concentrations (Angot et al., 2016a). At DC, these advections of warm and moist air masses are confirmed by an increase of temperature at 10 m a.g.l. and a high integrated water vapor column (Angot et al., 2016b). Finally, based on a statistical analysis of source and sink regions, Pfaffhuber et al. (2012) showed that transport from lower-latitude regions are frequently associated with the highest Hg(0) concentrations at TR.

During the winter expedition ANTXXIX/6 on board R/V Polarstern over the Weddell Sea (Figure 6-1), Nerentorp Mastromonaco et al. (2016) observed depletions of Hg(0) characterized by strong correlations with O_3. This is the first evidence of Hg(0) depletions occurring in winter. The authors propose a dark mechanism involving Br_2. AMDEs in Antarctica are operationally defined as Hg(0) concentrations below 0.60 ng m^{-3} (Pfaffhuber et al., 2012). Based on this threshold and on the O_3 signal, there is no evidence of Hg(0) depletions occurring during months of complete darkness at the three ground-based Antarctic sites.

6.3.2.1.2 Springtime AMDEs

Before going further, it should be noted that TR is not a coastal station. It is located at an elevation of 1275 m and approximately 220 km from the Antarctic coast. Contrarily, DDU is located on a small island about one km offshore from the Antarctic mainland.

AMDEs are observed at TR in positive correlation with O_3 (r up to 0.56, p value < 0.001, Spearman test). Based on the 0.60 ng m^{-3} threshold (see previous section), AMDEs occur in 2 % of the springtime observations, in line with the occurrence frequency of 5 % reported by Pfaffhuber et al. (2012) from February 2007 to June 2011. Based on a statistical analysis of source and sink regions, Pfaffhuber et al. (2012) indicated that the spring Hg(0) sink, caused

by AMDEs, is mainly located within sea-ice-dense areas surrounding Queen Maud Land. AMDEs at TR are weaker and less frequent when compared to the Arctic (see section 6.3.1.1.2) likely partly due to the location of the station not being exposed directly to depletion events but rather to transport of mercury-depleted air masses (Pfaffhuber et al., 2012). In contrast, AMDEs occur in 28 % of the observations from 28 August to 5 October 2013 during the spring expedition ANTXXIX/7 over sea-ice areas of the Weddell Sea. At DDU, on the other side of the Antarctic continent, data covering the spring period are scarce (Figure 6-3). As indicated by Angot et al. (2016a), the absence of depletions in spring 2012 tends to suggest that AMDEs, if any, are not very frequent at DDU. Several studies reported a less efficient bromine chemistry in East compared to West Antarctica due to a less sea-ice coverage (Theys et al., 2011; Legrand et al., 2016a). However, Angot et al. (2016a) reported low Hg(0) concentrations (0.71 ± 0.11 ng m^{-3}) and a significant positive correlation with O_3 (r up to 0.65, p value < 0.0001, Spearman test) in springtime oceanic air masses, likely due to bromine chemistry.

6.3.2.1.3 Boundary layer dynamics on the Antarctic Plateau in fall

The fall maximum at DC likely partly results from a low boundary layer oxidative capacity under low solar radiation limiting Hg(0) oxidation. Additionally, at DC, weak turbulence and mixing and strong temperature gradients near the surface are favored by light wind and clear sky conditions (Argentini et al., 2013). The surface-based temperature inversions were characterized by Pietroni et al. (2012) over the course of a year. In summer, a convective boundary layer characterized by a maximum depth of 200-400 m (Argentini et al., 2005) develops around midday. In winter, strong temperature inversions allow for a mixing depth of a few tens of meters only. Based on the limited area model MAR (Modèle Atmosphérique Régional), Angot et al. (2016b) indicated that the fall distinct maximum of Hg(0) concentrations is concomitant with the time when the boundary layer lowers to ~ 50 m on average and no longer exhibits a pronounced diurnal cycle. Hg(0) is thus suddenly dispersed into a reduced volume of air, limiting the dilution. Similarly, several studies showed that NO_x mixing ratios are enhanced when the boundary layer is shallow (Neff et al., 2008; Frey et al., 2013).

6.3.2.1.4 Extremely active processes in summer

Summertime Hg(0) concentrations at the three ground-based sites exhibit a high variability (Figure 6-2b), suggesting extremely active processes at this time of the year. Undetected from March to October, a diurnal cycle characterized by a noon Hg(0) maximum is observed in summer at DDU and DC over the 2012-2015 period (Angot et al., 2016a; Angot et al., 2016b). At DC (DDU), Hg(0) concentrations range from ~ 0.6 ng m^{-3} (~ 0.7 ng m^{-3}) on average at night to ~ 1.0 ng m^{-3} (~ 1.1 ng m^{-3}) on average around midday. Conversely, there is no diurnal variation in Hg(0) concentrations at TR, in good agreement with observations reported by Pfaffhuber et al. (2012) from February 2007 to June 2011. Similarly, there is no mention of a daily cycle at NM, Terra Nova Bay, and McMurdo where summer

campaigns were carried out (Ebinghaus et al., 2002b; Temme et al., 2003; Sprovieri et al., 2002; Brooks et al., 2008b). The absence of diurnal cycle at TR can be attributed to the absence of sources/sinks for Hg(0) with a diurnal cycle in the vicinity of the site (Pfaffhuber et al., 2012). The mean summertime Hg(0) concentration is significantly (p value < 0.0001, Mann-Whitney test) lower at DC (0.78 ± 0.46 ng m^{-3}) than at DDU (0.88 ± 0.32 ng m^{-3}) and TR (0.89 ± 0.29 ng m^{-3}), suggesting a more intense oxidation of Hg(0). The boundary layer oxidative capacity has been shown to be high in summer on the Antarctic Plateau with elevated levels of OH, O_3, NO_x, and RO_2 radicals (Davis et al., 2001; Grannas et al., 2007; Eisele et al., 2008; Kukui et al., 2014; Frey et al., 2015). Angot et al. (2016b) performed Hg(0) measurements in both the atmospheric boundary layer and the interstitial air of the snowpack, and analyzed total mercury in surface snow samples. The authors, in good agreement with Brooks et al. (2008a) and Dommergue et al. (2012), suggested that the observed summertime Hg(0) diurnal cycle at DC might be due to a dynamic daily cycle of Hg(0) oxidation, deposition to the snowpack, and reemission from the snowpack. Similarly, a recent study (Wang et al., 2016) reported a Hg(0) diurnal cycle at Kunlun station (80°25 S, 77°6 E) located near Dome A (80°22 S, 77°27 E) – the highest elevation point on the Antarctic Plateau (4090 m). This suggests that the dynamic daily cycle of Hg(0) oxidation, deposition to the snowpack, and reemission from the snowpack probably occurs throughout the Antarctic Plateau. Based on an analysis of air mass back trajectories, Angot et al. (2016a) showed that measurements at DDU on the East Antarctic coast are dramatically influenced by air masses exported from the Antarctic Plateau by strong katabatic winds. The advection of inland air masses enriched in oxidants – NO_x, O_3, and OH (Grilli et al., 2013; Kukui et al., 2012) – and Hg(II) species likely results in the buildup of an atmospheric reservoir of Hg(II) species at DDU, as supported by elevated levels of total mercury in surface snow samples (Angot et al., 2016a). The diurnal cycle observed at DDU – regardless of wind speed and direction – might result from a local dynamic cycle of oxidation/deposition/reemission in the presence of elevated levels of Hg(II) species along with emissions of mercury from ornithogenic soils – formed by an accumulation of penguin excreta.

Hg(0) depletion events occur each year in summer at DC with Hg(0) concentrations remaining low (~ 0.40 ng m^{-3}) for several weeks. These depletion events do not resemble to the ones observed in the Arctic. They are not associated with depletions of O_3, and occur as air masses stagnate over the Plateau which could favor an accumulation of oxidants within the shallow boundary layer (Angot et al., 2016b). At TR, Pfaffhuber et al. (2012) reported episodic low Hg(0) concentrations in summer, anticorrelated with O_3, and associated with the transport of inland air masses. Results at TR (Pfaffhuber et al., 2012) and DDU (Angot et al., 2016a), along with observations from earlier studies at other coastal Antarctic sites (Sprovieri et al., 2002; Temme et al., 2003), demonstrate that the inland atmospheric reservoir can influence the cycle of atmospheric mercury at a continental scale, especially in areas influenced by recurrent katabatic winds.

Additionally, Pfaffhuber et al. (2012) indicated that the ocean is a source of mercury to TR. Similarly, at DDU, Angot et al. (2016a) reported elevated (1.04 ± 0.29 ng m^{-3}) Hg(0)

concentrations in oceanic air masses along with a significant positive correlation between Hg(0) and the daily averaged percentage of oceanic air masses (r = 0.50, *p* value < 0.0001, Spearman test). These results are in line with the summer Hg(0) enhancement in the Arctic likely partly due to oceanic evasion from ice-free open waters (see section 6.3.1.1.3).

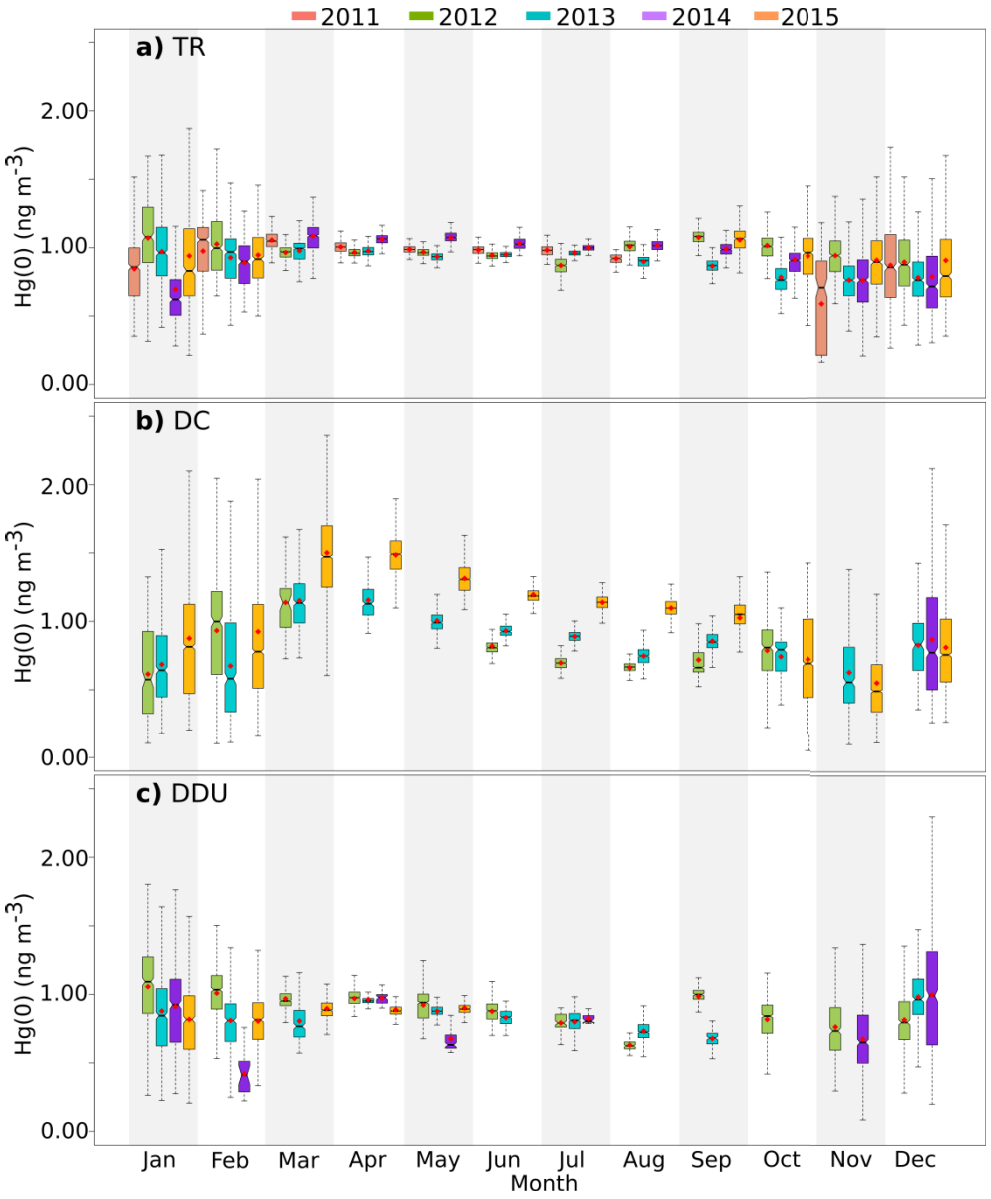

Figure 6-9: Box and whisker plots presenting the monthly Hg(0) concentration distribution at ground-based Antarctic sites **a)** TR, **b)** DC, and **c)** DDU in 2011 (pink), 2012 (green), 2013 (turquoise), 2014 (purple), and 2015 (orange). ◆: mean. Bottom and top of the box: first and third quartiles. Band inside the box: median. Ends of the whiskers: lowest (highest) datum still within the 1.5 interquartile range of the lowest (upper) quartile. Outliers are not represented.

6.3.2.2 Comparison with models

Table 6-4 displays goodness-of-fit statistics between monthly-averaged modeled and observed data in 2013. ECHMERIT slightly underestimates Hg(0) concentrations at the three ground-based Antarctic sites. Contrarily, the three other global models overestimate Hg(0)

levels, suggesting an underestimation of sinks. The ability of the four models to reproduce the observed seasonality of Hg(0) concentrations at ground-based Antarctic sites in 2013 is shown in Figure 6-6b and discussed in the following sections. The interannual variability of the monthly Hg(0) concentration distribution at Antarctic ground-based sites as simulated by GEM-MACH-Hg and GEOS-Chem is displayed in Figure 6-7b while Table 6-5 shows the percent bias between hourly averaged modeled and observed data on a seasonal basis from 2011 to 2014.

6.3.2.2.1 Seasonal variation

a) Winter

GEOS-Chem, GEM-MACH-Hg, and GLEMOS overestimate year 2013 Hg(0) concentrations in winter at the three ground-based stations (Figure 6-6a). This trend repeats year after year for GEOS-Chem and GEM-MACH-Hg (Table 6-5). The most striking result, however, is the modeled gradual increase of Hg(0) concentrations over the course of winter at the three ground-based sites according to ECHMERIT, GEOS-Chem, and GEM-MACH-Hg. A mean gradual increase of 9 %, 19 %, and 11 % is predicted by the three models, respectively, from May to August. GLEMOS, however, predicts a mean gradual decrease of 5 % over the course of winter at the three sites. It is to be noted (see section 6.3.2.1.1) that Hg(0) concentrations are constant from May to August at TR, exhibit a gradual 30 % decrease at DC possibly due to the dry deposition of Hg(0), and a gradual 20 % decrease at DDU due to advection of inland air masses. All in all, the four models misrepresent the decreasing trend at DC and DDU. This might be due to several factors including underestimation of concentrations of oxidants over the East Antarctic Plateau in this period of the year, omission of heterogeneous mechanisms, and significant bias in southern hemisphere emissions, including oceanic evasion. The strong increase (19 %) of Hg(0) concentrations from May to August predicted by GEOS-Chem is not restricted to the Antarctic continent but is obtained for the whole Southern Hemisphere (Fig. 3 in Song et al., 2015). The emission inversion performed by Song et al. (2015) overturns the seasonality of oceanic emissions and better reproduces the ground-based Hg(0) observations in the southern hemisphere midlatitudes and at TR. Further work, including sensitivity tests, is needed to explain the discrepancies between observed and modeled trends.

Additionally, all of the four models are unable to capture the differences in trends observed at the three ground-based sites (constant *vs.* decreasing concentrations). As discussed in section 6.3.2.1.1, TR, contrarily to DDU, is not significantly influenced by inland air masses. This large-scale airflow pattern will have to be captured by models in order to better reproduce observations. Interestingly, Zatko et al. (2016) calculated the annual mean surface wind convergence/divergence over the Antarctic continent using GEOS-Chem. The results – consistent with those by Parish and Bromwich (1987) and Parish and Bromwich (2007) – correctly indicate that the large-scale airflow pattern in Antarctica flows from the East Antarctic Plateau towards the coastal margins and accurately highlight major regions of wind convergence. The findings from this study can be used as the basis for future research.

b) Spring

Based on the 0.60 ng m^{-3} threshold, GEM-MACH-Hg and GEOS-Chem do not predict any AMDE at TR over the 2011-2014 period. Considering the low occurrence frequency based on observations (2 %, see section 6.3.2.1.2), this result is not unreasonable. Similarly, GEM-MACH-Hg does not predict any AMDE at DDU. However, GEOS-Chem predicts AMDEs in 1.5 % of the springtime observations at DDU. This overprediction of AMDEs at DDU likely results from the constant value of 5 pptv of BrO added in the springtime Antarctic boundary layer. While Saiz-Lopez et al. (2007) reported a spring maximum of up to 7 pptv at Halley Station (75°35 S, 26°30 W, West Antarctic coast), Legrand et al. (2016a) suggested a BrO mixing ratio ≤ 1 pptv at DDU (East Antarctic coast) in spring using an offline chemistry transport model. Based on the oxygen and nitrogen isotope analysis of airborne nitrate, Savarino et al. (2007) provided further evidence for low BrO levels in the vicinity of DDU.

c) Fall

None of the four models capture the fall maximum at DC (Figure 6-6b). While a spatially and temporally resolved distribution of concentrations of oxidants on the East Antarctic Plateau is needed, the boundary layer dynamics must also be taken into account. Based on the work by Lin and McElroy (2010), Zatko et al. (2016) incorporated a calculation of the boundary layer height across Antarctica and Greenland into GEOS-Chem. One could also rely on model outputs from the limited area model MAR, validated against observations at DC (Gallée and Gorodetskaya, 2010; Gallée et al., 2015). This model agrees very well with observations and provides reliable and useful information about surface turbulent fluxes, vertical profiles of vertical diffusion coefficients and boundary layer height.

d) Summer

The daily variation of Hg(0) concentrations was investigated based on hourly averaged data provided by GEOS-Chem and GEM-MACH-Hg. The two models are not able to reproduce the noon maximum observed at DC and DDU in summer (see section 6.3.2.1.4) suggesting that the dynamic daily cycle of deposition and reemission at the air-snow interface is not captured by the models. The bidirectional exchange of Hg(0) is complex and influenced by multiple environmental variables (*e.g.*, UV intensity, temperature, atmospheric turbulence, presence of reactants) limiting the accuracy of flux modeling (Zhu et al., 2016). The work carried out by Durnford et al. (2012) in the Arctic and by Zatko et al. (2016) in Antarctica could be good starting points for future research. The former developed a new dynamic physically based snowpack model to determine the fate of mercury deposited onto snowpacks; the latter incorporated an idealized snowpack along with a snow radiative transfer model (Zatko et al., 2013) into GEOS-Chem to investigate the impact of snow nitrate photolysis on the boundary layer chemistry across Antarctica.

6.3.2.2.2 Reactive Mercury and deposition

According to Figure 6-8b, ECHMERIT predicts low RM concentrations during the whole 2013 year at the three ground-based stations (annual averages of 10, 7, and 6 pg m^{-3} at TR, DC, and DDU, respectively). GEOS-Chem predicts a peak in spring at the three sites (up to ~ 160 pg m^{-3} on average October at DC) and quite elevated concentrations in summer and fall (~ 85 pg m^{-3} on average). GEM-MACH-Hg predicts increased concentrations in summer at TR and DDU only. Finally, GLEMOS predicts a more intense summer peak at DC (up to ~ 130 pg m^{-3} on average in November) than at DDU and TR. Measurements of RM are scarce in Antarctica and have never been reported on a year-round basis. RM concentrations ranging from 100 to 1000 pg m^{-3} have been reported in summer at South Pole (Brooks et al., 2008a) and several studies have reported elevated concentrations at coastal sites in spring during the AMDEs season (165 pg m^{-3} on average at McMurdo (Brooks et al., 2008b)) and in summer (mean RGM concentration of 116 pg m^{-3} at Terra Nova Bay (Sprovieri et al., 2002); RGM and Hg(p) concentrations ranging from 5 to > 300 pg m^{-3} and from 15 to 120 pg m^{-3}, respectively, at Neumayer (Temme et al., 2003)). These results along with the seasonal pattern of Hg(0) reported in section 6.3.2.1 suggest that the atmospheric boundary layer is enriched in RM in summer, especially on the Antarctic Plateau, and that the four models tend to underestimate the summertime concentrations. Year-round measurements are needed to further evaluate the accuracy of models predictions.

The total (wet + dry) deposition flux for year 2013 is equal to 1.0, 3.3, 2.5, and 3.9 µg m^{-2} yr^{-1} at TR, 0.8, 1.5, 0.8, and 1.1 µg m^{-2} yr^{-1} at DC, and 4.3, 9.7, 9.7, and 4.1 µg m^{-2} yr^{-1} at DDU according to GLEMOS, GEOS-Chem, GEM-MACH-Hg, and ECHMERIT, respectively. Deposition during summertime accounts for 73, 53, 68, and 35 % of the total deposition at TR, 58, 50, 37, and 35 % at DC, and 58, 61, 89, and 28 % at DDU according to GLEMOS, GEOS-Chem, GEM-MACH-Hg, and ECHMERIT, respectively. There are no measurements of wet and dry deposition in Antarctica except from Angot et al. (2016b) who reported a Hg(0) dry deposition velocity of 9.3×10^{-5} cm s^{-1} in winter at DC. Similarly to the Arctic (see section 6.3.1.2.2), deposition of mercury is typically inferred from concentrations of total mercury in the snowpack. To the best of our knowledge, results found in Angot et al. (2016b) are the only reported over various seasons. Higher total mercury concentrations in surface snow samples in summer suggest an enhanced deposition in this period of the year. Alternatively, deposition of mercury can be inferred from the biomonitoring of Antarctic macrolichens and mosses (Bargagli, 2016b). Large-scale and long-term biomonitoring surveys of mercury deposition have been performed in Victoria Land (Bargagli et al., 1993; Bargagli et al., 2005). While all four models predict higher total mercury deposition for year 2013 at high Arctic (ALT, SND, NYA) *vs.* Antarctic ground-based sites, significantly higher mercury concentrations in Antarctic *vs.* northern hemisphere lichens suggest otherwise (Bargagli et al., 1993).

Wet deposition accounts for 14, 53, 47, and 0 % of the total (wet + dry) flux at TR, 35, 7, 14, and 0 % at DC, and 68, 57, 60, and 8 % at DDU according to GLEMOS, GEOS-Chem,

GEM-MACH-Hg, and ECHMERIT, respectively. The amount of precipitation is equal to 214, 242, 291, and 1127 mm yr^{-1} at TR, 33, 29, 24, and 60 mm yr^{-1} at DC, and 643, 792, 895, and 1751 mm yr^{-1} at DDU according to GLEMOS, GEOS-Chem, GEM-MACH-Hg, and ECHMERIT, respectively. Ground-based measurements of precipitation are sparse and difficult to obtain in Antarctica. Strong winds in coastal regions make it difficult to tell the difference between blowing snow and precipitation (Palerme et al., 2014). On the Antarctic Plateau, a significant part of the precipitation falls in the form of ice crystals (diamond dust) under clear-sky conditions (Bromwich, 1988; Fujita and Abe, 2006). Satellite observations of precipitation in Antarctica by active sensors are now possible (Liu, 2008; Stephens et al., 2008). According to Palerme et al. (2014), the mean annual snowfall rate is < 20 mm water equivalent yr^{-1} at DC and ranges from 20 to 100 mm yr^{-1} at TR, and from 500 to 700 mm yr^{-1} at DDU. The low amount of precipitation at DC might, however, be offset by the high mercury-capture efficiency of ice crystals (Douglas et al., 2008) that are frequently observed at that site (Bromwich, 1988; Fujita and Abe, 2006).

6.4 Summary and future perspectives

The data compiled in this study represent the latest available in polar regions. While the Arctic is a semi-enclosed ocean almost completely surrounded by land, Antarctica is a land mass – covered with an immense ice shelf – surrounded by ocean. Therefore, the cycle of atmospheric mercury in the two regions presents both similarities and differences. Springtime AMDEs are observed in both regions at coastal sites (see sections 6.3.1.1.2 and 6.3.2.1.2). Their frequency and magnitude depend on parameters such as sea-ice dynamics, temperature, and concentration of bromine species, and exhibit a significant but poorly understood interannual variability. Additionally, coastal sites in the two regions are influenced by both snowpack reemission and oceanic evasion of Hg(0) in summer (see sections 6.3.1.1.3 and 6.3.2.1.4). As evidenced in section 6.3.1.1.3, the summertime enhancement of Hg(0) concentrations exhibits a significant but little understood interannual variability at Arctic sites. The cycle of atmospheric mercury differs between the Arctic and Antarctica, primarily because of their different geography. Arctic sites are significantly influenced by mercury emissions from northern hemisphere midlatitudes – especially in winter (see section 6.3.1.1.1). Coastal Antarctic sites are significantly influenced by the reactivity of atmospheric mercury observed on the Antarctic Plateau due to the large-scale airflow pattern flowing from the East Antarctic ice sheet towards the coastal margins (katabatic winds). As discussed in section 6.3.2.1, the cycle of atmospheric mercury on the Antarctic Plateau is surprising and involves yet unraveled mechanisms in winter and a daily bidirectional exchange of Hg(0) at the air-snow interface in summer.

From the comparison of multi-model simulations with observations, we identified whether the processes that affect Hg(0) seasonality and interannual variability, including mercury oxidation, deposition and reemission, are appropriately understood and represented in the

models. Generally, models reproduce quite fairly the observed seasonality at Arctic sites but fail to reproduce it at Antarctic sites. In order for the models to reproduce the seasonality of Hg(0) concentrations in Antarctica, parameterization of the boundary layer dynamics (see section 6.3.2.2.1) and of the large-scale airflow pattern (see above) is needed. Moreover, reaction pathways might be missing or inappropriately incorporated in models. Heterogeneous reactions, although poorly understood (Subir et al., 2012), might be required to explain the reactivity on the Antarctic Plateau. Additionally, while NO_x chemistry was shown to prevail upon halogens chemistry in East Antarctica in summer (Legrand et al., 2009; Grilli et al., 2013) it is currently incorporated in none of the four global models.

Based on this study, the following research gaps need to be addressed:

1. Improving the spatial resolution of RM measurements. There are presently no year-round data available in Antarctica. The Tekran speciation unit suffers from significant biases and interferences, is expensive and labor-intensive, and requires trained operators. Passive samplers, such as polyethersulfone cation exchange membranes, could provide an alternative (Huang et al., 2014) but further tests are needed to assess their collection efficiency and potential biases.

2. Unraveling of Hg(II) speciation. The exact speciation – expected to vary with space and time – remains unknown. Identification of Hg(II) species in ambient air emerges as one of the priorities for future research (Gustin et al., 2015). Recent advancement on analytical techniques may offer new insights into Hg(II) speciation (Huang et al., 2013; Jones et al., 2016) but further research is still needed. Such advancement will greatly improve our understanding of atmospheric redox processes.

3. Improving the spatial resolution of measurements of total mercury in snow samples. These measurements are an alternative to wet and dry deposition measurements – difficult to perform in polar regions.

4. Investigation of the fundamental environmental processes driving the interannual variability of Hg(0) concentrations, especially at Arctic sites. Further work is needed to establish the degree to which temperature and sea-ice dynamics across the Arctic alters mercury chemistry in spring and summer. This will also open up new opportunities to explore the influence of climate change on the cycle of mercury in polar regions.

5. Investigation (and quantification) of the oceanic fluxes of Hg(0) during oceanographic campaigns across the Arctic and Austral oceans. This will largely reduce the uncertainty in the mercury budget estimation in polar regions.

6. Reducing uncertainties in existing kinetic parameters and quantitatively investigate the effect of temperature on the rate constants (Subir et al., 2011). Limited data are available for temperature applicable to atmospheric conditions, especially in polar regions. Achieving this will largely reduce uncertainties in atmospheric models.

7. Investigation of the influence of atmospheric surfaces (*e.g.*, aerosols, clouds, ice, snow covers, ice crystals). This is a major gap for adequate modeling of mercury cycling (Subir et al., 2012) and studies addressing this are critically needed.

Acknowledgements

HA, OM, and AD thank the overwintering crew: S. Aguado, D. Buiron, N. Coillard, G. Dufresnes, J. Guilhermet, B. Jourdain, B. Laulier, S. Oros, A. Thollot, and N. Vogel at DDU, S. Aubin, A. Barbero, N. Hueber, C. Lenormant, and R. Jacob at DC. This work contributed to the EU-FP7 project Global Mercury Observation System (GMOS, www.gmos.eu) and has been supported by a grant from Labex OSUG@2020 (Investissements d'avenir – ANR10 LABX56), and the Institut Universitaire de France. Logistical and financial support was provided by the French Polar Institute IPEV (Program 1028, GMOstral). KAP thanks the Norwegian Environmental Agency and the Norwegian Antarctic Research Expeditions for long-term financial support of Norwegian mercury measurements and in particular the technicians J.H. Wasseng and A. Bäcklund at NILU for their excellent care taking of the Tekran monitors. NES and SS acknowledge support from the US National Science Foundation Atmospheric Chemistry Program under grant no 1053648.

6.5 Résumé des principaux résultats et conclusions de l'article

L'article ci-avant propose une compilation des données récentes (2011-2015) de concentrations en espèces mercurielles et de flux de dépôts en régions polaires. Alors que l'Arctique est principalement un océan entouré de terres, l'Antarctique est quant à lui un continent entouré par un océan et au centre duquel culmine une calotte glaciaire. Le cycle atmosphérique du mercure présente ainsi à la fois des similitudes et des différences en ces deux régions du globe. Des épisodes de déplétion de mercure (AMDE) peuvent être observés, aux deux pôles, au printemps en régions côtières. La fréquence et l'ampleur de ces épisodes de déplétion dépendent de paramètres tels que la dynamique de la glace de mer, la température et la concentration en espèces bromées réactives. Il en résulte une variabilité interannuelle encore peu comprise à l'heure actuelle. Les sites côtiers, tant en Arctique qu'en Antarctique, sont également sujets, en été, à des réémissions de mercure par le manteau neigeux et les eaux océaniques de surface. Les concentrations en Hg(0) sont maximales en été aux sites arctiques mais la variabilité interannuelle demeure peu comprise. Les principales différences observées proviennent, pour l'essentiel, de la géographie des deux régions. Les sites arctiques sont significativement impactés, surtout en hiver, par les émissions de mercure en provenance des régions industrialisées de l'Hémisphère Nord. En raison des vents catabatiques, les sites antarctiques côtiers sont quant à eux significativement impactés par la réactivité atmosphérique du mercure observée sur la calotte glaciaire (voir chapitre 5).

Grâce à la comparaison des données d'observations avec les sorties de différents modèles globaux, l'article ci-avant permet d'évaluer si les processus responsables des variations saisonnières et interannuelles des concentrations en espèces mercurielles sont correctement paramétrés au sein des modèles. Tandis que les modèles reproduisent plutôt correctement la saisonnalité des concentrations aux sites arctiques, ils s'avèrent pour l'heure inopérants en Antarctique. Une meilleure paramétrisation des fluctuations de la couche limite atmosphérique et de la dynamique des masses d'air semble nécessaire. De plus, les mécanismes réactionnels pourraient s'avérer trop simplistes, en omettant notamment les réactions d'oxydation par les NO_x.

L'article ci-avant permet enfin d'identifier un certain nombre de lacunes concernant notre compréhension du cycle atmosphérique du mercure en régions polaires et de proposer des axes de recherche à privilégier :

1. Etendre la couverture spatiale du suivi des concentrations en espèces divalentes. Il n'y a, à l'heure actuelle, aucune donnée disponible sur une année complète en Antarctique. L'unité de spéciation souffrant de biais et interférences importants (voir section 3.2.1.4), étant coûteuse et nécessitant la présence d'opérateurs qualifiés, l'utilisation d'échantillonneurs passifs pourrait être une alternative intéressante (Huang et al., 2014). Une évaluation de leurs performances est cependant nécessaire.

2. Identifier la spéciation du mercure divalent gazeux. Les nouvelles techniques actuellement en cours de développement (Huang et al., 2013; Jones et al., 2016) pourraient permettre des avancées considérables dans ce domaine.

3. Etendre la couverture spatiale du suivi des concentrations en mercure total dans la couche superficielle du manteau neigeux. La quantification directe des flux de dépôts secs et humides étant difficile à mettre en place en régions polaires, ces mesures sont une alternative abordable.

4. Déterminer la nature des processus responsables de la variabilité interannuelle des concentrations en Hg(0), en particulier en Arctique. Des études complémentaires sont nécessaires afin d'établir l'influence de la dynamique de la glace de mer sur la réactivité du mercure au printemps et en été. De telles études pourraient permettre d'étudier les conséquences possibles des changements climatiques sur le cycle du mercure en régions polaires.

5. Quantifier les flux de Hg(0) en provenance des eaux océaniques de surface au cours de campagnes océanographiques en Arctique et autour du continent antarctique.

6. Réduire les incertitudes au niveau des constantes de réactions d'oxydoréduction et étudier leur évolution sur une large gamme de température (Subir et al., 2011).

7. Améliorer nos connaissances des réactions de chimie hétérogène (Subir et al., 2012), notamment sur les surfaces communes en régions polaires (p. ex. neige, cristaux de glace).

7 Conclusion et Perspectives

7.1 Conclusion générale

Le mercure est préoccupant à l'échelle mondiale de par sa propagation atmosphérique sur de longues distances, loin des sources d'émissions, sa persistance dans l'environnement, son potentiel de bioaccumulation dans les chaînes alimentaires aquatiques et ses effets néfastes sur la santé humaine. Les modèles atmosphériques, utilisés pour retracer son cheminement depuis les sources d'émissions jusqu'aux dépôts au sein des écosystèmes, sont entachés de fortes incertitudes en raison notamment de notre compréhension partielle des processus atmosphériques (réactions d'oxydo-réduction, dépôts, réémissions) et du manque de données d'observations à l'échelle planétaire. Dans le cadre du programme GMOS et avec le soutien logistique et financier de l'IPEV, trois stations de mesures ont été installées par le LGGE début 2012 ; la première sur l'Ile d'Amsterdam (AMS) dans la couche limite marine subantarctique, les deux autres sur le continent antarctique : à Dumont d'Urville (DDU) sur la côte Est et à Concordia (DC) sur la calotte glaciaire à plus de 3200 m d'altitude. Nous disposons ainsi aujourd'hui de séries temporelles pluriannuelles uniques de concentrations en espèces mercurielles atmosphériques et de flux de dépôts humides (Figure 3-7) permettant d'évaluer et contraindre les modèles atmosphériques. A partir de ces données, l'objectif principal de ces travaux de thèse a été d'améliorer notre compréhension du cycle atmosphérique du mercure dans ces zones reculées de l'Hémisphère Sud.

Les principaux résultats obtenus à AMS sont résumés par la Figure 7-1. Les quatre années de suivi des espèces divalentes avec une unité de spéciation révèlent des concentrations de l'ordre du pg m^{-3}, c'est-à-dire au niveau des limites de détection instrumentales. Malgré des cumuls de précipitations importants, les flux de dépôts humides quantifiés depuis 2013 s'avèrent faibles (1,6-2,0 µg m^{-2} an^{-1}) en raison d'une concentration moyenne pondérée en mercure total peu élevée (~ 2 ng L^{-1}). Ces résultats suggèrent une réactivité atmosphérique *in situ* limitée dans cette zone de l'océan Indien. Les concentrations en Hg(0) sont par ailleurs très stables (1,04 ± 0,07 ng m^{-3} entre janvier 2012 et fin juillet 2016) ce qui corrobore cette hypothèse. Bien que non quantifié dans le cadre de cette étude, il semble peu probable que le flux de dépôts secs soit plus important que le flux de dépôts humides au vu des conditions météorologiques dans le secteur d'AMS (bruine très fréquente). Les réémissions de Hg(0) par les sols ont par ailleurs certainement peu d'influence sur le signal enregistré à AMS compte tenu des rares pics de concentrations en ^{220}Rn observés (traceur de masses d'air continentales locales). Les échanges de Hg(0) à l'interface air-océan n'ont pas été étudiés, la station de mesures étant située à plus de 55 m au-dessus du niveau de la mer. Notre compréhension des mécanismes d'oxydo-réduction dans cette région du globe demeure à ce jour partielle compte-tenu i) des difficultés rencontrées avec l'unité de spéciation (limite de détection élevée, concentrations probablement sous-estimées,

fonctionnement erratique de l'instrument), ii) de l'absence totale, pendant la durée de l'étude, de mesures de concentrations en oxydants et iii) de notre incapacité à déterminer la spéciation exacte du Hg(II). La détermination des mécanismes réactionnels nécessiterait des outils et des études complémentaires (voir section 7.2 Perspective). Ces travaux de thèse montrent par ailleurs qu'AMS, une des îles les plus isolées au monde, n'est qu'occasionnellement influencée par des masses d'air continentales polluées. A l'inverse, les stations de mesures situées à Cape Point en Afrique du Sud et à Cape Grim en Tasmanie, nécessitent l'acquisition de données complémentaires (p. ex. CO, ^{222}Rn, direction du vent, teneur en aérosols) permettant de filtrer les données. La station d'AMS permet la mesure directe du bruit de fond atmosphérique aux moyennes latitudes de l'Hémisphère Sud et il s'agit ainsi d'un site clé pour la surveillance, sur le long terme, des concentrations atmosphériques en Hg(0). Compte tenu de la stabilité du signal et des contraintes budgétaires, un suivi à haute fréquence temporelle (pas de temps 5 min) des concentrations en Hg(0) ne semble pas nécessaire.

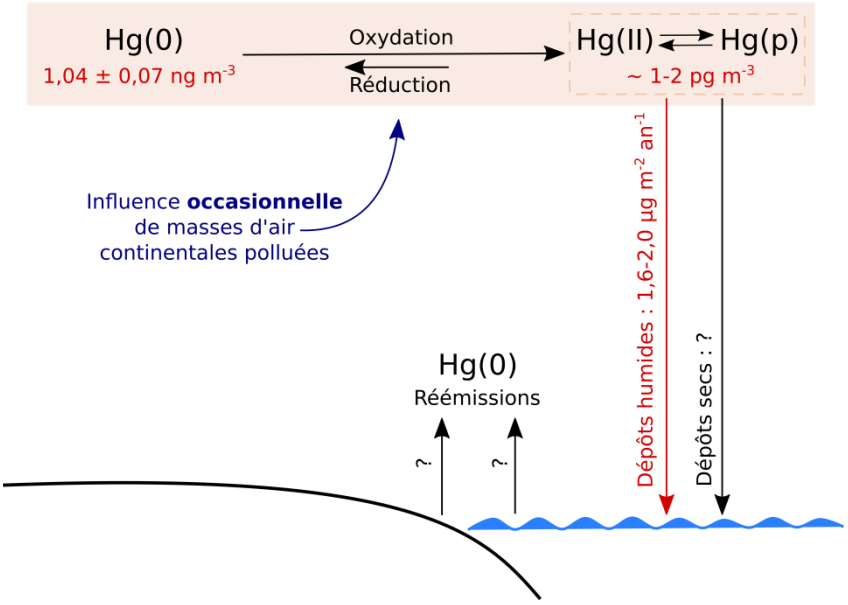

Figure 7-1: Cycle atmosphérique du mercure à AMS. Récapitulatif des principaux résultats.

Les principaux résultats obtenus en Antarctique sont résumés par la Figure 7-2. Les données acquises à DC démontrent l'existence d'une réactivité atmosphérique intense sur la calotte glaciaire pendant l'été en raison, notamment, des concentrations élevées en oxydants, de la dynamique de la couche limite atmosphérique et des échanges d'espèces mercurielles à l'interface air-neige. Bien que non mesurées dans le cadre de cette étude, nous faisons l'hypothèse de concentrations élevées en espèces divalentes atmosphériques en été. Cette hypothèse se base sur les concentrations élevées en mercure total mesurées dans les couches superficielles du manteau neigeux (jusqu'à ~ 74 ng L^{-1}) et sur les concentrations en espèces divalentes mesurées à Pôle Sud (0,10–1,00 ng m^{-3}) par Brooks et al. (2008a). Les tests préliminaires réalisés au cours de la campagne d'été 2014 avec des filtres PES corroborent cette hypothèse (concentrations de l'ordre de 400 pg m^{-3}, voir section 5.1.6.3.1). L'analyse des concentrations en Hg(0) à différentes profondeurs dans l'air du manteau neigeux a permis de mettre en évidence l'existence de réactions d'oxydo-réduction quelle que soit la saison.

Bien que les transitions restent inexpliquées, l'équilibre entre oxydation et réduction varie en fonction de la profondeur et d'une saison à une autre. En été, les concentrations en Hg(0) sont maximales dans les couches superficielles du manteau neigeux et des processus de réémissions provoquent un pic de concentration dans la couche limite atmosphérique à la mi-journée. En hiver, en l'absence de réémissions de Hg(0) par le manteau neigeux, nous avons pu observer une diminution progressive de la concentration en Hg(0) dans la couche limite atmosphérique. Ce phénomène pourrait s'expliquer par un dépôt sec de Hg(0) au cours de l'hiver. De même qu'à AMS, notre compréhension des mécanismes d'oxydo-réduction demeure à ce jour partielle compte tenu i) de l'absence de suivi sur une année complète au moins des concentrations en espèces divalentes et en oxydants, ii) de notre incapacité à déterminer la spéciation exacte du Hg(II) et iii) de notre compréhension limitée des processus de chimie hétérogène, notamment sur les surfaces couramment rencontrées en Antarctique (p. ex. neige, cristaux de glace). Les données acquises, en parallèle, à la station côtière de DDU et l'analyse de cryptogames (mousses, lichens; Bargagli, 2016a) démontrent que les processus observés sur la calotte glaciaire influent sur le cycle du mercure à l'échelle continentale, en raison des forts vents catabatiques qui s'écoulent vers les côtes, et engendrent des dépôts d'espèces divalentes au sein des écosystèmes côtiers. L'influence de ces processus, et notamment le rôle du manteau neigeux en période de fonte, sur le cycle biogéochimique du mercure à plus large échelle demeure cependant inconnue. Comme indiqué au sein du Chapitre 5, il serait intéressant de réaliser des simulations à l'aide de modèles couplés océan-atmosphère. Le suivi des concentrations en Hg(0) n'est plus effectif à DDU mais est toujours en cours à DC. L'intérêt stratégique de cette station est double ; il s'agit dans un premier temps d'une station de bruit de fond atmosphérique qui permettra de suivre l'évolution, sur le long terme, des concentrations en Hg(0) aux hautes latitudes de l'Hémisphère Sud. La calotte glaciaire antarctique est en outre un véritable laboratoire à ciel ouvert permettant d'étudier plus avant la réactivité atmosphérique du mercure.

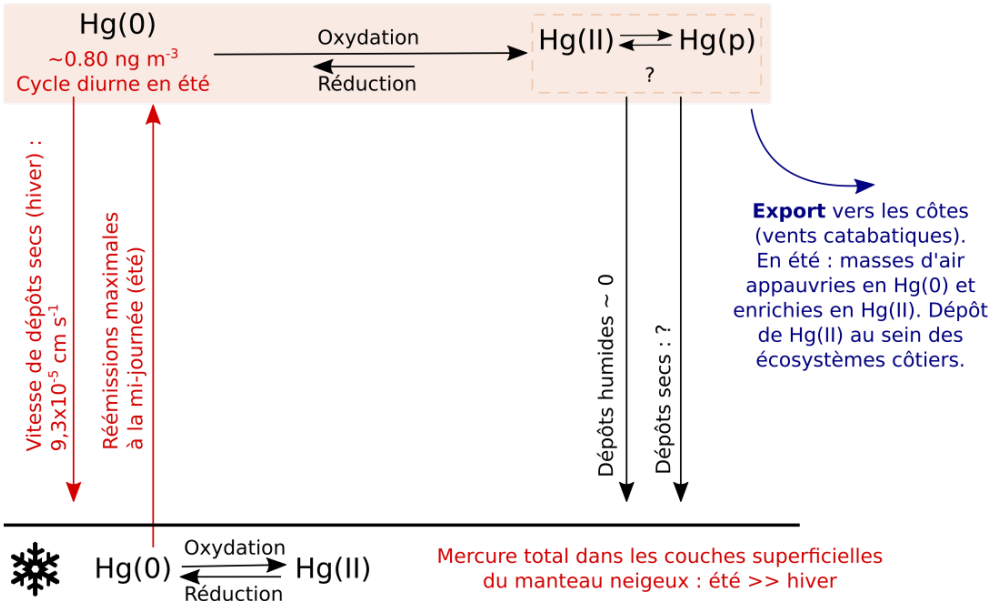

Figure 7-2: Cycle atmosphérique à DC. Récapitulatif des principaux résultats.

La comparaison des données d'observations en régions polaires avec les sorties de différents modèles globaux, proposée au sein du Chapitre 6, a déjà permis d'identifier un certain nombre de lacunes concernant notre compréhension du cycle atmosphérique du mercure en régions polaires et de proposer des axes de recherche à privilégier. La section 7.2 ci-dessous présente des perspectives d'ordre plus général qui m'apparaissent prioritaires.

7.2 Perspectives

Grâce à la mise en place de différents programmes d'observations du mercure (voir section 2.2) et notamment GMOS, nous disposons désormais d'une base de données solide de concentrations en espèces mercurielles et de flux de dépôts humides à l'échelle planétaire. Plutôt que de démultiplier le nombre de stations de mesures, il m'apparaît désormais primordial de maintenir le fonctionnement d'un certain nombre de stations sentinelles, judicieusement choisies, afin de suivre l'évolution sur le long terme et à l'échelle planétaire des concentrations en Hg(0). Afin de réduire les incertitudes en termes de flux, il apparaît de plus indispensable de mesurer en ces différentes stations les concentrations en espèces mercurielles atmosphériques (Hg(0), Hg(II) et Hg(p)) ainsi que les dépôts secs et humides. Afin d'étendre, à moindre coût, la couverture spatiale du suivi des concentrations en espèces divalentes à toutes ces stations sentinelles, le développement de techniques alternatives à l'unité de spéciation s'avère nécessaire (voir ci-après).

Une base de données solide de concentrations en espèces mercurielles et de flux de dépôts humides étant désormais disponible pour évaluer et contraindre les modèles atmosphériques, la plus forte incertitude émane à présent de notre compréhension toujours partielle des processus atmosphériques et notamment des réactions d'oxydo-réduction. Les trois axes de recherche détaillés ci-après permettraient, à mon sens, d'aller vers une meilleure compréhension de ces réactions.

Axe 1 : Suivi des concentrations en espèces divalentes et en oxydants.

L'utilisation de membranes échangeuses de cations en polyétersulfone (PES) est relativement répandues pour la collecte des espèces divalentes gazeuses (p. ex. Ebinghaus et al., 1999; Caldwell et al., 2006; Lyman et al., 2007; Lyman et al., 2009; Lyman et al., 2010a; Castro et al., 2012; Huang et al., 2012; Peterson et al., 2012). Des études de terrain et en laboratoire ont par ailleurs montré que ces membranes PES collectent 1,3 à 3,7 fois plus de Hg(II) que les dénudeurs enduits de KCl utilisés dans les unités de spéciation (Huang et al., 2013). D'après une étude réalisée par Lyman et al. (2009), ces membranes auraient une affinité similaire pour $HgCl_2$, $HgBr_2$ et HgO et celle-ci ne serait pas dépendante de la concentration en Hg(0). Ces membranes sont utilisées depuis décembre 2015 à AMS et DC (voir section 4.1.5.2, section 5.1.6.3.1 et Annexe 3). Les premiers résultats devraient être connus courant 2017. Si les différents tests d'assurance qualité s'avèrent satisfaisants (voir

Annexe 3), ces membranes pourraient être utilisées pour un suivi, à moindre coût, des espèces divalentes de par le monde.

Comme indiqué au sein de la section 7.1, le suivi des concentrations en oxydants fait souvent défaut lorsqu'il s'agit d'évaluer les mécanismes d'oxydation prépondérants. Il s'avère ainsi nécessaire de mettre en place des campagnes destinées à la fois à la mesure des concentrations en espèces mercurielles atmosphériques et en oxydants. Bien que des études de terrain et de modélisation aient montré que l'oxydation de Hg(0) par des espèces bromées réactives est prédominante en régions polaires, dans la haute troposphère ainsi qu'au sein de la couche limite marine (voir section 2.1.1), on s'est assez régulièrement heurté à des limites de détection trop élevées pour BrO en Antarctique (Grilli et al., 2013; Nerentorp Mastromonaco et al., 2016). Des avancées technologiques récentes ont cependant déjà permis d'abaisser cette limite de détection de l'ordre de 2 pptv (Saiz-Lopez et al., 2007; Grilli et al., 2013) à 0,3-0,6 pptv (Wang et al., 2015).

Axe 2 : Identification de la spéciation du mercure divalent gazeux.

La spéciation exacte du Hg(II) demeure inconnue. L'identification des espèces divalentes gazeuses présentes dans l'atmosphère est cependant primordiale afin d'améliorer notre compréhension du cycle biogéochimique du mercure (Gustin and Jaffe, 2010). Huang et al. (2013) ont développé une méthode basée sur la collecte des espèces divalentes sur des membranes nylon (porosité 0,2 µm) et l'identification des composés par désorption thermique. Il est à noter que cette méthode ne permet pas la quantification des composés et repose sur l'existence de standards. Pour l'heure, seuls les profils de thermo-désorption de $HgCl_2$, $HgBr_2$ et HgO sont connus. Jones et al. (2016) ont quant à eux récemment développé une méthode d'identification et de quantification des espèces divalentes par GC/MS. Cette méthode est cependant limitée, à l'heure actuelle, par la présence d'interférences lors de l'analyse en lien avec la nature du support de collecte utilisé (notamment les membranes nylon). Tout comme la méthode par désorption thermique, celle-ci repose sur l'existence de standards. Pour l'heure, seuls des tests visant à identifier et quantifier $HgCl_2$, $HgBr_2$, HgO et $Hg(NO_3)_2$ ont été réalisés. On s'attend à ce que la nature des espèces divalentes gazeuses présentes dans l'atmosphère varie en fonction des sites et des saisons (Huang et al., 2013). Le système de collecte doit ainsi être facilement déployable de par le monde et ne pas engendrer d'interférences lors de l'analyse (si analyse par GC/MS). Le développement de ces deux méthodes constitue une avancée considérable mais des études complémentaires sont de mise. La mise au point de sources de calibration pour une plus vaste gamme d'espèces divalentes gazeuses s'avère notamment nécessaire.

Axe 3 : Identification des processus et études cinétiques.

Le mercure possède sept isotopes stables (^{196}Hg, ^{198}Hg, ^{199}Hg, ^{200}Hg, ^{201}Hg, ^{202}Hg et ^{204}Hg) dont l'abondance peut être mesurée de manière précise (0,01 %) par spectrométrie de masse (Blum and Bergquist, 2007; Epov et al., 2011). Le concept de fractionnement isotopique rend compte des variations dans la répartition des isotopes d'un élément. On

distingue deux types de fractionnement : dépendant ou indépendant de la masse (MDF (« Mass Dependent Fractionation ») et MIF (« Mass Independent Fractionation »), respectivement). Diverses études ont permis de mettre en évidence le fait que les réactions d'oxydo-réduction, les processus d'adsorption-désorption ou de volatilisation peuvent engendrer un MDF et ainsi une variation de la signature isotopique δ^{202}Hg (p. ex. Bergquist and Blum, 2007; Zheng et al., 2007; Demers et al., 2013; Fu et al., 2016b). La réduction photochimique du mercure en phase aqueuse et au sein du manteau neigeux engendrerait par ailleurs un MIF des isotopes impairs et ainsi une variation des signatures isotopiques Δ^{199}Hg et Δ^{201}Hg (Bergquist and Blum, 2007; Zheng and Hintelmann, 2009). Les dépôts humides sont quant à eux associés à des MIF des isotopes pairs et ainsi à une variation des signatures isotopiques Δ^{200}Hg et Δ^{204}Hg (Gratz et al., 2010; Chen et al., 2012; Demers et al., 2013). D'après Chen et al. (2012), cela pourrait être dû à des réactions de photo-oxydation de Hg(0) au niveau de la tropopause. Plus récemment, Sun et al. (2016) ont montré que l'oxydation de Hg(0) par Br engendre un ratio Δ^{199}Hg/Δ^{201}Hg de 1,64 ± 0,30 (2σ) contre 1,89 ± 0,18 (2σ) lors de l'oxydation par Cl. Ces résultats suggèrent des mécanismes de MIF différents. L'analyse isotopique permet ainsi de renseigner quant à la nature des transformations physico-chimiques subies par le mercure ou quant aux sources d'émissions potentielles (Sonke et al., 2013). Les filtres PES, collectés notamment à AMS et DC depuis décembre 2015 (voir Axe 1), pourraient permettre une analyse isotopique du mercure divalent. Afin de disposer d'une quantité de matière suffisante pour l'analyse, la mise en place de filtres plus grands (90 mm de diamètre) et d'un débit de collecte plus élevé (4,0-4,5 L min^{-1}) s'avèreraient nécessaires.

Comme déjà discuté au sein de la section 2.1, la détermination expérimentale ou théorique des constantes de réaction associées à l'oxydation ou à la réduction des espèces mercurielles est un exercice difficile et les sources d'incertitudes sont nombreuses (Subir et al., 2011; Ariya et al., 2015). Il en résulte des constantes pouvant varier d'un ou deux ordres de grandeurs d'une étude à une autre (Tableau 2-1). Il s'avère essentiel de réduire l'incertitude sur ces constantes de réaction et d'étudier leur évolution sur une large gamme de température. L'atmosphère étant un milieu hétérogène et le cycle du mercure incluant des échanges aux interfaces (voir section 2.1.3), nous devons de plus améliorer nos connaissances des réactions de chimie hétérogène (Subir et al., 2012).

Références bibliographiques

ECMWF: European Centre for Medium-Range Weather Forecasts. http://www.ecmwf.int/en/forecasts/datasets, access: 20 January 2016.

Aas, W.: Data Quality 2004, Quality assurance and field comparisons, EMEP/CCC-Report 4/2006, NILU, Kjeller, Norway 2006.

Adams, J. W., Holmes, N. S., and Crowley, J. N.: Uptake and reaction of HOBr on frozen and dry NaCl/NaBr surfaces between 253 and 233 K, Atmos. Chem. Phys., 2, 79-91, 10.5194/acp-2-79-2002, 2002.

Agnan, Y., Le Dantec, T., Moore, C. W., Edwards, G. C., and Obrist, D.: New constraints on terrestrial surface-atmosphere fluxes of gaseous elemental mercury using a global database, Environmental Science and Technology, 50, 507-524, 2016.

Albert, M. R., and Shultz, E. F.: Snow and firn properties and air-snow transport processes at Summit, Greenland, Atmospheric Environment, 36, 2789-2797, 2002.

AMAP: Human Health in the Arctic. Arctic Monitoring and Assessment Programme (AMAP), Oslo, Norway, 165pp, 2015.

Amos, H. M., Jacob, D. J., Holmes, C. D., Fisher, J. A., Wang, Q., Yantosca, R. M., Corbitt, E. S., Galarneau, E., Rutter, A. P., Gustin, M. S., Steffen, A., Schauer, J. J., Graydon, J. A., St. Louis, V. L., Talbot, R. W., Edgerton, E. S., Zhang, Y., and Sunderland, E. M.: Gas-particle partitioning of atmopheric Hg(II) and its effect on global mercury deposition, Atmospheric Chemistry and Physics, 12, 591-603, 2012.

Amos, H. M., Jacob, D. J., Streets, D. G., and Sunderland, E. M.: Legacy impacts of all-time anthropogenic emissions on the global mercury cycle, Global biogeochemical cycles, 27, 1-12, doi: 10.1002/gbc.20040, 2013.

Amos, H. M., Jacob, D. J., Kocman, D., Horowitz, H. M., Zhang, Y., Dutkiewicz, S., Horvat, M., Corbitt, E. S., Krabbenhoft, D. P., and Sunderland, E. M.: Global biogeochemical implications of mercury discharges from rivers and sediment burial, Environmental science & technology, 48, 9514-9522, 2014.

Amos, H. M., Sonke, J. E., Obrist, D., Robins, N., Hagan, N., Horowitz, H. M., Mason, R. P., Witt, M. L. I., Hedgecock, I. M., Corbitt, E. S., and Sunderland, E. M.: Observational and modeling constraints on global anthropogenic enrichment of mercury, Environmental Science and Technology, 49, 4036-4047, 2015.

Amyot, M., Gill, G. A., and Morel, F. M. M.: Production and loss of dissolved gaseous mercury in coastal seawater, Environmental Science and Technology, 31, 3606-3611, 1997.

Amyot, M., Lean, D. R., Poissant, L., and Doyon, M.-R.: Distribution and transformation of elemental mercury in the St. Lawrence River and Lake Ontario, Canadian Journal of Fisheries and Aquatic Sciences, 57, 155-163, 2000.

Anderson, P. S., and Neff, W. D.: Boundary layer physics over snow and ice, Atmospheric Chemistry and Physics, 8, 3563-3582, 2008.

Andersson, M. E., Sommar, J., Gårdfeldt, K., and Linfqvist, O.: Enhanced concentrations of dissolved gaseous mercury in the surface waters of the Arctic Ocean, Marine Chemistry, 110, 190-194, 2008.

Andresen, S., Rosendal, G. K., and Skjaerseth, J. B.: Why negociate a legally binding mercury convention?, International Environmental Agreements: Politics, Law and Economics, 10.1007/s10784-012-9198-6, 2012.

Angot, H., Barret, M., Magand, O., Ramonet, M., and Dommergue, A.: A 2-year record of atmospheric mercury species at a background Southern Hemisphere station on Amsterdam Island, Atmospheric Chemistry and Physics 14, 11461-11473, 2014.

Angot, H., Dion, I., Vogel, N., Magand, O., Legrand, M., and Dommergue, A.: Atmospheric mercury record at Dumont d'Urville, East Antarctic coast: continental outflow and oceanic influences, Atmospheric Chemistry and Physics, 16, 8265-8279, doi:10.5194/acp-16-8265-2016, 2016a.

Angot, H., Magand, O., Helmig, D., Ricaud, P., Quennehen, B., Gallée, H., Del Guasta, M., Sprovieri, F., Pirrone, N., Savarino, J., and Dommergue, A.: New insights into the atmospheric mercury cycling in central Antarctica and implications on a continental scale, Atmospheric Chemistry and Physics 16, 8249-8264, doi:10.5194/acp-16-8249-2016, 2016b.

Appleton, A., Ashton, M., Kantai, T., Mwangi, W., Ripley, K., and Vavilov, A. A.: Summary of the 25th session of the UNEP governing council/global ministerial environment forum: 16-20 February 2009, Earth Negotiations Bulletin, 16, 1-16, 2009.

Argentini, S., Viola, A., Sempreviva, A. M., and Petenko, I.: Summer boundary-layer height at the plateau site of Dome C, Antarctica, Boundary-Layer Meteorology, 115, 409-422, 2005.

Argentini, S., Petenko, I., Viola, A., Mastrantonio, G., Pietroni, I., Casasanta, G., Aristidi, E., and Ghenton, C.: The surface layer observed by a high-resolution sodar at Dome C, Antarctica, Annals of geophysics, 56, F0557, doi:10.4401/ag-6347, 2013.

Ariya, P. A., Khalizov, A., and Gidas, A.: Reactions of gaseous mercury with atomic and molecular halogens: kinetics, product studies, and atmospheric implications, The Journal of Physical Chemistry A, 106, 7310-7320, 2002.

Ariya, P. A., Dastoor, A. P., Amyot, M., Schroeder, W. H., Barrie, L., Anlauf, K., Raofie, F., Ryzhkov, A., Davignon, D., Lalonde, J., and Steffen, A.: The arctic: a sink for mercury, Tellus, 56B, 397-403, 2004.

Ariya, P. A., Peterson, K., Snider, G., and Amyot, M.: Mercury chemical transformation in the gas, aqueous and heterogeneous phases: state-of-the-art science and uncertainties, in: Mercury fate and transport in the global atmosphere, edited by: Pirrone, N., and Mason, R. P., Springer, New York, 2009.

Ariya, P. A., Amyot, M., Dastoor, A., Deeds, D., Feinberg, A., Kos, G., Poulain, A. J., Ryjkov, A., Semeniuk, K., Subir, M., and Toyota, K.: Mercury physicochemical and biogeochemical transformation in the atmopshere and at atmospheric interfaces: a review and future directions, Chemical Reviews, 115, 3760-3802, doi: 10.1021/cr500667e, 2015.

Aspmo, K., Gauchard, P.-A., Steffen, A., Temme, C., Berg, T., Bahlmann, E., Banic, C., Dommergue, A., Ebinghaus, R., Ferrari, C., Pirrone, N., Sprovieri, F., and Wibetoe, G.: Measurements of atmospheric mercury species during an international study of mercury depletion events at Ny-Ålesund, Svalbard, spring 2003. How reproductible are our present methods?, Atmospheric Environment, 39, 7607-7619, 2005.

Aspmo, K., Temme, C., Berg, T., Ferrari, C., Gauchard, P.-A., Faïn, X., and Wibetoe, G.: Mercury in the atmosphere, snow and melt water ponds in the north atlantic ocean during Arctic summer, Environmental Science and Technology, 40, 4083-4089, 2006.

Axelrad, D. A., Bellinger, D. C., Ryan, L. M., and Woodruff, T. J.: Dose-response relationship of prenatal mercury exposure and IQ: an integrative analysis of epidemiologic data, Environmental health perspectives, 609-615, 2007.

Baker, P. G. L., Brunke, E.-G., Slemr, F., and Crouch, A. M.: Atmospheric mercury measurements at Cape Point, South Africa, Atmospheric Environment, 36, 2459-2465, 2002.

Bakir, F., Damluji, S. F., Amin-Zaki, L., Murtadha, M., Khalidi, A., and al-Rawi, N. Y.: Methylmercury poisoning in Iraq, Science, 18&, 230-241, 1973.

Balabanov, N. B., Shepler, B. C., and Peterson, K. A.: Accurate Global Potential Energy Surface and Reaction Dynamics for the Ground State of HgBr2, The Journal of Physical Chemistry A, 109, 8765-8773, 10.1021/jp053415l, 2005.

Balkanski, Y. J., and Jacob, D. J.: Transport of continental air to the subantarctic indian ocean, Tellus, 42B, 62-75, 1990.

Banic, C., Beauchamp, S., Tordon, R., Schroeder, W., Steffen, A., Anlauf, K., and Wong, H.: Vertical distribution of gaseous elemental mercury in Canada, Journal of Geophysical Research: Atmospheres, 108, 10.1029/2002JD002116, 2003.

Bargagli, R., Battisti, E., Focardi, S., and Formichi, P.: Preliminary data on environmental distribution of mercury in northern Victoria Land, Antarctica, Antarctic Science, 5, 3-8, 1993.

Bargagli, R., Agnorelli, C., Borghini, F., and Monaci, F.: Enhanced deposition and bioaccumulation of mercury in antarctic terrestrial ecosystems facing a coastal polynya, Environmental Science and Technology, 39, 8150-8155, 2005.

Bargagli, R.: Atmospheric chemistry of mercury in Antarctica and the role of cryptogams to assess deposition patterns in coastal ice-free areas, Chemosphere, 163, 202-208, http://dx.doi.org/10.1016/j.chemosphere.2016.08.007, 2016a.

Bargagli, R.: Moss and lichen biomonitoring of atmospheric mercury: a review, Science of the Total Environment, 572, 216-231, 2016b.

Barrie, L. A., Hoff, R. M., and Daggupaty, S. M.: Arctic Air Chemistry Proceedings of the Second SymposiumThe influence of mid-latitudinal pollution sources on haze in the Canadian arctic, Atmospheric Environment (1967), 15, 1407-1419, http://dx.doi.org/10.1016/0004-6981(81)90347-4, 1981.

Bartels-Rausch, T., Krysztofiak, G., Bernhard, A., Schläppi, M., Schwikowski, M., and Ammann, M.: Phototoinduced reduction of divalent mercury in ice by organic matter, Chemosphere, 82, 199-203, 2011.

Bash, J. O., Miller, D. R., Meyer, T. H., and Bresnahan, P. A.: Northeast United States and Southeast Canada natural mercury emissions estimated with a surface emission model, Atmospheric Environment, 38, 5683-5692, 2004.

Bauer, D., D'Ottone, L., Campuzano-Jost, P., and Hynes, A. J.: Gas phase elemental mercury: a comparison of LIF detection techniques and study of the kinetics of reaction with the hydroxyl radical, Journal of Photochemistry and Photobiology A: Chemistry, 157, 247-256, 2003.

Bauguitte, S. J.-B., Bloss, W. J., Evans, M. J., Salmon, R. A., Anderson, P. S., Jones, A. E., Lee, J. D., Saiz-Lopez, A., Roscoe, H. K., Wolff, E. W., and Plane, J. M. C.: Summertime NOx measurements during the CHABLIS campaign: can source and sink estimates unravel observed diurnal cycles?, Atmospheric Chemistry and Physics, 12, 989-1002, 2012.

Beal, S., Osterberg, E. C., Zdanowicz, C., and Fisher, D.: An ice core perspective on mercury pollution during the past 600 years, Environmental Science and Technology, 49, 7641-7647, 2015.

Bellanger, M., Pichery, C., Aerts, D., Berglund, M., Castano, A., Cejchanova, M., Crettaz, P., Davidson, F., Esteban, M., Fischer, M. E., Gurzau, A. E., Halzlova, K., Katsonouri, A., Knudsen, L. E., Kolossa-Gehring, M., Koppen, G., Ligocka, D., Miklavcic, A., Reis, M. F., Rudnai, P., Tratnik, J. S., Weihe, P., Budtz-Jorgensen, E., Grandjean, P., and DEMO/COPHES: Economic benefits of methylmercury exposure control in Europe: monetary value of neurotoxicity prevention, Environmental Health, 12, http://www.ehjournal.net/content/12/11/13, 2013.

Benoit, J. M., Gilmour, C., Heyes, A., Mason, R. P., and Miller, C.: Geochemical and biological controls over methylmercury production and degradation in aquatic systems, in: Biochemistry of environmental important trace elements, edited by: Chai, Y., and Braids, O. C., American Chemical Society, Washington DC, 262-297, 2003.

Berg, T., Bartnicki, J., Munthe, J., Lattila, H., Hrehoruk, J., and Mazur, A.: Atmospheric mercury species in the European Arctic: measurements and modelling, Atmospheric Environment, 35, 2569-2582, 2001.

Berg, T., Sekkesæter, S., Steinnes, E., Valdal, A.-K., and Wibetoe, G.: Springtime depletion of mercury in the European Arctic as observed at Svalbard, Science of The Total Environment, 304, 43-51, http://dx.doi.org/10.1016/S0048-9697(02)00555-7, 2003a.

Berg, T., Sommar, J., Wängberg, Gardfeldt, K., Munthe, J., and Schroeder, B.: Arctic mercury depletion events at two elevations as observed at the Zeppelin Station and Dirigibile Italia, Ny-Ålesund, spring 2002, J. Phys. IV France, 107, 151-154, 2003b.

Berg, T., Kallenborn, R., and Manø, S.: Temporal trends in atmospheric heavy metal and organochlorine concentrations at Zeppelin, Svalbard, Arctic, Antarctic, and Alpine Research, 36, 284-291, 2004.

Berg, T., Aspmo, K., and Steinnes, E.: Transport of Hg from atmospheric mercury depletion events to the mainland of Norway and its possible influence on Hg deposition, Geophysical research letters, 35, L09802, doi:10.1029/2008GL033586, 2008.

Berg, T., Pfaffhuber, K. A., Cole, A. S., Engelsen, O., and Steffen, A.: Ten-year trends in atmospheric mercury concentrations, meteorological effects and climate variables at Zeppelin, Ny-Alesund, Atmospheric Chemistry and Physics, 13, 6575-6586, 2013.

Bergquist, B. A., and Blum, J. D.: Mass-dependent and-independent fractionation of Hg isotopes by photoreduction in aquatic systems, Science, 318, 417-420, 2007.

Bey, I., Jacob, D. J., Yantosca, R. M., Logan, J. A., Field, B. D., Fiore, A. M., li, Q., Liu, H. Y., Mickley, L. J., and Schultz, M. G.: Global modeling of tropospheric chemistry with assimilated meteorology: model description and evaluation, Journal of geophysical research, 106, 23,073-023,095, 2001.

Bilello, M. A.: Prevailing wind directions in the Arctic Ocean, Corps of Engineers, U. S. Army: Hanover, New Hampshire, 38, 1973.

Blanchard, P., Froude, F., Martin, J., Dryfhout-Clark, H., and Woods, J.: Four years of continuous total gaseous mercury (TGM) measurements at sites in Ontario, Canada, Atmospheric Environment, 36, 3735-3743, 2002.

Bloom, N. S., and Fitzgerald, W. F.: Determination of volatile mercury species at the picogram level by low temperature gas chromatography with cold-vapor atomic fluorescence detection, Analytica Chimica Acta, 208, 151-161, 1988.

Bloss, W. J., Lee, J. D., Heard, D. E., Salmon, R. A., Bauguitte, S. J.-B., Roscoe, H. K., and Jones, A. E.: Observations of OH and HO_2 radicals in coastal Antarctica, Atmospheric Chemistry and Physics, 7, 4171-4185, 2007.

Blum, J. D., and Bergquist, B. A.: Reporting of variations in the natural isotopic composition of mercury, Analytical and Bioanalytical Chemistry, 388, 353-359, 2007.

Bocquet, F., Helmig, D., and Oltmans, S. J.: Ozone in interstitial air of the mid-latituden seasonal snowpack at Niwot Ridge, Colorado, Arctic, Antarctic, and Alpine Research, 39, 375-387, 2007.

Bose-O'Reilly, S., Schierl, R., Nowak, D., Siebert, U., William, J. F., Owi, F. T., and Ir, Y. I.: A preliminary study on health effects in villagers exposed to mercury in a small-scale artisanal gold mining area in Indonesia, Environmental Research, 149, 274-281, http://dx.doi.org/10.1016/j.envres.2016.04.007, 2016.

Bottenheim, J. W., and Chan, E.: A trajectory study into the origin of spring time Arctic boundary layer ozone depletion, Journal of Geophysical Research: Atmospheres, 111, 10.1029/2006JD007055, 2006.

Bourgeois, Q., and Bey, I.: Pollution transport efficiency toward the Arctic: senstivity to aerosol scavenging and source regions, Journal of geophysical research, 116, D08213, 10.1029/2010JD015096, 2011.

Bromwich, D., Guo, Z., Bai, L., and Chen, Q.: Modeled antarctic precipitation. Part I: spatial and temporal variability., J. Climate, 17, 427-447, 2004.

Bromwich, D. H.: Snowfall in high southern latitudes, Rev. Geophys., 26, 149-168, http://dx.doi.org/10.1029/RG026i001p00149, 1988.

Bromwich, D. H.: An extraordinary katabatic wind regime at Terra Nova Bay, Antarctica, Monthly Weather Review, 117, 688-695, 1989.

Brooks, S., Saiz-Lopez, A., Skov, H., Lindberg, S. E., Plane, J. M. C., and Goodsite, M. E.: The mass balance of mercury in the springtime arctic environment, Geophysical research letters, 33, L13812, doi: 10.1029/2005GL025525, 2006a.

Brooks, S. B., Saiz-Lopez, A., Skow, H., Lindberg, S. E., Plane, J. M. C., and Goodsite, M. E.: The mass balance of mercury in the springtime arctic environment, Geophysical research letters, 32, 2006b.

Brooks, S. B., Arimoto, R., Lindberg, S. E., and Southworth, G.: Antarctic polar plateau snow surface conversion of deposited oxidized mercury to gaseous elemental mercury with fractional long-term burial, Atmospheric Environment, 42, 2877-2884, 2008a.

Brooks, S. B., Lindberg, S. E., Southworth, G., and Arimoto, R.: Springtime atmospheric mercury speciation in the McMurdo, Antarctica coastal region, Atmospheric Environment, 42, 2885-2893, 2008b.

Brosset, C.: The behavior of mercury in the physical environment, Water, Air, and Soil Pollution, 34, 145-166, 1987.

Brunke, E.-G., Labuschagne, C., Parker, B., Scheel, H. E., and Whittlestone, S.: Baseline air mass selection at Cape Point, South Africa: application of ^{222}Rn and other filter criteria to CO_2, Atmospheric Environment, 38, 5693-5702, 2004.

Cadle, S. H.: Dry Deposition to Snowpacks, in: Seasonal Snowpacks: Processes of Compositional Change, edited by: Davies, T. D., Tranter, M., and Jones, H. G., Springer Berlin Heidelberg, Berlin, Heidelberg, 21-66, 1991.

Caldwell, C. A., Swartzendruber, P., and Prestbo, E.: Concentration and Dry Deposition of Mercury Species in Arid South Central New Mexico (2001−2002), Environmental Science & Technology, 40, 7535-7540, 10.1021/es0609957, 2006.

Calvert, J. G., and Lindberg, S. E.: Mechanisms of mercury removal by O_3 and OH in the atmosphere, Atmospheric Environment, 39, 3355-3367, 2005.

Carpi, A., and Lindberg, S. E.: Sunlight-mediated emission of elemental mercury from soil amended with municipal sewage sludge, Environmental Science & Technology, 31, 2085-2091, 1997.

Carpi, A., Fostier, A. H., Orta, O. R., dos Santos, J. C., and Gittings, M.: Gaseous mercury emissions from soil following forest loss and land use changes: Field experiments in the United States and Brazil, Atmospheric Environment, 96, 423-429, 2014.

Castro, M. S., Moore, C., Sherwell, J., and Brooks, S. B.: Dry deposition of gaseous oxidized mercury in Western Maryland, Science of The Total Environment, 417–418, 232-240, http://dx.doi.org/10.1016/j.scitotenv.2011.12.044, 2012.

Chapman, L., and Chan, H. M.: The influence of nutrition on methyl mercury intoxication, Environmental Health Perspectives, 108, 29-56, 2000.

Chen, D., Hale, R. C., La Guardia, M. J., Luellen, D., Kim, S., and Geisz, H. N.: Hexabromocyclododecane flame retardant in Antarctica: research station as sources, Environmental Pollution, 206, 611-618, 2015a.

Chen, H., Wang, Z., Li, J., Tang, X., Ge, B., Wu, X., Wild, O., and Carmichael, G.: GNAQPMS-Hg v1. 0, a global nested atmospheric mercury transport model: model description, evaluation and application to trans-boundary transport of Chinese anthropogenic emissions, Geoscientific Model Development, 8, 2857-2876, 2015b.

Chen, J., Hintelmann, H., Feng, X., and Dimock, B.: Unusual fractionation of both odd and even mercury isotopes in precipitation from Peterborough, ON, Canada, Geochimica et Cosmochimica Acta, 90, 33-46, 2012.

Chen, L., Zhang, Y., Jacob, D. J., Soerensen, A. L., Fisher, J. A., Horowitz, H. M., Corbitt, E. S., and Wang, X.: A decline in Arctic Ocean mercury suggested by differences in decadal trends of atmospheric mercury between the Arctic and northern midlatitudes, Geophysical research letters, 42, 6076–6083, 10.1002/2015GL064051, 2015c.

Choi, A. L., and Grandjean, P.: Methylmercury exposure and health effects in humans, Environmental Chemistry, 5, 112-120, 2008.

Choi, H.-D., Sharac, T. J., and Holsen, T. M.: Mercury deposition in the Adirondacks: a comparison between precipitation and throughfall, Atmospheric Environment, 42, 1818-1827, 2008.

Choi, H.-D., and Holsen, T. M.: Gaseous mercury emissions from unsterilized and sterilized soils: the effect of temperature and UV radiation, Environmental Pollution, 157, 1673-1678, 2009.

Clarkson, T. W., and Magos, L.: The toxicology of mercury and its chemical compounds, Critical reviews in toxicology, 36, 609-662, 2006.

Clever, H. L., Johnson, S. A., and Derrick, M. E.: The solubility of mercury and some sparingly soluble mercury salts in water and aqueous electrolyte solutions, Journal of physical and chemical reference data, 14, 631-680, 1985.

Clewell, H., Gearhart, J. M., Gentry, P. R., Covington, T. R., Van Landingham, C. B., Crump, K. S., and Shipp, A. M.: Evaluation of the uncertainty in an oral reference dose for methylmercury due to interindividual variability in pharmacokinetics, Risk Analysis, 19, 547-558, 1999.

Un seuil record de CO_2 franchi dans l'Hémisphère Sud: http://www2.cnrs.fr/presse/communique/4585.htm, access: 13 August 2016, 2016.

Cobbett, F. D., Steffen, A., Lawson, G., and Van Heyst, B. J.: GEM fluxes and atmospheric mercury concentrations (GEM, RGM and Hg(p)) in the Canadian Arctic at Alert, Nunavut, Canada (February–June 2005), Atmospheric Environment, 41, 6527-6543, http://dx.doi.org/10.1016/j.atmosenv.2007.04.033, 2007.

Cohen, L., Helmig, D., Neff, W. D., Grachev, A. A., and Fairall, C. W.: Boundary-layer dynamics and its influence on atmospheric chemistry at Summit, Greenland, Atmospheric Environment, 41, 5044-5060, 2007.

Cole, A. S., and Steffen, A.: Trends in long-term gaseous mercury observations in the Arctic and effects of temperature and other atmospheric conditions, Atmos. Chem. Phys., 10, 4661-4672, 10.5194/acp-10-4661-2010, 2010.

Cole, A. S., Steffen, A., Pfaffhuber, K. A., Berg, T., Pilote, M., Poissant, L., Tordon, R., and Hung, H.: Ten-year trends of atmospheric mercury in the high Arctic compared to Canadian sub-Arctic and mid-latitudes sites, Atmospheric Chemistry and Physics, 13, 1535-1545, 2013.

Cooke, W. F., Koffi, B., and Grégoire, J.-M.: Seasonality of vegetation fires in Africa from remote sensing data and application to a global chemistry model, Journal of geophysical research, 101, 21,051-021,065, 1996.

Corbitt, E. S., Jacob, D. J., Holmes, C. D., Streets, D. G., and Sunderland, E. M.: Global source - receptor relationship for mercury deposition under present-day and 2050 emissions scenarios, Environmental Science and Technology, 45, 10477-10484, 2011.

Cossa, D., Heimbürger, L.-E., Lannuzel, D., Rintoul, S. R., Butler, E. C. V., Bowie, A. R., Averty, B., Watson, R. J., and Remenyi, T.: Mercury in the Southern Ocean, Geochimica et Cosmochimica Acta, 75, 4037-4052, 2011.

Crump, K. S., Kjellström, T., Shipp, A. M., Silvers, A., and Stewart, A.: Influence of prenatal mercury exposure upon scholastic and psychological test performance: benchmark analysis of a New Zealand cohort, Risk Anal, 18, 701-713, 1998.

D'Amore, F., Bencardino, M., Cinnirella, S., Sprovieri, F., and Pirrone, N.: Data quality through a web-based QA/QC system: implementation for atmospheric mercury data from the Global Mercury Observation System, Environmental Science: Processes & Impacts, 17, 1482-1491, 2015.

Daniels, J. L., Longnecker, M. P., Rowland, A. S., Golding, J., and Team, A. S.: Fish intake during pregnancy and early cognitive development of offspring, Epidemiology, 15, 394-402, 2004.

Dastoor, A., Ryzhkov, A., Durnford, D., Lehnherr, I., Steffen, A., and Morrison, H.: Atmospheric mercury in the Canadian Arctic. Part II: Insight from modeling, Science of The Total Environment, 509–510, 16-27, http://dx.doi.org/10.1016/j.scitotenv.2014.10.112, 2015.

Dastoor, A. P., and Larocque, Y.: Global circulation of atmospheric mercury: a modelling study, Atmospheric Environment, 38, 147-161, 2004.

Dastoor, A. P., Davignon, D., Theys, N., Van Roozendael, M., Steffen, A., and Ariya, P. A.: Modeling dynamic exchange of gaseous elemental mercury at polar sunrise, Environmental Science and Technology, 42, 5183-5188, 2008.

Dastoor, A. P., and Durnford, D. A.: Arctic ocean: is it a sink or a source of atmospheric mercury?, Environmental Science and Technology, 48, 1707-1717, 2014.

Davies, D. K., Ilavajhala, S., Wong, M. M., and Justice, C. O.: Fire information for resource management system: archiving and distributing MODIS active fire data, IEEE Transactions on Geoscience and Remote Sensing, 47, 72-79, 2009.

Davis, D., Nowak, J. B., Chen, G., Buhr, M., Arimoto, R., Hogan, A., Eisele, F., Mauldin, L., Tanner, D., Shetter, R., Lefer, B., and McMurry, P.: Unexpected high levels of NO observed at South Pole, Geophysical research letters, 28, 3625-3628, 2001.

De Andrade, R. P., Michel, R. F. M., Schaefer, C. E. G. R., Simas, F. N. B., and Windmöller, C. C.: Hg distribution and speciation in Antarctic soils of the Fildes and Ardley peninsulas, King George Island, Antarctic Science, 24, 395-407, 2012.

De Simone, F., Gencarelli, C. N., Hedgecock, I. M., and Pirrone, N.: Global atmospheric cycle of mercury: a model study on the impact of oxidation mechanisms, Environmental Science and Pollution Research, 21, 4110-4123, 2014.

De Simone, F., Cinnirella, S., Gencarelli, C. N., Yang, X., Hedgecock, I. M., and Pirrone, N.: Model Study of Global Mercury Deposition from Biomass Burning, Environmental Science & Technology, 49, 6712-6721, 10.1021/acs.est.5b00969, 2015.

De Simone, F., Cinnirella, S., Gencarelli, C. N., Carbone, F., Hedgecock, I. M., and Pirrone, N.: Particulate-Phase Mercury Emissions during Biomass Burning and Impact on Resulting Deposition: a Modelling Assessment, Atmos. Chem. Phys. Discuss., 2016, 1-22, 10.5194/acp-2016-685, 2016a.

De Simone, F., Gencarelli, C. N., Hedgecock, I. M., and Pirrone, N.: A Modeling Comparison of Mercury Deposition from current Anthropogenic Mercury Emission Inventories, Environmental Science & Technology, 50, 5154-5162, 10.1021/acs.est.6b00691, 2016b.

Demers, J. D., Blum, J. D., and Zak, D. R.: Mercury isotopes in a forested ecosystem: Implications for air-surface exchange dynamics and the global mercury cycle, Global Biogeochemical Cycles, 27, 222-238, 2013.

Dibble, T. S., Zelie, M. J., and Mao, H.: Thermodynamics of reactions of ClHg and BrHg radicals with atmospherically abundant free radicals, Atmospheric Chemistry and Physics, 12, 10271-10279, 2012.

Domine, F., and Shepson, P. B.: Air-snow interactions and atmospheric chemistry, Science, 297, 1506-1510, 2002.

Domine, F., Albert, M., Huthwelker, T., Jacobi, H.-W., Kokhanovsky, A. A., Lehning, M., Picard, G., and Simpson, W. R.: Snow physics as relevant to snow photochemistry, Atmospheric Chemistry and Physics, 8, 171-208, 2008.

Dommergue, A., Ferrari, C. P., Gauchard, P.-A., and Boutron, C. F.: The fate of mercury species in a sub-arctic snowpack during snowmelt, Geophysical research letters, 30, 1621, 10.1029/2003GL017308, 2003a.

Dommergue, A., Ferrari, C. P., Poissant, L., Gauchard, P.-A., and Boutron, C. F.: Diurnal cycles of gaseous mercury within the snowpack at Kuujjuarapik/Whapmagoostui, Québec, Canada, Environmental Science and Technology, 37, 3289-3297, 2003b.

Dommergue, A., Bahlmann, E., Ebinghaus, R., Ferrari, C., and Boutron, C. F.: Laboratory simulation of Hg^0 emissions from a snowpack, Analytical and Bioanalytical Chemistry, 388, 319-327, 2007.

Dommergue, A., Larose, C., Faïn, X., Clarisse, O., Foucher, D., Hintelmann, H., Schneider, D., and Ferrari, C. P.: Deposition of Mercury Species in the Ny-Ålesund Area (79°N) and Their Transfer during Snowmelt, Environmental Science & Technology, 44, 901-907, 10.1021/es902579m, 2010a.

Dommergue, A., Sprovieri, F., Pirrone, N., Ebinghaus, R., Brooks, S., Courteaud, J., and Ferrari, C. P.: Overview of mercury measurements in the antarctic troposphere, Atmospheric Chemistry and Physics, 10, 3309-3319, 2010b.

Dommergue, A., Barret, M., Courteaud, J., Cristofanelli, P., Ferrari, C. P., and Gallée, H.: Dynamic recycling of gaseous elemental mercury in the boundary layer of the antarctic plateau, Atmospheric Chemistry and Physics, 12, 11027-11036, 2012.

Dommergue, A., Ferrari, C. P., Magand, O., Barret, M., Gratz, L. E., Pirrone, N., and Sprovieri, F.: Monitoring of gaseous elemental mercury in central Antarctica at Dome Concordia, E3S Web of Conferences. Proceedings of the 16th international conference on heavy metals in the environment, September 23-27, 2012, Rome, Italy, 1, doi: 10.1051/e3sconf/20130117003, 2013a.

Dommergue, A., Vogel, N., Ferrari, C. P., Magand, O., and Barret, M.: Preliminary results from a continuous record of atmospheric gaseous mercury at the coastal station Dumont d'Urville in Antarctica, E3S Web of Conferences. Proceedings of the 16th international conference on heavy metals in the environment, September 23-27, 2012, Rome, Italy, 1, doi: 10.1051/e3sconf/20130127005, 2013b.

Donohoue, D. L., Bauer, D., Cossairt, B., and Hynes, A. J.: Temperature and pressure dependent rate coefficients for the reaction of Hg with Br and the reaction of Br with Br: a pulsed laser photolysis-pulsed laser induced fluorescence study, Journal of physical chemistry, 110, 6623-6632, 2006.

Douglas, T. A., Sturm, M., Simpson, W. R., Blum, J. D., Alvarez-Aviles, L., Keeler, G. J., Perovich, D. K., Biswas, A., and Johnson, K.: Influence of snow and ice crystal formation and accumulation on mercury deposition to the Arctic, Environmental Science and Technology, 42, 1542-1551, 2008.

Douglas, T. A., Loseto, L. L., Macdonald, R. W., Outridge, P. M., Dommergue, A., Poulain, A. J., Amyot, M., Barkay, T., Berg, T., Chételat, J., Constant, P., Evans, M. J., Ferrari, C., Gantner, N., Johnson, M. S., Kirk, J., Kroer, N., Larose, C., Lean, D., Gissel Nielsen, T., Poissant, L., Rognerud, S., Skov, H., Sørensen, S., Wang, F., Wilson, S., and Zdanowicz, C.: The fate of mercury in Arctic terrestrial and aquatic ecosystems, a review, Environ. Chem., 9, 321-355, http://dx.doi.org/10.1071/EN11140, 2012.

Draxler, R. R., and Rolph, G. D.: HYSPLIT (HYbrid Single-Particle Lagrangian Integrated Trajectory) Model access via NOAA ARL READY Website

(http://www.arl.noaa.gov/HYSPLIT.php), last access: 24 October 2015. NOAA Air Resources Laboratory, College Park, MD. , 2013.

Driscoll, C. T., Mason, R. P., Chan, H. M., Jacob, D. J., and Pirrone, N.: Mercury as a global pollutant: sources, pathways, and effects, Environmental Science and Technology, 47, 4967-4983, 2013.

Dumarey, R., Temmerman, E., Dams, R., and Hoste, J.: The accuracy of the vapour injection calibration method for the determination of mercury by amalgamation/cold vapour atomic spectrometry, Analytica Chimica Acta, 170, 337-340, 1985.

Durnford, D., Dastoor, A., Figueras-Nieto, D., and Ryjkov, A.: Long range transport of mercury to the Arctic and across Canada, Atmospheric Chemistry and Physics, 10, 6063-6086, 2010.

Durnford, D., and Dastoor, A.: The behavior of mercury in the cryosphere: a review of what we know from observations, Journal of geophysical research, 116, doi:10.1029/2010JD014809, 2011.

Durnford, D., Dastoor, A., Ryzhkov, A., Poissant, L., Pilote, M., and Figueras-Nieto, D.: How relevant is the deposition of mercury onto snowpacks? – Part 2: A modeling study, Atmos. Chem. Phys., 12, 9251-9274, 10.5194/acp-12-9251-2012, 2012.

Dvonch, J. T., Graney, J. R., Marsik, F. J., Keeler, G. J., and Stevens, R. K.: An investigation of source-receptor relationships for mercury in south Florida using event precipitation data, Science of the Total Environment, 213, 95-108, 1998.

Ebinghaus, R., and Krüger, O.: Emission and local deposition estimates of atmospheric mercury in North-Western and Central Europe, in: Global and regional mercury cycles: Sources, fluxes and mass balances, Springer, 135-159, 1996.

Ebinghaus, R., Jennings, S. G., Schroeder, W. H., Berg, T., Donaghy, T., Guentzel, J., Kenny, C., Kock, H. H., Kvietkus, K., Landing, W., Mühleck, T., Munthe, J. P., E. M., Schneeberger, D., Slemr, F., Sommar, J., Urba, A., Wallschläger, D., and Xiao, Z.: International field intercomparison measurements of atmospheric mercury species at Mace Head, Ireland, Atmospheric Environment, 33, 3063-3073, 1999.

Ebinghaus, R., and Slemr, F.: Aircraft measurements of atmospheric mercury of southern and eastern Germany, Atmospheric Environment, 34, 895-903, 2000.

Ebinghaus, R., Kock, H. H., Coggins, A. M., Spain, T. G., Jennings, S. G., and Temme, C.: Long-term measurements of atmospheric mercury at Mace Head, Irish west coast, between 1995 and 2001, Atmospheric Environment, 36, 5267-5276, 2002a.

Ebinghaus, R., Kock, H. H., Temme, C., Einax, J. W., Löwe, A. G., Richter, A., Burrows, J. P., and Schroeder, W. H.: Antarctic springtime depletion of atmospheric mercury, Environmental Science and Technology, 36, 1238-1244, 2002b.

Ebinghaus, R., Jennings, S. G., Kock, H. H., Derwent, R. G., Manning, A. J., and Spain, T. G.: Decreasing trends in total gaseous mercury observations in baseline air at Mace Head, Ireland from 1996 to 2009, Atmospheric Environment, 45, 3475-3480, 2011.

EC: Regulation No. 1102/2008 of the European Parliament and of the Council on the banning of exports of metallic mercury and certain mercury compounds and mixtures and the safe storage of metallic mercury, Official Journal of the European Union, L 304, 75-79, 2008.

Eck, T. F., Holben, B. N., Reid, J. S., Mukelabai, M. M., Piketh, S. J., Torres, O., Jethva, H. T., Hyer, E. J., Ward, D. E., Dubovik, O., Sinyuk, A., Schafer, J. S., Giles, D. M., Sorokin, M., Smirnov, A., and Slutsker, I.: A seasonal trend of single scattering albedo in southern African biomass-burning particles: implications for satellite products biomass-burning sources, Journal of geophysical research, 118, 6414-6432, 2013.

Edgerton, E. S., Hartsell, B. E., and Jansen, J. J.: Mercury speciation in coal-fired power plant plumes observed at three surface sites in the southeastern US, Environmental science & technology, 40, 4563-4570, 2006.

Edwards, D. P., Emmons, L. K., Gille, J. C., Chu, A., Attié, J.-L., Giglio, L., Wood, S. W., Haywood, J., Deeter, M. N., Massie, S. T., Ziskin, D. C., and Drummond, J. R.: Satellite-observed pollution from southern hemisphere biomass burning, Journal of geophysical research, 111, 1-17, 2006.

Edwards, G. N.: Two cases of poisoning by mercuric methide, Saint Bartholomew's Hospital Report, 1, 141-150, 1865.

Eisele, F., Davis, D. D., Helmig, D., Oltmans, S. J., Neff, W., Huey, G., Tanner, D., Chen, G., Crawford, J. H., Arimoto, R., Buhr, M., Mauldin, L., Hutterli, M., Dibb, J., Blake, D., Brooks, S. B., Johnson, B., Roberts, J. M., Wang, Y., Tan, D., and Flocke, F.: Antarctic tropospheric chemistry (ANTCI) 2003 overview, Atmospheric Environment, 2008, 2749-2761, 2008.

EMEP manual for sampling and analysis: http://www.nilu.no/projects/ccc/manual/index.html, access: 02 August 2016, 2001.

Emmons, L. K., Walters, S., Hess, P. G., Lamarque, J. F., Pfister, G. G., Fillmore, D., Granier, C., Guenther, A., Kinnison, D., Laepple, T., Orlando, J., Tie, X., Tyndall, G., Wiedinmyer, C., Baughcum, S. L., and Kloster, S.: Description and evaluation of the Model for Ozone and Related chemical Tracers, version 4 (MOZART-4), Geosci. Model Dev., 3, 43-67, 10.5194/gmd-3-43-2010, 2010.

Endo, T., Hotta, Y., Haraguchi, K., and Sakata, M.: Mercury contamination in the red meat of whales and dolphins marketed for human consumption in Japan, Environmental science & technology, 37, 2681-2685, 2003.

Engstrom, D. R., Fitzgerald, W. F., Cooke, C. A., Lamborg, C. H., Drevnick, P. E., Swain, E. B., Balogh, S. J., and Balcom, P. H.: Atmospheric Hg Emissions from Preindustrial Gold and Silver Extraction in the Americas: A Reevaluation from Lake-Sediment Archives, Environmental Science & Technology, 48, 6533-6543, 10.1021/es405558e, 2014.

Enrico, M., Roux, G. L., Marusczak, N., Heimbürger, L.-E., Claustres, A., Fu, X., Sun, R., and Sonke, J. E.: Atmospheric Mercury Transfer to Peat Bogs Dominated by Gaseous Elemental Mercury Dry Deposition, Environmental Science & Technology, 50, 2405-2412, 10.1021/acs.est.5b06058, 2016.

Epov, V. N., Malinovskiy, D., Vanhaecke, F., Bégué, D., and Donard, O. F.: Modern mass spectrometry for studying mass-independent fractionation of heavy stable isotopes in environmental and biological sciences, Journal of Analytical Atomic Spectrometry, 26, 1142-1156, 2011.

Ericksen, J., Gustin, M., Schorran, D., Johnson, D., Lindberg, S., and Coleman, J.: Accumulation of atmospheric mercury in forest foliage, Atmospheric Environment, 37, 1613-1622, 2003.

EU: Council Directive 96/61/EC concerning integrated pollution prevention and control, Official Journal of the European Union, L 257, 1996.

EU: Directive 2000/60/EC of the European Parliament and of the Council establishing a framework for Community action in the field of water policy, Official Journal of the European Union, L 327, 1-73, 2000.

EU: Directive 2001/80/EC of the European Parliament and of the Council on the limitation of emissions of certain pollutants into the air from large combustion plants, Official Journal of the European Union, L 309, 22-30, 2001a.

EU: Regulation 466/2001/EC of the European Parliament and of the Council setting maximum levels for certain contaminants in foodstuffs, Official Journal of the European Communities, L77, 1-13, 2001b.

EU: Decision No 2455/2001/EC of the European Parliament and of the Council establishing the list of prioriry substances in the field of water policy and amending Directive 2000/60/EC, Official Journal of the European Union, L 331, 1-5, 2001c.

EU: Regulation 221/2002/EC of the European Parliament and of the Council amending Regulation (EC) No. 466/2001 setting maximum levels for certain contaminants in foodstuff, Official Journal of the European Communities, L37, 4-6, 2002.

EU: Directive 2004/107/EC of the European Parliament and of the Counci relating to arsenic, cadmium, mercury, nickel and polycyclic aromatic hydrocarbons in ambient air, Official Journal of the European Union, L 23, 3-16, 2004.

EU: Directive 2007/51/EC of the European Parliament and of the Council amending Council Directive 76/769/ECC relating to restrictions on the marketing of certain measuring devices containing mercury, Official Journal of the European Union, L 257, 13-15, 2007.

EU: Directive 2011/65/EU of the European Parliament and of the Council on the restriction of the use of certain hazardous substances in electrical and electronic equipment Official Journal of the European Union, L 174, 88-110, 2011.

EU: 2013/732/EU: Commissions Implementing Decision establishing the best available techniques (BAT) conclusions, under Directive 2010/75/EU of the European Parliament and of the Council on industrial emissions, for the production of chlor-alkali Official Journal of the European Communities, L332, 34-48, 2013.

Evers, D. C., Burgess, N. M., Champoux, L., Hoskins, B., Major, A., Goodale, W. M., Taylor, R. J., Poppenga, R., and Daigle, T.: Patterns and interpretation of mercury exposure in freshwater avian communities in northeastern North America, Ecotoxicology, 14, 193-221, 2005.

Evers, D. C., Keane, S. E., Basu, N., and Buck, D.: Evaluating the effectiveness of the Minamata Convention on Mercury: principles and recommendations for next steps, Science of the Total Environment, http://dx.doi.org/10.1016/j.scitotenv.2016.05.001, 2016.

Faïn, X., Grangeon, S., Bahlmann, E., Fritsche, J., Obrist, D., Dommergue, A., Ferrari, C., Cairns, W., Ebinghaus, R., Barbante, C., Cescon, P., and Boutron, C. F.: Diurnal production of gaseous mercury in the alpine snowpack before snowmelt, Journal of geophysical research, 112, doi:10.1029/2007JD008520, 2007.

Faïn, X., Ferrari, C., Dommergue, A., Albert, M., Battle, M., Arnaud, L., Barnola, J.-M., Cairns, W., Barbante, C., and Boutron, C. F.: Mercury in the snow and firn at Summit Station, Central Greenland, and implications for the study of past atmospheric mercury levels, Atmospheric Chemistry and Physics, 8, 3441-3457, 2008.

Favier, V., Agosta, C., Parouty, S., Durand, G., Delaygue, G., Gallée, H., Drouet, A.-S., Trouvilliez, A., and Krinner, G.: An updated and quality controlled surface mass balance dataset for Antarctica, The Cryosphere, 7, 583-597, 2013.

Feddersen, D., Talbot, R., Mao, H., and Sive, B. C.: Size distribution of particulate mercury in marine and coastal atmospheres, Atmospheric Chemistry and Physics, 12, 10899-10909, 2012.

Ferrari, C. P., Dommergue, A., Boutron, C. F., Skov, H., Goodsite, M. E., and Jensen, B.: Nighttime production of elemental gaseous mercury in interstitial air of snow at Station Nord, Greenland, Atmospheric Environment, 38, 2727-2735, 2004.

Ferrari, C. P., Gauchard, P.-A., Aspmo, K., Dommergue, A., Magand, O., Bahlmann, E., Nagorski, S., Temme, C., Ebinghaus, R., Steffen, A., Banic, C., Berg, T., Planchon, F., Barbante, C., Cescon, P., and Boutron, C. F.: Snow-to-air exchanges of mercury in an arctic seasonal snowpack in Ny-Alesund, Svalbard, Atmospheric Environment, 39, 7633-7645, 2005.

Ferrari, C. P., Padova, C., Faïn, X., Gauchard, P.-A., Dommergue, A., Aspmo, K., Berg, T., Cairns, W., Barbante, C., Cescon, P., Kaleschke, L., Richter, A., Wittrock, F., and Boutron, C. F.: Atmospheric mercury depletion event study in Ny-Alesund (Svalbard) in spring 2005. Deposition and transformation of Hg in surface snow during springtime, Science of the Total Environment, 397, 167-177, 2008.

Finley, B. D., Swartzendruber, P. C., and Jaffe, D. A.: Particulate mercury emissions in regional wildfire plumes observed at the mount bachelor observatory, Atmospheric Environment, 43, 6074-6083, 2009.

Fisher, J. A., Jacob, D. J., Soerensen, A. L., Amos, H. M., Steffen, A., and Sunderland, E. M.: Riverine source of Arctic Ocean mercury inferred from atmospheric observations, Nature Geosci, 5, 499-504, http://www.nature.com/ngeo/journal/v5/n7/abs/ngeo1478.html#supplementary-information, 2012.

Fisher, J. A., Jacob, D. J., Soerensen, A. L., Amos, H. M., Corbitt, E. S., Streets, D. G., Wang, Q., Yantosca, R. M., and Sunderland, E. M.: Factors driving mercury variability in the Arctic atmosphere and ocean over the past 30 years, Global biogeochemical cycles, 27, 1226-1235, 2013.

Fishman, J., Fakhruzzaman, K., Cros, B., and Nganga, D.: Identification of widespread pollution in the southern hemisphere deduced from satellite analyses, Science, 252, 1693-1696, 1991.

Fitzgerald, W. F., and Gill, G. A.: Subnanogram determination of mercury by two-stage gold amalgamation and gas detection applied to atmospheric analysis, Analytical chemistry, 51, 1714-1720, 1979.

La Russie convoite les ressources de l'Antarctique: http://www.lemonde.fr/planete/article/2011/10/22/la-russie-convoite-les-ressources-de-l-antarctique_1592344_3244.html, access: 28 July 2016, 2011.

France, J. L., King, M. D., Frey, M. M., Erbland, J., Picard, G., Preunkert, S., MacArthur, A., and Savarino, J.: Snow optical properties at Dome C (Concordia), Antarctica; implications for snow

emissions and snow chemistry of reactive nitrogen, Atmospheric Chemistry and Physics, 11, 9787-9801, 2011.

Frey, M. M., Brough, N., France, J. L., Anderson, P. S., Traulle, O., King, M. D., Jones, A. E., Wolff, E. W., and Savarino, J.: The diurnal variability of atmospheric nitrogen oxides (NO and NO2) above the Antarctic Plateau driven by atmospheric stability and snow emissions, Atmospheric Chemistry and Physics, 13, 3045-3062, 2013.

Frey, M. M., Roscoe, H. K., Kukui, A., Savarino, J., France, J. L., King, M. D., Legrand, M., and Preunkert, S.: Atmospheric nitrogen oxides (NO and NO_2) at Dome C, East Antarctica, during the OPALE campaign, Atmospheric Chemistry and Physics, 15, 7859-7875, 2015.

Friedli, H. R., Radke, L. F., Prescott, R., Li, P., Woo, J. H., and Carmichael, G. R.: Mercury in the atmosphere around Japan, Korea, and China as observed during the 2001 ACE-Asia field campaign: Measurements, distributions, sources, and implications, Journal of Geophysical Research: Atmospheres, 109, 10.1029/2003JD004244, 2004.

Friedli, H. R., Arellano, A. F., Cinnirella, S., and Pirrone, N.: Initial estimates of mercury emissions to the atmosphere from global biomass burning, Environmental Science and Technology, 43, 3507-3513, 2009a.

Friedli, H. R., Arellano, A. F., Cinnirella, S., and Pirrone, N.: Mercury emissions from global biomass burning: spatial and temporal distribution, in: Mercury fate and transport in the global atmosphere, edited by: Pirrone, N., and Mason, R. P., Springer 193-220, 2009b.

Fritsche, J., Obrist, D., and Alewell, C.: Evidence of microbial control of Hg0emissions from uncontaminated terrestrial soils, Journal of plant nutrition and soil science, 171, 200-209, 2008.

Fu, X., Marusczak, N., Heimbürger, L. E., Sauvage, B., Gheusi, F., Prestbo, E. M., and Sonke, J. E.: Atmospheric mercury speciation dynamics at the high-altitude Pic du Midi Observatory, southern France, Atmos. Chem. Phys., 16, 5623-5639, 10.5194/acp-16-5623-2016, 2016a.

Fu, X., Marusczak, N., Wang, X., Gheusi, F., and Sonke, J. E.: Isotopic Composition of Gaseous Elemental Mercury in the Free Troposphere of the Pic du Midi Observatory, France, Environmental Science & Technology, 10.1021/acs.est.6b00033, 2016b.

Fu, X. W., Feng, X., Dong, Z. Q., Yin, R. S., Wang, J. X., Yang, Z. R., and Zhang, H.: Atmospheric gaseous elemental mercury (GEM) concentrations and mercury depositions at a high-altitude mountain peak in south China, Atmospheric Chemistry and Physics, 10, 2425-2437, 2010.

Fujita, K., and Abe, O.: Stable isotopes in daily precipitation at Dome Fuji, East Antarctica, Geophysical research letters, 33, L18503, http://dx.doi.org/10.1029/2006GL026936, 2006.

Gallée, H., and Pettré, P.: Dynamical constraints on katabatic wind cessation in Adélie Land, Antarctica, Journal of the atmospheric sciences, 55, 1755-1770, 1998.

Gallée, H., and Gorodetskaya, I. V.: Validation of a limited area model over Dome C, Antarctic Plateau, during winter, Climate Dynamics, 34, 61-72, 2010.

Gallée, H., Preunkert, S., Argentini, S., Frey, M. M., Genthon, C., Jourdain, B., Pietroni, I., Casasanta, G., Barral, H., Vignon, E., Amory, C., and Legrand, M.: Characterization of the boundary layer at Dome C (East Antarctica) during the OPALE summer campaign, Atmospheric Chemistry and Physics, 15, 6225-6236, 2015.

Garbarino, J. R., Snyder-Conn, E., Leiker, T. J., and Hoffman, G. L.: Contaminants in Arctic snow collected over northwest Alaskan sea ice, Water Air & Soil Pollution, 139, 183-214, 2002.

Gårdfeldt, K., Sommar, J., Strömberg, D., and Feng, X.: Oxidation of atomic mercury by hydroxyl radicals and photoinduced decomposition of methylmercury in the aqueous phase, Atmospheric Environment, 35, 3039-3047, 2001.

Gårdfeldt, K., and Jonsson, M.: Is biomolecular reduction of Hg(II) complexes possible in aqueous systems of environmental importance, Journal of physical chemistry A, 107, 4478-4482, 2003.

Gauchard, P.-A., Aspmo, K., Temme, C., Steffen, A., Ferrari, C., Berg, T., Ström, J., Kaleschke, L., Dommergue, A., Bahlmann, E., Magand, O., Planchon, F., Ebinghaus, R., Banic, C., Nagorski, S., Baussand, P., and Boutron, C.: Study of the origin of atmospheric mercury depletion events recorded in Ny-Ålesund, Svalbard, spring 2003, Atmospheric Environment, 39, 7620-7632, http://dx.doi.org/10.1016/j.atmosenv.2005.08.010, 2005.

Gay, D. A., Schmeltz, D., Prestbo, E., Olson, J. R., Sharac, T., and Tordon, R.: The atmospheric mercury network: measurement and initial examination of an ongoing atmospheric mercury record across North America, Atmospheric Chemistry and Physics, 13, 11339-11349, 2013.

Gbor, P. K., Wen, D., Meng, F., Yang, F., Zhang, B., and Sloan, J. J.: Improved model for mercury emission, transport and deposition, Atmospheric Environment, 40, 973-983, 2006.

Genthon, C., Town, M. S., Six, D., Favier, V., Argentini, S., and Pellegrini, A.: Meteorological atmospheric boundary layer measurements and ECMWF analyses during summer at Dome C, Antarctica, Journal of geophysical research, 115, D05104, 10.1029/2009JD012741, 2010.

Genthon, C., Six, D., Gallée, H., Grigioni, P., and Pellegrini, A.: Two years of atmospheric boundary layer observations on a 45-m tower at Dome C on the Antarctic plateau, Journal of geophysical research: atmospheres, 118, 3218-3232, 2013.

Giang, A., and Selin, N. E.: Benefits of mercury controls for the United States, Proceedings of the National Academy of Sciences of the United States of America, www.pnas.org/cgi/doi/10.1073/pnas.1514395113, 2015.

Gibb, H., and O'Leary, K. G.: Mercury exposure and health impacts among individuals in the artisanal and small-scale gold mining community: a comprehensive review, Environmental Health Perspectives, 122, 667-672, 2014.

Gichuki, S. W., and Mason, R. P.: Wet and dry deposition of mercury in Bermuda, Atmospheric Environment, 87, 249-257, 2014.

Golding, J., Gregory, S., Iles-Caven, Y., Hibbeln, J., Emond, A., and Taylor, C. M.: Associations between prenatal mercury exposure and early child development in the ALSPAC study, NeuroToxicology, 53, 215-222, http://dx.doi.org/10.1016/j.neuro.2016.02.006, 2016.

Goodsite, M., Plane, J. M. C., and Skov, H.: Correction to a theoretical study of the oxidation of Hg0 to HgBr2 in the troposphere, Environmental Science & Technology, 46, 5262–5262, 2012.

Goodsite, M. E., Plane, J. M. C., and Skov, H.: A theoretical study of the oxidation of Hg^0 to $HgBr_2$ in the troposphere, Environmental Science and Technology, 38, 1772-1776, 2004.

Grandjean, P., Weihe, P., White, R. F., Debes, F., Araki, S., Yokoyama, K., Murata, K., Soerensen, N., Dahl, R., and Joergensen, P. J.: Cognitive deficit in 7-year-old children with prenatal exposure to methylmercury, Neurotoxicol Teratol, 19, 417-428, 1997.

Grandjean, P., Satoh, H., Murata, K., and Eto, K.: Adverse effects of methylmercury: environmental health research implications, Environmental Health Perspectives, 118, 1137-1145, 2010.

Grannas, A. M., Jones, A. E., Dibb, J., Ammann, M., Anastasio, C., Beine, H. J., Bergin, M., Bottenheim, J., Boxe, C. S., Carver, G., Chen, G., Crawford, J. H., Domine, F., Frey, M. M., Guzman, M. I., Heard, D. E., Helmig, D., Hoffmann, M. R., Honrath, R. E., Huey, L. G., Hutterli, M., Jacobi, H.-W., Klan, P., Lefer, B., McConnell, J. R., Plane, J. M. C., Sander, R., Savarino, J., Shepson, P. B., Simpson, W. R., Sodeau, J., Von Glasow, R., Weller, R., Wolff, E. W., and Zhu, T.: An overview of snow photochemistry: evidence, mechanisms and impacts, Atmospheric Chemistry and Physics, 7, 4329-4373, 2007.

Gratz, L. E., Keeler, G. J., Blum, J. D., and Sherman, L. S.: Isotopic composition and fractionation of mercury in Great Lakes precipitation and ambient air, Environmental science & technology, 44, 7764-7770, 2010.

Graydon, J. A., St Louis, V. L., Hintelmann, H., Lindberg, S. E., Sandilands, K. A., Rudd, J. W. M., Kelly, C. A., Hall, B. D., and Mowat, L. D.: Long-term wet and dry deposition of total and methyl mercury in the remote boreal ecoregion of Canada, Environmental Science & Technology, 42, 8345-8351, 2008.

Griffiths, T. R., and Anderson, R. A.: Tetrahalogenomercury (II) complexes. A study of their electronic spectra, formation constants, ionic strength, and cation effects, Canadian journal of chemistry, 69, 451-457, 1991.

Grilli, R., Legrand, M., Kukui, A., Méjean, G., Preunkert, S., and Romanini, D.: First investigations of IO, BrO, and NO2 summer atmospheric levels at a coastal East Antarctic site using mode-locked cavity enhanced absorption spectroscopy, Geophysical research letters, 40, 791-796, 2013.

Gros, V., Poisson, N., Martin, D., Kanakidou, M., and Bonsang, B.: Observations and modeling of the seasonal variation of surface ozone at Amsterdam Island: 1994-1996, Journal of geophysical research, 103, 28.103-109, 1998.

Gros, V., Bonsang, B., Martin, D., and Novelli, P. C.: Carbon monoxide short term measurements at Amsterdam Island: estimation of biomass burning rates, Chemosphere Global Change Sci., 1, 163-172, 1999.

Gschwend, P. M., Macfarlane, J. K., and Newman, K. A.: Volatile halogenated organic compounds released to seawater from temperate marine macroalgae, Science, 227, 1033-1035, 1985.

Gustin, M. S., Biester, H., and Kim, C. S.: Investigation of the light-enhanced emission of mercury from naturally enriched substrates, Atmospheric Environment, 36, 3241-3254, 2002.

Gustin, M. S., and Jaffe, D. A.: Reducing the uncertainty in measurement and understanding of mercury in the atmosphere, Environmental Science and Technology, 44, 2222-2227, 2010.

Gustin, M. S.: Exchange of mercury between the atmosphere and terrestrial ecosystems, Environmental chemistry and toxicology of mercury. Wiley, Hoboken, 423-452, 2011.

Gustin, M. S., Huang, J., Miller, M. B., Peterson, C., Jaffe, D. A., Ambrose, J., Finley, B. D., Lyman, S. N., Call, K., Talbot, R., Feddersen, D., Mao, H., and Lindberg, S. E.: Do we understand what the mercury speciation instruments are actually measuring? Results of RAMIX, Environmental Science and Technology, 47, 7295-7306, 2013.

Gustin, M. S., Amos, H. M., Huang, J., Miller, M. B., and Heidecorn, K.: Measuring and modeling mercury in the atmosphere: a critical review, Atmospheric Chemistry and Physics, 15, 5697-5713, 2015.

Gustin, M. S., Evers, D. C., Bank, M. S., Hammerschmidt, C. R., Pierce, A., Basu, N., Blum, J., Bustamante, P., Chen, C., Driscoll, C. T., Horvat, M., Jaffe, D., Pacyna, J., Pirrone, N., and Selin, N.: Importance of Integration and Implementation of Emerging and Future Mercury Research into the Minamata Convention, Environmental Science & Technology, 50, 2767-2770, 10.1021/acs.est.6b00573, 2016.

Hale, R. C., Kim, S. L., Harvey, E., La Guardia, M. J., Mainor, T. M., Bush, E. O., and Jacobs, E. M.: Antarctic research bases: local sources of polybrominated diphenyl ether (PBDE) flame retardants, Environmental Science and Technology, 42, 1452-1457, 2008.

Hall, B.: The gas phase oxidation of elemental mercury by ozone, Water, Air & Soil Pollution, 80, 301-315, 1995.

Han, Y., Huh, Y., Hong, S., Hur, S. D., Motoyama, H., Fujita, S., Nakazawa, F., and Fukui, K.: Quantification of total mercury in Antarctic surface snow using ICP-SF-MS: spatial variation from the coast to Dome Fuji, Bulletin of Korean Chemical Society, 32, 4258-4264, 2011.

Haq, I. U.: Argrosan poisoning in man, British medical journal, 1, 1579-1582, 1963.

Harada, M.: Minamata Disease: methylmercury poisoning in Japan caused by environmental pollution, Critical Reviews in Toxicology, 25, 1-24, 1995.

Harada, M., Hanada, M., Jajiri, M., Inoue, Y., Hotta, N., Fujino, T., Takaoka, S., and Ueda, K.: Mercury pollution in first nations groups in Ontario, Canada: 35 years of Canadian Minamata disease, Journal of Minamata Studies, 3, 3-10, 2011.

Hartman, J. S., Weisberg, P. J., Pillai, R., Ericksen, J. A., Kuiken, T., Lindberg, S. E., Zhang, H., Rytuba, J. J., and Gustin, M. S.: Application of a rule-based model to estimate mercury exchange for three background biomes in the continental United States, Environmental science & technology, 43, 4989-4994, 2009.

Hedgecock, I. M., and Pirrone, N.: Mercury and photochemistry in the marine boundary layer-modelling studies suggest the in situ production of reactive gas phase mercury, Atmospheric Environment, 35, 3055-3062, 2001.

Hedgecock, I. M., Pirrone, N., Sprovieri, F., and Pesenti, E.: Reactive gaseous mercury in the marine boundary layer: modelling and experimental evidence of its formation in the mediterranean region, Atmospheric Environment, 37, S41-S49, 2003.

Hedgecock, I. M., and Pirrone, N.: Chasing quicksilver: modeling the atmospheric lifetime of Hg(0) in the marine boundary layer at various latitudes, Environmental Science and Technology, 38, 69-76, 2004.

Heidam, N. Z., Wåhlin, P., and Christensen, J. H.: Tropospheric Gases and Aerosols in Northeast Greenland, Journal of the Atmospheric Sciences, 56, 261-278, doi:10.1175/1520-0469(1999)056<0261:TGAAIN>2.0.CO;2, 1999.

Heidam, N. Z., Christensen, J., Wåhlin, P., and Skov, H.: Arctic atmospheric contaminants in NE Greenland: levels, variations, origins, transport, transformations and trends 1990–2001, Science of The Total Environment, 331, 5-28, http://dx.doi.org/10.1016/j.scitotenv.2004.03.033, 2004.

Heintzenberg, J., Hansson, H. C., and Lannefors, H.: The chemical composition of arctic haze at Ny-Ålesund, Spitsbergen, Tellus, 33, 162-171, 10.1111/j.2153-3490.1981.tb01741.x, 1981.

Helmig, D., Oltmans, S. J., Carlson, D., Lamarque, J.-F., Jones, A., Labuschagne, C., Anlauf, K., and Hayden, K.: A review of surface ozone in the polar regions, Atmospheric Environment, 41, 5138-5161, 2007.

Helsel, D. R.: More than obvious: Better methods for interpreting nondetect data, Environmental Science and Technology, 39, 419A-423A, 2005.

Hirdman, D., Aspmo, K., Burkhart, J. F., Eckhardt, S., Sodemann, H., and Stohl, A.: Transport of mercury in the Arctic atmosphere: Evidence for a spring-time net sink and summer-time source, Geophysical research letters, 36, L12814, doi:10.1029/2009GL038345, 2009.

Hoegstroem, U.: Non-dimensional wind and temperature profiles in the atmosphere surface layer: a re-evaluation, Boundary-Layer Meteorology, 42, 55-78, 1988.

Holmes, C. D., Jacob, D. J., and Yang, X.: Global lifetime of elemental mercury against oxidation by atomic bromine in the free troposphere, Geophysical research letters, 33, L20808, 10.1029/2006GL027176, 2006.

Holmes, C. D., Jacob, D. J., Mason, R. P., and Jaffe, D. A.: Sources and deposition of reactive gaseous mercury in the marine atmosphere, Atmospheric Environment, 43, 2278-2285, 2009.

Holmes, C. D., Jacob, D. J., Corbitt, E. S., Mao, J., Yang, X., Talbot, R., and Slemr, F.: Global atmospheric model for mercury including oxidation by bromine atoms, Atmospheric Chemistry and Physics, 10, 12037-12057, 2010.

Horváth, O., and Vogler, A.: Photoredox chemistry of iodomercurate (II) complexes in acetonitrile, Inorganica chimica acta, 221, 79-84, 1994.

Huang, J., Choi, H.-D., Landis, M. S., and Holsen, T. M.: An application of passive samplers to understand atmospheric mercury concentration and dry deposition spatial distributions, Journal of Environmental Monitoring, 14, 2976-2982, 2012.

Huang, J., Miller, M. B., Weiss-Penzias, P., and Gustin, M. S.: Comparison of gaseous oxidized mercury measured by KCl-coated denuders, and nylon and cation exchange membranes, Environmental Science and Technology, 47, 7307-7316, 2013.

Huang, J., Lyman, S. N., Hartman, J. S., and Gustin, M. S.: A review of passive sampling systems for ambient air mercury measurements, Environmental Science: Processes & Impacts, 16, 374-392, 10.1039/C3EM00501A, 2014.

Huang, J., Kang, S., Zhang, Q., Guo, J., Sillanpää, M., Wang, Y., Sun, S., Sun, X., and Tripathee, L.: Characterizations of wet mercury deposition on a remote high-elevation site in the southeastern Tibetan Plateau, Environmental Pollution, 518-526, 2015.

Huey, L. G., Tanner, D. J., Slusher, D. L., Dibb, J. E., Arimoto, R., Chen, G., Davis, D., Buhr, M. P., Nowak, J. B., Mauldin, L., Eisele, F. L., and Kosciuch, E.: CIMS measurements of HNO_3 and SO_2 at the South Pole during ISCAT 2000, Atmospheric Environment, 38, 5411-5421, 2004.

Hutterli, M. A., McConnell, J. R., Chen, G., Bales, R. C., Davis, D. D., and Lenschow, D. H.: Formaldehyde and hydrogen peroxide in air, snow and intersitial air at South Pole, Atmospheric Environment, 38, 5439-5450, 2004.

Hynes, A. J., Donohoue, D. L., Goodsite, M. E., and Hedgecock, I. M.: Our current understanding of major chemical and physical processes affecting mercury dynamics in the atmosphere and at the air-water/terrestrial interfaces, in: Mercury fate and transport in the global atmosphere, edited by: Pirrone, N., and Mason, R. P., Springer, New York, 427-457, 2009.

Iverfeldt, Å., Munthe, J., Brosset, C., and Pacyna, J.: Long-term changes in concentration and deposition of atmospheric mercury over Scandinavia, Water, Air, and Soil Pollution, 80, 227-233, 1995.

Jadán Piedra, C., Sánchez, V., Vélez, D., and Devesa, V.: Reduction of mercury bioaccessibility using dietary strategies, LWT - Food Science and Technology, 71, 10-16, http://dx.doi.org/10.1016/j.lwt.2016.03.015, 2016.

Jaffe, D. A., Prestbo, E., Swartzendruber, P., Weiss-Penzias, P., Kato, S., Takami, A., Hatakeyama, S., and Kajii, Y.: Export of atmospheric mercury from Asia, Atmospheric Environment, 2005, 3029-3038, 2005.

Jaffe, D. A., Lyman, S., Amos, H. M., Gustin, M. S., Huang, J., Selin, N. E., Levin, L., Schure, A., Mason, R. P., Talbot, R., Rutter, A. P., Finley, B., Jaeglé, L., Shah, V., McClure, C., Ambrose, J., Gratz, L., Lindberg, S. E., Weiss-Penzias, P., Sheu, G.-R., Feddersen, D., Horvat, M., Dastoor, A., Hynes, A. J., Mao, H., Sonke, J. E., Slemr, F., Fisher, J. A., Ebinghaus, R., Zhang, B., and Edwards, D. P.: Progress on understanding atmospheric mercury hampered by uncertain measurements, Environmental Science and Technology, 48, 7204-7206, doi: 10.1021/es5026432, 2014.

Jalili, M. A., and Abbasi, A. H.: Poisoning by ethyl mercury toluence sulphonanilide, British journal of industrial medicine, 18, 303-308, 1961.

Jensen, S., and Jernelov, A.: Biological methylation of mercury in aquatic organisms, Nature, 223, 1453-1454, 1969.

Jin, M., Deal, C., Lee, S. H., Elliott, S., Hunke, E., Maltrud, M., and Jeffery, N.: Investigation of Arctic sea ice and ocean primary production for the period 1992–2007 using a 3-D global ice–ocean ecosystem model, Deep Sea Research Part II: Topical Studies in Oceanography, 81–84, 28-35, http://dx.doi.org/10.1016/j.dsr2.2011.06.003, 2012.

Joffre, S. M.: Modelling the dry deposition velocity of highly soluble gases to the sea surface, Atmospheric Environment (1967), 22, 1137-1146, http://dx.doi.org/10.1016/0004-6981(88)90343-5, 1988.

Johnson, K. P., Blum, J. D., Keeler, G. J., and Douglas, T. A.: Investigation of the deposition and emission of mercury in arctic snow during an atmospheric mercury depletion event, Journal of geophysical research, 113, doi: 10.1029/2008JD009893, 2008.

Jones, C. P., Lyman, S. N., Jaffe, D. A., Allen, T., and O'Neil, T. L.: Detection and quantification of gas-phase oxidized mercury compounds by GC/MS, Atmos. Meas. Tech., 9, 2195-2205, 10.5194/amt-9-2195-2016, 2016.

Jung, G., Hedgecock, I. M., and Pirrone, N.: ECHMERIT V1.0 – a new global fully coupled mercury-chemistry and transport model, Geosci. Model Dev., 2, 175-195, 10.5194/gmd-2-175-2009, 2009.

Jungwirth, P., and Tobias, D. J.: Specific ion effects at the air/water interface, Chemical reviews, 106, 1259-1281, 2006.

Kang, S., Huang, J., Wang, F., Zhang, Q., Zhang, Y., Li, C., Wang, L., Chen, P., Sharma, C. M., Li, Q., Sillanpää, M., Hou, J., Xu, B., and Guo, J.: Atmospheric mercury depositional chronology reconstructed from lake sediment and ice cores in the Himalayas and Tibetan Plateau, Environmental Science & Technology, 50, 2859-2869, 10.1021/acs.est.5b04172, 2016.

Karagas, M. R., Choi, A. L., Oken, E., Horvat, M., Schoeny, R., Kamai, E., Cowell, W., Grandjean, P., and Korrick, S.: Evidence on the human health effects of low-level methylmercury exposure, Environmental Health Perspectives, 120, 799-806, 2012.

Keeler, G., Gratz, L., and Al-Wali, K. I.: Long-term atmospheric mercury wet deposition at Underhill, Vermont, Ecotoxicology, 14, 71-83, 2005.

Kellerhals, M., Beauchamp, S. T., Belzer, W., Blanchard, P., Froude, F., Harvey, B., McDonald, K., Pilote, M., Poissant, L., Puckett, K., Schroeder, B., Steffen, A., and Tordon, R.: Temporal and spatial variability of total gaseous mercury in Canada: results from the Canadian Atmospheric Mercury Measurement Network (CAMNet), Atmospheric Environment, 37, 1003-1011, 2003.

Kerbrat, M., Legrand, M. P., S., Gallée, H., and Kleffmann, J.: Nitrous acid at Concordia (inland site) and Dumont d'Urville (coastal site), east antarctica, Journal of geophysical research, 117, doi:10.1029/2011JD017149, 2012.

Kessler, R.: The Minamata Convention on mercury: a first step toward protecting future generations, Environmental Health Perspectives, 121, A304-A309, 2013.

Khalil, M. A. K., and Rasmussen, R. A.: Sources, sinks, and seasonal cycles of atmospheric methane, Journal of geophysical research, 88, 5131-5144, 1983.

Kikuchi, T., Ikemoto, H., Takahashi, K., Hasome, H., and Ueda, H.: Parameterizing soil emission and atmospheric oxidation-reduction in a model of the global biogeochemical cycle of mercury, Environmental science & technology, 47, 12266-12274, 2013.

Kim, K.-H., Ebinghaus, R., Schroeder, W., Blanchard, P., Kock, H., Steffen, A., Froude, F., Kim, M.-Y., Hong, S., and Kim, J.-H.: Atmospheric mercury concentrations from several observatory sites in the Northern Hemisphere, Journal of Atmospheric Chemistry, 50, 1-24, 2005.

King, J. C., and Anderson, P. S.: Heat and water vapor fluxes and scalar roughness lengths over an Antarctic ice shelf, Boundary-Layer Meteorology, 69, 101-121, 1994.

King, J. C., and Turner, J.: Antarctic Meteorology and Climatology, Cambridge University Press, Cambridge, 409 pp., 1997.

King, J. C., Argentini, S. A., and Anderson, P. S.: Contrasts between the summertime surface energy balance and boundary layer structure at Dome C and Halley stations, Antarctica, Journal of geophysical research, 111, doi:10.1029/2005JD006130, 2006.

King, M. D., and Simpson, W. R.: Extinction of UV radiation in Arctic snow at Alert, Canada (82°N), Journal of geophysical research 106, 12499-12507, 2001.

Kirk, J. L., St. Louis, V. L., and Sharp, M. J.: Rapid Reduction and Reemission of Mercury Deposited into Snowpacks during Atmospheric Mercury Depletion Events at Churchill, Manitoba, Canada, Environmental Science & Technology, 40, 7590-7596, doi: 10.1021/es061299+, 2006.

Knightes, C. D.: Development and test application of a screening-level mercury fate model and tool for evaluating wildlife exposure risk for surface waters with mercury-contaminated sediments (SERAFM), Environmental Model Software, 23, 495-510, 2008.

Knightes, C. D., Sunderland, E., Barber, M. C., Johnston, J. M., and Ambrose, R. B. J.: Application of ecosystem-scale fate and bioaccumulation models to predict fish mercury response times to changes in atmospheric deposition, Environmental Toxicology and Chemistry, 28, 881-893, 2009.

Kock, H., Bieber, E., Ebinghaus, R., Spain, T., and Thees, B.: Comparison of long-term trends and seasonal variations of atmospheric mercury concentrations at the two European coastal monitoring stations Mace Head, Ireland, and Zingst, Germany, Atmospheric Environment, 39, 7549-7556, 2005.

Kocman, D., and Horvat, M.: A laboratory based experimental study of mercury emission from contaminated soils in the River Idrijca catchment, Atmospheric Chemistry and Physics, 10, 1417-1426, 2010.

König-Langlo, G., King, J. C., and Pettré, P.: Climatology of the three coastal Antarctic stations Dumont d'Urville, Neumayer, and Halley, Journal of geophysical research, 103, 10935-10946, 1998.

Koop, T., Kapilashrami, A., Molina, L. T., and Molina, M. J.: Phase transitions of sea-salt/water mixtures at low temperatures: implications for ozone chemistry in the polar marine boundary layer, Journal of geophysical research, 105, 26393–26402 10.1029/2000JD900413, 2000.

Kos, G., Ryzhkov, A., Dastoor, A., Narayan, J., Steffen, A., Ariya, P. A., and Zhang, L.: Evaluation of discrepancy between measured and modelled oxidized mercury species, Atmospheric Chemistry and Physics, 13, 4839-4863, 2013.

Kritz, M. A., Le Roulley, J.-C., and Danielsen, E. F.: The China Clipper - fast advective transport of radon-rich air from the Asian boundary layer to the upper troposphere near California, Tellus, 42B, 46-61, 1990.

Kukui, A., Legrand, M., Ancellet, G., Gros, V., Bekki, S., Sarda-Estève, R., Loisil, R., and Preunkert, S.: Measurements of OH and RO2 radicals at the coastal Antarctic site of Dumont d'Urville (East Antarctica) in summer 2010-2011, Journal of geophysical research, 117, D12310, doi:10.1029/2012JD017614, 2012.

Kukui, A., Legrand, M., Preunkert, S., Frey, M. M., Loisil, R., Gil Roca, J., Jourdain, B., King, M. D., France, J. L., and Ancellet, G.: Measurements of OH and RO_2 radicals at Dome C, East Antarctica, Atmospheric Chemistry and Physics, 14, 12373-12392, 2014.

Kunkely, H., Horváth, O., and Vogler, A.: Photophysics and photochemistry of mercury complexes, Coordination chemistry reviews, 159, 85-93, 1997.

Kuss, J., Zülicke, C., Pohl, C., and Schneider, B.: Atlantic mercury emission determined from continuous analysis of the elemental mercury sea-air concentration difference within transects between 50 N and 50 S, Global Biogeochemical Cycles, 25, 10.1029/2010GB003998, 2011.

Kwon, S. Y., and Selin, N. E.: Uncertainties in Atmospheric Mercury Modeling for Policy Evaluation, Current Pollution Reports, 2, 103-114, 10.1007/s40726-016-0030-8, 2016.

Lahoutifard, N., Sparling, M., and Lean, D.: Total and methy mercury patterns in Arctic snow during springtime at Resolute, Nunavut, Canada, Atmospheric Environment, 39, 7597-7606, 2005.

Lahoutifard, N., Poissant, L., and Scott, S. L.: Scavenging of gaseous mercury by acidic snow at Kuujjuarapik, Northern Québec, Science of the Total Environment, 355, 118-126, 2006.

Lalonde, J. D., Amyot, M., Kraepiel, A. M. L., and Morel, F. M. M.: Photooxidation of Hg(0) in artificial and natural waters, Environmental Science and Technology, 35, 1367-1372, 2001.

Lalonde, J. D., Poulain, A. J., and Amyot, M.: The role of mercury redox reactions in snow on snow-to-air mercury transfer, Environmental Science and Technology, 36, 174-178, 2002.

Lalonde, J. D., Amyot, M., Doyon, M.-R., and Auclair, J.-C.: Photo-induced Hg(II) reduction in snow from the remote and temperate experimental lakes area (Ontario, Canada), Journal of geophysical research, 108, doi:10.1029/2001JD001534, 2003.

Lambert, G., Polian, G., and Taupin, D.: Existence of periodicity in radon concentrations and in the large-scale circulation at latitudes between 40° and 70° south, Journal of geophysical research, 75, 2341-2345, 1970.

Lambert, G., Ardouin, B., and Sanak, J.: Atmospheric transport of trace elements toward Antarctica, Tellus B, 42, 76-82, 10.1034/j.1600-0889.1990.00009.x, 1990.

Lamborg, C. H., Rolfhus, K. R., Fitzgerald, W. F., and Kim, G.: The atmospheric cycling and air-sea exchange of mercury species in the south and equatorial atlantic ocean, Deep-Sea Research II, 46, 957-977, 1999.

Lamborg, C. H., Fitzgerald, W. F., Skoog, A., and Visscher, P. T.: The abundance and source of mercury-binding organic ligands in Long Island Sound, Marine Chemistry, 90, 151-163, 2004.

Lamborg, C. H., Hammerschmidt, C. R., Bowman, K. L., Swarr, G. J., Munson, K. M., Ohnemus, D. C., Lam, P. J., Heimbürger, L.-E., Rikjenberg, M. J. A., and Saito, M. A.: A global ocean inventory of anthropogenic mercury based on water column measurements, Nature, 512, 65-69, doi:10.1038/nature13563, 2014.

Landis, M. S., Stevens, R. K., Schaedlich, F., and Prestbo, E. M.: Development and characterization of an annular denuder methodology for the measurement of divalent inorganic reactive gaseous mercury in ambient air, Environmental Science and Technology, 36, 3000-3009, 2002.

Landis, M. S., Lynam, M. M., and Stevens, R. K.: The monitoring and modelling of Hg species in support of local, regional and global modelling, in: Dynamics of Mercury Pollution on Regional and Global Scales:, Springer, 123-151, 2005.

Larose, C., Dommergue, A., De Angelis, M., Cossa, D., Averty, B., Marusczak, N., Soumis, N., Schneider, D., and Ferrari, C.: Springtime changes in snow chemistry lead to new insights into mercury methylation in the Arctic, Geochimica et Cosmochimica Acta, 74, 6263-6275, 2010.

Laurier, F., Mason, R. P., Whalin, L., and Kato, S.: Reactive gaseous mercury formation in the north pacific ocean's marine boundary layer: a potential role of halogen chemistry, Journal of geophysical research, 108, 4529, doi: 10.1029/2003JD003625, 2003.

Laurier, F., and Mason, R. P.: Mercury concentration and speciation in the coastal and open ocean boundary layer, Journal of geophysical research, 112, doi: 10.1029/2006JD007320, 2007.

Legrand, M., Ducroz, F., Wagenbach, D., Mulvaney, R., and Hall, J.: Ammonium in coastal Antarctic aerosol and snow: role of polar ocean and penguin emissions, Journal of geophysical research, 103, 11043-11056, 1998.

Legrand, M., Sciare, J., Jourdain, B., and Genthon, C.: Subdaily variations of atmospheric dimethylsulfide, dimethylsulfoxide, methanesulfonate, and non-sea-salt sulfate aerosols in the atmospheric boundary layer at Dumont d'Urville (coastal Antarctica) during summer, Journal of geophysical research, 106, 14409-14422, 2001.

Legrand, M., Preunkert, S., Jourdain, B., Gallée, H., Goutail, F., Weller, R., and Savarino, J.: Year-round record of surface ozone at coastal (Dumont d'Urville) and inland (Concordia) sites in east antarctica, Journal of geophysical research, 114, D20306, doi:10.1029/2008JD011667, 2009.

Legrand, M., Gros, V., Preunkert, S., Sarda-Estève, R., Thierry, A.-M., Pépy, G., and Jourdain, B.: A reassessment of the budget of formic and acetic acids in the boundary layer at Dumont d'Urville

(coastal Antarctica): the role of penguin emissions on the budget of serveral oxygenated volatile organic compounds, Journal of geophysical research, 117, doi: 10.1029/2011JD017102, 2012.

Legrand, M., Yang, X., Preunkert, S., and Theys, N.: Year-round records of sea salt, gaseous, and particulate inorganic bromine in the atmospheric boundary layer at coastal (Dumont d'Urville) and central (Concordia) East Antarctic sites, Journal of geophysical research: atmospheres, 121, 997–1023, DOI: 10.1002/2015JD024066, 2016a.

Legrand, M. P., S., Savarino, J., Frey, M. M., Kukui, A., Helmig, D., Jourdain, B., Jones, A., Weller, R., Brough, N., and Gallée, H.: Inter-annual variability of surface ozone at coastal (Dumont d'Urville, 2004-2014) and inland (Concordia, 2007-2014) sites in East Antarctica, Atmospheric Chemistry and Physics, 16, 8053-8069, doi:10.5194/acp-16-8053-2016, 2016b.

Lei, H., Liang, X.-Z., Wuebbles, D., and Tao, Z.: Model analyses of atmospheric mercury: present air quality and effects of transpacific transport on the United States, Atmospheric Chemistry and Physics, 13, 10807-10825, 2013.

Li, C., Kang, S., Shi, G., Huang, J., Ding, M., Zhang, Q., Zhang, L., Guo, J., Xiao, C., Hou, S., Sun, B., Qin, D., and Ren, J.: Spatial and temporal variations of total mercury in Antarctic snow along the transect from Zhongshan station to Dome A, Tellus, 66, http://dx.doi.org/10.3402/tellusb.v66.25152, 2014.

Li, P., Feng, X., and Qiu, G.: Methylmercury exposure and health effects from rice and fish consumption: a review, International Journal of Environmental Research and Public Health, 7, 2666-2691, 2010.

Lin, C.-J., and Pehkonen, S. O.: Aqueous free radical chemistry of mercury in the presence of iron oxides and ambient aerosol, Atmospheric Environment, 31, 4125-4137, 1997.

Lin, C.-J., and Pehkonen, S. O.: Oxidation of elemental mercury by aqueous chlorine ($HOCl/OCl^-$): implications for tropospheric mercury chemistry, Journal of geophysical research, 103, 28,093-028,102, 1998.

Lin, C.-J., and Pehkonen, S. O.: The chemistry of atmospheric mercury: a review, Atmospheric Environment, 33, 2067-2079, 1999.

Lin, C.-J., Pongprueksa, P., Lindberg, S. E., Pehkonen, S. O., Byun, D., and Jang, C.: Scientific uncertainties in atmospheric mercury models I: model science evaluation, Atmospheric Environment, 40, 2911-2928, 2006.

Lin, C.-J., Gustin, M. S., Singhasuk, P., Eckley, C., and Miller, M.: Empirical models for estimating mercury flux from soils, Environmental science & technology, 44, 8522-8528, 2010a.

Lin, C.-J., Pan, L., Streets, D. G., Shetty, S. K., Jang, C., Feng, X., Chu, H.-W., and Ho, T. C.: Estimating mercury emission outflow from East Asia using CMAQ-Hg, Atmospheric Chemistry and Physics, 10, 1856-1864, 2010b.

Lin, J.-T., and McElroy, M. B.: Impacts of boundary layer mixing on pollutant vertical profiles in the lower troposphere: Implications to satellite remote sensing, Atmospheric Environment, 44, 1726-1739, http://dx.doi.org/10.1016/j.atmosenv.2010.02.009, 2010.

Lindberg, S. E., and Stratton, W. J.: Atmospheric mercury speciation: concentrations and behavior of reactive gaseous mercury in ambient air, Environmental Science and Technology, 32, 49-57, 1998.

Lindberg, S. E., Brooks, S., Lin, C.-J., Scott, K., Meyers, T., Chambers, L., Landis, M., and Stevens, R.: Formation of Reactive Gaseous Mercury in the Arctic: Evidence of Oxidation of Hg° to Gas-Phase Hg-II Compounds after Arctic Sunrise, Water, Air and Soil Pollution: Focus, 1, 295-302, doi: 10.1023/a:1013171509022, 2001.

Lindberg, S. E., Brooks, S., Lin, C.-J., Scott, K. J., Landis, M. S., Stevens, R. K., Goodsite, M. E., and Richter, A.: Dynamic oxidation of gaseous mercury in the arctic troposphere at polar sunrise, Environmental Science and Technology, 36, 1245-1256, 2002.

Lindberg, S. E., Bullock, R., Ebinghaus, R., Engstrom, D., Feng, X., Fitzgerald, W. F., Pirrone, N., Prestbo, E., and Seigneur, C.: A synthesis of progress and uncertainties in attributing the sources of mercury in deposition, Ambio, 36, 19-32, 2007.

Lindqvist, O., and Rodhe, H.: Atmospheric mercury - a review, Tellus, 37B, 136-159, 1985.

Lindqvist, O.: Mercury in the Swedish environment: recent research on causes, consequences and corrective methods, Water, Air & Soil Pollution, 55, 1-26, 1991.

Liu, G.: Deriving snow cloud characteristics from CloudSat observations, Journal of geophysical research, 113, D00A09, http://dx.doi.org/10.1029/2007JD009766, 2008.

Lohman, K., Seigneur, C., Edgerton, E., and Jansen, J.: Modeling mercury in power plant plumes, Environmental science & technology, 40, 3848-3854, 2006.

Lu, J. Y., Schroeder, W. H., Barrie, L. A., Steffen, A., Welch, H. E., Martin, K., Lockhart, L., Hunt, R. V., Boila, G., and Richter, A.: Magnification of atmospheric mercury deposition to polar regions in springtime: the link to tropospheric ozone depletion chemistry, Geophysical research letters, 28, 3219-3222, 2001.

Lu, J. Y., and Schroeder, W. H.: Annual time-series of total filterable atmospheric mercury concentrations in the Arctic, Tellus, 56B, 213-222, 2004.

Lyman, S. N., Gustin, M. S., Prestbo, E. M., and Marsik, F. J.: Estimation of Dry Deposition of Atmospheric Mercury in Nevada by Direct and Indirect Methods, Environmental Science & Technology, 41, 1970-1976, 10.1021/es062323m, 2007.

Lyman, S. N., Gustin, M. S., Prestbo, E. M., Kilner, P. I., Edgerton, E., and Hartsell, B.: Testing and Application of Surrogate Surfaces for Understanding Potential Gaseous Oxidized Mercury Dry Deposition, Environmental Science & Technology, 43, 6235-6241, 10.1021/es901192e, 2009.

Lyman, S. N., Gustin, M. S., and Prestbo, E. M.: A passive sampler for ambient gaseous oxidized mercury concentrations, Atmospheric Environment, 44, 246-252, http://dx.doi.org/10.1016/j.atmosenv.2009.10.008, 2010a.

Lyman, S. N., Jaffe, D. A., and Gustin, M. S.: Release of mercury halides from KCl denuders in the presence of ozone, Atmospheric Chemistry and Physics, 10, 8197-8204, 2010b.

Lyman, S. N., and Jaffe, D. A.: Formation and fate of oxidized mercury in the upper troposphere and lower stratosphere, Nature Geoscience, 5, 114-117, 2012.

Lynam, M. M., and Keeler, G. J.: Artifacts associated with the measurement of particulate mercury in an urban environment: The influence of elevated ozone concentrations, Atmospheric Environment, 39, 3081-3088, http://dx.doi.org/10.1016/j.atmosenv.2005.01.036, 2005.

Lynch, J. A., Horner, K. S., and Grimm, J. W.: Atmospheric deposition: spatial and temporal variations in Pennsylvania 2002, Penn State Institutes of the Environment, The Pennsylvania State University, University Park, PA, 231, 2003.

Magand, O., Genthon, C., Fily, M., Krinner, G., Picard, G., Frezzotti, M., and Ekaykin, A.: An up-to-date quality-controlled surface mass balance data set for the 90°-180°E Antarctica sector and 1950-2005 period, Journal of geophysical research, 112, doi: 10.1029/2006JD007691, 2007.

Mahaffey, K. R., Clickner, R. P., and Bodurow, C. C.: Blood organic mercury and dietary mercury intake: National Health and Nutrition Examination Survey, 1999 and 2000, Environmental health perspectives, 112, 562, 2004.

Mahaffey, K. R., Sunderland, E. M., Man Chan, H., Choi, A. L., Grandjean, P., Mariën, K., Oken, E., Sakamoto, M., Schoeny, R., Weihe, P., Yan, C.-H., and Yasutake, A.: Balancing the benefits of n-3 polyunsaturated fatty acids and the risks of methylmercury exposure from fish consumption, Nutrition Reviews, 69, 493-508, 2011.

Malcolm, E. G., and Keeler, G. J.: Evidence for a sampling artifact for particulate-phase mercury in the marine atmosphere, Atmospheric Environment, 41, 3352-3359, 2007.

Malcolm, E. G., Ford, A. C., Redding, T. A., Richardson, M. C., Strain, B. M., and Tetzner, S. W.: Experimental investigation of the scavenging of gaseous mercury by sea salt aerosol, Journal of atmospheric chemistry, 63, 221-234, 2009.

Mann, E., Mallory, M. L., Ziegler, S. E., Avery, T. S., Tordon, R., and O'Driscoll, N. J.: Photoreducible mercury loss from Arctic snow is influenced by temperature, and snow age, Environmental Science and Technology, 49, 12120-12126, 2015a.

Mann, E. A., Mallory, M. L., Ziegler, S. E., Tordon, R., and O'Driscoll, N. J.: Mercury in Artic snow: quantifying the kinetics of photochemical oxidation and reduction, Science of the Total Environment, 59, 115-132, 2015b.

Mann, J. L., Long, S. E., Shuman, C. A., and Kelly, W. E.: Determination of mercury content in a shallow firn core from Greenland by isotope dilution inductively coupled plasma mass spectrometry, Water Air & Soil Pollution, 163, 19-32, 2005.

Mao, H., and Talbot, R.: Speciated mercury at marine, coastal, and inland sites in New England - Part 1: Temporal variability, Atmospheric Chemistry and Physics, 12, 5099-5112, 2012.

Mason, R. P., Rolfhus, K. R., and Fitzgerald, W. F.: Methylated and elemental mercury cycling in surface and deep ocean waters of the north Atlantic, Water, Air & Soil Pollution, 80, 665-677, 1995.

Mason, R. P., Lawson, N. M., and Sheu, G. R.: Annual and seasonal trends in mercury deposition in Maryland, Atmospheric Environment, 34, 1691-1701, 2000.

Mason, R. P., Lawson, N. a., and Sheu, G.-R.: Mercury in the Atlantic Ocean: factors controlling air–sea exchange of mercury and its distribution in the upper waters, Deep Sea Research Part II: Topical Studies in Oceanography, 48, 2829-2853, 2001.

Mason, R. P., and Sheu, G.-R.: Role of the ocean in the global mercury cycle, Global biogeochemical cycles, 16, 1093, 2002.

Mason, R. P., Choi, A. L., Fitzgerald, W. F., Hammerschmidt, C. R., Lamborg, C. H., Soerensen, A. L., and Sunderland, E. M.: Mercury biogeochemical cycling in the ocean and policy implications, Environmental Research, 119, 101-117, 2012.

Mather, K. B., and Miller, G. S.: The problem of the katabatic winds on the coast of Terre Adélie, Polar Record, 13, 425-432, 1967.

Maturilli, M., Herber, A., and König-Langlo, G.: Climatology and time series of surface meteorology in Ny-Alesund, Svalbard, Earth System Science Data, 5, 155-163, 10.5194/essd-5-155-2013, 2013.

Mergler, D., Anderson, H. A., Chan, L. H. M., Mahaffey, K. R., Murray, M., Sakamoto, M., and Stern, A. H.: Methylmercury exposure and health effects in humans: a worldwide concern, AMBIO: A Journal of the Human Environment, 36, 3-11, 2007.

Micol, T., and Jouventin, P.: Long-term population trends in seven Antarctic seabirds at Pointe Géologie (Terre Adélie). Human impact compared with environmental change, Polar Biology, 24, 175-185, 2001.

Miller, E. K., Vanarsdale, A., Keeler, G. J., Chalmers, A., Poissant, L., Kamman, N. C., and Brulotte, R.: Estimation and mapping of wet and dry mercury deposition across northeastern North America, Ecotoxicology, 14, 53-70, 2005.

Miller, J. M., Moody, J. L., Harris, J. M., and Gaudry, A.: A 10-year trajectory flow climatology for Amsterdam island, 1980-1989, Atmospheric Environment, 27A, 1909-1916, 1993.

Monfray, P., Gaudry, A., Polian, G., and Lambert, G.: Seasonal variations of atmospheric CO_2 in the southern Indian Ocean, Tellus, 39B, 67-71, 1987.

Moore, C., and Carpi, A.: Mechanisms of the emission of mercury from soil: Role of UV radiation, Journal of Geophysical Research: Atmospheres, 110, 10.1029/2004JD005567, 2005.

Moore, C. W., Obrist, D., Steffen, A., Staebler, R. M., Douglas, T. A., Richter, A., and Nghiem, S. V.: Convective forcing of mercury and ozone in the Arctic boundary layer induced by leads in sea ice, Nature, 506, 81-84, 10.1038/nature12924, 2014.

Morel, F. M. M., Kraepiel, A. M. L., and Amyot, M.: The chemical cycle and bioaccumulation of mercury, Annual Review of Ecological Systems, 29, 543-566, 1998.

Morin, S., Savarino, J., Frey, M. M., Yan, N., Bekki, S., Bottenheim, J. W., and Martins, J. M. F.: tracing the origin and fate of NOx in the Arctic atmosphere using stable isotopes Science, 322, doi: 10.1126/science.1161910, 2008.

Mozaffarian, D., and Rimm, E. B.: Fish intake, contaminants, and human health: evaluating the risks and the benefits, Jama, 296, 1885-1899, 2006.

Muntean, M., Janssens-Maenhout, G., Song, S., Selin, N. E., Olivier, J. G., Guizzardi, D., Maas, R., and Dentener, F.: Trend analysis from 1970 to 2008 and model evaluation of EDGARv4 global gridded anthropogenic mercury emissions, Science of the Total Environment, 494-495, 337-350, 10.1016/j.scitotenv.2014.06.014, 2014.

Munthe, J., Xiao, Z. F., and Lindqvist, O.: The aqueous reduction of divalent mercury by sulfite, Water, Air & Soil Pollution, 56, 621-630, 1991.

Munthe, J.: The aqueous oxidation of elemental mercury by ozone, Atmospheric Environment, 26, 1461-1468, 1992.

Munthe, J., Kindbom, K., Kruger, O., Peterson, G., Pacyna, J., and Iverfeldt, Å.: Examining source-receptor relationships for mercury in Scandinavia, Water, Air & Soil Pollution, 1, 99-110, 2001a.

Munthe, J., Wängberg, I., Pirrone, N., Iverfeldt, Å., Ferrara, R., Ebinghaus, R., Feng, X., Gårdfeldt, K., Keeler, G. J., Lanzillotta, E., Lindberg, S. E., Lu, J., Mamane, Y., Prestbo, E., Schmolke, S., Schroeder, W. H., Sommar, J., Sprovieri, F., Stevens, R. K., Stratton, W. J., Tuncel, G., and Urba, A.: Intercomparison of methods for sampling and analysis of atmospheric mercury species, Atmospheric Environment, 35, 3007-3017, 2001b.

Munthe, J., Bishop, K., Driscoll, C., Graydon, J., Hultberg, H., Lindberg, S., Matzner, E., Porrari, P., Rea, P., Schwesig, D., St Louis, V., and Verta, M.: Input-output of mercury in forested catchments in Europe and North America, RMZ-Materials and Geoenvironment, 51, 1243-1246, 2004.

Munthe, J., Sprovieri, F., Horvat, M., and Ebinghaus, R.: SOPs and QA/QC protocols regarding measurements of TGM, GEM, RGM, TPM and mercury in precipitation in cooperation with WP3, WP4 and WP5. GMOS deliverable 6.1, CNR-IIA, IVL. http://www.gmos.eu, last access: 3 March 2014, 2011.

Murphy, D. M., Hudson, P. K., Thomson, D. S., Sheridan, P. J., and Wilson, J. C.: Observations of mercury-containing aerosols, Environmental Science and Technology, 40, 3163-3167, 2006.

Nakazawa, K., Nagafuchi, O., Kawakami, T., Inoue, T., Yokota, K., Serikawa, Y., Cyio, B., and Elvince, R.: Human health risk assessment of mercury vapor around artisanal small-sacle gold mining area, Palu city, Central Sulawesi, Indonesia, Ecotoxicology and Environmental Safety, 124, 155-162, 2016.

Nash, J. E., and Sutcliffe, J. V.: River flow forecasting through conceptual models part I — A discussion of principles, Journal of Hydrology, 10, 282-290, http://dx.doi.org/10.1016/0022-1694(70)90255-6, 1970.

Neff, W., Helmig, D., Grachev, A. A., and Davis, D.: A study of boundary layer behavior associated with high NO concentrations at the South Pole using a minisodar, tethered balloon, and sonic anemometer, Atmospheric Environment, 42, 2762-2779, 2008.

Ambient air quality - standard method for the determination of mercury deposition, 2010.

Nerentorp Mastromonaco, M., Gårdfeldt, K., Jourdain, B., Abrahamsson, K., Granfors, A., Ahnoff, M., Dommergue, A., Méjean, G., and Jacobi, H.-W.: Antarctic winter mercury and ozone depletion events over sea ice, Atmospheric Environment, 129, 125-132, 2016.

Neuman, J. A., Nowak, J. B., Huey, L. G., Burkholder, J. B., Dibb, J. E., Holloway, J. S., Liao, J., Peischl, J., Roberts, J. M., Ryerson, T. B., Scheuer, E., Stark, H., Stickel, R. E., Tanner, D. J., and Weinheimer, A.: Bromine measurements in ozone depleted air over the Arctic Ocean, Atmos. Chem. Phys., 10, 6503-6514, 10.5194/acp-10-6503-2010, 2010.

NGuyen, B. C., Mihalopoulos, N., and Belviso, S.: Seasonal variation of atmospheric dimethylsulfide at Amsterdam Island in the southern Indian Ocean, Journal of atmospheric chemistry, 11, 123-141, 1990.

Nguyen, Q. T., Skov, H., Sørensen, L. L., Jensen, B. J., Grube, A. G., Massling, A., Glasius, M., and Nøjgaard, J. K.: Source apportionment of particles at Station Nord, North East Greenland during 2008–2010 using COPREM and PMF analysis, Atmos. Chem. Phys., 13, 35-49, 10.5194/acp-13-35-2013, 2013.

Nie, Y., Liu, X., Sun, L., and Emslie, S. D.: Effect of penguin and seal excrement on mercury distribution in sediments from the Ross Sea region, East Antarctica, Science of the Total Environment, 433, 132-140, 2012.

Nriagu, J. O., and Becker, C.: Volcanic emissions of mercury to the atmosphere: global and regional inventories, Science of the Total Environment, 304, 3-12, 2003.

O'Concubhair, R., O'Sullivan, D. A., and Sodeau, J. R.: Dark oxidation of dissolved gaseous mercury in polar ice mimics, Environmental Science and Technology, 46, 4829-4836, 10.1021/es300309n, 2012.

O'Driscoll, N. J., Siciliano, S. D., Lean, D. R. S., and Amyot, M.: Gross photoreduction kinetics of mercury in temperate freshwater lakes and rivers: application to a general model of DGM dynamics, Environmental Science and Technology, 40, 837-843, 2006.

Obiri, S., Yeboah, P. O., Osae, S., and Adu-Kumi, S.: Levels of arsenic, mercury, cadmium, copper, lead, zinc and manganese in serum and whole blood of resident adults from mining and non-mining communities in Ghana, Environmental Science and Pollution Research, 1-9, 10.1007/s11356-016-6537-0, 2016.

Obrist, D., Moosmüller, H., Schürmann, R., Chen, L.-W. A., and Kreidenweis, S. M.: Particulate-phase and gaseous elemental mercury emissions during biomass combustion: controlling factors and correlation with particulate matter emissions, Environmental science & technology, 42, 721-727, 2007.

Obrist, D., Tas, E., Peleg, M., Matveev, V., Faïn, X., Asaf, D., and Luria, M.: Bromine-induced oxidation of mercury in the mid-latitude atmosphere, Nature Geoscience, 4, 22-26, 2011.

Ordonez, J. V., Carrillo, J. A., Miranda, M., and Gale, J. L.: Epidemiologic study of a disease believed to be encephalitis in the region of the highlands of Guatemala, Bol Oficina Sanit Panam, 60, 510-519, 1966.

Pacyna, E. G., Pacyna, J. M., Steenhuisen, F., and Wilson, S.: Global anthropogenic mercury emission inventory for 2000, Atmospheric Environment, 40, 4048-4063, 2006.

Pacyna, E. G., Pacyna, J. M., Sundseth, K., Munthe, J., Kindbom, K., Wilson, S., Steenhuisen, F., and Maxson, P.: Global emission of mercury to the atmosphere from anthropogenic sources in 2005 and projections to 2020, Atmospheric Environment, 44, 2487-2499, 2010.

Pal, B., and Ariya, P. A.: Studies of ozone initiated reactions of gaseous mercury: kinetics, product studies, and atmospheric implications, Physical Chemistry Chemical Physics, 6, 572-579, 2004a.

Pal, B., and Ariya, P. A.: Gas-phase $HO^{\cdot}$-initiated reactions of elemental mercury: kinetics, product studies, and atmospheric implications, Environmental Science and Technology, 38, 5555-5566, 2004b.

Palerme, C., Kay, J. E., Genthon, C., L'Ecuyer, T., Wood, N. B., and Claud, C.: How much snow falls on the Antarctic ice sheet?, The Cryosphere, 8, 1577-1587, 10.5194/tc-8-1577-2014, 2014.

Pan, L., Carmichael, G. R., Adhikary, B., Tang, Y., Streets, D., Woo, J.-H., Friedli, H. R., and Radke, L. F.: A regional analysis of the fate and transport of mercury in East Asia and an assessment of major uncertainties, Atmospheric Environment, 42, 1144-1159, 2008.

Parish, T. R., and Bromwich, D. H.: The surface windfield over the Antarctic ice sheets, Nature, 328, 51-54, 1987.

Parish, T. R., and Bromwich, D. H.: Reexamination of the near-surface airflow over the Antarctic continent and implications on atmospheric circulations at high southern latitudes, Monthly Weather Review, 135, 1961-1973, 2007.

Parrella, J. P., Jacob, D. J., Liang, Q., Zhang, Y., Mickley, L. J., Miller, B., Evans, M. J., Yang, X., Pyle, J. A., Theys, N., and Van Roozendael, M.: Tropospheric bromine chemistry: implications for present and pre-industrial ozone and mercury, Atmospheric Chemistry and Physics, 12, 6723-6740, 2012.

Pehkonen, S. O., and Lin, C.-J.: Aqueous photochemistry of mercury with organic acids, Journal of the Air & Waste Management Association, 48, 144-150, 1998.

Peleg, M., Matveev, V., Tas, E., Luria, M., Valente, R. J., and Obrist, D.: Mercury depletion events in the troposphere in mid-latitudes at the Dead Sea, Israel, Environmental science & technology, 41, 7280-7285, 2007.

Peleg, M., Tas, E., Obrist, D., Matveev, V., Moore, C., Gabay, M., and Luria, M.: Observational evidence for involvement of nitrate radicals in nighttime oxidation of mercury, Environmental Science and Technology, 49, 14008-14018, 2015.

Perovich, D. K.: Light reflection and transmission by a temperate snow cover, Journal of glaciology, 53, 201-210, 2007.

Petersen, G., Munthe, J., Pleijel, K., Bloxam, R., and Kumar, A. V.: A comprehensive Eulerian modeling framework for airborne mercury species: Development and testing of the Tropospheric Chemistry module (TCM), Atmospheric Environment, 32, 829-843, http://dx.doi.org/10.1016/S1352-2310(97)00049-6, 1998.

Petersen, P. B., and Saykally, R. J.: On the nature of ions at the liquid water surface, Annu. Rev. Phys. Chem., 57, 333-364, 2006.

Peterson, C., Alishahi, M., and Gustin, M. S.: Testing the use of passive sampling systems for understanding air mercury concentrations and dry deposition across Florida, USA, Science of The Total Environment, 424, 297-307, http://dx.doi.org/10.1016/j.scitotenv.2012.02.031, 2012.

Pettré, P., Payan, C., and Parish, T. R.: Interaction of katabatic flow woth local thermal effects in a coastal region of Adelie Land, East Antarctica, Journal of geophysical research, 98, 10429-10440, 1993.

Pfaffhuber, K. A., Berg, T., Hirdman, D., and Stohl, A.: Atmospheric mercury observations from Antarctica: seasonal variation and source and sink region calculations, Atmospheric Chemistry and Physics, 12, 3241-3251, 2012.

Pielke, R. A., Liston, G. E., Chapman, W. L., and Robinson, D. A.: Actual and insolation-weighted Northern Hemisphere snow cover and sea-ice between 1973-2002, Climate Dynamics, 22, 591-595, 2004.

Pietroni, I., Argentini, S., Petenko, I., and Sozzi, R.: Measurements and parametrizations of the atmospheric boundary-layer height at Dome C, Antarctica, Boundary-Layer Meteorology, 143, 189-206, 2012.

Pirrone, N., Ferrara, R., Hedgecock, I., Kallos, G., Mamane, Y., Munthe, J., Pacyna, J., Pytharoulis, I., Sprovieri, F., and Voudouri, A.: Dynamic processes of mercury over the Mediterranean region: results from the Mediterranean Atmospheric Mercury Cycle System (MAMCS) project, Atmospheric Environment, 37, 21-39, 2003.

Pirrone, N., Cinnirella, S., Feng, X., Finkelman, R., Friedli, H., Leaner, J., Mason, R., Mukherjee, A., Stracher, G., Streets, D., and Telmer, K.: Global mercury emissions to the atmosphere from anthropogenic and natural sources, Atmospheric Chemistry and Physics, 10, 5951-5964, 10.5194/acp-10-5951-2010, 2010.

Pirrone, N., Aas, W., Cinnirella, S., Ebinghaus, R., Hedgecock, I. M., Pacyna, J. M., Sprovieri, F., and Sunderland, E. M.: Toward the next generation of air quality monitoring: mercury, Atmospheric Environment, 80, 599-611, 2013.

Platt, U., and Janssen, C.: Observation and role of the free radicals NO_3, ClO, BrO and IO in the troposphere, Faraday Discuss., 100, 175-198, 1995.

Pöhler, D., Vogel, L., Frieß, U., and Platt, U.: Observation of halogen species in the Amundsen Gulf, Arctic, by active long-path differential optical absorption spectroscopy, Proceedings of the National Academy of Sciences, 107, 6582-6587, 2010.

Poissant, L., and Casimir, A.: Water-air and soil-air exchange rate of total gaseous mercury measured at background sites, Atmospheric Environment, 32, 883-893, 1998.

Poissant, L., and Pilote, M.: Time series analysis of atmospheric mercury in Kuujjuarapik/Whapmagoostui (Québec), J. Phys. IV France, 107, 1079-1082, 2003.

Poissant, L., Pilote, M., Beauvais, C., Constant, P., and Zhang, H. H.: A year of continuous measurements of three atmospheric mercury species (GEM, RGM and Hg_p) in southern Québec, Canada, Atmospheric Environment, 39, 1275-1287, 2005.

Polian, G., Lambert, G., Ardouin, B., and Jegou, A.: Long range transport of continental radon in subantarctic and antarctic areas, Tellus, Ser. B, 38, 178-189, 1986.

Poulain, A. J., Lalonde, J. D., Amyot, M., Shead, J. A., Raofie, F., and Ariya, P. A.: Redox transformations of mercury in an Arctic snowpack at springtime, Atmospheric Environment, 38, 6763-6774, 2004.

Poulain, A. J., Garcia, E., Amyot, M., Campbell, P. G. C., and Ariya, P. A.: Mercury distribution, partitioning and speciation in coastal vs. inland high Arctic snow, Geochim. Cosmochim. Acta, 71, 3419-3431, 2007.

Prather, K. A., Hatch, C. D., and Grassian, V. H.: Analysis of atmospheric aerosols, Annu. Rev. Anal. Chem., 1, 485-514, 2008.

Prestbo, E. M., and Gay, D. A.: Wet deposition of mercury in the U.S. and Canada, 1996–2005: Results and analysis of the NADP mercury deposition network (MDN), Atmospheric Environment, 43, 4223-4233, http://dx.doi.org/10.1016/j.atmosenv.2009.05.028, 2009.

Preunkert, S., Legrand, M., Pépy, G., Gallée, H., Jones, A., and Jourdain, B.: The atmospheric HCHO budget at Dumont d'Urville (East Antarctica): contribution of photochemical gas-phase production versus snow emissions, Journal of geophysical research: atmospheres, 118, 13319-13337, 2013.

Texte du Protocole au Traité sur l'Antarctique: http://www.ats.aq/documents/keydocs/vol_1/vol1_4_AT_Protocol_on_EP_f.pdf, access: 26 July 2016, 1991.

Pudasainee, D., Seo, Y.-C., Sung, J.-H., Jang, H.-N., and Gupta, R.: Mercury Co-beneficial Capture in Air Pollution Control Devices of Coal-fired Power Plants, International Journal of Coal Geology, in press, http://dx.doi.org/10.1016/j.coal.2016.08.013, 2016.

Pyle, D. M., and Mather, T. A.: The importance of volcanic emissions for the global atmospheric mercury cycle, Atmospheric Environment, 37, 5115-5124, 2003.

Rafaj, P., Bertok, I., Cofala, J., and Schöpp, W.: Scenarios of global mercury emissions from anthropogenic sources, Atmospheric Environment, 79, 472-479, 2013.

Raofie, F., and Ariya, P.: Kinetics and products study of the reaction of BrO radicals with gaseous mercury, Journal de Physique IV (Proceedings), 2003, 1119-1121,

Riaz, A., Khan, S., Shah, M. T., Li, G., Gul, N., and Shamshad, I.: Mercury contamination in the blood, urine, hair and nails of the gold washers and its human health risk during extraction of placer gold along Gilgit, Hunza and Indus rivers in Gilgit-Baltistan, Pakistan, Environmental Technology & Innovation, 5, 22-29, 2016.

Ricaud, P., Grigioni, P., Zbinden, R., Attié, J.-L., Genoni, L., Galeandro, A., Moggio, L., Montaguti, S., Petenko, I., and Legovini, P.: Review of tropospheric temperature, absolute humidity and integrated water vapor from the HAMSTRAD radiometer installed at Dome C, Antarctica, 2009-14, Antarctic Science, 27, 598-616, 2015.

Risch, M. R., Gay, D. A., Fowler, K. K., Keeler, G. J., Backus, S. M., Blanchard, P., Barres, J. A., and Dvonch, J. T.: Spatial patterns and temporal trends in mercury concentrations, precipitation depths, and mercury wet deposition in the North American Great Lakes region, 2002–2008, Environmental Pollution, 161, 261-271, http://dx.doi.org/10.1016/j.envpol.2011.05.030, 2012.

Rolph, G. D.: Real-time Environmental Applications and Display sYstem (READY) Website (http://www.ready.noaa.gov), last access: 24 February 2014. NOAA Air Resources Laboratory, College Park, MD. , 2013.

Rutter, A. P., and Schauer, J. J.: The impact of aerosol composition on the particle to gas partitioning of reactive mercury, Environmental Science and Technology, 41, 3934-3939, 2007a.

Rutter, A. P., and Schauer, J. J.: The effect of temperature on the gas-particle partitioning of reactive mercury in atmospheric aerosols, Atmospheric Environment, 41, 8647-8657, 2007b.

Rutter, A. P., Hanford, K. L., Zwers, J. T., and Perillo-Nicholas, A. L.: Evaluation of an offline method for the analysis of atmospheric reactive gaseous mercury and particulate mercury, Journal of the air and waste management association, 58, 377-383, 2008.

Rytuba, J. J.: Mercury from mineral deposits and potential environmental impact, Environmental Geology, 43, 326-338, 10.1007/s00254-002-0629-5, 2003.

Saiz-Lopez, A., Mahajan, A. S., Salmon, R. A., Bauguitte, S. J.-B., Jones, A. E., Roscoe, H. K., and Plane, J. M. C.: Boundary layer halogens in coastal antarctica, Science, 317, 348-351, 2007.

Sakata, M., Marumoto, K., Narukawa, M., and Asakura, K.: Regional variations in wet and dry deposition fluxes of trace elements in Japan, Atmospheric Environment, 40, 521-531, 2006.

Sander, R., Burrows, J., and Kaleschke, L.: Carbonate precipitation in brine – a potential trigger for tropospheric ozone depletion events, Atmos. Chem. Phys., 6, 4653-4658, 10.5194/acp-6-4653-2006, 2006.

Sanei, H., Outridge, P. M., Goodarzi, F., Wang, F., Armstrong, D., Warren, K., and Fishback, L.: Wet deposition mercury fluxes in the Canadian sub-Arctic and southern Alberta, measured using an automated precipitation collector adapted to cold regions, Atmospheric Environment, 44, 1672-1681, http://dx.doi.org/10.1016/j.atmosenv.2010.01.030, 2010.

Savarino, J., Kaiser, J., Morin, S., Sigman, D. M., and Thiemens, M. H.: Nitrogen and oxygen isotopic constraints on the origin of atmospheric nitrate in coastal Antarctica, Atmospheric Chemistry and Physics, 7, 1925-1945, 2007.

Scheuhammer, A.: The chronic toxicity of aluminium, cadmium, mercury, and lead in birds: a review, Environmental Pollution, 46, 263-295, 1987.

Scheuhammer, A. M., Meyer, M. W., Sandheinrich, M. B., and Murray, M. W.: Effects of environmental methylmercury on the health of wild birds, mammals, and fish, AMBIO: A Journal of the Human Environment, 36, 12-19, 2007.

Schroeder, W. H., Yarwood, G., and Niki, H.: Transformation processes involving mercury species in the atmosphere - results from a literature survey, Water, Air & Soil Pollution, 56, 653-666, 1991.

Schroeder, W. H., Anlauf, K. G., Barrie, L. A., Lu, J. Y., Steffen, A., Schneeberger, D. R., and Berg, T.: Arctic spingtime depletion of mercury, Nature, 394, 331-332, 1998.

Schroeder, W. H., and Munthe, J.: Atmospheric mercury - an overview, Atmospheric Environment, 32, 809-822, 1998.

Sciare, J., Mihalopoulos, N., and NGuyen, B. C.: Summertime seawater concentrations of dimethylsulfide in the western indian ocean: reconciliation of fluxes and spatial variability with long-term atmospheric observations, Journal of atmospheric chemistry, 32, 357-373, 1999.

Sciare, J., Mihalopoulos, N., and Baboukas, E.: Short-term variations of dimethylsulfide and its oxidation products at Amsterdam Island during summer time, Journal of atmospheric chemistry, 39, 281-302, 2001.

Sciare, J., Favez, O., Sarda-Estève, R., Oikonomou, K., Cachier, H., and Kazan, V.: Long-term observations of carbonaceous aerosols in the austral ocean atmosphere: evidence of a biogenic marine organic source, Journal of geophysical research, 114, D15302, doi: 10.1029/2009JD011998, 2009.

Seigneur, C., Vijayaraghavan, K., and Lohman, K.: Atmospheric mercury chemistry: Sensitivity of global model simulations to chemical reactions, Journal of Geophysical Research: Atmospheres, 111, 1-17, 2006.

Selin, H.: Global environmental law and treaty-making on hazardous substances: the Minamata Convention and mercury abatement, Global Environmental Politics, 14, doi: 10.1162/GLEP_a_00208, 2014a.

Selin, N. E., and Selin, H.: Global politics of mercury pollution: the need for multi-scale governance, RECIEL, 15, 258-269, 2006.

Selin, N. E., Jacob, D. J., Park, R. J., Yantosca, R. M., Strode, S., Jaeglé, L., and Jaffe, D. A.: Chemical cycling and deposition of atmospheric mercury: global constraints from observations, Journal of geophysical research, 112, D02308, doi: 10.1029/2006JD007450, 2007.

Selin, N. E., and Jacob, D. J.: Seasonal and spatial patterns of mercury wet deposition in the United States: constraints on the contribution from North American anthropogenic sources, Atmospheric Environment, 42, 5193-5204, 2008.

Selin, N. E., Jacob, D. J., Yantosca, R. M., Strode, S., Jaeglé, L., and Sunderland, E. M.: Global 3-D land-ocean-atmosphere model for mercury: present-day versus preindustrial cycles and anthropogenic enrichment factors for deposition, Global biogeochemical cycles, 22, GB2011, doi:10.1029/2007GB003040, 2008.

Selin, N. E.: Global biogeochemical cycling of mercury: a review, Annual Review of Environment and Resources, 34, 43-63, 2009.

Selin, N. E.: Science and strategies to reduce mercury risks: a critical review, Journal of Environmental Monitoring, 13, 2389-2399, 2011.

Selin, N. E.: Global change and mercury cycling: challenged for implementing a global mercury treaty, Environmental Toxicology and Chemistry, 33, 1202-1210, 2014b.

Seok, B., Helmig, D., Williams, M. W., Liptzin, D., and Chowanski, K. H., J.: An automated system for continuous measurements of trace gas fluxes through snow: an evaluation of the gas diffusion method at a subalpine forest site, Niwot Ridge, Colorado, Biogeochemistry, 95, 95-113, 2009.

Serrano, O., Martinez-Cortizas, A., Mateo, M. A., Biester, H., and Bindler, R.: Millennial scale impact on the marine biogeochemical cycle of mercury from early mining on the Iberian Peninsula, Global biogeochemical cycles, 27, 21-30, 2013.

Shanley, J. B., Engle, M., Scholl, M. A., Krabbenhoft, D. P., Brunette, R., Olson, M., and Conroy, M. E.: High mercury wet deposition at a "clean air" site in Puerto Rico, Environmental Science and Technology, 49, 12474-12482, 2015.

Shaw, G. E.: Evidence for a central Eurasian source area of Arctic haze in Alaska, Nature, 299, 815-818, 10.1038/299815a0, 1982.

Sherman, L. S., Blum, J. D., Johnson, K. P., Keeler, G. J., Barres, J. A., and Douglas, T. A.: Mass-independant fractionation of mercury isotopes in Arctic snow driven by sunlight, Nature Geoscience, 3, 173-177, 2010.

Shetty, S. K., Lin, C.-J., Streets, D. G., and Jang, C.: Model estimate of mercury emission from natural sources in East Asia, Atmospheric Environment, 42, 8674-8685, 2008.

Sheu, G.-R., Lin, N.-H., Wang, J.-L., Lee, C.-T., Yang, C.-F. O., and Wang, S.-H.: Temporal distribution and potential sources of atmospheric mercury measured at a high-elevation background station in Taiwan, Atmospheric Environment, 44, 2393-2400, 2010.

Sheu, G.-R., and Lin, N.-H.: Characterizations of wet mercury deposition to a remote islet (Pengjiayu) in the subtropical Northwest Pacific Ocean, Atmospheric Environment, 77, 474-481, 2013.

Shirsat, S. V., and Graf, H. F.: An emission inventory of sulfur from anthropogenic sources in Antarctica, Atmospheric Chemistry and Physics, 9, 3397-3408, 2009.

Si, L., and Ariya, P. A.: Reduction of oxidized mercury species by dicarboxylic acids (C_2-C_4): kinetic and product studies, Environmental Science and Technology, 42, 5150-5155, 2008.

Simpson, W. R., Carlson, D., Hönninger, G., Douglas, T. A., Sturm, M., Perovich, D., and Platt, U.: First-year sea-ice contact predicts bromine monoxide (BrO) levels at Barrow, Alaska better than potential frost flower contact, Atmospheric Chemistry and Physics, 7, 621-627, 2007a.

Simpson, W. R., Von Glasow, R., Riedel, K., Anderson, P. S., Ariya, P. A., Bottenheim, J., Burrows, J. P., Carpenter, L. J., Friess, U., Goodsite, M. E., Heard, D. E., Hutterli, M., Jacobi, H.-W., Kaleschke, L., Neff, W., Plane, J. M. C., Platt, U., Richter, A., Roscoe, H. K., Sander, R., Shepson, P. B., Sodeau, J., Steffen, A., Wagner, T., and Wolff, E. W.: Halogens and their role in polar boundary-layer ozone depletion, Atmospheric Chemistry and Physics, 7, 4375-4418, 2007b.

Skamarock, W. C., Klemp, J. B., Dudhia, J., Gill, D. O., Barker, D. M., Wang, W., and Powers, J. G.: A description of the advanced research WRF version 2. NCAR/TN-468+STR. NCAR Technical Note. Boulder, CO, USA, 2007.

Skov, H., Christensen, J. H., Goodsite, M. E., Heidam, N. Z., Jensen, B., Wåhlin, P., and Geernaert, G.: Fate of Elemental Mercury in the Arctic during Atmospheric Mercury Depletion Episodes and the Load of Atmospheric Mercury to the Arctic, Environmental Science & Technology, 38, 2373-2382, 10.1021/es030080h, 2004.

Skyllberg, U., Bloom, P. R., Qian, J., Lin, C.-M., and Bleam, W. F.: Complexation of mercury (II) in soil organic matter: EXAFS evidence for linear two-coordination with reduced sulfur groups, Environmental science & technology, 40, 4174-4180, 2006.

Slemr, F., Schuster, G., and Seiler, W.: Distribution, speciation, and budget of atmospheric mercury, Journal of atmospheric chemistry, 3, 407-434, 1985.

Slemr, F., Brunke, E.-G., Ebinghaus, R., Temme, C., Munthe, J., Wängberg, I., Schroeder, W. H., Steffen, A., and Berg, T.: Wordlwide trend of atmospheric mercury since 1977, Geophysical research letters, 30, 1516, 2003.

Slemr, F., Brunke, E.-G., Labuschagne, C., and Ebinghaus, R.: Total gaseous mercury concentrations at the Cape Point GAW station and their seasonality, Geophysical research letters, 35, L11807, doi: 10.1029/2008GL033741, 2008.

Slemr, F., Ebinghaus, R., Brenninkmeijer, C., Hermann, M., Kock, H., Martinsson, B., Schuck, T., Sprung, D., Velthoven, P. v., and Zahn, A.: Gaseous mercury distribution in the upper troposphere and lower stratosphere observed onboard the CARIBIC passenger aircraft, Atmospheric Chemistry and Physics, 9, 1957-1969, 2009.

Slemr, F., Angot, H., Dommergue, A., Magand, O., Barret, M., Weigelt, A., Ebinghaus, R., Brunke, E.-G., Pfaffhuber, K. A., Edwards, G., Howard, D., Powell, J., Keywood, M., and Wang, F.: Comparison of mercury concentrations measured at several sites in the Southern Hemisphere, Atmospheric Chemistry and Physics, 15, 3125-3133, 2015.

Schuster, D. L., Neff, W., Kim, S., Huey, L. G., Wang, F., Zeng, T., Tanner, D., Blake, D., Beyersdorf, A., Lefer, B., Crawford, J. H., Eisele, F., Mauldin, L., Kosciuch, E., Buhr, M., Wallace, H. W., and Davis, D. D.: Atmospheric chemistry results from the ANTCI 2005 Antarctic plateau airborne study, Journal of geophysical research, 115, doi:10.1029/2009JD012605, 2010.

Smith-Downey, N. V., Sunderland, E. M., and Jacob, D. J.: Anthropogenic impacts on global storage and emissions of mercury from terrestrial soils: Insights from a new global model, Journal of geophysical research, 115, 10.1029/2009JG001124, 2010.

Snider, G., Raofie, F., and Ariya, P. A.: Effects of relative humidity and CO (g) on the O 3-initiated oxidation reaction of Hg 0 (g): kinetic & product studies, Physical Chemistry Chemical Physics, 10, 5616-5623, 2008.

Soerensen, A. L., Skov, H., Jacob, D. J., Soerensen, B. T., and Johnson, M.: Global concentrations of gaseous elemental mercury and reactive gaseous mercury in the marine boundary layer, Environmental Science and Technology, 44, 7425-7430, 2010a.

Soerensen, A. L., Sunderland, E. M., Holmes, C. D., Jacob, D. J., Yantosca, R. M., Skov, H., Christensen, J. H., Strode, S. A., and Mason, R. P.: An improved global model for air-sea exchange of mercury: high concentrations over the north atlantic, Environmental Science and Technology, 44, 8574-8580, 2010b.

Soerensen, A. L., Jacob, D. J., Streets, D. G., Witt, M. L. I., Ebinghaus, R., Mason, R. P., Andersson, M., and Sunderland, E. M.: Multi-decadal decline of mercury in the North Atlantic atmosphere explained by changing subsurface seawater concentrations, Geophysical research letters, 39, doi:10.1029/2012GL053736, 2012.

Soerensen, A. L., Mason, R. P., Balcom, P. H., Jacob, D. J., Zhang, Y., Kuss, J., and Sunderland, E. M.: Elemental mercury concentrations and fluxes in the tropical atmosphere and ocean, Environmental Science & Technology, 48, 11312-11319, 10.1021/es503109p, 2014.

Soerensen, A. L., Jacob, D. J., Schartup, A. T., Fisher, J. A., Lehnherr, I., St. Louis, V. L., Heimbürger, L.-E., Sonke, J. E., Krabbenhoft, D. P., and Sunderland, E. M.: A mass budget for mercury and methylmercury in the Arctic Ocean, Global biogeochemical cycles, 30, 560–575, 10.1002/2015GB005280, 2016.

Sommar, J., Hallquist, M., Ljungström, E., and Lindqvist, O.: On the gas phase reactions between volatile biogenic mercury species and the nitrate radical, Journal of atmospheric chemistry, 27, 233-247, 1997.

Sommar, J., Gårdfeldt, K., Strömberg, D., and Feng, X.: A kinetic study of the gas-phase reactions between the hydroxyl radical and atomic mercury, Atmospheric Environment, 35, 3049-3054, 2001.

Sommar, J., Wängberg, I., Berg, T., Gårdfeldt, K., Munthe, J., Richter, A., Urba, A., Wittrock, F., and Schroeder, W. H.: Circumpolar transport and air-surface exchange of atmospheric mercury at Ny-Alesund (79°N), Svalbard, spring 2002, Atmos. Chem. Phys., 7, 151-166, 10.5194/acp-7-151-2007, 2007.

Sommar, J., Andersson, M. E., and Jacobi, H. W.: Circumpolar measurements of speciated mercury, ozone and carbon monoxide in the boundary layer of the Arctic Ocean, Atmos. Chem. Phys., 10, 5031-5045, 10.5194/acp-10-5031-2010, 2010.

Song, S., Selin, N. E., Soerensen, A. L., Angot, H., Artz, R., Brooks, S., Brunke, E.-G., Conley, G., Dommergue, A., Ebinghaus, R., Holsen, T. M., Jaffe, D. A., Kang, D., Kelley, P., Luke, W. T., Magand, O., Marumoto, K., Pfaffhuber, K. A., Ren, X., Sheu, G.-R., Slemr, F., Warneke, T., Weigelt, A., Weiss-Penzias, P., Wip, D. C., and Zhang, Q.: Top-down constraints on atmospheric mercury emissions and implications for global biogeochemical cycling, Atmospheric Chemistry and Physics, 15, 7103-7125, 2015.

Sonke, J. E., Heimbürger, L.-E., and Dommergue, A.: Mercury biogeochemistry: paradigm shifts, outstanding issues and research needs, Comptes Rendus Geoscience, 345, 213-224, 2013.

Spreen, G., Kaleschke, L., and Heygster, G.: Sea ice remote sensing using AMSR-E 89 GHz channels, Journal of geophysical research, 113, C02S03, http://dx.doi.org/10.1029/2005JC003384, 2008.

Sprovieri, F., Pirrone, N., Hedgecock, I. M., Landis, M. S., and Stevens, R. K.: Intensive atmospheric mercury measurements at Terra Nova Bay in antarctica during November and December 2000, Journal of geophysical research, 107, 4722, doi:10.1029/2002JD002057, 2002.

Sprovieri, F., Pirrone, N., Gårdfeldt, K., and Sommar, J.: Mercury speciation in the marine boundary layer along a 6000 km cruise path around the Mediterranean Sea, Atmospheric Environment, 37, S63-S71, 2003.

Sprovieri, F., Pirrone, N., Landis, M. S., and Stevens, R. K.: Oxidation of Gaseous Elemental Mercury to Gaseous Divalent Mercury during 2003 Polar Sunrise at Ny-Alesund, Environmental Science & Technology, 39, 9156-9165, 10.1021/es050965o, 2005a.

Sprovieri, F., Pirrone, N., Landis, M. S., and Stevens, R. K.: Atmospheric mercury behavior at different altitudes at Ny Alesund during Spring 2003, Atmospheric Environment, 39, 7646-7656, http://dx.doi.org/10.1016/j.atmosenv.2005.08.001, 2005b.

Sprovieri, F., Pirrone, N., Ebinghaus, R., Kock, H. H., and Dommergue, A.: A review of worldwide atmospheric mercury measurements, Atmospheric Chemistry and Physics, 10, 8245-8265, 2010.

Sprovieri, F., Pirrone, N., Bencardino, M., D'Amore, F., Angot, H., Barbante, C., Brunke, E.-G., Cabrera, F. A., Cairns, W., Comero, S., Diéguez, M., Dommergue, A., Ebinghaus, R., Feng, X. B., Fu, X., Garcia, P. E., Gawlik, B. M., Hageström, U., Hansson, K., Horvat, M., Kotnik, J., Labuschagne, C., Magand, O., Martin, L., Mashyanov, N., Mkololo, T., Munthe, J., Obolkin, V. A., Islas, M. R., Sena, F., Somerset, V., Spandow, P., Vardè, M., Walters, C., Wängberg, I., Weigelt, A., Yang, X., and Zhang, H.: Five-year records of total mercury deposition flux at GMOS sites in the Northern and Southern Hemispheres, Atmospheric Chemistry and Physics Discussions, doi:10.5194/acp-2016-517, in review, 2016a.

Sprovieri, F., Pirrone, N., Bencardino, M., D'Amore, F., Carbone, F., Cinnirella, S., Mannarino, V., Landis, M., Ebinghaus, R., Weigelt, A., Brunke, E.-G., Labuschagne, C., Martin, L., Munthe, J., Wängberg, I., Artaxo, P., Morais, F., Cairns, W., Barbante, C., Diéguez, M., Garcia, P. E., Dommergue, A., Angot, H., Magand, O., Skov, H., Horvat, M., Kotnik, J., Read, K. A., Neves, M., Gawlik, B. M., Sena, F., Mashyanov, N., Obolkin, V. A., Wip, D. C., Feng, X. B., Zhang, H., Ramachandran, R., Cossa, D., Knoery, J., Marusczak, N., Nerentorp Mastromonaco, M., and Nordstrøm, C.: Atmospheric mercury concentrations observed at ground-based monitoring sites globally distributed in the framework of the GMOS network, Atmospheric Chemistry and Physics Discussions, 10.5194/acp-2016-466, in review, 2016b.

Stamenkovic, J., Gustin, M. S., Arnone, J. A., Johnson, D. W., Larsen, J. D., and Verburg, P. S.: Atmospheric mercury exchange with a tallgrass prairie ecosystem housed in mesocosms, Science of the total environment, 406, 227-238, 2008.

Steen, A. O., Berg, T., Dastoor, A. P., Durnford, D. A., Hole, L. R., and Pfaffhuber, K. A.: Dynamic exchange of gaseous elemental mercury during polar night and day, Atmospheric Environment, 43, 5604-5610, http://dx.doi.org/10.1016/j.atmosenv.2009.07.069, 2009.

Steen, A. O., Berg, T., Dastoor, A. P., Durnford, D. A., Engelsen, O., Hole, L. R., and Pfaffhuber, K. A.: Natural and anthropogenic atmospheric mercury in the European Arctic: a fractionation study, Atmos. Chem. Phys., 11, 6273-6284, 10.5194/acp-11-6273-2011, 2011.

Steffen, A., Schroeder, W., Bottenheim, J., Narayan, J., and Fuentes, J. D.: Atmospheric mercury concentrations: measurements and profiles near snow and ice surfaces in the Canadian Arctic during Alert 2000, Atmospheric Environment, 36, 2653-2661, 2002.

Steffen, A., Schroeder, W. H., Edwards, G., and Banic, C.: Mercury throughout polar sunrise 2002, J. Phys. IV France, 107, 1267-1270, 2003.

Steffen, A., Schroeder, W., Macdonald, R., Poissant, L., and Konoplev, A.: Mercury in the Arctic atmosphere: An analysis of eight years of measurements of GEM at Alert (Canada) and a comparison with observations at Amderma (Russia) and Kuujjuarapik (Canada), Science of The Total Environment, 342, 185-198, http://dx.doi.org/10.1016/j.scitotenv.2004.12.048, 2005.

Steffen, A., Douglas, T., Amyot, M., Ariya, P. A., Aspmo, K., Berg, T., Bottenheim, J., Brooks, S., Cobbett, F., Dastoor, A., Dommergue, A., Ebinghaus, R., Ferrari, C., Gardfeldt, K., Goodsite, M. E., Lean, D., Poulain, A. J., Scherz, C., Skov, H., Sommar, J., and Temme, C.: A synthesis of atmospheric mercury depletion event chemistry in the atmosphere and snow, Atmospheric Chemistry and Physics, 8, 1445-1482, 2008.

Steffen, A., Scherz, T., Oslon, M., Gay, D. A., and Blanchard, P.: A comparison of data quality control protocols for atmospheric mercury speciation measurements, Journal of Environmental Monitoring, 14, 752-765, doi: 10.1039/c2em10735j, 2012.

Steffen, A., Bottenheim, J., Cole, A., Ebinghaus, R., Lawson, G., and Leaitch, W. R.: Atmospheric mercury speciation and mercury in snow over time at Alert, Canada, Atmospheric Chemistry and Physics, 14, 2219-2231, 2014.

Steffen, A., Lehnherr, I., Cole, A., Ariya, P., Dastoor, A., Durnford, D., Kirk, J., and Pilote, M.: Atmospheric mercury in the Canadian Arctic. Part I: A review of recent field measurements, Science of The Total Environment, 509–510, 3-15, http://dx.doi.org/10.1016/j.scitotenv.2014.10.109, 2015.

Stein, D. C., Swap, R. J., Greco, S., Piketh, S. J., Macko, S. A., Doddridge, B. G., Elias, T., and Bruintjes, R. T.: Haze layer characterization and associated meteorological controls along the eastern

coastal region of southern africa, Journal of geophysical research, 108, 8506, doi: 10.1029/2002JD003237, 2003.

Stephens, G. L., Vane, D. G., Tanelli, S., Eastwood, I., Durden, S., Rokey, M., Reinke, D., Partain, P., Mace, G. G., Austin, R., L'Ecuyer, T., Haynes, J., Lebsock, M., Suzuki, K., Waliser, D., Wu, D., Kay, J., Gettelman, A., Wang, Z., and Marchand, R.: CloudSat mission: performance and early science after the first year of operation, Journal of geophysical research, 113, D00A18, http://dx.doi.org/10.1029/2008JD009982, 2008.

Stohl, A.: Computation, accuracy and application of trajectories - a review and bibliography, Atmospheric Environment, 32, 947-966, 1998.

Stohl, A., Hittenberger, M., and Wotawa, G.: Validation of the Lagrangian particle dispersion model FLEXPART against large scale tracer experiments, Atmospheric Environment, 32, 4245-4264, 1998.

Stohl, A., and Thomson, D. J.: A density correction for Lagrangian particle dispersion models, Boundary-Layer Meteorology, 90, 155-167, 1999.

Stohl, A., Forster, C., Frank, A., Seibert, P., and Wotawa, G.: Technical note: the Lagrangian particle dispersion model FLEXPART version 6.2, Atmospheric Chemistry and Physics, 5, 2461-2474, 2005.

Streets, D. G., Hao, J., Wu, Y., Jiang, J., Chan, M., Tian, H., and Feng, X.: Anthropogenic mercury emissions in China, Atmospheric Environment, 39, 7789-7806, 2005.

Streets, D. G., Zhang, Q., and Wu, Y.: Projections of global mercury emissions in 2050, Environmental Science and Technology, 43, 2983-2988, 2009.

Streets, D. G., Devane, M. K., Lu, Z., Bond, T. C., Sunderland, E. M., and Jacob, D. J.: All-time releases of mercury to the atmosphere from human activities, Environmental Science and Technology, 45, 10485-10491, 2011.

Strode, S. A., Jaeglé, L., Selin, N. E., Jacob, D. J., Park, R. J., Yantosca, R. M., Mason, R. P., and Slemr, F.: Air-sea exchange in the glocal mercury cycle, Global biogeochemical cycles, 21, GB1017, doi: 10.1029/2006GB002766, 2007.

Subir, M., Ariya, P. A., and Dastoor, A.: A review of uncertainties in atmospheric modeling of mercury chemistry I. Uncertainties in existing kinetic parameters - fundamental limitations and the importance of heteregeneous chemistry, Atmospheric Environment, 45, 5664-5675, 2011.

Subir, M., Ariya, P. A., and Dastoor, A.: A review of the sources of uncertainties in atmospheric mercury modeling II. Mercury surface and heterogeneous chemistry - a missing link, Atmospheric Environment, 46, 1-10, 2012.

Sun, G., Sommar, J., Feng, X., Lin, C.-J., Ge, M., Wang, W., Yin, R., Fu, X., and Shang, L.: Mass-Dependent and -Independent Fractionation of Mercury Isotope during Gas-Phase Oxidation of Elemental Mercury Vapor by Atomic Cl and Br, Environmental Science & Technology, 10.1021/acs.est.6b01668, 2016.

Sunderland, E. M.: Mercury exposure from domestic and imported estuarine and marine fish in the US seafood market, Environmental health perspectives, 115, 235-242, 2007.

Sunderland, E. M., and Mason, R. P.: Human impacts on open ocean mercury concentrations, Global biogeochemical cycles, 21, GB4022, 2007.

Sunderland, E. M., Cohen, M. D., Selin, N. E., and Chmura, G. L.: Reconciling models and measurements to assess trends in atmospheric mercury deposition, Environmental Pollution, 156, 526-535, 2008.

Sunderland, E. M., Krabbenhoft, D. P., Moreau, J. W., Strode, S. A., and Landing, W. M.: Mercury sources, distribution, and bioavailability in the north pacific ocean: insights from data and models, Global biogeochemical cycles, 23, 2009.

Sunderland, E. M., and Selin, N. E.: Future tends in environmental mercury concentrations: implications for prevention strategies, Environmental Health, 12, 1-5, doi: 10.1186/1476-069X-12-2, 2013.

Swap, R. J., Annegarn, H. J., Suttles, J. T., King, M. D., Platnick, S., Privette, J. L., and Scholes, R. J.: Africa burning: a thematic analysis of the southern african regional science initiative (SAFARI 2000), Journal of geophysical research, 108, 8465, doi: 10.1029/2003JD003747, 2003.

Swartzendruber, P., Jaffe, D. A., Prestbo, E. M., Weiss-Penzias, P., Selin, N. E., Park, R. J., Jacob, D. J., Strode, S., and Jaeglé, L.: Observations of reactive gaseous mercury in the free

troposphere at the mount bachelor observatory, Journal of geophysical research, 111, 1-12, 10.1029/2006JD007415, 2006.

Tackett, P. J., Cavender, A. E., Keil, A. D., Shepson, P. B., Bottenheim, J. W., Morin, S., Deary, J., Steffen, A., and Doerge, C.: A study of the vertical scale of halogen chemistry in the Arctic troposphere during Polar Sunrise at Barrow, Alaska, Journal of Geophysical Research: Atmospheres, 112, 10.1029/2006JD007785, 2007.

Takizawa, Y., and Osame, M.: Understanding of Minamata disease: methylmercury poisoning in Minamata and Niigata, Japan, Japan Public Health Association, 2001.

Talbot, R., Mao, H., Scheuer, E., Dibb, J., and Avery, M.: Total depletion of Hg in the upper troposphere–lower stratosphere, Geophysical Research Letters, 34, 10.1029/2007GL031366, 2007.

Talbot, R., Mao, H., Feddersen, D., Smith, M., Kim, S. Y., Sive, B. C., Haase, K., Ambrose, J., Zhou, Y., and Russo, R.: Comparison of particulate mercury measured with manual and automated methods, Atmosphere, 2, 1-20, 2011.

Tarasick, D. W., and Bottenheim, J. W.: Surface ozone depletion episodes in the Arctic and Antarctic from historical ozonesonde records, Atmos. Chem. Phys., 2, 197-205, 10.5194/acp-2-197-2002, 2002.

Taylor, C. M., Golding, J., and Emond, A. M.: Blood mercury levels and fish consumption in pregnancy: risks and benefits for birth outcomes in a prospective observational birth cohort, International Journal of Hygiene and Environmental Health, 10.1016/j.ijheh.2016.05.004, 2016.

Tekran: Model 2537A - Principles of operation. Tekran Inc. Toronto, Canada, 1998.

Tekran: Tekran 2537 mercury monitor detection limit. Summary of known estimates, Tekran Instruments Corp., Toronto, ON, Canada., 2011.

Temme, C., Einax, J. W., Ebinghaus, R., and Schroeder, W. H.: Measurements of atmospheric mercury species at a coastal site in the antarctic and over the atlantic ocean during polar summer, Environmental Science and Technology, 37, 22-31, 2003.

Temme, C., Slemr, F., Ebinghaus, R., and Einax, J. W.: Distribution of mercury over the atlantic ocean in 1996 and 1999-2001, Atmospheric Environment, 37, 1889-1897, 2003a.

Temme, C., Ebinghaus, R., Einax, J. W., Steffen, A., and Schroeder, W. H.: Time series analysis of long-term data sets of atmospheric mercury concentrations, Analytical and bioanalytical chemistry, 380, 493-501, 2004.

Temme, C., Blanchard, P., Steffen, A., Banic, C., Beauchamp, S., Poissant, L., Tordon, R., and Wiens, B.: Trend, seasonal and multivariate analysis study of total gaseous mercury data from the Canadian atmospheric mercury measurement network (CAMNet), Atmospheric Environment, 41, 5423-5441, 2007.

Theys, N., Van Roozendael, M., Hendrick, F., Yang, X., De Smedt, I., Richter, A., Begoin, M., Errera, Q., Johnston, P. V., Kreher, K., and De Mazière, M.: Global observations of tropospheric BrO columns using GOME-2 satellite data, Atmospheric Chemistry and Physics, 11, 1791-1811, 2011.

Tokos, J. J., Hall, B. o., Calhoun, J. A., and Prestbo, E. M.: Homogeneous gas-phase reaction of Hg° with H2O2, 03, CH3I, and (CH3)2S: Implications for atmospheric Hg cycling, Atmospheric Environment, 32, 823-827, 1998.

Tossell, J. A.: Calculation of the energetics for oxidation of gas-phase elemental Hg by Br and BrO, The Journal of physical chemistry A, 107, 7804-7808, 2003.

Toyota, K., Dastoor, A., and Ryzhkov, A.: Air-snowpack exchange of bromine, ozone and mercury in the springtime Arctic simulated by the 1-D model PHANTAS - Part 2: mercury and its speciation, Atmospheric Chemistry and Physics, 14, 4135-4167, 2014.

Texte du Traité sur l'Antarctique: http://www.ats.aq/documents/keydocs/vol_1/vol1_2_AT_Antarctic_Treaty_f.pdf, access: 25 July 2016, 1959.

Travnikov, O., and Ilyin, I.: The EMEP/MSC-E Mercury Modelling System, in: Mercury Fate and Transport in the Global Atmosphere: Emissions, Measurements, and Models, edited by: Pirrone, N., and Mason, R. P., Springer, 571-587, 2009.

Travnikov, O., Dastoor, A., De Simone, F., Hedgecock, I. M., Pirrone, N., Ryjkov, A., Selin, N. E., Song, S., and Yang, X.: Multi-model study of mercury dispersion in the atmosphere: Atmospheric processes and model evaluation, in preparation.

UNEP: United Nations Environment Programme (UNEP), Global Mercury Assessment, Inter-organisation Programme for the sound management of chemicals, Geneva, 2002.

UNEP: Global Mercury Assessment 2013: Sources, Emissions, Releases and Environmental Transport. UNEP Chemicals Branch, Geneva, Switzerland, 44 pp., 2013a.

UNEP: Text of the Minamata Convention on Mercury for adoption by the Conference of Plenipotentiaries. unep.org. July 31, Available at: http://www.unep.org/hazardoussubstances/Portals/9/Mercury/Documents/dipcon/CONF_3_Minamata%20Convention%20on%20Mercury_final%2026%2008_e.pdf, last access: 27 March 2016, 2013b.

UNEP: Global mercury modelling: update of modelling results in the global mercury assessment 2013, 2015.

Urba, A., Kvietkus, K., Sakalys, J., Xiao, Z., and Lindqvist, O.: A new sensitive and portable mercury vapor analyzer GARDIS-1A, in: Mercury as a Global Pollutant, Springer, 1305-1309, 1995.

US EPA: Method 1631, Revision E: Mercury in water by oxidation, purge and trap, and cold vapor atomic fluorescence spectrometry, US Environmental Protection Agency, Office of Water, EPA 821-R-96-001, 46, 2002.

Van Loon, L., Mader, E., and Scott, S. L.: Reduction of the aqueous mercuric ion by sulfite: UV spectrum of $HgSO_3$ and its intramolecular redox reaction, Journal of physical chemistry A, 104, 1621-1626, 2000.

Vanarsdale, A. W., J., Keeler, G., Miller, E., Boulet, G., Brulotte, R., and Poissant, L.: Patterns of mercury deposition and concentration in northeastern North America, Ecotoxicology, 14, 37-52, 2005.

Varekamp, J. C., and Buseck, P. R.: Global mercury flux from volcanic and geothermal sources, Applied Geochemistry, 1, 65-73, 1986.

Verfaillie, D., Fily, M., Le Meur, E., Magand, O., Jourdain, B., Arnaud, L., and Favier, V.: Snow accumulation variability derived from radar and firn core data along a 600 km transect in Adelie Land, East Antarctic plateau, The Cryosphere, 6, 1345-1358, 2012.

Vermette, S., Lindberg, S. E., and Bloom, N. S.: Field tests for a regional mercury deposition network - sampling design and preliminary test results, Atmospheric Environment, 29, 1247-1251, 1995.

Vermette, S., Bloom, N., Tokos, J., Welker, M., Verry, S., and Lindberg, S.: The Mercury Deposition Network (NADP/MDN): Transition Phase, February 1995 to February 1996. National Atmospheric Deposition Program, Illinois Sate Water Survey, Champaign, IL., 1996.

Vijayaraghavan, K., Karamchandani, P., Seigneur, C., Balmori, R., and Chen, S. Y.: Plume-in-grid modeling of atmospheric mercury, Journal of Geophysical Research: Atmospheres, 113, 2008.

Wade, L.: Mercury pollution: gold's dark side, Science, 341, 1448-1449, 2013.

Wang, F., Saiz-Lopez, A., Mahajan, A. S., Gomez Martin, J. C., Armstrong, D., Lemes, M., Hay, T., and Prados-Roman, C.: Enhanced production of oxidised mercury over the tropical pacific ocean: a key missing oxidation pathway, Atmospheric Chemistry and Physics, 14, 1323-1335, 2014.

Wang, J., Zhang, L., and Xie, Z.: Total gaseous mercury along a transect from coastal to central Antarctic: Spatial and diurnal variations, Journal of Hazardous Materials, 317, 362-372, http://dx.doi.org/10.1016/j.jhazmat.2016.05.068, 2016.

Wang, P.: Atmospheric mercury speciation and aerosol properties at Ny-Alesund, Department of Chemistry, Norwegian University of Science and Technology, 130 pp., 2015.

Wang, S., Schmidt, J. A., Baidar, S., Coburn, S., Dix, B., Koenig, T. K., Apel, E., Bowdalo, D., Campos, T. L., Eloranta, E., Evans, M. J., DiGangi, J. P., Zondlo, M. A., Gao, R.-S., Haggerty, J. A., Hall, S. R., Hornbrook, R. S., Jacob, D. J., Morley, B., Pierce, B., Reeves, M., Romashkin, P., Ter Schure, A., and Volkamer, R.: Active and widespread halogen chemistry in the tropical and subtropical free troposphere, Proceedings of the National Academy of Sciences, 112, 9281-9286, 2015.

Wang, Z., and Pehkonen, S. O.: Oxidation of elemental mercury by aqueous bromine: atmospheric implications, Atmospheric Environment, 38, 3675-3688, 2004.

Wängberg, I., Munthe, J., Pirrone, N., Iverfeldt, Å., Bahlman, E., Costa, P., Ebinghaus, R., Feng, X., Ferrara, R., and Gårdfeldt, K.: Atmospheric mercury distribution in Northern Europe and in the Mediterranean region, Atmospheric Environment, 35, 3019-3025, 2001.

Wängberg, I., Munthe, J., Berg, T., Ebinghaus, R., Kock, H., Temme, C., Bieber, E., Spain, T., and Stolk, A.: Trends in air concentration and deposition of mercury in the coastal environment of the North Sea Area, Atmospheric Environment, 41, 2612-2619, 2007.

Wedeen, R. P.: Were the hatters of New Jersey "mad"?, American journal of industrial medicine, 16, 225-233, 1989.

Weigelt, A., Ebinghaus, R., Manning, A., Derwent, R., Simmonds, P., Spain, T., Jennings, S., and Slemr, F.: Analysis and interpretation of 18 years of mercury observations since 1996 at Mace Head, Ireland, Atmospheric Environment, 100, 85-93, 2015.

Weiss-Penzias, P., Jaffe, D. A., Swartzendruber, P., Hafner, W., Chand, D., and Prestbo, E.: Quantifying Asian and biomass burning sources of mercury using the Hg/CO ratio in pollution plumes observed at the Mount Bachelor observatory, Atmospheric Environment, 41, 4366-4379, 2007.

Weiss-Penzias, P., Amos, H. M., Selin, N. E., Gustin, M. S., Jaffe, D. A., Obrist, D., Sheu, G.-R., and Giang, A.: Use of a global model to understand speciated atmospheric mercury observations at five high-elevation sites, Atmospheric Chemistry and Physics, 15, 1161-1173, 2015.

Wennberg, P.: Atmospheric chemistry: Bromine explosion, Nature, 397, 299-301, 1999.

Whalin, L., Kim, E.-H., and Mason, R. P.: Factors influencing the oxidation, reduction, methylation and demethylation of mercury species in coastal waters, Marine Chemistry, 107, 278-294, 2007.

Whittlestone, S., Gras, J. L., and Siems, S. T.: Surface air mass origins during the first aerosol characterization experiment (ACE 1), Journal of geophysical research, 103, 16,341-316,350, 1998.

WHO: World Health Organization. Background and purpose of the WHO environmental health criteria programme. Environmental health criteria for mercury, 1976.

World Health Organization. Exposure to mercury: a major public health concern. Geneva.: http://www.who.int/ipcs/features/mercury.pdf access: 11 July 2016, 2007.

Williams, J., Gros, V., Bonsang, B., and Kazan, V.: HO cycle in 1997 and 1998 over the southern indian ocean derived from CO, radon, and hydrocarbon measurements made at Amsterdam island, Journal of geophysical research, 106, 12719-12725, doi: 10.1029/2001JD900116, 2001.

Witt, M. L. I., Mather, T. A., Baker, A. R., De Hoog, J. C. M., and Pyle, D. M.: Atmospheric trace metals over the south-west indian ocean: total gaseous mercury, aerosol trace metal concentrations and lead isotope ratios, Marine Chemistry, 121, 2-16, 2010.

Wolfe, M. F., Schwarzbach, S., and Sulaiman, R. A.: Effects of mercury on wildlife: a comprehensive review, Environmental toxicology and chemistry, 17, 146-160, 1998.

Wood, M., and Trip, L.: Examining fish consumption advisories related to mercury contamination in Canada, Environment Canada. http://www.ec.gc.ca/MERCURY/EN/efca.cfm, 2001.

Xia, C., Xie, Z., and Sun, L.: Atmospheric mercury in the marine boundary layer along a cruise path from Shanghai, China to Prydz Bay, Antarctica, Atmospheric Environment, 44, 1815-1821, 2010.

Xiao, W., Liu, S., Li, H., Xiao, Q., Wang, W., Hu, Z., Hu, C., Gao, Y., Shen, J., Zhao, X., Zhang, M., and Lee, X.: A flux-gradient system for simultaneous measurement of the CH_4, CO_2, and H_2O fluxes at a lake-air interface, Environmental Science and Technology, 48, 14490-14498, 2014.

Xiao, Z. F., Munthe, J., Stromberg, D., and Lindqvist, O.: Photochemical behavior of inorganic mercury compounds in aqueous solution, in: Mercury as a global pollutant - Integration and Synthesis, edited by: Watras, C. J., and Huckabee, J. W., Lewis Publishers, 581-592, 1994.

Xu, X., Yang, X., Miller, D. R., Helble, J. J., and Carley, R. J.: Formulation of bi-directional atmosphere-surface exchanges of elemental mercury, Atmospheric Environment, 33, 4345-4355, 1999.

Yang, X., Cox, R. A., Warwick, N. J., Pyle, J. A., Carver, G. D., O'Connor, F. M., and Savage, N. H.: Tropospheric bromine chemistry and its impacts on ozone: A model study, Journal of geophysical research, 110, D23311, 10.1029/2005JD006244, 2005.

Yang, Y.-K., Zhang, C., Shi, X.-J., Tao, L., and Wang, D.-Y.: Effect of organic matter and pH on mercury release from soils, Journal of Environmental Sciences, 19, 1349-1354, 2007.

Young, J. F., Wosilait, W. D., and Luecke, R. H.: Analysis of methylmercury disposition in humans utilizing a PBPK model and animal pharmacokinetic data, Journal of toxicology and environmental health. Part A., 63, 19-52, 2001.

Yu, J., Xie, Z., Kang, H., Li, Z., Sun, C., Bian, L., and Zhang, P.: High variability of atmospheric mercury in the summertime boundary layer through the central Arctic Ocean, Scientific Reports, 4, 6091, 10.1038/srep06091

http://www.nature.com/articles/srep06091#supplementary-information, 2014.

Yu, S., Mathur, R., Kang, D., Schere, K., and Tong, D.: A study of the ozone formation by ensemble back trajectory-process analysis using the Eta-CMAQ forecast model over the northeastern U.S. during the 2004 ICARTT period, Atmospheric Environment, 43, 355-363, 2009.

Zambrano-Bigiarini, M.: hydroGOF: Goodness-of-fit functions for comparison of simulated and observed hydrological time series. R package version 0.3-8. http://CRAN.R-project.org/package=hydroGOF, last access: 10 June 2016, 2014.

Zatko, M., Geng, L., Alexander, B., Sofen, E., and Klein, K.: The impact of snow nitrate photolysis on boundary layer chemistry and the recycling and redistribution of reactive nitrogen across Antarctica and Greenland in a global chemical transport model, Atmos. Chem. Phys., 16, 2819-2842, 10.5194/acp-16-2819-2016, 2016.

Zatko, M. C., Grenfell, T. C., Alexander, B., Doherty, S. J., Thomas, J. L., and Yang, X.: The influence of snow grain size and impurities on the vertical profiles of actinic flux and associated NOx emissions on the Antarctic and Greenland ice sheets, Atmospheric Chemistry and Physics, 13, 3547-3567, 2013.

Zhang, L., Wright, L. P., and Blanchard, P.: A review of current knowledge concerning dry deposition of atmospheric mercury, Atmospheric Environment, 43, 5853-5864, 2009.

Zhang, Y., Jaeglé, L., van Donkelaar, A., Martin, R. V., Holmes, C. D., Amos, H. M., Wang, Q., Talbot, R., Artz, R., Brooks, S., Luke, W., Holsen, T. M., Felton, D., Miller, E. K., Perry, K. D., Schmeltz, D., Steffen, A., Tordon, R., Weiss-Penzias, P., and Zsolway, R.: Nested-grid simulation of mercury over North America, Atmos. Chem. Phys., 12, 6095-6111, 10.5194/acp-12-6095-2012, 2012.

Zhang, Y., Jaeglé, L., Thompson, L., and Streets, D. G.: Six centuries of changing oceanic mercury, Global Biogeochemical Cycles, 28, 1251-1261, 2014.

Zhang, Y., Jacob, D. J., Horowitz, H. M., Chen, L., Amos, A., Krabbenhoft, D. P., Slemr, F., St Louis, V. L., and Sunderland, E. M.: Observed decrease in atmospheric mercury explained by global decline in anthropogenic emissions, Proceedings of the National Academy of Sciences of the United States of America, 113, 526-531, 2016.

Zhao, T., Gong, S., Bottenheim, J., McConnell, J., Sander, R., Kaleschke, L., Richter, A., Kerkweg, A., Toyota, K., and Barrie, L.: A three-dimensional model study on the production of BrO and Arctic boundary layer ozone depletion, Journal of Geophysical Research: Atmospheres, 113, 10.1029/2008JD010631, 2008.

Zheng, W., Foucher, D., and Hintelmann, H.: Mercury isotope fractionation during volatilization of Hg (0) from solution into the gas phase, Journal of Analytical Atomic Spectrometry, 22, 1097-1104, 2007.

Zheng, W., and Hintelmann, H.: Mercury isotope fractionation during photoreduction in natural water is controlled by its Hg/DOC ratio, Geochimica et Cosmochimica Acta, 73, 6704-6715, 2009.

Zhu, W., Sommar, J., Lin, C.-J., and Feng, X.: Mercury vapor air–surface exchange measured by collocated micrometeorological and enclosure methods–Part II: Bias and uncertainty analysis, Atmospheric Chemistry and Physics, 15, 5359-5376, 2015a.

Zhu, W., Sommar, J., Lin, C., and Feng, X.: Mercury vapor air–surface exchange measured by collocated micrometeorological and enclosure methods–Part I: Data comparability and method characteristics, Atmos. Chem. Phys, 15, 685-702, 2015b.

Zhu, W., Lin, C. J., Wang, X., Sommar, J., Fu, X., and Feng, X.: Global observations and modeling of atmosphere–surface exchange of elemental mercury: a critical review, Atmos. Chem. Phys., 16, 4451-4480, 10.5194/acp-16-4451-2016, 2016.

Liste des tableaux

Liste des figures

Liste des acronymes

AERONET : Aerosol robotic network

ALT : Alert (station de mesures au Canada)

AMAP : Arctic Monitoring and Assessment Programme

AMDE : Atmospheric Mercury Depletion Event

AMNet : Atmospheric mercury network

AMS : Ile d'Amsterdam (station de mesures au milieu de l'océan Indien)

ANCOVA : Analysis of covariance

AND : Andøya (station de mesures en Norvège)

ANR : Agence Nationale de la Recherche

AOD : Aerosol Optical Depth

BAR : Bariloche (station de mesures en Argentine)

BB : Biomass Burning

CAMNet : Canadian atmospheric mercury measurement network

CEA : Commissariat à l'énergie atomique et aux énergies alternatives

CMA : Col Margherita (station de mesures en Italie)

CNR-IIA : Instituto del Consiglio Nazionale delle Ricerche, Istituto sull'inquinamento atmosferico

CNRS : Centre National de la Recherche Scientifique

CPG : Cape Grim (station de mesures en Tasmanie)

CPT : Cape Point (station de mesures en Afrique du Sud)

CRDS : Cavity Ring-Down Spectroscopy

CRO : Archipel de Crozet

CST : Celestún (station de mesures au Mexique)

CSTP : Conditions Standard de Température et de Pression

CVAFS : Cold Vapor Atomic Fluorescence Spectrometer

DA : Dôme A en Antarctique

DC : Station Concordia (station de mesures située à Dôme C sur la calotte glaciaire antarctique)

DDU : Dumont d'Urville (station de mesures située sur la côte Est du continent antarctique)

DL : Detection Limit

DMS : Dimethylsulfide

ECCC : Environment and Climate Change Canada

ECMWF : European Centre for Medium-range Weather Forecast

EI : Exercice d'intercomparaison

EMEP : European Monitoring and Evaluation Programme

GC/MS : Gas Chromatography/Mass Spectrometry

GEM-MACH : Global environmental multi-scale modelling air quality and chemistry

GET : Géosciences Environnement Toulouse

GFS : Global Forecast System

GLEMOS : Global EMEP multi-media modelling system

GMOS : Global Mercury Observation System

GT : Groupe de travail

HA : Halley (station de mesures britannique en Antarctique)

HAMSTRAD : H_2O Antarctica microwave stratospheric and tropospheric radiometers

HBT : Ville d'Hobart en Tasmanie

Hg(0) : Mercure élémentaire gazeux

Hg(I) : Ion mercureux

Hg(II) : Mercure divalent gazeux

Hg_r(II) : Reducible divalent mercury

Hg_{nr}(II) : Non reducible divalent mercury

Hg(p) : Mercure divalent particulaire

Hg_{tot} : Mercure total

HYSPLIT : Hybrid single-particle Lagrangian integrated trajectory

ICOS : Integrated Carbon Observation System

INSU : Institut National des Sciences de l'Univers

IPEV : Institut polaire français Paul-Emile Victor

IPSL : Institut Pierre Simon Laplace

ISK : Iskrba (station de mesures en Slovénie)

IWV : Integrated Water Vapor

KER : Archipel des Kerguelen

LEFE : Les Enveloppes Fluides et l'Environnement

LGGE : Laboratoire de Glaciologie et Géophysique de l'Environnement

LIDAR : Light detection and ranging

LIS : Listvyanka (station de mesures en Russie)

LON : Longobucco (station de mesures en Italie)

MAL : Mont Ailao (station de mesures en Chine)

MAR : Modèle Atmosphérique Régional

MCH : Mont Changbai (station de mesures en Chine)

MDF : Mass Dependent Fractionation

MeHg : Méthylmercure (regroupe ici CH_3Hg^+ et $Hg(CH_3)_2$)

MHE : Mace Head (station de mesures en Irlande)

MIF : Mass Independent Fractionation

MIT : Massachussetts Institute of Technology

MM : McMurdo (station de mesures américaine en Antarctique)

MODIS : Moderate resolution imaging spectroradiometer

MOZART : Model for ozone and related chemical tracers

MWA : Mont Waliguan (station de mesures en Chine)

n-3 PUFA : n-3 polyacides gras insaturés à longue chaîne

NADP : National Atmospheric Deposition Program

NASA : National Aeronautics and Space Administration

NCEP : National Centre for Environmental Predictions

NILU : Norwegian Institute for Air Research

NIST : National Institute of Standards and Technology

NM : Neumayer (station de mesures allemande en Antarctique)

NOAA : National Oceanic and Atmospheric Administration

NPP : Net Primary Productivity

NSE : Nash-Sutcliffe efficiency

NYA : Ny-Ǻlesund (station de mesures au Spitsberg)

ODE : Ozone Depletion Event

OMS : Organisation Mondiale de la Santé (WHO en anglais)

p-TOMCAT : parallel-tropospheric off-line model of chemistry and transport

PAL : Pallas (station de mesures en Finlande)

PBIAS : percent bias

PBL : Planetary Boundary Layer

PBPK : Modèles pharmacocinétiques physiologiques

PES (membranes ou filtres) : Polyéthersulfone

PES : Potential Emission Sensitivities

PFA : Perfluoroalkoxy

PNUE : Programme des Nations Unies pour l'Environnement (UNEP en anglais)

POS : Procédures Opératoires Standard

PTFE : Polytétrafluoroéthylène

QA/QC : Quality Assurance/Quality Control

RAO : Råö (station de mesures en Suède)

READY : Real-time environmental applications and display system

RGM : Reactive Gaseous Mercury

RM : Reactive Mercury

RMSE : Root Mean Standard Error

RPF : Regenerable Particulate Filter

RUN : Ile de la Réunion

SIA : Snow interstitial Air

SIS : Sisal (station de mesures au Mexique)

SND : Villum Research Station at Station Nord (station de mesures au Groenland)

SP : Amundsen-Scott South Pole station

SRM : Standard Reference Material

SW : Shortwave radiation

TAAF : Terres Australes et Antarctiques Françaises

TGM : Total Gaseous Mercury

TNB : Terra Nova Bay (station de mesures italienne en Antarctique)

TR : Troll (station de mesures norvégienne en Antarctique)

UE : Union Européenne (EU en anglais)

US EPA : United States Environmental Protection Agency

UV : Rayonnements ultraviolets

UV-A : Ultraviolets proches du rayonnement visible (320-400 nm)

UV-B : Ultraviolets plus énergétiques (280-320 nm)

WD : Wind Direction

WRF : Weather Research and Forecast

WS : Wind Speed

ZG : Zhongshan (station de mesures chinoise en Antarctique)

Annexes

Annexe 1 : Atmospheric mercury concentrations observed at ground-based monitoring sites globally distributed in the framework of the GMOS network

Sprovieri, F., Pirrone, N., Bencardino, M., D'Amore, F., Carbone, F., Cinnirella, S., Mannarino, V., Landis, M., Ebinghaus, R., Weigelt, A., Brunke, E.-G., Labuschagne, C., Martin, L., Munthe, J., Wängerg, I., Artaxo, P., Morais, F., Cairns, W., Barbante, C., Diéguez, M., Garcia,, P. E., Dommergue, A., **Angot, H.**, Magand, O., Skov, H., Horvat, M., Kotnik, J., Read, K. A., Neves, L. M., Gawlik, B. M., Sena, F., Mashyanov, N., Obolkin, V. A., Wip, D., Feng, X. B., Zhang, H., Fu, X., Ramachandran, R., Cossa, D., Knoery, J., Marusczak, N., Nerentorp, M., Nordstrøm, C., Atmospheric Chemistry and Physics, 11915-11935, 2016.

Atmos. Chem. Phys., 16, 11915–11935, 2016
www.atmos-chem-phys.net/16/11915/2016/
doi:10.5194/acp-16-11915-2016
© Author(s) 2016. CC Attribution 3.0 License.

Atmospheric Chemistry and Physics Open Access EGU

Atmospheric mercury concentrations observed at ground-based monitoring sites globally distributed in the framework of the GMOS network

Francesca Sprovieri[1], Nicola Pirrone[2], Mariantonia Bencardino[1], Francesco D'Amore[1], Francesco Carbone[1], Sergio Cinnirella[1], Valentino Mannarino[1], Matthew Landis[3], Ralf Ebinghaus[4], Andreas Weigelt[4], Ernst-Günther Brunke[5], Casper Labuschagne[5], Lynwill Martin[5], John Munthe[6], Ingvar Wängberg[6], Paulo Artaxo[7], Fernando Morais[7], Henrique de Melo Jorge Barbosa[7], Joel Brito[7], Warren Cairns[8], Carlo Barbante[8,9], María del Carmen Diéguez[10], Patricia Elizabeth Garcia[10], Aurélien Dommergue[11,12], Helene Angot[11,12], Olivier Magand[12,11], Henrik Skov[13], Milena Horvat[14], Jože Kotnik[14], Katie Alana Read[15], Luis Mendes Neves[16], Bernd Manfred Gawlik[17], Fabrizio Sena[17], Nikolay Mashyanov[18], Vladimir Obolkin[19], Dennis Wip[20], Xin Bin Feng[21], Hui Zhang[21], Xuewu Fu[21], Ramesh Ramachandran[22], Daniel Cossa[23], Joël Knoery[24], Nicolas Marusczak[23], Michelle Nerentorp[25], and Claus Norstrom[13]

[1]CNR Institute of Atmospheric Pollution Research, Rende, Italy
[2]CNR Institute of Atmospheric Pollution Research, Rome, Italy
[3]Office of Research and Development, US Environmental Protection Agency, Research Triangle Park, NC, USA
[4]Helmholtz-Zentrum, Geesthacht, Germany
[5]Cape Point GAW Station, Climate and Environment Research & Monitoring, South African Weather Service, Stellenbosch, South Africa
[6]IVL, Swedish Environmental Research Inst. Ltd., Göteborg, Sweden
[7]University of Sao Paulo, Sao Paulo, Brazil
[8]University Ca' Foscari of Venice, Venice, Italy
[9]CNR Institute for the Dynamics of Environmental Processes, Venice, Italy
[10]INIBIOMA-CONICET-UNComa, Bariloche, Argentina
[11]Laboratoire de Glaciologie et Géophysique de l'Environnement, University Grenoble Alpes, Grenoble, France
[12]Laboratoire de Glaciologie et Géophysique de l'Environnement, CNRS, Grenoble, France
[13]Department of Environmental Science, Aarhus University, Aarhus, Denmark
[14]Jožef Stefan Institute, Lubliana, Slovenia
[15]NCAS, University of York, York, UK
[16]Cape Verde Observatory, INMG – São Vicente, Cabo Verde
[17]Joint Research Centre, Ispra, Italy
[18]St. Petersburg State University, St. Petersburg, Russia
[19]Limnological Institute SB RAS, Irkutsk, Russia
[20]Department of Physics, University of Suriname, Paramaribo, Suriname
[21]Institute of Geochemistry, State Key Laboratory of Environmental Geochemistry, Chinese Academy of Sciences, Guiyang, China
[22]Institute for Ocean Management, Anna University, Chennai, India
[23]LER/PAC, Ifremer,Centre Méditerranée, La Seyne-sur-Mer, France
[24]LBCM, Ifremer, Centre Atlantique, Nantes, France
[25]Chalmers University of Technology, Gothenburg, Sweden

Correspondence to: Francesca Sprovieri (f.sprovieri@iia.cnr.it)

Received: 31 May 2016 – Published in Atmos. Chem. Phys. Discuss.: 7 June 2016
Revised: 30 August 2016 – Accepted: 1 September 2016 – Published: 23 September 2016

Abstract. Long-term monitoring of data of ambient mercury (Hg) on a global scale to assess its emission, transport, atmospheric chemistry, and deposition processes is vital to understanding the impact of Hg pollution on the environment. The Global Mercury Observation System (GMOS) project was funded by the European Commission (http://www.gmos.eu) and started in November 2010 with the overall goal to develop a coordinated global observing system to monitor Hg on a global scale, including a large network of ground-based monitoring stations, ad hoc periodic oceanographic cruises and measurement flights in the lower and upper troposphere as well as in the lower stratosphere. To date, more than 40 ground-based monitoring sites constitute the global network covering many regions where little to no observational data were available before GMOS. This work presents atmospheric Hg concentrations recorded worldwide in the framework of the GMOS project (2010–2015), analyzing Hg measurement results in terms of temporal trends, seasonality and comparability within the network. Major findings highlighted in this paper include a clear gradient of Hg concentrations between the Northern and Southern hemispheres, confirming that the gradient observed is mostly driven by local and regional sources, which can be anthropogenic, natural or a combination of both.

1 Introduction

Mercury (Hg) is found ubiquitously in the atmosphere and is known to deposit to ecosystems, where it can be taken up into food webs and transformed to highly toxic species (i.e., methyl-Hg) which are detrimental to ecosystem and human health. A number of activities have been carried out since the late 1980s in developed countries within European and international strategies and programs (i.e., UNECE-CLRTAP, EU-Mercury Strategy; UNEP Governing Council) to elaborate possible mechanisms to reduce Hg emissions to the atmosphere from industrial facilities, trying to balance the increasing emissions in rapidly industrializing countries of the world (Pirrone et al., 2013, 2008, 2009; Pacyna et al., 2010). Hg displays complex speciation and chemistry in the atmosphere, which influences its transport and deposition on various spatial and temporal scales (Douglas et al., 2012; Goodsite et al., 2004, 2012; Lindberg et al., 2007; Soerensen et al., 2010a, b; Sprovieri et al., 2010b; Slemr et al., 2015). Most of Hg is observed in the atmosphere as Gaseous Elemental Mercury (GEM/Hg0), representing 90 to 99 % of the total with a terrestrial background concentration of approximately 1.5–1.7 ng m^{-3} in the Northern Hemisphere and between 1.0 and 1.3 ng m^{-3} in the Southern Hemisphere based on research studies published before Global Mercury Observation System (GMOS) (Lindberg et al., 2007; Sprovieri et al., 2010b). The results obtained from newly established GMOS ground-based sites show a background value in the Southern Hemisphere close to 1 ng m^{-3}, which is lower than that obtained in the past. Oxidized Hg species (gaseous oxidized mercury or GOM) and particulate bound mercury (PBM) contribute significantly to dry and wet deposition fluxes to terrestrial and aquatic receptors (Brooks et al., 2006; Goodsite et al., 2004, 2012; Hedgecock et al., 2006; Skov et al., 2006; Gencarelli et al., 2015; De Simone et al., 2015). Although in the past 2 decades a number of Hg monitoring sites have been established (in Europe, Canada, USA and Asia) as part of regional networks and/or European projects (i.e., MAMCS, MOE, MERCYMS) (Munthe et al., 2001, 2003; Wängberg et al., 2001, 2008; Pirrone et al., 2003; Steffen et al., 2008), the need to establish a global network to assess likely southern–northern hemispheric gradients and long-term trends has long been considered a high priority for policy and scientific purposes. The main reason is to make consistent and globally distributed Hg observations available that can be used to validate regional and global-scale models for assessing global patterns of Hg concentrations and deposition and re-emission fluxes. Therefore a coordinated global observational network for atmospheric Hg was established within the framework of the GMOS project (Seventh Framework Program – FP7) in 2010. The aim of GMOS was to provide high-quality Hg datasets in the Northern and Southern hemispheres for a comprehensive assessment of atmospheric Hg concentrations and their dependence on meteorology, long-range atmospheric transport and atmospheric emissions on a global scale (Sprovieri et al., 2013). This network was developed by integrating previously established ground-based atmospheric Hg monitoring stations with newly established GMOS sites in regions of the world where atmospheric Hg observational data were scarce, particularly in the Southern Hemisphere (Sprovieri et al., 2010b). The stations are located at both high altitude and high sea level locations, as well as in climatically diverse regions. The measurements from these sites have been used to validate regional- and global-scale atmospheric Hg models in order to improve our understanding of global Hg transport, deposition and re-emission, as well as to provide a contribution to future international policy development and implementation (Gencarelli et al., 2016; De Simone et al., 2016). The GMOS overarching objective to establish a global Hg monitoring network was achieved having in mind the need to assure high-quality observations in line with international quality assurance/quality control (QA/QC) standards and to fill the gap in terms of spatial coverage of measurements in the Southern Hemisphere where data were lacking or nonexistent. One of the major outcomes of GMOS has been an interoperable e-infrastructure developed following the Group on Earth Observations (GEO) data sharing and interoperability principles which allows us to provide support to UNEP for the implementation of the Minamata Convention (i.e., Article 22 to measure the effectiveness of

measures). Within the GMOS network, Hg measurements were in fact carried out using high-quality techniques by harmonizing the GMOS measurement procedures with those already adopted at existing monitoring stations around the world. Standard operating procedures (SOPs) and a QA/QC system were established and implemented at all GMOS sites in order to assure full comparability of network observations. To ensure a fully integrated operation of the GMOS network, a centralized online system (termed GMOS Data Quality Management, G-DQM) was developed for the acquisition of atmospheric Hg data in near real time and providing a harmonized QA/QC protocol. This novel system was developed for integrating data control and is based on a service-oriented approach that facilitates real-time adaptive monitoring procedures, which is essential for producing high-quality data (Cinnirella et al., 2014; D'Amore et al., 2015). GMOS activities are currently part of the GEO strategic plan (2016–2025) within the GEO flagship on "tracking persistent pollutants". The overall goal of this flagship is to support the development of GEOSS by fostering research and technological development on new advanced sensors for in situ and satellite platforms, in order to lower the management costs of long-term monitoring programs and improve spatial coverage of observations. In this paper we present for the first time a complete global dataset of Hg concentrations at selected ground-based sites in the Southern and Northern hemispheres and highlight its potential to support the validation of global-scale atmospheric models for research and policy scenario analysis.

2 Experimental

GMOS global network

The GMOS network currently consists of 43 globally distributed monitoring stations located both at sea level (i.e., Mace Head, Ireland; Calhau, Cabo Verde; Cape Point, South Africa; Amsterdam Island, southern Indian Ocean) and high-altitude locations, such as the Everest-K2 Pyramid station (Nepal) at 5050 m a.s.l. and the Mt. Waliguan (China) station at 3816 m a.s.l., as well as in climatically diverse regions, including polar areas such as Villum Research Station (VRS), Station Nord (Greenland), Pallas (Finland) and Dome Concordia and Dumont d'Urville stations in Antarctica. It is possible to browse the GMOS monitoring sites at the GMOS Monitoring Services web portal. The monitoring sites are classified as master (M) and secondary (S) with respect to the Hg measurement programs (Table 1). Master stations perform speciated Hg measurements and collect precipitation samples for Hg analysis whereas the secondary stations perform only total gaseous mercury (TGM)/GEM measurements and precipitation samples as well. Table 1 summarize key information about GMOS stations, such as (a) the location, elevation and type of monitoring stations; (b) new sites (master and/or secondary) established as part of GMOS; and (c) existing monitoring sites established by institutions that are part of European and international monitoring programs and managed by GMOS partners and GMOS external partners who have agreed to share their monitoring data and submit them to the central database following the interoperability principles and standards set in GEOSS (Group Earth Observation System of System). The GMOS objective of establishing a global Hg monitoring network was achieved always bearing in mind not only the necessity to provide intercomparable data worldwide but also international standards of intercomparability. In particular, GMOS attempts to comply with the data sharing principles set by the GEO that aim to develop the GEOSS through the use of "observation systems, which include ground-, air-, water- and space-based sensors, field surveys and citizen observatories. GEO works to coordinate the planning, sustainability and operation of these systems, aiming to maximize their added value and use." Additionally, GMOS makes use of "information and processing systems, which include hardware and software tools needed for handling, processing and delivering data from the observation systems to provide information, knowledge, services and products." In 2010 the Executive Committee of GEO selected GMOS as a showcase for the work plan (2012–2015) to demonstrate how GEOSS can support the convention and policies as well as pioneering activity in environmental monitoring using highly advanced e-infrastructure. More details about the sites can also be found at http://www.gmos.eu.

Eleven monitoring stations managed by external partners are included within the global network sharing their data with the GMOS central database. These new associated stations follow the "Governance and Data Policy of the Global Mercury Observation System" guidelines established by GMOS (Pirrone, 2012).

From the start of GMOS a small number of monitoring sites have been relocated or have become recently operational, but most of the sites have been fully operational for the entire project period and remain active. These original core group stations consist of 27 monitoring sites. Their spatial coverage is better throughout the Northern Hemisphere with 17 operational monitoring stations, whereas there are 5 sites in the tropical zone (area between the Tropic of Cancer ($+23°27'$) and the Tropic of Capricorn ($-23°27'$)), and 5 sites in the Southern Hemisphere. The sites in the Southern Hemisphere include new Hg stations, such as the GMOS site in Bariloche (Patagonia, Argentina), the station in Kodaicanal (South India) and the site on the Amsterdam Island (Terres Australes et Antarctiques Françaises, TAAF) in the southern Indian Ocean, and two sites in Antarctica at the Italian–French Dome Concordia station and at the French site Dumont d'Urville.

Table 1. Atmospheric ground-based sites locations that are part of the GMOS network and general characteristics of the sites (i.e., code, lat, long), including the type of monitoring station in respect to the Hg measurements carried out as speciated (M) or not (S). In bold, external GMOS partners are indicated.

Code	Site	Country	Elevation (m a.s.l.)	Lat (°)	Long (°)	GMOS site[a]
AMS	Amsterdam Island	Terres Australes et Antarctiques Françaises	70	−37.79604	77.55095	M
BAR	Bariloche	Argentina	801	−41.128728	−71.420100	M
CAL	Calhau	Cabo Verde	10	16.86402	−24.86730	S
CHE	**Cape Hedo**	**Japan**	**60**	**26.86430**	**128.25141**	**M**
CPT	Cape Point	South Africa	230	−34.353479	18.489830	S
CST	Celestún	Mexico	3	20.85838	−90.38309	S
CMA	Col Margherita	Italy	2545	46.36711	11.79341	S
DMC	Concordia Station	Antarctica	3220	−75.10170	123.34895	S
DDU	Dumont d'Urville	Antarctica	40	−66.66281	140.00292	S
EVK	Ev-K2	Nepal	5050	27.95861	86.81333	S
ISK	Iskrba	Slovenia	520	45.56122	14.85805	M
KOD	Kodaicanal	India	2333	10.23170	77.46524	M
LSM	La Seyne-sur-Mer	France	10	43.106119	5.885250	S
LIS[b]	Listvyanka	Russia	670	51.84670	104.89300	S
LON	Longobucco	Italy	1379	39.39408	16.61348	M
MHD	Mace Head	Ireland	8	53.32661	−9.90442	S
MAN	Manaus	Brazil	110	−2.89056	−59.96975	M
MIN	Minamata	Japan	20	32.23056	130.40389	M
MAL	Mt. Ailao	China	2503	24.53791	101.03024	S/M
MBA	**Mt. Bachelor**	**WA, USA**	**2743**	**43.977516**	**121.685968**	**M**
MCH	Mt. Changbai	China	741	42.40028	128.11250	M/S
MWA	Mt. Walinguan	China	3816	36.28667	100.89797	M
NIK[b]	Nieuw Nickerie	Suriname	1	5.95679	−57.03923	S
PAL	Pallas	Finland	340	68.00000	24.23972	S
RAO	Rao	Sweden	5	57.39384	11.91407	M
SIS	Sisal	Mexico	7	21.16356	−90.04679	S
VRS	Villum Research Station	Greenland	30	81.58033	−16.60961	S

[a] M indicates master, S indicates secondary. [b] These sites use Lumex, elsewhere Tekran.

3 Hg measurements methods

3.1 Field operation

All GMOS secondary sites used the Tekran continuous mercury vapor analyzer, model 2537A/B (Tekran Instruments Corp., Toronto, Ontario, Canada) with the exception of Listvyanka site (LIS), Russia, and Nieuw Nickerie site (NIK), Suriname, which used a Lumex RA-915+ mercury analyzer. The latter provides direct continuous GEM concentrations in air flow without Hg collection on sorbent traps (Sholupov and Ganeyev, 1995; Sholupov et al., 2004). GMOS master sites used the Tekran model 2537A/B mercury vapor analyzer coupled with their speciation system model 1130 for GOM and model 1135 for particulate boundaries mercury ($PBM_{2.5}$) with fractions less than 2.5 µm in diameter to prevent large particles from depositing on the KCl-coated denuder (Gustin et al., 2015). The principles and operation of the Tekran Hg speciation system are described in Landis et al. (2002). Data were captured using either personal computers or data loggers and were submitted to the GMOS Central database network (http://www.gmos.eu/sdi). During the implementation of the GMOS global network, harmonized SOPs as well as common QA/QC protocols were developed (Munthe et al., 2011; Brown et al., 2010a, b) according to measurement practices followed within existing European and American monitoring networks and based on the most recent literature (Brown et al., 2010b; Steffen et al., 2012; Gay et al., 2013). The GMOS SOPs were reviewed by both GMOS partners and external partners as experts in this issue and finally adopted within the GMOS network (Munthe et al., 2011). Full SOPs are available online (http://www.gmos.eu/sdi) and include sections on site selection, field operations, data management, field maintenance and reporting procedures. All monitoring sites strictly followed the GMOS SOPs to harmonize operations and ensure the comparability of all results obtained worldwide. At the GMOS master sites the Hg analyzers were operated in conjunction with the Tekran 1130/1135 speciation units, and therefore the TGM/GEM data for these

sites are explicitly referred to as GEM. GEM concentrations were also provided by the two secondary sites (LIS and NIK) which used the Lumex Hg analyzer (see the Lumex measurements principle in Sect. 2.2.2). Regarding the TGM/GEM at the other GMOS secondary sites, it has been discussed whether the Tekran 2537A/B instruments measure TGM = GEM + GOM or GEM only (Slemr et al., 2011, 2015); considering that previous modeling studies and experimental measurements highlighted that particularly at remote/background monitoring sites the oxidized fraction of the TGM is less than 2 % (Gustin et al., 2015), we consider the Tekran 2537A/B data to represent GEM. This is also in line with a study recently published by Slemr et al. (2015) which reports a comparison of Hg concentrations at several GMOS sites in the Southern Hemisphere. Following the SOPs implemented at all GMOS sites, the Hg analyzers used at the secondary sites were operated without the speciation units but using the PTFE (Teflon) filters to protect the instrument from sea salt and other particles intrusion. Slemr et al. (2015) assumed that the surface active GOM in the humid air of the marine boundary layer (MBL) at several GMOS secondary sites, mostly located at the coastline (i.e., Cape Point (South Africa), Cape Grim (Australia) as well as Sisal (Mexico), Nieuw Nickerie (Paramaribo), Calhau (Cabo Verde), etc.), has been filtered out together with particulate matter (PM), partly by the sea salt particles loaded PTFE filter and partly on the walls of the inlet tubing. Consequently, they assumed that measurements at the secondary sites represent GEM only and are thus directly comparable to those at remote master sites. In contrast, the observations made by Temme et al. (2003) at Troll (Antarctica) suggested that at the low temperature and humidity prevailing at this site, GOM passed the inlet tubing and the PTFE filter, thus measuring TGM and not GEM. Taking into account these findings, Slemr et al. (2015) calculated for the GMOS master site on Amsterdam Island (AMS) a value of GOM less than 1 % of TGM compared to the other secondary sites in the Southern Hemisphere, including Troll, therefore highlighting a value which is insignificant when compared with the uncertainties discussed in the available peer-reviewed literature (Slemr et al., 2015). Since we compare results at various stations, in this work we have taken into account analysis of both systematic and random uncertainties associated with the measurements as well as published results of Tekran intercomparison exercises as reported and discussed elsewhere (Slemr et al., 2015, and references there in).

3.2 GEM measurements method

Amalgamation with gold is the principle method used to sample Hg0 for atmospheric measurements worldwide (Gustin et al., 2015). The most widely used automated instrument is the Tekran 2537A/B analyzer (Tekran Instrument Corp., Ontario, Canada) which performs amalgamation on dual gold cartridges used alternately and thermal desorption (at 500 °C) to provide continuous GEM measurements. One trap is sampling while the other is heated, releasing Hg0 into an inert carrier gas (usually ultra-high-purity argon); quantification is by cold vapor atomic fluorescence spectroscopy (CVAFS) at 253.7 nm (Landis et al., 2002). Concentrations are expressed in ng m^{-3} at standard temperature and pressure (STP, 273.15 K, 1013.25 hPa). The sampling interval is between 5 and 15 min based on location logistics and meteorological conditions. Taking into account the elevation of some monitoring sites in the network (i.e., Ev-K2CNR, Nepal (5050 m a.s.l.), Mt. Waliguan, China (3816 m a.s.l.), and Concordia Station (3220 m a.s.l.)), the Tekran 2537A/B analyzers have been operated with a 15 min sample time resolution at a flow rate of 0.8 L min^{-1}. Following the SOPs the Tekran analyzers also perform automatic internal permeation source calibrations every 71 h, and the best estimate of the method detection limit is 0.1 ng m^{-3} at a flow rate of 1 L min^{-1}. The alternative automated instrument to measure continuous GEM concentrations is the Lumex RA-915AM, which is based on the use of differential atomic absorption spectrometry with direct Zeeman effect, providing a detection limit lower than 1 ng m^{-3} (Sholupov and Ganeyev, 1995; Sholupov et al., 2004). Comparison studies between the Tekran 2537 and the RA-915AM performed during EN 15852 standard development showed good agreement of the monitoring data obtained with these systems (Brown et al., 2010b).

3.3 GEM/GOM/PBM measurements method

Speciated atmospheric Hg measurements were performed using the Tekran Hg speciation system units (models 1130 and 1135) coupled to a Tekran 2537A/B analyzer. PBM and GOM concentrations are expressed in picograms per cubic meter (pg m^{-3}) at STP (273.15 K, 1013.25 hPa). At most GMOS sites, the speciation units were located on the rooftop of the station and connected to a Tekran 2537A/B analyzer through a heated PTFE line (50 °C, 10 m in length). The sampling time resolution, due to some technical/location issues, was set equal to 5, 10 and 15 min for GEM (see tables in the Supplement) and equal to 1, 2 and 3 h for GOM and PBM. Speciation measurements were performed following the GMOS SOPs and procedure as described elsewhere (Landis et al., 2002) using a size-selective impactor inlet (2.5 µm cutoff aerodynamic diameter at 10 L min^{-1}), a KCl-coated quartz annular denuder in the 1130 unit and a quartz regenerable particulate filter (RPF) in the 1135 unit.

3.4 Quality assurance and quality control procedures

In terms of network data acquisition, QA/QC implementation procedures and data management, the worldwide configuration of the GMOS network was a challenge for all scientists and site operators involved in GMOS. The traditional approaches to Hg monitoring QA/QC management

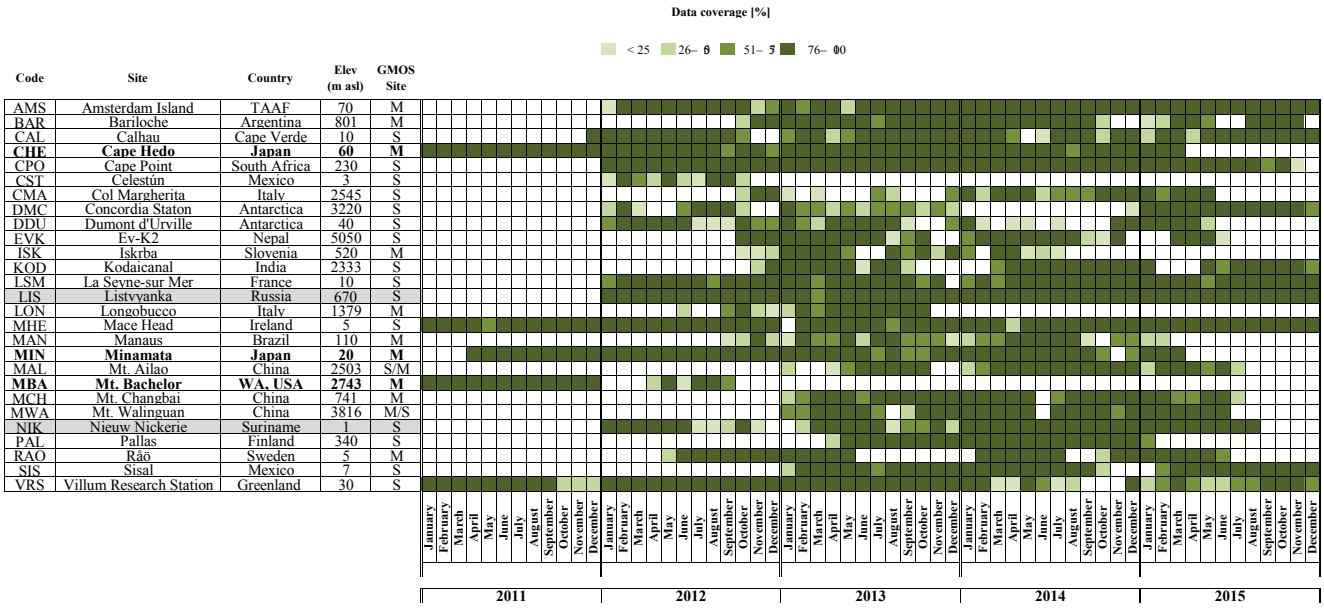

Figure 1. Coverage and consistency (%), on monthly basis, of GEM data collected at some of the ongoing GMOS secondary stations during the period 2011–2015.

that were primarily site specific and manually implemented were no longer easily applicable or sustainable when applied to a global network with the number and size of data streams generated from the monitoring stations in near real time. The G-DQM system was designed to automate the QA process, making it available on the web with a user-friendly interface to manage all the QC steps from initial data transmission through final expert validation. From the user's point of view, G-DQM is a web-based application, developed using an approach based on Software as a Service (SaaS) (D'Amore et al., 2015). G-DQM is part of the GMOS cyber-infrastructure (CI), which is a research environment that supports advanced data acquisition, storage, management, integration, mining and visualization, built on an IT infrastructure (Cinnirella et al., 2014; D'Amore et al., 2015).

4 Results and discussion

4.1 GMOS data coverage and consistency

Almost all GMOS stations provide near-real-time raw data that are archived and managed by GMOS-CI. Figures 1 and 2, over the 2011–2015 period and at some of the ongoing secondary and master GMOS stations, show the elemental and speciated Hg raw data coverage, respectively. For each station the coverage of raw data was generated considering the percentage of the real available raw data in respect to the total potential number of data points on monthly basis. During the first year of the project a number of sites were being established and/or equipped and not enough data were available to support broad network spatial analysis. In 2011 (at the effectively starting of the project) only four monitoring sites produced Hg measurements and, step by step, an increasing number of stations have been established and added to the network in 2012. Therefore, we evaluated the years 2013 and 2014 due to major data coverage (%) of the observations. In fact, our statistical evaluations/calculations are related to this period for all the ground-based sites taken into account within the GMOS network in order to harmonize the discussion and compare the results worldwide.

4.2 Northern–southern hemispheric gradients

A summary of descriptive statistics based on monthly and annual averages from all GMOS sites is presented in Tables S1 and S2 in the Supplement. The 2013 and 2014 annual mean concentrations of 1.55 and 1.51 ng m^{-3}, respectively, for the sites located in the Northern Hemisphere were calculated by averaging the 13 site means for both years. Similar calculations were made for the Southern Hemisphere and the tropics (see Tables S1 and S2). Annual mean concentrations of 1.23 and 1.22 ng m^{-3} for 2013 and 2014, respectively, were obtained in the tropical zone and 0.93 and 0.97 ng m^{-3} for the Southern Hemisphere. Figure 3 shows the GEM yearly distribution for 2013 (blue) and 2014 (green). The sites have been organized in the graphic as well as in the tables according to their latitude from those in the Northern Hemisphere to those in the tropics and in the Southern Hemisphere. The data so far do not cover a long enough timespan to investigate temporal trends, but some attempts have been previously made for the more established sites, such as Mace Head (MHD), Ireland (Ebinghaus et al., 2011; Weigelt et al., 2015), and Cape

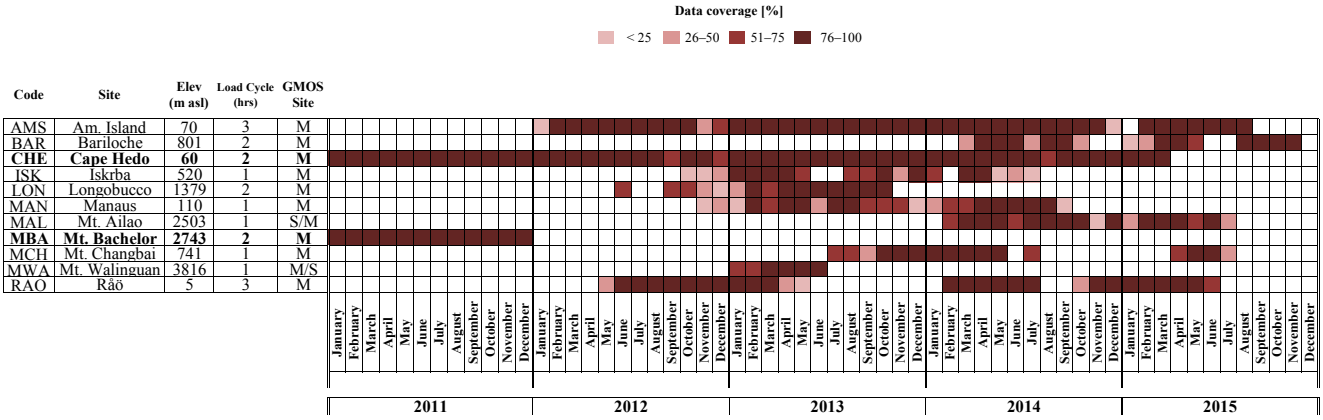

Figure 2. Coverage and consistency, on monthly basis, of GOM/PBM data collected at some of the ongoing GMOS master stations during the period 2011–2015.

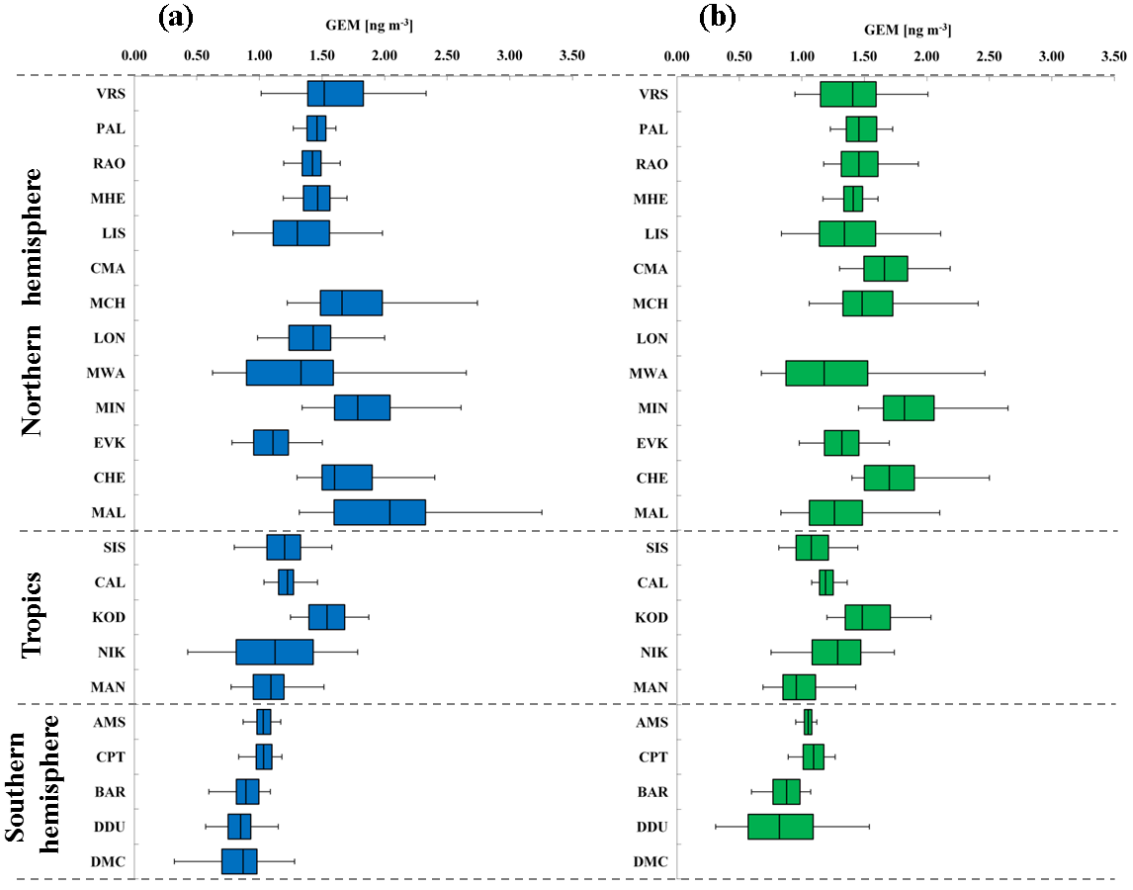

Figure 3. Box-and-whisker plots of gaseous elemental mercury yearly distribution (GEM, ng m^{-3}) at all GMOS stations for **(a)** 2013 and **(b)** 2014. The sites are organized according to their latitude from the northern to the southern locations. Each box includes the median (midline) and 25th and 75th percentiles (box edges), 5th and 95th percentiles (whiskers).

Point (CPT), South Africa (Slemr et al., 2015). At MHD the annual baseline GEM means observed by (Ebinghaus et al., 2011) decreased from 1.82 ng m^{-3} at the start of the record in 1996 to 1.4 ng m^{-3} in 2011, showing a downwards trend of 1.4–1.8 % per year. Both a downward trend of 1.6 % at MHD from 2013 and 2014 and the slight increase in Hg concentrations seen by Slemr et al. (2015) at CPT from 2007 to 2013 continued through the end of 2014. Some debate re-

mains as to whether anthropogenic emissions are increasing or decreasing (Lindberg et al., 2002; Selin et al., 2008; Pirrone et al., 2013). A clear gradient of GEM concentrations between the Northern and Southern hemispheres is seen in the data for both 2013 and 2014, in line with previous studies (Soerensen et al., 2010a, b; Sommar et al., 2010; Lindberg et al., 2007; Sprovieri et al., 2010b).

The 13 northern sites had significantly higher median concentrations than the southern sites did. The north–south gradient is clearly evident in Fig. 4 where the probability density functions (PDFs) of the data are reported. The datasets have been divided into three principal groups related to the latitude: north samples, tropical samples and south samples. The histograms, normalized to the unit area, have been constructed following the Scott rule for the bin width ΔW: $\Delta W = 3.5\sigma/\sqrt[3]{n}$, where σ represents the standard deviation and n the number of samples. This choice is optimal when dealing with normal distributed samples since it minimizes the integrated mean squared error of the density estimate and is then fitted through a normal distribution (full line in Fig. 4), obtained through the classical maximum likelihood estimation method. Since a clear overlap can be observed between the three datasets presented in Fig. 4, in order to make the distinction between the distributions clear we perform the standard Student t test against the null hypothesis (h_0) that the three distributions come from the same mother distribution with the same mean (μ_0) and unknown standard deviation (σ_0).

For every case the null hypothesis (h_0) can be rejected, as the means of the three distribution are significantly different, with a 99 % confidence level. If X_N, X_S and X_T are the mean of the experimental measures, respectively, for the northern, southern and tropical groups, the confidence intervals evaluated from the t test are reported in Table 2. The interpretations of the results clearly demonstrate that $X_N > X_T > X_S$ (Table 2), so that a significant gradient exists in the GEM concentrations from the Northern Hemisphere to the Southern Hemisphere. Due to the significant difference in the PDFs, the probability p (p value) of observing a test statistic as extreme as, or more extreme than, the observed value under the null hypothesis is close to zero. Thus the validity of the null hypothesis should be rejected. The spatial gradient observed from northern to southern regions is highlighted in both Figs. 5 and 6, which also report the statistical monthly distribution of GEM values obtained for 2013 and 2014, respectively, at all GMOS sites in the Northern and Southern hemispheres as well as in the tropical area.

4.2.1 Seasonal pattern analysis in the Northern Hemisphere

Statistics describing the spatial and temporal distribution of GEM concentrations at all GMOS sites for 2013 and 2014 are summarized in Fig. 3 whereas Figs. 5 and 6 show the monthly statistical GEM distribution for both years considered. The GEM concentrations highlight that the mean GEM values of most of the GMOS sites were between 1.3 and 1.6 ng m^{-3}, with a typical interquartile range of about 0.25 ng m^{-3}. Only a few sites have shown a mean values above 1.6 ng m^{-3}, such as MCH, MIN and MAL, and only the EVK site, located at 5050 m a.s.l. in the Eastern Himalaya of Nepal, reported mean values below 1.3 ng m^{-3}. This value is comparable with free tropospheric concentrations measured in August 2013 over Europe (Weigelt et al., 2016). The mean GEM concentration observed at EVK is less than the reported background GEM concentration for the Northern Hemisphere (1.5–1.7 ng m^{-3}) and more similar to expected background levels of GEM in the Southern Hemisphere (1.1–1.3 ng m^{-3}) (Lindberg et al., 2007; Pirrone, 2016). The values between 1.3 and 1.6 ng m^{-3} observed at the other GMOS sites in the Northern Hemisphere are comparable to the concentrations measured at the long-term monitoring stations at Mace Head, Ireland (Ebinghaus et al., 2011; Slemr et al., 2011; Weigelt et al., 2015), and Zingst, Germany (Kock et al., 2005). GEM concentration means are also in good agreement with the overall mean concentrations observed at multiple sites in the Canadian Atmospheric Mercury Measurement Network (CAMNet) (1.58 ng m^{-3}) reported by Temme et al. (2007) and those reported from Arctic stations in this pa-

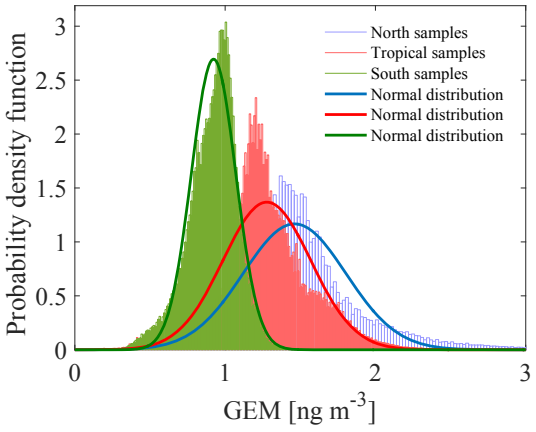

Figure 4. Probability density functions (PDFs) of the GEM data (ng m^{-3}) for the northern, southern and tropical sample groups (dash dotted lines). Full lines the normal distribution fit of the samples.

Table 2. The mean (X) of the experimental measures for the northern (X_N), southern (X_S) and tropical (X_T) groups and the confidence intervals evaluated from the Student t test among them.

Difference between means	Minimum of the confidence interval	Maximum of the confidence interval
$X_N - X_S$	0.590	0.592
$X_N - X_T$	0.225	0.229
$X_T - X_S$	0.362	0.365

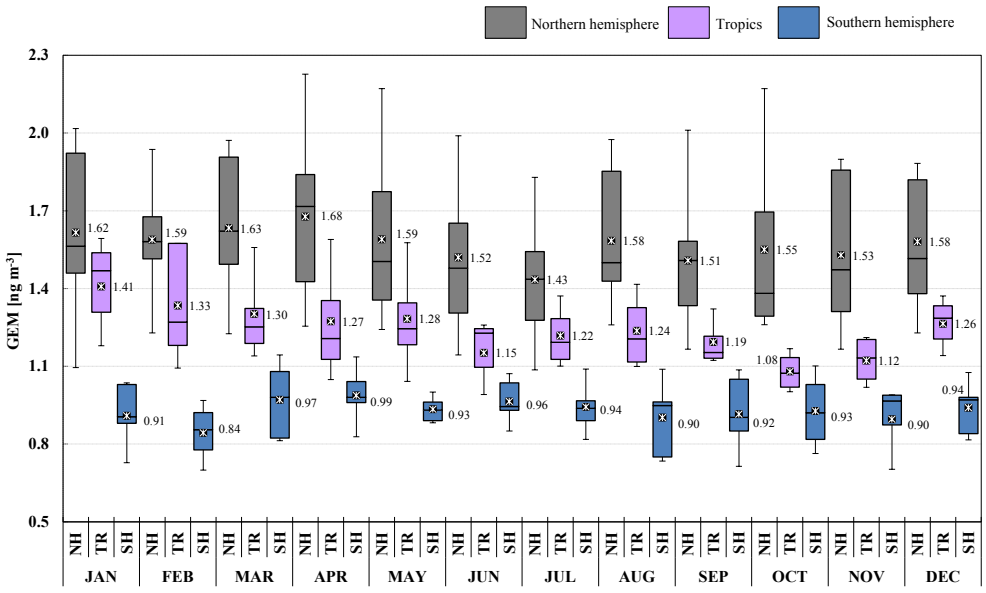

Figure 5. Monthly statistical distribution and spatial gradient for 2013 year from Northern Hemisphere to Southern Hemisphere.

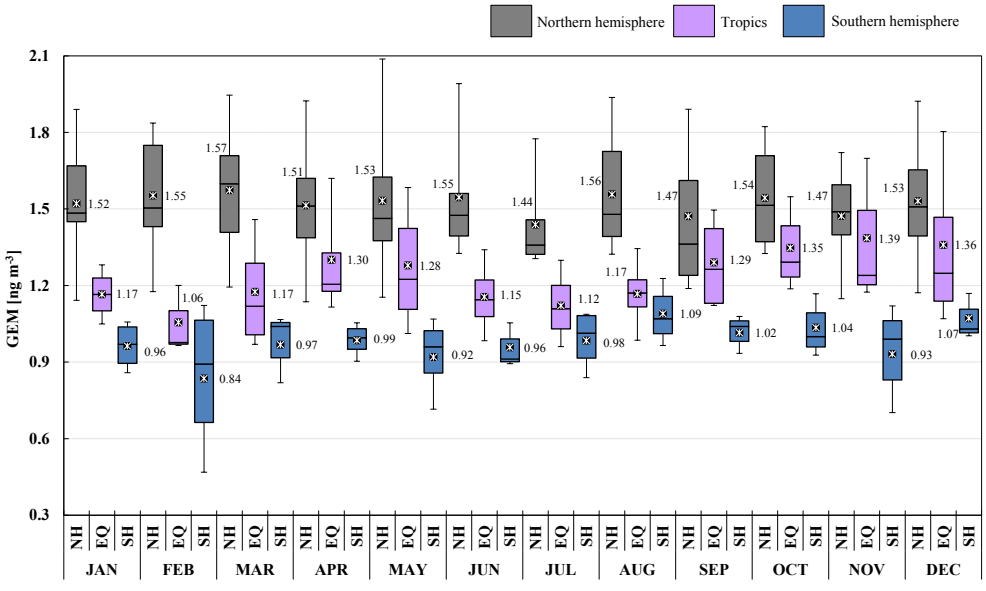

Figure 6. Monthly statistical distribution and spatial gradient for 2014 from Northern Hemisphere to Southern Hemisphere.

per (VRS, PAL). Seasonal variations of GEM concentrations have also been observed at all GMOS sites in the Northern Hemisphere. Most sites show higher concentrations during the winter and spring and lower concentrations in summer and fall seasons (Figs. 5 and 6). However, few sites such as VRS, Station Nord (northeastern Greenland: 81°36′ N, 16°40′ W), show a slightly different seasonal variation. In winter this high Arctic site (VRS) is sporadically impacted by episodic transport of pollution mainly due to high atmospheric pressure systems over Siberia and low pressure systems over the North Atlantic (Skov et al., 2004; Nguyen et al., 2013). During the spring (April–May) and summer (August–September) seasons GEM concentrations show a higher variability with low concentrations near the instrumental detection limit due to episodic atmospheric Hg depletion events (AMDEs) that occur in the spring (Skov et al., 2004; Sprovieri et al., 2005a, b; Hedgecock et al., 2008; Steffen et al., 2008; Dommergue et al., 2010a) and high GEM concentrations (2 ng m^{-3}) in June and July, probably due to GEM emissions from snow and ice surfaces (Poulain et al., 2004; Sprovieri et al., 2005a, b, 2010b; Dommergue et al., 2010b; Douglas et al., 2012) and Hg evasion from the Arc-

tic Ocean (Fisher et al., 2012; Dastoor and Durnford, 2014). Models of the MBL that simulate the temporal variations of Hg species (Hedgecock and Pirrone, 2005, 2004; Holmes et al., 2009; Soerensen et al., 2010b) show that photo-induced oxidation of GEM by Br can reproduce the diurnal variation of GOM observed in the MBL during cruise measurements better than other oxidation candidates (Hedgecock and Pirrone, 2005; Sprovieri et al., 2010a) and also the seasonal variation (Soerensen et al., 2010b). Although Br is currently considered to be the globally most important oxidant for determining the lifetime of GEM in the atmosphere, there are also other possible candidates that can enhance Hg oxidation (Hynes et al., 2009; Ariya et al., 2008; Subir et al., 2011, 2012). The lack of a full understanding of the reaction kinetics and fate of atmospheric Hg highlights the need to have a global observation system as presented here in order to calibrate and constrain atmospheric box and global/regional-scale models (Hedgecock and Pirrone, 2005; Dastoor et al., 2008).

4.2.2 GMOS sites in Asia

As can be seen in Fig. 3, the group with the highest GEM median variability and maximum concentrations is in Asia, which includes the following sites: Mt. Ailao (MAL), Mt. Changbai (MCH), Mt. Waliguan (MWA) and Minamata (MIN), where 95th percentile values ranged from 3.26 to 2.74 ng m^{-3} in 2013 (Table S2). These sites are often impacted by air masses that have crossed emission source regions (AMAP/UNEP, 2013). GEM concentrations recorded at all remote Chinese sites (MAL, MCH and MWA) are elevated compared to that observed at background/remote areas in Europe and North America, and at others sites in the Northern Hemisphere (Fu et al., 2012a, b, 2015). A previous study by Fu et al. (2012a) at MWA suggested that long-range atmospheric transport of GEM from industrial and urbanized areas in northwestern China and northwestern India contributed significantly to the elevated GEM at MWA. MAL station is located in Southwest China, at the summit of Ailao Mountain National Nature Reserve, in central Yunnan province. It is a remote station, isolated from industrial sources and populated regions in China. Kunming, one of the largest cities in Southwest China, is located 180 km to the northeast of the MAL site. The winds are dominated by the Indian summer monsoon (ISM) in warm seasons (May to October), and the site is mainly impacted by Hg emission from eastern Yunnan, western Guizhou and southern Sichuan of China and the northern part of the Indochinese Peninsula. In cold seasons the impact of emissions from India and northwestern part of the Indochinese Peninsula increased and played an important role in elevated GEM observed at MAL (Zhang et al., 2016). However, most of the important Chinese anthropogenic sources of Hg and other air pollutants are located to the north and east of the station, whereas anthropogenic emissions from southern and western Yunnan province are fairly low (Wu et al., 2006; Kurokawa et al., 2013; Zhang et al., 2016). Average atmospheric GEM concentrations during this study calculated for MWA and MAL during 2013 and 2014 are in good agreement with those observed during previous measurements at both sites from October 2007 to September 2009 at MWA and from September 2011 to March 2013 at MAL (Fu et al., 2015; Zhang et al., 2016). Also the overall mean GEM concentration observed in 2013 and 2014 at MCH background air pollution site (1.66 ± 0.48 ng m^{-3} in 2013 and 1.48 ± 0.42 ng m^{-3} in 2014, respectively) is in good agreement with the overall mean value recorded earlier from 24 October 2008 to 31 October 2010 (1.60 ± 0.51 ng m^{-3}, Fu et al., 2012b). Fu et al. (2012a) highlighted a higher mean TGM concentration of 3.58 ± 1.78 ng m^{-3} observed from August 2005 to July 2006 that was probably due to surface winds circulation with effect of regional emission sources, such as the large iron mining district in the northern part of North Korea and two large power plants and urban areas to the southwest of the sampling site.

In summary, the observed concentrations are a function of site location relative to both natural and anthropogenic sources, elevation and local conditions (i.e., meteorological parameters), often showing links to the patterns of regional air movements and long-range transport. Seasonal variations at ground-based remote sites in China have been observed. At MCH GEM was significantly higher during cold seasons compared to that recorded in warm seasons (from April to September) whereas the reverse has been observed at the other two Chinese GMOS sites.

In order to statistically check the difference of GEM concentrations among the three Chinese sites an alternative statistical test has been performed, since in this case the distributions are strongly non-normal.

As in the previous case we construct the unit-area histogram, then we fit with a log-normal distribution. It is worth noting that in this case the histograms has been constructed by manually setting the bin width ΔW. With this choice the total number of bins can be evaluated as

$$n = (X_{\max} - X_{\min})/\Delta W = 61. \quad (1)$$

By looking at Fig. 7, is easy to notice that the skewness ($\mu_3/\sigma^3 \sim 2$ where μ_3 is third-order moment of the distribution and σ is the standard deviation) and the kurtosis ($\mu_4/\mu_2^2 \sim 10$ where μ_i is the ith-order moment of the distribution) are far from being zero. In the following the alternative is briefly described. Let us consider a pair of our three time series, namely X_i ($i = 1, 2$), which corresponds to independent random samples described by the log-normal distributions. Then the random variables $Y_i = \ln(X_i)$ are close to normal distribution with means μ_i and variances σ_i^2, namely $Y_i \sim N(\mu_i, \sigma_i^2)$.

Since $\eta_i = \exp(\mu_i + 0.5\sigma_i^2)$ is the expectation value for X_i, the problem of our interest is then to test the null hy-

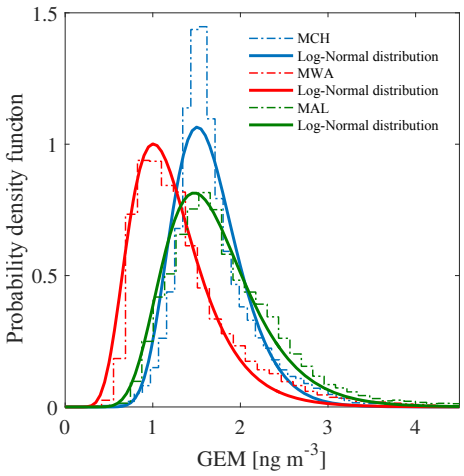

Figure 7. Probability density functions (PDFs) of the GEM data (ng m^{-3}) for the Chinese sample groups (dash dotted lines). Full lines the log-normal distribution fit of the samples.

Table 3. Differences between the η_i obtained for MCH, MWA and MAL, confidence intervals and associated p values.

Difference of η_i	Minimum of the confidence interval	Maximum of the confidence interval	P
$\eta_{MCH} - \eta_{MWA}$	0.285	0.286	1
$\eta_{MCH} - \eta_{MAL}$	0.043	0.043	1
$\eta_{MWA} - \eta_{MAL}$	0.328	0.329	1

pothesis on $\eta_2 - \eta_1$. More formally, we test $H_0 : \theta \leq 0$, where $\theta = \eta_2 - \eta_1$. In other words, we test the null hypothesis to see if there is a significant difference in the sample means. Using the algorithm described in Krishnamoorthya and Mathewb (2003) and Abdollahnezhad et al. (2012), specifically designed to perform the inference on difference of means of two log-normal distributions, we obtain the estimates for the p-values which are close to 1 and the confidence intervals, calculated at a confidence level of 95 % (reported in Table 3).

From the statistical results we can conclude that a clear distinction exists between the MWA site and the other two (MCH, MAL) as shown from the values in Table 3. However, despite the large overlap in the samples distributions of MCH and MAL the difference in their η_i (η_{MCH} and η_{MAL}, respectively) is also significant, with a smaller confidence interval.

Several hypothesis have been made to explain the seasonal variations of GEM in China, including seasonal changes in anthropogenic GEM emissions and natural emissions. The seasonal emission changes mainly resulted from coal combustion for urban and residential heating during cold seasons. This source lacks emission control devices and releases large amounts of Hg, leading to elevated GEM concentrations in the area and thus at MCH (Feng et al., 2004; Fu et al., 2008a, b, 2010). Conversely, GEM at MAL and MWA was higher in warm seasons than in cold seasons. These findings highlight that emissions from domestic heating during the winter could not explain the lower winter GEM concentrations observed at MWA and MAL, but there might be other not-yet-understood factors that played a key role in the observed GEM seasonal variations at these sites, such as the monsoonal winds influence which can change the source–receptor relationship at observational sites and subsequently the seasonal GEM trends (An, 2000; Fu et al., 2015). Among the remote Chinese sites, MAL started as secondary site and in 2014 was upgraded to a master site; conversely, MWA started as a master site and then became a secondary site whereas MCH operated continuously as a master site. Therefore, PBM and GOM concentrations have been measured during the years 2013 and 2014 at all Chinese sites even if not continuously (see Fig. 2 for Hg speciation data coverage). The GOM and PBM concentrations measured at these sites were substantially elevated compared to the background values in the Northern Hemisphere, from 1.8 to 42.8 pg m^{-3} and from 40.4 to 167.4 pg m^{-3} at the MCH and MWA, respectively, in 2013. The 2014 PBM maxima were 44.2 and 45.0 pg m^{-3} at MCH and MAL, respectively. Regional anthropogenic emissions and long-range transport from domestic source regions are likely to be the primary causes of these elevated values (Sheu et al., 2013). Seasonal variations of PBM observed at the Chinese master sites mostly showed lower concentrations in summer and higher concentrations (up to 1 order of magnitude higher) in winter and fall (Wang et al., 2006, 2007; Fu et al., 2008b; Zhu et al., 2014; Xu et al., 2015; Xiu et al., 2009; Zhang et al., 2013). The higher PBM in winter was likely caused by direct PBM emissions, formation of secondary particulate Hg via gas–particle partitioning and a lack of wet scavenging processes (Wang et al., 2006; Fu et al., 2008b; Zhu et al., 2014). PBM has an atmospheric residence time ranging from a few hours to several days and can therefore be transported to the remote sites when conditions are favorable (Sheu et al., 2013). Atmospheric PM pollution is of special concern in China due to the spatial distribution of anthropogenic emission concentrations of PM2.5 in heavily populated areas of eastern and northern China, which are among the highest in the world (van Donkelaar et al., 2010). The GOM concentrations observed at both master sites show high variability and several episodes with high GOM values were probably due to local emission sources (such as domestic heating in small settlements) rather than to long-range transport from industrial and urbanized areas (Fu et al., 2015). GOM has a shorter atmospheric residence time that limits long-range transport (Lindberg and Stratton, 1998; Pirrone et al., 2008). However, with low RH and high winds, the possibility of regional transport of GOM cannot be ruled out. For example, the observations at MWA exhibit a number of high GOM events related to air plumes originating from industrial and urbanized centers that are about 90 km east of the sampling site (Fu et al., 2012a; Pirrone, 2016). MWA is a remote site situated at the edge of the northeastern part of

the Qinghai–Xizang (Tibet) plateau. The monitoring station is relatively isolated from industrial point sources and there are no known local Hg sources around the site. Most of the Chinese industrial and populated regions associated with anthropogenic Hg emissions are situated to the east of MWA. Predominantly winds are from the west to southwest in cold seasons and the east in warm seasons (Pirrone, 2016). East Asia is, in fact, the largest Hg source region in the world, contributing to nearly 50 % of the global anthropogenic Hg emissions to the atmosphere (Streets et al., 2005, 2011; Pirrone et al., 2010; Lin et al., 2010).

4.2.3 Seasonal pattern analysis in the Southern Hemisphere

For the sites located in the Southern Hemisphere, the GEM concentrations highlight that the mean GEM values ranged between 0.84 and 1.09 ng m^{-3}, in both 2013 and 2014, with a typical interquartile range of about 0.25 ng m^{-3} (see Figs. 3, 5 and 6). The mean GEM concentrations observed at the southern sites are lower than those reported in the Northern Hemisphere but in good agreement with the southern hemispherical background (1.1 ng m^{-3}) (Lindberg et al., 2007; Sprovieri et al., 2010b; Lindberg et al., 2002; Dommergue et al., 2010b; Angot et al., 2014; Slemr et al., 2015; Soerensen et al., 2010a) and the expected range for remote sites in the Southern Hemisphere. As in the Northern Hemisphere, a seasonal variation of GEM concentrations was observed in the Southern Hemisphere. In particular, GEM concentrations from the coastal Global Atmosphere Watch station, Cape Point (CPT), South Africa, show seasonal variations with maxima during austral winter and minima in summer. The site is located in a nature reserve at the southernmost tip of the Cape Peninsula on a hill, 230 m a.s.l. It is characterized by dry summers with moderate temperatures and increased precipitation (cold fronts) during austral winter. During the summer months, biomass burning events sometimes occur within the southwestern Cape region, affecting GEM levels. The dominant wind direction at CPT is from the southeastern sector, advecting clean maritime air from the South Atlantic Ocean (Brunke et al., 2004, 2012) which occurs primarily during austral summer (December till February). Furthermore, the station is also at times subjected to air from the northern sector, mainly during austral winter. During such continental airflow events, anthropogenic emissions from the industrialized area in Gauteng, 1500 km to the northeast of CPT, can sometimes be observed (Brunke et al., 2012; Slemr et al., 2015). The GEM seasonal variability at CPT is hence in good agreement with the prevailing climatology at the site. Also GEM data at Amsterdam Island followed a similar trend, with slightly but significantly higher concentrations in winter (July–September) than in summer (December–February). Amsterdam Island is a remote and very small island of 55 km^2 with a population of about 30 residents, located in the southern Indian Ocean at 3400 and 5000 km downwind from the nearest lands, Madagascar and South Africa, respectively (Angot et al., 2014). GEM concentrations at AMS were remarkably steady with an average hourly mean concentration of 1.03 ± 0.08 ng m^{-3} and a range of 0.72–1.55 ng m^{-3}. A small seasonal cycle has been observed by Angot et al. (2014) and despite the remoteness of the island, wind sector analysis, air mass back trajectories and satellite observations suggest the presence of a long-range contribution from the southern African continent to the GEM regional/global budget from July to September during the biomass burning season extended from May to October (Angot et al., 2014). The higher GEM concentrations at AMS are comparable with those recorded at Calhau (Cabo Verde), Nieuw Nickerie (Paramaribo) and Sisal (Mexico) in the tropical zone, whereas the lower concentrations of GEM observed, less than 1 ng m^{-3}, were associated with air masses coming from southern Indian Ocean and the Antarctic continent. Bariloche (BAR) master site in North Patagonia also shows higher concentrations during the austral winter (from end of May to September) and lower concentrations in other seasons (Diéguez et al., 2015). The Patagonian site has been established inside Nahuel Huapi National Park, a well-protected natural reserve, located east of the Patagonian Andes. The area is included in the Southern Volcanic Zone (SVZ) of the Andes, under the influence of at least three active volcanoes with high eruption frequency located at the west of the Andes cordillera (Daga et al., 2014). The climate of the region is influenced by the year-round strong westerly winds blowing from the Pacific which discharge the humidity in a markedly seasonal way (fall–winter) in the western area of the park. GEM records at BAR station show background concentrations comparable to those found in Antarctica and other remote locations of the South Hemisphere with concentrations ranging between 0.2 and 1.3 ng m^{-3}, with an annual mean of 0.89 ± 0.15 ng m^{-3}. Previous records of GEM concentrations from a short-term survey in 2007 along a longitudinal transect across the Andes with Bariloche as the eastern endpoint reported concentrations below 2 ng m^{-3} close to BAR (Higueras et al., 2014). In this survey, the highest GEM concentrations were recorded in the proximity and downwind from the volcanic area, reaching concentrations up to 10 ng m^{-3} (Higueras et al., 2014). Similarly to the seasonal trends at other GMOS sites in the Southern Hemisphere, GEM concentrations were at their lowest level in summer on the Antarctic Plateau at Concordia Station (DMC, altitude 3220 m) but at their highest level in fall (Angot et al., 2016b). GEM concentrations reached levels of 1.2 ng m^{-3} from mid-February to May (fall) likely due to a low boundary layer oxidative capacity under low solar radiation limiting GEM oxidation and/or a shallow boundary layer ($\sim$ 50 m in average) limiting the dilution. In summer (November to mid-February), the DMC GEM data showed a high variability with a concentration range varying from below the detection limit to levels comparable to those recorded at midlatitude background Southern Hemisphere stations due

to an intense chemical exchange at the air/snow interface. Additionally, the mean summertime GEM concentration at DMC was ∼ 25 % lower than at other Antarctic stations in the same period of the year, suggesting a continuous oxidation of GEM as a result of the high oxidative capacity of the Antarctic plateau boundary layer in summer. GEM depletion events occurred each year in summer (January–February 2012 and 2013) with GEM concentrations remaining low (∼ 0.40 ng m^{-3}) for several weeks. These depletion events did not resemble the ones observed in the Arctic. They were not associated with depletion of ozone and occurred as air masses stagnated over the Plateau, which could favor an accumulation of oxidants within the shallow boundary layer. These observations suggest that the inland atmospheric reservoir in Antarctica is depleted in GEM and enriched in GOM in summer. Measurements at DDU on the East Antarctic coast were dramatically influenced by air masses exported from the Antarctic Plateau by strong katabatic winds (Angot et al., 2016a). These results, along with observations from earlier studies, demonstrate that, in Antarctica, the inland atmospheric reservoir can influence the cycle of atmospheric Hg at a continental scale (Sprovieri et al., 2002; Temme et al., 2003; Pfaffhuber et al., 2012; Angot et al., 2016b, a). Observations at DDU also highlighted that the Austral Ocean is a net source of GEM in summer and a net sink in spring, likely due to enhanced oxidation by halogens over sea-ice-covered areas.

4.2.4 Seasonal pattern analysis in the tropical zone

Relatively few observations of atmospheric Hg had been carried out in the tropics, before the start of GMOS. Until recently atmospheric Hg data for the tropics were only available from short-term measurement campaigns. To date, therefore, there is no information in the tropical area that can be used to establish long-term trends. Observations in this region may provide a valuable input to our understanding of key exchange processes that take place in the Hg cycle considering that the Intertropical Convergence Zone (ITCZ) passes twice each year over this region and the northern and southern hemispheric air masses may well influence the evolution of Hg concentrations observed in this region. As can be seen in Fig. 3, five GMOS sites are located in the tropics: Sisal (SIS) in Mexico, Nieuw Nickerie (NIK) in Suriname, Manaus (MAN) in Brazil, Calhau (CAL) in Cabo Verde and southern Kodaikanal (KOD) in southern India. GEM concentrations observed in 2013 and 2014 at all sites are comparable with Hg levels recorded at remote sites in the Southern Hemisphere (1.1 to 1.3 ng m^{-3}; Lindberg et al., 2007). Among these sites, the Kodaikanal site (KOD) shows the highest monthly mean GEM concentrations (see Figs. 5 and 6 as well as Tables S1 and S2) ranging between 1.25 ng m^{-3} (5th percentile) to 1.87 ng m^{-3} (95th percentile) during 2013 with an annually based statistic mean of 1.54 ± 0.20 ng m^{-3} and between 1.20 ng m^{-3} (5th percentile) to 2.03 ng m^{-3} (95th percentile) during 2014 with an annually average of 1.48 ± 0.26 ng m^{-3}. KOD is a Global Atmospheric Watch (GAW) regional site which is operated by the Indian Meteorological Department. It is worthwhile to point out that the other tropical GMOS sites are close to sea level and on the coast, whereas KOD is a high-altitude site (2333 m a.s.l.). Therefore different meteo-climatic conditions influence the long-range transport of air masses to this site. This site is also influenced by anthropogenic sources such as the well-known, but not close, Hg thermometer plant, 2150 m far away from the monitoring station at Kodaikanal (Karunasagar et al., 2006). Due to this anthropogenic influence, atmospheric Hg concentrations from 3 to 8 ng m^{-3} for the years 2000 and 2001 have been reported (Rajgopal and Mascarenhas, 2006). India is the third largest hard coal producer in the world after the People's Republic of China and the USA (Pirrone et al., 2010; Mason, 2009; Penney and Cronshaw, 2015). For the past 3 decades, India has increased the production of metals, cement, fertilizers and electricity through burning of coal, natural gas and oil, becoming one of the most rapidly growing economies (Mukherjee et al., 2009; Karunasagar et al., 2006). Relatively little attention has been paid to potential Hg pollution problems due to mining operations, metal smelting, energy and fuel consumption, which could impact on ecosystem health (Mohan et al., 2012). Hg concentrations are in fact enhanced in India due to industrial emissions of Hg mostly from coal combustion (the major source category (48 %), followed by waste disposal (31 %), the iron and steel industry, chloralkali plants, the cement industry and other minor sources (i.e., clinical thermometers) (Mukherjee et al., 2008; UNEP, 2008). Unfortunately, details of Hg emissions from these facilities and atmospheric Hg data in general are scarce. Therefore it is necessary for India as well as for the other place in the world where Hg measurement are yet lacking to generate continuous data, which can then be used by scientists for modeling applications to improve emission inventories in order to prevent inaccurate assessments of Hg emission and deposition.

GEM levels observed at Sisal (SIS), Mexico, were below the expected global average concentration (∼ 1.5 ng m^{-3}). Monthly mean GEM concentrations ranged between 1.0 and 1.47 ng m^{-3} in 2013 with an annual average of 1.20 ± 0.24 ng m^{-3} (5th and 95th percentiles: 0.8 and 1.58 ng m^{-3}), whereas in 2014 the range varied from 0.82 to 1.45 ng m^{-3}, with an annual average of 1.11 ± 0.37 ng m^{-3} (5th and 95th percentiles: 0.82 and 1.45 ng m^{-3}). GEM measurements at SIS showed, in addition, very little variability over the sampling period, indicating that this relatively remote site on the Yucatán Peninsula was not subject to any significant anthropogenic sources of Hg at all. During 2013 and 2014, the SIS site was typically influenced by the marine air originating from the Atlantic Ocean before entering the Gulf of Mexico (Sena et al., 2015). Average GEM concentrations reported at SIS are lower than those recorded in other rural places in Mexico, such as Puerto Angel (on the Pacific

coast in Oaxaca state) and Huejutla (a rural area in the state of Hidalgo), where average values of 1.46 and 1.32 ng m^{-3} were determined, respectively (de la Rosa et al., 2004). Low GEM concentrations were recorded in 2013 during the later part of the wet season (July/October). Those values may indicate a slight decrease, probably due to deposition processes since the site is a coastal station and subject to frequent episodes with high humidity caused by rain (Sprovieri et al., 2016). These findings have also been confirmed through wind roses and backward trajectories that show the predominant wind direction from east-southeast most of the time and sometimes from east-northeast (Atlantic Ocean) (Sprovieri et al., 2016). In addition, the ITCZ moves north of the Equator passing over the Yucatán peninsula during the northern hemispheric summer, causing tropical rain events which could contribute to the slight decrease of Hg concentrations. Highest GEM levels were observed during the winter period (December–January) in 2013, whereas 2014 had the lowest GEM concentration in January and higher GEM levels during spring and summer. The background Hg concentrations measured at Sisal are closely comparable to those recorded at Nieuw Nickerie (NIK), Paramaribo, Suriname, located on the northeastern coast of the South American continent, the first long-term measurement site in the tropics which has been in operation since 2007 (Müller et al., 2012). Analysis of data shows that the annual mean GEM for 2013 and 2014 at NIK are a little lower than those at SIS: 1.13 ± 0.42 and 1.28 ± 0.46 ng m^{-3}, respectively (see Tables S1 and S2). NIK is also a background site because most of the time the air masses arriving at the site come from the clean marine air of the Atlantic Ocean and the influence of possible local anthropogenic sources and continental air is minimal. As the ITCZ crosses Suriname twice each year, the NIK site samples both northern and southern hemispheric air masses. Occasionally higher values are seen: 1.57 ng m^{-3} in February/March 2013 and 1.51 in August/September 2014 (see Figs. S1 and S2). Manaus (MAN) in Amazonia (Brazil) is a GMOS master site located in the Amazon region, an area with a history of important land use change and significant artisanal and small-scale gold mining activities since the 1980s. Burning of natural vegetation to produce agriculture lands or pastures represents an important diffuse source of Hg to the atmosphere in Brazil (Lacerda et al., 2004; do Valle et al., 2005). The analysis of atmospheric Hg species at this site is thus important for the determination of the dynamics of atmospheric Hg. Annual mean Hg concentrations in 2013 and 2014 at MAN are slightly lower than those at both SIS and NIK, with little variability between the two years (see Tables S1 and S2). The measurements from MAN station may therefore suggest that although the Hg emissions from regional biomass burning and artisanal and small-scale gold mining represent the major emission sources in the Amazon basin as reported in a study performed by Artaxo et al. (2000), they may not have a significant impact locally but contribute to the global Hg background (concerning Hg from biomass burning see De Simone et al. (2015). Unfortunately the emissions from both these sources are associated with large uncertainties and vary over time. Quantifying their impact in South America is extremely important and there is a strong case for expanding the number of GMOS measurement sites in the region. MAN is in fact a very remote site, inside the campus of the Embrapa Amazonia Oriental and upwind from the three main gold mining areas in the Amazon basin, which are located in Rondonia, Mato Grosso and in the south of the Parà states (Artaxo et al., 2000). Previous Hg measurements performed by Artaxo et al. (2000) during an aircraft experiment over different sites in the Amazon basin highlighted Hg concentrations between 0.5 and 2 ng m^{-3} at pristine sites (and among them also MAN) not impacted by air masses enriched with emissions from gold mining areas and/or biomass burning. Those data collected from August to September 1995 are comparable to ours observed in 2013 and 2014 at MAN during the same period, whereas other sites over areas with intense biomass burning and near areas with strong Hg emissions (Alta Floresta and Rondonia, for example) reported very high Hg levels (5–14 ng m^{-3})(Artaxo et al., 2000). These high Hg concentrations were never observed at MAN during the 2013 and 2014 period. Monthly mean GEM concentrations at MAN ranged between 1.01 and 1.18 ng m^{-3} in 2013 and between 0.94 and 1.10 ng m^{-3} in 2014. Also PBM and GOM recorded during 2013 show little variation and varied between 1.35 and 12.70 pg m^{-3} (5th and 95th percentile, respectively) with a median value of 3.17 pg m^{-3}. In 2014, the range was from 0.53 to 5.24 pg m^{-3} (5th and 95th percentile, respectively) with a median value of 1.48 pg m^{-3}. The MAN Hg concentrations therefore seem not to be influenced by regional emissions. However, a number of parameters, such as the intense air mass convection occurring in the Amazon basin and meteorological condition in general, clearly contribute to the observed Hg concentrations, and they do not necessarily reflect only regional emissions (Artaxo et al., 2000; do Valle et al., 2005). Most of the air masses that reach the site in 2013 and 2014 come from tropical Atlantic and travel for about 1500 km over pristine forest before reaching the site (Artaxo et al., 2015); the prevailing winds during the wet seasons (from January–March) were from north-northeast, northeast and east-northeast, whereas during the dry seasons (from August to October) they were from north and north-northeast as well as north-northwest (Artaxo et al., 2015).

The Cape Verde Atmospheric Observatory's Calhau Station (CAL) contributes data from the eastern tropical Atlantic Ocean, where GMOS provides the only existing dataset. CAL is an important GAW station located on Sao Vicente Island, approximately 50 m from the coastline. GEM measurements from 2012 to 2014 were broadly consistent with previously published oceanographic campaign measurements in the region, with typical Hg values between 1.1 and 1.4 ng m^{-3}. The prevailing wind was from the northeast open ocean, bringing air masses from the tropical Atlantic and

from the African continent (Mendes, 2014). Due to its relatively long residence time in the atmosphere, the ground-level background GEM concentration tends to be relatively constant over the year in tropical regions, unlike midlatitude and polar regions where a more noticeable seasonal variation has been observed. When compared with measurements from cruise campaigns from North to South Atlantic, we can see that the GEM data at CAL are similar to previously reported South Atlantic data, where Hg concentrations are lower than the northern part of the Atlantic. Monthly mean GEM concentrations in 2013 ranged from 1.12 to 1.38 ng m^{-3}, with an annually based mean of 1.22 ± 0.14 ng m^{-3} (5th and 95th percentile equal to 1.04 and to 1.46 ng m^{-3}, respectively), whereas in 2014 the monthly mean observed varied from 1.12 to 1.33 ng m^{-3}, with an annually based mean of 1.20 ± 0.09 ng m^{-3} (5th and 95th percentile equal to 1.08 and to 1.36 ng m^{-3}, respectively). The highest GEM concentrations in air originating from central Africa have been recorded at CAL when the relative humidity was lowest (occasionally during dust events) (Carpenter, 2011). All tropical GMOS sites show little atmospheric Hg variability through both the years (2013 and 2014) with small GEM fluctuations during the months, which agrees well with a relatively long atmospheric lifetime of Hg in the background troposphere and small variations in the source strength (Ebinghaus et al., 2002). However, clear diurnal cycles of Hg have been conversely observed.

5 Conclusions

The higher Hg concentrations and spatiotemporal variability observed in the Northern Hemisphere compared to the tropical area and Southern Hemisphere confirm that the majority of emissions and re-emissions are located in the Northern Hemisphere. The inter-hemispherical gradient with higher GEM concentrations in the Northern Hemisphere has remained nearly constant over the years, confirmed by the observations carried out in the Southern Hemisphere and other locations where previously GMOS Hg measurements were lacking or absent. Previous results on all cruises carried out over the oceans highlighted that in the Northern Hemisphere GEM mean values are almost generally higher than those obtained in the Southern Hemisphere, with a rather homogeneous distribution of GEM in the Southern Hemisphere. The stability of these background concentrations can be seen as evidence that the atmospheric lifetime of Hg is reasonably long to explain the extent of its dispersion but would not be in accord with the most recent theoretical and experimental studies of the reaction rates of Hg with atmospheric oxidants. The oxidation of atmospheric Hg can occur with extraordinary rapidity in the polar troposphere during the springtime Hg depletion events as well as within the MBL due to the reactions between Hg and bromine compounds, although there are other possible reactants that can enhance Hg oxidation depending upon environmental factors and setting. These uncertainties highlight several Hg issue which have to be improved to better understand the atmospheric transport and transformation mechanisms of Hg. One such issue concerns the chemical composition of the oxidized phase of atmospheric Hg, GOM and PBM, which are currently operationally defined but still not well understood. Field and laboratory studies highlighted analytical interferences within the methods currently adopted to measure oxidized Hg species which suggest the variation of the chemical compounds across space and time. This has significant implications for refining existing measurement methods and developing new techniques/methodologies capable of distinguishing between Hg compounds within different environmental compartments. Knowing the precise chemical composition of GOM would immediately provide impetus to those who study reaction kinetics to refine rate constants and reaction mechanisms as well as allow modeling studies chemical mechanisms to be verified, thus improving our understanding of the important processes characterizing the atmospheric transport and transformation of Hg. The variation of observed Hg concentration across GMOS network shows increased amplitude in areas strongly influenced by anthropogenic sources. There are, however, uncertainties in the emission estimates especially for the tropical region and the Southern Hemisphere and not enough long-term information in either areas to identify long-term trends. The lack of an advanced global emission inventory for regional- and global-scale models application represented another important objective of the GMOS network. In the last years several modeling studies have highlighted the discrepancy between modeled and observed concentrations of GEM at background sites primarily due to existing gaps in biomass burning, artisanal small-scale gold mining and open-coal bed fire contributions within the emission inventories for anthropogenic sources. Therefore, long-term atmospheric Hg measurements across the GMOS global network and additional new GMOS ground-based sites increasingly incorporated into strategic areas are crucial to continue in the next future in order to provide high-quality measurement datasets which can give new insights and information about the worldwide trends of atmospheric Hg. The overarching benefit of this coordinated Hg monitoring network would clearly be the advancement of knowledge about Hg processes on a global scale due to model/measurement comparisons, models development and validation on different spatial and temporal scales, and assessing trends with significant implications within the Task Force on Hemispheric Transport of Air Pollutants (HTAP-TF) in the context of a global model intercomparison aimed to study long-range transport pathways of pollutants and their precursors. The experience gained during GMOS, the development of SOPs for Hg monitoring and the establishment of the Spatial Data Infrastructure (SDI; http://www.gmos.eu/sdi/) (along GEOSS lines), which includes the G-DQM system, provide a template to aid coun-

tries complying with the requirements of Article 22 of the Minamata Convention.

6 Data availability

Mercury data discussed in this manuscript are reported within the GMOS central database and are available upon request at http://sdi.iia.cnr.it/geoint/publicpage/GMOS/gmos_historical.zul (GMOS Database, 2014). The GMOS database coordinated by the CNR-IIA is part of the GMOS Cyber-Infrastructure (CI), which supports advanced data acquisition, storage, management, integration, mining and visualization. All GMOS stations provide near-real-time raw data that are archived and managed for the QA/QC process by the GMOS-Data Quality Managment System (G-DQM), a web-based application which is part of the GMOS-CI, developed by the CNR-IIA in 2011, and is currently ongoing.

The Supplement related to this article is available online at doi:10.5194/acp-16-11915-2016-supplement.

Acknowledgements. The number of people and institutions to acknowledge for their great contribution during field studies is quite significant for a project like GMOS, but we greatly acknowledge the European Commission for funding GMOS as part of the FP7 (contract no. 26511). Special thanks to those research scientists and technicians that helped to set up aircraft-based platform for UTLS measurements, ground-based sites in remote locations including EV-K2 in Karakorum, Amsterdam Island and Dome C in Antarctica, and all those involved in GMOstral 1028 (IPEV) project for field logistics and technical support.

Edited by: N. Pirrone
Reviewed by: T. Dvonch, J. Pacyna, and one anonymous referee

References

Abdollahnezhad, K., Babanezhad, M., and Jafari, A. A.: Inference on Difference of Means of two Log-Normal Distributions; A Generalized Approach, Journal of Statistical and Econometric Methods, 1, 125–131, 2012.

AMAP/UNEP: Technical Background Report for the Global Mercury Assessment 2013, Tech. rep., Arctic Monitoring and Assessment Programme, Oslo, Norway/UNEP Chemicals Branch, Geneva, Switzerland, 2013.

An, Z.: The history and variability of the East Asian paleomonsoon climate, Quaternary Sci. Rev., 19, 171–187, doi:10.1016/S0277-3791(99)00060-8, 2000.

Angot, H., Barret, M., Magand, O., Ramonet, M., and Dommergue, A.: A 2-year record of atmospheric mercury species at a background Southern Hemisphere station on Amsterdam Island, Atmos. Chem. Phys., 14, 11461–11473, doi:10.5194/acp-14-11461-2014, 2014.

Angot, H., Dion, I., Vogel, N., Legrand, M., Magand, O., and Dommergue, A.: Multi-year record of atmospheric mercury at Dumont d'Urville, East Antarctic coast: continental outflow and oceanic influences, Atmos. Chem. Phys., 16, 8265–8279, doi:10.5194/acp-16-8265-2016, 2016a.

Angot, H., Magand, O., Helmig, D., Ricaud, P., Quennehen, B., Gallée, H., Del Guasta, M., Sprovieri, F., Pirrone, N., Savarino, J., and Dommergue, A.: New insights into the atmospheric mercury cycling in central Antarctica and implications on a continental scale, Atmos. Chem. Phys., 16, 8249–8264, doi:10.5194/acp-16-8249-2016, 2016b.

Ariya, P., Skov, H., Grage, M., and Goodsite, M.: Gaseous elemental mercury in the ambient atmosphere: review of the application of theoretical calculations and experimental studies for determination of reaction coefficients and mechanisms with halogens and other reactants, Adv. Quantum Chem., 55, 43–55, doi:10.1016/S0065-3276(07)00204-3, 2008.

Artaxo, P., de Campos, R., Fernandes, E., Martins, J., Xiao, Z., Lindqvist, O., Fernàndez-Jimènez, M., and Maenhaut, W.: Large scale mercury and trace element measurements in the Amazon basin, Atmos. Environ., 34, 4085–4096, 2000.

Artaxo, P., de Brito, J. F., Barbosa, H., Morais, F., Sprovieri, F., and Bencardino, M.: Mercury concentrations in Central Amazon Basin, available at: http://www.gmos.eu/public/artaxo_poster_2015.pdf (last access: 4 September 2016), 2015.

Brooks, S., Saiz-Lopez, A., Skov, H., Lindberg, S., Plane, J., and Goodsite, M.: The mass balance of mercury in the springtime arctic environment, J. Environ. Monitor., 33, L13812, doi:10.1029/2005GL025525, 2006.

Brown, R., Pirrone, N., van Hoek, C., Horvat, M., Kotnik, J., Wängberg, I., Corns, W., Bieber, E., and Sprovieri, F.: Standardization of a European measurement method for the determination of total gaseous mercury: results of the field trial campaign and determination of a measurement uncertainty and working range, Accredit. Qual. Assur., 15, 359–366, doi:10.1007/s00769-010-0636-2, 2010a.

Brown, R., Pirrone, N., van Hoek, C., Sprovieri, F., Fernandez, R., and Toté, K.: Standardisation of a European measurement method for the determination of mercury in deposition: results of the field trial campaign and determination of a measurement, J. Environ. Monitor., 12, 689–695, doi:10.1039/b924955a, 2010b.

Brunke, E.-G., Labuschagne, C., Parker, B., Scheel, H., and Whittlestone, S.: Baseline air mass selection at Cape Point, South Africa: application of ^{222}Rn and other filter criteria to CO_2, Atmos. Environ., 38, 5693–5702, doi:10.1016/j.atmosenv.2004.04.024, 2004.

Brunke, E.-G., Ebinghaus, R., Kock, H. H., Labuschagne, C., and Slemr, F.: Emissions of mercury in southern Africa derived from long-term observations at Cape Point, South Africa, Atmos. Chem. Phys., 12, 7465–7474, doi:10.5194/acp-12-7465-2012, 2012.

Carpenter, L. J.: Seasonal characteristics of tropical marine boundary layer air measured at the Cape Verde Atmospheric Observatory, J. Atmos. Chem., 67, 87–140, doi:10.1007/s10874-011-9206-1, 2011.

Cinnirella, S., D'Amore, F., Bencardino, M., Sprovieri, F., and Pirrone, N.: The GMOS cyber(e)-infrastructure: advanced services for supporting science and policy, Environ. Sci. Pollut. R., 21, 4193–4208, doi:10.1007/s11356-013-2308-3, 2014.

Daga, R., Guevara, S., Poire, D., and Arribére, M.: Characterization of tephras dispersed by the recent eruptions of volcanoes Calbuco (1961), Chaitén (2008) and Cordón Caulle Complex (1960 and 2011), in Northern Patagonia, J. S. Am. Earth Sci., 49, 1–14, doi:10.1016/j.jsames.2013.10.006, 2014.

D'Amore, F., Bencardino, M., Cinnirella, S., Sprovieri, F., and Pirrone, N.: Data quality through a web-based QA/QC system: implementation for atmospheric mercury data from the Global Mercury Observation System, Environmental Sciences: Processes and Impacts, 17, 1482–1492, doi:10.1039/C5EM00205B, 2015.

Dastoor, A. and Durnford, D.: Arctic Ocean: Is it a sink or a source of atmospheric mercury?, Environ. Sci. Technol., 48, 1707–1717, 2014.

Dastoor, A., Davignon, D., Theys, N., Roozendael, M. V., Steffen, A., and Ariya, P.: Modeling dynamic exchange of gaseous elemental mercury at polar sunrise, Environ. Sci. Technol., 42, 1482–1492, doi:10.1021/es800291w, 2008.

de la Rosa, D., Volke-Sepulveda, T., Solarzano, G., Green, C., Tordon, R., and Beauchamp, S.: Survey of atmospheric total gaseous mercury in Mexico, Atmos. Environ., 38, 4839–4846, 2004.

De Simone, F., Cinnirella, S., Gencarelli, C. N., Yang, X., Hedgecock, I. M., and Pirrone, N.: Model Study of Global Mercury Deposition from Biomass Burning, Environ. Sci. Technol., 49, 6712–6721, 2015.

De Simone, F., Cinnirella, S., Gencarelli, C. N., Carbone, F., Hedgecock, I. M., and Pirrone, N.: Particulate-Phase Mercury Emissions during Biomass Burning and Impact on Resulting Deposition: a Modelling Assessment, Atmos. Chem. Phys. Discuss., doi:10.5194/acp-2016-685, in review, 2016.

Diéguez, M., García, P., and Sprovieri, F.: Atmospheric mercury fluxes in North Patagonia: first continuous records of the EMMA station (Global Mercury Observation System, Bariloche, Argentina), in: proceedings ICMGP, 14–19 June 2015, Jeju, Republic of Korea, 2015.

Dommergue, A., Larose, C., Fain, X., Clarisse, O., Foucher, D., Hintelmann, H., Schneider, D., and Ferrari, C.: Deposition of mercury species in the Ny-Alesund area (79° N) and their transfer during snowmelt, Environ. Sci. Technol., 44, 901–907, doi:10.1021/es902579m, 2010b, 2010a.

Dommergue, A., Sprovieri, F., Pirrone, N., Ebinghaus, R., Brooks, S., Courteaud, J., and Ferrari, C. P.: Overview of mercury measurements in the Antarctic troposphere, Atmos. Chem. Phys., 10, 3309–3319, doi:10.5194/acp-10-3309-2010, 2010b.

Douglas, T., Loseto, L., MacDonald, R., Outridge, P., Dommergue, A., and Poulain, A.: The fate of mercury in Arctic terrestrial and aquatic ecosystems, a review, Environ. Chem., 9, 321–355, doi:10.1071/en11140, 2012.

do Valle, C., Santana, G., Augusti, R., EgrejaFilho, F., and Windmoller, C.: Speciation and quantification of mercury in Oxisol, Ultisol, and Spodosol from Amazon (Manaus, Brazil), Chemosphere, 58, 779–792, 2005.

Ebinghaus, R., Kock, H. H., Coggins, A. M., Spain, T. G., Jennings, S. G., and Temme, C.: Long-term measurements of atmospheric mercury at Mace Head, Irish west coast, between 1995 and 2001, Atmos. Environ., 36, 5267–5276, 2002.

Ebinghaus, R., Jennings, S., Kock, H., Derwent, R., Manning, A., and Spain, T.: Decreasing trends in total gaseous mercury observations in baseline air at Mace Head, Ireland from 1996 to 2009, Atmos. Environ., 45, 3475–3480, 2011.

Feng, X., Shang, L., Wang, S., Tang, S., and Zheng, W.: Temporal variation of total gaseous mercury in the air of Guiyang, China, J. Geophys. Res.-Atmos., 109, D03303, doi:10.1029/2003JD004159, 2004.

Fisher, J. A., Jacob, D. J., Soerensen, A. L., Amos, H. M., Steffen, A., and Sunderland, E. M.: Riverine source of Arctic Ocean mercury inferred from atmospheric observations, Nat. Geosci., 5, 499–504, doi:10.1038/NGEO1478, 2012.

Fu, X., Feng, X., Zhu, W., Wang, S., and Lu, J.: Total gaseous mercury concentrations in ambient air in the eastern slope of Mt. Gongga, South-Eastern fringe of the Tibetan plateau, China, Atmos. Environ., 42, 970–979, 2008a.

Fu, X., Feng, X., Zhu, W., Zheng, W., Wang, S., and Lu, J. Y.: Total particulate and reactive gaseous mercury in ambient air on the eastern slope of the Mt. Gongga area, China, Appl. Geochem., 23, 408–418, 2008b.

Fu, X. W., Feng, X., Dong, Z. Q., Yin, R. S., Wang, J. X., Yang, Z. R., and Zhang, H.: Atmospheric gaseous elemental mercury (GEM) concentrations and mercury depositions at a high-altitude mountain peak in south China, Atmos. Chem. Phys., 10, 2425–2437, doi:10.5194/acp-10-2425-2010, 2010.

Fu, X. W., Feng, X., Liang, P., Deliger, Zhang, H., Ji, J., and Liu, P.: Temporal trend and sources of speciated atmospheric mercury at Waliguan GAW station, Northwestern China, Atmos. Chem. Phys., 12, 1951–1964, doi:10.5194/acp-12-1951-2012, 2012a.

Fu, X. W., Feng, X., Shang, L. H., Wang, S. F., and Zhang, H.: Two years of measurements of atmospheric total gaseous mercury (TGM) at a remote site in Mt. Changbai area, Northeastern China, Atmos. Chem. Phys., 12, 4215–4226, doi:10.5194/acp-12-4215-2012, 2012b.

Fu, X. W., Zhang, H., Yu, B., Wang, X., Lin, C.-J., and Feng, X. B.: Observations of atmospheric mercury in China: a critical review, Atmos. Chem. Phys., 15, 9455–9476, doi:10.5194/acp-15-9455-2015, 2015.

Gay, D. A., Schmeltz, D., Prestbo, E., Olson, M., Sharac, T., and Tordon, R.: The Atmospheric Mercury Network: measurement and initial examination of an ongoing atmospheric mercury record across North America, Atmos. Chem. Phys., 13, 11339–11349, doi:10.5194/acp-13-11339-2013, 2013.

Gencarelli, C., Simone, F. D., Hedgecock, I., Sprovieri, F., Yang, X., and Pirrone, N.: European and Mediterranean mercury modelling: Local and long-range contributions to the deposition flux, Atmos. Environ., 117, 162–168, doi:10.1016/j.atmosenv.2015.07.015, 2015.

Gencarelli, C. N., Bieser, J., Carbone, F., De Simone, F., Hedgecock, I. M., Matthias, V., Travnikov, O., Yang, X., and Pirrone, N.: Sensitivity model study of regional mercury dispersion in the atmosphere, Atmos. Chem. Phys. Discuss., doi:10.5194/acp-2016-663, in review, 2016.

GMOS Database: Land-based Monitoring Sites, available at: http://sdi.iia.cnr.it/geoint/publicpage/GMOS/gmos_historical.zul, last access: 28 December 2014.

Goodsite, M., Plane, J., and Skov, H.: A theoretical study of the oxidation of Hg^0 to $HgBr_2$ in the troposphere, Environ. Sci. Technol., 38, 1772–1776, doi:10.1021/es034680s, 2004.

Goodsite, M., Plane, J., and Skov, H.: Correction to a theoretical study of the oxidation of Hg^0 to $HgBr_2$ in the troposphere, Environ. Sci. Technol., 46, 5262–5262, doi:10.1021/es301201c, 2012.

Gustin, M. S., Amos, H. M., Huang, J., Miller, M. B., and Heidecorn, K.: Measuring and modeling mercury in the atmosphere: a critical review, Atmos. Chem. Phys., 15, 5697–5713, doi:10.5194/acp-15-5697-2015, 2015.

Hedgecock, I. and Pirrone, N.: Modelling chemical and physical processes of Hg compounds in the marine boundary layer, in: Dynamics of Mercury Pollution on Regional and Global Scales, edited by: Pirrone, N. and Mahaffey, K., Springer Verlag Publishers, Norwell, USA, 2005.

Hedgecock, I. M. and Pirrone, N.: Chasing Quicksilver: Modeling the Atmospheric Lifetime of Hg0(g) in the Marine Boundary Layer at Various Latitudes, Environ. Sci. Technol., 38, 69–76, 2004.

Hedgecock, I. M., Pirrone, N., Trunfio, G. A., and Sprovieri, F.: Integrated mercury cycling, transport, and air-water exchange (MECAWEx) model, J. Geophys. Res.-Atmos., 111, D20302, doi:10.1029/2006JD007117, 2006.

Hedgecock, I. M., Pirrone, N., and Sprovieri, F.: Chasing quicksilver northward: mercury chemistry in the Arctic troposphere, Environ. Chem., 5, 131–134, 2008.

Higueras, P., Oyarzun, R., Kotnik, J., Esbrí, J., Martínez-Coronado, A., Horvat, M., López-Berdonces, M., Llanos, W., Vaselli, O., Nisi, B., Mashyanov, N., Ryzov, V., Spiric, Z., Panichev, N., McCrindle, R., Feng, X., Fu, X., Lillo, J., Loredo, J., García, M., Alfonso, P., Villegas, K., Palacios, S., Oyarzún, J., Maturana, H., Contreras, F., Adams, M., Ribeiro-Guevara, S., Niecenski, L., Giammanco, S., and Huremović, J.: A compilation of field surveys on gaseous elemental mercury (GEM) from contrasting environmental settings in Europe, South America, South Africa and China: separating fads from facts, Environ. Geochem. Health, 36, 713–734, doi:10.1007/s10653-013-9591-2, 2014.

Holmes, C. D., Jacob, D. J., Mason, R. P., and Jaffe, D. A.: Sources and deposition of reactive gaseous mercury in the marine atmosphere, Atmos. Environ., 43, 2278–2285, 2009.

Hynes, A. J., Donohoue, D. L., Goodsite, M. E., and Hedgecock, I. M.: Our current understanding of major chemical and physical processes affecting mercury dynamics in the atmosphere and at the air-water/terrestrial interfaces, in: Mercury Fate and Transport in the Global Atmosphere: Emissions, Measurements and Models, edited by: Pirrone, N. and Mason, R. P., chap. 14, 427–457, Springer, New York, USA, 2009.

Karunasagar, D., Krishna, M. B., Anjaneyalu, Y., and Arunachalam, J.: Studies of mercury pollution in a lake due to a thermometer factory situated in a tourist resort; Kodaikanal, India, Environ. Pollut., 143, 153–158, 2006.

Kock, H., Bieber, E., Ebinghaus, R., Spain, T., and Thees, B.: Comparison of long-term trends and seasonal variations of atmospheric mercury concentrations at the two European coastal monitoring stations Mace Head, Ireland, and Zingst, Germany, Atmos. Environ., 39, 7549–7556, 2005.

Krishnamoorthya, K. and Mathewb, T.: Inferences on the means of lognormal distributions using generalized p-values and generalized confidence intervals, J. Stat. Plan. Infer., 115, 103–121, doi:10.1016/S0378-3758(02)00153-2, 2003.

Kurokawa, J., Ohara, T., Morikawa, T., Hanayama, S., Janssens-Maenhout, G., Fukui, T., Kawashima, K., and Akimoto, H.: Emissions of air pollutants and greenhouse gases over Asian regions during 2000–2008: Regional Emission inventory in ASia (REAS) version 2, Atmos. Chem. Phys., 13, 11019–11058, doi:10.5194/acp-13-11019-2013, 2013.

Lacerda, L., de Souzab, M., and Ribeiro, M.: The effects of land use change on mercury distribution in soils of Alta Floresta, Southern Amazon, Environ. Pollut., 129, 247–255, 2004.

Landis, M., Stevens, R., Schaedlich, F., and Prestbo, E.: Development and characterization of an annular denuder methodology for the measurement of divalent inorganic reactive gaseous mercury in ambient air, Environ. Sci. Technol., 36, 3000–3009, doi:10.1021/es015887t, 2002.

Lin, C.-J., Pan, L., Streets, D. G., Shetty, S. K., Jang, C., Feng, X., Chu, H.-W., and Ho, T. C.: Estimating mercury emission outflow from East Asia using CMAQ-Hg, Atmos. Chem. Phys., 10, 1853–1864, doi:10.5194/acp-10-1853-2010, 2010.

Lindberg, S. and Stratton, W.: Atmospheric mercury speciation: concentrations and behavior of reactive gaseous mercury in ambient air, Environ. Sci. Technol., 32, 49–57, doi:10.1021/es970546u, 1998.

Lindberg, S., Brooks, S., Lin, C., Scott, K., Landis, M., Stevens, R., and Goodsite, M.: Dynamic oxidation of gaseous mercury in the arctic troposphere at polar sunrise, Environ. Sci. Technol., 36, 1245–1256, 2002.

Lindberg, S., Bullock, R., Ebinghaus, R., Engstrom, D., Feng, X., Fitzgerald, W., Pirrone, N., Prestbo, E., and Seigneur, C.: A synthesis of progress and uncertainties in attributing the sources of mercury in deposition, Environ. Sci. Technol., 36, 19–33, doi:10.1579/0044-7447(2007)36[19:ASOPAU]2.0.CO;2, 2007.

Mason, R. P.: Mercury emissions from natural processes and their importance in the global mercury cycle, in: Mercury Fate and Transport in the Global Atmosphere: Emissions, Measurements and Models, edited by: Pirrone, N. and Mason, R. P., chap. 7, 173–191, Springer, New York, USA, 2009.

Mendes, N. L. S.: Total Gaseous Mercury (TGM) measurements at the Cape Verde Atmospheric Observatory (CVAO), Tech. rep., University of York, Chemistry (York), available at: http://etheses.whiterose.ac.uk/6616/ (last access: 15 June 2016), 2014.

Mohan, M., Deepa, M., Ramasamy, E., and Thomas, A.: Accumulation of mercury and other heavy metals in edible fishes of Cochin backwaters, Southwest India, Environ. Monit. Assess., 184, 4233–4245, doi:10.1007/s10661-011-2258-5, 2012.

Mukherjee, A., Bhattacharya, P., Sarkar, A., and Zevenhoven, R.: Mercury emissions from industrial sources in India, in: Mercury Fate and Transport in the Global Atmosphere: Measurements, models and policy implications, edited by: Pirrone, N. and Mason, R., UNEP, available at: http://www.unep.org/chemicalsandwaste/Portals/9/Mercury/Documents/Full_Report.pdf (last access: 10 April 2015), 2008.

Mukherjee, A. B., Bhattacharya, P., Sarkar, A., and Zevenhoven, R.: Mercury Emissions from Industrial Sources in India and its Effects in the Environment, in: Mercury Fate and Transport in the Global Atmosphere: Emissions, Measurements, and Models, edited by: Pirrone, N. and Mason, R., 3–49, Springer, New York, USA, 2009.

Müller, D., Wip, D., Warneke, T., Holmes, C. D., Dastoor, A., and Notholt, J.: Sources of atmospheric mercury in the tropics: continuous observations at a coastal site in Suriname, Atmos. Chem. Phys., 12, 7391–7397, doi:10.5194/acp-12-7391-2012, 2012.

Munthe, J., Wängberg, I., Pirrone, N., Iverfeldt, A., Ferrara, R., Ebinghaus, R., Feng, X., Gårdfeldt, K., Keeler, G., Lanzillotta,

E., Lindberg, S. E., Lu, J., Mamane, Y., Prestbo, E., Schmolke, S., Schroeder, W. H., Sommar, J., Sprovieri, F., Stevens, R. K., Stratton, W., Tuncel, G., and Urba, A.: Intercomparison of methods for sampling and analysis of atmospheric mercury species, Atmos. Environ., 35, 3007–3017, 2001.

Munthe, J., Wängberg, I., Iverfeldt, A., Lindqvist, O., Stomberg, D., Sommar, J., Gårdfeldt, K., Petersen, G., Ebinghaus, R., Prestbo, E., Larjava, K., and Siemens, V.: Distribution of atmospheric mercury species in Northern Europe: final results from the MOE project, Atmos. Environ., 37, 9–20, 2003.

Munthe, J., Sprovieri, F., Horvat, M., and Ebinghaus, R.: SOPs and QA/QC protocols regarding measurements of TGM, GEM, RGM, TPM and mercury in precipitation in cooperation with WP3, WP4 and WP5, GMOS deliverable 6.1, CNR-IIA, IVL, available at: http://www.gmos.eu (last access: 10 October 2015), 2011.

Nguyen, Q. T., Skov, H., Sørensen, L. L., Jensen, B. J., Grube, A. G., Massling, A., Glasius, M., and Nøjgaard, J. K.: Source apportionment of particles at Station Nord, North East Greenland during 2008–2010 using COPREM and PMF analysis, Atmos. Chem. Phys., 13, 35–49, doi:10.5194/acp-13-35-2013, 2013.

Pacyna, E., Pacyna, J., Sundseth, K., Munthe, J., Kindbom, K., Wilson, S., Steenhuisen, F., and Maxson, P.: Global emission of mercury to the atmosphere from anthropogenic sources in 2005 and projections to 2020, Atmos. Environ., 44, 2487–2499, doi:10.1016/j.atmosenv.2009.06.009, 2010.

Penney, K. and Cronshaw, I.: Coal in India 2015, Tech. rep., Australian Government – Department of Industry and Science, availalbe at: http://www.industry.gov.au/Office-of-the-Chief-Economist/Publications/Documents/Coal-in-India.pdf (last access: 10 May 2016), 2015.

Pfaffhuber, K. A., Berg, T., Hirdman, D., and Stohl, A.: Atmospheric mercury observations from Antarctica: seasonal variation and source and sink region calculations, Atmos. Chem. Phys., 12, 3241–3251, doi:10.5194/acp-12-3241-2012, 2012.

Pirrone, N.: GMOS DATA POLICY, available at: http://www.gmos.eu/public/GMOS-Governance_Data_Policy_rev160705.pdf (last access: 22 May 2015), 2012.

Pirrone, N.: Atmospheric mercury at High Altitude sites: transport patterns and emission source regions, Special Issue: Global Mercury Observation System – Atmosphere (GMOS-A), in preparation, 2016.

Pirrone, N., Ferrara, R., Hedgecock, I., Kallos, G., Mamane, Y., Munthe, J., Pacyna, J., Pytharoulis, I., Sprovieri, F., Voudouri, A., and Wängberg, I.: Dynamic Processes of Mercury Over the Mediterranean Region: results from the Mediterranean Atmospheric Mercury Cycle System (MAMCS) project, Atmos. Environ., 37, 21–39, doi:10.1016/S1352-2310(03)00251-6, 2003.

Pirrone, N., Hedgecock, I., and Sprovieri, F.: Atmospheric mercury, easy to spot and hard to pin down: impasse?, Atmos. Environ., 42, 8549–8551, doi:10.1016/j.atmosenv.2008.09.004, 2008.

Pirrone, N., Cinnirella, S., Feng, X., Finkelman, R., Friedli, H., Leaner, J., Mason, R., Mukherjee, A., Stracher, G., Streets, D., and Telmer, K.: Global mercury emissions to the atmosphere from natural and anthropogenic sources, in: Mercury Fate and Transport in the Global Atmosphere: Emissions, Measurements, and Models, edited by: Pirrone, N. and Mason, R., 3–49, Springer, New York, USA, 2009.

Pirrone, N., Cinnirella, S., Feng, X., Finkelman, R. B., Friedli, H. R., Leaner, J., Mason, R., Mukherjee, A. B., Stracher, G. B., Streets, D. G., and Telmer, K.: Global mercury emissions to the atmosphere from anthropogenic and natural sources, Atmos. Chem. Phys., 10, 5951–5964, doi:10.5194/acp-10-5951-2010, 2010.

Pirrone, N., Aas, W., Cinnirella, S., Ebinghaus, R., Hedgecock, I., Pacyna, J., Sprovieri, F., and Sunderland, E.: Toward the next generation of air quality monitoring: Mercury, Atmos. Environ., 80, 599–611, doi:10.1016/j.atmosenv.2013.06.053, 2013.

Poulain, A., Lalonde, J., Amyot, M., Shead, J., Raofie, F., and Ariya, P.: Redox transformations of mercury in an Arctic snowpack at springtime, Atmos. Environ., 38, 6763–6774, doi:10.1016/j.atmosenv.2004.09.013, 2004.

Rajgopal, T. and Mascarenhas, H. R. P.: Epidemiologicalsurveillance of employees in a mercury thermometer plant: An occupational health study, Indian J. Occup. Environ. Med., 10, 11–18, 2006.

Selin, N. E., Jacob, D. J., Yantosca, R. M., Strode, S., Jaeglé, L., and Sunderland, E. M.: Global 3-D land-ocean-atmosphere model for mercury: Present-day versus preindustrial cycles and anthropogenic enrichment factors for deposition, Global Biogeochem. Cy., 22, GB2011, doi:10.1029/2007GB003040, 2008.

Sena, F., Umlauf, G., Ruiz, A. A., Islas, M. R., Trejo, J. A. V., Cabrera, F. A., and Vargas, I. O.: Wet deposition and atmospheric mercury monitoring in Sisal, Yucatán, México, as part of the Global Mercury Observation System (GMOS), Tech. rep., JRC – EUROPEAN COMMISION, doi:10.2788/823558, 2015.

Sheu, G., Lin, N., Lee, C., Wang, J., Chuang, M., Wang, S., Chi, K., and Ou-Yang, C.: Distribution of atmospheric mercury in northern Southeast Asia and South China Sea during Dongsha Experiment, Atmos. Environ., 78, 174–183, doi:10.1016/j.atmosenv.2012.07.002, 2013.

Sholupov, S. and Ganeyev, A.: Zeeman atomic absorption spectrometry using high frequency modulated light polarization, Spectrochim. Acta B, 50, 1227–1236, doi:10.1016/0584-8547(95)01316-7, 1995.

Sholupov, S., Pogarev, S., Ryzhov, V., Mashyanov, N., and Stroganov, A.: Zeeman atomic absorption spectrometer RA-915+ for direct determination of mercury in air and complex matrix samples, Fuel Process. Technol., 85, 473–485, doi:10.1016/j.fuproc.2003.11.003, 2004.

Skov, H., Christensen, J. H., Goodsite, M. E., Heidam, N. Z., Jensen, B., Wåhlin, P., and Geernaert, G.: Fate of Elemental Mercury in the Arctic during Atmospheric Mercury Depletion Episodes and the Load of Atmospheric Mercury to the Arctic, Environ. Sci. Technol., 38, 2373–2382, 2004.

Skov, H., Goodsite, M., Lindberg, S., Meyers, T., Landis, M., Larsen, M., and McConville, G.: The fluxes of Reactive Gaseous mercury measured with a newly developed method using relaxed eddy accumulation, Atmos. Environ., 40, 5452–5463, doi:10.1016/j.atmosenv.2006.04.061, 2006.

Slemr, F., Brunke, E.-G., Ebinghaus, R., and Kuss, J.: Worldwide trend of atmospheric mercury since 1995, Atmos. Chem. Phys., 11, 4779–4787, doi:10.5194/acp-11-4779-2011, 2011.

Slemr, F., Angot, H., Dommergue, A., Magand, O., Barret, M., Weigelt, A., Ebinghaus, R., Brunke, E.-G., Pfaffhuber, K. A., Edwards, G., Howard, D., Powell, J., Keywood, M., and Wang, F.: Comparison of mercury concentrations measured at several sites

in the Southern Hemisphere, Atmos. Chem. Phys., 15, 3125–3133, doi:10.5194/acp-15-3125-2015, 2015.

Soerensen, A., Skov, H., Soerensen, D. J. B., and Johnson, M.: Global concentrations of gaseous elemental mercury and reactive gaseous mercury in the marine boundary layer, Environ. Sci. Technol., 44, 7425–7430, doi:10.1021/es903839n, 2010a.

Soerensen, A., Sunderland, E., Holmes, C., Jacob, D., Yantosca, R., Skov, H., Christensen, J., Strode, S., and Mason, R.: An improved global model for air-sea exchange of mercury: high concentrations over the North Atlantic, Environ. Sci. Technol., 44, 8574–8580, doi:10.1021/es102032g, 2010b.

Sommar, J., Andersson, M. E., and Jacobi, H.-W.: Circumpolar measurements of speciated mercury, ozone and carbon monoxide in the boundary layer of the Arctic Ocean, Atmos. Chem. Phys., 10, 5031–5045, doi:10.5194/acp-10-5031-2010, 2010.

Sprovieri, F., Pirrone, N., Hedgecock, I., Landis, M., and Stevens, R.: Intensive atmospheric mercury measurements at Terra Nova Bay in antarctica during November and December 2000, J. Geophys. Res., 107, ACH 20-1–ACH 20-8, doi:10.1029/2002JD002057, 2002.

Sprovieri, F., Pirrone, N., Landis, M., and Stevens, R.: Oxidation of gaseous elemental mercury to gaseous divalent mercury during 2003 polar sunrise at Ny-Alesund, Environ. Sci. Technol., 39, 9156–9165, doi:10.1021/es050965o, 2005a.

Sprovieri, F., Pirrone, N., Landis, M., and Stevens, R.: Atmospheric mercury behaviour at different altitudes at NyAlesund during Spring 2003, Atmos. Environ., 39, 7646–7656, doi:10.1016/j.atmosenv.2005.08.001, 2005b.

Sprovieri, F., Hedgecock, I. M., and Pirrone, N.: An investigation of the origins of reactive gaseous mercury in the Mediterranean marine boundary layer, Atmos. Chem. Phys., 10, 3985–3997, doi:10.5194/acp-10-3985-2010, 2010a.

Sprovieri, F., Pirrone, N., Ebinghaus, R., Kock, H., and Dommergue, A.: A review of worldwide atmospheric mercury measurements, Atmos. Chem. Phys., 10, 8245–8265, doi:10.5194/acp-10-8245-2010, 2010b.

Sprovieri, F., Gratz, L., and Pirrone, N.: Development of a ground based atmospheric monitoring network for the Global Mercury Observation System (GMOS), in: E3S web Conference, doi:10.1051/e3sconf/20130117007, 2013.

Sprovieri, F., Pirrone, N., Bencardino, M., D'Amore, F., Angot, H., Barbante, C., Brunke, E.-G., Arcega-Cabrera, F., Cairns, W., Comero, S., Diéguez, M. D. C., Dommergue, A., Ebinghaus, R., Feng, X. B., Fu, X., Garcia, P. E., Gawlik, B. M., Hageström, U., Hansson, K., Horvat, M., Kotnik, J., Labuschagne, C., Magand, O., Martin, L., Mashyanov, N., Mkololo, T., Munthe, J., Obolkin, V., Islas, M. R., Sena, F., Somerset, V., Spandow, P., Vardè, M., Walters, C., Wängberg, I., Weigelt, A., Yang, X., and Zhang, H.: Five-year records of Total Mercury Deposition flux at GMOS sites in the Northern and Southern Hemispheres, Atmos. Chem. Phys. Discuss., doi:10.5194/acp-2016-517, in review, 2016.

Steffen, A., Douglas, T., Amyot, M., Ariya, P., Aspmo, K., Berg, T., Bottenheim, J., Brooks, S., Cobbett, F., Dastoor, A., Dommergue, A., Ebinghaus, R., Ferrari, C., Gardfeldt, K., Goodsite, M. E., Lean, D., Poulain, A. J., Scherz, C., Skov, H., Sommar, J., and Temme, C.: A synthesis of atmospheric mercury depletion event chemistry in the atmosphere and snow, Atmos. Chem. Phys., 8, 1445–1482, doi:10.5194/acp-8-1445-2008, 2008.

Steffen, A., Scherz, T., Olson, M., Gay, D., and Blanchard, P.: A comparison of data quality control protocols for atmospheric mercury speciation measurements, J. Environ. Monitor., 14, 752–765, 2012.

Streets, D. G., Hao, J., Wu, Y., Jiang, J., Chan, M., Tian, H., and Feng, X.: Anthropogenic mercury emissions in China, Atmos. Environ., 39, 7789–7806, 2005.

Streets, D. G., Devane, M. K., Lu, Z., Bond, T. C., Sunderland, E. M., and Jacob, D. J.: All-Time Releases of Mercury to the Atmosphere from Human Activities, Environ. Sci. Technol., 45, 10485–10491, 2011.

Subir, M., Ariya, P. A., and Dastoor, A. P.: A review of uncertainties in atmospheric modeling of mercury chemistry I. Uncertainties in existing kinetic parameters – Fundamental limitations and the importance of heterogeneous chemistry, Atmos. Environ., 45, 5664–5676, 2011.

Subir, M., Ariya, P. A., and Dastoor, A. P.: A review of the sources of uncertainties in atmospheric mercury modeling II. Mercury surface and heterogeneous chemistry – A missing link, Atmos. Environ., 46, 1–10, 2012.

Temme, C., Einax, J. W., Ebinghaus, R., and Schroeder, W. H.: Measurements of Atmospheric Mercury Species at a Coastal Site in the Antarctic and over the South Atlantic Ocean during Polar Summer, Environ. Sci. Technol., 37, 22–31, 2003.

Temme, C., Blanchard, P., Steffen, A., Banic, C., Beauchamp, S., Poissant, L., Tordon, R., and Wiens, B.: Trend, seasonal and multivariate analysis study of total gaseous mercury data from the Canadian atmospheric mercury measurement network (CAMNet), Atmos. Environ., 41, 5423–5441, 2007.

UNEP: UNEP: Mercury fate and transport in the global atmosphere: Measurements, models and policy implications, Tech. rep., UNEP Global Mercury Partnership Mercury Air Transport and Fate Research partnership area, http://www.unep.org/gc/gc22/Document/UNEP-GC22-INF3.pdf (last access: 10 June 2016), 2008.

van Donkelaar, A., Martin, R., Brauer, M., Kahn, R., Levy, R., and Verduzco, C.: Global estimates of ambient fine particulate matter concentrations from satellite-based aerosol optical depth: development and application, Environ. Health Persp., 118, 847–855, doi:10.1289/ehp.0901623., 2010.

Wang, Z., Zhang, X., Chen, Z., and Zhang, Y.: Mercury concentrations in size-fractionated airborne particles at urban and suburban sites in Beijing, Atmos. Environ., 40, 2194–2201, doi:10.1016/j.atmosenv.2005.12.003, 2006.

Wang, Z., Chen, Z., Duan, N., and Zhang, X.: Gaseous elemental mercury concentration in atmosphere at urban and remote sites in China, J. Environ. Sci., 19, 176–180, doi:10.1016/S1001-0742(07)60028-X, 2007.

Wängberg, I., Munthe, J., Pirrone, N., Iverfeldt, A., Bahlman, E., Costa, P., Ebinghaus, R., Feng, X., Ferrara, R., Gardfeldt, K., Kock, H., Lanzillotta, E., Mamane, Y., Mas, F., Melamed, E., Osnat, Y., Prestbo, E., Sommar, J., Schmolke, S., Spain, G., Sprovieri, F., and Tuncel, G.: Atmospheric mercury distribution in Northern Europe and in the Mediterranean region, Atmos. Environ., 35, 3019–3025, 2001.

Wängberg, I., Munthe, J., Amouroux, D., Andersson, M., Fajon, V., Ferrara, R., Gårdfeldt, K., Horvat, M., Mamane, Y., Melamed, E., Monperrus, M., Ogrinc, N., Yossef, O., Pirrone, N., Sommar, J.,

and Sprovieri, F.: Atmospheric mercury at mediterranean coastal stations, Environ. Fluid Mech., 8, 101–116, 2008.

Weigelt, A., Ebinghaus, R., Manning, A., Derwent, R., Simmonds, P., Spain, T., Jennings, S., and Slemr, F.: Analysis and interpretation of 18 years of mercury observations since 1996 at Mace Head, Ireland, Atmos. Environ., 100, 85–93, doi:10.1016/j.atmosenv.2014.10.050, 2015.

Weigelt, A., Ebinghaus, R., Pirrone, N., Bieser, J., Bödewadt, J., Esposito, G., Slemr, F., van Velthoven, P. F. J., Zahn, A., and Ziereis, H.: Tropospheric mercury vertical profiles between 500 and 10 000 m in central Europe, Atmos. Chem. Phys., 16, 4135–4146, doi:10.5194/acp-16-4135-2016, 2016.

Wu, Y., Wang, S., Streets, D. G., Hao, J., Chan, M., and Jiang, J.: Trends in Anthropogenic Mercury Emissions in China from 1995 to 2003, Environ. Sci. Technol., 40, 5312–5318, 2006.

Xiu, G., Cai, J., Zhang, W., Zhang, D., Bueler, A., Lee, S., Shen, Y., Xu, L., Huang, X., and Zhang, P.: Speciated mercury in size-fractionated particles in Shanghai ambient air, Atmos. Environ., 43, 3145–3154, doi:10.1016/j.atmosenv.2008.07.044, 2009.

Xu, L., Chen, J., Yang, L., Niu, Z., Tong, L., Yin, L., and Chen, Y.: Characteristics and sources of atmospheric mercury speciation in a coastal city, Xiamen, China, Chemosphere, 119, 530–539, doi:10.1016/j.chemosphere.2014.07.024, 2015.

Zhang, H., Fu, X., Lin, C.-J., Shang, L., Zhang, Y., Feng, X., and Lin, C.: Monsoon-facilitated characteristics and transport of atmospheric mercury at a high-altitude background site in southwestern China, Atmos. Chem. Phys. Discuss., doi:10.5194/acp-2016-506, in review, 2016.

Zhang, L., Wang, S. X., Wang, L., and Hao, J. M.: Atmospheric mercury concentration and chemical speciation at a rural site in Beijing, China: implications of mercury emission sources, Atmos. Chem. Phys., 13, 10505–10516, doi:10.5194/acp-13-10505-2013, 2013.

Zhu, J., Wang, T., Talbot, R., Mao, H., Yang, X., Fu, C., Sun, J., Zhuang, B., Li, S., Han, Y., and Xie, M.: Characteristics of atmospheric mercury deposition and size-fractionated particulate mercury in urban Nanjing, China, Atmos. Chem. Phys., 14, 2233–2244, doi:10.5194/acp-14-2233-2014, 2014.

Annexe 2 : Fiche de maintenance

Onglet 1 – Id & 2537 (A REMPLIR)

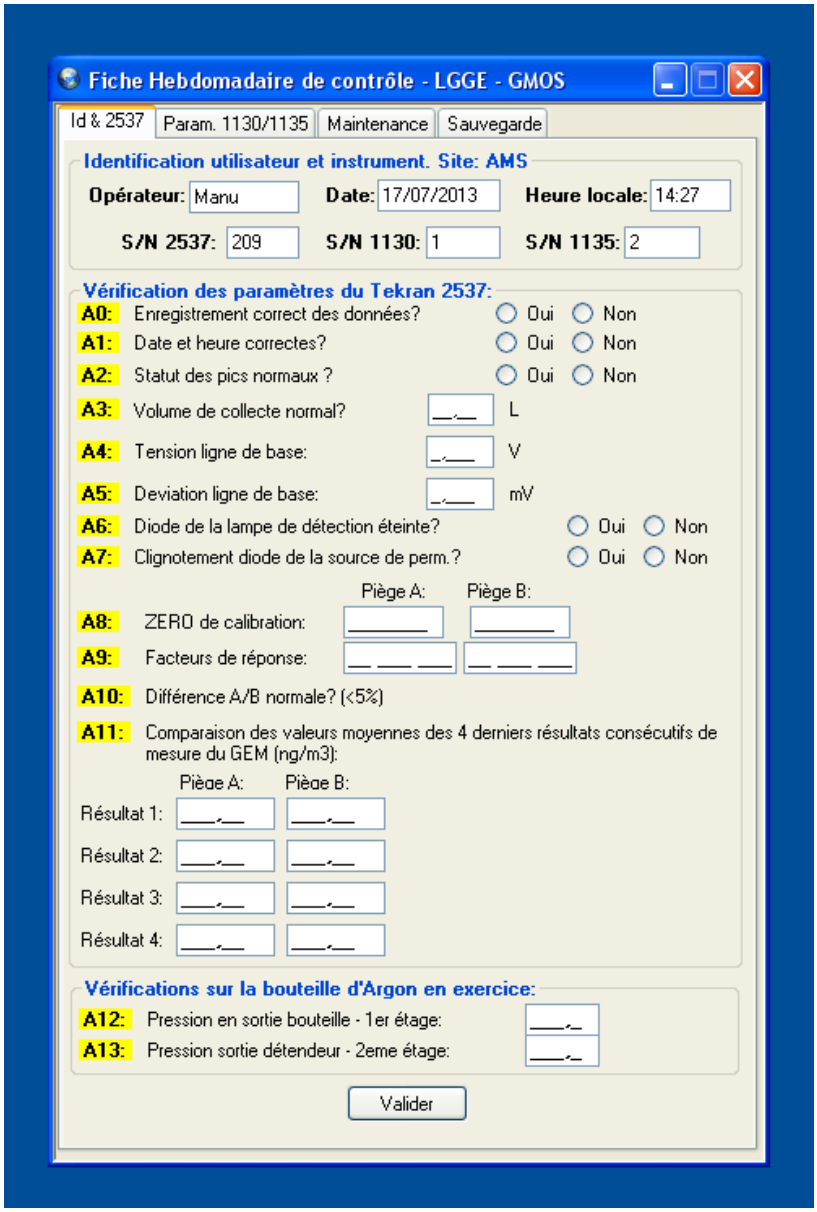

Onglet 2 – Param. 1130/1135 (NE PAS REMPLIR A AMS)

Onglet 3 – Maintenance (A REMPLIR)

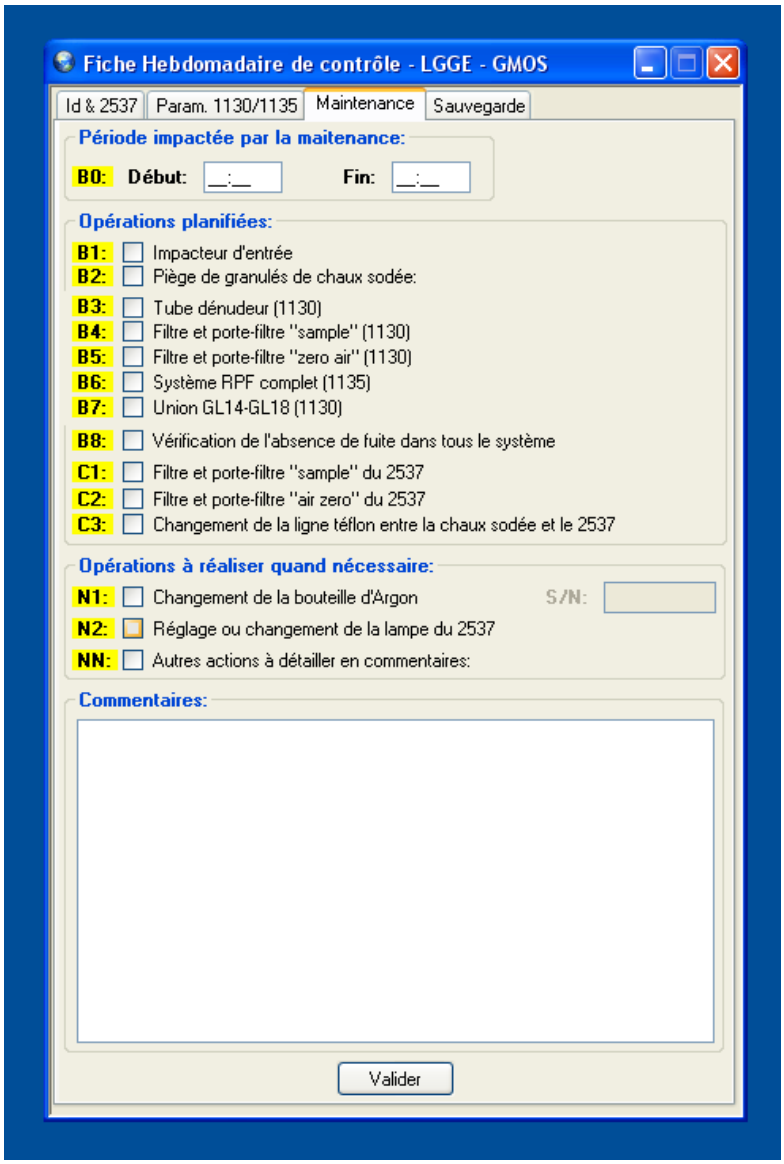

<u>Onglet 4</u> – Sauvegarde (A REMPLIR)

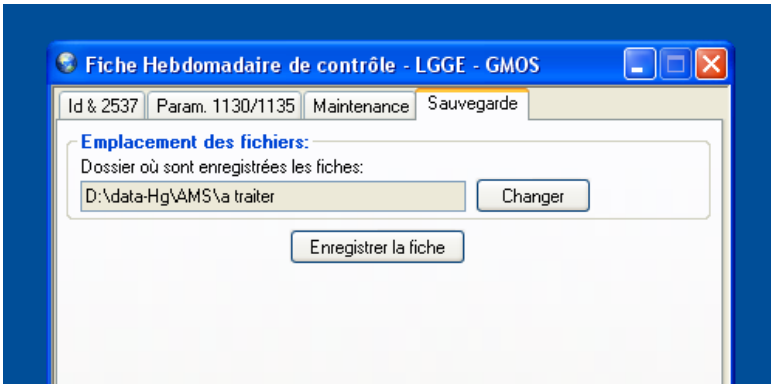

Voir directement sur site pour le dossier de stockage des fichiers de maintenance.

Annexe 3 : Protocole d'utilisation des filtres PES à AMS et DC

Compte tenu de la porosité des filtres (0,45 µm), nous estimons que le Hg(p) est collecté conjointement avec le Hg(II) par filtration. Nous mesurerions ainsi des concentrations en mercure réactif (Hg(II) + Hg(p)). Le protocole mis en place aux deux sites ainsi que les tests d'assurance qualité réalisés ou à réaliser sont décrits au sein des sections ci-après.

A. Protocole d'échantillonnage et de conservation des filtres

L'ensemble porte-filtre + filtre PES en amont de la ligne d'échantillonnage est changé toutes les deux semaines afin de permettre la collecte d'une quantité suffisante de mercure réactif pour l'analyse chimique du filtre. Après retrait de l'ensemble porte-filtre + filtre PES en place depuis deux semaines, les noix de serrage sont protégées avec du parafilm et l'ensemble est temporairement stocké dans une double gaine plastique propre. De retour au laboratoire, le filtre PES est précautionneusement retiré du porte-filtre à l'aide d'une pince PTFE propre et déposé dans une boîte de pétri propre. Après identification du filtre (numéro, date), la boîte est scotchée et parafilmée. Celle-ci est alors conservée sur site au congélateur dans une double gaine plastique thermo-soudée. Le rapatriement des filtres vers la métropole est assuré dans un container à -20 °C. L'analyse des filtres collectés à AMS et DC depuis décembre 2015 devrait débuter début 2017.

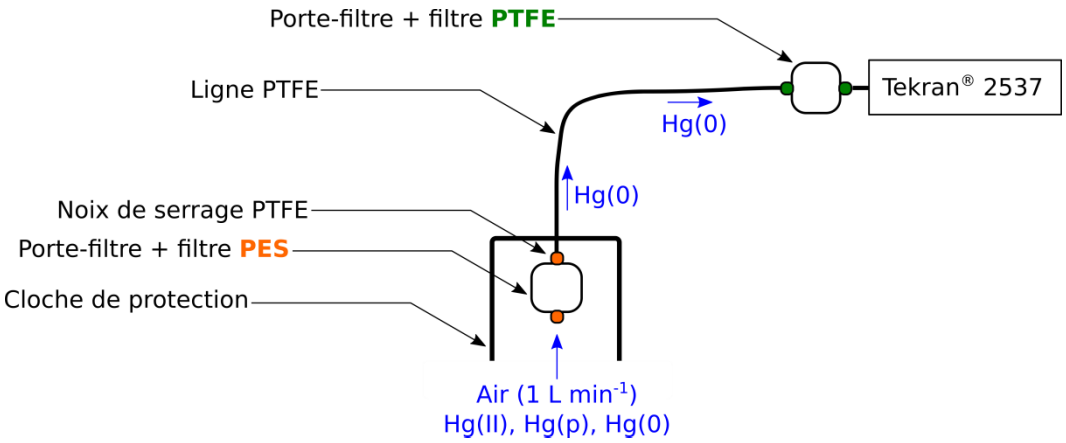

Figure 1: Schéma de la ligne d'échantillonnage et d'analyse mise en place à AMS et DC depuis décembre 2015. L'analyseur Tekran® 2537 est désormais relié à une cloche de prélèvement *via* une ligne PTFE (chauffée à AMS, non chauffée à DC). Cette cloche abrite une membrane échangeuse de cations en polyétersulfone (PES) de porosité 0,45 µm et de 47 mm de diamètre censée piéger les espèces divalentes gazeuses et particulaires. L'analyseur est en outre protégé, en amont immédiat, par un filtre PTFE de porosité 0,2 µm.

Une fois le filtre PES retiré et stocké, le porte-filtre est nettoyé selon un protocole strict incluant un trempage de 12 h dans un bain d'acide et des rinçages à l'eau milliQ et au méthanol. Un nouveau filtre PES est alors introduit à l'aide d'une pince PTFE. L'ensemble

est parafilmé et conservé dans un double sachet Ziploc® à l'abri de la lumière avant mise en place ultérieure en amont de la ligne d'échantillonnage.

B. Tests d'assurance qualité réalisés

Des blancs de terrain sont réalisés comme suit à chaque changement de l'ensemble porte-filtre + filtre PES. Après désinstallation de l'ensemble en place depuis deux semaines (voir section ci-avant), un nouvel ensemble destiné à la réalisation du blanc est mis en place. Celui-ci est laissé en place pendant 5 min mais sans pompage, c'est-à-dire sans remise en route du Tekran® 2537. Après ce laps de temps, l'ensemble porte-filtre + filtre PES est désinstallé et le filtre conservé selon le protocole décrit au sein de la section précédente. Un nouvel ensemble propre est alors mis en place afin de collecter le mercure réactif au cours des deux semaines suivantes.

Afin d'évaluer si la collecte des espèces ayant une affinité avec les filtres PES est optimale, le filtre PTFE situé en amont immédiat du Tekran® 2537 a été remplacé par un filtre PES. Pendant 4 mois (soit 8 échantillons intégrés sur deux semaines), deux filtres PES ont ainsi été mis en place en série à AMS et à DC. D'après les tests réalisés par Huang et al. (2013), la quantité de mercure réactif sur le second filtre devrait être négligeable mais ce test simple permettra de s'en assurer. Ce test ne permet en revanche pas de s'assurer que toutes les espèces divalentes présentes dans l'atmosphère sont effectivement piégées par les filtres (Figure 2).

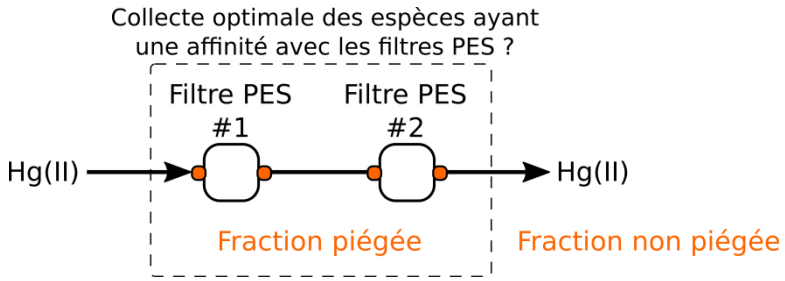

Figure 2: Schéma récapitulatif des fractions d'espèces divalentes piégées ou non par les filtres PES mis en place à AMS et DC.

Les résultats de ces différents tests devraient être connus courant 2017. Même si un gros effort a déjà été réalisé en termes d'assurance qualité, la mise en place d'un certain nombre de tests complémentaires s'avère nécessaire. Une liste (non exhaustive) e st proposée ci-après.

C. Tests d'assurance qualité à réaliser

1) Influence du mode (température, luminosité) et de la durée de conservation des filtres sur les résultats ? 2) Les filtres PES piègent-ils une fraction de Hg(0) ? 3) Les filtres PES piègent-ils l'intégralité des espèces divalentes présentes dans l'atmosphère ? 4) Influence du débit sur le taux de collecte du mercure réactif ? 5) Influence de la durée d'exposition du filtre sur le taux de collecte du mercure réactif ?

Annexe 4 : Five-year records of total mercury deposition flux at GMOS sites in the Northern and Southern Hemispheres

Sprovieri, F., Pirrone, N., Bencardino, M., D'Amore, F., **Angot, H.**, Barbante, C., Brunke, E.-G., Cabrera, F. A., Cairns, W., Comero, S., Diéguez, M. D. C., Dommergue, A., Ebinghaus, R., Feng, X. B., Fu; X., Garcia, P. E., Gawlik, B. M., Hageström, U., Hansson, K., Horvat, M., Kotnik, J., Labuschagne, C., Magand, O., Martin, L., Mashyanov, N., Mkololo, T., Munthe, J., Obolkin, V., Islas, M. R., Sena, F., Somerset, V., Spandow, P., Vardè, M., Walters, C., Wängberg, I., Weigelt, A., Yang, X., Zhang, H., Atmospheric Chemistry and Physics Discussions, doi: 10.5194/acp-2016-517, in review, 2016.

Atmos. Chem. Phys. Discuss., doi:10.5194/acp-2016-517, 2016
Manuscript under review for journal Atmos. Chem. Phys.
Published: 20 July 2016
© Author(s) 2016. CC-BY 3.0 License.

Atmospheric Chemistry and Physics Discussions

Five-year records of Total Mercury Deposition flux at GMOS sites in the Northern and Southern Hemispheres

Francesca Sprovieri[1], Nicola Pirrone[2], Mariantonia Bencardino[1], Francesco D'Amore[1], Helene Angot[3,4], Carlo Barbante[17,10], Ernst-Günther Brunke[5], Flor Arcega-Cabrera[15], Warren Cairns[17], Sara Comero[8], María del Carmen Diéguez[7], Aurélien Dommergue[3,4], Ralf Ebinghaus[6], Xin Bin Feng[12], Xuewu Fu[12], Patricia Elizabeth Garcia[7], Bernd Manfred Gawlik[8], Ulla Hageström[9], Katarina Hansson[9], Milena Horvat[11], Jože Kotnik[11], Casper Labuschagne[5], Olivier Magand[4,3], Lynwill Martin[5], Nikolay Mashyanov[13], Thumeka Mkololo[5], John Munthe[9], Vladimir Obolkin[16], Martha Ramirez Islas[14], Fabrizio Sena[8], Vernon Somerset[5], Pia Spandow[9], Massimiliano Vardè[1,17], Chavon Walters[5], Ingvar Wängberg[9], Andreas Weigelt[6], Xu Yang[12], and Hui Zhang[12]

[1]CNR Institute of Atmospheric Pollution Research, Rende, Italy
[2]CNR Institute of Atmospheric Pollution Research, Rome, Italy
[3]Univ. Grenoble Alpes, Laboratoire de Glaciologie et Géophysique de l'Environnement, Grenoble, France
[4]CNRS, Laboratoire de Glaciologie et Géophysique de l'Environnement, Grenoble, France
[5]Cape Point GAW Station, Climate and Environ. Research & Monitoring, South African Weather Service
[6]Helmholtz-Zentrum Geesthacht, Germany
[7]INIBIOMA-CONICET-UNComa, Bariloche, Argentina
[8]Joint Research Centre, Italy
[9]IVL, Swedish Environmental Research Inst. Ltd., Sweeden
[10]University Ca' Foscari of Venice, Italy
[11]Jožef Stefan Institute, Lubliana, Slovenia
[12]State Key Laboratory of Environmental Geochemistry, Inst. of Geochemistry, Chinese Academy of Sciences
[13]St. Petersburg State University, Russia
[14]Instituto Nacional de Ecología y Cambio Climático (INECC), Mexico
[15]Universidad Nacional Autónoma de México (UNAM), Unidad de Química, Sisal, Mexico
[16]Limnological Institute (LIN), Siberian Branch of the Russian Academy of Sciences (SB RAS), Russia
[17]CNR Institute for the Dynamics of Environmental Processes, Venice, Italy

Correspondence to: Francesca Sprovieri (f.sprovieri@iia.cnr.it)

Abstract. The atmospheric deposition of mercury (Hg) occurs via several mechanisms including dry and wet scavenging by precipitation events. In an effort to understand the atmospheric cycling and seasonal depositional characteristics of Hg, wet deposition samples were collected for approximately five years at 17 selected GMOS monitoring sites located in the Northern and Southern Hemispheres in the framework of the Global Mercury Observation System (GMOS) project. Total mercury (THg) exhibited annual and seasonal patterns in Hg wet deposition samples. Inter-annual differences in total wet deposition are mostly linked with precipitation volume, with the greatest deposition flux occurring in the wettest years. This data set provides a new insight into baseline concentrations of THg concentrations in precipitation worldwide, particularly in regions, such as the Southern Hemisphere and tropical areas where wet deposition as well as atmospheric Hg species were not investigated before, opening the way for future and additional simultaneous measurements across the GMOS network as well as new findings in future modeling studies.

Atmos. Chem. Phys. Discuss., doi:10.5194/acp-2016-517, 2016
Manuscript under review for journal Atmos. Chem. Phys.
Published: 20 July 2016
© Author(s) 2016. CC-BY 3.0 License.

Atmospheric Chemistry and Physics Discussions

1 Introduction

Mercury (Hg) is a persistent pollutant of global concern due to its toxicity and its capacity to bioaccumulate aquatic food chains with serious consequences on human and wildlife health (Driscoll et al., 2013). Long-range atmospheric transport is the main pathway for contamination of remote ecosystems, therefore atmospheric deposition is the primary indicator for the understanding of its impact on aquatic and terrestrial ecosystems (Schroeder and Munthe, 1998; Lindberg et al., 2002). Hg exists in the atmosphere mainly in three operationally defined forms: gaseous elemental mercury (GEM),oxidized gaseous mercury (GOM), and particulate bound mercury (PBM). Globally, GEM is the predominant form whereas GOM and PBM are thought to be rapidly dry deposited and wet scavenged by precipitation (Lindberg et al., 2007). Due to the current lack of existing direct and accurate measurements of Hg dry deposition (Gustin et al., 2012; Zhang et al., 2012), the investigation of Hg fluxes to terrestrial and aquatic surfaces in different part of the world are mainly performed by wet deposition measurements (Gratz et al., 2009; Feng et al., 2009). Hg wet deposition represents the air-to-surface flux in precipitation (Lindberg et al., 2007). Previous studies suggested that the magnitude of Hg wet deposition varies geographically and seasonally due to climatic conditions, atmospheric chemistry, and human influences i.e. emissions of Hg from anthropogenic sources (Vanarsdale et al., 2005; Selin and Jacob, 2008; Prestbo and Gay, 2009). Current annual atmospheric deposition of Hg has been estimated to be 3200 $Mg\ y^{-1}$ deposited on land and 3700 $Mg\ y^{-1}$ into oceans (Mason et al., 2012). The preindustrial deposition rate has been estimated to be 1000 $Mg\ y^{-1}$ deposited on land and 2500 $Mg\ y^{-1}$ into oceans (Selin, 2009). Developed countries in North America and Europe have reduced their anthropogenic Hg use and emissions (Hylander, 2001), but Hg use and emission are still occurring widely around the world (Pacyna et al., 2010; Pirrone et al., 2010). In North America seasonal patterns in wet deposition are observed in both depositional flux and concentration with the highest values in summer and lowest values in winter (Pacyna et al., 2010; Mason et al., 2000);(Keeler et al., 2005; Choi et al., 2008; Prestbo and Gay, 2009). Explanations for this observation include more effective Hg scavenging by rain compared to snow (Keeler et al., 2005; Selin and Jacob, 2008), and a greater availability of soluble Hg due to convective transport in summer events (Keeler et al., 2005; Strode et al., 2007, 2008). Geographic differences in Hg wet deposition may be explained in part by the proximity to atmospheric sources. Results from the National Atmospheric Deposition Program's (NADP) Mercury Deposition Network (MDN) sites in the Northeastern United States exhibit a geographic trend with southern and coastal sites receiving higher Hg concentrations and depositional fluxes (Vanarsdale et al., 2005; Prestbo and Gay, 2009) due to their location nearer to the East coast megalopolis and downwind of anthropogenic emission sources such as coal burning power plants and waste incinerators. In addition, gaseous evasion of Hg from marine waters is a significant global source of atmospheric Hg and may also contribute to elevated depositional fluxes in coastal regions (Mason and Sheu, 2002). A similar pattern exists in northern Europe with a clear gradient in atmospheric concentrations and deposition (Munthe et al., 2003). Hg wet deposition data are therefore important for verifying atmospheric models, understanding the biogeochemical cycling of Hg on a regional/global scale, and investigating ecosystem impacts. Regional monitoring networks with properly chosen monitoring sites can provide accurate estimates of wet deposition at regional scales. Long-term Hg wet deposition measurements exist at many locations within the United States as part of the MDN or in Europe as part of the EMEP program; however, before the establishment of the global Hg network by the GMOS,

Atmos. Chem. Phys. Discuss., doi:10.5194/acp-2016-517, 2016
Manuscript under review for journal Atmos. Chem. Phys.
Published: 20 July 2016
© Author(s) 2016. CC-BY 3.0 License.

Atmospheric Chemistry and Physics Discussions

Table 1. Key information on the 17 GMOS monitoring sites

		Code	Name	Country	Lat	Lon	Elev.	Collector Type	Type*
Northern Hemisphere	1	NYA	Ny-Ålesund	Norway	78,90	11,88	12	bulk-modified	M
	2	PAL	Pallas	Finland	68,00	24,24	340	bulk-modified	S
	3	RAO	Råö	Sweden	57,39	11,91	5	bulk-modified	M
	4	MHE	Mace Head	Ireland	53,33	-9,91	5	wet-only	S
	5	LIS	Listvyanka	Russia	51,85	104,89	670	wet-only	S
	6	CMA	Col Margherita	Italy	46,37	11,79	2545	bulk-modified	S
	7	ISK	Iskrba	Slovenia	45,56	14,86	520	wet-only	M
	8	MCH	Mt. Changbai	China	42,40	128,11	741	wet-only	M/S
	9	LON	Longobucco	Italy	39,39	16,61	1379	wet-only	M
	10	MWA	Mt. Waliguan	China	36,29	100,90	3816	wet-only	M
	11	MAL	Mt. Ailao	China	24,54	101,03	2503	wet-only	S/M
Tropics	12	SIS	Sisal	Mexico	21,16	-90,05	7	wet-only	S
	13	CST	Celestún	Mexico	20,86	-90,38	3	wet-only	S
Southern Hemisphere	14	AMS	Amsterdam Island	TAAF	-37,80	77,55	70	wet-only	M
	15	CPT	Cape Point	South Africa	-34,35	18,49	230	wet-only	S
	16	CGR	Cape Grim	Australia	-40,68	144,69	94	bulk-modified	S
	17	BAR	Bariloche	Argentina	-41,13	-71,42	801	wet-only	M

* M=Master;S= Secondary

long-term of ambient Hg concentrations and measurements of Hg wet deposition fluxes were lacking (Lindberg et al., 2007; Selin, 2009; Zhang and Wright, 2009). Although a number of monitoring stations have been established to better understand the impact of Hg wet deposition on ecosystems in many countries in the Northern Hemisphere (Wängberg et al., 2007; Prestbo and Gay, 2009; Sanei et al., 2010) several regions of the world (i.e., regions which are becoming increasingly impacted by anthropogenic activities in general), and prevalently the Tropical zone and the Southern Hemisphere, were lacking in wet deposition data available, in terms of concentrations and deposition Hg fluxes.

To address this concern, seasonal and annual variations of Hg wet deposition and concentration at 17 ground-based sites in the Northern and Southern Hemispheres were monitored as a part of GMOS (www.gmos.eu). Here an overview of the seasonal/annual Hg wet deposition patterns across the 17 sites, is presented, briefly examining meteorological/climatological conditions, as well as indicators of anthropogenic air mass sources and/or atmospheric chemical conditions in relation to Hg wet deposition results observed. This study is the first multi-year comparison of Hg wet deposition worldwide and provides insights into annual and seasonal variations, as well as spatial gradient in Hg deposition patterns.

Atmos. Chem. Phys. Discuss., doi:10.5194/acp-2016-517, 2016
Manuscript under review for journal Atmos. Chem. Phys.
Published: 20 July 2016
© Author(s) 2016. CC-BY 3.0 License.

Atmospheric Chemistry and Physics Discussions

Table 2. Annual wet deposition flux [$\mu g m^{-2} yr^{-1}$], cumulative rainfall amounts [mm], number of sampling days [d], weighted THg concentrations [$ng L^{-1}$] and average wet deposition flux normalized to the number of sampling days [$ng m^{-2} d^{-1}$] observed at the 17 GMOS ground-based monitoring sites for 2011 and 2012. Measures in bold are related to the calculations based on a restricted number of sampling days, therefore statistically less representative than the others

		2011					2012				
		Annual Wet Dep. Flux [$\mu g m^{-2} yr^{-1}$]	Rainfall [mm]	ndays [d]	Weighted HgT [$ng L^{-1}$]	Aver. Wet Dep. Flux [$ng m^{-2} d^{-1}$]	Annual Wet Dep. Flux [$\mu g m^{-2} yr^{-1}$]	Rainfall [mm]	ndays [d]	Weighted HgT [$ng L^{-1}$]	Aver. Wet Dep. Flux [$ng m^{-2} d^{-1}$]
Northern Hemisphere	NYA	-	-	-	-	-	0,9	238,6	350	3,8	2,6
	PAL	2,9	407,4	363	7,1	8,0	1,9	278,6	332	6,8	5,7
	RAO	5,8	646,6	364	8,9	15,8	6,5	621,8	366	10,4	17,8
	MHE	-	-	-	-	-	0,9	393,7	113	2,2	7,6
	LIS	-	-	-	-	-	**0,2**	**17,4**	**18**	**9,7**	**9,4**
	CMA	-	-	-	-	-	-	-	-	-	-
	ISK	5,1	680,2	224	7,5	22,7	8,4	1349,7	363	6,2	23,2
	MCH	2,8	264,6	119	10,6	23,6	4,8	569,4	228	8,4	21,1
	LON	-	-	-	-	-	**0,3**	**88,2**	**19**	**3,9**	**18,1**
	MWA	-	-	-	-	-	0,3	79,5	127	4,3	2,7
	MAL	4,3	1543,2	222	2,8	19,5	3,2	971,5	202	3,3	16,1
Tropics	SIS	-	-	-	-	-	-	-	-	-	-
	CST	-	-	-	-	-	2,4	297,1	155	8,1	15,5
Southern Hemisphere	AMS	-	-	-	-	-	-	-	-	-	-
	CPT	0,3	133,5	119	2,1	2,4	3,8	260,3	147	14,6	25,8
	CGR	-	-	-	-	-	-	-	-	-	-
	BAR	-	-	-	-	-	-	-	-	-	-

Table 3. Annual wet deposition flux [$\mu g m^{-2} yr^{-1}$], cumulative rainfall amounts [mm], number of sampling days [d], weighted THg concentrations [$ng L^{-1}$] and average wet deposition flux normalized to the number of sampling days [$ng m^{-2} d^{-1}$] observed at the 17 GMOS ground-based monitoring sites for 2013, 2014 and 2015. Measures in bold are related to the calculations based on a restricted number of sampling days, therefore statistically less representative than the others

		2013					2014					2015				
		Annual Wet Dep. Flux [*]	Rainfall [mm]	ndays [d]	Weighted HgT [$ng L^{-1}$]	Aver. Wet Dep. Flux [**]	Annual Wet Dep. Flux [*]	Rainfall [mm]	ndays [d]	Weighted HgT [$ng L^{-1}$]	Aver. Wet Dep. Flux [**]	Annual Wet Dep. Flux [*]	Rainfall [mm]	ndays [d]	Weighted HgT [$ng L^{-1}$]	Aver. Wet Dep. Flux [**]
Northern Hemisphere	NYA	0,9	225,4	243	4,1	3,8	1,7	293,3	357	5,7	4,7	0,8	171,7	180	4,4	4,2
	PAL	1,3	298,1	368	4,5	3,6	2,3	379,1	353	6,1	6,5	-	-	-	-	-
	RAO	4,2	515,2	365	8,2	11,5	6,3	631,6	365	9,9	17,2	-	-	-	-	-
	MHE	4,8	1048,8	363	8,2	13,3	4,1	623,3	119	6,6	34,7	-	-	-	-	-
	LIS	**0,1**	**47,5**	**8**	**2,6**	**15,6**	-	-	-	-	-	-	-	-	-	-
	CMA	-	-	-	-	-	4,4	559,5	219	7,8	20,0	-	-	-	-	-
	ISK	7,2	1364,4	350	5,3	20,6	10,0	1631,1	350	6,1	28,6	3,0	991,8	330	3,0	9,1
	MCH	1,2	300,4	121	3,9	9,6	**1,0**	**177,0**	**85**	**5,4**	**11,3**	-	-	-	-	-
	LON	3,1	472,6	208	6,6	15,0	-	-	-	-	-	-	-	-	-	-
	MWA	0,4	60,0	146	6,4	2,6	**2,2**	**144,9**	**93**	**15,0**	**23,3**	-	-	-	-	-
	MAL	5,5	1042,0	289	5,3	19,2	**0,2**	**30,0**	**66**	**6,7**	**3,0**	-	-	-	-	-
Tropics	SIS	7,4	669,6	361	11,0	20,5	6,5	712,5	368	9,1	17,7	-	-	-	-	-
	CST	**0,1**	**6,2**	**13**	**13,5**	**6,5**	-	-	-	-	-	-	-	-	-	-
Southern Hemisphere	AMS	1,95	833,2	272	2.34	7,2	1,55	864,1	328	1,80	4,7	-	-	-	-	-
	CPT	5,2	264,9	140	19,6	37,1	0,57	310,4	133	1,84	5,8	0,6	216,9	98	3,0	6,6
	CGR	3,1	775,6	290	4,0	10,6	3,8	562,3	337	6,7	11,2	3,1	477,4	247	6,5	12,6
	BAR	-	-	-	-	-	**0,1**	**258,6**	**91**	**0,4**	**1,1**	0,5	840,3	169	0,6	3,0

*uom: [$\mu g m^{-2} yr^{-1}$]
**uom: [$ng m^{-2} d^{-1}$]

Atmos. Chem. Phys. Discuss., doi:10.5194/acp-2016-517, 2016
Manuscript under review for journal Atmos. Chem. Phys.
Published: 20 July 2016
© Author(s) 2016. CC-BY 3.0 License.

Atmospheric Chemistry and Physics Discussions

2 Experimental

2.1 GMOS ground-based monitoring sites

The global Hg monitoring network has been established in the framework of the GMOS and presented in (Sprovieri et al., 2016). It has been developed by integrating previously on-going ground-based Hg monitoring stations as part of regional networks with those established as part of GMOS also in regions of the world where atmospheric Hg measurements were previously limited. To date the GMOS network consists of 43 monitoring stations worldwide distributed and located in climatically diverse regions, including polar areas (Sprovieri et al., 2016). In the present study we refer the discussion on Hg wet deposition to a representative number of 17 ground-based sites distributed in the Northern and Southern Hemispheres. Table 1 provides key information on the 17 monitoring sites such as, their location (i.e., Country, coordinates etc.), elevation (m. asl) and type of monitoring stations, Master and Secondary sites in respect to the atmospheric Hg measurements performed (Hg speciation and TGM/GEM measurements, respectively) along with THg wet deposition sampling.

2.2 Sample collection, analytical procedure, and QA/QC

Precipitation samples were collected across the sites primarily using wet-only collectors, (i.e., N-CON MDN or the Eigenbrodt NSA 171 wet-only samplers). Where necessary, due to site constraints or operator availability, few GMOS sites (Table 1) alternatively collected bulk precipitation samples. Within GMOS special attention was paid in respect to protocols harmonization, data quality collection and data management in order to assure a full comparability of site specific observational datasets. During the implementation stage of the GMOS global network, harmonized Standard Operating Procedures (SOPs) as well as common Quality Assurance/Quality Control (QA/QC) protocols have been addressed (Munthe et al., 2011) in accordance with the measurement practice adopted in well-established regional monitoring networks and based on the most recent literature (Brown et al., 2010a, b; Steffen et al., 2012; Gay et al., 2013). For THg in precipitation an ad-hoc Standard Operating Procedure has been developed and adopted within the network, and furthermore the management of the measurement program at most of the GMOS sites consisting in analysis of all precipitation samples, cleaning procedures, distribution of the sample bottles to all sites, have been performed by three reference laboratories (IVL, Sweden; CNR-IIA, Italy, and IJS, Slovenia) whereas the precipitation samples related to some other GMOS sites, in Russia (Listvyanka), in China (Mt. Walinguan, Mt. Ailao, and Mt. Changbai), and in South Africa (Cape Point) have been analyzed by local laboratories. The analytical performance and the QA/QC of the analysis carried out by the reference laboratories as well as by the local laboratories were confirmed by the results achieved during International Inter-comparison exercises for Hg in water (i.e., Brooks Rand Instruments Inter-laboratory Comparison Study). GMOS sites predominantly collected bi-weekly samples. However, considering the spatial distribution and the diversity of meteorological parameters and conditions characterizing the monitoring sites locations, the sampling frequency was sometime different across the sites. THg concentrations in precipitation samples, refrigerated and kept in the dark before the analysis (to avoid photo-induced reduction of the Hg in the precipitation sample), were determined according to the U.S. EPA Method 1631 (version E) (1631, 2002): each sample was first oxidized by BrCl (0.5 mL/100 mL sample), followed by neutralization with hydroxylamine hydrochloride ($NH_2OH \cdot HCl$). Stanneous chloride ($SnCl_2$) was

Atmos. Chem. Phys. Discuss., doi:10.5194/acp-2016-517, 2016
Manuscript under review for journal Atmos. Chem. Phys.
Published: 20 July 2016
© Author(s) 2016. CC-BY 3.0 License.

Atmospheric Chemistry and Physics Discussions

then added to the sample to reduce $Hg^{2+}_{(aq)}$ to $Hg^{0}_{(g)}$ which was quantified by Cold Vapor Atomic Fluorescence Spectrometry (CVAFS) using a Tekran Mercury Analysis System Model 2600 (Tekran Inc. Corporation, Canada). Working Hg standards solutions were obtained from a Standard Reference Material (SRM) produced by accredited laboratory (ISO/IEC 17025). Calibration standards were analyzed in the range from 0.2 to 100 ng/L (Recovery 93-109%). The standard curve was used within the coefficient of determination (r^2) greater than 0.998 (linear). Initial (IPR) and ongoing precision and recovery (OPR) solutions (5 ppt) were analyzed prior to the analysis of samples and again after every 12 samples (Recovery 91-103%). These values were within the quality control acceptance criteria for performance in the EPA Method 1631e. The method detection limit (MDL; 40 CFR 136, Appendix B) for Hg has been determined to be 0.02 ng/L. The minimum level of quantification (ML) has been established as 0.05 ng/L for THg. The QA/QC of the analysis were obtained using replicates, method blanks, field blanks, initial/ongoing precision recovery (IPR/OPR) standards, matrix spikes and certified reference materials (CRMs) with different certified Hg concentrations. Method and field blanks were always below the respective MDL, indicating minimal contamination during sampling, transport, and treatment for this study. Additionally, the sampling train materials [i.e., fluorinated polyethylene (FLPE) bottles, cylindrical glass funnels, Teflon adapters along with the glass capillary S-shaped tubes (to prevent loss of mercury from the sample) etc.] were thoroughly acid-cleaned and rinsed with ultra-pure water in the Hg laboratory before and after sampling steps, and randomly tested for Hg concentrations; they were always below the MDL. All of these materials have been triple-bagged in zip-type plastic bags to keep them clean prior to use in the field. The results of "blanks" analysis allowed us to exclude possible contamination of all samples during different steps.

2.3 Hg wet deposition flux calculation

Considering the geographical distribution of the 17 sites located at different latitude and longitude, and therefore, under different meteorological and climatologically conditions, the precipitation was not collected over an entire year at each station due to limited amount of precipitation samples occurring during specific periods (i.e., dry seasons). Therefore, Hg flux was necessarily estimated based on the volume-weighted mean (VWM) concentration and the annual total precipitation amount collected at each site. The annual THg wet deposition flux can be approximated by the following equation:

$$F_W = C_{H_{gx}} \sum_{i=1}^{i=n} P^i 1/1000$$

where F_W is the annual THg wet deposition flux ($\mu g m^{-2} yr^{-1}$),and $C_{H_{gx}}$ is the volume-weighted mean (VWM) concentration of THg (ngL^{-1}).$P^i(mm; 1mm = 1Lm^{-2})$ represents the precipitation amount associated to each wet deposition sample.

3 Hg wet deposition patterns and inter-annual variability

The annual variations in THg concentration and wet deposition recorded at all 17 monitoring GMOS sites are summarized in Tables 2 and 3. Tables 2 and 3 list the monitoring sites according to their latitude and for each site, rain amounts collected, the number of the sampling days as well as the annual wet deposition flux and average THg wet deposition flux calculated for the period 2011-2015. The latter was calculated taking into account the number of sampling days at each site for each sample.

Atmos. Chem. Phys. Discuss., doi:10.5194/acp-2016-517, 2016
Manuscript under review for journal Atmos. Chem. Phys.
Published: 20 July 2016
© Author(s) 2016. CC-BY 3.0 License.

Atmospheric Chemistry and Physics Discussions

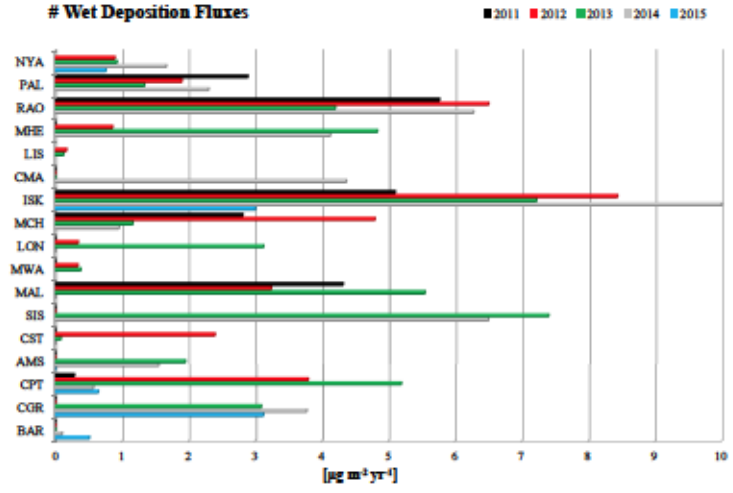

Figure 1. Annual THg wet deposition flux ($\mu gm^{-2}yr^{-1}$) during 2011 – 2015 at the 17 GMOS sites

Annual THg wet deposition fluxes are shown in Figure 1.The Hg deposition at each site tends to vary from year to year, but to a different degree at different locations. It is well known that the magnitude of Hg wet deposition varies geographically and seasonally due to different meteorological and climatic conditions, atmospheric chemistry, and anthropogenic influences (Vanarsdale et al., 2005; Selin and Jacob, 2008; Prestbo and Gay, 2009). Therefore, considering the 10 sites distributed in the Northern Hemisphere, the discussion of the results will be separately related to the seven European sites and the three Chinese sites (see Tables 2 and 3) as well as those located in the tropical area and the sites distributed in the Southern Hemisphere. Considering the THg wet deposition from 2012 to 2014 at the European sites, there appears to be a geographical trend with an increase in Hg deposition from north (Arctic area, i.e., Ny Alesund, Pallas etc.) to south in the Northern Hemisphere (i.e., Rao, Mace Head, Listvyanka, Col Margherita, Longobucco). At the Chinese sites as well as at lower latitude (i.e., Tropical area and Southern Hemisphere) no spatial trend has been observed. However, it is important to point out that the sites in the Southern Hemisphere are limited in number compared to those in the Northern Hemisphere and the data coverage is less complete for each year considered. This makes detailed evaluation of spatial trends at the southern sites difficult. In addition, apart from Cape Point (CPT), no historical records of THg deposition exist for the new stations established in the GMOS project.

The geographical trend observed at the European stations with higher deposition of Hg in southern sites than in the north is in line with emission patterns with the main source areas in central and eastern Europe. The present data in combination with ground-based atmospheric Hg measurements performed within the GMOS project during 2012 - 2015 period indicate that these findings are in good agreement with the geographical distribution of atmospheric Hg with a downward gradient from the Northern to the Southern Hemisphere (Sprovieri et al., 2016). Figure 1 shows from 2012 to 2014 (the period with

Atmos. Chem. Phys. Discuss., doi:10.5194/acp-2016-517, 2016
Manuscript under review for journal Atmos. Chem. Phys.
Published: 20 July 2016
© Author(s) 2016. CC-BY 3.0 License.

Atmospheric Chemistry and Physics Discussions

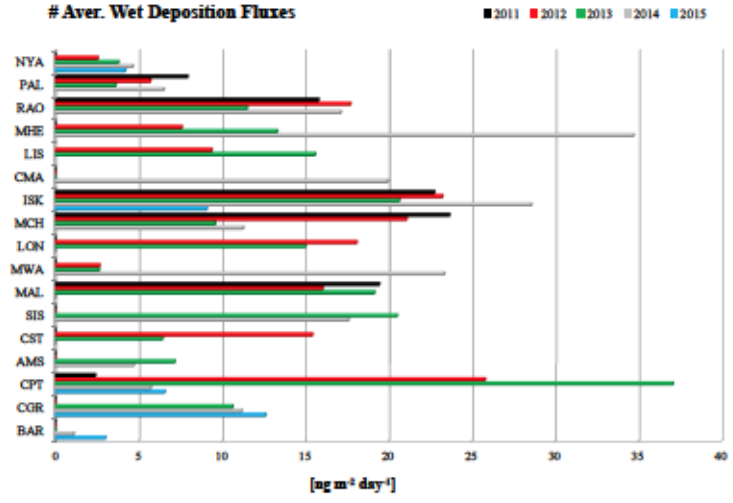

Figure 2. Average THg wet deposition Flux ($\mu gm^{-2}d^{-1}$) calculated during 2011-2015 at the 17 GMOS sites

more data coverage) a general increasing of THg wet deposition from Ny Alesund station (Norway) to Iskrba; this finding is particularly evident during the 2013 for sites at lower latitudes (i.e., Mace Head, Ireland, Col Margherita and Longobucco, Italy). This patterns is not apparent for other sites such as Listvyanka (Russia) indicating the influence of other emission sources or atmospheric transport pathways. In order to compare THg wet deposition at all sites and look for a confirmed geographical trend in Europe, average wet deposition values were calculated ($ngm^{-2}d^{-1}$) normalizing the calculations on the effective number of sampling days. The results are shown in Figure 2. Comparing annual average wet deposition flux as is shown in Figure 1, and considering for example the 2013 period common to most of European sites, all measurements performed in the Northern Hemisphere, apart Col Margherita, where data is missing for that period, generally fits into a clear south to north decreasing trend. Deposition of atmospheric Hg at any given location is influenced by factors such as: (a) atmospheric Hg concentration depending upon the local, regional and global sources; (b) site location in relation to the predominant wind direction in relation to the source areas; (c) precipitation amount which removes Hg from the atmosphere, and (d) length of precipitation events which affect Hg concentrations.

In particular, Hg concentrations appear to be higher at the beginning of a precipitation event (i.e., rain or snow), and lower at the end of a precipitation event (Keeler et al., 2005; Gratz et al., 2009; Prestbo and Gay, 2009; Chen et al., 2014). This is most evident during periods of prolonged precipitation (i.e., over a period of several days). It is obvious therefore that the Hg deposition obtained at some sites, is strongly influenced by the precipitation amounts. The annual deposition amounts during the 2011-2015 period is reported in Figure 3 which shows the influence of the precipitation amount on Hg deposition between, for example, Rao (Sweden) site and Pallas (Finland) site. The THg wet deposition fluxes recorded during 2011, 2012,

Atmos. Chem. Phys. Discuss., doi:10.5194/acp-2016-517, 2016
Manuscript under review for journal Atmos. Chem. Phys.
Published: 20 July 2016
© Author(s) 2016. CC-BY 3.0 License.

Atmospheric Chemistry and Physics Discussions

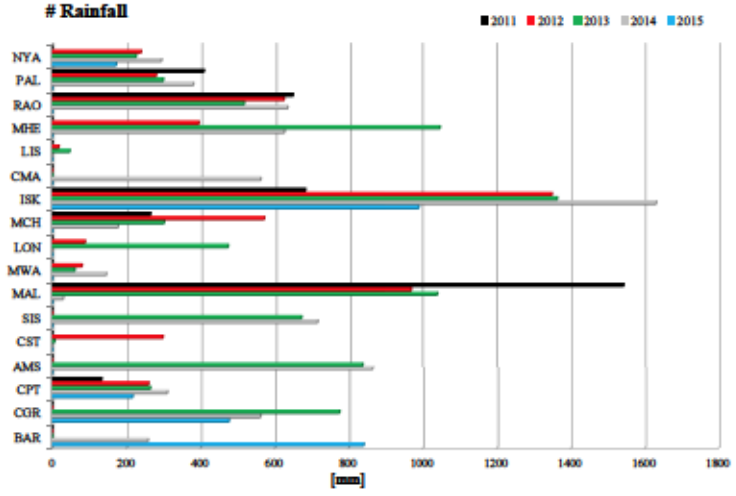

Figure 3. Precipitation amounts collected at all GMOS sites during 2011-2015

2013, and 2014 were respectively 5.8 $\mu gm^{-2}y^{-1}$, 6.5 $\mu gm^{-2}y^{-1}$, 4.2 $\mu gm^{-2}y^{-1}$,and 6.3 $\mu gm^{-2}y^{-1}$ at Rao site. This is more than two times higher than at Pallas during the same years (2.9 $\mu gm^{-2}y^{-1}$, 1.9 $\mu gm^{-2}y^{-1}$, 1.3 $\mu gm^{-2}y^{-1}$ and 2.3 $\mu gm^{-2}y^{-1}$), and since the precipitation amounts are also a factor of two higher at Rao site in comparison to Pallas, the Hg deposition results seem to be consistent with this increase in the south compared to the northern sites. These findings also confirmed the results obtained by (Munthe et al., 2007) during an assessment on available Hg data in precipitation carried out from 1996 to 2002 at five Scandinavian EMEP monitoring stations, and among them also at Rao and Pallas GMOS sites. (Munthe et al., 2007) highlights, in fact, that the highest annual Hg wet deposition and yearly averaged THg concentrations in precipitation have been recorded at the southern Scandinavian coastal sites where the highest average annual deposition amounts also occurred. The annually based THg wet deposition flux ($\mu gm^{-2}y^{-1}$) calculated, conversely, at Mt. Changbai, Mt. Walinguan and Mt. Ailao show no significant geographical trend with high variability and notable differences in concentrations among the sites during the same period. These stations are all remote sites in China, and considering the 2012, 2013, and 2014 period which is the most representative in terms of number of samples recorded, it is possible to see (Figure 2) that the averaged THg wet deposition fluxes ($ngm^{-2}d^{-1}$) in remote areas of China were not significantly higher than the values observed at the rest of the GMOS sites (i.e., ISK, MHE, RAO). At the sites located at lower latitude and Southern Hemisphere the relationship between precipitation amount and deposition was not as evident as in the Northern hemisphere. At the Sisal monitoring station (SIS), a coastal site of the Tropical area located on the Yucatan peninsula (Gulf of Mexico), the 2013 annual wet THg deposition flux was 67.34 $\mu gm^{-2}y^{-1}$ and the average wet Hg deposition flux was 20.5 $ngm^{-2}d^{-1}$ whereas the rainfall amounts was 669.6 mm which is lower than the rainfall recorded at the remote southern sites, such as Amsterdam

Atmos. Chem. Phys. Discuss., doi:10.5194/acp-2016-517, 2016
Manuscript under review for journal Atmos. Chem. Phys.
Published: 20 July 2016
© Author(s) 2016. CC-BY 3.0 License.

Atmospheric Chemistry and Physics Discussions

Island (833.6 mm rainfall), and Cape Grim (775.6 mm rainfall) where the annual wet Hg deposition flux recorded were considerably lower at 1.95 and 3.1 $\mu gm^{-2}y^{-1}$, respectively, and the average wet Hg deposition flux as well at 7.2 and 10.6 $\mu gm^{-2}y^{-1}$, respectively (see Tables 2 and 3). The 2013 and 2014 annual wet deposition flux recorded at SIS are comparable or higher than those observed at most GMOS sites in the Northern and Southern Hemisphere (Tables 2 and 3). Because of the Hg deposition at any given location is dependent upon both THg concentrations (which has a geographical component) in precipitation and precipitation amounts (Munthe et al., 2007), the results obtained across the sites located from the Tropical area to the Southern Hemisphere highlighted that in this case, the geographical component in terms of local meteorology and local emission sources, has had a higher influence on the THg results. During the sampling period SIS was typically influenced by air masses originated from Atlantic Ocean coming from east-south-east, but crossing the Caribbean Islands and/or Central/South America with occasional air masses coming from east-north-east mostly during the winter period crossing the south of Florida and Caribbean Archipelago prior to arrive at the monitoring site (Sena et al., 2015; Sprovieri et al., 2016). Very few Hg deposition measurements have been performed at tropical latitudes (Hansen and Gay, 2013; Shanley et al., 2008);(Shanley et al., 2015). (Shanley et al., 2015) in a study over seven years (2005-2012) on Hg wet deposition at Puerto Rico (Caribbean Archipelago, US) highlighted that despite receiving prevailing unpolluted air off the Atlantic Ocean from northeasterly trade winds, wet Hg deposition recorded at the site was about 30% higher than that observed in Florida and the Gulf Coast, which in turn, are the highest deposition areas in the U.S., and thus greater than at all other MDN sites. The wet Hg deposition map from the MDN, in fact, shows a general pattern of relatively low deposition over the western U.S. ($\sim 2-5\mu gm^{-2}y^{-1}$) and higher in the eastern U.S. (6-15 $\mu gm^{-2}y^{-1}$) due to increasing precipitation and location of important anthropogenic Hg sources. In addition, in the Eastern U.S. a north-south latitudinal gradient exists in wet Hg loading, with wet deposition reaching a maximum in the SE U.S. over Florida (Prestbo and Gay, 2009; Selin, 2014). Despite its unpolluted, tropical setting, Puerto Rico seems to fit as a southern extension to a latitudinal gradient of increasing Hg deposition from north to south in the eastern U.S. (Shanley et al., 2015). The high wet Hg deposition at SIS can be directly linked to the meteo-climatic conditions and pressure systems typical of the tropics. The higher THg wet deposition observed at latitudes lower than south of Florida and or Mexico, such as Puerto Rico (27.9 $\mu gm^{-2}y^{-1}$) an unpolluted tropical site crossed often by air masses detected at SIS prevalently in summer and fall and few in winter, also suggests that frequent high convective clouds in this subtropical region likely access the reservoir of oxidized Hg species in the upper free troposphere (Guentzel et al., 2001; Driscoll et al., 2013; Nair et al., 2013). (Shanley et al., 2015) found that the high Hg deposition was not correlated to GOM at ground level but to the maximum height of rain detected within clouds (obtained from the echo tops using the NOA-NEXRAD radar station) suggesting that droplets in high convective cloud tops scavenged GOM from above the mixing layer (Shanley et al. (2015) and references therein). Numerous studies suggest in fact that the upper free troposphere holds a large pool of GOM that has been oxidized from the global Hg pool (Driscoll et al., 2013; Swartzendruber et al., 2006; Weiss-Penzias et al., 2009) and that frequent high convective clouds occurring in tropical regions, particularly closer to the Equator, scavenge GOM by precipitation being readily soluble (Lindberg et al., 2007; Selin and Jacob, 2008; Holmes et al., 2010). Closer to the equator, the Hadley cell structure indeed gives way to the Intertropical Convergence Zone (ICT), and the atmospheric circulation there may affect upper-atmosphere Hg levels. The few measurements in the Northern-Hemisphere tropics, such as SIS, generally indicate lower

Atmos. Chem. Phys. Discuss., doi:10.5194/acp-2016-517, 2016
Manuscript under review for journal Atmos. Chem. Phys.
Published: 20 July 2016
© Author(s) 2016. CC-BY 3.0 License.

Atmospheric Chemistry and Physics Discussions

Hg fluxes than those measured at lower tropical latitude probably due to fewer convective rain events with clouds that reach the upper atmosphere (Shanley et al. (2015) and references therein). The higher annual wet Hg deposition observed at SIS compared to the other GMOS sites could be also due to a contribution of air masses crossing areas with discrete anthropogenic emission sources, particularly in late spring and summer, such as the metropolitan area of San Juan and/or minor industrial plants in Fajardo and Antille Islands, and/or from air masses crossing, particularly in winter, several coal power plants and waste incinerations in the southern United States and southern Florida (Latysh and Wetherbee, 2007). In addition, also legal and/or illegal gold mining activities which are widespread (Veiga et al., 2006; Sprovieri et al., 2016) in the southern regions of the Yucatan peninsula (i.e., Nicaragua; Guatemala, etc.) could contribute to the Hg wet deposition at SIS. The southern sites, AMS, CPT, CGR, and Bariloche (BAR), Argentina are more remote compared to SIS. AMS is a very small island located in the southern Indian Ocean where atmospheric Hg concentrations recorded during the same period were remarkably steady with annual median of 1.03±0.10 ngm^{-3} and lower than those recorded at the Tropical sites (Angot et al., 2014);(Sprovieri et al., 2016) but slightly higher than annual averages and medians recorded at Cape Grim in 2013 (Slemr et al., 2014). Both AMS and Cape Grim for most of the time receive clean marine air masses (Slemr et al., 2014; Angot et al., 2014). Previous studies (Mason and Sheu, 2002; Sprovieri et al., 2003; Holmes et al., 2009; Sprovieri et al., 2010b, a) analyzed atmospheric observations of GOM from Mediterranean, Pacific and Atlantic cruises in terms of Hg chemistry and deposition in the marine atmosphere, and suggested that elevated levels of halogen atoms, and in particular of Br in the marine boundary layer (MBL) are an important source of GOM from oxidation of GEM, that more readily deposited throughout sea-salt aerosols followed by aerosol deposition. GEM evasion from marine waters therefore, could represent a significant source of atmospheric Hg which contributes to depositional fluxes in marine regions (Mason and Sheu, 2002), such as Amsterdam Island, and Cape Grim. In 2013, among the Southern sites, the highest annual and average THg wet deposition flux have been recorded at CPT (5.2 $\mu gm^{-2}y^{-1}$ and 37.1 $ngm^{-2}d^{-1}$) which salso showed the lowest both deposition amount (264.9 mm) and the number of sampling days (Tables 2 and 3) compared to AMS (with annual wet deposition flux of 1.95 $\mu gm^{-2}y^{-1}$ and 7.2 $ngm^{-2}d^{-1}$, considering a rainfall of 833.2 mm) and CGR (with wet deposition flux of 3.1 $\mu gm^{-2}y^{-1}$ and 10.6 $ngm^{-2}d^{-1}$, considering a rainfall of 775.6 mm). These findings have not been observed at CPT in 2014 with the lowest annual wet deposition flux (0.57 $\mu gm^{-2}y^{-1}$) and comparable precipitation amounts and number of sampling days of the year before (see Tables 2 and 3).

CPT is situated on the southern tip of South Africa (Sprovieri et al., 2016; Brunke et al., 2016), and during the wetter season (May till October) normally precipitation increased due to the passage of cold fronts moving from West to East (Brunke et al., 2016). (Brunke et al., 2004) highlighted that CPT receives clean marine air most of the time whereas continental and polluted air masses are observed at the site more frequently during the winter period with air masses advected to the station from north to north-western (Rautenbach and Smith, 2001; Brunke et al., 2004) region where the Gauteng and Mpumalanga provinces are located. These south African areas represent the major anthropogenic Hg sources with former mine dumps from gold mining and large coal-burning power stations (Dabrowski et al., 2008). Therefore, the highest annual average THg wet deposition flux observed at CPT in 2013 compared to the other southern sites which received more precipitation amounts than the CPT site seem to be prevalently influenced by regional/large scale emission sources during the sampling period. Measurements of atmospheric Hg deposition in Bariloche (BAR), Argentina have been carried out for the first time from 2014 till 2015. BAR site

Atmos. Chem. Phys. Discuss., doi:10.5194/acp-2016-517, 2016
Manuscript under review for journal Atmos. Chem. Phys.
Published: 20 July 2016
© Author(s) 2016. CC-BY 3.0 License.

Atmospheric Chemistry and Physics Discussions

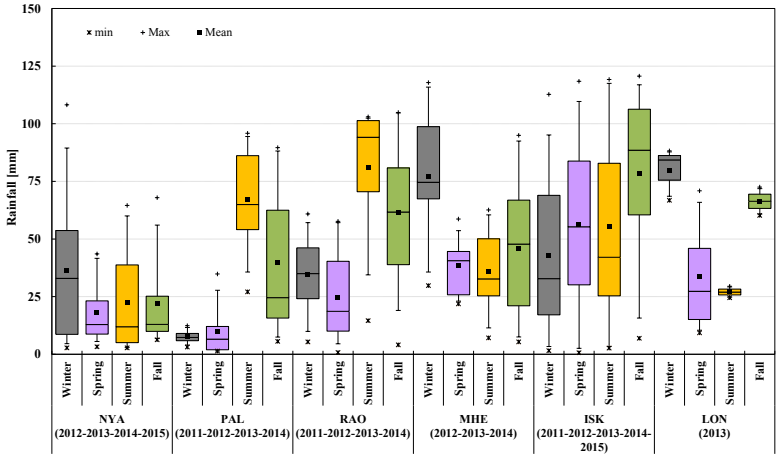

Figure 4. Seasonal distribution of rainfall amounts, at the European GMOS sites from 2011 to 2015

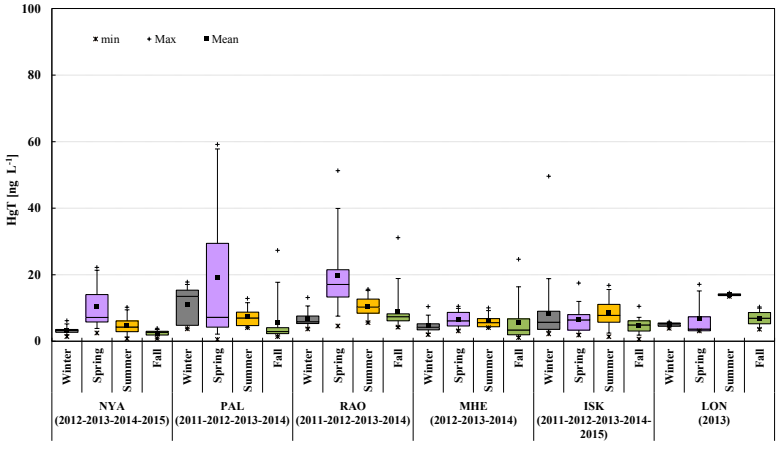

Figure 5. Seasonal distribution of volume-weighted THg concentration in precipitation at the European GMOS sites from 2011 to 2015

Atmos. Chem. Phys. Discuss., doi:10.5194/acp-2016-517, 2016
Manuscript under review for journal Atmos. Chem. Phys.
Published: 20 July 2016
© Author(s) 2016. CC-BY 3.0 License.

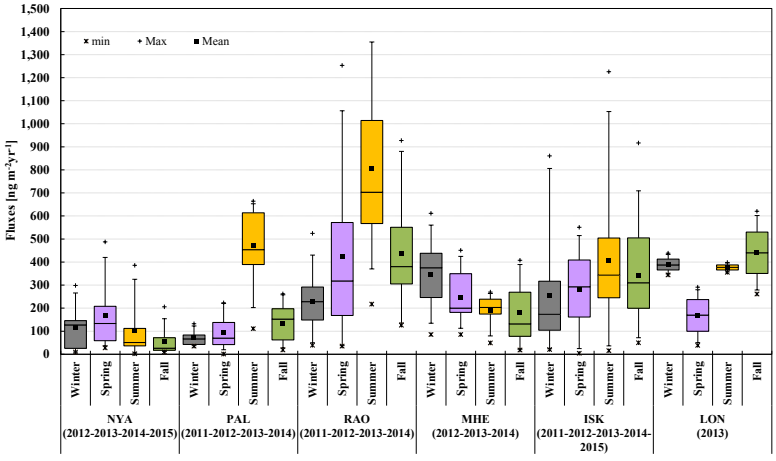

Figure 6. Seasonal distribution of THg wet deposition flux at the European GMOS sites from 2011 to 2015

has been established inside a well protected natural reserve in Northern Patagonia, on the shore of Gutierrez River at south-east of the Nahuel Huapi lake. GEM records at BAR station resemble background concentrations comparable to levels found in Antarctica and other remote locations of the South Hemisphere with annual mean GEM concentrations of 0.9 ± 0.14 ngm^{-3} (Diéguez et al., 2015; Sprovieri et al., 2016). The annual THg wet deposition flux calculated at BAR in 2014 was very low (0.1 $\mu gm^{-2}yr^{-1}$), however, it is necessary to point out that the number of samples carried out during the year was scarce (n = 91), therefore, the average wet deposition flux value (1.1 $ngm^{-2}d^{-1}$) obtained is less representative than that recorded in 2015 (3.0 $ngm^{-2}d^{-1}$) calculated over a number of sampling days of nearly 50% of the year. The 2015 THg wet deposition flux was 0.5 $\mu gm^{-2}yr^{-1}$ and an average wet deposition flux of 3.0 $ngm^{-2}d^{-1}$ which is lower than those recorded at the other southern GMOS sites with a comparable number of sampling days and, conversely, more close to the value observed in the Arctic, at Ny Alesund station (4.2 $ngm^{-2}d^{-1}$).

4 Seasonal patterns and Influence of meteorological conditions on Hg wet deposition

4.1 European Stations

In this study, seasons are delineated according to the metereological definition. Since THg wet deposition flux depends on the total precipitation amount and the concentration of total Hg in that precipitation, the seasonal cycles of both these parameters are shown along with the cycles of Hg wet deposition in Figures 4, 5, 6 and 7.

Atmos. Chem. Phys. Discuss., doi:10.5194/acp-2016-517, 2016
Manuscript under review for journal Atmos. Chem. Phys.
Published: 20 July 2016
© Author(s) 2016. CC-BY 3.0 License.

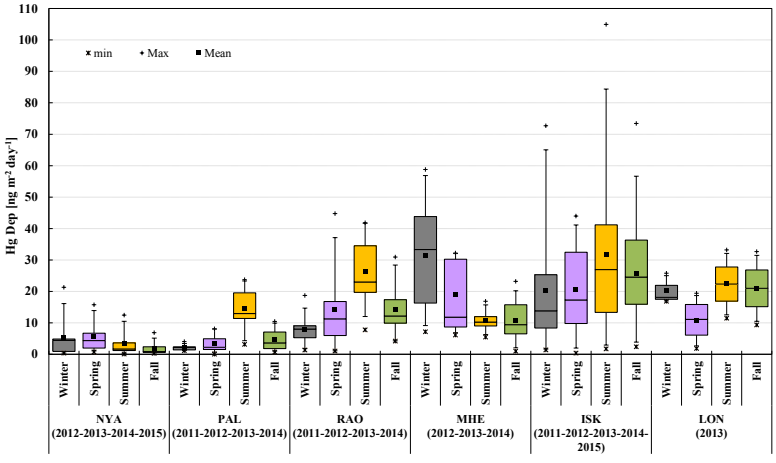

Figure 7. Seasonal distribution of THg wet deposition flux averaged on the number of sampling days, at the European GMOS sites from 2011 to 2015

Seasonal trends of THg in precipitation are clearly evident at all sites, with increased Hg concentrations and deposition observed during spring and summer months at most of them, implying a significant dependence on meteorological conditions throughout the years. The seasonal variability in Hg concentrations and Hg deposition has been reported in previous studies in North America (Hoyer et al., 1995; Landis and Keeler, 1997) and Europe (Iverfeldt, 1991; Munthe et al., 2007). The warm month maximum in seasonal THg wet deposition is predominant at most European GMOS sites, except at Mace Head (MHE) and Longobucco (LON) where the maximum THg wet deposition occurs during the winter and the fall seasons, respectively. However, the patterns of THg concentrations and precipitation amounts reveal that at most of the sites, the seasonal THg wet deposition maximum corresponds to the maximum in precipitation amounts collected, except at Ny Alesund (NYA), Iskrba (ISK) and LON. Therefore, the dominant factor in determining the Hg wet deposition loading recorded at all the European sites was generally related to the amounts of precipitation collected. Hg concentrations in rainfall at NYA peaked in spring, and decreased through the summer, in fall and winter seasons (Figure 5). Rainfall mean were fairly equally distributed in all seasons except the winter season. Thus, wet Hg loading was highest in spring, intermediate in winter and summer and lowest in fall (Figures 6 and 7). High levels of soluble species could in general be due to direct enhanced atmospheric oxidation of GEM to GOM, which occurs in regions with high concentrations of oxidants such as polar regions during springtime (where AMDEs occur, such as NYA). At Pallas (PAL), Hg concentrations in rainfall increased through the winter, peaking in spring, and decreased through the summer and fall. Rainfall was not fairly equally distributed in all seasons but lowest values were

Atmos. Chem. Phys. Discuss., doi:10.5194/acp-2016-517, 2016
Manuscript under review for journal Atmos. Chem. Phys.
Published: 20 July 2016
© Author(s) 2016. CC-BY 3.0 License.

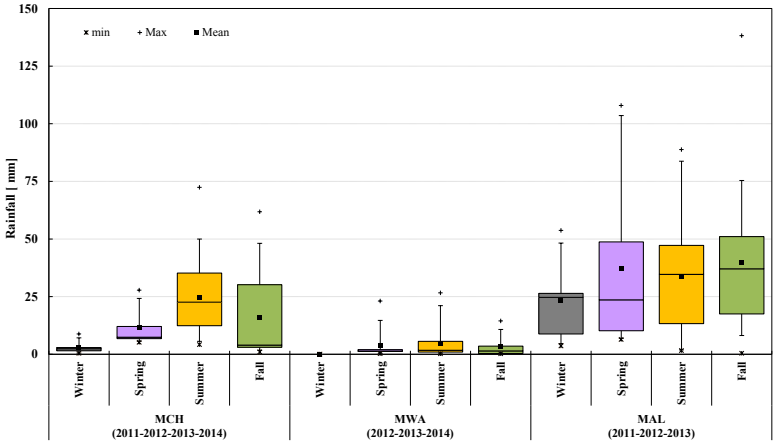

Figure 8. Seasonal distribution of rainfall amounts, at the three Chinese GMOS sites from 2011 to 2014

recorded during winter and spring and highest rainfall was observed in summer followed by a decreasing during the fall season. Thus, wet Hg loading was highest in summer, intermediate in fall, and lowest in winter and spring (Figures 6 and 7).

Similar rainfall behavior was observed at RAO, where Hg concentrations in rainfall peaked in spring, and decreased in fall and winter through the summer season. Therefore, wet Hg loading was highest in summer and the lowest in winter with intermediate values in spring and fall. At MHE, Hg concentrations in rainfall increased through the winter, peaked in spring, and decreased through the summer and fall seasons. Rainfall mean was fairly equally distributed in all seasons except the winter season. Thus, wet Hg loading was highest in winter, intermediate in spring and summer, and the lowest in fall (Figures 6 and 7). At ISK, Hg concentrations in rainfall increased from the winter, peaked in summer through spring, and decreased in fall. Rainfall mean was fairly equally distributed in spring and summer seasons except the winter season which shows the lowest rainfall whereas they peaked in fall season. Thus, wet Hg loading increased from the winter, peaked in summer through spring, and decreased in fall, following the same behavior of Hg concentrations in rainfall. (Figure 4). LON shows highest seasonal THg wet deposition in autumn and the lowest during spring. In this latter case, it is necessary to point out that these results are related to one year (2013) in contrast to the other sites in which all precipitation samples were grouped and analyzed season by season for a period of three to five years. Among the European sites the highest THg wet deposition have been recorded at the remote RAO and PAL stations during the more photochemically active summer months, whereas lower amounts were found in deposited in the colder months. In addition, rainfall amount during summer seems to be identified as the overriding factor controlling wet Hg loading at these sites. The lowest concentrations and total wet deposition were seen in winter months at most of sites. The seasonal pattern in the atmospheric Hg, with highest precipitation concentrations and wet deposition typically seen

Atmos. Chem. Phys. Discuss., doi:10.5194/acp-2016-517, 2016
Manuscript under review for journal Atmos. Chem. Phys.
Published: 20 July 2016
© Author(s) 2016. CC-BY 3.0 License.

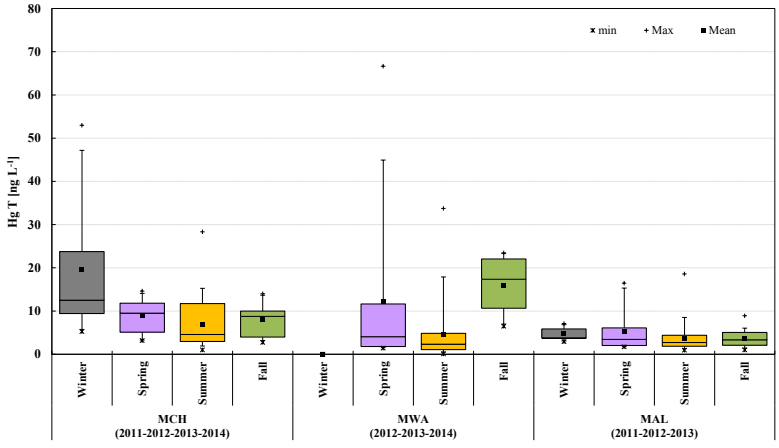

Figure 9. Seasonal distribution of volume-weighted THg concentration in precipitation at the three Chinese GMOS sites from 2011 to 2014

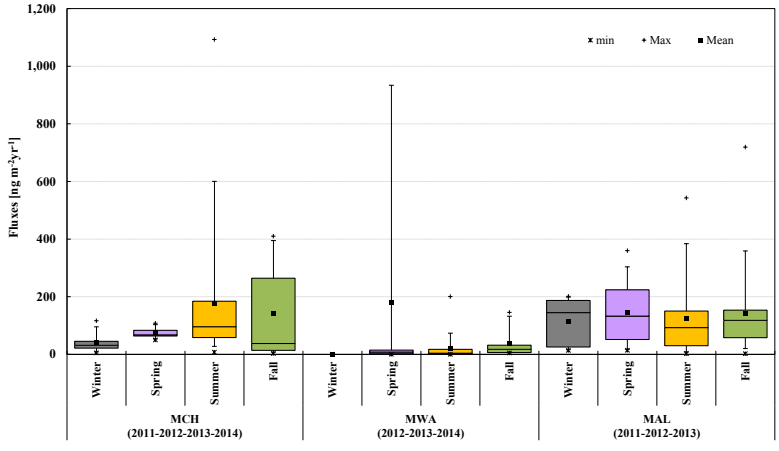

Figure 10. Seasonal distribution of THg wet deposition flux at the three Chinese GMOS sites from 2011 to 2014

Atmos. Chem. Phys. Discuss., doi:10.5194/acp-2016-517, 2016
Manuscript under review for journal Atmos. Chem. Phys.
Published: 20 July 2016
© Author(s) 2016. CC-BY 3.0 License.

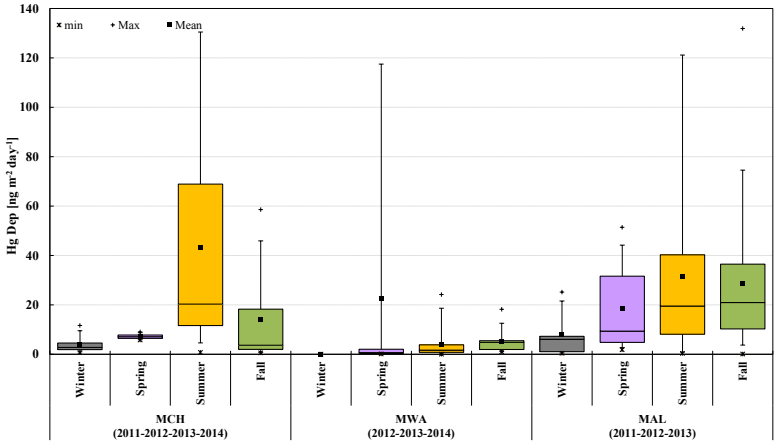

Figure 11. Seasonal distribution of THg wet deposition flux averaged on the number of sampling days, at the three Chinese GMOS sites from 2011 to 2014

in summer and lowest concentrations and wet deposition in winter, was believed partly to be the result of increased convection and mixing during the warmer summer months which can increase the ability of the air to transport Hg over longer distances, leading to greater precipitation amounts that remove Hg from the atmosphere. This may also indicate the role of precipitation type in the amount of Hg wet deposition, as rain may have a greater capacity to scavenge and hold different forms of Hg than snow. Higher Hg deposition, typically observed during the warmer months, was likely the result of a mix of meteorological, source emission, and atmospheric chemistry influences. For example, it is widely known that the concentrations of oxidants such as ozone, OH radicals, and acids that oxidize GEM to GOM are higher during warmer months and would lead to elevated concentrations of oxidized species (Schroeder and Munthe, 1998; Lin and Pehkonen, 1999). Scavenging of soluble oxidized Hg species has also been considered to be more efficient in summertime precipitation events than in winter due to differences in the cloud microphysical processing between rain and frozen precipitation (Hoyer et al., 1995).

4.2 Chinese Stations

China has been regarded as one of the largest atmospheric Hg emission sources region in the world (Streets et al., 2005; Wu et al., 2006). However, limited monitoring sites and data are available to understand Hg deposition patterns in China. Few previous measurements of THg deposition in China have been conducted in remote areas like Mt. Fanjing (Xiao et al., 1998), Mt. Leigong (Fu et al., 2010), Wujiang River basin (Guo et al., 2008), and Mt. Gongga (Fu et al., 2008, 2010) in southwestern China, as well as at Mt. Changbai (Wan et al., 2009) in northeastern China. In order to evaluate the spatial and temporal

Atmos. Chem. Phys. Discuss., doi:10.5194/acp-2016-517, 2016
Manuscript under review for journal Atmos. Chem. Phys.
Published: 20 July 2016
© Author(s) 2016. CC-BY 3.0 License.

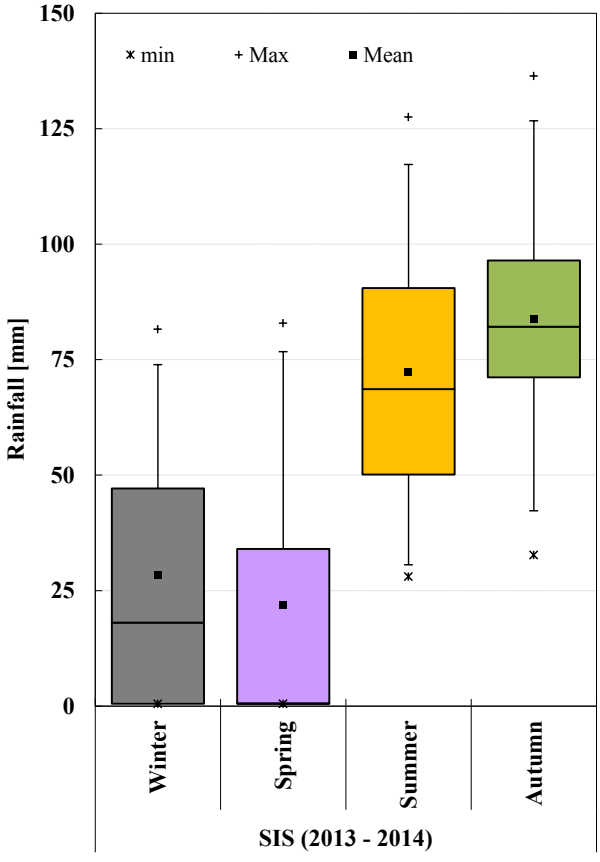

Figure 12. Seasonal distribution of rainfall amounts, at the tropical GMOS site (Sisal, Mexico) in 2013 and 2014

distribution of THg at the three GMOS Asian stations, all measurements performed from 2011 to 2014 at Mt. Changbai (MCH), Mt. Walinguan (MWA), and Mt. Ailao (MAL) were grouped by season and by site (Figures 8, 9, 10 and 11). Seasonal variations of THg in precipitation were observed at the three Chinese sites (Figure 9). The results obtained during the sampling period were similar to the seasonal variations of THg in precipitation in other Chinese regions, such as Wujiang River Basin, Guizhou, China, but in contrast to the observations in North America (Landis et al., 2002), Adirondacks (Choi et al., 2008) and Great

Atmos. Chem. Phys. Discuss., doi:10.5194/acp-2016-517, 2016
Manuscript under review for journal Atmos. Chem. Phys.
Published: 20 July 2016
© Author(s) 2016. CC-BY 3.0 License.

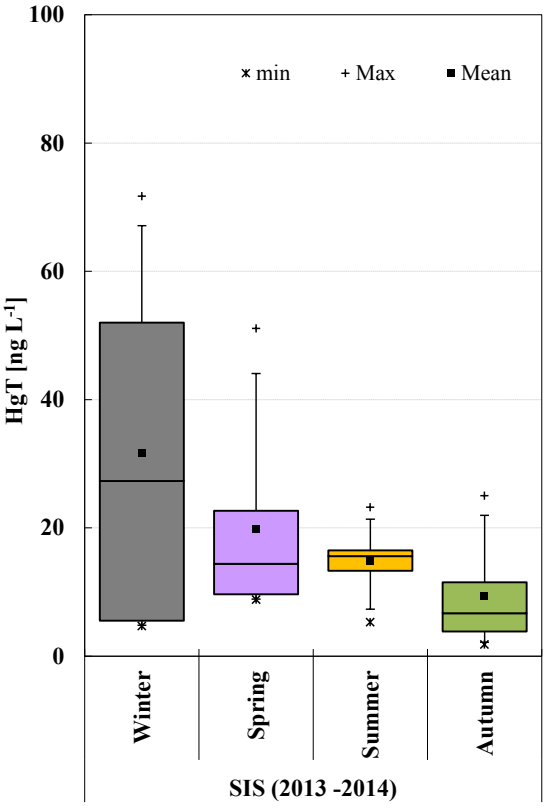

Figure 13. Seasonal distribution of volume-weighted THg concentration in precipitation, at the tropical GMOS site (Sisal, Mexico) in 2013 and 2014

Lakes region (Hall et al., 2005), which found increased THg concentration during summer months (Prestbo and Gay, 2009). Geographic differences in Hg wet deposition worldwide may be explained in part by the proximity to atmospheric sources and regional difference in anthropogenic emission sources. Atmospheric Hg species, in particular, GEM and PBM have been found to be substantially increased over recent years in both remote and urban areas of China, especially in central and eastern China,

Atmos. Chem. Phys. Discuss., doi:10.5194/acp-2016-517, 2016
Manuscript under review for journal Atmos. Chem. Phys.
Published: 20 July 2016
© Author(s) 2016. CC-BY 3.0 License.

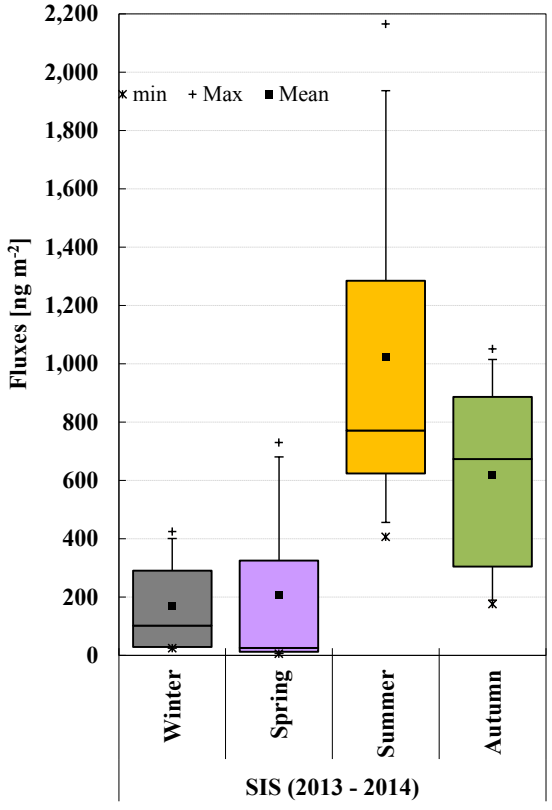

Figure 14. Seasonal distribution of THg wet deposition flux, at the tropical GMOS site (Sisal, Mexico) in 2013 and 2014

compared to those observed in North America and Europe which reported opposite long-term trends (Fu et al., 2015).The increasing trend in China is possibly caused by the increase in anthropogenic Hg emissions in the past decade, and indicates that the influence of regional emissions on Hg levels in China exceed global emission influence ((Lindberg et al., 2007) and references therein). The seasonal variation of weighted THg concentration observed in precipitation with highest value in winter and lowest in summer (see Figures 8, 9, 10 and 11), could be attributed in a first instance, to lower rainy amounts collected

Atmos. Chem. Phys. Discuss., doi:10.5194/acp-2016-517, 2016
Manuscript under review for journal Atmos. Chem. Phys.
Published: 20 July 2016
© Author(s) 2016. CC-BY 3.0 License.

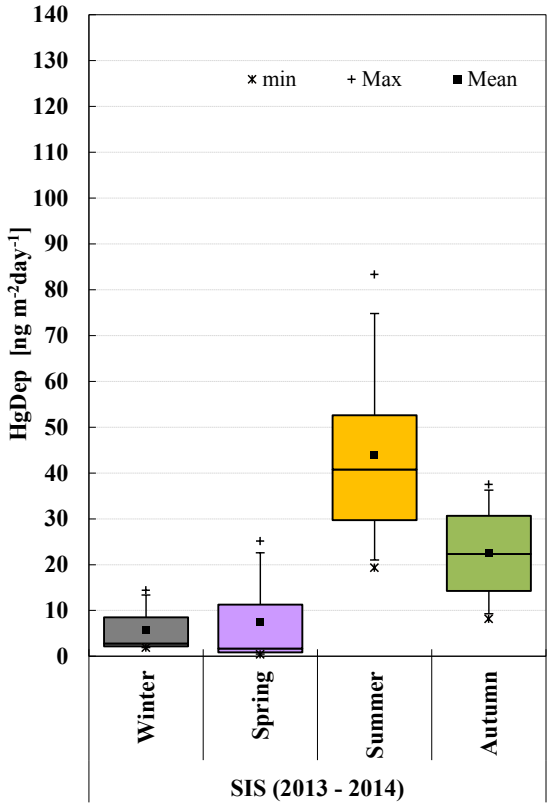

Figure 15. Seasonal distribution of THg wet deposition flux averaged on the number of sampling days, at the tropical GMOS site (Sisal, Mexico) in 2013 and 2014

in winter. The results obtained at the three Chinese sites show in fact that the THg concentrations varied with rain amount. In particular, at MCH, THg concentrations slightly increased in autumn, peaked during the winter season, and decreased during spring and summer when the lowest values were recorded. The reverse trend has been observed in precipitation amount through the seasons. Average THg wet deposition trend ($ngm^{-2}d^{-1}$) is comparable with that of the precipitation amount, with values

Atmos. Chem. Phys. Discuss., doi:10.5194/acp-2016-517, 2016
Manuscript under review for journal Atmos. Chem. Phys.
Published: 20 July 2016
© Author(s) 2016. CC-BY 3.0 License.

of THg flux increased from winter, through spring, and peaked in summer. Ruling out the winter season at MWA during which very few rainy samples have been collected, thus not representative for the present discussion, weighted THg concentrations peaked in fall and decreased during spring with lowest values in summer period. Therefore, wet Hg loading was highest in spring, intermediate in fall and lowest in summer. The positive or negative correlation between THg concentrations and the precipitation amount has not been obviously observed at MAL where the rainy samples show a fairly variability during all seasons with lowest average rainfall in winter and the highest in fall, whereas THg concentrations showed high values in winter and lowest in fall, and wet Hg loading was highest in summer, intermediate in fall and spring and the lowest values were recorded in winter. (Fu et al., 2015) highlight significant positive correlations between rainwater THg concentrations and PBM and GOM concentrations, resulting in positive correlations between wet deposition fluxes and PBM and GOM concentrations. This has been explained by the authors with the washout process of PBM and GOM during rain events which could contribute to enhance Hg wet deposition in China, particularly in urban areas where PBM and GOM concentrations are much higher. In remote areas of China, however, washout of elevated atmospheric PBM does not seem to drive a notable increase in Hg wet deposition flux, probably due to the low washout rate of PBM during rain events at high altitude monitoring sites, such as MAL and MWA where low-level clouds reduced the contribution of Hg washout (Lee et al., 2001; Seigneur et al., 2004). (Guo et al., 2008) in a previous study in Guizhou on Hg in precipitation also pointed out that maximum THg concentrations in rainy samples during winter may be related to coal burning in domestic activities. Similar conclusions have also been reported in a study performed by Wang et al. (2012) at three Chinese sites (urban, residential and near-remote sites) in Chongqing province from 2010 to 2011, where they also found a high correlation between THg and particulate Hg (PBM) concentrations, suggesting that THg concentration in precipitation may be influenced by the PBM concentration. Additionally, comparable seasonal behavior of Hg concentrations in precipitation with our results have been also observed, but with annual mean THg concentrations (ngL-1) significantly higher than those observed at MCH, MWA, and MAL sites which are located in remote Chinese areas. The seasonal pattern in deposition flux observed at the remote MCH, MAL, and MWA are comparable with those observed at remote sites of Europe and North America (Choi et al., 2008; Mason et al., 2000; Keeler et al., 2005; Sanei et al., 2010; Lombard et al., 2011), with maximum values during warmer months (Figures 8, 9, 10 and 11). It was suggested by (Keeler et al., 2005) and (Mason et al., 2000) that this annual maximum was mainly due to more effective scavenging by rain in summer than by snow in the cold season (Sorensen et al., 1994; Mason et al., 2000; Keeler et al., 2005; Selin and Jacob, 2008).Mercury is not incorporated into cold cloud precipitation as efficiently as in warm cloud precipitation (Landis et al., 2002). Other explanations for this observation have been addressed by the authors including a greater availability of soluble Hg due to convective transport in summer events (Guentzel et al., 2001; Keeler et al., 2005), and a summer increase in Hg-containing soil derived particles in the atmosphere (Sorensen et al., 1994).

4.2.1 Tropical Station: SISAL, Mexico

Hg deposition measurements are rare in tropical latitudes, with very few scientific publications in the past decade (Shanley et al. (2015) and references therein). The tropics are a particularly important region regarding global atmospheric chemistry. Due to intense ultraviolet radiation and high water vapor concentrations, high OH concentrations oxidize inorganic and organic gases,

Atmos. Chem. Phys. Discuss., doi:10.5194/acp-2016-517, 2016
Manuscript under review for journal Atmos. Chem. Phys.
Published: 20 July 2016
© Author(s) 2016. CC-BY 3.0 License.

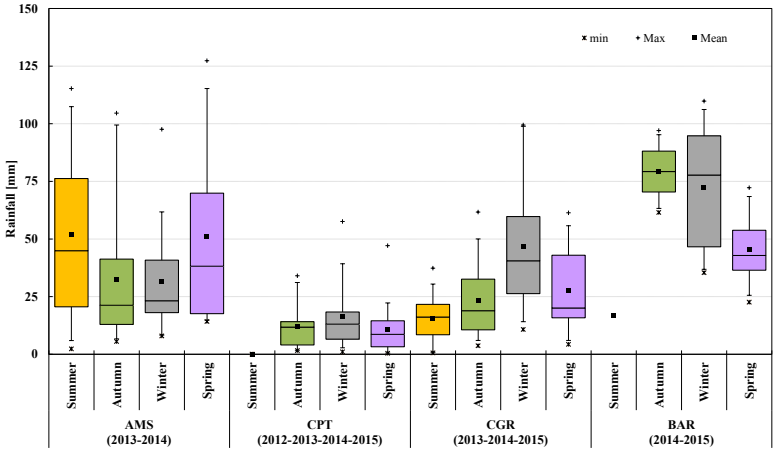

Figure 16. Seasonal distribution of rainfall amounts,at the four GMOS sites in the Southern Hemisphere from 2012 to 2015

and induce an efficient removal from the atmosphere of the oxidized products (Shanley et al. (2015) and references therein). Strong convective events in the tropical regions leads to huge volumes of air being drawn out of the sub-cloud layer with the resultant chemical composition of the precipitation coming from the capture of gases and small particles by the liquid phases of cloud and rain. Hg deposition measurements started in Mexico at Celestùn station (CST) in 2012 (see Table 1), but after a short time period of sampling, the monitoring station changed the location with SIS, therefore, we refer the discussion to the SIS data related to both 2013 and 2014 years during which sufficient precipitation samples have been recorded. Despite receiving unpolluted air off the Atlantic Ocean from northeasterly and southeasterly trade winds, during most of the years (Sena et al., 2015), the site recorded higher wet Hg deposition fluxes during summer and fall compared to those observed during the other seasons. The SIS high Hg deposition rates, comparable to other sites in the Northern Hemisphere, such as the Chinese sites (i.e., MWA) or European sites (i.e., ISK) that sometimes are also impacted by anthropogenic emissions, are driven in part by high rainfall events more intense during summer and fall, and less during winter and spring period. The high wet Hg deposition flux at this site suggests that other tropical areas may be hotspots for Hg deposition as well. A number of studies have suggested that this could be due to higher precipitation and the scavenging ratios from the global pool in the sub-tropical free troposphere where high concentrations of oxidized Hg species exist (Guentzel et al., 2001; Seigneur et al., 2004; Selin and Jacob, 2008). These findings were also highlighted in previous studies in south of Florida and the Gulf of Mexico coastal areas confirming that local and regional Hg emissions play only a minor role on wet Hg deposition (Guentzel et al., 2001; Sillman et al., 2013) suggesting that the primary source of scavenged oxidized Hg could be the global pool.

Weather patterns in SIS exhibit a seasonality annual rainfall, with highest rainfall from June/July through October/November.

Atmos. Chem. Phys. Discuss., doi:10.5194/acp-2016-517, 2016
Manuscript under review for journal Atmos. Chem. Phys.
Published: 20 July 2016
© Author(s) 2016. CC-BY 3.0 License.

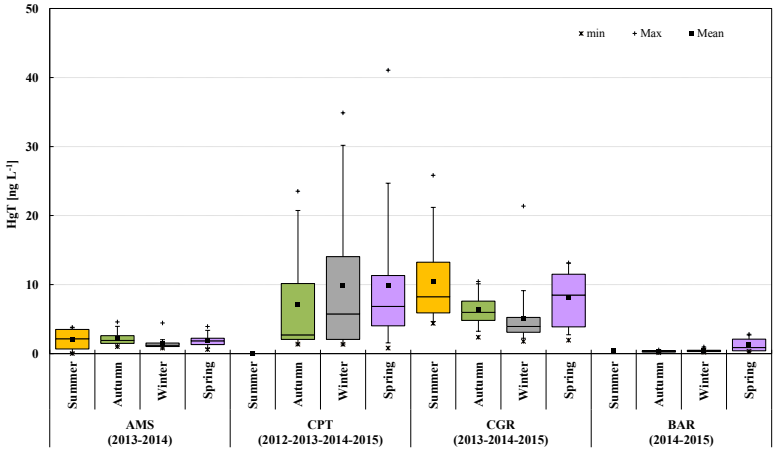

Figure 17. Seasonal distribution of volume-weighted THg concentration in precipitation, at the four GMOS sites in the Southern Hemisphere from 2012 to 2015

Summer tropical waves and systems characterized by deep convection and low pressure produced greater rainfall. During summer and fall, the site indeed receives rainfall from deep convection associated with tropical waves embedded in the prevailing easterly airflow. THg concentrations were higher in low volume samples. With larger storms Hg concentrations were diluted, this means that rainout of Hg was maximum (the decreasing of Hg concentrations with the increasing of the rainfall depth). Weighted THg concentrations in rainfall (ngL^{-1}) increased from the fall, peaked in winter, and decreased through the spring and summer. On average terms THg in wet deposition was highest in summer, intermediate in fall, and lowest in spring and winter (Figures 12, 13, 14 and 15). The higher summer Hg deposition flux is not driven by higher Hg concentrations in rainfall since the highest Hg concentrations in rain samples occurred in winter (Figures 12, 13, 14 and 15). Different mechanisms leading to enhanced Hg concentrations in rain during the winter including greater anthropogenic emissions are probably associated with higher use of fossil flues in power plants during the cold season. As reported in Section 3 relating to the annual wet deposition patterns, the THg wet deposition observed at SIS could also be influenced by air masses crossing particularly in winter the southern Unite States and southern Florida where several coal power plants and waste incinerations (Latysh and Wetherbee, 2007) are located. The high wet deposition of Hg during the rainy seasons (May/June to October/November), in contrast, could be due to more efficient scavenging processes of reactive gaseous mercury from the free troposphere by tall convective thunderstorms, and the concentration of GOM by the sea breeze effect, where the diurnal alternation of onshore and offshore winds can lead to a buildup of pollutants in the air mass. Greater information on Hg deposition and cycling is needed

Atmos. Chem. Phys. Discuss., doi:10.5194/acp-2016-517, 2016
Manuscript under review for journal Atmos. Chem. Phys.
Published: 20 July 2016
© Author(s) 2016. CC-BY 3.0 License.

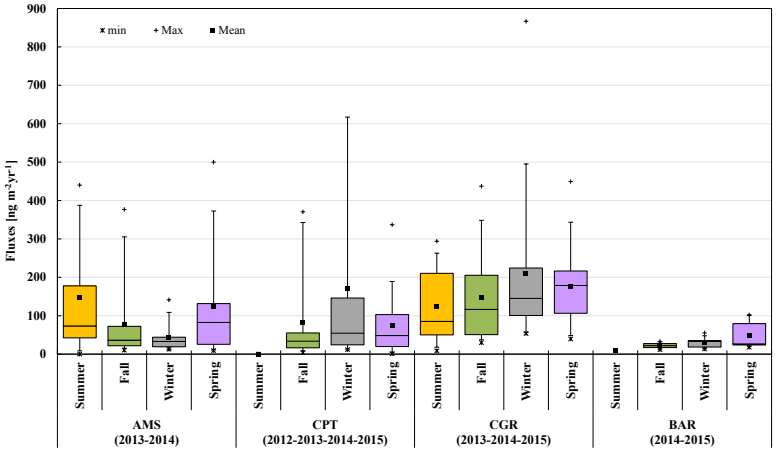

Figure 18. Seasonal distribution of THg wet deposition flux, at the four GMOS sites in the Southern Hemisphere from 2012 to 2015

in tropical regions, where populations are more likely to be exposed to Hg through fish consumption and artisanal gold mining activity.

4.2.2 Southern Hemisphere Stations

In remote areas far from any local sources, atmospheric deposition has been recognized as the main source of Hg to the ocean (Lindberg et al., 2007; Pirrone et al., 2008). Hg can then be reemitted back to the atmosphere via gas exchange, and modeling studies suggest that reemission from oceans is a major contributor to atmospheric concentrations of GEM, particularly in the Southern Hemisphere where oceans were shown to contribute more than half of the surface atmospheric concentration ((Strode et al., 2007) and references therein). In the Southern Hemisphere we considered the four monitoring sites, Amsterdam Island (AMS), southern Indian Ocean, CPT, South Africa, Cape Grim (CGR), Australia, and Bariloche (BAR), Argentina which recorded a representative number of samples over the 2012-2015 period. Figures 16, 17, 18 and 19 show the box plots related to rainfall, THg concentrations in precipitation as well as wet deposition flux of Hg recorded at the four southern sites. An NSA-171 (Eigenbrodt) collector was set up at AMS at the beginning of the 2013. The GMOS site experiences a mild oceanic climate with monthly median air temperature ranged from 11 °C in austral winter to 17 °C in austral summer and frequent presence of clouds (Sciare et al., 2009). In 2013 and 2014 AMS displays the highest precipitation amounts collected during the warmer seasons (spring and summer) (Fig. 16, 17). Also the THg wet deposition flux patterns follow the same trend observed for the rainfall highlighting that the main factor driving the flux seems to be the amount of rain collected (Fig. 18). The THg fluxes

Atmos. Chem. Phys. Discuss., doi:10.5194/acp-2016-517, 2016
Manuscript under review for journal Atmos. Chem. Phys.
Published: 20 July 2016
© Author(s) 2016. CC-BY 3.0 License.

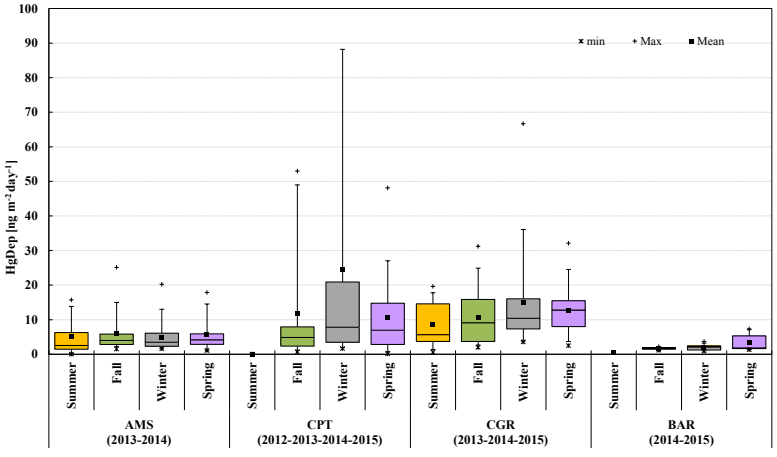

Figure 19. Seasonal distribution of THg wet deposition flux averaged on the number of sampling days, at the four GMOS sites in the Southern Hemisphere from 2012 to 2015

pattern seems to be in agreement with the results of atmospheric Hg speciation measurements carried out during the same period at AMS, and in particular with the GOM seasonal pattern observed since January 2012 by (Angot et al., 2014) that highlighted a higher frequency of GOM events between December and March (summer). However, additional and integrated measurements in ambient air and rainwater samples to improve our understanding of deposition processes and oxidation mechanisms should be addressed. The variation of Hg concentrations in precipitation and Hg wet deposition fluxes driven by the precipitation amounts collected at AMS occurred also at CPT where, apart the dry summer season, Hg concentrations in precipitation, Hg wet deposition fluxes as well as the precipitation amounts, followed the same trend during the rainy season (May till October), with a maximum in wintertime for all the parameters recorded. CPT experiences a Mediterranean-type climate that is characterized by rather dry summers comprising moderate temperatures. The austral autumn to spring season normally experience increased precipitation due to the passage of cold fronts moving from West to East, therefore, CPT generally receives clean marine air from the Atlantic Ocean whereas continental and polluted air masses are observed at the site more frequently, mainly during the winter period (Brunke et al., 2004, 2016), due to the prevailing air masses from the north to northwestern sector (Rautenbach and Smith, 2001; Brunke et al., 2004). The highest THg concentrations and wet deposition fluxes recorded during the winter season could be due also to the contribution of polluted air masses crossing Cape Town metropolitan area before arriving at the stations. However, in a previous study on GEM concentrations and THg in precipitation carried out over a period of seven years (2007-2013) by (Brunke et al., 2016) highlighted that GEM, THg, CO and 222Rn levels within the urban-marine events observed at CPT did not substantially differ from those seen in the marine rain episodes, concluding that no significant local

Atmos. Chem. Phys. Discuss., doi:10.5194/acp-2016-517, 2016
Manuscript under review for journal Atmos. Chem. Phys.
Published: 20 July 2016
© Author(s) 2016. CC-BY 3.0 License.

anthropogenic influences were detected on THg concentrations. Conversely, a significant positive correlation was found CPT between GEM and THg concentrations, and with the Southern Oscillation Index (SOI), suggesting that both GEM and THg concentrations are primarily influenced by large scale meteorology which in turn controls Hg emission sources in terms, for example, of enhanced sea surface temperature that could increase large scale droughts leading to a raised biomass burning (Brunke et al., 2016).

Measurements of atmospheric Hg deposition in Australia have never been reported before (Jardine and Bunn, 2010). From 2013 till 2015, at Cape Grim GAW Station (CGR), located on the north-western coast of Tasmania, Australia, highest value in rainfall have been observed during winter an lowest in summer, whereas Hg concentrations peaked in summer and dropped to lowest values in winter (see Fig. 16, 17, 18 and 19). The trend of Hg wet deposition fluxes conversely seems to be driven by the precipitation amounts even if a small seasonal variability of Hg loading was displayed. Indeed, an increase in precipitation volume results in an increase of the Hg deposition flux. This is accompanied by a decrease in Hg concentrations in rain, probably due to the dilution of the washout loading (Prestbo and Gay, 2009). This means that any changes in meteorological conditions, especially precipitation, complicate the interpretation of GMOS observations at different latitude and might mask any trends due to change in Hg emissions. At BAR the highest precipitation amounts in 2014 and 2015 were collected during the fall and winter seasons and decreased in spring when the highest THg concentrations occurred (see Fig. 16, 17, 18 and 19). Therefore, the seasonal THg wet deposition peaked in spring and decreased during the cold seasons. It is necessary to point out, however, that in 2014 at BAR no samples have been recorded in fall and summer as well as in 2015, during the same seasons the number of sampling days was very low particularly in summer. This means that further measurements and studies are needed to draw any conclusion and improve our understanding of deposition processes and oxidation mechanisms in this region. There are very few previous observations of Hg wet deposition in the Southern Hemisphere, and this makes difficult any comparison of data recorded during GMOS. The results observed at the four southern GMOS sites highlighted that the magnitude of wet deposition is affected by two main factors: amount of precipitation and the THg concentration in precipitation influenced by soluble Hg species (oxidized Hg) in the atmosphere. High levels of soluble species could in general be due to direct anthropogenic emissions of Hg oxidized species or by enhanced atmospheric oxidation of GEM to GOM, which occurs in regions with high concentrations of oxidants such as southern locations (where more solar radiation occurs) or polar regions during springtime (where AMDEs occur).

5 Conclusions

Mercury deposition measurements are critical for constructing an accurate global Hg budget and to model the benefits or consequences of changes in Hg emissions, for example, as proscribed by the Minamata Convention. Early models of wet Hg deposition had few measurements for calibration or validation, and tended to overestimate the influence of local emission sources. A synthesis of all available Hg measurements in precipitation from GMOS network is presented, including trends and seasonal cycles. These results provide a set of data for modeling applications to fully understand THg wet deposition patterns as well as the transformation and deposition mechanisms of atmospheric Hg. With broad geographic coverage including mostly

Atmos. Chem. Phys. Discuss., doi:10.5194/acp-2016-517, 2016
Manuscript under review for journal Atmos. Chem. Phys.
Published: 20 July 2016
© Author(s) 2016. CC-BY 3.0 License.

background and remote sites with few local or regional sources, GMOS's observation network gives important insights to evaluate future Hg trends on global scale. The results on THg wet deposition carried out in this study open the way for new avenues in future modeling studies as well as highlight the need of additional and integrated measurements in ambient air and rainwater samples to improve our understanding of deposition processes and oxidation mechanisms. These new observations in fact, give scientists and modelers some insight into baseline concentrations of THg concentrations in precipitation and depositional fluxes especially in the tropical area, and in the Southern Hemisphere where wet deposition as well as atmospheric Hg species were not investigated before. Greater information on Hg deposition and cycling is obviously needed in these regions. Moving forward, in addition to continued monitoring GMOS sites, integration with other ground-based monitoring sites at strategic locations along with integrations with atmospheric Hg species and other key oxidants, identification of the compounds making up GOM and PBM continue to be needed. Knowledge of these exact chemical species would also lead to improved understanding of the chemistry and wet and dry deposition processes of oxidized Hg specie in different air masses. Wet deposition measurements worldwide would assist modelers in constraining the atmospheric Hg budget on global scale, as would additional direct measurements of dry deposition across the GMOS network.

Acknowledgements. This work was funded by the FP7 (2010-2015) Global Mercury Observation System (GMOS) project. We thank all GMOS external Partners for providing high quality-controlled wet deposition measurements as well as we would like to acknowledge and thank all the site operators for the GMOS global network. AD, OM, HA thank the French Polar Institute IPEV(Program 1028, GMOStral), the LEFE CNRS/INSU (program SAMOA) and the overwintering crew at Amsterdam Island. The CNR-IIA research staff thanks also F. Cofone, A. Servidio, and A. Rosselli for their technical support for the laboratory work carried out on the samples from AMS, LON, CMA, and Mexican Stations.

Atmos. Chem. Phys. Discuss., doi:10.5194/acp-2016-517, 2016
Manuscript under review for journal Atmos. Chem. Phys.
Published: 20 July 2016
© Author(s) 2016. CC-BY 3.0 License.

Atmospheric Chemistry and Physics Discussions

References

1631, U. E. M.: Revision E, Mercury in water by Oxidation, Purge and Trap, and Cold Vapor atomic Fluorescence Spectrometry, Tech. rep., United States Environmental Protection Agency, 2002.

Angot, H., Barret, M., Magand, O., Ramonet, M., and Dommergue, A.: A 2-year record of atmospheric mercury species at a background Southern Hemisphere station on Amsterdam Island, Atmos. Chem. Phys., 14, 11 461–11 473, doi:10.5194/acp-14-11461-2014, 2014.

Brown, R., Pirrone, N., van Hoek, C., Horvat, M., Kotnik, J., Wangberg, I., Corns, W., Bieber, E., and Sprovieri, F.: Standardization of a European measurement method for the determination of total gaseous mercury: results of the field trial campaign and determination of a

Monitoring, 12, 689–695, doi:10.1039/b924955a, 2010b.

Brunke, E., Labuschagne, C., Parker, B., Scheel, H., and Whittlestone, S.: Baseline air mass selection at Cape Point, South Africa: application of 222Rn and other filter criteria to CO2, Atmos. Environ., 38, 5693–5702, doi:10.1016/j.atmosenv.2004.04.024, 2004.

Brunke, E., Walters, C., Mkololo, T., Martin, L., Labuschagne, C., Silwana, B., Slemr, F., Weigelt, A., Ebinghaus, R., and Somerset, V.: Somerset Mercury in the atmosphere and in rainwater at Cape Point, South Africa Atmospheric Environment, 125, 24–32, 2016.

Chen, L., Wang, H. H., Liu, J. F., Tong, Y. D., Ou, L. B., Zhang, W., Hu, D. Chen, C., and Wang, X.: Intercontinental transport and deposition patterns of atmospheric mercury from anthropogenic emissions, Atmos. Chem. Phys., 14, 1818 – 1827, 2014.

Choi, H.-D., Sharac, T. J., and Holsen, T. M.: Mercury deposition in the Adirondacks: A comparison between precipitation and throughfall, Atmospheric Environment, 42, 1818 – 1827, 2008.

Dabrowski, J., Ashton, P., Murray, K., Leaner, J., and Mason, R.: Anthropogenic mercury emissions in South Africa: coal combustion in power plants., Atmos. Environ., 42, 6620–6626, 2008.

Diéguez, M., García, P., and Sprovieri, F.: Atmospheric mercury fluxes in North Patagonia: first continuous records of the EMMA station (Global Mercury Observation System, Bariloche, Argentina), in proceedings ICMGP, 2015.

Driscoll, C., Mason, R., Chan, H., Jacob, D., and Pirrone, N.: Mercury as a global pollutant: sources, pathways, and effects, Environmental Science & Technology, 47, 4967–4983, doi:10.1021/es305071v, 2013.

Feng, X. F. X., Dong, Z., Yin, R., amd ZR Yang, J. W., and Zhang, H.: Atmospheric total gaseous mercury (TGM) concentrations and wet and dry deposition of mercury at a high-altitude mountain peak in south China, Atmospheric Chemistry and Physics, 9, 23 465–23 504, 2009.

Fu, X., Feng, X., and Wang, S.: Exchange fluxes of Hg between surfaces and atmosphere in the eastern flank of Mount Gongga, Sichuan province, southwestern China, Geophys Res, 23, 408 – 418, doi:10.1029/2008JD009814, 2008.

Fu, X., Feng, X., Dong, Z., Yin, R., Wang, J., Yang, Z., and Zhang, H.: Atmospheric gaseous elemental mercury (GEM) concentrations and mercury depositions at a high-altitude mountain peak in south China, Atmospheric Chemistry and Physics, 10, 2425 – 2437, doi:10.5194/acp-10-2425-2010, 2010.

Fu, X., Zhang, H., Yu, B., Wang, X., Lin, C., and Feng, X.: Observations of atmospheric mercury in China: a critical review, Atmospheric Chemistry and Physics, 15, 9455–9476, doi:10.5194/acp-15-9455-2015, 2015.

© Author(s) 2016. CC-BY 3.0 License.

Gay, D., Schmeltz, D., Prestbo, E., Olson, M., Sharac, T., and Tordon, R.: The atmospheric mercury network: measurement and initial examination of an ongoing atmospheric mercury record across North America, Atmospheric Chemistry and Physics, 13, 10 521–10 546, 2013.

Gratz, L. E., Keeler, G. J., and Miller, E. K.: Long-term relationships between mercury wet deposition and meteorology, Atmospheric Environment, 43, 6218 – 6229, 2009.

Guentzel, J. L., Landing, W. M., Gill, G. A., and Pollman, C. D.: Processes Influencing Rainfall Deposition of Mercury in Florida, Environmental Science & Technology, 35, 863 – 873, 2001.

Guo, Y., Feng, X., Li, Z., He, T., Yan, H., Meng, B., Zhang, J., and Qiu, G.: Distribution and wet deposition fluxes of total and methyl mercury in Wujiang River basin, Guizhou, China, Atmosperic Environment, 42, 7096–7103, 2008.

Gustin, M. S., Weiss-Penzias, P. S., and Peterson, C.: Investigating sources of gaseous oxidized mercury in dry deposition at three sites across Florida, USA, Atmospheric Chemistry and Physics, 12, 9201–9219, 2012.

Hall, B. D., Manolopoulos, H., Hurley, J. P., Schauer, J. J., St.Louis, V. L., Kenski, D., Graydon, J., Babiarz, C. L., Cleckner, L. B., and Keeler, G. J.: Methyl and total mercury in precipitation in the Great Lakes region, Atmos. Environ., 39, 7557–7569, 2005.

Hansen, A. and Gay, D.: Observations of mercury wet deposition in Mexico, Environ. Sci. Pollut. Res., 20, 8316–8325, doi:10.1007/s11356-013-2012-3, 2013.

Holmes, C. D., Jacob, D. J., Mason, R. P., and Jaffe, D. A.: Sources and deposition of reactive gaseous mercury in the marine atmosphere, Atmospheric Environment, 43, 2278 – 2285, 2009.

Holmes, C. D., Jacob, D. J., Corbitt, E. S., Mao, J., Yang, X., Talbot, R., and Slemr, F.: Global atmospheric model for mercury including oxidation by bromine atoms, Atmospheric Chemistry and Physics, 10, 12 037 – 12 057, 2010.

Hoyer, M., Burke, J., and Keeler, G.: Atmospheric sources, transport and deposition of mercury inMichigan: two years if event precipitation, Water Air Soil Pollut., 80, 199–208, 1995.

Hylander, L.: Global mercury pollution and its expected decrease after a mercury trade ban. Water Air Soil Pollut, Water, Air, and Soil Pollution, 125, 334–334, 2001.

Iverfeldt, A.: Mercury in forest canopy through fall water and its relation to atmospheric deposition, Water Air and Soil Pollution, 56, 553–564, 1991.

Jardine, T. D. and Bunn, S. E.: Northern Australia, whither the mercury?, CSIRO, Marine and Freshwater Research, 61, doi:10.1071/MF09126, 2010.

Keeler, G., Gratz, L., and Al-wali, K.: Long-term Atmospheric Mercury Wet Deposition at Underhill, Vermont, Ecotoxicology, 14, 71–83, 2005.

Landis, M., Stevens, R., Schaedlich, F., and Prestbo, E.: Development and characterization of an annular denuder methodology for the measurement of divalent inorganic reactive gaseous mercury in ambient air, Environmental Science & Technology, 36, 3000–3009, doi:10.1021/es015887t, 2002.

Landis, M. S. and Keeler, G. J.: Critical evaluation of a modified automatic wet-only precipitation collector for mercury and trace element determinations, Environmental Science & Technology, 31, 2610–2615, doi:10.1021/Es9700055, 1997.

Latysh, N. E. and Wetherbee, G. A.: NADP-MDN Report: External Quality Assurance Programs Managed by the U.S. Geological Survey in Support of the National Atmospheric Deposition Program/Mercury Deposition Network, Tech. rep., United States Geological Survey (USGS) and U. S. Department of the Interior, 2007.

Atmos. Chem. Phys. Discuss., doi:10.5194/acp-2016-517, 2016
Manuscript under review for journal Atmos. Chem. Phys.
Published: 20 July 2016
© Author(s) 2016. CC-BY 3.0 License.

Atmospheric Chemistry and Physics Discussions

Lee, D. S., Nemitz, E., Fowler, D., and Kingdon, R. D.: Modelling atmospheric mercury transport and deposition across Europe and the UK, Atmos. Environ., 35, 5455–5466, doi:10.1016/S1352-2310(01)00284-9, 2001.

Lin, C. and Pehkonen, S.: The chemistry of atmospheric mercury: a review, Atmospheric Environment, 33, 2067–2079, 1999.

Lindberg, S., Brooks, S., Lin, C., Scott, K., Landis, M., Stevens, R., and Goodsite, M.: Dynamic oxidation of gaseous mercury in the arctic troposphere at polar sunrise, Environmental Science and Technology, 36, 1245–1256, 2002.

Lindberg, S., Bullock, R., Ebinghaus, R., Engstrom, D., Feng, X., Fitzgerald, W., Pirrone, N., Prestbo, E., and Seigneur, C.: A synthesis of progress and uncertainties in attributing the sources of mercury in deposition, AMBIO: A Journal of the Human Environment, 36, 19–33, 2007.

Lombard, M. A. S., Bryce, J. G., Mao, H., and Talbot, R.: Mercury deposition in Southern New Hampshire, 2006–2009, Atmos.Chem. Phys., 11, 7657–7668, doi:10.5194/acp-11-7657-2011, 2011.

Mason, R. and Sheu, G.: Role of the ocean in the global mercury cycle, Global Biogeochem. Cy., 16, 1093, doi:10.1029/2001gb001440, 2002.

Mason, R., Lawson, N., and Sheu, G.: Annual and seasonal trends in mercury deposition in Maryland, Atmospheric Environment, 34, 1691–1701, doi:10.1016/S1352-2310(99)00428-8, 2000.

Mason, R., Choi, A., Fitzgerald, W., Hammerschmidt, C., Soerensen, C. L. A., and Sunderland, E.: Environ Res, Global Biogeochem. Cy., 119, 101–117, 2012.

Munthe, J., Wangberg, I., Iverfeldt, A., Lindqvist, O., Stomberg, D., Sommar, J., Gårdfeldt, K., Petersen, G., Ebinghaus, R., Prestbo, E., Larjava, K., and Siemens, V.: Distribution of atmospheric mercury species in Northern Europe: final results from the MOE project, Atmospheric Environment, 37, 9 – 20, 2003.

Munthe, J., Wängberg, I., Rognerud, S., Fjeld, E., Verta, M., Porvari, P., and M., M.: Mercury in Nordic Ecosystem., Tech. rep., IVL Report B1761, 2007.

Munthe, J., Sprovieri, F., Horvat, M., and Ebinghaus, R.: SOPs and QA/QC protocols regarding measurements of TGM, GEM, RGM, TPM and mercury in precipitation in cooperation with WP3, WP4 and WP5, GMOS deliverable 6.1, CNR-IIA, IVL, 2011.

Nair, U., Wu, Y., Holmes, C., Schure, A. T., Kallos, G., and Walters, J.: Cloud-resolving simulations of mercury scavenging and deposition in thunderstorms, Atmos. Chem. Phys., 13, 10 143–10 157., 2013.

Pacyna, E., Pacyna, J., Sundseth, K., Munthe, J., Kindbom, K., Wilson, S., Steenhuisen, F., and Maxson, P.: Global emission of mercury to the atmosphere from anthropogenic sources in 2005 and projections to 2020, Atmos. Environ., 44, 2487–2499, doi:10.1016/j.atmosenv.2009.06.009, 2010.

Pirrone, N., Hedgecock, I., and Sprovieri, F.: Atmospheric mercury, easy to spot and hard to pin down: impasse?, Atmospheric Environment, 42, 8549–8551, doi:10.1016/j.atmosenv.2008.09.004, 2008.

Pirrone, N., Cinnirella, S., Feng, X., Finkelman, R., Friedli, H., Leaner, J., Mason, R., Mukherjee, A., Stracher, G., Streets, D., and Telmer, K.: Global mercury emissions to the atmosphere from anthropogenic and natural sources, Atmos. Chem. Phys, 10, 5951–5964, doi:10.5194/acp-10-5951-2010, 2010.

Prestbo, E. M. and Gay, D. A.: Wet deposition of mercury in the U.S. and Canada, 1996–2005: Results and analysis of the NADP mercury deposition network (MDN), Atmospheric Environment, 43, 4223 – 4233, 2009.

Rautenbach, C. d. and Smith, I.: Teleconnections between global sea-surface temperatures and the interannual variablility of observed and model simulated rainfall over southern Africa, J. Hydrol., 254, 1–15, 2001.

© Author(s) 2016. CC-BY 3.0 License.

Sanei, H., Outridge, P., Goodarzi, F., Wang, F., Armstrong, D., Warren, K., and Fishback, L.: Wet deposition mercury fluxes in the Canadian sub-Arctic and southern Alberta, measured using an automated precipitation collector adapted to cold regions, Atmospheric Environment, 44, 1672–1681, 2010.

Schroeder, W. and Munthe, J.: Atmospheric mercury – An overview, Atmospheric Environment, 32, doi:10.1016/S1352-2310(97)00293-8, 1998.

Sciare, J., Favez, O., Sarda-Estève, R., Oikonomou, K., Cachier, H., and Kazan, V.: Long-term observations of carbonaceous aerosols in the austral ocean atmosphere: evidence of a biogenic marine organic source, J. Geophys. Res., 114, D15 302, doi:10.1029/2009JD011998, 2009.

Seigneur, C., Vijayaraghavan, K., Lohman, K., Karamchandani, P., and Scott, C.: Global Source Attribution for Mercury Deposition in the United States, Environmental Science & Technology, 38, 555–569, 2004.

Selin, N. E.: Global Biogeochemical Cycling of Mercury: A Review, Annual Review of Environment and Resources, 34, 43–63, 2009.

Selin, N. E.: Global change and mercury cycling: Challenges for implementing a global mercury treaty, Environmental Toxicology and Chemistry, 33, 1202–1210, doi:10.1002/etc.2374, http://dx.doi.org/10.1002/etc.2374, 2014.

Selin, N. E. and Jacob, D. J.: Seasonal and spatial patterns of mercury wet deposition in the United States: Constraints on the contribution from North American anthropogenic sources, Atmospheric Environment, 42(21), 5193–5204, 2008.

Sena, F., Umlauf, G., Ruiz, A. A., Islas, M. R., Trejo, J. A. V., Cabrera, F. A., and Vargas, I. O.: Wet deposition and atmospheric mercury monitoring in Sisal, Yucatán, México, as part of the Global Mercury Observation System (GMOS), Tech. rep., JRC - EUROPEAN COMMISION, 2015.

Shanley, J., Mast, M., Campbell, D., Aiken, G., Krabbenhoft, D., Hunt, R., Walker, J., Schuster, P., Chalmers, A., Aulenbach, B., Peters, N., Marvin-DiPasquale, M., Clow, D., and Shafer, M.: Comparison of total mercury and methylmercury cycling at five sites using the small watershed approach, Environ. Pollut., 154, 143–154, 2008.

Shanley, J., Engle, M., M, S., Krabbenhoft, D., Brunette, R., Olson, M., and Conroy, M.: High Mercury Wet Deposition at a "Clean Air" Site in Puerto Rico, Environ. Sci. Technol., pp. 12 474–12 482, 2015.

Sillman, S., Marsik, F., Dvonch, J. T., and Keeler, G. J.: Assessing atmospheric deposition of mercury in Florida, USA: Local versus global sources and models versus measurements, E3S Web of Conferences 2013, 1, 07008., 2013.

Slemr, F., Weigelt, A., Ebinghaus, R., Brenninkmeijer, C., Baker, A., Schuck, T., Rauthe-Schoch, A., Riede, H., Leedham, E., Hermann, M., van Velthoven, P., Oram, D., O'Sullivan, D., Dyroff, C., Zahn, A., and Ziereis, H.: Mercury Plumes in the Global Upper Troposphere Observed during Flights with the CARIBIC Observatory from May 2005 until June 2013, Atmosphere-Basel, 5, 342–369, doi:10.3390/Atmos5020342, 2014.

Sorensen, J. A., Glass, G. E., and Schmidt, K.: Regional patternsof wet mercury deposition, Environ. Sci. Tech., 12, 2025–2032, 1994.

Sprovieri, F., Pirrone, N., Gårdfeldt, K., and Sommar, J.: Mercury speciation in the marine boundary layer along a 6000km cruise path around the Mediterranean Sea, Atmospheric Environment, 37, 63 – 71, 2003.

Sprovieri, F., Hedgecock, I., and N., P.: An Investigation of the origins of reactive gaseous mercury in the Mediterranean marine boundary layer, Atmospheric Chemistry and Physics, 10, 3985–3997, doi:10.5194/acp-10-3985-2010, 2010a.

Sprovieri, F., Pirrone, N., Ebinghaus, R., and Kock, H.: A review of worldwide atmospheric mercury measurements, Atmospheric Chemistry and Physics, 10, 8245–8265, doi:10.5194/acp-10-8245-2010, 2010b.

Sprovieri, F., Pirrone, N., Bencardino, M., D'Amore, F., Carbone, F., Cinnirella, S., Mannarino, V., Landis, M., Ebinghaus, R., Weigelt, A., Brunke, E.-G., Labuschagne, C., Martin, L., Munthe, J., Wängberg, I., Artaxo, P., Morais, F., Cairns, W., Barbante, C., del Car-

© Author(s) 2016. CC-BY 3.0 License.

men Diéguez, M., Garcia, P. E., Dommergue, A., Angot, H., Magand, O., Skov, H., Horvat, M., Kotnik, J., Read, K. A., Neves, L. M., Gawlik, B. M., Sena, F., Mashyanov, N., Vladimir, Obolkin, A., Wip, D., Feng, X. B., Zhang, H., Fu, X., Ramachandran, R., Cossa, D., Knoery, J., Marusczak, N., Nerentorp, M., , and Norstrom, C.: Atmospheric Mercury Concentrations observed at ground-based monitoring sites globally distributed in the framework of the GMOS network, ACPD, Special Issue: Global Mercury Observation System – Atmosphere (GMOS-A), doi:10.5194/acp-2016-466, 2016.

Steffen, A., Scherz, T., Olson, M., Gay, D., and Blanchard, P.: A comparison of data quality control protocols for atmospheric mercury speciation measurements, Journal of Environmental Monitoring, 14, 752–765, 2012.

Streets, D. G., Hao, J., Wu, Y., Jiang, J., Chan, M., Tian, H., and Feng, X.: Anthropogenic mercury emissions in China, Atmospheric Environment, 39, 7789 – 7806, 2005.

Strode, S. A., Jaeglé, L., Selin, N. E., Jacob, D. J., Park, R. J., Yantosca, R. M., Mason, R. P., and Slemr, F.: Air-sea exchange in the global mercury cycle, Global Biogeochem. Cycles, 21, GB1017–, doi:10.1029/2006GB002766, 2007.

Strode, S. A., Jaeglé, L., Jaffe, D. A., Swartzendruber, P. C., Selin, N. E., Holmes, C., and Yantosca, R. M.: Trans-Pacific transport of mercury, J. Geophys. Res., 113, D15 305–, doi:10.1029/2007JD009428, 2008.

Swartzendruber, P. C., Jaffe, D. A., Prestbo, E. M., Weiss-Penzias, P., Selin, N. E., Park, R., Jacob, D. J., Strode, S., and Jaeglé, L.: Observations of reactive gaseous mercury in the free troposphere at the Mount Bachelor Observatory, Journal Of Geophysical Research - Atmospheres, 111, –, 2006.

Vanarsdale, A., Weiss, J., Keeler, G., Miller, E., Boulet, G., Brulotte, R., and Poissant, L.: Patterns of mercury deposition and concentration in northeastern North America, Ecotoxicology, 14, 37–52, doi:10.1007/s10646-004-6258-x, 2005.

Veiga, M., Maxson, P., and Hylander, L.: Origin of Mercury in Artisanal Gold Mining, Journal of Cleaner Production, 14, 436–447, 2006.

Wan, Q., Feng, X. B., Lu, J. L., Zheng, W., Song, X. J., Han, S. J., , and Xu, H.: Atmospheric mercury in Changbai mountain area, northeastern China I: The seasonal distribution pattern of total gaseous mercury and its potential sources, Environ. Res., 109, 201–206, 2009.

Wängberg, I., Munthe, J., Berg, T., Ebinghaus, R., Kock, H., Temme, C., Bieber, E., Spain, T., and Stolk, A.: Trends in air concentration and deposition of mercury in the coastal environment of the North Sea Area, Atmospheric Environment, 41, 2612–2619, 2007.

Weiss-Penzias, P., Gustin, M., and Lyman, S.: Observations of speciated atmospheric mercury at three sites in Nevada: Evidence for a free tropospheric source of reactive gaseous mercury, Geophys. Res., 114, 2612–2619, 2009.

Wu, Y., Wang, S., Streets, D. G., Hao, J., Chan, M., and Jiang, J.: Trends in Anthropogenic Mercury Emissions in China from 1995 to 2003, Environmental Science & Technology, 40, 5312–5318, 2006.

Xiao, Z., Sommar, J., Lindqvist, O., and Tan, H.and He, J.: tmospheric mercury deposition on Fanjing Mountain Nature Reserve, Guizhou, China, A, Chemosphere, 36, 2191–2200, 1998.

Zhang, L. and Wright, L.: A review of current knowledge concerning dry deposition of atmospheric mercury, Atmospheric Environment, 43, 5853–5864, doi:10.1016/j.atmosenv.2009.08.019, 2009.

Zhang, L., Blanchard, P., Gay, D., Prestbo, E., Risch, M., Johnson, D., Narayan, J., Zsolway, R., Holsen, T., Miller, E., Castro, M., Graydon, J., Louis, V., and Dalziel, J.: Estimation of speciated and total mercury dry deposition at monitoring locations in eastern and central North America, Atmospheric Chemistry and Physics, 12, 4327–4340, doi:10.5194/acp-12-4327-2012, 2012.

Annexe 5 : Comparison of mercury concentrations measured at several sites in the Southern Hemisphere

Slemr, F., **Angot, H.**, Dommergue, A., Magand, O., Barret, M., Weigelt, A., Ebinghaus, R., Brunke, E.-G., Pfaffhuber, K. A., Edwards, G., Howard, D., Powell, J., Keywood, M., Wang, F., Atmospheric Chemistry and Physics, 15, 3125-3133, 2015.

Atmos. Chem. Phys., 15, 3125–3133, 2015
www.atmos-chem-phys.net/15/3125/2015/
doi:10.5194/acp-15-3125-2015
© Author(s) 2015. CC Attribution 3.0 License.

Atmospheric Chemistry and Physics
Open Access

Comparison of mercury concentrations measured at several sites in the Southern Hemisphere

F. Slemr[1], H. Angot[2], A. Dommergue[2,3], O. Magand[3], M. Barret[2,3], A. Weigelt[4], R. Ebinghaus[4], E.-G. Brunke[5], K. A. Pfaffhuber[6], G. Edwards[7], D. Howard[7], J. Powell[8], M. Keywood[8], and F. Wang[9]

[1]Max-Planck-Institute for Chemistry, Hahn-Meitner-Weg 1, 55128 Mainz, Germany
[2]Université Grenoble Alpes, LGGE, 38041 Grenoble, France
[3]CNRS, LGGE, 38041 Grenoble, France
[4]Helmholtz-Zentrum Geesthacht (HZG), Institute of Coastal Research, Max-Planck-Strasse 1, 21502 Geesthacht, Germany
[5]South African Weather Service c/o CSIR, P.O. Box 320, Stellenbosch 7599, South Africa
[6]Norwegian Institute for Air Research (NILU), P.O. Box 100, 2027 Kjeller, Norway
[7]Macquarie University, Environmental Science, Sydney, NSW, Australia
[8]CSIRO Ocean and Atmosphere Flagship Research, Aspendale, VIC, Australia
[9]Centre for Earth Observation Science, Department of Environment and Geography, University of Manitoba, Winnipeg, MB, R3T 2N2, Canada

Correspondence to: F. Slemr (franz.slemr@mpic.de)

Received: 6 October 2014 – Published in Atmos. Chem. Phys. Discuss.: 3 December 2014
Revised: 7 February 2015 – Accepted: 25 February 2015 – Published: 19 March 2015

Abstract. Our knowledge of the distribution of mercury concentrations in air of the Southern Hemisphere was until recently based mostly on intermittent measurements made during ship cruises. In the last few years continuous mercury monitoring has commenced at several sites in the Southern Hemisphere, providing new and more refined information. In this paper we compare mercury measurements at several remote sites in the Southern Hemisphere made over a period of at least 1 year at each location. Averages of monthly medians show similar although small seasonal variations at both Cape Point and Amsterdam Island. A pronounced seasonal variation at Troll research station in Antarctica is due to frequent mercury depletion events in the austral spring. Due to large scatter and large standard deviations of monthly average median mercury concentrations at Cape Grim, no systematic seasonal variation could be found there. Nevertheless, the annual average mercury concentrations at all sites during the 2007–2013 period varied only between 0.85 and 1.05 ng m^{-3}. Part of this variability is likely due to systematic measurement uncertainties which we propose can be further reduced by improved calibration procedures. We conclude that mercury is much more uniformly distributed throughout the Southern Hemisphere than the distributions suggested by measurements made onboard ships. This finding implies that smaller trends can be detected in shorter time periods. We also report a change in the trend sign at Cape Point from decreasing mercury concentrations in 1996–2004 to increasing concentrations since 2007.

1 Introduction

Our knowledge of the distribution of mercury in air over the Southern Hemisphere is mostly based on measurements made during ship cruises. According to the most comprehensive review of shipboard measurements made between 1990 and 2009 by Soerensen et al. (2012) mercury concentrations varied between 0.72 ng m^{-3} reported by Kuss et al. (2011) for the southern Atlantic Ocean and 2.20 ng m^{-3} observed by Xia et al. (2010) over the southeastern Indian Ocean. These data were collected in different areas during different seasons, typically over a period of 1 or 2 months. Only a few of these measurements were accompanied by measurements of tracers specific to anthropogenic pollution

and the influence from the ship such as CO, nitrogen oxides, and particles. Consequently, the influence of sources such as from biomass burning, regional pollution, and pollution from the ship itself could not be properly filtered out from the data. Part of the reported variability may also be due to the use of frequently undeclared and non-uniform standard conditions under which these concentrations are reported. Mercury concentrations in ng m^{-3} are usually reported at a standard pressure of 1013 hPa and a standard temperature of 273.14 K. However, some researchers and organisations use 293.14 K or 298.14 K. Since the same concentrations reported at 273.14 and 298.14 K differ by almost 10 %, the non-uniform standard conditions alone would prevent the detection of the statistically significant decrease in annual median mercury concentrations at Cape Point from $\sim$ 1.3 ng m^{-3} in 1996 to below 1.2 ng m^{-3} in 2004 (Slemr et al., 2008). Lastly, averages and standard deviations are quite frequently quoted without the number of measurements on which they are based. This means that the averages or medians cannot be weighed by the number of the measurements. It also makes statistical tests for the differences of averages impossible. It is not surprising that, using such data, Soerensen et al. (2012) concluded that no significant trend in the Southern Hemisphere could be detected so far. While we agree with this conclusion, a qualification is required: the quality of the data used by Soerensen et al. (2012) does not allow detection of trends smaller than their variability, i.e. some 50 % or even more. Consequently, with trends of up to $\sim$ 2 % per year (Slemr et al., 2008; Ebinghaus et al., 2011), it would take several decades to detect trends from measurements onboard ships.

Recently, mercury has been measured continuously at several remote sites in the Southern Hemisphere over periods of a year or more. In this paper we will compare these measurements in terms of their monthly and annual statistics. We selected stations which are either baseline stations (Amsterdam Island, Troll research station in Antarctica) or where additional measurements (e.g. CO, ^{222}Rn, wind direction, aerosol) allow us to filter out baseline conditions (Cape Point and Cape Grim). The results show that atmospheric mercury is more uniformly distributed over the Southern Hemisphere than the measurements onboard ships suggest. Stationary sites with continuous and reproducible measurements of higher quality over longer periods allow for the detection of smaller trends in shorter time periods.

2 Experimental

Figure 1 shows the location of the sites whose data are used in this paper: Amsterdam Island, Cape Grim, Cape Point, Troll research station, and Galápagos Archipelago.

The Cape Point site (CPT, 34°21′ S, 18°29′ E) is operated as one of the Global Atmospheric Watch (GAW) baseline monitoring observatories of the World Meteorological Organization (WMO). The station is located on the southern tip of the Cape Peninsula within the Cape Point National Park on top of a peak 230 m a.s.l. and about 60 km south of Cape Town. The station has been in operation since the end of the 1970s and its current continuous measurement portfolio includes Hg, CO, O_3, CH_4, N_2O, ^{222}Rn, CO_2, several halocarbons, particles, and meteorological parameters. The station receives clean marine air masses for most of the time. Occasional events with continental and polluted air can easily be filtered out using a combination of the CO and ^{222}Rn measurements (Brunke et al., 2004). Gaseous elemental mercury (GEM) was measured by a manual amalgamation technique (Slemr et al., 2008) between September 1995 and December 2004 and has been measured by the automated Tekran 2537B instrument (Tekran Inc., Toronto, Canada) since March 2007. Only the Tekran data are reported here. These data were obtained in compliance with the standard operating procedures of the GMOS (Global Mercury Observation System, www.gmos.eu) project. The instrument has been run with a 15 min sampling frequency. For data analysis, 30 min averages were used. On average, 30 % of the data were classified as baseline using the ^{222}Rn $\leq$ 250 mBq m^{-3} criterion.

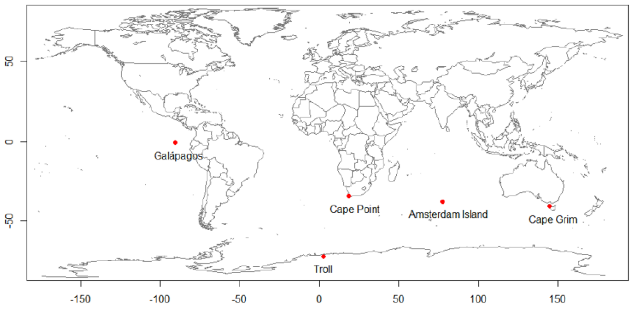

Figure 1. The location of the sites whose data are reported in this paper.

Amsterdam Island (AMS, 37°48′ S, 77°33′ E) is a small isolated island (55 km^2) located in the Indian Ocean 3400 km east of Madagascar. AMS is a GAW global station established in 1967. The climate of Amsterdam Island is mild oceanic, with frequent presence of clouds. Measurements are performed at Pointe Bénédicte station, which is located 2 km west of the Saint Martin de Viviès base on the edge of a cliff 55 m a.s.l. (GPS coordinates: 37°48′ S, 77°33′ E). GEM has been measured using a Tekran 2537B connected to a Tekran 1130/1135 speciation unit since January 2012 with a 5 min sampling frequency. For data analysis, 1 h averages were used. Details on operation and calibration procedures are given in Angot et al. (2014) and follow GMOS standard operating procedures. The station receives clean marine air masses almost all the time.

The Norwegian Antarctic Troll research station (TRS) is located in Queen Maud Land at 72°01′ S and 2°32′ E at an elevation of 1275 m and about 220 km from the Antarctic coast.

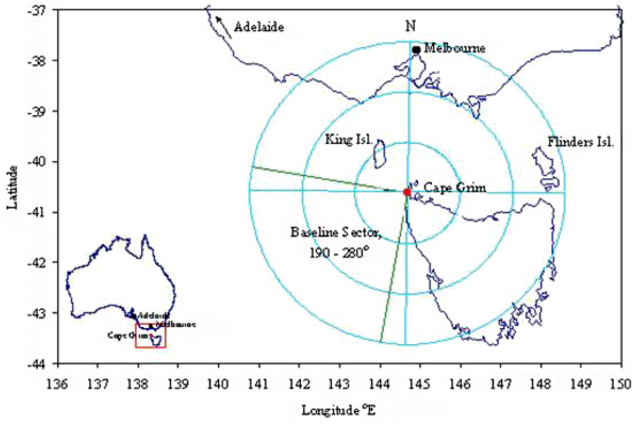

Figure 2. Location of the Cape Grim station and definition of the baseline sector.

The station has been in operation since January/February 2007 and its current continuous measurements include mercury, CO, O_3, particles, greenhouse gases, hydrocarbons, persistent organic compounds (POPs) and meteorological parameters (Hansen et al., 2009; Pfaffhuber et al., 2012). Mercury has been measured using the Tekran 2537B instrument since February 2007 with a 5 min sampling frequency. For data analysis, 1 h averages were used. The original mercury concentrations were reported at a standard temperature of 293.14 K and were converted to the standard temperature of 273.14 K to be comparable with all other data reported here.

The Cape Grim Baseline Air Pollution Station is located on the north-western coast of Tasmania, Australia (40°41′ S, 144°41′ E, Fig. 2). The Cape Grim Baseline Air Pollution Station was established in 1976 to monitor and study global atmospheric composition and is part of the WMO GAW programme. Measurements at Cape Grim include greenhouse gases such as CO_2, CH_4, N_2O, O_3, reactive nitrogen oxides, stratospheric ozone depleting chemicals such as chlorofluorocarbons (CFCs), radon, and GEM. The Tekran 2537A instrument was run with 5 min sampling time. For data analysis, 15 min averages were used. Additionally, meteorological parameters are measured, such as wind speed and direction, rainfall, temperature, humidity, air pressure, solar radiation, along with condensation nuclei (CN) concentration (particles greater than 10 nm), ultrafine condensation nuclei concentration (greater than 3 nm), aerosol absorption, aerosol scattering, cloud condensation nuclei concentration and rainfall chemical composition. Baseline conditions are defined as those with wind directions at 50 m altitude lying between 190 and 280°. In addition, CN should be less than a threshold concentration determined from 5 years of CN data for the current month based on the 90th percentile of CN hourly medians for this period, interpolated using cubic splines to give daily values (Fig. 2). During 2011–2013, the station received baseline marine air for 33 % of the time.

All mercury measurements reported here were made by an automated dual channel, single amalgamation, cold vapour atomic fluorescence analyser (Tekran-Analyzer model 2537 A or B, Tekran Inc., Toronto, Canada). The instrument features two gold cartridges. While one is adsorbing mercury during a sampling period, the other is being thermally desorbed using argon as a carrier gas. Mercury is detected using cold vapour atomic fluorescence spectroscopy (CVAFS). The functions of the cartridges are then interchanged, allowing continuous sampling of the incoming air stream. The instrument can be combined with a speciation unit (Tekran 1130/1135) consisting of a denuder, aerosol filter and pyrolyser that enables a determination of GEM, gaseous oxidised mercury (GOM), and particle-bound mercury (PM, < 2.5 µm) typically every 2–3 h (Landis et al., 2002). Operation and calibration of the instruments follow established and standardised procedures (e.g. Steffen and Schroeder, 1999). All mercury concentrations reported here are given in ng m^{-3} at 273.14 K and 1013 hPa.

In this paper we compare measurements at different sites in terms of monthly and annual average and median concentrations. Random uncertainties of individual measurements will average out and all we have to discuss are thus the systematic uncertainties, i.e. biases. The Tekran analyser is a complex instrument and the systematic uncertainties of its measurements depend on the operation procedure, the performance of the instrument, and the experience of its operators. All instruments used in this study are equipped with an internal mercury permeation source that is used to check and adjust periodically the instrument span and zero, typically every 25–72 h depending on the standard operating procedures that are used. This periodical internal calibration removes drifts both in span and zero that are caused mostly by the temperature and ageing of the fluorimeter lamp. The permeation rate of ~ 1 pg Hg s^{-1} is, however, too low to allow a gravimetric determination of the permeation rate within a reasonable time period, as is usually done when certifying permeation devices for other gases (Barratt, 1981). Consequently, the permeation rate is calibrated every 6–12 months by repeated injection (at least 10 injections) of known volumes of gas saturated with mercury vapour at a known temperature. A skilled operator can achieve an individual injection precision of ~ 3 %, resulting in an uncertainty of ~ 1 % for 10 injections. The flow rate uncertainty of ~ 1 % represents the second major contribution to the overall systematic uncertainty (Widmer et al., 1982). Adding smaller contributions from uncertainties associated with the injected volume and the temperature of the mercury vapour saturating device yields an overall systematic uncertainty of ~ 3 %. We consider this to be the lower limit of the overall systematic uncertainty because this estimate assumes ideal performances of the instrument, its internal permeation device, the calibration mercury vapour saturating device, the injection syringes, as well as of the instrument operators.

A comprehensive analysis of all random and systematic uncertainties involved in a single manual determination of mercury concentration in air is given by Brown et al. (2008), who estimated the combined relative uncertainty to be 16.7 % at the concentration of 1.2 ng m^{-3}. This uncertainty includes the uncertainty from different published mercury vapour pressure curves and can be reduced to 12.6 % when one vapour pressure curve is accepted to be correct, as is the case here. This uncertainty analysis, however, is not directly applicable to measurements with the Tekran instrument because most items in the uncertainty budget are random rather than systematic. The combined systematic uncertainty (square root of the sum of uncertainties in quadrature) from uncertainties in flow calibration (2 %) and detector calibration (7 %) would be ∼ 7 %. Since one vapour pressure curve was used, the 5.5 % uncertainty in the saturated mercury concentration can be neglected. The overall systematic uncertainty would then be ∼ 3 % and is comparable to our estimate.

Contributions of deviations from an ideal performance, such as slow deactivation of the traps, difference between the concentrations from the two traps, contamination of the switching valves and traps, and leaks (Steffen et al., 2012), are difficult to quantify. Thus we take published results of Tekran instrument intercomparisons as a measure of practically achievable systematic uncertainty. In an intercomparison described by Ebinghaus et al. (1999) three Tekran instruments that were operated side by side at Mace Head were biased by 0.02–0.11 ng m^{-3} (median 0.01–0.13 ng m^{-3}) against each other. With an average concentration of 1.75 ng m^{-3}, this represents the highest systematic uncertainty of ∼ 6 %. Two Tekran instruments were run side by side for 4 days at a site in Tuscany in June 1998 (Munthe et al., 2001) with an average bias of 9 %. Mercury was measured by five Tekran instruments for 28 days within a 6-week period in May and June 2006 at German EMEP station Waldhof (Aas et al., 2006). The median concentrations were 2.02, 1.88, 1.77, 1.70, and 1.69 ng m^{-3}, and their average was 1.81 ± 0.14 ng m^{-3}. The average bias was thus ∼ 8 % and the bias between the instruments with the lowest and highest readings was ∼ 18 % (related to the average concentrations). In summary, based on experimental evidence, we can expect an average systematic uncertainty of ∼ 10 %, in extreme cases up to 20 %.

Despite using the same instrumentation, the measurements may target different mercury species at different sites, depending on their configuration and/or local conditions. At Amsterdam Island the instrument was operated with the Tekran 1130/1135 speciation unit. It showed GOM concentrations of less than 5 pg m^{-3} representing less than 1 % of the total gaseous mercury (TGM) concentrations of ∼ 1 ng m^{-3} (Angot et al., 2014). The data for Amsterdam Island presented here are stated explicitly as GEM. The instruments at Cape Point, Cape Grim, and Troll research station are operated without speciation units but with PTFE (Teflon) filters to protect the instrument from sea salt and other particles. Although not proven, we assume that the surface active GOM in the humid air of the marine boundary layer at Cape Point and Cape Grim will be filtered out together with PM, partly by the salt particle loaded PTFE filter (denuders coated with KCl are used to adsorb GOM (Landis et al., 2002)) and partly on the walls of the inlet tubing. Consequently, we assume that measurements at Cape Point and Cape Grim represent GEM only and are thus directly comparable to those at Amsterdam Island. Although at Troll research station the same configuration with a PTFE filter is used, measurements by Temme et al. (2003) showed that at the low temperature and humidity prevailing at this site, GOM passed the inlet tubing and the PTFE filter. The measurements at Troll research station are thus assumed to represent TGM. As the GOM concentrations at Amsterdam Island in particular and in the marine boundary layer in general are below 10 pg m^{-3} (Soerensen et al., 2010; Angot et al., 2014), the difference between TGM and GEM at Amsterdam Island, Cape Grim and Cape Point is usually less than 1 %, which is insignificant when compared with the uncertainties discussed above. Consequently, GEM measurements at Cape Point, Cape Grim and Amsterdam Island are comparable to TGM measured at Troll research station. We caution, however, that recent studies have shown that the KCl-coated denuder in the Tekran speciation technique does not efficiently collect all GOM (Gustin et al., 2013; Huang et al., 2013; Ambrose et al., 2013). The bias between the TGM measurements at Troll research station and GEM measurements at all other stations can thus be larger.

The pair data difference tests were done using a *t* test (Kaiser and Gottschalk, 1972). A Mann–Kendal test for trend detection and the estimate of Sen's slope were made using the program by Salmi et al. (2002).

3 Results and discussion

3.1 Comparison of seasonal variations

Figure 3 shows seasonal variation of median mercury concentrations at Amsterdam Island, Cape Point, Cape Grim, and Troll research station in Antarctica during 2011–2013. Plotted are the averages of monthly median mercury concentrations and their standard deviations. We prefer here the use of monthly medians because they are less influenced by extreme values. The medians for Cape Point and Cape Grim were calculated both from unfiltered data and data filtered using the ^{222}Rn ≤ 250 mBq m^{-3} criterion for Cape Point and the baseline criteria mentioned above for Cape Grim. Pair tests for systematic differences between the monthly medians of filtered and unfiltered data (Kaiser and Gottschalk, 1972) did not show any significant difference (significance level < 95 %) at both sites. Thus pollution events occasionally observed at Cape Point (Brunke et al. 2012; Slemr et

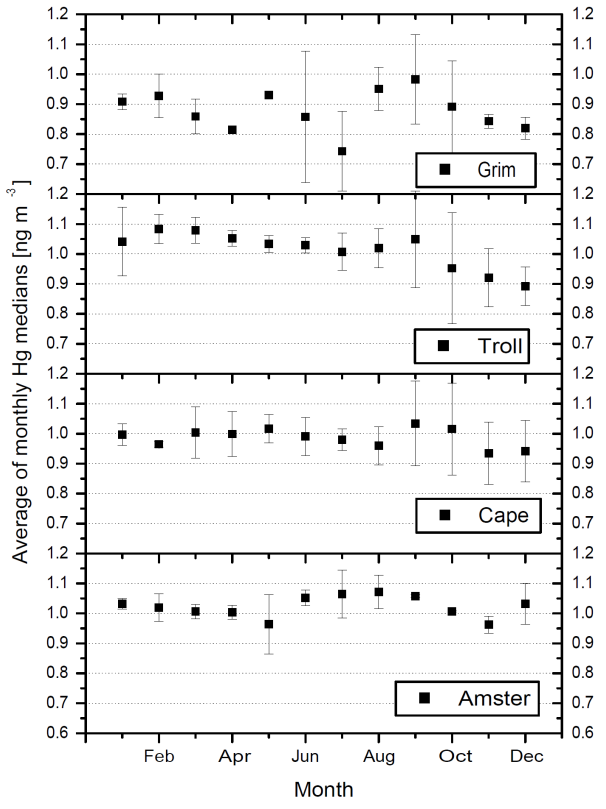

Figure 3. Seasonal variation of average monthly medians of mercury concentrations in 2011–2013 at Cape Point (no data in February 2011) and Troll research station (no data in September and October 2011). At Amsterdam Island the data cover only the 28 January 2012 to 31 December 2013 period and, at Cape Grim, data from January to August and November 2011, and April, May and October 2013 are missing. Bars denote the standard deviation of the monthly averages.

al., 2013) and at Cape Grim have no substantial influence on the monthly medians of mercury concentrations. This finding also has implications for the data from Amsterdam Island: if the influence of continental air masses is unimportant at Cape Point located on the coast of South Africa and at Cape Grim near the Australian continent, even less influence can be expected at Amsterdam Island, an isolated island in the middle of the Indian Ocean. Consequently, medians of unfiltered data from all sites were used when constructing this figure.

The smallest seasonal variation, within $\sim 0.1\,\mathrm{ng\,m^{-3}}$, is observed at Cape Point and Amsterdam Island, and the data which vary around $1\,\mathrm{ng\,m^{-3}}$ are very similar. In fact, a pair test for the differences in monthly medians (23 months) revealed no significant difference (significance level $< 95\,\%$) between the measurements at Amsterdam Island and Cape Point. Standard deviations of monthly medians averaged over 3 years (2011–2013) at Cape Point tend to be somewhat larger than those averaged over 2 years at Amsterdam Island, possibly due to inter-annual variations. Taking the standard deviations into account, there is no seasonal variation discernible at both sites.

The seasonal variation at Troll research station is, at $\sim 0.2\,\mathrm{ng\,m^{-3}}$, substantially larger, whereas the monthly standard deviations are comparable to those at Cape Point. Minimum values are observed in October, November, and December, which are the months with frequent mercury depletion events in Antarctica (Temme et al., 2003; Pfaffhuber et al., 2012), and maximum values tend to occur in February and March and are, at $\sim 1.1\,\mathrm{ng\,m^{-3}}$, somewhat higher than at Cape Point and Amsterdam Island. In November and December the monthly average concentrations are, at $\sim 0.9\,\mathrm{ng\,m^{-3}}$, somewhat lower than at Cape Point and Amsterdam Island but comparable when averaged over the whole year (see Table 1). A pair test for differences in monthly medians at Cape Point, Amsterdam Island, and Troll research station revealed no statistically significant difference between them in the 2011–2013 period (33 months for Cape Point vs. Troll, 24 months for Amsterdam Island vs. Troll). There is a significant difference ($> 99\,\%$, 79 months) between medians at Cape Point and Troll research station over the period 2007–2013, which might be due to different trends at both sites.

Cape Grim data show the largest seasonal variation of $\sim 0.25\,\mathrm{ng\,m^{-3}}$, the largest monthly standard deviations, and the lowest annual average concentration of $\sim 0.85\,\mathrm{ng\,m^{-3}}$ of all four sites, some 15 % below the annual mean concentrations at all other sites. Large standard deviations in September and October coincide with similar variability at Troll research station and Cape Point. Large and random scatter of the monthly values in other months suggests that the data from Cape Grim are not as homogeneous as those from other sites. Pair tests for differences in monthly medians detected a highly significant systematic difference between data from Cape Point and Amsterdam Island on the one hand and those from Cape Grim on the other (Cape Point vs. Cape Grim: $> 99.9\,\%$, 23 months; Amsterdam Island vs. Cape Grim: $> 99.9\,\%$, 21 months). Without additional QA/QC effort we cannot find out how many of these differences between the data from Cape Grim and from the other three sites are due to regional differences and/or due to the systematic uncertainties discussed in the experimental section.

3.2 Comparison of annual averages

The annual averages and medians for the Amsterdam Island, Cape Point, Cape Grim, and Troll research stations are given in Table 1. The table also contains an average of monthly medians for March, April, May, June, and October 2011 for Galápagos Archipelago (Wang et al., 2014). Located just south of the Equator, Galápagos Archipelago may be influenced by northern hemispheric air, especially in January, when the intertropical convergence zone (ITCZ) is at its southernmost position (Wang et al., 2014). The band of mixed northern and southern hemispheric air at ITCZ in the

Table 1. Comparison of annual average and median mercury concentrations at Amsterdam Island, Cape Point, Cape Grim, Troll research station, and Galápagos Archipelago. Hourly data were available for Amsterdam Island and Troll research station, half-hourly data for Cape Point, 5–15 min data for Cape Grim, and monthly averages for Galápagos Archipelago. All concentrations are given in ng m^{-3} at 273.14 K and 1013 hPa.

Site	2011		2012		2013	
	Average and standard deviation	Median, number of measurements	Average and standard deviation	Median, number of measurements	Average and standard deviation	Median, number of measurements
Cape Point	0.923 ± 0.106	0.934, 13 918	1.017 ± 0.095	1.018, 15 040	1.052 ± 0.160	1.040, 7809
Amsterdam Island	No data	No data	1.025 ± 0.065[a]	1.028, 6164[a]	1.028 ± 0.096	1.027, 7410
Cape Grim	0.959 ± 0.146[b]	0.976, 3692[b]	0.872 ± 0.130	0.854, 35 097	0.848 ± 0.112[c]	0.858, 36 310[c]
Troll	1.032 ± 0.192	1.061, 5876	1.052 ± 0.160	1.040, 7809	0.970 ± 0.162	1.000, 8196
Galápagos Archipelago	1.054 ± 0.087[d]	1.041, 5 months[d,e]	No data	No data	No data	No data

[a] Temporal coverage 28 January 2012–31 December 2012.
[b] Only September, October and December covered by measurements.
[c] No data in April, May and October.
[d] Only March, April, May, June, and October data were considered; February eliminated because of ITCZ proximity.
[e] Average of monthly medians.

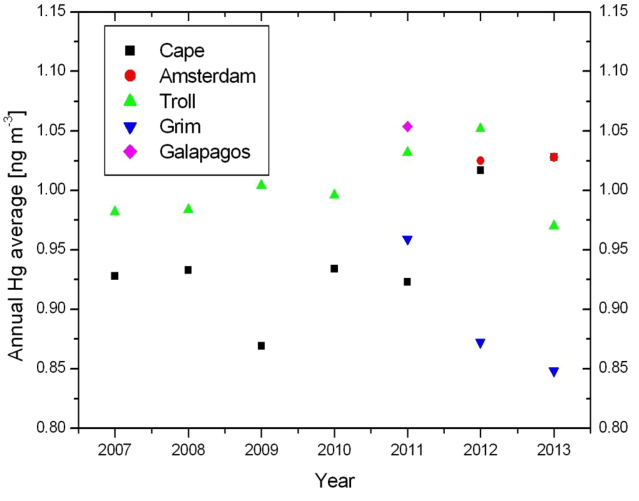

Figure 4. Annual average mercury concentrations at Cape Point, Amsterdam Island, Cape Grim, Troll research station and Galapagos Archipelago (Wang et al., 2014). Note that the 2013 annual averages at Cape Point and Amsterdam Island fall together.

marine boundary layer over the Atlantic Ocean tends to be quite narrow, usually less than 500 km broad (Slemr et al., 1985). If the same applies for the region around Galápagos Archipelago, then data from December, January and February could have been influenced by northern hemispheric air. Thus data for February 2011, although available, were not included.

Figure 4 shows an overview of the average mercury concentrations measured at different southern hemispheric sites during 2007–2013. It does not show the average mercury concentration of 1.32 ± 0.23 ng m^{-3} measured at a coastal site in Suriname for the season when the ITCZ is located north of the site and air originates from the South Atlantic (Müller et al., 2012). As the ITCZ moves seasonally over the site in Suriname, the influence of northern hemispheric air is greater than at Galápagos Archipelago. Moreover, this site is also influenced by emissions from large-scale biomass burning in the Amazonas region (Ebinghaus et al., 2007; Müller et al, 2012). And last but not least, no annual statistics for southern hemispheric air can be made for Suriname because only seasonal concentrations are available. For these reasons, the measurements at Suriname are not included in further discussion.

Most of the annual medians and averages for individual sites in Table 1 differ by less than 0.02 ng m^{-3}, implying that the data are nearly normally distributed. Only at the Troll research station do the differences between annual medians and averages tend to be larger, while the medians tend to exceed the averages (in 6 of the 7 years). This is probably due to the extremely low values during the depletion events which occur during the Antarctic spring.

The annual averages and medians at Amsterdam Island and Cape Point differ by 0.01 and 0.01 ng m^{-3}, respectively, in 2012, and by 0.02 and 0.01 ng m^{-3}, respectively, in 2013. When compared over the overlapping period in 2012 (28 January–31 December), the averages and medians at both sites differed merely by 0.00 and 0.01 ng m^{-3}, respectively. The differences between Troll research station and the two other stations (Amsterdam Island and Cape Point) are substantially larger, by as much as 0.11 and 0.13 ng m^{-3} for 2011 averages and medians, respectively. In 2012 and 2013 the differences are below 0.1 ng m^{-3}. Annual averages over the period of 2007–2013 show that the difference between Cape Point and Troll research station never exceeded 0.14 ng m^{-3}, reached in 2009, and the average difference was 0.06 ng m^{-3}. The highest difference in medians was 0.20 ng m^{-3}, also in 2009, and the average difference was 0.08 ng m^{-3}.

Larger concentration differences are observed between Cape Grim and all other sites in 2011–2013. The annual

averages and medians at Cape Grim were lower than at Amsterdam Island by 0.15 and 0.17 ng m^{-3}, respectively, in 2012, and by 0.18 and 0.17 ng m^{-3}, respectively, in 2013. The differences in annual averages and medians at Cape Grim and Cape Point were somewhat lower in 2012 and somewhat higher in 2013 than the corresponding differences between Cape Grim and Amsterdam Island. In 2011, data for Cape Grim and Cape Point overlap only for the period from September 6 to October 19. In this period, the average and median concentrations at Cape Grim were, at 1.03 ± 0.11 ($n = 2328$) and 1.04 ng m^{-3}, respectively, substantially higher than 0.86 ± 0.07 ($n = 1474$) and 0.86 ng m^{-3}, respectively, at Cape Point.

Figure 4 shows that the annual average mercury concentrations at all sites vary within ~ 0.2 ng m^{-3} from 0.85 ng m^{-3} (Cape Grim in 2013) to ~ 1.05 ng m^{-3} (Galápagos Archipelago in 2011 and Troll research station in 2012). It is not clear how much of this variability is real or due to systematic uncertainty issues discussed in the experimental chapter. We believe that both components contribute and that the real variability of the annual average or median mercury concentrations at southern hemispheric sites not influenced by local and regional pollution is lower. Assuming a systematic uncertainty of ~ 10 % (see Experimental), the real variability at 1 ng m^{-3} in the Southern Hemisphere would be ~ 0.1 ng m^{-3}. This number can be viewed as a preliminary threshold for judging how representative the trends observed at any background site in the Southern Hemisphere are. With this threshold, much smaller trends at shorter time periods can be detected by long-term measurements at several sites when compared to shipboard measurements as reviewed by Soerensen et al. (2012).

3.3 Trend at Cape Point

Figure 4 shows an overall tendency of annual average mercury concentrations for Cape Point to increase with time. The Mann–Kendall test applied to annual averages and medians for 2007–2013 does not reveal a significant trend. However, when applied to monthly medians and averages, the trend is highly significant (at 99.99 % significance level for averages and at 99.96 % for medians). Senn's slope calculated from monthly averages is 0.018 ng m^{-3} yr^{-1} (0.008–0.026 ng m^{-3} yr^{-1} at a significance level of 95 %) and, from monthly medians, 0.016 ng m^{-3} yr^{-1} (0.007–0.025 ng m^{-3} yr^{-1}). This is the first analysis suggesting that mercury concentrations are increasing, as would be expected based on increasing worldwide anthropogenic emissions (Streets et al., 2009; Muntean et al., 2014). A decreasing trend of -0.015 ng m^{-3} yr^{-1} was derived from annual medians at Cape Point in the years 1996–2004 (Slemr et al., 2008), implying that the turning point was located between 2004 and 2007.

No trend could be detected in annual and monthly data from Troll research station over the same period: seven annual averages and medians are not sufficient for trend detection as they were for Cape Point, and the trend in monthly averages and medians is probably masked by the strong seasonal variation. All other southern hemispheric data sets are too short for any trend detection.

Over 7 years of measurements at Cape Point the concentrations had increased by 0.12 ng m^{-3} when calculated from the trend of the monthly averages and 0.11 ng m^{-3} from the trend of the monthly medians. The changing trend from a decrease during the 1996–2004 period to an increase during 2007–2013 at Cape Point is not the only sign that the hemispheric trends in mercury concentrations are changing. An analysis of 1996–2013 data from Mace Head, classified according to the geographical origin of the air masses, showed a) that the downward trend of mercury concentration in air masses originating from over the Atlantic Ocean south of 28° N is substantially lower than for all other classes originating north of 28° N and b) that all downward trends for air masses originating from north of 28° N are decelerating (Weigelt et al., 2015). The apparent inconsistency that no decelerating trend for air masses from south of 28° N was found can be explained by the fact that the changes of a smaller trend are likely to be more difficult to detect.

4 Conclusions

We compared mercury concentrations measured at Cape Point, Amsterdam Island, Cape Grim, and Troll research station in Antarctica. Amsterdam Island and Troll research station are background stations per se, and at Cape Point and Cape Grim the influence of local and regional pollution can be eliminated by using filters such as CO and ^{222}Rn or wind direction and aerosol concentrations. No systematic difference was found between the unfiltered and filtered monthly median mercury concentrations at Cape Point and Cape Grim. We find that in terms of annual averages and medians the gradients of background mercury concentrations within the Southern Hemisphere are small and do not exceed 0.2 ng m^{-3}. Taking into account a systematic measurement uncertainty of ~ 0.1 ng m^{-3}, the real variability could be as low as 0.1 ng m^{-3}. This is much lower than the variability of shipboard mercury measurements on which the discussions of secular trends of mercury concentrations have relied so far. Consequently, smaller trends at shorter time periods can be detected by increasingly available long-term measurements at background sites in the Southern Hemisphere. The preliminary threshold of ~ 0.1 ng m^{-3} for trend detection will further decrease when the comparability of the data sets improves.

The discussion of the measurement uncertainties shows a large difference between a small theoretical uncertainty and the much larger uncertainty achieved experimentally during several intercomparisons. Sampling flow rate can be precisely calibrated, and thus we believe that most of the "sur-

plus" uncertainty comes from the behaviour and calibration of the Tekran internal permeation source. The issues related to the injection of known amounts of mercury are relatively well known (for example, not all syringes and replacement needles are suitable) and the uncertainty caused by them can be reduced by meticulous work. To the best of our knowledge we could not find any information about the dynamical behaviour of the internal permeation source that would enable one to calculate how much time is needed to stabilise the permeation rate (Barratt, 1981). Working practice, however, suggests that the time needed to stabilise the permeation rate increases with the decreasing permeation rate. We surmise that the very small permeation rate of the device in the Tekran instrument needs days rather than hours to stabilise within a 1 % margin required for precision measurements (Barratt, 1981). We thus conclude that the limited time of the cruises and the field conditions onboard ships are at least partly responsible for the large spread of the data from shipborne measurements.

We also report here an increasing trend for mercury concentrations at Cape Point for the period 2007–2013. No significant trend could be detected in mercury concentrations measured at Troll research station in Antarctica over the same period, but this is at least partly due to pronounced seasonal variations at Troll. As mercury concentrations at Cape Point decreased over the period 1996–2004, we conclude that the trend must thus have changed in direction between 2004 and 2007. Such change is qualitatively consistent with the trend changes observed at Mace Head in the Northern Hemisphere (Weigelt et al., 2014).

Acknowledgements. This work contributes to European Community FP7 project Global Mercury Observation System (GMOS). For Amsterdam Island, logistical support and financial support were provided by French Polar Institute IPEV (program 1028, GMOStral). Financial support was also provided by a grant from Labex OSUG@2020 (ANR10 LABX56) and LEFE CNRS/INSU (program SAMOA). We deeply thank the overwintering staff: B. Bouillard, J. Chastain, E. Coz, A. Croguennoc, M. Le Dréau, and V. Lucaire. Aurélien Dommergue acknowledges the Institut Universitaire de France. The Australian Bureau of Meteorology in Australia and CSIRO are also thanked for their continuous support of Cape Grim station. We also sincerely thank the staff at Cape Grim, S. Cleland, J. Ward, N. Sommerville and S. Baley. We acknowledge the support of the Cape Grim Science program student scholarship program. For Troll, financial support to sustain measurements is given through the Norwegian Antarctic Research Expeditions (NARE) programme administered by the Norwegian Polar Institute (NPI). We are very grateful for the technical support offered by the overwintering NPI staff at Troll. The NILU field team, but especially Jan H. Wasseng, is thanked for annual maintenance of the equipment at the Troll station.

The article processing charges for this open-access publication have been covered by the Max Planck Society.

Edited by: A. Dastoor

References

Aas, W. (Ed.): Data Quality 2004, Quality Assurance, and Field Comparisons, EMEP/CCC-Report 4/2006, NILU, Kjeller, Norway 2006.

Ambrose, J. L., Lyman, S. N., Huang, J., Gustin, M. S., and Jaffe, D. A.: Fast time resolution oxidized mercury measurements during the Reno Atmospheric Mercury Intercomparison Experiment (RAMIX), Environ. Sci. Technol. 47, 7285–7294, 2013.

Angot, H., Barret, M., Magand, O., Ramonet, M., and Dommergue, A.: A 2-year record of atmospheric mercury species at a background Southern Hemisphere station on Amsterdam Island, Atmos. Chem. Phys., 14, 11461–11473, doi:10.5194/acp-14-11461-2014, 2014.

Barratt, R. S.: The preparation of standard gas mixtures, Analyst, 106, 817–849, 1981.

Brown, R. J. C., Brown, A. S., Yardley, R. E., Corns, W. T., and Stockwell, P. B.: A practical uncertainty budget for ambient mercury vapour measurement, Atmos. Environ. 42, 2504–2517, 2008.

Brunke, E.-G., Labuschagne, C., Parker, B., Scheel, H. E., and Whittlestone, S.: Baseline air mass selection at Cape Point, South Africa: Application of ^{222}Rn and other filter criteria to CO_2, Atmos. Environ., 38, 5693–5702, 2004.

Brunke, E.-G., Ebinghaus, R., Kock, H. H., Labuschagne, C., and Slemr, F.: Emissions of mercury in southern Africa derived from long-term observations at Cape Point, South Africa, Atmos. Chem. Phys., 12, 7465–7474, doi:10.5194/acp-12-7465-2012, 2012.

Ebinghaus, R., Jennings, S. G., Schroeder, W. H., Berg, T., Donaghy, T., Guentzel, J., Kenny, C., Kock, H. H., Kvietkus, K., Landing, W., Mühleck, T., Munthe, J., Prestbo, E. M., Schneeberger, D., Slemr, F., Sommar, J., Urba, A., Wallschläger, D., and Xiao, Z.: International field intercomparison measurements of atmospheric mercury species, Atmos. Environ. 33, 3063–3073, 1999.

Ebinghaus, R., Jennings, S. G., Kock, H. H., Derwent, R. G., Manning, A. J., and Spain, T. G.: Decreasing trend in total gaseous mercury observations in baseline air at Mace Head, Ireland, from 1996 to 2009, Atmos. Environ., 45, 3475–3480, 2011.

Ebinghaus, R., Slemr, F., Brenninkmeijer, C. A. M., van Velthoven, P., Zahn, A., Hermann, M., O' Sullivan, D. A., and Oram, D. E.: Emission of gaseous mercury from biomass burning in South America in 2005 observed during CARIBIC flights, Geophys. Res. Lett. 34, L08813, doi:10.1029/2006GL028866, 2007.

Gustin, M. S., Huang, J., Miller, M. B., Peterson, C., Jaffe, D. A., Ambrose, J., Finley, B. D., Lyman, S. N., Call, K., Talbot, R., Feddersen, D., Mao, H., and Lindberg, S. E.: Do we understand what the mercury speciation instruments are actually measuring? Results of RAMIX, Environ. Sci. Technol. 47, 7295–7306, 2013.

Hansen, G., Aspmo, K., Berg, T., Edvardsen, K., Fiebig, M., Kallenborn, R., Krognes, T., Lunder, C., Stebel, K., Schmidbauer, N.,

Solberg, S., Espen Yttri, K.: Atmospheric monitoring at the Norwegian Antarctic station Troll: measurement programme and first results, Polar. Res., 28, 353–363, 2009.

Huang, J., Miller, M. B., Weiss-Penzias, P., and Gustin, M. S.: Comparison of gaseous oxidized Hg measured by KCl-coated denuders, and nylon and cation exchange membranes, Environ. Sci. Technol., 47, 7307–7316, 2013.

Kaiser, R. and Gottschalk, G.: Elementare Tests zur Beurteilung von Meßdaten, Bibliographisches Institut, Mannheim, 1972.

Kuss, J., Zülicke, C., Pohl, C., and Schneider, B.: Atlantic mercury emission determined from continuous analysis of the elemental mercury sea-air concentration difference within transects between 50° N and 50° S, Global Biogeochem. Cy., 25, GB3021, doi:10.1029/2010GB003998, 2011.

Landis, M. S., Stevens, R. K., Schaedlich, F.,and Prestbo, E. M.: Development and characterization of an annular denuder methodology for the measurement of divalent inorganic reactive mercury in ambient air, Environ. Sci. Technol. 36, 3000–3009, 2002.

Müller, D., Wip, D., Warneke, T., Holmes, C. D., Dastoor, A., and Notholt, J.: Sources of atmospheric mercury in the tropics: continuous observations at a coastal site in Suriname, Atmos. Chem. Phys., 12, 7391–7397, doi:10.5194/acp-12-7391-2012, 2012.

Muntean, M., Janssens-Maenhout, G., Song, S., Selin, N. E., Olivier, J. G. J., Guizzardi, D., Maas, R., and Dentener, F.: Trend analysis from 1970 to 2008 and model evaluation of EDGARv4 global gridded anthropogenic mercury emissions, Sci. Tot. Environ., 494–495, 337–350, 2014.

Munthe, J., Wängberg, I., Pirrone, N., Iverfeldt, A., Ferrara, R., Ebinghaus, R., Feng, X., Gardfeldt, K., Keeler, G., Lanzillotta, E., Lindberg, S. E., Lu, J., Mamane, Y., Prestbo, E., Schmolke, S., Schroeder, W. H., Sommar, J., Sprovieri, F., Stevens, R. K., Stratton, W., Tuncel, G., and Urba, A.: Intercomparison of methods for sampling and analysis of atmospheric mercury species, Atmos. Environ. 35, 3007–3017, 2001.

Pfaffhuber, K. A., Berg, T., Hirdman, D., and Stohl, A.: Atmospheric mercury observations from Antarctica: seasonal variation and source and sink region calculations, Atmos. Chem. Phys., 12, 3241–3251, doi:10.5194/acp-12-3241-2012, 2012.

Salmi, T., Määttä, A., Anttila, P., Ruoho-Airola, T., and Amnell, T.: Detecting trends of annual values of atmospheric pollutants by the Mann-Kendall test and Sen's slope estimates – the Excel template application Makesens, Finnish Meteorological Institute, Helsinki, Finland, 2002.

Slemr, F., Schuster, G., and Seiler, W.: Distribution, speciation, and budget of atmospheric mercury, J. Atmos. Chem. 3, 407–434, 1985.

Slemr, F., Brunke, E.-G., Labuschagne, C., and Ebinghaus, R.: Total gaseous mercury concentrations at the Cape Point GAW station and their seasonality, Geophys. Res. Lett. 35, L11807, doi:10.1029/2008GL033741, 2008.

Slemr, F., Brunke, E.-G., Ebinghaus, R., and Kuss, J.: Worldwide trend of atmospheric mercury since 1995, Atmos. Chem. Phys., 11, 4779–4787, doi:10.5194/acp-11-4779-2011, 2011.

Slemr, F., Brunke, E.-G., Whittlestone, S., Zahorowski, W., Ebinghaus, R., Kock, H. H., and Labuschagne, C.: ^{222}Rn-calibrated mercury fluxes from terrestrial surface of southern Africa, Atmos. Chem. Phys., 13, 6421–6428, doi:10.5194/acp-13-6421-2013, 2013.

Soerensen, A. L., Skov, H., Jacob, D. J., Soerensen, B. T., and Johnson, M. S.: Global concentrations of gaseous elemental mercury and reactive gaseous mercury in the marine boundary layer, Environ. Sci. Technol. 44, 7425–7430, 2010.

Soerensen, A. L., Jacob, D. J., Streets, D. G., Witt, M. L. I., Ebinghaus, R., Mason, R. P., Andersson, M., and Sunderland, E. M.: Multi-decadal decline of mercury in the North-Atlantic atmosphere explained by changing subsurface seawater concentrations, Geophys. Res. Lett. 39, L21810, doi:10.1029/2012GL053736, 2012.

Steffen, A. and Schroeder, W.: Standard operation procedures manual for total gaseous mercury measurements, Canadian Mercury Measurement Network (CAMNet), Version 4.0, March 1999.

Steffen, A., Scherz, T., Olson, M., Gay, D., and Blanchard, P.: A

Streets, D. G., Zhang, Q., and Wu, Y.: Projections of global mercury emissions in 2050, Environ. Sci. Technol. 43, 2983–2988, 2009.

Temme, C., Einax, J. W., Ebinghaus, R., and Schroeder, W. H.: Measurements of atmospheric mercury species at a coastal site in the Antarctic and over the South Atlantic Ocean during polar summer, Environ. Sci. Technol. 37, 22–31, 2003.

Wang, F., Saiz-Lopez, A., Mahajan, A. S., Gómez Martín, J. C., Armstrong, D., Lemes, M., Hay, T., and Prados-Roman, C.: Enhanced production of oxidised mercury over the tropical Pacific Ocean: a key missing oxidation pathway, Atmos. Chem. Phys., 14, 1323–1335, doi:10.5194/acp-14-1323-2014, 2014.

Weigelt, A., Ebinghaus, R., Manning, A. J., Derwent, R. G., Simmonds, P. G., Spain, T. G., Jennings, S. G., and Slemr, F.: Analysis and interpretation of 18 years of mercury observations since 1996 at Mace Head at the Atlantic Ocean coast of Ireland, Atmos. Environ. 100, 85–93, 2015.

Widmer, A. E., Fehlmann, R., and Rehwald, W.: A calibration system for calorimetric mass flow devices, J. Phys. E: Sci. Instrum., 15, 213–220, 1982.

Xia, C., Xie, Z., and Sun, L.: Atmospheric mercury in the marine boundary layer along a cruise path from Shanghai, China, to Prydz Bay, Antarctica, Atmos. Environ., 44, 1815–1821, 2010.

Annexe 6 : Top-down constraints on atmospheric mercury emissions and implications for global biogeochemical cycling

Song, S., Selin, N. E., Soerensen, A. L., **Angot, H.**, Artz, R., Brooks, S., Brunke, E.-G., Conley, G., Dommergue, A., Ebinghaus, R., Holsen, T. M., Jaffe, D. A., Kang, S., Kelley, P., Luke, W. T., Magand, O., Marumoto, K., Pfaffhuber, K. A., Ren, X., Sheu, G.-R., Slemr, F., Warneke, T., Weigelt, A., Weiss-Penzias, P., Wip, D. C., Zhang, Q., Atmospheric Chemistry and Physics, 15, 7103-7125, 2015.

Atmos. Chem. Phys., 15, 7103–7125, 2015
www.atmos-chem-phys.net/15/7103/2015/
doi:10.5194/acp-15-7103-2015
© Author(s) 2015. CC Attribution 3.0 License.

Atmospheric Chemistry and Physics
Open Access

Top-down constraints on atmospheric mercury emissions and implications for global biogeochemical cycling

S. Song[1], N. E. Selin[1,2], A. L. Soerensen[3,4], H. Angot[5], R. Artz[6], S. Brooks[7], E.-G. Brunke[8], G. Conley[9], A. Dommergue[5], R. Ebinghaus[10], T. M. Holsen[11], D. A. Jaffe[12,13], S. Kang[14,15], P. Kelley[6,16], W. T. Luke[6], O. Magand[5], K. Marumoto[17], K. A. Pfaffhuber[18], X. Ren[6,16], G.-R. Sheu[19], F. Slemr[20], T. Warneke[21], A. Weigelt[10], P. Weiss-Penzias[22], D. C. Wip[23], and Q. Zhang[24]

[1]Department of Earth, Atmospheric and Planetary Sciences, Massachusetts Institute of Technology, Cambridge, MA, USA

[2]Engineering Systems Division, Massachusetts Institute of Technology, Cambridge, MA, USA

[3]Department of Environmental Health, Harvard School of Public Health, Boston, MA, USA

[4]Department of Applied Environmental Science, Stockholm University, Stockholm, Sweden

[5]Univ. Grenoble Alpes, CNRS, LGGE, Grenoble, France

[6]Air Resources Laboratory, National Oceanic and Atmospheric Administration, College Park, MD, USA

[7]Department of Mechanical, Aerospace and Biomedical Engineering, University of Tennessee Space Institute, Tullahoma, TN, USA

[8]South African Weather Service c/o CSIR, Stellenbosch, South Africa

[9]Center for Air Quality, Ohio University, Athens, OH, USA

[10]Institute of Coastal Research, Helmholtz-Zentrum Geesthacht, Geesthacht, Germany

[11]Department of Civil and Environmental Engineering, Clarkson University, Potsdam, NY, USA

[12]School of Science, Technology, Engineering and Mathematics, University of Washington, Bothell, WA, USA

[13]Department of Atmospheric Sciences, University of Washington, Seattle, WA, USA

[14]State Key Laboratory of Cryospheric Sciences, Cold and Arid Regions Environmental and Engineering Research Institute, Chinese Academy of Sciences (CAS), Lanzhou, China

[15]CAS Center for Excellence in Tibetan Plateau Earth Sciences, Chinese Academy of Sciences, Beijing, China

[16]Cooperative Institute for Climate and Satellites, University of Maryland, College Park, MD, USA

[17]Environmental Chemistry Section, National Institute for Minamata Disease, Kumamoto, Japan

[18]Norwegian Institute for Air Research (NILU), Tromsø, Norway

[19]Department of Atmospheric Sciences, National Central University, Jhongli, Taiwan

[20]Max Planck Institute for Chemistry, Air Chemistry Division, Mainz, Germany

[21]Institute of Environmental Physics, University of Bremen, Bremen, Germany

[22]Microbiology and Environmental Toxicology, University of California, Santa Cruz, CA, USA

[23]Anton de Kom Universiteit van Suriname, Paramaribo, Suriname

[24]Key Laboratory of Tibetan Environment Changes and Land Surface Processes, Institute of Tibetan Plateau Research, Chinese Academy of Sciences, Beijing, China

Correspondence to: S. Song (song33@mit.edu)

Received: 26 November 2014 – Published in Atmos. Chem. Phys. Discuss.: 25 February 2015
Revised: 13 May 2015 – Accepted: 09 June 2015 – Published: 30 June 2015

Abstract. We perform global-scale inverse modeling to constrain present-day atmospheric mercury emissions and relevant physiochemical parameters in the GEOS-Chem chemical transport model. We use Bayesian inversion methods combining simulations with GEOS-Chem and ground-based Hg^0 observations from regional monitoring networks and individual sites in recent years. Using optimized emissions/parameters, GEOS-Chem better reproduces these ground-based observations and also matches regional over-water Hg^0 and wet deposition measurements. The optimized global mercury emission to the atmosphere is $\sim 5.8\,Gg\,yr^{-1}$. The ocean accounts for $3.2\,Gg\,yr^{-1}$ (55 % of the total), and the terrestrial ecosystem is neither a net source nor a net sink of Hg^0. The optimized Asian anthropogenic emission of Hg^0 (gas elemental mercury) is 650–1770 $Mg\,yr^{-1}$, higher than its bottom-up estimates (550–800 $Mg\,yr^{-1}$). The ocean parameter inversions suggest that dark oxidation of aqueous elemental mercury is faster, and less mercury is removed from the mixed layer through particle sinking, when compared with current simulations. Parameter changes affect the simulated global ocean mercury budget, particularly mass exchange between the mixed layer and subsurface waters. Based on our inversion results, we re-evaluate the long-term global biogeochemical cycle of mercury, and show that legacy mercury becomes more likely to reside in the terrestrial ecosystem than in the ocean. We estimate that primary anthropogenic mercury contributes up to 23 % of present-day atmospheric deposition.

1 Introduction

Mercury (Hg) is a ubiquitous trace metal that cycles between the atmosphere, ocean, land, and biosphere (Selin, 2009). Atmospheric mercury transports globally (Driscoll et al., 2013) and, in aquatic systems, can be converted to methylmercury, a bioaccumulative toxic compound (Mergler et al., 2007). Human activities have strongly affected the mercury global cycle by both unintentional and intentional releases (Streets et al., 2011). Since mercury deposited to terrestrial and ocean surfaces can remobilize, the atmosphere continues to be affected by its historical releases (Lindberg et al., 2007; Amos et al., 2013). Atmosphere–surface fluxes of mercury are still poorly constrained, limiting our ability to fully understand timescales of its global biogeochemical cycle (Pirrone et al., 2010; Mason et al., 2012). A better knowledge of these fluxes is important for assessing its impacts on humans and evaluating the effectiveness of policy actions (Selin, 2014).

Current estimates of mercury fluxes to the atmosphere are mainly built on a bottom-up approach. Anthropogenic inventories are based on emission factors, activity levels, and abatement efficiency (Pacyna et al., 2010; S. Wang et al., 2014; Muntean et al., 2014). Flux estimates from ocean and terrestrial surfaces extrapolate limited direct measurements to larger scales and use simplified process models (Mason, 2009; Kuss et al., 2011). The top-down or inverse approach, combining observations and atmospheric modeling, has been widely used to derive sources and sinks of greenhouse gases and ozone-depleting substances (Gurney et al., 2002; Xiao et al., 2010). Inverse studies have addressed mercury at a regional scale (Roustan and Bocquet, 2006; Krüger et al., 1999). For example, a hybrid inversion combining back trajectories and a regional chemical transport model (CTM) identified Hg^0 emission using year-long urban observations (de Foy et al., 2012). This scheme was expanded to estimate sources of oxidized Hg (de Foy et al., 2014).

In this paper, we apply a top-down approach at global scale to quantitatively estimate present-day mercury emission sources (emission inversion) as well as key parameters in a CTM (parameter inversion), in order to better constrain the global biogeochemical cycle of mercury. Section 2 describes the overall methodology. We combine ground-based observations of atmospheric Hg^0 (Sect. 2.1) and simulations with the GEOS-Chem global CTM (Sect. 2.2). Reference (also known as a priori) emissions are from GEOS-Chem parameterizations and agree well with bottom-up estimates (Sect. 2.3). We adopt a Bayesian inversion method (Sect. 2.4) to obtain the optimized (a posteriori) emissions, with a monthly time step, taking into account uncertainties associated with both reference emissions and ground-based observations (Sect. 2.6). Section 3 presents results and discussion. Comparisons of observations and model outputs are given in Sect. 3.1. The optimized emissions from ocean and terrestrial surfaces and from anthropogenic sources are shown in Sect. 3.2. We use results of the emission inversion to identify key uncertain model parameters, and optimize them in the parameter inversion (Sects. 2.5 and 3.3). Finally, we discuss implications of our inversion results for the global biogeochemical mercury cycle (Sect. 3.4) and summarize our conclusions (Sect. 4).

2 Methods

2.1 Atmospheric mercury observations

Tropospheric mercury exists mainly as gaseous elemental mercury (GEM) but also as two operationally defined species, gaseous oxidized mercury (GOM) and particle-bound mercury (PBM) (Valente et al., 2007). Manual methods of measuring GEM or total gaseous mercury (TGM = GEM + GOM) were applied in the 1970s (Slemr et al., 1981). High-frequency measurements (time resolution < 1 h, e.g., using Tekran automated ambient air analyzers) became available in the 1990s and have substantially replaced manual sampling (time resolution of about several hours). We only use GEM and TGM observations in this study because we are not able to quantify the uncertainty in GOM and PBM measurements (Jaffe et al., 2014; McClure et al., 2014).

We identify high-frequency observations of GEM and TGM concentration for our inversions using two criteria. First, we choose sites in rural/remote areas not strongly affected by local emissions. Second, we require that observations at different sites are minimally correlated (Brunner et al., 2012). Data sets are drawn from the Atmospheric Mercury Network (AMNet) (Gay et al., 2013), the Canadian Measurement Networks (including the Canadian Air and Precipitation Monitoring Network (CAPMoN) and other sites sponsored by Environment Canada) (Cole et al., 2014), and the European Monitoring and Evaluation Programme (EMEP) (Tørseth et al., 2012). We use data from 2009 to 2011, when all these networks were active. To expand spatial coverage of observations, we also collected data from individual sites for recent years (2007–2013). Some sites are included in the Global Mercury Observation System (GMOS) (Pirrone et al., 2013). All sites use Tekran analyzers, operated in sampling intervals of 5–30 min. We calculate Pearson's correlation coefficients between each pair of sites using hourly data. Several sites are excluded due to strong correlations within each other, as shown in Table S1 in the Supplement. Table 1 shows the names, locations, and affiliated networks of the 27 ground-based sites used in our inversion. Site locations are also plotted in Fig. 1. For most of these sites GEM data are used, and for a few sites where GEM data are not available we use TGM data (see Table 1). The concentration difference between measured GEM and TGM concentrations in remote near-surface air is usually $<1\,\%$ (Lan et al., 2012; Fu et al., 2012a; Weigelt et al., 2013; Steffen et al., 2014) and thus we do not distinguish between measured GEM and TGM concentrations and use Hg^0 to represent them in the paper. These sites are all uncorrelated or only weakly correlated ($-0.3 < r < 0.4$, $n = 10^3$–10^4) (see Table S2 in the Supplement).

Original observational data are converted into hourly averages and then into monthly averages (Fig. S1 in the Supplement). We require >30 min data to derive an hourly average and >10-day data to derive a monthly average. Where full data are available, median values are used to suppress the influence of high Hg^0 due to local or regional pollution events (Weigelt et al., 2013; Jaffe et al., 2005) or occasional low Hg^0 due to non-polar depletion events (Brunke et al., 2010). For a few individual sites (see Table 1), the original data are not available and monthly arithmetic means are used. Finally, multiple-year averages are calculated. Hg^0 concentrations are given in nanograms per cubic meter at standard temperature and pressure.

Four polar sites are included (ALT, ZEP, and ADY in the Arctic and TRS in Antarctica, see Table 1). Episodically low Hg^0 is observed at these sites in polar spring (Cole et al., 2013; Pfaffhuber et al., 2012). These atmospheric mercury depletion events (AMDEs) result from rapid Hg^0 oxidation and deposition driven by halogens (Steffen et al., 2008). Volatilization of the deposited Hg and the large quantities of imported mercury from circumpolar rivers to the Arctic Ocean are hypothesized to contribute to the observed summer Hg^0 peak in the Arctic region (Dastoor and Durnford, 2013; Fisher et al., 2012). The lack of understanding of the above physical and chemical processes limits GEOS-Chem's ability to reproduce Hg^0 in the polar spring and summer. For these reasons we remove Hg^0 data at polar sites for this period (i.e., March–September in the Arctic and October–March in Antarctica).

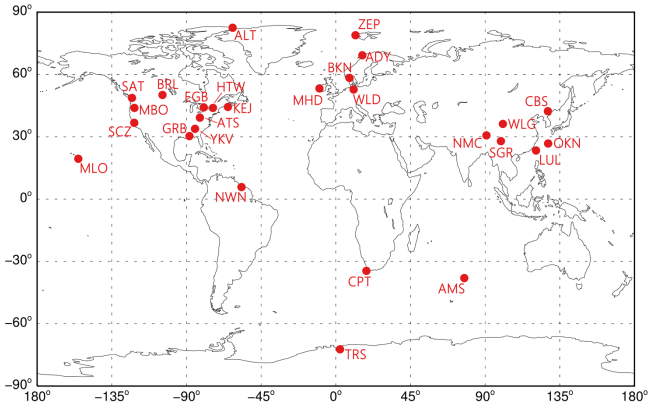

Figure 1. Locations of ground-based observational sites.

We also include three mountaintop sites (LUL, MBO, and MLO, see Table 1). These sites are affected by upslope surface air during the day and downslope air from the free troposphere at night (Sheu et al., 2010; Fu et al., 2010). The downslope air usually contains higher levels of GOM than the upslope air due to oxidation of Hg^0 to GOM in the free troposphere (Timonen et al., 2013). Therefore, Hg^0 at mountaintop sites peaks in the afternoon whereas GOM peaks between midnight and early morning (Fig. S2 in the Supplement), showing an opposite diurnal pattern to most low-elevation sites (Lan et al., 2012). The minimum hourly Hg^0 at night is calculated to be $\sim 90\,\%$ of the all-day average. Thus, to represent Hg^0 modeled at a vertical layer in the free troposphere (this layer is obtained by matching observed air pressure), the observed mountaintop Hg^0 data are multiplied by 0.9.

We do not use over-water Hg^0 observations (i.e., from ship cruises) in the inversion because they are very limited and usually cover large areas, making their observational errors difficult to estimate. Instead, we use over-water observations as an independent check of our inversion results. The North Atlantic Ocean is the most densely sampled ocean basin. Soerensen et al. (2012) assembled Hg^0 measurements from 18 ship cruises in this region during 1990–2009 and found a statistically significant decrease of -0.046 ± 0.010 ng m^{-3} yr^{-1}. However, previous GEOS-Chem simulations of Hg^0 concentration did not take this multidecadal trend into account in evaluating its seasonal variability (Soerensen et al., 2010a). Here we add a new ship cruise and adjust observed Hg^0 concentrations (Hg^0_{obs}) from

Table 1. Information for ground-based observational sites of atmospheric mercury.

ID[a,b]	Location	Time period	Lat	Long	Alt[c]	Network[d]	Observational errors[e]			Mismatch error (σ_{MM})[e]	NRMSE[f]		
							σ_{IP}	σ_{IC}	σ_{SF}		reference simulation	emission inversion	parameter inversion
ALT	Alert, NU, Canada	2009	83	−62	210	1	28	138	3	36	0.06	0.03	0.02
ZEP	Zeppelin, Ny-Ålesund, Norway	2009–2011	79	12	474	2	34	169	6	14	0.13	0.19	0.18
ADY	Andøya, Norway	2010–2011	69	16	380	2	36	181	4	13	0.16	0.22	0.23
BKN	Birkenes, Norway	2010–2011	58	8	219	2	36	178	6	32	0.19	0.22	0.24
MHD	Mace Head, Ireland	2009–2011	53	−10	15	2	29	145	5	8	0.08	0.08	0.09
WLD	Waldhof, Germany	2009–2011	53	11	74	2	33	163	10	114	0.14	0.10	0.12
BRL	Bratt's Lake, SK, Canada	2009–2010	50	−105	587	1	25	127	5	23	0.18	0.11	0.13
SAT	Saturna, BC, Canada	2009–2010	49	−123	178	1	28	140	8	28	0.16	0.12	0.13
KEJ	Kejimkujik, NS, Canada	2009–2011	44	−65	158	3	28	138	6	14	0.07	0.05	0.09
EGB	Egbert, ON, Canada	2009–2010	44	−80	251	1	25	126	5	49	0.21	0.11	0.11
MBO	Mt. Bachelor, OR, USA	2009–2010	44	−122	2763	4	26	128	6	10	0.04	0.04	0.06
HTW	Huntington Wildlife Forest, NY, USA	2009–2011	44	−74	502	3	26	131	8	29	0.13	0.06	0.08
CBS	Mt. Changbai, JL, China	2008–2010	42	128	741	4	32	160	14	134	0.17	0.16	0.23
ATS	Athens Super Site, OH, USA	2009–2011	39	−82	274	3	28	137	6	39	0.17	0.04	0.07
SCZ	Santa Cruz, CA, USA	2010–2011	37	−122	150	3	30	148	5	23	0.07	0.05	0.04
WLG	Waliguan, QH, China	2007–2008	36	101	3816	4	38	188	20	223	0.21	0.26	0.24
YKV	Yorkville, GA, USA	2009–2011	34	−85	394	3	24	122	6	48	0.30	0.15	0.13
NMC	Nam Co Lake, XZ, China	2011–2013	31	91	4730	4	25	124	6	23	0.07	0.06	0.07
GRB	Grand Bay NERR, MS, USA	2009–2011	30	−88	1	3	28	141	5	41	0.08	0.07	0.08
SGR	Shangri-La, YN, China	2009–2010	28	100	3580	4	50	250	30	544	0.37	0.40	0.37
OKN	Okinawa, Japan	2009–2011	27	128	60	4	39	195	13	37	0.24	0.24	0.22
LUL	Mt. Front Lulin, Taiwan	2009–2011	24	121	2862	4	29	145	12	52	0.12	0.13	0.13
MLO	Mauna Loa, HI, USA	2011	20	−156	3384	3	25	123	16	8	0.11	0.13	0.11
NWN	Nieuw Nickerie, Suriname	2007–2008	6	−57	5	4	25	126	22	105	0.22	0.13	0.18
CPT	Cape Point, South Africa	2009–2011	−34	18	230	4	18	91	4	13	0.26	0.08	0.16
AMS	Amsterdam Island, Indian Ocean	2012–2013	−38	78	55	4	21	103	3	7	0.16	0.08	0.07
TRS	Troll Research Station, Antarctica	2009–2011	−72	3	1275	4	22	107	3	33	0.15	0.13	0.09
Avg.							29	146	8	63	0.16	0.13	0.14

[a] Observational sites without original data are MBO, CBS, WLG, NMC, SGR, LUL, and NWN. [b] Observational sites where we use TGM data are ALT, BRL, SAT, EGB, CBS, WLG, NMC, SGR, and NWN. For all other sites, we use GEM data. [c] Unit for altitude is meters. [d] Network affiliations: (1) Canadian networks, (2) EMEP, (3) AMNet, and (4) individual observational sites. More information about these individual sites can be found in Weiss-Penzias et al. (2006) for MBO, Fu et al. (2012b) for CBS, Fu et al. (2012a) for WLG, Zhang et al. (2015) for SGR, MOEJ (2013) for OKN, Sheu et al. (2010) for LUL, Müller et al. (2012) for NWN, Slemr et al. (2011) for CPT, Angot et al. (2014) for AMS, and Slemr et al. (2015) for the Southern Hemispheric sites. [e] Unit for errors is picograms per cubic meter. [f] Equation of NRMSE (quantity without unit) is given in Sect. 3.1.

all 19 ship cruises to Hg^0 levels consistent with year 2009 based on a fitted decline trend (Table S3 and Fig. S3 in the Supplement). Seasonal variation is estimated by dividing the normalized Hg^0 (Hg^0_{nor}) by month of measurement. As shown in Fig. 2, Hg^0_{nor} are smaller and show less seasonal variability compared to Hg^0_{obs}.

2.2 GEOS-Chem model

GEOS-Chem (v9-02) is a CTM driven by assimilated meteorological fields from the NASA Goddard Earth Observing System (Bey et al., 2001). The original GEOS-5 has a resolution of $1/2° \times 2/3°$ and is degraded to $2° \times 2.5°$ for input into our simulations. The GEOS-Chem global mercury simulation was described and evaluated in Selin et al. (2007) and Strode et al. (2007), with updates by Selin et al. (2008), Holmes et al. (2010), Soerensen et al. (2010b), and Amos et al. (2012). It couples a three-dimensional atmosphere, a two-dimensional mixed layer slab ocean, and a two-dimensional terrestrial reservoir. For consistency with most ground-based observations, we use meteorological years 2009–2011 for analysis after a spin-up period of 4 years.

Three mercury tracers (representing GEM, GOM, and PBM) are simulated in the atmosphere in GEOS-Chem. Models have assumed that Hg^0 is oxidized by OH, ozone, and/or halogens (Lei et al., 2013; De Simone et al., 2014; Travnikov and Ilyin, 2009; Durnford et al., 2010; Grant et al., 2014). Some studies suggested the gas-phase reaction with Br was the most important Hg^0 oxidation process globally (Seigneur and Lohman, 2008; Hynes et al., 2009), and here we use Br as the only oxidant of Hg^0 (Holmes et al., 2010; Goodsite et al., 2012). Tropospheric Br fields are archived from a full chemistry GEOS-Chem simulation (Parrella et al., 2012). Models also hypothesize gas- and/or aqueous-phase reductions of oxidized Hg and scale their kinetics to match atmospheric observations (Holmes et al., 2010; Pongprueksa et al., 2011; Selin et al., 2007). However, an accurate determination of potential pathways is lacking (Subir et al., 2011, 2012), and their atmospheric relevance is unknown (Gårdfeldt and Jonsson, 2003). Thus, we do not include atmospheric reduction of oxidized Hg in our simulations.

2.3 Emission inversion: reference emissions

For our reference emissions, we use parameterizations in GEOS-Chem with improvements from recent literature. As shown in Table 2, the global mercury emission is estimated as 6.0 Gg yr^{-1}, with an uncertainty range of 0.4–12.2 Gg yr^{-1}. Mercury released via natural processes is assumed to be entirely Hg^0 (Stein et al., 1996), while a small fraction of anthropogenic mercury is in oxidized forms. Anthropogenic emission is unidirectional, but air–surface exchange is bidirectional (emission and deposition) (Xu et al., 1999; Gustin et al., 2008). A positive net emission from a surface means it is a net source of Hg^0, whereas a negative value means it is a net sink. We describe below our reference emissions for individual sources.

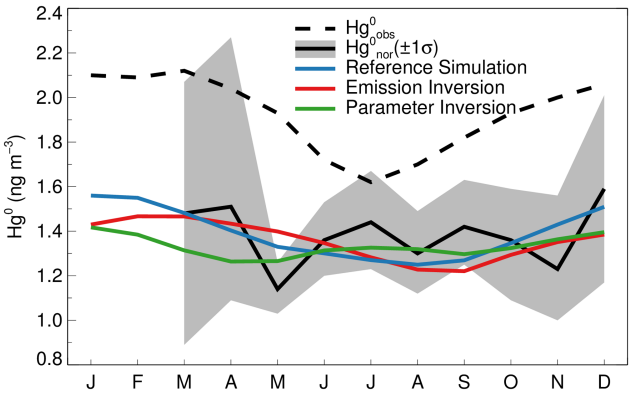

Figure 2. Observed and modeled monthly Hg^0 concentrations over the North Atlantic Ocean. The observational data and related references are given in the Supplement. Hg^0_{obs} are the concentrations observed from 19 ship cruises during 1990–2009, whereas Hg^0_{nor} are the concentrations normalized to levels consistent with year 2009. The gray shaded region shows the 1σ error of Hg^0_{nor}, which is composed of the observational error, mismatch error, and regression error.

2.3.1 Anthropogenic sources

We use the anthropogenic emission inventory based on activity data for year 2010, developed by AMAP/UNEP (2013). As shown in Table 2, the total anthropogenic emission is 1960 Mg yr^{-1}, with an uncertainty range of 1010–4070 Mg yr^{-1} (AMAP/UNEP, 2013). We do not optimize oxidized mercury emissions (accounting for 19 % of the total anthropogenic sources) because this form has a short atmospheric lifetime (days to weeks) and may not significantly contribute to observed TGM concentrations. The geospatial distribution for emissions from contaminated sites (Kocman et al., 2013) is not available for this inventory, and we distribute this small source (80 Mg yr^{-1}) based on the locations of mercury mines (Selin et al., 2007). We do not consider in-plume reduction of oxidized Hg emitted from coal-fired power plants (Y. Zhang, et al., 2012). About 50 % of global emissions are from Asia (defined as 65–146° E, 9° S–60° N), and a small fraction are from Europe and North America (together < 10 %). For other regions like Africa and South America, there is no effective observational site to constrain emissions (Fig. 1). Thus, only anthropogenic emissions from Asia are optimized in the inversion, but we still include other regions' anthropogenic emissions in the GEOS-Chem simulations.

Table 2. Global mercury emissions into the atmosphere ($Mg\,yr^{-1}$).[a]

Source	Included in inversion?[b]	Reference emission	Optimized emission
Anthropogenic[c]		1960 (420–3510)	2250 (1150–3360)
Asia	Y	770 ± 390	1060 ± 110
Other regions	N	760	760
Contaminated sites	N	80 (70–100)	80 (70–100)
Oxidized Hg	N	350	350
Net ocean		2990 (470–5510)	3160 (1160–5160)
Net NH ocean	Y	1230 ± 630	1670 ± 530
Net SH ocean	Y	1760 ± 880	1490 ± 680
Net terrestrial[d]		1070 (−510 to 3130)	340 (−590 to 1750)
Soil	Y	1680 ± 840	860 ± 440
Prompt re-emission	N	520	500
Hg^0 dry deposition	N	−1430	−1320
Geogenic	N	90 (60–600)	90 (60–600)
Biomass burning	N	210	210
TOTAL[e]		6020 (380–12150)	5750 (1720–10270)

[a] Flux values in parentheses indicate estimated uncertainty ranges. For sources included in the inversion, "average ± SD" is shown. The uncertainty ranges of contaminated sites and geogenic emissions are from AMAP/UNEP (2013) and Mason (2009), respectively. If the uncertainty range of a source is not available, we assume that its SD is a half of its best estimate. [b] Only selected mercury emission sources are included in the inversion, see Sect. 2.3.4. [c] Oxidized Hg emissions from anthropogenic sources are not included in the inversion. "Asia" and "Other regions" (except Asia) refer to emissions of Hg^0. [d] Because air–terrestrial interactions are bi-directional, we assume that uncertainties of prompt re-emission and Hg^0 deposition have been covered by that of soil emission. [e] Total mercury emissions are the sum of anthropogenic, net ocean, and net terrestrial emissions.

2.3.2 Ocean

The mixed layer (ML) slab ocean model in GEOS-Chem is described in Soerensen et al. (2010b). Net Hg^0 emission from ocean surfaces is determined by the supersaturation of Hg^0_{aq} in the ML relative to the atmosphere and the air–sea exchange rate. Hg^0_{aq} in the ML is mainly produced by the net photolytic and biotic reduction of Hg^{2+}_{aq}. Atmospheric deposition accounts for most Hg^{2+}_{aq} inputs into the ML, but subsurface waters also contribute a considerable fraction. The ML interacts with subsurface waters through entrainment/detrainment of the ML and wind-driven Ekman pumping.

We improve several parameterizations in GEOS-Chem based on recent findings. (1) Basin-specific subsurface water mercury concentrations are updated according to new measurements (Lamborg et al., 2012; Munson, 2014), as shown in the Supplement, Fig. S4. (2) Soerensen et al. (2010b) used the Wilke–Chang method for estimating the Hg^0_{aq} diffusion coefficient (D_{Hg}) (Wilke and Chang, 1955), but this estimate was believed to be too high (Loux, 2004). We adopt a revised D_{Hg} derived by molecular dynamics (MD) simulation (Kuss et al., 2009). As shown in the Supplement, Fig. S5, compared to the Wilke–Chang method, the MD simulation obtains a D_{Hg} that agrees much better with laboratory results (Kuss, 2014). (3) Particulate mercury (Hg^P_{aq}) sinking from the ML is estimated by linking the organic carbon export (biological pump) and Hg^P_{aq} : C ratios. Soerensen et al. (2010b) used the model of Antia et al. (2001) for estimating carbon export fluxes, giving a global total of $23\,Gt\,C\,yr^{-1}$. However, this estimate is mainly based on the flux measurement data from much deeper depths and may not well represent carbon export from the ML. Different models suggest global carbon export fluxes ranging from 5 to $20\,Gt\,C\,yr^{-1}$ with a best estimate of $11\,Gt\,C\,yr^{-1}$ (Sanders et al., 2014; Henson et al., 2011). Thus, we multiply carbon export fluxes in GEOS-Chem by a factor of 0.47 ($11\,Gt\,C\,yr^{-1}/23\,Gt\,C\,yr^{-1}$) to match this best estimate.

Net global ocean emission of $2990\,Mg\,yr^{-1}$ from the improved GEOS-Chem (considered as reference emission, shown in Table 2) compares favorably with best estimates of $2680\,Mg\,yr^{-1}$ using a bottom-up approach (Pirrone et al., 2010; Mason, 2009). Due to their different seasonal characteristics, we divide the global ocean into the NH (Northern Hemisphere) and SH (Southern Hemisphere) oceans and optimize their emissions separately.

2.3.3 Terrestrial ecosystem

Although atmosphere–terrestrial Hg^0 exchange is bi-directional, only recently developed exchange models have coupled deposition (downward) and emission (upward) fluxes and dynamically estimated net fluxes by gradients be-

tween air Hg^0 and "compensation points" inferred from surface characteristics (Bash, 2010; Bash et al., 2007). Because their complex parameterizations lack field data for verification (X. Wang et al., 2014), such exchange models have not been incorporated into current global CTMs. As described in Selin et al. (2008) and Holmes et al. (2010), GEOS-Chem treats emission and deposition fluxes of Hg^0 separately. Only dry deposition is considered for Hg^0 due to its low Henry's law constant (Lin and Pehkonen, 1999). Net emission from terrestrial surfaces (E_{net}) represents the sum of these processes: volatilization from soil (E_{soil}), prompt re-emission of deposited Hg (E_{pr}), geogenic activity (E_{gg}), biomass burning (E_{bb}), and dry deposition to surfaces (E_{ddHg^0}).

$$E_{net} = E_{soil} + E_{pr} + E_{gg} + E_{bb} - E_{ddHg^0} \quad (1)$$

Soil emission (E_{soil}) is specified as a function of solar radiation and soil Hg concentration:

$$E_{soil}\,(ng\,m^{-2}\,h^{-1}) = \beta C_{soil} \exp(1.1 \times 10^{-3} \times R_g), \quad (2)$$

where C_{soil} is soil Hg concentration ($ng\,g^{-1}$) and R_g is the solar radiation flux at the ground ($W\,m^{-2}$). GEOS-Chem assumes a global average soil concentration of $43\,ng\,g^{-1}$ for preindustrial conditions and derives its spatial distribution from the local equilibrium between emission and deposition. The scaling factor β ($1.2 \times 10^{-2}\,g\,m^{-2}\,h^{-1}$) is obtained from the global mass balance of the preindustrial simulation. Selin et al. (2008) assumed that present-day soil mercury reservoir and emission have both increased by 15 % compared to the preindustrial period and distributed this global average increase according to the present-day deposition pattern of anthropogenic emission. However, by linking soil mercury with organic carbon pools, Smith-Downey et al. (2010) estimated that present-day Hg storage in organic soils has increased by 20 % while soil emission by 190 %. Mason and Sheu (2002) suggested doubled soil emissions compared to preindustrial times. Thus, following Smith-Downey et al. (2010), we assume a 190 % global increase in the present day, and distribute this increase according to the anthropogenic emission deposition pattern. The present-day reference soil emission is calculated to be $1680\,Mg\,yr^{-1}$.

An additional $520\,Mg\,yr^{-1}$ is emitted from the soil, vegetation, and snow (E_{pr}) through rapid photoreduction of recently deposited oxidized Hg (Fisher et al., 2012). Geogenic emission (E_{gg}) is set as $90\,Mg\,yr^{-1}$, consistent with its best bottom-up estimate (Mason, 2009; Bagnato et al., 2014). Biomass burning (E_{bb}) of $210\,Mg\,yr^{-1}$ is estimated using the Global Fire Emissions Database version 3 of CO (van der Werf et al., 2010) and a Hg : CO ratio of $100\,nmol\,mol^{-1}$ (Holmes et al., 2010). This amount falls at the lower end of bottom-up estimates (Friedli et al., 2009). Dry deposition of Hg^0 is estimated using a resistance-in-series scheme (Wesely, 1989) and has a downward flux of $1430\,Mg\,yr^{-1}$. Using Eq. (1), net emission of Hg^0 from terrestrial surfaces is calculated to be $1070\,Mg\,yr^{-1}$ in GEOS-Chem (Table 2), at the lower end of the bottom-up estimates (1140–5280 $Mg\,yr^{-1}$) (Mason, 2009; Pirrone et al., 2010) and also lower than $1910\,Mg\,yr^{-1}$ by Kikuchi et al. (2013) using a different empirical mechanism (Lin et al., 2010).

2.3.4 Sources included in emission inversion

Because of limitations in both observations and the CTM, only anthropogenic emission from Asia, ocean evasion (separated into the NH and SH), and soil emission are optimized in the emission inversion (see Table 2). The remaining sources are still included in the simulation but not inverted because they are too diffusely distributed, their magnitude is small, and/or observations are not sensitive to them (Chen and Prinn, 2006). The seasonal sources (the NH ocean, SH ocean, and soil) usually have strong spatiotemporal variations and the inversion optimizes their monthly magnitudes and uncertainties. For the aseasonal Asian anthropogenic emission, the inversion optimizes its annual magnitude and uncertainty.

2.4 Bayesian inversion method

We use a Bayesian method to invert emissions and parameters with a weighted least-squares technique (Ulrych et al., 2001). The unknowns (correction factors for reference emissions and parameters) are contained in a state vector $\boldsymbol{x}$ and their a priori errors (uncertainties in reference emissions and parameters) in a matrix $\mathbf{P}$. In the emission inversion, as we include one aseasonal source (Asian anthropogenic emission) and three monthly sources (the NH ocean, SH ocean, and soil), the vector $\boldsymbol{x}$ contains 37 elements. $\mathbf{P}$ is a 37×37 diagonal matrix with each diagonal element equal to the square of 1σ a priori error of the corresponding element in $\boldsymbol{x}$ (see Sect. 2.6.1).

Our inversion method assumes a linear relationship between the observation vector $\boldsymbol{y}^{obs}$ and $\boldsymbol{x}$, as shown in the measurement equation:

$$\boldsymbol{y}^{obs} = \boldsymbol{y}^{ref} + \mathbf{H}\boldsymbol{x} + \boldsymbol{\varepsilon}, \quad (3)$$

where $\boldsymbol{y}^{ref}$ contains monthly Hg^0 concentrations modeled by GEOS-Chem using the reference emissions and parameters. The vectors $\boldsymbol{y}^{obs}$ and $\boldsymbol{y}^{ref}$ both have 12 (number of months per year) × 27 (number of observational sites) = 324 elements. $\boldsymbol{\varepsilon}$ represents the model and observational errors which will be discussed in detail in Sect. 2.6.

The state vector $\boldsymbol{x}$ is related to monthly Hg^0 concentrations by the sensitivity matrix $\mathbf{H}$, in which the elements are written as

$$\mathbf{h}_{ij} = \frac{\boldsymbol{y}_i - \boldsymbol{y}_i^{ref}}{\boldsymbol{x}_j - \boldsymbol{x}_j^{ref}} \approx \frac{\partial \boldsymbol{y}_i}{\partial \boldsymbol{x}_j}, \quad (4)$$

where i and j are indices for the observational and state vectors, respectively. $\mathbf{H}$ describes how monthly Hg^0 concentrations at different observational sites respond to changes in the

state vector $\boldsymbol{x}$ (for examples see the Supplement, Fig. S6). The GEOS-Chem CTM acts as a mathematical operator relating the emissions/parameters to monthly Hg^0 concentrations. For the emission inversion, sensitivities for the seasonal and aseasonal sources are generated by two different types of simulations. The aseasonal Asian anthropogenic emission is perturbed above the reference level by 50 %, and we run the GEOS-Chem CTM until steady state is reached. For the seasonal sources (e.g., the NH ocean emission from March), a 1-month pulse of Hg^0 is emitted, and we track modeled Hg^0 concentrations by GEOS-Chem for the next 3 years. After this, we assume that the perturbed concentrations at all observational sites will exponentially decrease (Saikawa et al., 2012).

The objective function $\mathbf{J}$ with respect to $\boldsymbol{x}$ is

$$\mathbf{J}(\boldsymbol{x}) = \boldsymbol{x}^T\mathbf{P}^{-1}\boldsymbol{x} + (\mathbf{H}\boldsymbol{x} - \boldsymbol{y}^{\mathrm{obs}} + \boldsymbol{y}^{\mathrm{ref}})^T \mathbf{R}^{-1}(\mathbf{H}\boldsymbol{x} - \boldsymbol{y}^{\mathrm{obs}} + \boldsymbol{y}^{\mathrm{ref}}), \quad (5)$$

where $\mathbf{R}$, a diagonal 324×324 matrix, represents errors related to observations and the CTM and will be described in detail in Sect. 2.6. By minimizing $\mathbf{J}$, we obtain the expression for the optimal estimate of the state $\boldsymbol{x}$:

$$\boldsymbol{x} = (\mathbf{H}^T\mathbf{R}^{-1}\mathbf{H} + \mathbf{P}^{-1})^{-1}\mathbf{H}^T\mathbf{R}^{-1}(\boldsymbol{y}^{\mathrm{obs}} - \boldsymbol{y}^{\mathrm{ref}}), \quad (6)$$

$$\mathbf{Q} = (\mathbf{H}^T\mathbf{R}^{-1}\mathbf{H} + \mathbf{P}^{-1})^{-1}, \quad (7)$$

where the matrix $\mathbf{Q}$ contains the a posteriori errors of $\boldsymbol{x}$. The size of $\mathbf{Q}$ is the same as the matrix $\mathbf{P}$. Each diagonal element in $\mathbf{Q}$ is the square of 1σ a posteriori error of the corresponding element in $\boldsymbol{x}$. A detailed mathematical derivation of the above equations can be found in Wunsch (2006). As shown in Eqs. (6) and (7), several vectors and matrices need to be calculated during the optimization procedure, including the observational vector $\boldsymbol{y}^{\mathrm{obs}}$ and its error matrix $\mathbf{R}$, the error matrix $\mathbf{P}$ of the a priori state, the sensitivity matrix $\mathbf{H}$, and the vector $\boldsymbol{y}^{\mathrm{ref}}$ which is obtained from the reference simulation of the GEOS-Chem CTM.

2.5 Parameter inversion

As described in Sect. 3.2.1, based on results of ocean evasion in our emission inversion and sensitivity tests of model parameters, we identify two ocean parameters in GEOS-Chem for improvement: the rate constant of dark oxidation of Hg^0_{aq} (denoted as K_{OX2}, following notations in Soerensen et al., 2010b) and the partition coefficient between Hg^{2+}_{aq} and Hg^P_{aq} (denoted as K_D). For simplicity they are expressed in decimal logarithms ($-\log K_{OX2}$ and $\log K_D$).

A $-\log K_{OX2}$ (s^{-1}) of 7.0 is specified in GEOS-Chem (Soerensen et al., 2010b). From a survey of laboratory studies (see details in the Supplement) (Amyot et al., 1997; Lalonde et al., 2001, 2004; Qureshi et al., 2010), we suggest that this value is too low and that a more appropriate range of $-\log K_{OX2}$ is 4.0–6.0. The chemical mechanisms for dark oxidation of Hg^0_{aq} remain unclear. OH generated from photochemically produced H_2O_2 via the Fenton reaction may oxidize Hg^0_{aq} in dark conditions (Zhang and Lindberg, 2001; Zepp et al., 1992). Light irradiation before a dark period is needed, and dark oxidation kinetics depend on intensity and duration of light (Qureshi et al., 2010; Batrakova et al., 2014). Future work could include a more mechanistic representation of this process as laboratory studies become available.

K_D ($= C_s/C_dC_{SPM}$) describes the affinity of aqueous Hg^{2+} for suspended particulate matter (SPM), where C_s, C_d, and C_{SPM} are the concentrations of Hg^P_{aq}, Hg^{2+}_{aq}, and SPM, respectively. GEOS-Chem uses a $\log K_D$ ($L\,kg^{-1}$) of 5.5 based on measurements in the North Pacific and North Atlantic oceans (Mason and Fitzgerald, 1993; Mason et al., 1998).

In the parameter inversion, we attempt to constrain these two ocean model parameters using the Bayesian approach described in Sect. 2.4. For consistency with sources in the emission inversion, two other parameters are included, i.e., emission ratios for soil (ER_{Soil}) and Asian anthropogenic sources (ER_{Asia}). It is noted that the emission inversion and parameter inversion are carried out separately. Because the responses of Hg^0 concentrations to changes in ocean parameters are nonlinear, as shown in the Supplement Fig. S7, we use a two-step iterative inversion method (Prinn et al., 2011). At each iteration step, the sensitivity matrix $\mathbf{H}$ is estimated by linearizing the nonlinear function around the current parameter estimate. In the parameter inversion, the state vector $\boldsymbol{x}$ contains four elements (corresponding to the four parameters), and $\mathbf{P}$ and $\mathbf{Q}$ are 4×4 matrices.

2.6 Error representation

Successful estimation of $\boldsymbol{x}$ (Eq. 6) and its uncertainty $\mathbf{Q}$ (Eq. 7) depends on reasonable representations of all relevant errors, including the a priori errors associated with reference emissions/parameters (contained in $\mathbf{P}$) and errors related to Hg^0 observations and the CTM (contained in $\mathbf{R}$). $\mathbf{R}$ consists of three parts: observational errors, model–observation mismatch errors, and model errors.

2.6.1 Errors in reference emission and parameters

For the emission inversion, we set the 1σ errors in reference emissions as 50 % in order to match uncertainties in their estimates using bottom-up approaches (see Table 2). For example, the reference emissions and 1σ errors for the NH and SH oceans are 1230 ± 630 and $1760 \pm 880\,Mg\,yr^{-1}$, respectively. The uncertainty range of reference emission from the global ocean is estimated as 470–5510 $Mg\,yr^{-1}$, comparing very well with 780–5280 $Mg\,yr^{-1}$ from bottom-up estimates (Mason, 2009; Pirrone et al., 2010). For the parameter inversion, the a priori estimates of two ocean model parameters

are taken from literature reviews (Batrakova et al., 2014): $-\log K_{OX2}$ (5.0 ± 1.0) and $\log K_D$ (5.3 ± 0.4). The a priori uncertainties of ER_{Soil} and ER_{Asia} are chosen as 50 %, the same as in the emission inversion.

2.6.2 Observational errors

Observational errors for ground-based sites determine their relative importance in deriving the optimized state. As shown in Eq. (8), the total observational errors (σ_{TOT}) contain instrumental precision (σ_{IP}), intercomparison (σ_{IC}), and sampling frequency errors (σ_{SF}) (Rigby et al., 2012; Chen and Prinn, 2006).

$$\sigma_{TOT} = \sqrt{\sigma_{IP}^2 + \sigma_{IC}^2 + \sigma_{SF}^2} \quad (8)$$

The instrumental precision (σ_{IP}) of high-frequency Hg^0 measurements using the Tekran instrument is ~ 2 % (Poissant et al., 2005). Here an intercomparison error (σ_{IC}) is used to represent the comparability of Hg^0 concentrations measured by different research groups using the Tekran instrument. In principle, it includes several inaccuracies during the measurement process (e.g., the instrument's flow control and the permeation source rate for the automated calibration) and also arises from the different data management and quality control protocols taken by different research groups (Steffen et al., 2012). Its value has been assessed during several field intercomparisons (Temme et al., 2006; Aspmo et al., 2005; Munthe et al., 2001; Ebinghaus et al., 1999; Schroeder et al., 1995). Hg^0 concentrations measured by different groups have a relative SD of reproducibility of 1–9 %, and we choose a generous uniform intercomparison error of 10 %. Sampling frequency error (σ_{SF}) reflects the ability of each site to capture the overall variability of Hg^0 concentration in 1 month and is calculated as the monthly SD divided by the square root of the number of valid hourly data points in this month (Rigby et al., 2012). Table 1 shows observational errors at each site, averaged over 2009–2011. The total observational errors are dominated by intercomparison errors. The other two types of errors have small contributions.

2.6.3 Model–observation mismatch errors

The mismatch error (σ_{MM}) exists because an observation is made at a single point in space, but its corresponding grid box in model represents a large volume of air. We estimate σ_{MM} as the SD of monthly Hg^0 concentrations in the eight surrounding grid boxes (at the same vertical layer) from the reference simulation (Chen and Prinn, 2006). As shown in Table 1, σ_{MM} values are larger over strongly emitting continental areas (e.g., SGR and WLG) and smaller over remote marine areas (e.g., CPT and AMS).

2.6.4 Model errors

All existing CTMs including GEOS-Chem are imperfect, due to both errors in meteorological data driving the CTMs and errors induced by their parameterizations of physical and chemical processes. The former type of model errors is termed "forcing errors" and the latter "process errors" (Locatelli et al., 2013). Physical processes consist of horizontal/vertical resolution, advection/convection, turbulence, planetary boundary layer mixing, etc. The CTM for Hg is subject to large process errors due to highly uncertain atmospheric chemistry. Recent studies have shown that Br concentration may be significantly underestimated in GEOS-Chem (Parrella et al., 2012; Gratz et al., 2015) and that current Br-initiated oxidation mechanisms are incomplete in describing all possible radical reactions (Dibble et al., 2012; F. Wang, et al., 2014). In order to provide a preliminary assessment of the effect of Br oxidation chemistry on our inversion, we perform an additional parameter inversion including six new elements in the state vector $\boldsymbol{x}$, and each of them represents Br columns in a 30° latitudinal band (see results in Sect. 3.3 and Fig. S8 in the Supplement).

Quantifying model errors requires incorporating many CTMs which are driven by different meteorology and which contain different parameterizations (Prinn, 2000). Multi-CTM intercomparison studies have been performed for CO_2 and CH_4 (Gurney et al., 2002; Baker et al., 2006; Locatelli et al., 2013), suggesting that model errors can impact inverted emissions. Few other global CTMs exist for Hg (Bullock et al., 2008, 2009). Due to our inability to quantify model errors using a single CTM, model errors are not incorporated in our inversion, like many other inverse studies (Huang et al., 2008; Xiao et al., 2010; Rigby et al., 2012). As a result, $\mathbf{R}$ in Eq. (5) only includes observational errors and model–observation mismatch errors.

3 Results and discussion

3.1 Emission inversion: model–observation comparison

We first test whether the comparison between ground-based Hg^0 observations and model outputs improves when using optimized emissions, compared to reference emissions. Figure 3 shows the modeled and observed Hg^0 concentrations at all 27 sites. To quantify model performance, we calculate the normalized root mean square error (NRMSE) for each site:

$$\mathrm{NRMSE} = \frac{\sqrt{\frac{1}{n}\sum_{i=1}^{n}\left(X_{\mathrm{obs},i} - X_{\mathrm{mod},i}\right)^2}}{\frac{1}{n}\sum_{i=1}^{n} X_{\mathrm{obs},i}}, \quad (9)$$

where $X_{\mathrm{obs},i}$ and $X_{\mathrm{mod},i}$ are the observed and modeled Hg^0 concentrations at the ith month (n in total), respectively. As

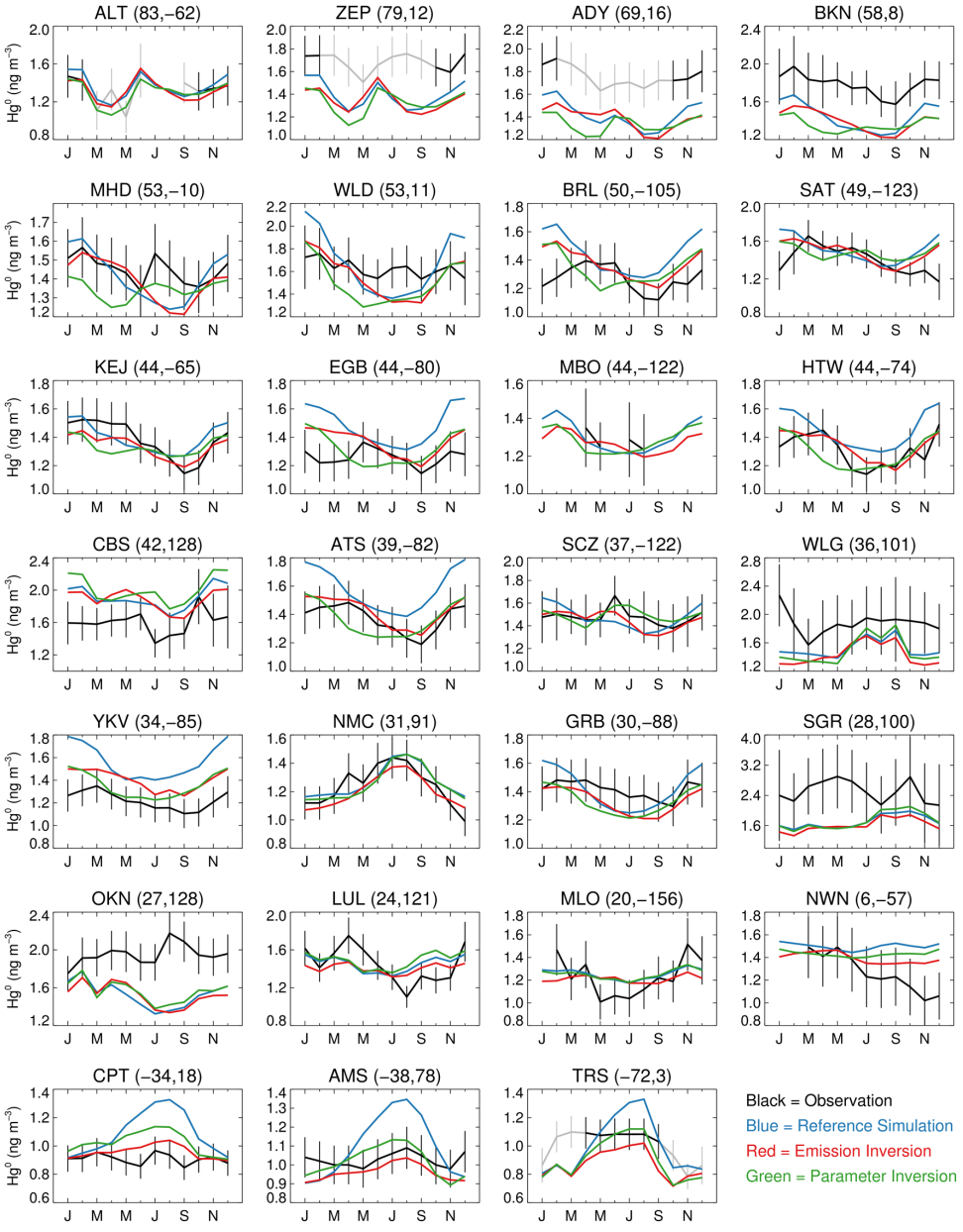

Figure 3. Monthly Hg^0 concentrations for all ground-based observational sites. Note different scales on vertical axes. Error bars correspond to the total errors described in Sect. 2.6. The two numbers in parentheses after the name of each site are its latitude and longitude. For polar sites (ALT, ZEP, ADY, and TRS), the gray color shows the observed Hg^0 concentrations that are not used in our inversions due to AMDEs, as shown in Sect. 2.1.

shown in Table 1, an average NRMSE of 0.13 is obtained for the emission inversion, smaller than that of 0.16 for the reference simulation, indicating that the emission inversion can better reproduce ground-based observations. While this is a relatively small uncertainty reduction (−0.03), we do not expect better performance for our inversion. This is because errors in Hg^0 observations (as described above, and in Table 1) are roughly 13 %, which constrain the optimization. Our inversion brings the average NRMSE within the observation error.

The NRMSEs are not reduced for all 27 sites (see Table 1). For three Nordic sites (ZEP, ADY, and BKN) and four Asia-Pacific sites (WLG, SGR, LUL, and MLO), the NRMSEs increase. Hg^0 concentrations are $\sim 1.8\,ng\,m^{-3}$ at the three Nordic sites, higher than the modeled values (Fig. 3) from both reference simulation and emission inversion, and also higher than those measured at many background sites

in Europe (Ebinghaus et al., 2011; Kentisbeer et al., 2014; Weigelt et al., 2013). Part of the differences may be explained by a positive bias in the instrumentation of these Nordic observations when compared to other laboratories (Temme et al., 2006). It is also possible that GEOS-Chem cannot sufficiently capture local meteorology and/or emissions at these sites. For the Asia-Pacific sites, the reference simulation underestimates Hg^0 at SGR (−32 %, calculated as $(\mathbf{y}^{\mathrm{ref}}/\mathbf{y}^{\mathrm{obs}} - 1) \times 100\,\%$, hereinafter the same) and WLG (−19 %) and predicts comparable values at MLO (+2 %) and LUL (+0 %). Such discrepancies likely arise from unknown intercomparison errors and are influenced by local emission and meteorology factors not captured by the CTM (Fu et al., 2012b; Wan et al., 2009). These sites are operated by three different laboratories but, to the best of our knowledge, no field intercomparisons have been conducted among these laboratories.

Figure 4 compares monthly Hg^0 observations with model simulations for sites aggregated into four regions: Asia-Pacific, North America, Europe, and Southern Hemisphere. The emission inversion significantly improves the comparison for the SH sites (CPT, AMS, and TRS, see Table 1). In the reference simulation, Hg^0 concentrations at the SH sites vary seasonally, with a high in austral winter ($\sim 1.3\,\mathrm{ng\,m^{-3}}$) and a low in austral summer ($\sim 0.9\,\mathrm{ng\,m^{-3}}$). However, observed Hg^0 shows little seasonal variation with monthly concentrations of $\sim 1.0\,\mathrm{ng\,m^{-3}}$. The emission inversion reduces the Hg^0 concentration in austral winter and fits the observations much better (the average NRMSE decreases from 0.19 to 0.10). As shown in Fig. 3, all three SH sites show improvement after optimization.

The emission inversion also improves the comparison for sites in North America (the average NRMSE decreases from 0.13 to 0.08). Hg^0 data at a total of 11 sites are available, including five coastal sites (ALT, SAT, KEJ, SCZ, and GRB), five inland sites (BRL, EGB, HTW, ATS, and YKV), and one mountaintop site (MBO) (see Fig. 1 and Table 1). Hg^0 at the coastal and inland sites are observed to be 1.41 ± 0.04 and $1.29 \pm 0.06\,\mathrm{ng\,m^{-3}}$, respectively. This coastal–inland difference in observation is consistent with results of Cheng et al. (2014), who found that air masses from open ocean at the site KEJ had $0.06\,\mathrm{ng\,m^{-3}}$ higher Hg^0 concentrations than those originating over land. The reference simulation and emission inversion both obtain comparable Hg^0 concentrations at the coastal sites (1.43 ± 0.06 and $1.38 \pm 0.07\,\mathrm{ng\,m^{-3}}$). At the inland sites, the emission inversion predicts Hg^0 concentrations ($1.38 \pm 0.03\,\mathrm{ng\,m^{-3}}$) closer to observations than the reference simulation ($1.50 \pm 0.06\,\mathrm{ng\,m^{-3}}$).

Over-water Hg^0 observations serve as an independent test of the emission inversion. As shown in Fig. 2, Hg^0 concentrations over the North Atlantic Ocean from both the reference simulation and the emission inversion fall within 1σ uncertainty ranges of Hg^0_{nor}. The NRMSEs for the reference simulation and the emission inversion are 0.09 and 0.10, respectively. Thus, using Hg^0 emissions constrained by ground-based observations, GEOS-Chem still matches these regional over-water observations.

We additionally test the performance of the inversion by comparison with regional wet deposition data. Since most oxidized Hg is formed from the oxidation of Hg^0, changing Hg^0 emissions may have an effect on modeled oxidized Hg and its subsequent deposition. We compare model results to the observed wet deposition fluxes from NADP/MDN (2012), as shown in the Supplement, Fig. S9. We use the monitoring sites active in 2009–2011 ($n = 126$). Both the reference simulation and the emission inversion fit observations well ($R \approx 0.7$, NRMSE ≈ 0.3). Accordingly, the effect of the inversion on the NADP/MDN (National Atmospheric Deposition Program/Mercury Deposition Program) wet deposition fluxes is insignificant.

3.2 Emission inversion: optimized emissions

The annual reference and optimized emissions of mercury are shown in Table 2. The relationship $\bar{\sigma} = \sqrt{n \sum_{i=1}^{n} \sigma_t^2}$, where $n = 12$ months and σ_t is monthly error, is used to compute the annual uncertainty for seasonal processes (Chen and Prinn, 2006). The uncertainty of the aseasonal source (annual Asian anthropogenic emission) is obtained directly from Eq. (7). The global optimized mercury emission is $\sim 5.8\,\mathrm{Gg\,yr^{-1}}$, with an uncertainty range of 1.7–10.3 $\mathrm{Gg\,yr^{-1}}$. Compared to our reference emission of $\sim 6.0\,\mathrm{Gg\,yr^{-1}}$ (uncertainty range: 0.4–12.2 $\mathrm{Gg\,yr^{-1}}$), the emission inversion results in a slightly smaller value and also reduces its uncertainty range. The optimized value is smaller than previous estimates of $7.5\,\mathrm{Gg\,yr^{-1}}$ by Pirrone et al. (2010) using a bottom-up approach. The emission inversion increases emissions from anthropogenic sources and ocean surfaces but decreases those from terrestrial surfaces. The ocean accounts for more than half (55 %) of the total, while the terrestrial surface contributes only a small fraction (6 %).

3.2.1 Ocean

Net Hg^0 evasion from the global ocean is optimized by the emission inversion as $3160\,\mathrm{Mg\,yr^{-1}}$, with an uncertainty range of 1160–5160 $\mathrm{Mg\,yr^{-1}}$ (Table 2). The NH and SH oceans contribute similar amounts to the total but, on an area basis, evasion from the NH ocean is higher since it is 30 % smaller. We are able to reduce ocean evasion uncertainty from 50 to 40 % by using top-down constraints.

Figure 5 shows the monthly reference and optimized emissions of seasonal sources. We find, for both hemispheres, that the emission inversion generally results in increased ocean emissions in summer and decreased emissions in winter, compared to the reference simulation. As a result, we hypothesize that one or more ocean processes that affect the

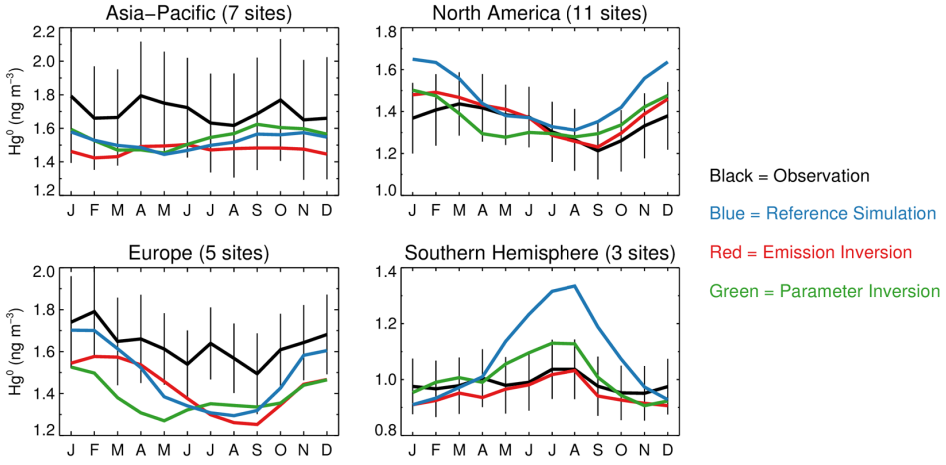

Figure 4. Averaged monthly observations and model simulations of Hg^0 concentrations for the ground-based observational sites in the four regions (Asia-Pacific: 45° E–140° W, 0–90° N; North America: 140–45° W, 15–90° N; Europe: 15° W–45° E, 15–90° N, and the Southern Hemisphere). Note different scales on vertical axes. Hg^0 observations are shown with total errors as described in Sect. 2.6.

seasonal behavior of aqueous mercury and its evasion are not well-represented in GEOS-Chem. We therefore conduct a series of sensitivity studies of model parameters to test their potential effects on the seasonal pattern of ocean emission. We also compare the parameter values used in GEOS-Chem with their possible ranges in a recent review (Batrakova et al., 2014). The tested model parameters in GEOS-Chem include rates of redox chemical reactions and physical processes in the ML and subsurface mercury concentrations affecting physical exchange between the ML and subsurface waters. Through these sensitivity tests and literature review, we identify two processes as candidates for improvement, the rate constant of dark oxidation of Hg^0_{aq} (K_{OX2}) and the partition coefficient between Hg^{2+}_{aq} and Hg^P_{aq} (K_D). We optimize these two ocean model parameters in the parameter inversion, as described in Sect. 2.5.

3.2.2 Terrestrial ecosystem

As shown in Table 2, the emission inversion reduces soil emissions of Hg^0 by about 50 %, from 1680 ± 840 to $860 \pm 440\,Mg\,yr^{-1}$. Using Eq. (1), the optimized net emission flux from terrestrial surfaces (E_{net}) is $340\,Mg\,yr^{-1}$. If we do not consider geogenic activities ($90\,Mg\,yr^{-1}$) and biomass burning ($210\,Mg\,yr^{-1}$), the E_{net2} (calculated as $E_{soil} + E_{pr} - E_{ddHg^0}$ and representing net emissions from soils/vegetation) is almost zero after optimization. Thus, terrestrial surfaces are neither a net source nor a net sink of Hg^0. This is in contrast to bottom-up estimates that the terrestrial surface is a net source of about $2000\,Mg\,yr^{-1}$ (Pirrone et al., 2010; Mason, 2009).

Vegetation is now believed to serve as a net sink of atmospheric Hg^0 through foliar uptake and sequestration (Gustin et al., 2008; Stamenkovic and Gustin, 2009; X. Wang et al., 2014). Although its size has not been well quantified, we suggest that this sink is important in global mass balance since litterfall transfers 2400–6000 Mg Hg yr^{-1} to terrestrial surfaces (Gustin et al., 2008). Air–soil flux measurements show that Hg^0 emissions from background soils generally dominate over dry deposition (Obrist et al., 2014; Edwards and Howard, 2013; Park et al., 2013; Denkenberger et al., 2012; Ericksen et al., 2006). Our result of a smaller soil Hg source is consistent with a study by Obrist et al. (2014), which suggested that Hg was unlikely to be re-emitted once incorporated into soils and that terrestrial Hg emission was restricted to surface layers (Demers et al., 2013). Our result is also in agreement with estimates of terrestrial fluxes of southern Africa using Hg^0 correlations with ^{222}Rn, a radioactive gas of predominantly terrestrial origin (Slemr et al., 2013). Considering that soil is a smaller source while vegetation a sink of Hg^0, our result that the terrestrial ecosystem is neither a net source nor a net sink of Hg^0 is reasonable, implying that the magnitudes of soil emission and dry deposition of Hg^0 (primarily to vegetation) are similar. We evaluate dry deposition fluxes modeled by GEOS-Chem against data in L. Zhang et al. (2012), which estimated fluxes at sites in North America and obtained good agreements with surrogate surface and litterfall measurements (Graydon et al., 2008; Lyman et al., 2007). As shown in the Supplement, Fig. S10, there is no bias in the average dry deposition flux at eight background sites, indicating that $\sim 1400\,Mg\,yr^{-1}$ (modeled by GEOS-Chem) may be reasonable estimates for both emission and dry deposition of Hg^0.

3.2.3 Anthropogenic emission from Asia

Table 3 summarizes Asian emissions of Hg^0 (only GEM) estimated by several recent bottom-up emission inventories and modeling studies. These inventories reported Asian anthro-

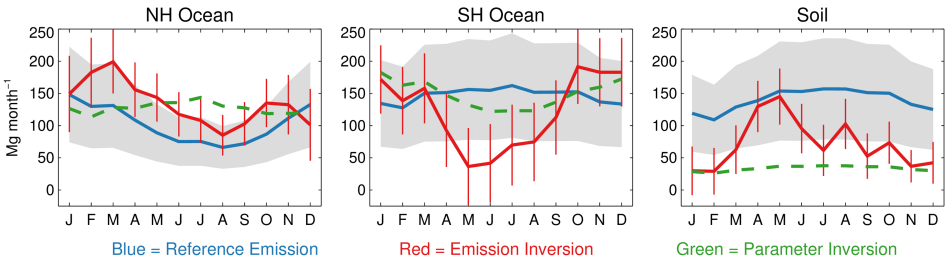

Figure 5. Monthly emissions for the three seasonal sources (NH ocean, SH ocean, and soil) from the reference simulation (blue solid lines), emission inversion (red solid lines), and parameter inversion (green dashed lines). The gray shaded regions and red error bars indicate 1σ uncertainties for the reference emissions and emission inversion, respectively.

Table 3. Comparison of Asian Hg^0 emissions ($Mg\,yr^{-1}$) from recent studies.[a]

Reference	Base year	Anthropogenic	Net terrestrial[b]	Net ocean[b]	Total
		Emission inventories			
Streets et al. (2009)[c]	2006	800			
Streets et al. (2011)[c]	2008	700			
Muntean et al. (2014)	2008	580			
AMAP/UNEP (2013)	2010	770			
Rafaj et al. (2013)[c]	2010	550–750			
		Other studies			
Pan et al. (2007)[d]	1999			420	2270
Shetty et al. (2008)[d]	2001		710	120	
Strode et al. (2008)	2004	890–990			1260–1450
Fu et al. (2015)[e]	2007–2010				1590–1870
This study					
Reference emission	2009–2011	770 ± 390	360	230	1360
Emission inversion	2009–2011	1060 ± 110	130	300	1490
Inversion using different Asian sites	2009–2011	650–1770	0–230	260–300	1180–2030

[a] Here Hg^0 only refers to gaseous elemental mercury. [b] Net terrestrial and ocean emissions are from the Asian domain. [c] Estimated values from tables and figures in the references. [d] An east Asian domain is used in these studies. Their terrestrial and ocean surfaces are smaller than those of the Asia domain. [e] The Asian domain includes mainland China, southern Asia, Indochinese Peninsula, and central Asia, and does not include ocean surfaces.

pogenic emissions ranging from 550 to 800 $Mg\,yr^{-1}$. In our model simulations, the reference emission of 770 $Mg\,yr^{-1}$ follows AMAP/UNEP (2013). The emission inversion using all 27 sites increases this value to 1060 ± 110 $Mg\,yr^{-1}$. Uncertainty in Asian anthropogenic emission should be larger than that obtained using our inversion method, because emission estimates are sensitive to the Asia-Pacific sites used in the inversion. As discussed above, model performance at several Asia-Pacific sites is affected by unknown intercomparison errors and local emission and meteorological factors not captured by GEOS-Chem. To obtain a more accurate estimate of uncertainty, we perform seven emission inversions, each including only one Asia-Pacific site.

As shown in Table 3, these inversions result in Asian anthropogenic emissions of Hg^0 ranging from 650 to 1770 $Mg\,yr^{-1}$. Comparing this range to its bottom-up inventory estimates of 550–800 $Mg\,yr^{-1}$, we suggest that it is very likely to be underestimated. We estimate total (anthropogenic + natural + legacy) Hg^0 emission in Asia as 1180–2030 $Mg\,yr^{-1}$. Our uncertainty ranges cover those in Strode et al. (2008), which estimated total Asian emission of 1260–1450 $Mg\,yr^{-1}$ with 890–990 $Mg\,yr^{-1}$ from anthropogenic sources, by comparing GEOS-Chem to the observed Hg : CO ratio at sites OKN and MBO. Pan et al. (2007) assimilated aircraft observations into a regional CTM and estimated total Hg^0 emission in east Asia as 2270 $Mg\,yr^{-1}$, at the upper end of our range. Fu et al. (2015) obtained a total Hg^0 emission in Asia of 1590–1870 $Mg\,yr^{-1}$, which compared well with our range, using the Hg^0 : CO and Hg^0 : CO_2 slopes observed at ground-based sites and inventories of CO and

CO_2. Shetty et al. (2008) estimated natural terrestrial emission in east Asia was about 710 Mg yr^{-1}, much higher than our 0–230 Mg yr^{-1} in a larger domain. The difference is due to their larger estimation of vegetation evapotranspiration (630 Mg yr^{-1}).

3.3 Parameter inversion

Results of the parameter inversion are presented in Table 4. The a posteriori K_{OX2} of 6×10^{-6} s^{-1} is much larger than its current value (1×10^{-7} s^{-1}) in GEOS-Chem, suggesting that Hg^0_{aq} dark oxidation in the ML is more important than previously thought. The a posteriori log K_D of 4.2 is lower than seawater values in the literature (Fitzgerald et al., 2007; Batrakova et al., 2014) but agrees with the lower end of freshwater measurements (Amos et al., 2014). We attribute this discrepancy to several simplifying assumptions in GEOS-Chem. K_D is linked to the estimates of SPM concentrations in the ML and organic carbon export. As described above, the amount of organic carbon export is very uncertain (5–20 Gt C yr^{-1}). A smaller organic carbon export may correspond to a larger log K_D. The uncertain spatial and seasonal variations of carbon export may also affect the estimate of log K_D. In addition, there are no available global data sets of SPM in the ML. GEOS-Chem derives SPM concentrations from MODIS satellite chlorophyll *a* and C : Chl *a* ratios (Soerensen et al., 2010b). Thus, the uncertain SPM fields may also affect log K_D. As for the other two parameters (ER_{Soil} and ER_{Asia}), the parameter inversion decreases soil emission but increases Asian anthropogenic emission, consistent with the emission inversion (see Table 4).

Similar to our model–observation comparison for the emission inversion, we run GEOS-Chem using optimized parameters and calculate the NRMSEs for all ground-based sites (Table 1). A smaller average NRMSE of 0.14 for the parameter inversion than that of 0.16 for the reference simulation shows improvement in model performance. GEOS-Chem simulations using optimized parameters also match regional over-water Hg^0 (NRMSE = 0.10, Fig. 2) and wet deposition measurements (Fig. S9 in the Supplement). In addition, we evaluate the optimized model against recent surface ocean measurements of total aqueous mercury (Hg^T_{aq}), Hg^0_{aq}, and Hg^P_{aq} (Table 5). For Hg^T_{aq}, 50 and 75 % (6 and 8 out of 12) of the modeled data from the reference and optimized simulations, respectively, are within measurement ranges. For Hg^0_{aq}, 60 % (6 out of 10) of the modeled data from both simulations are within measurement ranges. For Hg^P_{aq}, the reference simulation predicts a higher value while the parameter inversion predicts a lower value than the only measurement data. These results suggest that the parameter inversion is comparable or potentially better than the reference simulation with regard to modeling surface ocean mercury.

Optimizing the two ocean model parameters, $-\log K_{OX2}$ and log K_D, changes the global ocean Hg budget in GEOS-Chem, as shown in Fig. 6. Sources of Hg_{aq} in the ML include deposition of oxidized Hg and physical transport from subsurface waters. They are balanced by Hg^0 evasion and Hg^P_{aq} sinking. In the reference simulation, although deposition (20.2 Mmol yr^{-1}) accounts for most ML Hg_{aq} inputs, the two physical transport processes, entrainment/detrainment of the ML and Ekman pumping, together supply a considerable amount (F_{INT}: 6.1 Mmol yr^{-1}) from subsurface waters. This upward flux is a result of the gradient in Hg^T_{aq} between the ML (0.8 pM) and subsurface waters (1.1 pM). Hg^0 evasion and Hg^P_{aq} sinking remove 14.9 and 11.4 Mmol yr^{-1} from the ML, respectively. The combined effect of the larger K_{OX2} and smaller K_D in the parameter inversion is, in the ML, that Hg^{2+}_{aq} increases from 0.69 to 0.95 pM, Hg^P_{aq} decreases from 0.05 to 0.004 pM, and Hg^0_{aq} remains 0.06 pM. Hg^P_{aq} sinking becomes a smaller sink (1.7 Mmol yr^{-1}) due to the lower K_D. Physical transport contributes a downward flux (−1.5 Mmol yr^{-1}) since the gradient of Hg^T_{aq} between the ML (1.0 pM) and subsurface waters (1.1 pM) is diminished.

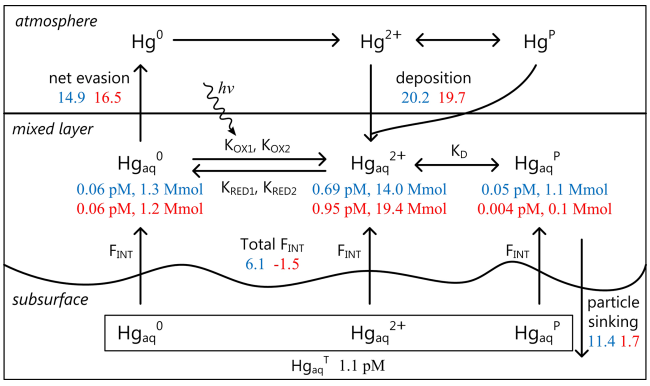

Figure 6. Global ocean mercury budget modeled by GEOS-Chem. Blue color indicates the reference simulation and red color the parameter inversion. Fluxes are in megamoles per year. Notations in this figure follow Soerensen et al. (2010b). F_{INT} denotes net fluxes from subsurface waters through entrainment/detrainment of the mixed layer and Ekman pumping.

Physical transport and Hg^P_{aq} sinking affect seasonal variations of simulated Hg^0 evasion from the ocean (Soerensen et al., 2010b). In summer, enhanced biological productivity increases Hg^P_{aq} sinking and decreases Hg^0 evasion by shifting speciated Hg_{aq} equilibrium in the ML towards Hg^0_{aq} loss. During winter months, the ML deepens and Hg_{aq} in subsurface waters invade the ML by entrainment; additionally, Hg^0 evasion will be enhanced if subsurface waters contain higher Hg^T_{aq}. In the parameter inversion, physical transport and Hg^P_{aq} sinking are both weakened, as described above. As a result, the parameter inversion overturns seasonality of simulated ocean evasions in both hemispheres (Fig. 5), agreeing with results from the emission inversion.

As described in Sect. 2.6.4, we conduct an additional parameter inversion including six new elements representing Br

Table 4. Evolution of the parameters' estimates in the parameter inversion.

Parameter	A priori	First iteration	Before second iteration*	A posteriori
$-\log K_{OX2}$	5.0 ± 1.0	5.1 ± 0.1	5.1 ± 1.0	5.2 ± 0.1 ($K_{OX2} = 6 \times 10^{-6}\ s^{-1}$)
$\log K_D$	5.3 ± 0.4	4.4 ± 0.2	4.4 ± 0.2	4.2 ± 0.2 ($K_D = 1.6 \times 10^4\ L\ kg^{-1}$)
ER_{Soil}	1.0 ± 0.5	0.37 ± 0.08	0.37 ± 0.19	0.24 ± 0.1 (soil emission decreases by 76 %)
ER_{Asia}	1.0 ± 0.5	1.7 ± 0.1	1.7 ± 0.9	1.9 ± 0.1 (Asian anthropogenic emission increases by 90 %)

* For the second iteration, we use the best estimates derived from the first iteration, but larger parameter uncertainties. The uncertainty of 1.0 for $-\log K_{OX2}$ is the same as that for the a priori estimate. The uncertainties for ER_{Soil} and ER_{Asia} are chosen as 50 % of their best estimates, consistent with the emission inversion. The uncertainty for $\log K_D$ is chosen as 0.2 because it is approaching the lower end (4.2) of the possible values in the literature survey.

Table 5. Recent surface ocean mercury measurements and simulated concentrations.[a]

Location	Date	Latitude, longitude	Measurement	Reference simulation[b]	Parameter inversion[b]	Ref.[c]
			Hg^T_{aq} (pM)			
Atlantic Ocean	Nov 2008	15–50° N, 20–5° W	0.8–3.0	**0.64**	0.89	(1)
		30–15° S, 0–15° E	0.4–2.8	0.48	0.97	(1)
	Apr–May 2009	15–50° N, 25–5° W	0.4–2.3	**0.34**	0.82	(1)
		50–15° S, 65–20° W	0.5–1.5	0.68	0.89	(1)
	Oct–Nov 2005	20° S–35° N, 25° W–10° E	0.5–4.5	0.63	1.2	(2)
	Jun 2008	32° N, 64° W	0.6–1.0	0.65	**1.2**	(3)
	Sep 2008–2009	25–35° N, 65–60° W	0.6–0.9	**0.95**	**1.2**	(4)
	Aug 2010	30–32° N, 65–60° W	1.2–1.6	**0.91**	1.2	(4)
Pacific Ocean	Mar 2006	20–50° N, 152° W	0.5–1.9	0.96	1.2	(5)
	May 2009	30° N, 140° W	0.2–0.4	**0.80**	**1.1**	(6)
	Oct 2011	15° S–17° N, 175–155° W	< 0.5	**0.83**	**1.1**	(7)
Southern Ocean	Mar–Apr 2008	66–44° S, 140–147° E	0.6–2.8	0.85	1.1	(8)
			Hg^0_{aq} (fM)			
Atlantic Ocean	Nov 2008	15–50° N, 20–5° W	30–140	52	51	(1)
		30–15° S, 0–15° E	15–30	**38**	**68**	(1)
	Apr–May 2009	15–50° N, 25–5° W	15–40	27	**55**	(1)
		50–15° S, 65–20° W	10–70	54	59	(1)
	Jul 2005	60° N, 40° W–5° E	30–90	**22**	83	(9)
	Sep 2008–2009	25–35° N, 65–60° W	80–170	80	87	(4)
	Jun 2009	32° N, 64° W	105–135	**55**	**90**	(4)
	Aug 2010	30–32° N, 65–60° W	130–260	**77**	**94**	(4)
Pacific Ocean	Oct 2011	15S–17° N, 175–155° W	< 100	71	81	(7)
Southern Ocean	Mar–Apr 2008	66–44° S, 140–147° E	< 280	72	58	(8)
			Hg^P_{aq} (fM)			
Pacific Ocean	Oct 2011	15° S–17° N, 175–155° W	20–50	**70**	**5**	(7)

[a] $1\ pM = 10^{-9}\ mol\ m^{-3}$; $1\ fM = 10^{-12}\ mol\ m^{-3}$. [b] Numbers in bold represent the modeled concentrations that are out of the corresponding measurement ranges. [c] References: (1) Kuss et al. (2011), (2) Pohl et al. (2011), (3) Lamborg et al. (2012), (4) Soerensen et al. (2013), (5) Sunderland et al. (2009), (6) Hammerschmidt and Bowman (2012), (7) Munson (2014), (8) Cossa et al. (2011), and (9) Andersson et al. (2011).

columns in different latitudinal bands. As shown in the Supplement, Fig. S8, $-\log K_{OX2}$ is found to be strongly correlated with Br columns at 30–60° N, 30° S–0°, and 60–30° S. The other three factors, $\log K_D$, ER_{Soil}, and ER_{Asia}, have no or weak correlations with Br columns. Thus, we suggest that the inversion results of smaller terrestrial emissions and larger Asian anthropogenic emissions are not likely to be affected by the uncertainty in atmospheric chemistry, but the poor understanding of atmospheric chemistry may limit our ability to further constrain specific ocean model parameters.

3.4 Implications for the Hg biogeochemical cycle

We use the box model developed by Amos et al. (2013, 2014) to explore the long-term impact of our inverted emissions and parameters on the global biogeochemical cycling of mercury. This seven-box model dynamically couples the atmosphere, three terrestrial reservoirs (fast, slow, and armored), and three ocean reservoirs (surface, subsurface, and deep). All rate coefficients of Hg mass between reservoirs are assumed to be of the first order. The simulation is initialized with geogenic emissions to represent the natural mercury cycle and, after reaching steady state, it is driven by historical anthropogenic emissions (Streets et al., 2011; Horowitz et al., 2014).

Two box-model simulations are performed. The first uses rate coefficients from the present-day global budget in the reference simulation. The second uses those from our emission and parameter inversions and has higher anthropogenic emissions, lower re-emission from terrestrial surfaces, and less sinking out of the surface ocean than the first one does (Table S4 in the Supplement). The second simulation obtains larger terrestrial mercury reservoirs, highlighting their important role in sequestering legacy mercury. The oceans are a smaller mercury reservoir of ~ 1700 Mmol in the second simulation, compared to that of ~ 2000 Mmol in the first simulation. The former number is more consistent with the estimates of about 1300–1400 Mmol by Lamborg et al. (2014) and Zhang et al. (2014). The first box-model simulation shows that 18 % of present-day atmospheric deposition is from primary anthropogenic emissions, 76 % is legacy, and 6 % is natural (i.e., geogenic emissions). Applying our inversion results into the box model, the second simulation suggests that primary anthropogenic emissions account for a larger fraction (18–23 %) of present-day atmospheric deposition. Legacy releases of mercury contribute a smaller proportion (72–76 %) but still play a major role.

4 Summary and conclusion

Here, we perform global-scale inverse modeling combining ground-based Hg^0 observations and GEOS-Chem mercury simulations. Using Bayesian inversion methods, we are able to constrain present-day mercury emission fluxes from major sources (emission inversion) and relevant key parameters in GEOS-Chem (parameter inversion), and reduce uncertainties associated with these fluxes and parameters.

The emission inversion better reproduces the ground-based Hg^0 observations (particularly for sites in the Southern Hemisphere and North America) than the reference simulation and also matches measured Hg^0 over the North Atlantic Ocean and wet deposition fluxes in North America. We obtain a global Hg emission of $5.8\,\mathrm{Gg\,yr^{-1}}$ (uncertainty range: 1.7–$10.3\,\mathrm{Gg\,yr^{-1}}$), smaller than the estimate of $7.5\,\mathrm{Gg\,yr^{-1}}$ using a bottom-up approach (Pirrone et al., 2010). The global ocean accounts for $3.2\,\mathrm{Gg\,yr^{-1}}$ Hg (55 % of the total). The terrestrial ecosystem is neither a net source nor a net sink of atmospheric Hg^0, in contrast to its bottom-up estimate as a significant source (Pirrone et al., 2010). The optimized Asian anthropogenic emissions range from 650 to $1770\,\mathrm{Mg\,yr^{-1}}$, suggesting that bottom-up inventories (550–$800\,\mathrm{Mg\,yr^{-1}}$) may have underestimated their value. The total Asian Hg^0 emission (including anthropogenic, natural and legacy sources) is estimated as 1180–$2030\,\mathrm{Mg\,yr^{-1}}$, consistent with recent studies (Fu et al., 2015; Strode et al., 2008; Pan et al., 2007).

The emission inversion changes seasonal patterns of ocean emissions in both hemispheres. We identify and constrain two ocean model parameters in GEOS-Chem that can explain this seasonal pattern, the rate constant of dark oxidation of Hg^0_{aq} (K_{OX2}) and the partition coefficient between Hg^{2+}_{aq} and Hg^P_{aq} (K_D). The a posteriori K_{OX2} ($6 \times 10^{-6}\,\mathrm{s^{-1}}$) is larger than its current value in GEOS-Chem ($1 \times 10^{-7}\,\mathrm{s^{-1}}$), suggesting that dark oxidation of Hg^0_{aq} is more important than previously thought. The a posteriori $\log K_D$ (4.2) is smaller than its a priori (5.3), leading to less Hg^P_{aq} sinking out of the mixed layer. These changes in parameters affect the simulated global ocean mercury budget, especially mass exchange between the mixed layer and subsurface waters. The parameter inversion changes seasonality of ocean emissions in both hemispheres, agreeing with results from the emission inversion.

Our inversion results suggest changes in our understanding of the timescales of cycling between different mercury reservoirs. Based on these changes, the long-term biogeochemical box-model simulations result in larger estimated terrestrial mercury pools and smaller ocean mercury pools. Legacy mercury accounts for a smaller fraction of present-day atmospheric deposition than previous estimates, whereas the contribution of primary anthropogenic emissions becomes larger (up to 23 %).

Our inversion results identify specific knowledge gaps in mercury observation and modeling that currently limit our ability to constrain the biogeochemical cycle of mercury. First, and most important, effective inversions are hampered by the uncertain atmospheric Hg measurements, particularly the large intercomparison errors in measured GEM. Only a few experiments have been made to evaluate the comparability of mercury measurements (Gustin et al., 2013). Our results show that intercomparison errors (about 10 %) dominate the total observational errors and thus limit the uncertainty reduction possible by our inverse approach. Our inversions only lead to moderate reductions of the average NRMSE (Sect. 3.1). Therefore, research aimed at quantifying and reducing the intercomparison errors should be given high priority by the mercury measurement community. Second, observational sites are sparse in some regions (e.g., the Southern Hemisphere). More sites in these regions are necessary to further constrain emissions. Third, the uncertainty in atmospheric mercury chemistry also affects our inversion re-

sults (specifically, in constraining ocean model parameters). Improving our understanding of atmospheric mercury chemistry at both global and regional scales (e.g., the polar regions) requires a combination of both measurement and modeling advances.

The Supplement related to this article is available online at doi:10.5194/acp-15-7103-2015-supplement.

Acknowledgements. This work is supported by the US NSF Atmospheric Chemistry Program #1053648. A. Dommergue, O. Magand, and H. Angot acknowledge the EU-FP7 project GMOS, Labex OSUG@2020 (ANR10 LABX56) and LEFE CNRS/INSU (program SAMOA) for funding, and the French Polar Institute IPEV (Program 1028, GMOStral) for logistical and financial support. S. Kang and Q. Zhang acknowledge support by project NSFC (41225002). We thank Environment Canada, Ministry of the Environment (Japan), the SEARCH network (sponsored by Southern Company and EPRI), X. Feng and X. Fu (IGCAS, China), K. Crist (Ohio University), and all other investigators for providing observational data, H. Amos (Harvard) for assistance and helpful discussions on the global biogeochemical box model, and J. Kuss (IOW, Germany), C. D. Holmes (FSU), Y. Zhang and E. S. Corbitt (Harvard) for helpful discussions. We also thank two anonymous referees for their helpful comments.

Edited by: A. Dastoor

References

AMAP/UNEP: Technical Background Report for the Global Mercury Assessment 2013, Arctic Monitoring and Assessment Programme, Oslo, Norway/UNEP Chemicals Branch Geneva, Switzerland, vi + 263 pp., 2013.

Amos, H. M., Jacob, D. J., Holmes, C. D., Fisher, J. A., Wang, Q., Yantosca, R. M., Corbitt, E. S., Galarneau, E., Rutter, A. P., Gustin, M. S., Steffen, A., Schauer, J. J., Graydon, J. A., Louis, V. L. St., Talbot, R. W., Edgerton, E. S., Zhang, Y., and Sunderland, E. M.: Gas-particle partitioning of atmospheric Hg(II) and its effect on global mercury deposition, Atmos. Chem. Phys., 12, 591–603, doi:10.5194/acp-12-591-2012, 2012.

Amos, H. M., Jacob, D. J., Streets, D. G., and Sunderland, E. M.: Legacy impacts of all-time anthropogenic emissions on the global mercury cycle, Global Biogeochem. Cy., 27, 410–421, doi:10.1002/gbc.20040, 2013.

Amos, H. M., Jacob, D. J., Kocman, D., Horowitz, H. M., Zhang, Y., Dutkiewicz, S., Horvat, M., Corbitt, E. S., Krabbenhoft, D. P., and Sunderland, E. M.: Global biogeochemical implications of mercury discharges from rivers and sediment burial, Environ. Sci. Technol., 48, 9514–9522, doi:10.1021/es502134t, 2014.

Amyot, M., Gill, G. A., and Morel, F. M. M.: Production and loss of dissolved gaseous mercury in coastal seawater, Environ. Sci. Technol., 31, 3606–3611, doi:10.1021/es9703685, 1997.

Andersson, M. E., Sommar, J., Gårdfeldt, K., and Jutterström, S.: Air–sea exchange of volatile mercury in the North Atlantic Ocean, Mar. Chem., 125, 1–7, doi:10.1016/j.marchem.2011.01.005, 2011.

Angot, H., Barret, M., Magand, O., Ramonet, M., and Dommergue, A.: A 2-year record of atmospheric mercury species at a background Southern Hemisphere station on Amsterdam Island, Atmos. Chem. Phys., 14, 11461–11473, doi:10.5194/acp-14-11461-2014, 2014.

Antia, A. N., Koeve, W., Fischer, G., Blanz, T., Schulz-Bull, D., Schölten, J., Neuer, S., Kremling, K., Kuss, J., Peinert, R., Hebbeln, D., Bathmann, U., Conte, M., Fehner, U., and Zeitzschel, B.: Basin-wide particulate carbon flux in the Atlantic Ocean: Regional export patterns and potential for atmospheric CO_2 sequestration, Global Biogeochem. Cy., 15, 845–862, doi:10.1029/2000gb001376, 2001.

Aspmo, K., Gauchard, P.-A., Steffen, A., Temme, C., Berg, T., Bahlmann, E., Banic, C., Dommergue, A., Ebinghaus, R., Ferrari, C., Pirrone, N., Sprovieri, F., and Wibetoe, G.: Measurements of atmospheric mercury species during an international study of mercury depletion events at Ny-Ålesund, Svalbard, spring 2003. How reproducible are our present methods?, Atmos. Environ., 39, 7607–7619, doi:10.1016/j.atmosenv.2005.07.065, 2005.

Bagnato, E., Tamburello, G., Avard, G., Martinez-Cruz, M., Enrico, M., Fu, X., Sprovieri, M., and Sonke, J. E.: Mercury fluxes from volcanic and geothermal sources: an update, Geological Society, London, Special Publications, 410, 263–285, doi:10.1144/sp410.2, 2014.

Baker, D. F., Law, R. M., Gurney, K. R., Rayner, P., Peylin, P., Denning, A. S., Bousquet, P., Bruhwiler, L., Chen, Y. H., Ciais, P., Fung, I. Y., Heimann, M., John, J., Maki, T., Maksyutov, S., Masarie, K., Prather, M., Pak, B., Taguchi, S., and Zhu, Z.: TransCom 3 inversion intercomparison: Impact of transport model errors on the interannual variability of regional CO_2 fluxes, 1988–2003, Global Biogeochem. Cy., 20, GB1002, doi:10.1029/2004gb002439, 2006.

Bash, J. O.: Description and initial simulation of a dynamic bidirectional air-surface exchange model for mercury in Community Multiscale Air Quality (CMAQ) model, J. Geophys. Res.-Atmos., 115, D06305, doi:10.1029/2009jd012834, 2010.

Bash, J. O., Bresnahan, P., and Miller, D. R.: Dynamic surface interface exchanges of mercury: A review and compartmentalized modeling framework, J. Appl. Meteorol. Clim., 46, 1606–1618, doi:10.1175/jam2553.1, 2007.

Batrakova, N., Travnikov, O., and Rozovskaya, O.: Chemical and physical transformations of mercury in the ocean: a review, Ocean Sci., 10, 1047–1063, doi:10.5194/os-10-1047-2014, 2014.

Bey, I., Jacob, D. J., Yantosca, R. M., Logan, J. A., Field, B. D., Fiore, A. M., Li, Q., Liu, H. Y., Mickley, L. J., and Schultz, M. G.: Global modeling of tropospheric chemistry with assimilated meteorology: Model description and evaluation, J. Geophys. Res.-Atmos., 106, 23073–23095, doi:10.1029/2001jd000807, 2001.

Brunke, E.-G., Labuschagne, C., Ebinghaus, R., Kock, H. H., and Slemr, F.: Gaseous elemental mercury depletion events observed at Cape Point during 2007–2008, Atmos. Chem. Phys., 10, 1121–1131, doi:10.5194/acp-10-1121-2010, 2010.

Brunner, D., Henne, S., Keller, C. A., Reimann, S., Vollmer, M. K., O'Doherty, S., and Maione, M.: An extended Kalman-filter for regional scale inverse emission estimation, Atmos. Chem. Phys., 12, 3455–3478, doi:10.5194/acp-12-3455-2012, 2012.

Bullock, O. R., Atkinson, D., Braverman, T., Civerolo, K., Dastoor, A., Davignon, D., Ku, J.-Y., Lohman, K., Myers, T. C., Park, R. J., Seigneur, C., Selin, N. E., Sistla, G., and Vijayaraghavan, K.: The North American Mercury Model Intercomparison Study (NAMMIS): Study description and model-to-model comparisons, J. Geophys. Res.-Atmos., 113, D17310, doi:10.1029/2008jd009803, 2008.

Bullock, O. R., Atkinson, D., Braverman, T., Civerolo, K., Dastoor, A., Davignon, D., Ku, J.-Y., Lohman, K., Myers, T. C., Park, R. J., Seigneur, C., Selin, N. E., Sistla, G., and Vijayaraghavan, K.: An analysis of simulated wet deposition of mercury from the North American Mercury Model Intercomparison Study, J. Geophys. Res.-Atmos., 114, D08301, doi:10.1029/2008jd011224, 2009.

Chen, Y.-H. and Prinn, R. G.: Estimation of atmospheric methane emissions between 1996 and 2001 using a three-dimensional global chemical transport model, J. Geophys. Res., 111, D10307, doi:10.1029/2005jd006058, 2006.

Cheng, I., Zhang, L., Mao, H., Blanchard, P., Tordon, R., and Dalziel, J.: Seasonal and diurnal patterns of speciated atmospheric mercury at a coastal-rural and a coastal-urban site, Atmos. Environ., 82, 193–205, doi:10.1016/j.atmosenv.2013.10.016, 2014.

Cole, A. S., Steffen, A., Pfaffhuber, K. A., Berg, T., Pilote, M., Poissant, L., Tordon, R., and Hung, H.: Ten-year trends of atmospheric mercury in the high Arctic compared to Canadian sub-Arctic and mid-latitude sites, Atmos. Chem. Phys., 13, 1535–1545, doi:10.5194/acp-13-1535-2013, 2013.

Cole, A. S., Steffen, A., Eckley, C. S., Narayan, J., Pilote, M., Tordon, R., Graydon, J. A., St. Louis, V. L., Xu, X., and Branfireun, B. A.: A survey of mercury in air and precipitation across Canada: patterns and trends, Atmosphere, 5, 635–668, doi:10.3390/atmos5030635, 2014.

Cossa, D., Heimbürger, L.-E., Lannuzel, D., Rintoul, S. R., Butler, E. C. V., Bowie, A. R., Averty, B., Watson, R. J., and Remenyi, T.: Mercury in the Southern Ocean, Geochim. Cosmochim. Ac., 75, 4037–4052, doi:10.1016/j.gca.2011.05.001, 2011.

Dastoor, A. P. and Durnford, D. A.: Arctic Ocean: Is it a sink or a source of atmospheric mercury?, Environ. Sci. Technol., 48, 1707–1717, doi:10.1021/es404473e, 2013.

de Foy, B., Wiedinmyer, C., and Schauer, J. J.: Estimation of mercury emissions from forest fires, lakes, regional and local sources using measurements in Milwaukee and an inverse method, Atmos. Chem. Phys., 12, 8993–9011, doi:10.5194/acp-12-8993-2012, 2012.

de Foy, B., Heo, J., and Schauer, J. J.: Estimation of direct emissions and atmospheric processing of reactive mercury using inverse modeling, Atmos. Environ., 85, 73–82, doi:10.1016/j.atmosenv.2013.11.070, 2014.

Demers, J. D., Blum, J. D., and Zak, D. R.: Mercury isotopes in a forested ecosystem: Implications for air-surface exchange dynamics and the global mercury cycle, Global Biogeochem. Cy., 27, 222–238, doi:10.1002/gbc.20021, 2013.

Denkenberger, J. S., Driscoll, C. T., Branfireun, B. A., Eckley, C. S., Cohen, M., and Selvendiran, P.: A synthesis of rates and controls on elemental mercury evasion in the Great Lakes Basin, Environ. Pollut., 161, 291–298, doi:10.1016/j.envpol.2011.06.007, 2012.

De Simone, F., Gencarelli, C. N., Hedgecock, I. M., and Pirrone, N.: Global atmospheric cycle of mercury: a model study on the impact of oxidation mechanisms, Environ. Sci. Pollut. R., 21, 4110–4123, doi:10.1007/s11356-013-2451-x, 2014.

Dibble, T. S., Zelie, M. J., and Mao, H.: Thermodynamics of reactions of ClHg and BrHg radicals with atmospherically abundant free radicals, Atmos. Chem. Phys., 12, 10271–10279, doi:10.5194/acp-12-10271-2012, 2012.

Driscoll, C. T., Mason, R. P., Chan, H. M., Jacob, D. J., and Pirrone, N.: Mercury as a global pollutant: sources, pathways, and effects, Environ. Sci. Technol., 47, 4967–4983, doi:10.1021/es305071v, 2013.

Durnford, D., Dastoor, A., Figueras-Nieto, D., and Ryjkov, A.: Long range transport of mercury to the Arctic and across Canada, Atmos. Chem. Phys., 10, 6063–6086, doi:10.5194/acp-10-6063-2010, 2010.

Ebinghaus, R., Jennings, S. G., Schroeder, W. H., Berg, T., Donaghy, T., Guentzel, J., Kenny, C., Kock, H. H., Kvietkus, K., Landing, W., Mühleck, T., Munthe, J., Prestbo, E. M., Schneeberger, D., Slemr, F., Sommar, J., Urba, A., Wallschläger, D., and Xiao, Z.: International field intercomparison measurements of atmospheric mercury species at Mace Head, Ireland, Atmos. Environ., 33, 3063–3073, doi:10.1016/S1352-2310(98)00119-8, 1999.

Ebinghaus, R., Jennings, S. G., Kock, H. H., Derwent, R. G., Manning, A. J., and Spain, T. G.: Decreasing trends in total gaseous mercury observations in baseline air at Mace Head, Ireland from 1996 to 2009, Atmos. Environ., 45, 3475–3480, doi:10.1016/j.atmosenv.2011.01.033, 2011.

Edwards, G. C. and Howard, D. A.: Air-surface exchange measurements of gaseous elemental mercury over naturally enriched and background terrestrial landscapes in Australia, Atmos. Chem. Phys., 13, 5325–5336, doi:10.5194/acp-13-5325-2013, 2013.

Ericksen, J. A., Gustin, M. S., Xin, M., Weisberg, P. J., and Fernandez, G. C. J.: Air–soil exchange of mercury from background soils in the United States, Sci. Total Environ., 366, 851–863, doi:10.1016/j.scitotenv.2005.08.019, 2006.

Fisher, J. A., Jacob, D. J., Soerensen, A. L., Amos, H. M., Steffen, A., and Sunderland, E. M.: Riverine source of Arctic Ocean mercury inferred from atmospheric observations, Nat. Geosci., 5, 499–504, doi:10.1038/ngeo1478, 2012.

Fitzgerald, W. F., Lamborg, C. H., and Hammerschmidt, C. R.: Marine biogeochemical cycling of mercury, Chem. Rev., 107, 641–662, doi:10.1021/cr050353m, 2007.

Friedli, H. R., Arellano, A. F., Cinnirella, S., and Pirrone, N.: Initial estimates of mercury emissions to the atmosphere from global biomass burning, Environ. Sci. Technol., 43, 3507–3513, doi:10.1021/es802703g, 2009.

Fu, X. W., Feng, X., Dong, Z. Q., Yin, R. S., Wang, J. X., Yang, Z. R., and Zhang, H.: Atmospheric gaseous elemental mercury (GEM) concentrations and mercury depositions at a high-altitude mountain peak in south China, Atmos. Chem. Phys., 10, 2425–2437, doi:10.5194/acp-10-2425-2010, 2010.

Fu, X. W., Feng, X., Liang, P., Deliger, Zhang, H., Ji, J., and Liu, P.: Temporal trend and sources of speciated atmospheric mercury at Waliguan GAW station, Northwestern China, Atmos. Chem. Phys., 12, 1951–1964, doi:10.5194/acp-12-1951-2012, 2012a.

Fu, X. W., Feng, X., Shang, L. H., Wang, S. F., and Zhang, H.: Two years of measurements of atmospheric total gaseous mercury (TGM) at a remote site in Mt. Changbai area, Northeastern China, Atmos. Chem. Phys., 12, 4215–4226, doi:10.5194/acp-12-4215-2012, 2012b.

Fu, X. W., Zhang, H., Lin, C.-J., Feng, X. B., Zhou, L. X., and Fang, S. X.: Correlation slopes of GEM / CO, GEM / CO_2, and GEM / CH_4 and estimated mercury emissions in China, South Asia, the Indochinese Peninsula, and Central Asia derived from observations in northwestern and southwestern China, Atmos. Chem. Phys., 15, 1013–1028, doi:10.5194/acp-15-1013-2015, 2015.

Gårdfeldt, K. and Jonsson, M.: Is bimolecular reduction of Hg(II) complexes possible in aqueous systems of environmental importance, J. Phys. Chem. A, 107, 4478–4482, doi:10.1021/jp0275342, 2003.

Gay, D. A., Schmeltz, D., Prestbo, E., Olson, M., Sharac, T., and Tordon, R.: The Atmospheric Mercury Network: measurement and initial examination of an ongoing atmospheric mercury record across North America, Atmos. Chem. Phys., 13, 11339–11349, doi:10.5194/acp-13-11339-2013, 2013.

Goodsite, M. E., Plane, J. M. C., and Skov, H.: Correction to a theoretical study of the oxidation of Hg^0 to $HgBr_2$ in the troposphere, Environ. Sci. Technol., 46, 5262–5262, doi:10.1021/es301201c, 2012.

Grant, S. L., Kim, M., Lin, P., Crist, K. C., Ghosh, S., and Kotamarthi, V. R.: A simulation study of atmospheric mercury and its deposition in the Great Lakes, Atmos. Environ., 94, 164–172, doi:10.1016/j.atmosenv.2014.05.033, 2014.

Gratz, L. E., Shah, V., Ambrose, J. L., Jaffe, D. A., Jaeglé, L., Stutz, J., Festa, J., Spolaor, M., Tsai, C., Selin, N. E., Song, S., Zhou, X., Weinheimer, A., Knapp, D., Montzka, D., Flocke, F., Campos, T., Apel, E., Hornbrook, R., Blake, N., Hall, S., Tyndall, G., Reeves M., Stechman, D., and Stell, M.: Oxidation of mercury by bromine in the subtropical Pacific free troposphere, Nat. Geosci., in review, 2015.

Graydon, J. A., St. Louis, V. L., Hintelmann, H., Lindberg, S. E., Sandilands, K. A., Rudd, J. W. M., Kelly, C. A., Hall, B. D., and Mowat, L. D.: Long-term wet and dry deposition of total and methyl mercury in the remote boreal ecoregion of Canada, Environ. Sci. Technol., 42, 8345–8351, doi:10.1021/es801056j, 2008.

Gurney, K. R., Law, R. M., Denning, A. S., Rayner, P. J., Baker, D., Bousquet, P., Bruhwiler, L., Chen, Y.-H., Ciais, P., Fan, S., Fung, I. Y., Gloor, M., Heimann, M., Higuchi, K., John, J., Maki, T., Maksyutov, S., Masarie, K., Peylin, P., Prather, M., Pak, B. C., Randerson, J., Sarmiento, J., Taguchi, S., Takahashi, T., and Yuen, C.-W.: Towards robust regional estimates of CO_2 sources and sinks using atmospheric transport models, Nature, 415, 626–630, doi:10.1038/415626a, 2002.

Gustin, M. S., Lindberg, S. E., and Weisberg, P. J.: An update on the natural sources and sinks of atmospheric mercury, Appl. Geochem., 23, 482–493, doi:10.1016/j.apgeochem.2007.12.010, 2008.

Gustin, M. S., Huang, J., Miller, M. B., Peterson, C., Jaffe, D. A., Ambrose, J., Finley, B. D., Lyman, S. N., Call, K., Talbot, R., Feddersen, D., Mao, H., and Lindberg, S. E.: Do we understand what the mercury speciation instruments are actually measuring? Results of RAMIX, Environ. Sci. Technol., 47, 7295–7306, doi:10.1021/es3039104, 2013.

Hammerschmidt, C. R. and Bowman, K. L.: Vertical methylmercury distribution in the subtropical North Pacific Ocean, Mar. Chem., 132–133, 77–82, doi:10.1016/j.marchem.2012.02.005, 2012.

Henson, S. A., Sanders, R., Madsen, E., Morris, P. J., Le Moigne, F., and Quartly, G. D.: A reduced estimate of the strength of the ocean's biological carbon pump, Geophys. Res. Lett., 38, L04606, doi:10.1029/2011gl046735, 2011.

Holmes, C. D., Jacob, D. J., Corbitt, E. S., Mao, J., Yang, X., Talbot, R., and Slemr, F.: Global atmospheric model for mercury including oxidation by bromine atoms, Atmos. Chem. Phys., 10, 12037–12057, doi:10.5194/acp-10-12037-2010, 2010.

Horowitz, H. M., Jacob, D. J., Amos, H. M., Streets, D. G., and Sunderland, E. M.: Historical mercury releases from commercial products: global environmental implications, Environ. Sci. Technol., 48, 10242–10250, doi:10.1021/es501337j, 2014.

Huang, J., Golombek, A., Prinn, R., Weiss, R., Fraser, P., Simmonds, P., Dlugokencky, E. J., Hall, B., Elkins, J., Steele, P., Langenfelds, R., Krummel, P., Dutton, G., and Porter, L.: Estimation of regional emissions of nitrous oxide from 1997 to 2005 using multinetwork measurements, a chemical transport model, and an inverse method, J. Geophys. Res.-Atmos., 113, D17313, doi:10.1029/2007jd009381, 2008.

Hynes, A., Donohoue, D., Goodsite, M., and Hedgecock, I.: Our current understanding of major chemical and physical processes affecting mercury dynamics in the atmosphere and at the air-water/terrestrial interfaces, in: Mercury Fate and Transport in the Global Atmosphere, edited by: Mason, R. and Pirrone, N., Springer US, New York, NY, USA, 427–457, 2009.

Jaffe, D., Prestbo, E., Swartzendruber, P., Weiss-Penzias, P., Kato, S., Takami, A., Hatakeyama, S., and Kajii, Y.: Export of atmospheric mercury from Asia, Atmos. Environ., 39, 3029–3038, doi:10.1016/j.atmosenv.2005.01.030, 2005.

Jaffe, D. A., Lyman, S., Amos, H. M., Gustin, M. S., Huang, J., Selin, N. E., Levin, L., ter Schure, A., Mason, R. P., Talbot, R., Rutter, A., Finley, B., Jaeglé, L., Shah, V., McClure, C., Ambrose, J., Gratz, L., Lindberg, S., Weiss-Penzias, P., Sheu, G.-R., Feddersen, D., Horvat, M., Dastoor, A., Hynes, A. J., Mao, H., Sonke, J. E., Slemr, F., Fisher, J. A., Ebinghaus, R., Zhang, Y., and Edwards, G.: Progress on understanding atmospheric mercury hampered by uncertain measurements, Environ. Sci. Technol., 48, 7204–7206, doi:10.1021/es5026432, 2014.

Kentisbeer, J., Leeson, S. R., Malcolm, H. M., Leith, I. D., Braban, C. F., and Cape, J. N.: Patterns and source analysis for atmospheric mercury at Auchencorth Moss, Scotland, Environ. Sci.-Process Impacts, 16, 1112–1123, doi:10.1039/c3em00700f, 2014.

Kikuchi, T., Ikemoto, H., Takahashi, K., Hasome, H., and Ueda, H.: Parameterizing soil emission and atmospheric oxidation-reduction in a model of the global biogeochemical cycle of mercury, Environ. Sci. Technol., 47, 12266–12274, doi:10.1021/es401105h, 2013.

Kocman, D., Horvat, M., Pirrone, N., and Cinnirella, S.: Contribution of contaminated sites to the global mercury budget, Environ. Res., 125, 160–170, doi:10.1016/j.envres.2012.12.011, 2013.

Krüger, O., Ebinghaus, R., Kock, H. H., Richter-Politz, I., and Geilhufe, C.: Inverse modelling of gaseous mercury emissions at the

contaminated industrial site BSL Werk Schkopau, in: Mercury Contaminated Sites - Characterization, Risk Assessment and Remediation, edited by: Ebinghaus, R., Turner, R. R., Lacerda, D., Vasiliev, O., and Salomons, W., Springer Environmental Science, Springer, Heidelberg, 377–392, 1999.

Kuss, J.: Water–air gas exchange of elemental mercury: An experimentally determined mercury diffusion coefficient for Hg^0 water–air flux calculations, Limnol. Oceanogr., 59, 1461–1467, doi:10.4319/lo.2014.59.5.1461, 2014.

Kuss, J., Holzmann, J., and Ludwig, R.: An elemental mercury diffusion coefficient for natural waters determined by molecular dynamics simulation, Environ. Sci. Technol., 43, 3183–3186, doi:10.1021/es8034889, 2009.

Kuss, J., Zülicke, C., Pohl, C., and Schneider, B.: Atlantic mercury emission determined from continuous analysis of the elemental mercury sea-air concentration difference within transects between 50° N and 50° S, Global Biogeochem. Cy., 25, GB3021, doi:10.1029/2010gb003998, 2011.

Lalonde, J. D., Amyot, M., Kraepiel, A. M. L., and Morel, F. M. M.: Photooxidation of Hg(0) in artificial and natural waters, Environ. Sci. Technol., 35, 1367–1372, doi:10.1021/es001408z, 2001.

Lalonde, J. D., Amyot, M., Orvoine, J., Morel, F. M. M., Auclair, J.-C., and Ariya, P. A.: Photoinduced oxidation of Hg^0(aq) in the waters from the St. Lawrence Estuary, Environ. Sci. Technol., 38, 508–514, doi:10.1021/es034394g, 2004.

Lamborg, C. H., Hammerschmidt, C. R., Gill, G. A., Mason, R. P., and Gichuki, S.: An intercomparison of procedures for the determination of total mercury in seawater and recommendations regarding mercury speciation during GEOTRACES cruises, Limnol. Oceanogr.-Meth., 10, 90–100, doi:10.4319/lom.2012.10.90, 2012.

Lamborg, C. H., Hammerschmidt, C. R., Bowman, K. L., Swarr, G. J., Munson, K. M., Ohnemus, D. C., Lam, P. J., Heimburger, L.-E., Rijkenberg, M. J. A., and Saito, M. A.: A global ocean inventory of anthropogenic mercury based on water column measurements, Nature, 512, 65–68, doi:10.1038/nature13563, 2014.

Lan, X., Talbot, R., Castro, M., Perry, K., and Luke, W.: Seasonal and diurnal variations of atmospheric mercury across the US determined from AMNet monitoring data, Atmos. Chem. Phys., 12, 10569–10582, doi:10.5194/acp-12-10569-2012, 2012.

Lei, H., Liang, X.-Z., Wuebbles, D. J., and Tao, Z.: Model analyses of atmospheric mercury: present air quality and effects of transpacific transport on the United States, Atmos. Chem. Phys., 13, 10807–10825, doi:10.5194/acp-13-10807-2013, 2013.

Lin, C. J. and Pehkonen, S. O.: The chemistry of atmospheric mercury: a review, Atmos. Environ., 33, 2067–2079, doi:10.1016/s1352-2310(98)00387-2, 1999.

Lin, C.-J., Gustin, M. S., Singhasuk, P., Eckley, C., and Miller, M.: Empirical models for estimating mercury flux from soils, Environ. Sci. Technol., 44, 8522–8528, doi:10.1021/es1021735, 2010.

Lindberg, S., Bullock, R., Ebinghaus, R., Engstrom, D., Feng, X., Fitzgerald, W., Pirrone, N., Prestbo, E., and Seigneur, C.: A synthesis of progress and uncertainties in attributing the sources of mercury in deposition, AMBIO: A Journal of the Human Environment, 36, 19–33, doi:10.1579/0044-7447(2007)36[19:asopau]2.0.co;2, 2007.

Locatelli, R., Bousquet, P., Chevallier, F., Fortems-Cheney, A., Szopa, S., Saunois, M., Agusti-Panareda, A., Bergmann, D., Bian, H., Cameron-Smith, P., Chipperfield, M. P., Gloor, E., Houweling, S., Kawa, S. R., Krol, M., Patra, P. K., Prinn, R. G., Rigby, M., Saito, R., and Wilson, C.: Impact of transport model errors on the global and regional methane emissions estimated by inverse modelling, Atmos. Chem. Phys., 13, 9917–9937, doi:10.5194/acp-13-9917-2013, 2013.

Loux, N. T.: A critical assessment of elemental mercury air/water exchange parameters, Chem. Spec. Bioavailab., 16, 127–138, doi:10.3184/095422904782775018, 2004.

Lyman, S. N., Gustin, M. S., Prestbo, E. M., and Marsik, F. J.: Estimation of dry deposition of atmospheric mercury in Nevada by direct and indirect methods, Environ. Sci. Technol., 41, 1970–1976, doi:10.1021/es062323m, 2007.

Mason, R.: Mercury emissions from natural processes and their importance in the global mercury cycle, in: Mercury Fate and Transport in the Global Atmosphere, edited by: Mason, R. and Pirrone, N., Springer US, New York, NY, USA, 173–191, 2009.

Mason, R. P. and Fitzgerald, W. F.: The distribution and biogeochemical cycling of mercury in the equatorial Pacific Ocean, Deep-Sea Res. Pt. I, 40, 1897–1924, doi:10.1016/0967-0637(93)90037-4, 1993.

Mason, R. P. and Sheu, G. R.: Role of the ocean in the global mercury cycle, Global Biogeochem. Cy., 16, 1093, doi:10.1029/2001gb001440, 2002.

Mason, R. P., Rolfhus, K. R., and Fitzgerald, W. F.: Mercury in the North Atlantic, Mar. Chem., 61, 37–53, doi:10.1016/S0304-4203(98)00006-1, 1998.

Mason, R. P., Choi, A. L., Fitzgerald, W. F., Hammerschmidt, C. R., Lamborg, C. H., Soerensen, A. L., and Sunderland, E. M.: Mercury biogeochemical cycling in the ocean and policy implications, Environ. Res., 119, 101–117, doi:10.1016/j.envres.2012.03.013, 2012.

McClure, C., Jaffe, D. A., and Edgerton, E. S.: Evaluation of the KCl denuder method for gaseous oxidized mercury using $HgBr_2$ at an in-service AMNet site, Environ. Sci. Technol., 48, 11437–11444, doi:10.1021/es502545k, 2014.

Mergler, D., Anderson, H. A., Chan, L. H. M., Mahaffey, K. R., Murray, M., Sakamoto, M., and Stern, A. H.: Methylmercury exposure and health effects in humans: a worldwide concern, AMBIO: A Journal of the Human Environment, 36, 3–11, doi:10.1579/0044-7447(2007)36[3:meahei]2.0.co;2, 2007.

MOEJ: Ministry of the Environment, Japan: Monitoring results of atmosphere mercury background concentration, available at: http://www.env.go.jp/press/press.php?serial=16473 (last access: 25 June 2015), 2013 (in Japanese).

Müller, D., Wip, D., Warneke, T., Holmes, C. D., Dastoor, A., and Notholt, J.: Sources of atmospheric mercury in the tropics: continuous observations at a coastal site in Suriname, Atmos. Chem. Phys., 12, 7391–7397, doi:10.5194/acp-12-7391-2012, 2012.

Munson, K. M.: Transformations of mercury in the marine water column, PhD Thesis, Joint Program in Oceanography (Massachusetts Institute of Technology, Department of Earth, Atmospheric, and Planetary Sciences; and the Woods Hole Oceanographic Institution), available at: http://hdl.handle.net/1721.1/87513 (last access: 25 June 2015), 2014.

Muntean, M., Janssens-Maenhout, G., Song, S., Selin, N. E., Olivier, J. G. J., Guizzardi, D., Maas, R., and Dentener, F.: Trend analysis from 1970 to 2008 and model evaluation of EDGARv4 global gridded anthropogenic mercury emissions, Sci. Total En-

viron., 494–495, 337–350, doi:10.1016/j.scitotenv.2014.06.014, 2014.

Munthe, J., Wängberg, I., Pirrone, N., Iverfeldt, Å., Ferrara, R., Ebinghaus, R., Feng, X., Gårdfeldt, K., Keeler, G., Lanzillotta, E., Lindberg, S. E., Lu, J., Mamane, Y., Prestbo, E., Schmolke, S., Schroeder, W. H., Sommar, J., Sprovieri, F., Stevens, R. K., Stratton, W., Tuncel, G., and Urba, A.: Intercomparison of methods for sampling and analysis of atmospheric mercury species, Atmos. Environ., 35, 3007–3017, doi:10.1016/S1352-2310(01)00104-2, 2001.

NADP/MDN: Mercury Deposition Network, National Atmospheric Deposition Program, available at: http://nadp.sws.uiuc.edu/mdn/ (last access: 25 June 2015), 2012.

Obrist, D., Pokharel, A. K., and Moore, C.: Vertical profile measurements of soil air suggest immobilization of gaseous elemental mercury in mineral soil, Environ. Sci. Technol., 48, 2242–2252, doi:10.1021/es4048297, 2014.

Pacyna, E. G., Pacyna, J. M., Sundseth, K., Munthe, J., Kindbom, K., Wilson, S., Steenhuisen, F., and Maxson, P.: Global emission of mercury to the atmosphere from anthropogenic sources in 2005 and projections to 2020, Atmos. Environ., 44, 2487–2499, doi:10.1016/j.atmosenv.2009.06.009, 2010.

Pan, L., Chai, T., Carmichael, G. R., Tang, Y., Streets, D., Woo, J.-H., Friedli, H. R., and Radke, L. F.: Top-down estimate of mercury emissions in China using four-dimensional variational data assimilation, Atmos. Environ., 41, 2804–2819, doi:10.1016/j.atmosenv.2006.11.048, 2007.

Park, S.-Y., Kim, P.-R., and Han, Y.-J.: Mercury exchange flux from two different soil types and affecting parameters, Asian J. Atmos. Environ., 7, 199–208, doi:10.5572/ajae.2013.7.4.199, 2013.

Parrella, J. P., Jacob, D. J., Liang, Q., Zhang, Y., Mickley, L. J., Miller, B., Evans, M. J., Yang, X., Pyle, J. A., Theys, N., and Van Roozendael, M.: Tropospheric bromine chemistry: implications for present and pre-industrial ozone and mercury, Atmos. Chem. Phys., 12, 6723–6740, doi:10.5194/acp-12-6723-2012, 2012.

Pfaffhuber, K. A., Berg, T., Hirdman, D., and Stohl, A.: Atmospheric mercury observations from Antarctica: seasonal variation and source and sink region calculations, Atmos. Chem. Phys., 12, 3241–3251, doi:10.5194/acp-12-3241-2012, 2012.

Pirrone, N., Cinnirella, S., Feng, X., Finkelman, R. B., Friedli, H. R., Leaner, J., Mason, R., Mukherjee, A. B., Stracher, G. B., Streets, D. G., and Telmer, K.: Global mercury emissions to the atmosphere from anthropogenic and natural sources, Atmos. Chem. Phys., 10, 5951–5964, doi:10.5194/acp-10-5951-2010, 2010.

Pirrone, N., Aas, W., Cinnirella, S., Ebinghaus, R., Hedgecock, I. M., Pacyna, J., Sprovieri, F., and Sunderland, E. M.: Toward the next generation of air quality monitoring: Mercury, Atmos. Environ., 80, 599–611, doi:10.1016/j.atmosenv.2013.06.053, 2013.

Pohl, C., Croot, P. L., Hennings, U., Daberkow, T., Budeus, G., and Loeff, M. R. v. d.: Synoptic transects on the distribution of trace elements (Hg, Pb, Cd, Cu, Ni, Zn, Co, Mn, Fe, and Al) in surface waters of the Northern- and Southern East Atlantic, J. Marine Syst., 84, 28–41, doi:10.1016/j.jmarsys.2010.08.003, 2011.

Poissant, L., Pilote, M., Beauvais, C., Constant, P., and Zhang, H. H.: A year of continuous measurements of three atmospheric mercury species (GEM, RGM and Hgp) in southern Québec, Canada, Atmos. Environ., 39, 1275–1287, doi:10.1016/j.atmosenv.2004.11.007, 2005.

Pongprueksa, P., Lin, C. J., Singhasuk, P., Pan, L., Ho, T. C., and Chu, H. W.: Application of CMAQ at a hemispheric scale for atmospheric mercury simulations, Geosci. Model Dev. Discuss., 4, 1723–1754, doi:10.5194/gmdd-4-1723-2011, 2011.

Prinn, R. G.: Measurement equation for trace chemicals in fluids and solution of its inverse, in: Inverse Methods in Global Biogeochemical Cycles, Geophys. Monogr. Ser., AGU, Washington, DC, USA, 3–18, 2000.

Prinn, R. G., Heimbach, P., Rigby, M., Dutkiewicz, S., Melillo, J. M., Reilly, J. M., Kicklighter, D. W., and Waugh, C.: A strategy for a global observing system for verification of national greenhouse gas emissions, MIT Joint Program on the Science and Policy of Global Change, available at: http://globalchange.mit.edu/research/publications/2161 (last access: 25 June 2015), 2011.

Qureshi, A., O'Driscoll, N. J., MacLeod, M., Neuhold, Y.-M., and Hungerbühler, K.: Photoreactions of mercury in surface ocean water: gross reaction kinetics and possible pathways, Environ. Sci. Technol., 44, 644–649, doi:10.1021/es9012728, 2010.

Rafaj, P., Bertok, I., Cofala, J., and Schöpp, W.: Scenarios of global mercury emissions from anthropogenic sources, Atmos. Environ., 79, 472–479, doi:10.1016/j.atmosenv.2013.06.042, 2013.

Rigby, M., Manning, A. J., and Prinn, R. G.: The value of high-frequency, high-precision methane isotopologue measurements for source and sink estimation, J. Geophys. Res.-Atmos., 117, D12312, doi:10.1029/2011jd017384, 2012.

Roustan, Y. and Bocquet, M.: Inverse modelling for mercury over Europe, Atmos. Chem. Phys., 6, 3085–3098, doi:10.5194/acp-6-3085-2006, 2006.

Saikawa, E., Rigby, M., Prinn, R. G., Montzka, S. A., Miller, B. R., Kuijpers, L. J. M., Fraser, P. J. B., Vollmer, M. K., Saito, T., Yokouchi, Y., Harth, C. M., Mühle, J., Weiss, R. F., Salameh, P. K., Kim, J., Li, S., Park, S., Kim, K.-R., Young, D., O'Doherty, S., Simmonds, P. G., McCulloch, A., Krummel, P. B., Steele, L. P., Lunder, C., Hermansen, O., Maione, M., Arduini, J., Yao, B., Zhou, L. X., Wang, H. J., Elkins, J. W., and Hall, B.: Global and regional emission estimates for HCFC-22, Atmos. Chem. Phys., 12, 10033–10050, doi:10.5194/acp-12-10033-2012, 2012.

Sanders, R., Henson, S. A., Koski, M., De La Rocha, C. L., Painter, S. C., Poulton, A. J., Riley, J., Salihoglu, B., Visser, A., Yool, A., Bellerby, R., and Martin, A. P.: The biological carbon pump in the North Atlantic, Prog. Oceanogr., 129, 200–218, doi:10.1016/j.pocean.2014.05.005, 2014.

Schroeder, W. H., Keeler, G., Kock, H., Roussel, P., Schneeberger, D., and Schaedlich, F.: International field intercomparison of atmospheric mercury measurement methods, Water Air Soil Poll., 80, 611–620, doi:10.1007/bf01189713, 1995.

Seigneur, C. and Lohman, K.: Effect of bromine chemistry on the atmospheric mercury cycle, J. Geophys. Res.-Atmos., 113, D23309, doi:10.1029/2008jd010262, 2008.

Selin, N. E.: Global biogeochemical cycling of mercury: a review, Annu. Rev. Env. Resour., 34, 43–63, doi:10.1146/annurev.environ.051308.084314, 2009.

Selin, N. E.: Global change and mercury cycling: Challenges for implementing a global mercury treaty, Environ. Toxicol. Chem., 33, 1202–1210, doi:10.1002/etc.2374, 2014.

Selin, N. E., Jacob, D. J., Park, R. J., Yantosca, R. M., Strode, S., Jaeglé, L., and Jaffe, D.: Chemical cycling and deposition of atmospheric mercury: Global constraints

from observations, J. Geophys. Res.-Atmos., 112, D02308, doi:10.1029/2006jd007450, 2007.

Selin, N. E., Jacob, D. J., Yantosca, R. M., Strode, S., Jaeglé, L., and Sunderland, E. M.: Global 3-D land-ocean-atmosphere model for mercury: Present-day versus preindustrial cycles and anthropogenic enrichment factors for deposition, Global Biogeochem. Cy., 22, GB2011, doi:10.1029/2007gb003040, 2008.

Shetty, S. K., Lin, C.-J., Streets, D. G., and Jang, C.: Model estimate of mercury emission from natural sources in East Asia, Atmos. Environ., 42, 8674–8685, doi:10.1016/j.atmosenv.2008.08.026, 2008.

Sheu, G.-R., Lin, N.-H., Wang, J.-L., Lee, C.-T., Ou Yang, C.-F., and Wang, S.-H.: Temporal distribution and potential sources of atmospheric mercury measured at a high-elevation background station in Taiwan, Atmos. Environ., 44, 2393–2400, doi:10.1016/j.atmosenv.2010.04.009, 2010.

Slemr, F., Seiler, W., and Schuster, G.: Latitudinal distribution of mercury over the Atlantic Ocean, J. Geophys. Res.-Oceans, 86, 1159–1166, doi:10.1029/JC086iC02p01159, 1981.

Slemr, F., Brunke, E.-G., Ebinghaus, R., and Kuss, J.: Worldwide trend of atmospheric mercury since 1995, Atmos. Chem. Phys., 11, 4779–4787, doi:10.5194/acp-11-4779-2011, 2011.

Slemr, F., Brunke, E.-G., Whittlestone, S., Zahorowski, W., Ebinghaus, R., Kock, H. H., and Labuschagne, C.: ^{222}Rn-calibrated mercury fluxes from terrestrial surface of southern Africa, Atmos. Chem. Phys., 13, 6421–6428, doi:10.5194/acp-13-6421-2013, 2013.

Slemr, F., Angot, H., Dommergue, A., Magand, O., Barret, M., Weigelt, A., Ebinghaus, R., Brunke, E.-G., Pfaffhuber, K. A., Edwards, G., Howard, D., Powell, J., Keywood, M., and Wang, F.: Comparison of mercury concentrations measured at several sites in the Southern Hemisphere, Atmos. Chem. Phys., 15, 3125–3133, doi:10.5194/acp-15-3125-2015, 2015.

Smith-Downey, N. V., Sunderland, E. M., and Jacob, D. J.: Anthropogenic impacts on global storage and emissions of mercury from terrestrial soils: Insights from a new global model, J. Geophys. Res.-Biogeo., 115, G03008, doi:10.1029/2009jg001124, 2010.

Soerensen, A. L., Skov, H., Jacob, D. J., Soerensen, B. T., and Johnson, M. S.: Global concentrations of gaseous elemental mercury and reactive gaseous mercury in the marine boundary layer, Environ. Sci. Technol., 44, 7425–7430, doi:10.1021/es903839n, 2010a.

Soerensen, A. L., Sunderland, E. M., Holmes, C. D., Jacob, D. J., Yantosca, R. M., Skov, H., Christensen, J. H., Strode, S. A., and Mason, R. P.: An improved global model for air-sea exchange of mercury: high concentrations over the North Atlantic, Environ. Sci. Technol., 44, 8574–8580, doi:10.1021/es102032g, 2010b.

Soerensen, A. L., Jacob, D. J., Streets, D. G., Witt, M. L. I., Ebinghaus, R., Mason, R. P., Andersson, M., and Sunderland, E. M.: Multi-decadal decline of mercury in the North Atlantic atmosphere explained by changing subsurface seawater concentrations, Geophys. Res. Lett., 39, L21810, doi:10.1029/2012gl053736, 2012.

Soerensen, A. L., Mason, R. P., Balcom, P. H., and Sunderland, E. M.: Drivers of surface ocean mercury concentrations and air–sea exchange in the West Atlantic Ocean, Environ. Sci. Technol., 47, 7757–7765, doi:10.1021/es401354q, 2013.

Stamenkovic, J. and Gustin, M. S.: Nonstomatal versus stomatal uptake of atmospheric mercury, Environ. Sci. Technol., 43, 1367–1372, doi:10.1021/es801583a, 2009.

Steffen, A., Douglas, T., Amyot, M., Ariya, P., Aspmo, K., Berg, T., Bottenheim, J., Brooks, S., Cobbett, F., Dastoor, A., Dommergue, A., Ebinghaus, R., Ferrari, C., Gardfeldt, K., Goodsite, M. E., Lean, D., Poulain, A. J., Scherz, C., Skov, H., Sommar, J., and Temme, C.: A synthesis of atmospheric mercury depletion event chemistry in the atmosphere and snow, Atmos. Chem. Phys., 8, 1445–1482, doi:10.5194/acp-8-1445-2008, 2008.

Steffen, A., Scherz, T., Olson, M., Gay, D., and Blanchard, P.: A comparison of data quality control protocols for atmospheric mercury speciation measurements, J. Environ. Monit., 14, 752–765, doi:10.1039/c2em10735j, 2012.

Steffen, A., Bottenheim, J., Cole, A., Ebinghaus, R., Lawson, G., and Leaitch, W. R.: Atmospheric mercury speciation and mercury in snow over time at Alert, Canada, Atmos. Chem. Phys., 14, 2219–2231, doi:10.5194/acp-14-2219-2014, 2014.

Stein, E. D., Cohen, Y., and Winer, A. M.: Environmental distribution and transformation of mercury compounds, Crit. Rev. Env. Sci. Tec., 26, 1–43, doi:10.1080/10643389609388485, 1996.

Streets, D. G., Zhang, Q., and Wu, Y.: Projections of global mercury emissions in 2050, Environ. Sci. Technol., 43, 2983–2988, doi:10.1021/es802474j, 2009.

Streets, D. G., Devane, M. K., Lu, Z., Bond, T. C., Sunderland, E. M., and Jacob, D. J.: All-time releases of mercury to the atmosphere from human activities, Environ. Sci. Technol., 45, 10485–10491, doi:10.1021/es202765m, 2011.

Strode, S. A., Jaeglé, L., Selin, N. E., Jacob, D. J., Park, R. J., Yantosca, R. M., Mason, R. P., and Slemr, F.: Air-sea exchange in the global mercury cycle, Global Biogeochem. Cy., 21, GB1017, doi:10.1029/2006gb002766, 2007.

Strode, S. A., Jaeglé, L., Jaffe, D. A., Swartzendruber, P. C., Selin, N. E., Holmes, C., and Yantosca, R. M.: Trans-Pacific transport of mercury, J. Geophys. Res.-Atmos., 113, D15305, doi:10.1029/2007jd009428, 2008.

Subir, M., Ariya, P. A., and Dastoor, A. P.: A review of uncertainties in atmospheric modeling of mercury chemistry I. Uncertainties in existing kinetic parameters – Fundamental limitations and the importance of heterogeneous chemistry, Atmos. Environ., 45, 5664–5676, doi:10.1016/j.atmosenv.2011.04.046, 2011.

Subir, M., Ariya, P. A., and Dastoor, A. P.: A review of the sources of uncertainties in atmospheric mercury modeling II. Mercury surface and heterogeneous chemistry – A missing link, Atmos. Environ., 46, 1–10, doi:10.1016/j.atmosenv.2011.07.047, 2012.

Sunderland, E. M., Krabbenhoft, D. P., Moreau, J. W., Strode, S. A., and Landing, W. M.: Mercury sources, distribution, and bioavailability in the North Pacific Ocean: Insights from data and models, Global Biogeochem. Cy., 23, GB2010, doi:10.1029/2008gb003425, 2009.

Temme, C., Ebinghaus, R., Kock, H. H., Schwerin, A., and Bieber, E.: Field intercomparison of mercury measurements within EMEP (executive summary), available at: http://www.nilu.no/projects/ccc/qa/files/EMEP-QA_Hg_UBA.doc (last access: 25 June 2015), 2006.

Timonen, H., Ambrose, J. L., and Jaffe, D. A.: Oxidation of elemental Hg in anthropogenic and marine airmasses, Atmos. Chem. Phys., 13, 2827–2836, doi:10.5194/acp-13-2827-2013, 2013.

Tørseth, K., Aas, W., Breivik, K., Fjæraa, A. M., Fiebig, M., Hjellbrekke, A. G., Lund Myhre, C., Solberg, S., and Yttri, K. E.: Introduction to the European Monitoring and Evaluation Programme (EMEP) and observed atmospheric composition change during 1972–2009, Atmos. Chem. Phys., 12, 5447–5481, doi:10.5194/acp-12-5447-2012, 2012.

Travnikov, O. and Ilyin, I.: The EMEP/MSC-E mercury modeling system, in: Mercury Fate and Transport in the Global Atmosphere, edited by: Mason, R. and Pirrone, N., Springer US, New York, NY, USA, 571–587, 2009.

Ulrych, T., Sacchi, M., and Woodbury, A.: A Bayes tour of inversion: A tutorial, Geophysics, 66, 55–69, doi:10.1190/1.1444923, 2001.

Valente, R. J., Shea, C., Lynn Humes, K., and Tanner, R. L.: Atmospheric mercury in the Great Smoky Mountains compared to regional and global levels, Atmos. Environ., 41, 1861–1873, doi:10.1016/j.atmosenv.2006.10.054, 2007.

van der Werf, G. R., Randerson, J. T., Giglio, L., Collatz, G. J., Mu, M., Kasibhatla, P. S., Morton, D. C., DeFries, R. S., Jin, Y., and van Leeuwen, T. T.: Global fire emissions and the contribution of deforestation, savanna, forest, agricultural, and peat fires (1997–2009), Atmos. Chem. Phys., 10, 11707–11735, doi:10.5194/acp-10-11707-2010, 2010.

Wan, Q., Feng, X. B., Lu, J. L., Zheng, W., Song, X. J., Han, S. J., and Xu, H.: Atmospheric mercury in Changbai Mountain area, northeastern China I. The seasonal distribution pattern of total gaseous mercury and its potential sources, Environ. Res., 109, 201–206, doi:10.1016/j.envres.2008.12.001, 2009.

Wang, F., Saiz-Lopez, A., Mahajan, A. S., Gómez Martín, J. C., Armstrong, D., Lemes, M., Hay, T., and Prados-Roman, C.: Enhanced production of oxidised mercury over the tropical Pacific Ocean: a key missing oxidation pathway, Atmos. Chem. Phys., 14, 1323–1335, doi:10.5194/acp-14-1323-2014, 2014.

Wang, S., Zhang, L., Wang, L., Wu, Q., Wang, F., and Hao, J.: A review of atmospheric mercury emissions, pollution and control in China, Front. Environ. Sci. Eng., 8, 631–649, doi:10.1007/s11783-014-0673-x, 2014.

Wang, X., Lin, C.-J., and Feng, X.: Sensitivity analysis of an updated bidirectional air–surface exchange model for elemental mercury vapor, Atmos. Chem. Phys., 14, 6273–6287, doi:10.5194/acp-14-6273-2014, 2014.

Weigelt, A., Temme, C., Bieber, E., Schwerin, A., Schuetze, M., Ebinghaus, R., and Kock, H. H.: Measurements of atmospheric mercury species at a German rural background site from 2009 to 2011 – methods and results, Environ. Chem., 10, 102–110, doi:10.1071/EN12107, 2013.

Weiss-Penzias, P., Jaffe, D. A., Swartzendruber, P., Dennison, J. B., Chand, D., Hafner, W., and Prestbo, E.: Observations of Asian air pollution in the free troposphere at Mount Bachelor Observatory during the spring of 2004, J. Geophys. Res.-Atmos., 111, D10304, doi:10.1029/2005jd006522, 2006.

Wesely, M. L.: Parameterization of surface resistances to gaseous dry deposition in regional-scale numerical models, Atmos. Environ., 23, 1293–1304, doi:10.1016/0004-6981(89)90153-4, 1989.

Wilke, C. R. and Chang, P.: Correlation of diffusion coefficients in dilute solutions, AIChE J., 1, 264–270, doi:10.1002/aic.690010222, 1955.

Wunsch, C.: Discrete inverse and state estimation problems: with geophysical fluid applications, Cambridge University Press, New York, USA, 43–69, 2006.

Xiao, X., Prinn, R. G., Fraser, P. J., Weiss, R. F., Simmonds, P. G., O'Doherty, S., Miller, B. R., Salameh, P. K., Harth, C. M., Krummel, P. B., Golombek, A., Porter, L. W., Butler, J. H., Elkins, J. W., Dutton, G. S., Hall, B. D., Steele, L. P., Wang, R. H. J., and Cunnold, D. M.: Atmospheric three-dimensional inverse modeling of regional industrial emissions and global oceanic uptake of carbon tetrachloride, Atmos. Chem. Phys., 10, 10421–10434, doi:10.5194/acp-10-10421-2010, 2010.

Xu, X., Yang, X., R. Miller, D., Helble, J. J., and Carley, R. J.: Formulation of bi-directional atmosphere-surface exchanges of elemental mercury, Atmos. Environ., 33, 4345–4355, doi:10.1016/S1352-2310(99)00245-9, 1999.

Zepp, R. G., Faust, B. C., and Hoigne, J.: Hydroxyl radical formation in aqueous reactions (pH 3–8) of iron(II) with hydrogen peroxide: the photo-Fenton reaction, Environ. Sci. Technol., 26, 313–319, doi:10.1021/es00026a011, 1992.

Zhang, H. and Lindberg, S. E.: Sunlight and Iron(III)-induced photochemical production of dissolved gaseous mercury in freshwater, Environ. Sci. Technol., 35, 928–935, doi:10.1021/es001521p, 2001.

Zhang, H., Fu, X. W., Lin, C.-J., Wang, X., and Feng, X. B.: Observation and analysis of speciated atmospheric mercury in Shangri-La, Tibetan Plateau, China, Atmos. Chem. Phys., 15, 653–665, doi:10.5194/acp-15-653-2015, 2015.

Zhang, L., Blanchard, P., Gay, D. A., Prestbo, E. M., Risch, M. R., Johnson, D., Narayan, J., Zsolway, R., Holsen, T. M., Miller, E. K., Castro, M. S., Graydon, J. A., Louis, V. L. St., and Dalziel, J.: Estimation of speciated and total mercury dry deposition at monitoring locations in eastern and central North America, Atmos. Chem. Phys., 12, 4327–4340, doi:10.5194/acp-12-4327-2012, 2012.

Zhang, Y., Jaeglé, L., van Donkelaar, A., Martin, R. V., Holmes, C. D., Amos, H. M., Wang, Q., Talbot, R., Artz, R., Brooks, S., Luke, W., Holsen, T. M., Felton, D., Miller, E. K., Perry, K. D., Schmeltz, D., Steffen, A., Tordon, R., Weiss-Penzias, P., and Zsolway, R.: Nested-grid simulation of mercury over North America, Atmos. Chem. Phys., 12, 6095–6111, doi:10.5194/acp-12-6095-2012, 2012.

Zhang, Y., Jaeglé, L., Thompson, L., and Streets, D. G.: Six centuries of changing oceanic mercury, Global Biogeochem. Cy., 28, 1251–1261, doi:10.1002/2014gb004939, 2014.

Résumé

Le mercure (Hg) est un métal émis dans l'atmosphère par des sources naturelles et anthropiques. Il est préoccupant à l'échelle mondiale de par sa propagation atmosphérique sur de longues distances, loin des sources d'émissions, sa persistance dans l'environnement, son potentiel de bioaccumulation dans les chaînes alimentaires aquatiques et ses effets néfastes sur la santé humaine. Les modèles atmosphériques, utilisés pour retracer son cheminement depuis les sources d'émissions jusqu'aux dépôts au sein des écosystèmes, sont entachés de fortes incertitudes en raison notamment de notre compréhension partielle des processus atmosphériques (réactions d'oxydo-réduction, dépôts, réémissions) et du manque de données d'observations à l'échelle planétaire. L'objectif de ces travaux de thèse est d'améliorer notre compréhension du cycle atmosphérique du Hg en trois sites reculés de l'Hémisphère Sud : l'île d'Amsterdam (AMS) en plein océan Indien, Concordia (DC) sur la calotte glaciaire antarctique et Dumont d'Urville (DDU) sur la côte Est du continent. Les données acquises à AMS démontrent une réactivité atmosphérique limitée du Hg dans cette région du globe. L'île étant faiblement et rarement influencée par des masses d'air continentales polluées, il s'agit d'un site clé pour la surveillance, sur le long terme, du bruit de fond atmosphérique aux moyennes latitudes de l'Hémisphère Sud. Les données acquises en Antarctique démontrent l'existence de processus inédits en termes de réactivité dans l'atmosphère et à l'interface air-neige. Les processus observés sur la calotte glaciaire influent par ailleurs sur le cycle du Hg à l'échelle continentale du fait des forts vents catabatiques. Ces avancées scientifiques permettront, à terme, de contraindre et d'améliorer les modèles atmosphériques globaux.

Abstract

Mercury (Hg) is a metal emitted by both natural and anthropogenic sources. It is of global concern owing to its long-range atmospheric transport, its persistence in the environment, its ability to bioaccumulate in ecosystems, and its negative effects on human health. Large uncertainties associated with atmospheric models – that trace the link from emissions to deposition of Hg onto environmental surfaces – arise as a result of our incomplete understanding of atmospheric processes (oxidation pathways, deposition, and re-emission) and of the scarcity of monitoring data at a global scale. The aim of this PhD work is to improve our understanding of the atmospheric Hg cycling at three remote sites of the Southern Hemisphere: Amsterdam Island (AMS) in the Indian Ocean, Concordia (DC) on the East Antarctic ice sheet, and Dumont d'Urville (DDU) on the East Antarctic coast. Data acquired at AMS suggest a limited atmospheric reactivity of Hg in this part of the globe. The advection of polluted continental air masses being scarce, AMS is a key site for the long-term monitoring of the atmospheric background in the Southern Hemisphere mid-latitudes. Data acquired in Antarctica highlight the occurrence of unprecedented processes in the atmosphere and at the air-snow interface. Due to katabatic winds flowing out from the East Antarctic ice sheet down the steep vertical drops along the coast, processes observed at DC influence the cycle of atmospheric Hg on a continental scale. These scientific breakthroughs will ultimately lead to improved global transport and deposition models.